Translation control to improve oncolytic virus efficacy and regulate inflammatory diseases

HUY-DUNG HOANG

Thesis submitted to the University of Ottawa

in partial fulfillment of the requirements for the degree of

Doctor of Philosophy,

with specialization in Biochemistry

Department of Biochemistry, Microbiology and Immunology

Faculty of Medicine

University of Ottawa

Ottawa, Ontario, Canada

© Huy-Dung Hoang, Ottawa, Canada 2021

Abstract

Translation control is crucial during virus-host interaction, in which the host relies on the translation machinery to mount an antiviral response or induce the inflammation response to reduce virus spread, while the virus aims to take control of this system to thwart the host defense while producing viral progeny. The field of oncolytic virus (OV) therapy relies on replicating, engineered viruses that preferentially infect tumor cells to induce direct oncolysis or promote an antitumor immune response. Despite the importance of translation control in virus-host interaction, not much has been described on the interaction at the translation level between OV and cancer cells. I propose that this knowledge gap could reveal significant improvements in OV efficacy in treating cancer. In my first study, I set out to characterize the translatome of an infection-resistant breast cancer cell line infected by three clinically advanced OVs to identify residual antiviral activity in cancer cells regulated by translation control. I found the inositol phosphatase *Inpp5e* to be a novel antiviral gene that is translationally induced during infection via a transcript variant shift. Mechanistically, I showed that the majority of *Inpp5e* transcripts in uninfected cells contain a long 5' UTR that harbor four translationally inhibitory upstream reading frames (uORF). Yet, OV infection induced the expression of a shorter 5' UTR with a spliced intron that removes three uORFs, derepressing the translation of *Inpp5e* mRNA. CRISPR-Cas9 knockout of *Inpp5e* also enhanced the infectivity of oncolytic HSV1 and VSV. My study suggests the existence of a class of translationally regulated antiviral genes in cancer cells. In my second study, I sought to adapt the translation of transgenes to the unique translation condition imposed by the infecting virus via the incorporation of a viral 5'UTR. I identified HSV1 5'UTRs by locating the transcription start site of most HSV1 genes using RNA-seq data, then determined the 5'UTR of US11 as a potent translation enhancer during HSV1 infection. Incorporation of this 5'UTR into the transgene expression cassette inserted into the HSV1 genome enhanced transgene expression significantly at the translation level. In my third study, I set out to explore the mechanism of miR-223 mediated inflammation inhibition. miR-223 is a protective miRNA in the context of atherogenesis via suppressing inflammatory signaling. Using transcriptome and translatome profiling (RNA-seq and Ribo-seq), I found that the inhibitory effect of miR-223 on inflammation occurs primarily at the translation level. Overall, my work highlights the importance of translation control in OV-cancer cells interaction, as well as in inflammation-related diseases.

ACKNOWLEDGEMENT

"*No man is an island, entire of itself*", John Donne.

This thesis is built upon the support of the Alain lab current and past members, the thriving scientific and collegial environment of Children's Hospital of Eastern Ontario Research Institute II, fruitful collaborations and mentorships from scientists and students at the University of Ottawa, and the body of knowledge accumulated by the tireless works of many scientists across the world.

To Dr. Tommy Alain, my journey would not be possible without you offering me the chance to be a member of your lab. Your patience and trust, despite my novice beginning and complete lack of background in virus and translation regulation, allowed me to fully grow my inquisitive spirit and to pursue my own curiosity. I cannot imagine a better environment to conduct my Ph.D.

To the senior members of the Alain lab, Dr. Tyson Graber, Dr. Bruno Fonseca, and Jian-Jun Jia, I would like to thank you for your endless patience and inspiration in passing your way of science to me. I learned a lot about how to be a scientist from you.

I would like to thank my Thesis Advisory Committee members, Drs. Katey Rayner, Marceline Côté, and John Copeland for their critical discussion, scientific support and inspiration. I would like to especially thank Dr. Rayner for introducing me to Tommy when I was looking for a Ph.D student opening in Canada, which turned out to be an extraordinary journey, and for your support in collaboration with your lab.

To the trainees of the 4th floor of RI II, thank you for being my companions, sharing the ebb and flow of our trainee life. My journey through Ph.D would be less exciting without you.

To Lynn Kyte, Keith Wilson, and the support staff of CHEO RI II, thank you for taking great care of the Research Institute. The RI II appears to descend into chaos every time you take a vacation.

To my dad, mom and Trúc, thank you for being my family. Your ever unconditional support is instrumental for me to become who I am today, I owe my success to you.

Last but foremost, to My-Anh, I thank you for sharing our life through thick and thin. No word is needed between us, but I cherish every moment we spent together and look forward to many more.

TABLE OF CONTENTS

Abstract.....II
ACKNOWLEDGEMENT..... III
List of Abbreviations..... IX
List of Figures.....XV
List of Tables.....XVII
CHAPTER 1. Introduction..... 1
1.1. Basic of translation control in eukaryotic cells..... 3
1.1.1 The canonical cap-dependent translation control in mammalian cells..... 3
1.1.2. To translate the messenger: various mechanisms to modulate the translation rate of a mRNA..... 8
1.1.3. Suppressing translation during stress: the integrated stress response 14
1.2. The unique translation environment of the infected cells..... 16
1.2.1. The translation control arm of the antiviral response..... 17
1.2.2. The virus strikes back: viral strategies to control the host's translation machinery 23
1.3 Translation control in oncolytic viruses 28
1.3.1. A brief introduction of oncolytic viruses..... 28
1.3.2. On tumor selectivity of oncolytic viruses..... 29
1.3.3. Engineering oncolytic viruses 33
1.3.4. The knowledge gap of translation regulation in virus-host interaction and OV design: challenges and potentials..... 35
1.4. Translation control of the inflammation response via miRNAs 38
1.4.1. Translation control and the innate immunity..... 38
1.4.2. miRNA as a player in translation control of the inflammation response 40
1.4.3. Atherosclerosis and inflammation..... 41
1.5. Summary 42
CHAPTER 2. Induction of an Alternative mRNA 5' Leader Enhances Translation of the Ciliopathy Gene *Inpp5e* and Resistance to Oncolytic Virus Infection..... 44
2.1. Author contributions..... 44
2.2. Abstract 44
2.3. Introduction 45
2.4. Materials and Methods 47
2.4.1. Cell culture and viruses 53
2.4.2. Lentivirus production and plasmids 54

2.4.3. Poly(I:C) treatment 55
2.4.4. Polysome profiling 55
2.4.5. Metabolic labeling and cell viability 55
2.4.6. Ribosome profiling 56
2.4.7. Mapping and analysis of ribosome profiling data 57
2.4.8. Functional analysis of DEGs 57
2.4.9. Immunocytochemistry 58
2.4.10. Western blotting 59
2.4.11. Quantitative RT-PCR (RT-qPCR) and Droplet Digital RT-PCR (RT-ddPCR) 59
2.4.12. CAT translation reporter assays 60
2.4.13. CRISPR/Cas9-mediated gene knockout 61
2.4.14. Live cell monitoring of virus spread 62
2.4.15. Plaque assays 62
2.4.16. Binding assays 63
2.4.17. Quantification and Statistical Analyses 63
2.4.18. Data and Code Availability 63
2.5. Results 64
2.5.1. Transcription and translation are uncoupled in response to oncolytic virus infection of 4T1 cells 64
2.5.2. Genes of the common translatome between all three infections function in pathways not previously associated with viral infections 67
2.5.3. Oncolytic viruses de-repress translation of host mRNAs enriched in uORFs 69
2.5.4. INPP5E is translationally induced during the host antiviral response 73
2.5.5. Expression of an alternative 5’ leader during infection releases Inpp5e from uORF-mediated translational repression 77
2.5.6. INPP5E functions as an antiviral effector that modifies viral binding 83
2.6. Discussion 87
2.7. Acknowledgements 102
CHAPTER 3. A Viral Leader Sequence Enhances Translation of GM-CSF Encoded Within Oncolytic HSV1 103
3.1. Author contributions 103
3.2. Abstract 103
3.3. Introduction 104
3.4. Materials and Methods 106
3.4.1. Cell culture and viruses 106

3.4.2. Plasmid construction 106
3.4.3. RNA-seq mapping and TSS identification 108
3.4.4. CAT reporter assay 108
3.4.5. Quantitative RT-PCR 109
3.4.6. Western Blot 109
3.4.7. Live-cell monitoring of GFP expression 110
3.4.8. Generating recombinant HSV1 viruses 110
3.4.9. Plaque titration 111
3.4.10. Polysome fractionation 111
3.4.11. GM-CSF quantification 112
3.4.12. Single step-growth curve and monitoring HSV1 genes expression 112
3.4.13. Data and Code Availability 112
3.4.14. Statistical analyses 112
3.5. Results 113
3.5.1. Determining HSV1 mRNA leader sequence 113
3.5.2. The US11 leader enhances translation of downstream ORFs in HSV1-infected cells 117
3.5.3. The US11 leader enhances transgene protein expression from a recombinant HSV1 genome 122
3.5.4. The HSV1 US11 leader confers increased translation efficiency on the downstream transgene in a HSV1 dependent manner 127
3.6. Discussion 131
3.7. Acknowledgements 149
CHAPTER 4. miR-223 Exerts Translational Control of Cholesterol Efflux and Inflammatory Pathways to Protect from Atherosclerosis 150
4.1. Author contributions 150
4.2. Abstract 150
4.3. Introduction 152
4.4. Materials and Methods 155
4.4.1. Reagents 155
4.4.2. Mice 155
4.4.3. Macrophage isolation and polarization 155
4.4.4. Cell transfection with miRNA mimics 156
4.4.5. Cholesterol efflux 156
4.4.6. miRNA and gene expression analysis 156

4.4.7. Western blot analysis 157
4.4.8. Atherosclerosis PCR pathway array analysis 158
4.4.9. Atherosclerosis studies 158
4.4.10. Gene expression analysis in mouse aorta 159
4.4.11. Ribosome profiling 160
4.4.12. Statistics 161
4.5. Results 162
4.5.1. miR-223 positively regulates ABCA1 expression and promotes macrophage cholesterol efflux in vitro 162
4.5.1. miR-223 suppresses macrophage pro-inflammatory activation and promotes macrophage polarization toward the anti-inflammatory phenotype in vitro 165
4.5.3. Deletion of miR-223 in BM-derived cells promotes atherogenesis and enhances inflammatory signaling 168
4.5.4. Global analysis of transcription and translation regulation by miR-223 in macrophages 172
4.6. Discussion 178
4.7. Acknowledgements 188
CHAPTER 5. General Discussion 189
5.1. Enhancing therapeutic efficacy of OVs via targeting *Inpp5e* and other translationally induced antiviral genes 190
5.2. Translational derepression/upregulation as a novel mechanism for antiviral gene expression 193
5.3. Translational adaptation as an approach to tailor oncolytic viruses 197
5.4. On the effect of miRNA-mediated translation control of the immune response 200
5.6. Conclusion 201
REFERENCES 202
APPENDICES 226
6.1 Quercetin Induces Pannexin 1 Expression via an Alternative Transcript with a Translationally Active 5'Leader in Rhabdomyosarcoma (Co-First Author article) 226
6.1.1 Abstract 227
6.1.2. Introduction 228
6.1.3. Materials and Methods 230
6.1.4. Results 237
6.1.5. Discussion 246
6.1.6. Acknowledgements 251

6.1.7. References 226
6.2. Battling for Ribosomes: Translational Control at the Forefront of the Antiviral Response 272
6.2.1 Author contributions 272
6.2.2. Abstract 272
6.2.3. Parasitizing protein synthesis 273
6.2.4. A brief introduction to eukaryotic mRNA translation 274
6.2.5. Translational control at the forefront of the antiviral response 277
6.2.6. Viruses fight back: Viral manipulation of host translation 292
6.2.7. Studying translation during viral infection: Technological progress and limits 300
6.2.8. Perspectives 307
6.2.9. Acknowledgments 310
6.2.10. References 319
6.3. Emerging translation strategies during virus–host interaction 333
6.3.1 Author contributions 333
6.3.2. Abstract 333
6.3.3. INTRODUCTION 334
6.3.4. EMERGING TRANSLATION STRATEGIES DURING VIRUS–HOST INTERACTION 339
6.3.5. CONCLUSION AND PERSPECTIVE 355
6.3.6. Acknowledgments 357
6.3.7. References 357
6.4 Copyrights 367
6.5. Curriculum vitae 374

List of Abbreviations

4E-BP	eIF4E binding protein
4EHP	eIF4E homologous protein
5-FC	5-fluorocytosine
5-FU	5-fluorouracil
5'TOP motif	5'terminal oligo pyrimidine motif
ABETA	amyloid beta
AGO2	argonaute 2
APC	antigen-presenting cell
ARE	AU-rich element
ATF4	activating transcription factor 4
BiP	binding immunoglobulin protein/immunoglobulin heavy chain binding protein
CAI	codon adaptation index
CCL15	C-C motif ligand 15
CCR4-NOT	carbon catabolite repression 4 - negative on TATA-less
CD	cytosine deaminase
CD38	cluster of differentiation 38
CD4	cluster of differentiation 4
CD8	cluster of differentiation 8
CDK1	cyclin dependent kinase 1
CDS	coding sequence
CHOP	C/EBP homologous protein
CP	ceruloplasmin
CRM1	chromosome protein maintenance 1
CXCL10	C-X-C motif chemokine ligand 10
Cyr61	cysteine-rich angiogenic inducer 61
DAMP	damage-associated molecular pattern
dNTP	deoxynucleoside triphosphate
dsRNA	double-stranded RNA

E1A	early region 1 A
E1B	early region 1 B
eEF	eukaryotic elongation factor
EGFR	epithelial growth factor receptor
eIF2	eukaryotic initiation factor 2
eIF3	eukaryotic initiation factor 3
eIF4A	eukaryotic initiation factor 4A
eIF4B	eukaryotic initiation 4B
eIF4F	eukaryotic initiation factor 4F
eIF4G	eukaryotic initiation factor 4G
ER	endoplasmic reticulum
eRF1	eukaryotic release factor 1
eRF3	eukaryotic release factor 3
ERPS	glutamyl-prolyl tRNA synthetase
FGF	fibroblast growth factor
GADD34	growth-arrest and DNA damage-inducible protein 34
GAIT	IFN-γ activated inhibitor of translation
GAPDH	glyceraldehyde 3-phosphate dehydrogenase
GCN2	general control non-depressible 2
GCPR	G-coupled protein receptor
GDP	guanosine diphosphate
GM-CSF	granulocyte-macrophage colony-stimulating factor
GTP	guanosine triphosphate
GW182	glycine-tryptophane protein of 182 kDa
HCMV	human cytomegalovirus
HIV	human immunodeficiency virus
hnRNP A1	heterogeneous nuclear ribonucleoprotein A1
HRI	heme-regulated inhibitor
HSV1	herpes simplex virus 1
HuR	human antigen R

IAV	influenza A virus
ICI	immune checkpoint inhibitor
ICP34.5	infected cell protein 34.5
IE	immediate early
IFIT	interferon induced protein with tetratricopeptide repeat
IFN	interferon
IL12	interleukin 12
IL2	interleukin 2
INPP5B	inositol polyphosphate-5-phosphatase B
INPP5D	inositol polyphosphate-5-phosphatase D
INPP5E	inositol polyphosphate-5-phosphatase E
IRAK1	interleukin 1 receptor associated kinase 1
IRES	internal ribosome entry site
IRF7	IFN regulator factor 7
ISG	interferon stimulated gene
ISG15	interferon stimulated gene 15
ISR	integrated stress response
ITAF	IRES trans-acting factor
KLF2	Kruppel-like factor 2
LARP1	La-related protein 1
LPS	lipopolysaccharide
LST8	lethal with Sec13 protein 8
m7G	7-methylguanosine
MCMV	murine cytomegalovirus
Met-tRNAi	initiator methionine-tRNA
MeV	measle virus
miRNA	microRNA
MORM	mental retardation, truncal obesity, retinal dystrophy and micropenis
mRNA	messenger RNA
mTORC1	mechanistic target of rapamycin complex 1

myc	myelocytomatosis oncogene
NAP1L1	nucleosome assembly protein 1-like 1
NDV	Newcastle disease virus
NF-κB	nuclear factor kappa-light-chain-enhancer of activated B cells
NIS	Na(sodium)-iodine symporter
NPM1	nucleophosmin 1
NS1	non-structural protein 1
NXF1	nuclear RNA export factor 1
ORF	open reading frame
OV	oncolytic virus
PABP	poly(A) binding protein
PAMP	pathogen-associated molecular pattern
PB1	polymerase basic protein 1
PDCD4	programmed cell death protein 4
PERK	PKR-like ER kinase
PI(4,5)P2	phosphatidyl-inositol-4,5-biphosphate
PI3K	phosphoinositide 3 kinase
PIC	preinitiation complex
PKR	protein kinase R
pORF	primary open reading frame
PP1	protein phosphatase 1
pre-miRNA	premature microRNA
pri-miRNA	primary microRNA
PTEN	phosphatase and tensin homolog
RACK1	receptor of activated protein kinase 1
Raptor	regulatory protein associated with mTOR
Ras	rat sarcoma
RB	retinoblastoma
RBP	RNA-binding protein
Rev	regulator of expression of viral protein

RGNNV	red-spotter grouper nervous necrosis virus
Ribo-seq	ribosome profiling/ribosome footprint sequencing
RISC	RNA-induced silencing complex
RNA-seq	RNA sequencing
rRNA	ribosomal RNA
RTK	receptor tyrosine kinase
S6K1	protein S6 kinase 1
SG	stress granule
SHIP1	Src homology 2 (SH2)-domain containing inositol 5-phosphatase 1
shRNA	short hairpin RNA
SINV	SINV
siRNA	short interfering RNA
SPI-1	serine protease inhibitor 1
SPI-2	serine protease inhibitor 2
ssRNA	single-stranded RNA
TAA	tumor associated antigen
TBEV	tick-borne encephalitis virus
TC	ternary complex
TERT	telomerase reverse transcriptase
TIA1	T-cell-restricted intracellular antigen-1
TIAR	TIA1-related protein
TK	thymidine kinase
TLR	toll-like receptor
TP53	tumor protein 53
TRAF6	tumor necrosis factor receptor (TNFR)-associated factor 6
tRNA	transfer RNA
TSC1/2	tuberous sclerosis 1/2
TSS	transcription start site
TTP	tristetraprolin
T-VEC	talimogene laherparepvec

uORF	upstream open reading frame
UPR	unfolded protein response
UTR	untranslated region
UV	ultraviolet
VACV	vaccinia virus
VEGF	vascular endothelial growth factor
Vhs	virion-host shutoff
VSV	vesicular stomatitis virus
WNV	West-Nile virus

List of Figures

Figure 1.1: Assembling the translation machinery 7

Figure 1.2: Mechanism of uORF-mediated translation inhibition 12

Figure 1.3. Translational control during viral infection 20

Figure 2.1. Transcription and translation are uncoupled in response to oncolytic virus infection of 4T1 cells 66

Figure 2.2. Genes of the common translatome between all three infections function in pathways not previously associated with viral infections 68

Figure 2.3. Oncolytic viruses de-repress translation of host mRNAs enriched in uORFs 72

Figure 2.4. INPP5E is translationally induced during the host antiviral response 76

Figure 2.5. Expression of an alternative 5′ leader during infection releases Inpp5e from uORF-mediated translational repression 79

Figure 2.6. INPP5E acts as an antiviral effector that modifies viral binding 85

Figure 2.7. Model of translationally induced antiviral genes in cancer cells via isoform switch 92

Figure S2.1. Quality control of the ribosome profiling experiments. 93

Figure S2.2. The cellular response to infection exhibits an antiviral state at the transcriptional level 94

Figure S2.3. Characterizing cis-elements in the common translationally regulated transcripts 95

Figure S2.4. CRISPR-Cas9 knock-out of INPP5E in 4T1 cells 96

Figure S2.5. Evidence of variant switching with infection 97

Figure S2.6. Characterizing the role of candidate proteins in modifying viral infection 98

Figure 3.1. Characterizing HSV1 individual transcript from RNA-seq coverage 117

Figure 3.2. HSV1 US11 and UL27 leader sequences mediate enhanced expression of protein reporters in HSV1-infected mammalian cells 121

Figure 3.3. A recombinant HSV1 virus exhibits a US11 leader-dependent boost in GM-CSF expression 126

Figure 3.4. The HSV1 US11 leader confers increased translation efficiency of the downstream transgene 131

Figure S3.1. Examples of spliced junction detected on known HSV1 spliced transcripts 138

Figure S3.2. Full RNA-seq coverage of HSV1 genome 139

Figure S3.3. Relative mRNA expression level of the 10 late genes selected as candidates 143

Figure S3.4. Translation reporter screen for HSV1 leader that enhance translation during HSV infection 144

Figure S3.5. US11 leader enhancement is robust in different cell types and species 146

Figure 4.1. miR-223 positively regulates ABCA1 expression and promotes macrophage cholesterol efflux 165

Figure 4.2. miR-223 suppresses macrophage pro-inflammatory activation and promotes macrophage polarization toward the anti-inflammatory phenotype 169

Figure 4.3. Deletion of miR-223 in BM cells promotes atherogenesis and enhances inflammatory signaling 171

Figure 4.4. Global analysis of transcription and translation regulation in miR-223-/- BMDMs 175

Figure 4.5. Ingenuity Pathway Analysis revealed activation of inflammation signaling at the transcription and translation level in BMDMs 178

Figure S4.1. The expression of Abca1 and macrophage activation markers 184

Figure S4.2. Body weight, plasma cholesterol and circulating levels of most leukocytes and lymphocytes are unchanged in mice receiving miR-223 BM 185

Figure S4.3. Indirect regulation of atherosclerosis gene expression by miR-223 186

Figure S4.4. RNAseq and Riboseq analysis of gene expression in BMDMs 187

Figure S4.5. Ingenuity Pathway Analysis characterize the effect of miR-223 removal on BMDMs 189

List of Tables

Table S2.1 TE and RNA Expression of All Genes in Virus- versus Mock-Infected 4T1 Cells, Related to Figure 2.1E ..... (attached file)

Table S2.2 List of Common and Unique Sets of DEGs between Viral Infections at the Transcriptional and Translational Levels, Related to Figure 2.2A ..... (attached file)

Table S2.3 GO Terms Enriched for the DEGs Commonly Regulated by All Three Viruses at the Transcriptional and Translational Levels, Related to Figures 2B and 2C ..... (attached file)

Table S2.4 Oligonucleotides used in this study, related to Figures 2.4-6..... 101

Table 3.1: Identified HSV1 TSS in this study 136

Table 3.2: Sequence of HSV1 leader identified in this study ..... (attached file)

Table S3.1. Oligonucleotides used in this study 147

Table 4.1. Most significantly different genes (up- or down-regulated) in miR-223-/- macrophages 173

CHAPTER 1. Introduction

The central dogma of molecular biology describes the flow of information in a cell: information is stored in a permanent form in DNA, which is accessed via transcription into the temporary molecule messenger RNA (mRNA) that is then translated into protein, the primary structural and functional molecule of the cell. The dogma also presents a fascinating fact about life: approximately 3.1 billion base pairs in our DNA encode *us* including every aspect of our life, from the fertilization of the fetus to the full development of the body with precise spatial and temporal orchestration of hundreds of different cell types, how our body exchange energy and material with the environment, fight pathogens, and most definitely our consciousness that is unique amongst animal to the best of our knowledge, are concisely encrypted in this string of nucleotides. How can so little space encode so much information? Following the sequencing of the human genome, transcription profiling studies provided a glimpse at how the complexity of life is contained in the compactness of the genome: the key to the extraordinary coding capacity of the genome may lie in gene expression regulation that dictates which gene and how much of it is expressed. This can result in an almost infinite number of combinations of possible gene expression patterns that define each cell, cellular state and cell process. Since then, gene expression has proven itself to be much more complicated. Various extra layers of gene expression regulations have been discovered and incorporated before and after transcriptional regulation since the central dogma's inception: epigenetic, alternative splicing, nuclear export, post-transcription modification/epitranscriptomic, mRNA translation, and protein stability have all been shown to contribute to different phenotypes in mammalian cells. Each extra layer of gene expression regulation adds one more dimension to exponentially increase the number of possible cellular states and types that can be encoded by the genome, bringing biology closer and closer to

understanding and modeling life. Amongst known gene regulation mechanisms, mRNA translation is perhaps one of the most critical layers of regulation that define mammalian gene expression. It was found early that mRNA and protein levels are poorly correlated in bacteria[1], yeast[1–3], *Arabidopsis thaliana*[4], *Drosophila melanogaster*, and *Caenorhabditis elegans*[5], and recently mammalian cells[6], suggesting that the regulation of translation output plays an essential role in shaping the cellular proteome and phenotype. Indeed, translation control was found to be involved in every aspect of mammalian cells and organisms, from virus-host interaction, embryo development to memory and learning[7].

Translation control plays a crucial role in virus infection: being an incomplete life form that exists strictly by using their genetic material to hijack the host cell, viruses make the host translation machinery a primary target to usurp for the ultimate purpose of transforming the host cell into a virus-producing factory[8]. Yet, upon sensing the invader, the host cell also relies on the translation machinery to mount an emergency response. The innate antiviral immunity, activated minutes to hours after viral infection, depends on the translation machinery to produce antiviral proteins to fight the viruses. The antiviral response can even include a global shutoff of protein synthesis to restrict viral replication in the infected cells. These opposing forces from both the host and the virus create a unique translation environment in the infected cells, yet this area of translation control remains poorly explored comparing to the more rigorously studied transcriptional control of the antiviral state and interferon stimulated genes (ISGs).

In the last two decades, we have learned to harness viruses as powerful tools to treat human diseases; the most notable uses are as gene therapy vectors, replicating vaccines, and oncolytic agents targeting cancer. These applications inevitably find themselves in the poorly charted zone of gene expression control during virus-host interaction, where understanding and adapting

virotherapies to the conditions of the infected cells are crucial for the efficacy of the methods. Thus, studying translation control in infected cells will benefit not only the treatment of viral diseases, but also the development of more effective virotherapies. Additionally, dysregulation of translation control was found to be responsible for the development of various diseases and dysfunctions, most notably cancer, cardiovascular disease, and abnormal developmental processes[9]. The dysregulation of translation control in cancer is well established, with uncontrolled activation of various signaling pathways found in a range of cancer types. Another particularly interesting disease, atherosclerosis, is intimately connected to inflammation, which in turn is regulated via translation control. Thus, a detailed understanding of the role of translation regulation in human diseases will undisputedly benefit us on the path to find effective treatments for various maladies.

1.1. Basic of translation control in eukaryotic cells

1.1.1 The canonical cap-dependent translation control in mammalian cells

At the center of the mammalian translation control is the mechanism of cap-dependent translation. A prototypical mammalian mRNA consists of the following elements, listed from a 5' to 3' order: a 5' cap, the 5' untranslated region (UTR), the primary open reading frame (ORF) followed by a 3'UTR that terminates with a poly(A) stretch. At the 5' termini, a 7-methylguanosine (m^7G) is linked to the first ribonucleotide of the mRNA via a triphosphate link and is called the 5' cap, which is important for the stability and translation of the mRNA. Immediately after the 5' cap is the 5'UTR, which contains various sequences and structural *cis*-elements that influence the translation initiation step. Interestingly, despite its name, the 5'UTR can harbor small upstream open reading frame(s) (uORF) that can be translated[10]. The primary ORF begins at a start codon, canonically an AUG codon with a strong Kozak context (gccgccRccAUGG in human, where R is

a purine) but can alternatively be a CUG or other alternative start codons and ends with a stop codon. The 3'UTR region follows the ORF and might include *cis*-elements that modify the translation and stability of the mRNA, most importantly miRNA binding sites and RNA-binding protein (RBP) binding sites. Finally, at the 3' end of the mRNA is a long chain of adenine bases, added after transcription and is important for the circularization of the mRNA, which again affects translation and stability[11].

The cap-dependent translation is conserved in eukaryotic cells and can be divided into three steps: translation initiation, elongation, and termination (**Figure 1.1**)[8]. Translation initiation is the rate-limiting step and is strictly regulated, responsible for assembling an elongation-competent 80S ribosome at the translation start site from the 40S and 60S ribosomal subunits. The initiation step starts with the docking of the eIF4F (eukaryotic initiation factor 4F) complex at the 5' cap via interaction of the cap-binding protein eIF4E (eukaryotic initiation factor 4E) with the 7-methylguanosine cap. The complex also includes the scaffolding protein eIF4G (eukaryotic initiation factor 4G) that serves as an assembling platform for other initiating factors, and the RNA helicase eIF4A (eukaryotic initiation factor 4A) that helps resolve secondary structures in the 5'UTR. The 40S subunit is charged with an initiator methionine-tRNA (Met-tRNAi), provided by the ternary complex (TC) that is composed of the three eIF2 subunits: eIF2α, eIF2β, and eIF2γ. The initiation factors eIF1, eIF1A, eIF3, and eIF5 facilitate the association of the TC to the 40S subunit, forming the 43S preinitiation complex (PIC). This complex is then assembled on the eIF4F complex via eIF4G-eIF3 interaction, and the mRNA strand is situated into the mRNA channel of the 40S subunit so that the Met-tRNAi can inspect the nucleotide sequence[12]. The 43S PIC then starts scanning the mRNA from the 5' termini, seeking a strong base pairing with the Met-tRNAi. Although an AUG in a strong Kozak context (gccgccRccAUGG) was initially thought

to be the only codon capable of base pairing with Met-tRNAi, recent studies have found that other codons, including CUG, GUG or UUG, can also serve as alternative start codons, albeit to a lesser extent[13,14]. Engagement of the 43S PIC with a start codon triggers hydrolysis of GTP to GDP, forming the 48S pre-initiation complex. The eIFs are then released while the 60S subunit is simultaneously recruited via the help of eIF5 and eIF5B, which forms an elongation-competent 80S ribosome. It is important to note that of the released eIFs, the eIF2.GDP is recycled by the guanidine nucleotide exchange factor eIF2B, which replaces the GDP with GTP and makes eIF2 ready for a new round of initiation. The recycling of eIF2 is a critical step in regulating translation initiation via the phosphorylation of the α subunit of eIF2 at serine 51 (P-eIF2α), which enhances the affinity of eIF2 for eIF2B and effectively trapping eIF2B as well as eIF2 in the inactive GDP-bound state. This will be discussed in more details later in this thesis.

Translation elongation and termination are relatively simpler than the initiation step. The elongation step starts with the delivery of an amino acyl-tRNA by eukaryotic elongation factor (eEF) 1A to the A-site of the ribosome. Peptidyl bond is formed between the amino acid or peptide chain at the P- sites and the aa-tRNA at the A-site. The translocase eEF2 then rachets the ribosome toward the 3’ end of the mRNA in a GTP-dependent manner, positioning the peptidyl-tRNA to the P-site and the de-acylated tRNA to the E-site, freeing the A-site for the next round of elongation. The termination step takes place when a stop codon (UGA, UAG or UAA) reaches the A-site of the ribosome. A translation termination complex, consisting of the GTPase eukaryotic release factor 3 (eRF3) and the tRNA-mimic eRF1, is delivered to the A-site. Recognition of a stop codon by eRF1 triggers GTP hydrolysis and dissociation of eRF3. The eRF1 then catalyzes the release of the polypeptide chain from the tRNA at the P-site. The ATPase ABCE1 further facilitates peptide release and mediates the dissociation of the 80S ribosome for recycling[15].

CHAPTER 1

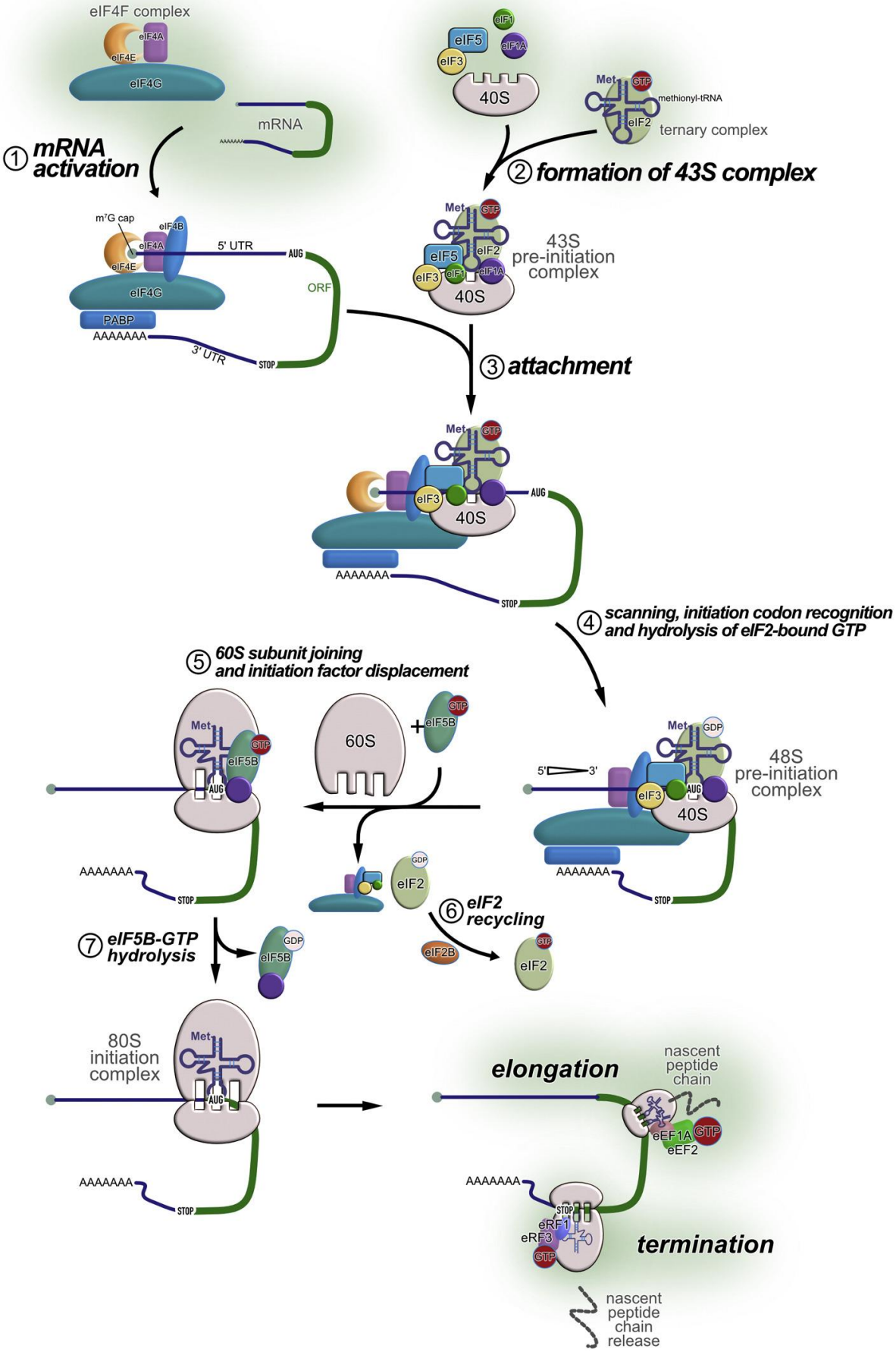
eIF4F complex
eIF4A
eIF4E
eIF4G
mRNA
① mRNA activation
eIF1
eIF5
eIF1A
eIF3
40S
Met
GTP
methionyl-tRNA
eIF2
ternary complex
② formation of 43S complex
m7G cap
eIF4B
5' UTR
AUG
ORF
PABP
AAAAAAA
3' UTR
STOP
43S pre-initiation complex
③ attachment
④ scanning, initiation codon recognition and hydrolysis of eIF2-bound GTP
⑤ 60S subunit joining and initiation factor displacement
60S
eIF5B
GDP
eIF2
48S pre-initiation complex
5'
3'
⑥ eIF2 recycling
eIF2B
⑦ eIF5B-GTP hydrolysis
80S initiation complex
elongation
nascent peptide chain
eEF1A
eEF2
termination
eRF1
eRF3
nascent peptide chain release

Figure 1.1: Assembling the translation machinery. Translation initiation is highly regulated and can be divided into seven steps. (1) mRNA activation: The eIF4F complex interacts with the m^7G cap structure at the 5′ terminus of the mRNA; this cap-binding complex comprises the cap-binding protein eIF4E, the scaffold protein eIF4G, and the RNA helicase eIF4A. The closed loop model is illustrated, where eIF4G interactions with PABP bound to the poly(A) tail effectively circularize the mRNA and synergistically enhance initiation. (2) Formation of the 43S preinitiation complex: The TC made up of eIF2-GTP bound to Met-tRNAi joins with the 40S small ribosomal subunit along with eIF1, eIF1A, eIF5, and eIF3. (3) Attachment: The 43S complex is recruited to the eIF4F-activated mRNA through interactions between eIF3 subunits and eIF4G. (4) Scanning, initiation codon recognition and hydrolysis of eIF2-bound GTP: The 43S complex scans the 5′ UTR of the mRNA in a 5′ to 3′ direction until it reaches an initiation (start) codon. Engagement of the initiation codon by the Met-tRNAi anticodon triggers hydrolysis of GTP bound to eIF2, forming the 48S pre-initiation complex. (5) 60S subunit joining and initiation factor displacement: The eIFs are released concurrently with recruitment of the 60S ribosomal subunit which is mediated by eIF5B-GTP together with eIF1A which displace eIF2-GDP. (6) eIF2 recycling: The GEF activity of eIF2B converts eIF2-GDP back to eIF2-GTP, allowing it to participate in another round of initiation. (7) eIF5B-GTP hydrolysis: GTP hydrolysis and release of eIF5B and eIF1A forms the elongation-competent 80S initiation complex. Next, elongation is mediated by aminoacyl-tRNA delivered through eEF1A, ribosome-catalyzed peptide bond formation and eEF2-mediated ribosome translocation. Following multiple cycles of elongation, the ribosome reaches a stop codon. Here, termination of translation ensues with recruitment of the tRNA mimic eRF1 together with the GTPase eRF3, which triggers release of the peptide from the ribosome. Figure reprinted from Hoang *et al*., 2018[8] with permission from Journal of Molecular Biology.

1.1.2. To translate the messenger: various mechanisms to modulate the translation rate of an mRNA

Although it was generally thought to be generally constant, translation rate is now understood to vary widely between different cellular states or between transcripts in the same cell. In a most detailed study so far of gene expression in mammalian cells using genome-wide quantification of mRNA and protein levels, Schwanhausser *et al.* found that the median transcription rate is about two transcripts per hour, with the specific rate ranging from 0.1 to 10 mRNAs/hour. Yet, the median translation rate is approximately 140 protein molecules per mRNA per hour, and the actual range spans four orders of magnitude from 1 to 10^4 proteins per mRNA per hour, which is significantly more dynamic than transcription[16]. This study, together with others, suggests that translational output varies greatly between individual mRNAs and is a powerful regulatory layer of gene expression in mammalian cells. Various mechanisms are responsible for controlling the translation rate of an mRNA, primarily via signaling of the mTORC1 (mechanistic target of rapamycin complex 1) axis, the integrated stress response (ISR), and *cis*-elements in the UTRs of mRNA that regulate translation *per se* or via interaction with miRNAs as well was RBPs. Additionally, the field of translation control also continuously discovers novel mechanisms that affect translation, such as m6A-methylation of mRNA or tRNA fragments. The most relevant and well-studied mechanisms will be discussed in the following section.

Controlling translation initiation via mTORC1

The mTORC1 complex is at the center of an extended signaling network that senses environmental conditions and regulates cell growth and proliferation accordingly. The complex is formed from the mechanistic target of rapamycin (mTOR), Raptor (regulatory protein associated

with mTOR), and LST8 (lethal with Sec13 protein 8)[17–19]. It receives signaling inputs from growth factors, amino acids, energy, oxygen and stress, and regulates protein synthesis, anabolism and catabolism, and protein turnover[20]. Regarding protein synthesis, mTORC1 controls mRNA translation rate via its downstream kinase substrates/effectors, most importantly S6K1 (protein S6 kinase 1), 4E-BPs (eIF4E binding proteins), and LARP1 (LA-related protein 1)[21–24]. mTORC1 phosphorylates S6K1 on Thr389 residue, enabling its kinase activity on downstream substrates, including the translation initiation factor eIF4B and the ribosomal protein S6 to promote elongation[21]. Additionally, S6K1 also phosphorylates and induces the degradation of PDCD4 (programmed cell death protein 4), an inhibitor of eIF4A and eIF4B[25]. The 4E-BPs family consists of three members including 4E-BP1, 2 and 3 that are inhibitors of translation initiation: the hypo-phosphorylated forms of 4E-BPs bind to eIF4E and inhibit cap-dependent translation[26]. Phosphorylation of 4E-BPs by mTORC1 at multiple sites mediates its release from eIF4E and thus stimulates translation. Recently, I contributed to the discovery that LARP1 is a phospho-substrate of mTORC1 that also mediates translation of a subset of mRNAs containing the 5'TOP (terminal oligo pyrimidine) motif, a motif commonly found at the 5' end of mRNAs of ribosomal proteins and translation factors that are important for cell growth[24,27]. Although the mechanism of LARP1-mediated translation regulation is not yet clear, the protein is found to bind to the 5' cap of mRNAs containing a 5'TOP motif, competing with eIF4E for cap binding[28] and in doing so, effectively decreasing translation initiation of this subset of transcripts. However, binding of LARP1 to TOP mRNAs also promotes mRNA stability[24,29]. On the other hand, the most recent findings show that phosphorylation of LARP1 by mTORC1 promotes its release from the 5' cap and allows translation of TOP mRNAs[30].

Tailoring ribosome load via *cis*-elements on the 5'UTR

Flanking the coding sequence (CDS) are the 5' and 3'UTRs, described initially as non-coding regions that do not contain information for protein synthesis but are critical for ribosome recruitment to the CDS as well as mRNA stability via various *cis*-elements. These sequences affect translation through forming secondary structures or directly interacting with scanning ribosomes or other cellular factors such as miRNA complexes and RBPs. They act in concert with or independent of the cap-dependent translation initiation regulation, and sometimes even bypass cap-dependent initiation to modify translation of the main CDS. As these *cis*-elements are specific for each mRNA, they provide a mean to regulate specific subsets of mRNAs on top of the global control via translation initiation. In certain conditions, these *cis*-elements can even induce translation of specific mRNAs while global translation is inhibited.

The 5'UTR region is crucial for initiating translation as it includes the 5' cap structure required for the assembly of the translation initiation complex, and it is scanned by the 43S PIC for the appropriate start codon to begin translation. Expectedly, the sequence of the 5'UTR can heavily influence the initiation process. These sequences can be loosely termed translational *cis*-elements of the 5'UTR. The most well-understood *cis*-elements in the 5'UTR are the 5'TOP motif, uORF and IRES (internal ribosome entry site), which will be discussed in the following section. Other *cis*-elements will also be briefly mentioned.

5'TOP motif: Immediately following the m^7G cap, the 5'TOP motif consists of an invariable 5'-cytidine accompanied by a tract of pyrimidines. It is particularly found on mRNAs encoding for ribosomal proteins and translation factors, and the 5'TOP motif often defines the most sensitive group of mRNAs to mTORC1-mediated translation control[23,31]. LARP1, a recently discovered mTORC1 effector, was found to be the main factor regulating TOP mRNA translation[24,27,28]. The DM15 region of LARP1 recognizes and binds to the 5'TOP motif, together with the m^7G cap,

which displaces eIF4E and thus inhibits translation initiation. Activation of mTORC1 decreases LARP1 association with the cap of 5'TOP mRNAs due to phosphorylation of LARP1 by mTORC1[24,30]. Therefore, the 5'TOP motif provides a mechanism for mTORC1 via LARP1 to specifically turn on/off the synthesis of ribosomal proteins and translation factors.

uORF: Recent genome-wide ribosome profiling studies revealed extensive translation activity in the 5'UTR on very short open reading frame termed uORFs, estimated to be present in approximately 50% of all 5'UTRs[13,32,33]. Additionally, these studies revealed an unexpected observation that non-AUG start codons are responsible for 20-70% translation initiation, with CUG, GUG and UUG being the most prevalent alternative translation initiation sites[13,32]. The primary effect of uORF is believed to be translational inhibition of the primary ORF via competition for scanning 43S PIC with the primary ORF's start codon (**Figure 1.2**). Recognition of the uORF start codon initiates the assembly of the full 80S ribosome and translation of the uORF, followed by the dissociation of the ribosome at the uORF stop codon. In the presence of a uORF, the primary ORF can still be translated by two main mechanisms: leaky scanning of the 43S PIC or re-initiation of the 40S subunit. Leaky scanning occurs as the uORF start codon usually is in a suboptimal context for recognition by the 43S PIC, thus a fraction of scanning PICs bypasses the uORF and starts translation at the downstream start codon of the primary ORF. Re-initiation occurs after the 80S ribosome is dissociated at the stop codon of the uORF, when the 40S subunit reacquires a ternary complex and starts scanning again, eventually initiating translation at the start codon of downstream pORF[34]. Although a uORF is generally an inhibitory element for translation, the presence of multiple uORFs can confer a translation advantage in stress conditions, where P-eIF2α induces the expression of certain transcripts[35]. Additionally, an alternative transcription start

site or alternative splicing that removes or adds sequences to the 5'UTR can also change the uORF composition, thus modulating the translation activity of the corresponding transcript.

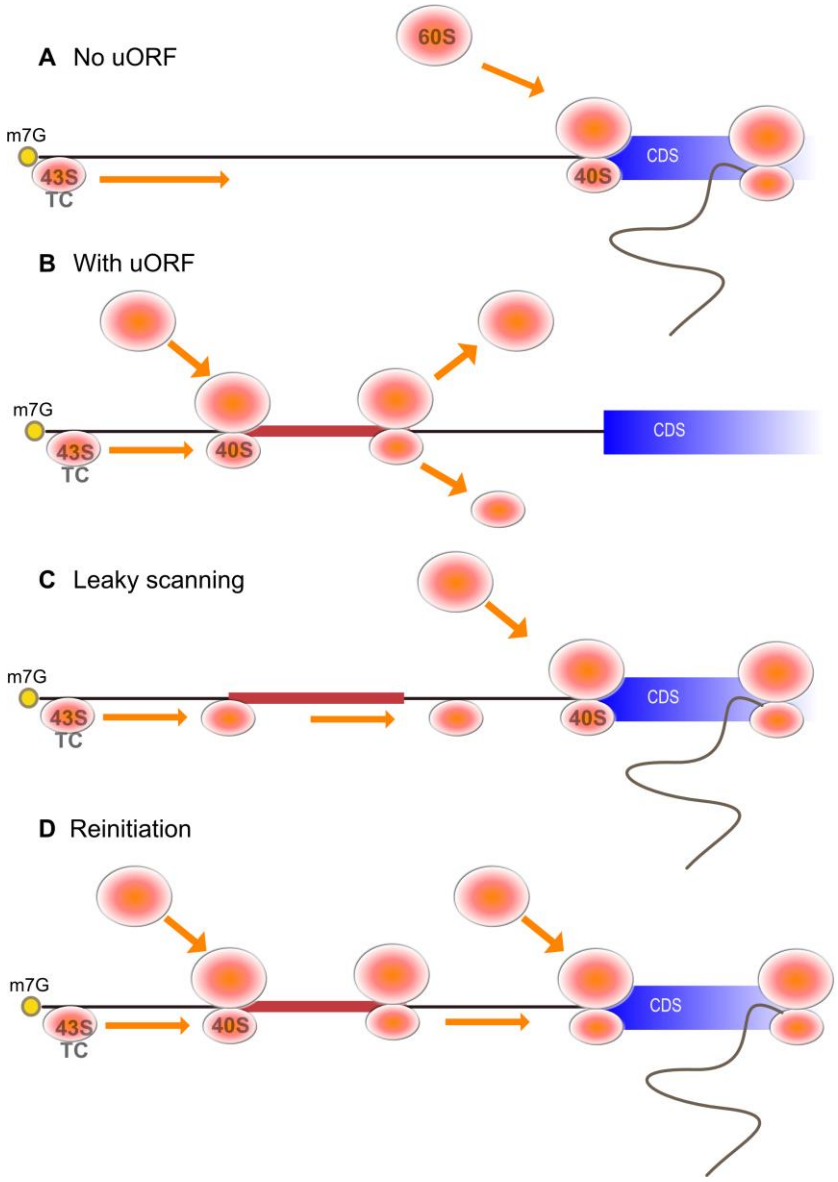

Figure 1.2: Mechanism of uORF-mediated translation inhibition. (A) Canonical 43S scanning where the 43S pre-initiation complex scans the 5'UTR for a strong translation initiation site (often an AUG with strong Kozak context) where it recruits the 60S ribosome to assemble an elongating-competent 80S ribosome. (B) When a uORF is present, the translation initiation site of the uORF is recognized by a fraction of scanning 43S, initiate translation and cause dissociation of the ribosomal subunit at the stop codon, reducing translation from the primary ORF. (C) Certain stress conditions increase leaky scanning, where the scanning 43S ignores an upstream start codon

and initiates translation at a downstream start codon, derepressing uORF-mediated translation inhibition. (D) On rare occasions, the 40S stays on the mRNA after ribosome dissociation at the stop codon and continues to scan the mRNA, acquires a new TC, and starts a new cycle of translation at a downstream start codon.

IRES: First described in a viral mRNA, IRESes are RNA sequences capable of forming secondary structures that initiate ribosome scanning with only a fraction of the required translation initiation factors and ribosome subunits, thus bypassing the need for the complete set of initiation factors used in cap-dependent translation initiation[36]. Due to the capacity to initiate translation without the 5' cap, IRES-mediated translation is categorized as cap-independent translation. Viral IRESes are generally classified into four types based on their requirement of translation factors[8,36]. These viral IRESes maintain the translation of the viral mRNAs during the antiviral and infected stages of the cells where cap-dependent translation is generally inhibited by the antiviral response or by viral proteins, giving viral mRNAs an edge to compete for the translation machinery and resources over cellular mRNAs. Cellular IRESes are less conserved and cannot be clearly classified, yet can be divided into two types, with type I requiring additional IRES trans-acting factors (ITAFs) for recruiting ribosomes, while type II containing short *cis*-elements that can base-pair with 18S rRNA[37]. Similar to viral IRESes, cellular IRESes are believed to become relevant during stress conditions where cap-dependent translation is suppressed, maintaining translation of a subset of stress-related or apoptotic transcripts[38,39]. The mechanism of cellular IRES-mediated translation control is also less well-understood compared to viral IRES-mediated translation.

1.1.3. Suppressing translation during stress: the integrated stress response

While translation of cellular mRNAs is activated during growth and proliferation to produce more proteins to accommodate increased cellular demands, cells usually respond to various stress conditions by tuning down protein synthesis. The regulation of protein synthesis in response to stress is regulated by an extensive signaling network termed the integrated stress response (ISR), which converges on the translation initiation factor eIF2α[40]. Various stressors are sensed by four eIF2α kinases: general control non-derepressible 2 (GCN2), protein kinase R(PKR), PKR-like ER

kinase (PERK), and heme-regulated inhibitor (HRI). These kinases share a similar activation mechanism, in which they dimerize and autophosphorylate for activation. The stress sensing mechanisms, however, are different for each kinase. GCN2 senses amino acid deprivation via its binding to deacylated tRNA, an indication of insufficient amino acid supply for amino acyl-tRNA synthetases[41]. UV irradiation also activates GCN2, but the mechanism is not clear[42]. Virus infection is sensed by PKR via its interaction with mostly double-stranded RNA (dsRNA), a nucleic acid product commonly found during a virus replication cycle but not in uninfected cells[43]. PERK is the sensor of the unfolded protein response (UPR), a condition in which the endoplasmic reticulum is overloaded with newly synthesized proteins and that in turn causes an accumulation of misfolded proteins. The luminal domain of PERK is normally associated with immunoglobulin heavy chain binding protein (BiP). BiP is dissociated from PERK during ER stress, leading to the inactivation of PERK[44,45]. Unfolded proteins can also act as a PERK ligands, activating PERK upon interaction[46]. Lastly, HRI is an eIF2α kinase that is specifically expressed in red blood cells, and senses oxidative stress via its interaction with heme, the iron-containing porphyrin co-factor that mediates oxygen binding to hemoglobin. Upon activation, these eIF2α kinases phosphorylate eIF2α at serine 51, enhancing its binding with the guanine nucleotide exchange factor eIF2B and trapping this molecule in a complex with P-eIF2α-GDP to impede the recycling of eIF2α to the active GTP bound form needed for ternary complex (TC) formation. Thus, phosphorylation of eIF2α by its kinases inhibits global protein synthesis via depletion of the pool of active TC. However, a subset of mRNAs is translationally activated during P-eIF2α conditions. One primary mechanism of translation de-repression during ISR conditions involved uORF and was discovered by studying translation control of a main ISR transcription factor, activating transcription factor 4 (ATF4). The 5'UTR of *Atf4* contains 2 uORFs, of which uORF1 is standalone while uORF2

overlaps with the primary ORF but is on a different reading frame than the pORF. During normal conditions where TC is abundant, scanning PIC initiates translation at the start codon of uORF1, and the ribosome is dissociated at its stop codon. The 40S then continues scanning and picks up another TC for reinitiation and recognizes the start codon of uORF2. Due to the difference in the reading frame, ribosomes that recognize uORF2 bypass the start codon of the primary ORF, effectively preventing translation of *Atf4*. During stress conditions, there is a scarcity of TC, thus the 40S ribosome dissociating from the stop codon of uORF1 takes longer to reassociate with an active TC. Some of these ribosomes continue to scan pass the start codon of uORF2 before acquiring a TC, thus are capable of reaching the start codon of the primary ORF and translating *Atf4*[47]. This uORF-mediated translation de-repression appears not to be unique for *Atf4* but widespread in a subset of stress related genes, suggesting a common mechanism for stress-induced translation[48].

1.2. The unique translation environment of the infected cells

Translation control is at the forefront of virus-host interactions. All viruses completely rely on the host translation machinery during their infection cycle. Global translation can be turned on and off faster than transcription, providing a more effective mechanism to respond to a virus infection. Early sensing of virus infection often results in a global translation shutoff to limit virus replication. On the other hand, when an infection is successfully established, viruses have evolved diverse mechanisms to evade the host's translation shutoff while redirecting the host translation machinery away from host mRNAs to translate viral mRNAs. This interplay warrants a unique translation environment where virus and host compete for the control of the translation machinery, the outcome of which decides the fate of the infected cell. Additionally, understanding this translation environment is essential for virus-related medical applications, especially when

translation enhancing elements that function in normal cells might not be applicable in infected cells. This section will discuss the two aspects of this translation environment: the translation control arm of the antiviral response where the host cell attempts to restrict early infection and the diverse strategies that viruses employ to take control of the translation machinery.

1.2.1. The translation control arm of the antiviral response

Upon sensing of viral infection, the translation environment in the host cell can be modulated by several responses. I will primarily describe here two main pathways: activation of mTORC1 and phosphorylation of eIF2α via the ISR. Other cellular processes such as stress granule formation, induction of tRNA fragments, modulation of cellular tRNA pool, or mRNA methylation can also contribute to modulate translation control of the antiviral state (**Figure 1.3**)

Activation of the mTORC1 signaling pathway

At the center of cellular metabolism and protein synthesis, mTORC1 was also shown to be critical for the antiviral response. The mTORC1 is likely activated very early during the infection cycle. One upstream signaling axis of mTORC1 is the PI3K/Akt signaling axis, mostly responsible for transmitting extracellular cues by receptor tyrosine kinases (RTKs) and G-coupled protein receptors (GCPRs)[49]. Interestingly, several reports have shown that a virus infection was shown to be able to trigger a period of transient PI3K/AKT activation, probably due to the virus interaction with cellular receptors[50–52]. Interferon and the virus sensors toll-like receptors (TLRs) can also activate mTORC1, providing a mechanism to sustain mTORC1 activity later in infection[53]. The activation of mTORC1 in turn is essential for the translation of effector genes of the antiviral response.

Studies using genetic disruption as well pharmacological inhibitions of upstream signaling factors or downstream effectors of mTORC1 suggest that the activation of mTORC1 is required for the expression of key transcription factors of the antiviral response, ISGs, cytokines and chemokines. For example, deletion of mTORC1 upstream inhibitors tuberous sclerosis 1/2 (TSC1/2) or the downstream effectors 4E-BPs resulted in enhanced expression of ISG15 and CXCL10 upon interferon treatment[54]. 4E-BP1/2 double knockout was also shown to enhance translation of the key interferon transcription factor IRF7 and confer resistance to VSV (versicular stomatitis virus) infection[55]. Additionally, inhibitors of mTORC1 such as rapamycin were found to inhibit interferon production[56,57].

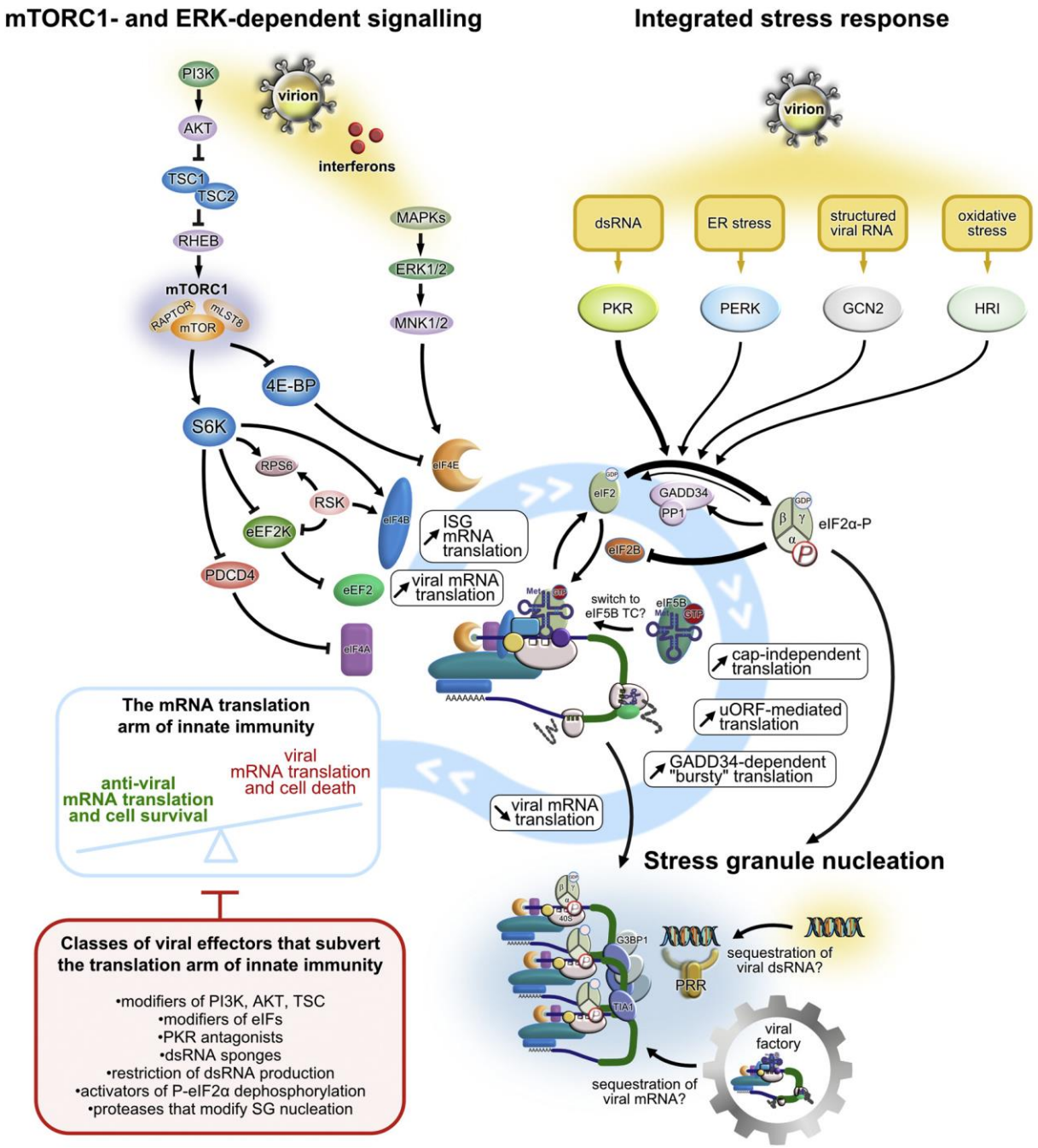
mTORC1- and ERK-dependent signalling
Integrated stress response
PI3K
AKT
TSC1
TSC2
RHEB
mTORC1
RAPTOR
mLST8
mTOR
virion
interferons
MAPKs
ERK1/2
MNK1/2
4E-BP
S6K
RPS6
RSK
eEF2K
PDCD4
eIF4E
eIF4B
eEF2
eIF4A
ISG mRNA translation
viral mRNA translation
dsRNA
ER stress
structured viral RNA
oxidative stress
PKR
PERK
GCN2
HRI
eIF2
GADD34
PP1
eIF2B
eIF2α-P
switch to eIF5B TC?
eIF5B
cap-independent translation
uORF-mediated translation
GADD34-dependent "bursty" translation
viral mRNA translation
The mRNA translation arm of innate immunity
anti-viral mRNA translation and cell survival
viral mRNA translation and cell death
Stress granule nucleation
G3BP1
TIA1
PRR
sequestration of viral dsRNA?
viral factory
sequestration of viral mRNA?
Classes of viral effectors that subvert the translation arm of innate immunity
•modifiers of PI3K, AKT, TSC
•modifiers of eIFs
•PKR antagonists
•dsRNA sponges
•restriction of dsRNA production
•activators of P-eIF2α dephosphorylation
•proteases that modify SG nucleation

Figure 1.3. Translational control during viral infection. mRNA translation (*center*) is perturbed during virus infection (*following in a clockwise direction from top left*) via mTORC1- and ERK-dependent signaling pathways, the integrated stress response, and stress granule (SG) nucleation. The PI3K–mTORC1 signaling pathway is activated during infection with various viruses (denoted by "virion") or by autocrine and/or paracrine interferons. ERK–MNK signaling can also be activated and results in phosphorylation of eIF4E, although the consequences of this modification are unclear. Viruses can also induce the integrated stress response by activating the eIF2α kinases: PKR is the major target, being activated by viral dsRNA, while PERK, GCN2, and HRI are activated via ER stress, structured viral RNA or oxidative stress, respectively. Any or all of these activities result in phosphorylation of eIF2α which inhibits the GEF activity of eIF2B, thus inhibiting translation initiation. An alternative ternary complex consisting of eIF5B–GTP–Met–$tRNA_i$ may also facilitate translation of transcripts in the context of high P-eIF2α, ostensibly in a cap-independent manner. Dephosphorylation of P-eIF2α by the specific binding of GADD34–PP1 can result in phases of phosphorylation/dephosphorylation which prevent a tonic brake on cellular mRNA translation. This cycling may thus promote uORF-mediated and/or so-called bursty translation which allows for the synthesis of antiviral proteins while keeping a phasic brake on viral mRNA translation. P-eIF2α and subsequent translation inhibition promotes SG nucleation which may serve an antiviral role by minimizing viral mRNA translation and maximizing activation of PRRs by viral dsRNA. SGs might sequester viral dsRNA and mRNAs and this function could be facilitated through close association with viral factories. (*Boxed region; red*) Classes of viral effectors that can subvert the translational arm of innate immunity, thus favoring viral propagation (see text for details). (*Boxed region; light blue)* Viral infection acts to re-program host mRNA translation and constitutes the translation arm of innate immunity which contributes to cell survival. Subversion of this arm by viral effectors can tip the balance, increasing viral mRNA translation, replication and eventually cell death. Figure reprinted from Hoang *et al*., 2018[8] with permission from Journal of Molecular Biology.

Shunting translation initiation via phosphorylation of eIF2α

The activation of the ISR is the second most well-characterized translation control mechanism in response to virus infection. As described above, the ISR senses various types of stress via four main eIF2α kinases and phosphorylates eIF2α, turning off global protein synthesis. The particular environment of P-eIF2α also favors a subset of transcripts that contains multiples uORFs in their 5'UTRs, allowing for a mechanism of stress-related translation de-repression. The PKR is the primary sensor of virus replication in host cells via its affinity for dsRNA and 5'-triphosphate capped ssRNA (single-stranded RNA), nucleic acid products of viral genome replication[58,59]. Binding to its ligand triggers dimerization and autophosphorylation, activating PKR's kinase activity[60]. The capacity of PKR to sense abnormal cytoplasmic RNA molecules places it at the center of ISR-mediated antiviral response, yet other kinases can also be activated during virus infection. An infection commonly causes ER stress due to the overloading of viral proteins in the ER, activating PERK in the process[61]. Viral structured genomic RNAs can also activate GCN2, such as in the case of Sindbis virus (SINV) or murine cytomegalovirus (MCMV)[62,63]. Though HRI was initially thought to be expressed only in erythrocytes and not known to be involved in virus-host interaction, interestingly, overexpression of this kinase in the orange-spotted grouper (*Epinephelus coioides*) protects the fish from infection by red-spotted grouper nervous necrosis virus (RGNNV)[64]. Turning off global translation via P-eIF2α appears to be an effective way to restrict translation of viral transcripts[65]. Additionally, this condition allows for translation de-repression of certain stress-related regulators such as the pro-survival gene ATF4 or the pro-apoptotic genes GADD34 (growth-arrest and DNA damage-inducible protein 34) and CHOP (C/EBP homologous protein) via a uORF-mediated mechanism as discussed above[66–68]. This mechanism might be important for maintaining cellular homeostasis during viral stress but

might also be usurped by the virus for replication such as in the case of ATF4 in HCMV infection[69]. Notably, certain viruses also appear to incorporate a uORF-mediated translation control to their transcripts, possibly to adapt to the ISR condition of the infected cells[70].

Other translation control mechanisms of host cell during the antiviral state

Although activation of mTORC1 and ISR are the two main translation mechanisms activated during the antiviral state, other translation processes also occur in the infected cells, but the outcomes are not as well understood. Formation of stress granules (SGs) was observed in cells infected with various viruses[71,72]. Although the role of SGs in virus-host interaction is not clearly understood, one implication on translation control of this cellular process is perhaps via the sequestration of naked viral RNAs by SG proteins. Supporting this notion, the SG proteins TIA1 and TIAR were found to directly bind to viral RNA of West Nile virus (WNV) or tick-born encephalitis virus (TBEV)[73,74]. Certain viruses form virus factories in infected cells, which are subcellular loci that are enriched with viral proteins and nucleic acids and serve as assembling sites for virions. SGs or SG proteins were found to colocalize with virus factories, perhaps due to the high concentration of viral RNAs that could serve as SG nucleation points, suggesting a role of SGs in interfering with virus replication[75,76].

Transcription activation of ISGs is an integrated part of the antiviral state. A subset of ISGs was recently found to be involved in modifying translation of host or viral mRNAs. Some proteins in the interferon-induced protein with tetratricopeptide repeats (IFIT) family bind to eIF3 to inhibit translation. They also form a complex with viral 5'-ppp mRNAs, specifically inhibiting virus mRNAs translation[77]. Additionally, the endoribonuclease RNAse L can also inhibit global protein synthesis via degradation of rRNAs and mRNAs[78]. Moreover, the protein ISG15 was shown to

modify the eIF4E homologous protein (4EHP) by a process called ISGylation, enhancing 4EHP binding affinity to mRNA 5'cap[79] and potentially alter cap-dependent translation initiation.

1.2.2. The virus strikes back: viral strategies to control the host's translation machinery

Despite various strategies deployed by the host to restrict mRNA translation in the infected cells, viruses have co-evolved and adapted counterstrategies to maintain translation of viral mRNAs even in the host's antiviral states. As viral mRNAs are astoundingly diverse, ranging from uncapped polycistronic mRNAs with no 5' nor 3'UTRs to capped monocistronic mRNAs with UTRs and introns, translation strategies employed by viruses to usurp the protein synthesis machinery are as varied and unique for each virus. Some of these strategies are also remarkably unconventional and are not observed outside of the infected cells. I will describe some strategies below.

Modulating cap-dependent translation initiation

As mTORC1 is the primary hub to regulate cap-dependent translation in cells, signaling pathways through this complex are often targeted by viruses attempting to take control of the host's translation machinery. One strategy employed by viruses is to inhibit mTORC1 in order to restrict cap-dependent translation and also potentially thwart the translation of antiviral transcripts in infected cells. For example, the VSV matrix protein was found to suppress protein synthesis via dephosphorylation and activation of 4E-BP1, potentially by inhibiting phosphorylation of AKT and activation of mTORC1[80–82]. On the other hand, other viruses opt to enhance mTORC1 activity to boost translation in combination with other methods to restrict translation of host mRNAs. Various viruses were found to encode proteins that target specific molecules along the PI3K/Akt/mTORC1 signaling pathway to stimulate mTORC1, such as the herpes simplex virus 1

(HSV1) US3, human cytomegalovirus (HCMV) UL38, or influenza A virus (IAV) NS1 proteins[83–85]. In the well-studied case of HSV1, host transcripts might be targeted for degradation early in the infection cycle by the viral host shut-off protein (Vhs), thus leaving the activation of mTORC1 to benefit viral mRNA translation exclusively[86].

Viruses can also inhibit host translation by directly targeting the components of the eukaryotic translation initiation complex. For example, the scaffolding protein eIF4G is targeted for degradation by a range of viral proteins such as the poliovirus 2A protease or a number of proteases from retroviruses[87,88]. Alternatively, certain viral proteins can interact with eIF4G and restrict its interaction with other initiation factors[89]. Similarly, initiation factors such as eIF4E, eIF3, or PABP are also targets of viral proteins[90–92].

Evolving cis-element in the 5'UTR to enhance translation

Many viruses develop specific elements in their 5'UTRs to enhance translation in the specific conditions of the infected cells. The most well-studied example of such elements is the IRES, sequences that form secondary structures capable of initiating translation in a cap-independent manner to take advantage of the deficiency of initiation factors necessary for cap-dependent translation in the infected cell. As discussed above, a viral IRES is capable of initiating translation on an mRNA with only a subset of initiation factors, and some IRESes can recruit ribosomes by themself. Viral IRESes are more structurally conserved than cellular IRESes and can be classified into four types based on their requirement for eIFs[8]. Type I viral IRESes require all eIFs except for eIF4E and allows for ribosome scanning for the initiating codon. Type I IRESes are particularly found in the *Enterovirus* genus, such as poliovirus. Type II viral IRESes (found in the *Cardiovirus* and *Aphthovirus* genus) are similar to type I viral IRESes in the requirement for all eIFs apart from eIF4E, but interestingly recruit ribosomes directly to the initiating codon. Type

III IRESes are found in a wide range of viruses belonging to the *Flaviviridae*, *Picornaviridae* and *Dicistroviridae* families. This type of IRESes requires a smaller subset of eIFs (eIF2, eIF3 and eIF5) and does not require ribosome scanning. Finally, type IV viral IRESes (found in the *Dicistroviridae* and *Nyamiviridae* families) are the most structurally sophisticated IRESes and bypass the requirement for all eIFs and also do not require the use of Met-tRNAi[93].

Other *cis*-elements in the 5'UTR that can enhance translation have also been reported in some viruses, yet their mechanisms of action are only poorly or partially understood. One particularly curious example is the non-templated poly(A) leader that is found in the 5'UTRs of mRNAs of vaccinia virus late genes. This poly(A) element is not encoded in the vaccinia genome, but added to the 5' end of vaccinia virus mRNAs due to slipping of the virus polymerase on a poly(T) motif of the promoter region[94–96]. Interestingly, this poly(A) motif enhances translation in vaccinia-infected cells using a non-canonical cap-dependent mechanism that excludes the need for eIF3 and eIF4F[97,98]. The exact mechanism of poly(A) motif-mediated translation enhancement is still poorly understood, but it is proposed to be related to phosphorylation of the host small ribosomal protein RACK1 (receptor of activated protein kinase 1) by the vaccinia kinase B1[99]. Another example of virus translation enhancer in the 5'UTR is found in the mRNA encoding the nucleocapsid protein of measle virus (MeV). The first 15 residues at the 5' end of this mRNA can form a short stem-loop structure that recruits the La/SSB auto-antigen protein, which in turn promotes selective translation of this mRNA in the translation shutoff environment of MeV-infected cells[100].

Overriding eIF2α phosphorylation

Phosphorylation of eIF2α by the ISR is the main mechanism to shut down global translation in infected cells. Viruses also developed mechanisms to prevent or reverse P-eIF2α. As dsRNA

produced during virus replication is the substrate of the eIF2α kinase PKR, various viral proteins can bind to dsRNA and mask it from PKR recognition, such as US11, TRS1, NS1, σ3 and E3 of HSV1, HCMV, IAV, reovirus, and VACV, respectively[101–105]. More interestingly, some viruses produce structured viral RNAs that antagonize instead of activating PKR upon binding, effectively serving as RNA-based inhibitors of PKR[106–108]. Viruses can also produce proteins that directly bind to PKR to impair its function[109–112]. Additionally, certain viral proteins including HSV1 ICP34.5, African swine fever virus (ASFV) DP71L and papillomavirus E6 promote the dephosphorylation of P-eIF2α directly, or increase the activity of the phosphatase PP1 on P-eIF2α to facilitate its dephosphorylation[113–115].

Compartmentalization of translation

Aside from modulating translation signaling pathways and evolving viral mRNAs to compete for ribosomes, many viruses can also spatially reorganize translation in favor of their mRNAs in the host cell, whether by specifically recruiting the translation apparatus to loci enriched in viral mRNAs or by restricting the access of host mRNAs to the translation apparatus.

As mentioned previously, certain viruses compartmentalize their replication in viral factories in the host cytoplasm, which are subcellular loci enriched in viral nucleic acids and proteins, and selectively recruit host proteins to assist in the process. Although translation compartmentalization in viral factories is still poorly understood, it was found that the translation initiation factors eIF4E and eIF4G are recruited to the viral factory of poxviruses[116]. Additionally, measuring protein synthesis activity *in cellulo* also showed a higher synthesis rate inside viral factories of vaccinia virus (VACV) and reovirus[117,118]. Thus, observations from these studies suggest that selective recruitment of translation factors to viral factories can serve as a mechanism to spatially favor the translation of viral mRNAs, while exhausting the resources for host mRNA translation.

Another commonly observed strategy to spatially separate host mRNAs from the translation apparatus is by impeding the mRNA nuclear export process while selectively exporting viral mRNAs to the cytoplasm, therefore exclusively retaining the access of the translation machinery for viral mRNAs. Nuclear export is frequently hijacked by various RNA and DNA viruses, mostly via viral proteins that interact with nuclear export proteins. For example, the IAV NS1 protein partially localizes to the nucleus of infected cells and was shown to form a complex with the nuclear export factors to inhibit nuclear export[119]. Similarly, the matrix protein M of VSV can also relocate to the nucleus via its nuclear localization signal where it interacts with the nuclear export protein RAE1, resulting in impaired nuclear export of host mRNAs[120,121]. Interestingly, as antiviral genes are transcribed and translated during infection, blocking of nuclear export also seems to impair the antiviral response in infected cells. The viral proteins NS1 and M (of IAV and VSV, respectively) are also inhibitors of interferon (IFN) production[122,123]. In the case of the VSV M protein, the mutation at the methionine residue 51 that removes its capacity to impair nuclear export[124] also render the protein unable to thwart IFN production in infected cells[123]. In addition to blocking host nuclear export, viruses may also seek to rather promote viral mRNA export. For example, the HIV1 Rev protein recognizes a specific sequence called rev-responsive-element on unspliced viral mRNAs and facilitates the export of these mRNAs via its interaction with the nuclear export receptor CRM1[125]. In the case of HSV1, the infected cell protein (ICP) 27 was also shown to be crucial for the export of HSV1 mRNAs from the nucleus. The N-terminal RGG RNA binding motif of ICP27 recognizes GC-rich sequences[126], and directs the bound mRNAs to export via interaction with the export factor REF and the export receptor NXF1[126–129]. In summary, translation control is a crucial facet of the virus-host interaction that defines both the host antiviral

response and the virus replication. We will next explore the current state of knowledge of translation control in oncolytic viruses.

1.3 Translation control in oncolytic viruses

1.3.1. A brief introduction of oncolytic viruses

OVs are wild-type or engineered viruses that preferentially replicate in tumor cells while sparing non-cancerous cells. Infection of cancer cells with these viruses leads to direct tumor cell lysis (oncolysis) and necrosis, resulting in the release of a mixture of pathogen-associated molecular patterns (PAMPs), damage-associated molecular patterns (DAMPs), virus antigens, tumor antigens and cytokines. This mixture creates an ideal condition to turn the tumor microenvironment into a pro-immunogenic milieu and invites the attention of cell-mediated immunity: antigen-presenting cells (APCs) phagocyte both viruses and tumor antigens, presenting these antigens to helper T-cells ($CD4^+$) and cytotoxic T-cells ($CD8^+$). Recognition of tumor antigens by these immune cells triggers an antitumor immune response that can then target uninfected or relapsed tumors[130,131].

The history of OVs dates back to the early 20th century with anecdotal observations of a correlation between viral infection/inoculation and tumor remission[132]. Yet, with rudimentary approaches of that time, such as the application of crude virus lysates on tumor tissues, the efficacy of OVs remained dubious and side effects related to virus infection were widespread[132,133]. It was not until the generation of an attenuated oncolytic HSV1 via disruption of the virus gene thymidine kinase (TK), which eliminates neurovirulence but retains the virus infectivity in glioblastoma, that the modern era of OVs begun[134]. Since then, the field has made impressive strides, evolved into an emerging therapeutic avenue for cancer treatment with close to one hundred clinical trials

involving OVs as monotherapies or in combination with other therapeutics[135]. Improvements have been made on tumor specificity, safety as well as oncolytic potency, and combinations of OVs with other therapies such as immune checkpoint inhibitor (ICI) are also currently explored. More than 14 different species of viruses have been developed as OV backbones, ranging from human viruses (*e.g.*, HSV1, reovirus, adenovirus), vaccine strains (*e.g.* Measles virus, vaccinia virus) to non-human viruses (*e.g.* vesicular stomatitis virus, Maraba virus, NDV, Myxoma). Genetic engineering has also allowed for the incorporation of transgenes to enhance antitumor immune response, tumor cytotoxicity, viral spread, as well as for *in vivo* monitoring of virus infection. The most important landmark of OVs came in 2015 when T-VEC, an engineered oncolytic HSV1 that expresses the transgene granulocyte-macrophage colony-stimulating factor (GM-CSF), was approved by the U.S. Food and Drug Administration (FDA) for the treatment of unresectable melanoma[136,137]. In this trial, comparing to the control arm with recombinant GM-CSF treatment, T-VEC improved overall survival and produced a superior response rate. Specifically, 16.9% of patients in the T-VEC treated group achieved a complete response rate (the disappearance of all lesions) as compared to 0.7% of patients in the control arm. With various other OVs in different stages of clinical trials, T-VEC is likely to be the first of an emerging class of biologics available for the treatment of cancer.

1.3.2. On tumor selectivity of oncolytic viruses

Tumor selectivity, or oncotropism, refers to the capacity of OVs to specifically infect and replicate in tumor cells and is a crucial characteristic of a safe and efficient OV. It has been observed that several wild-type viruses have a natural tropism for tumor cells, such as reovirus, VSV, Newcastle disease virus (NDV) or parvovirus, suggesting that the tumor provides a favorable condition for virus entry and replication. Indeed, various hallmarks of cancer also support

productive viral infection, including deregulation of the immune response, deregulation of cellular metabolism, evasion of death pathways, enhanced proliferation, and dysregulated translation[138,139], proposing that cancer cells are a better substrate for virus replication than untransformed cells. Additionally, a subset of viruses also evolved mechanisms to bypass cellular checkpoints and to promote uncontrolled cellular growth, such as suppressing apoptosis or p53-mediated cell cycle arrest. Thus, it is possible to restrict the infection of an engineered virus to cancer cells where these checkpoints are dysregulated by removing these viral genes.

A critical and perhaps most supportive characteristic of cancer cells for viral infection is the general suppression or insensitivity to the IFN signaling pathway[140–145]. The mechanism underlying this inhibition is not clear, but it might provide the tumor with an evolution fitness by avoiding immune clearance[146,147]. A number of recent studies discovered that cancer cells might enter a "viral-mimicry" state, characterized by activation of the antiviral response without infection[148]. This viral-mimicry state can be attributed to the transcription activation of endogenous retroviral elements upon treatment with certain drugs[149,150]. Alternatively, the exchange of naked RNA species in the tumor microenvironment via exosome can also activate the antiviral state[151,152]. As the antiviral state is detrimental for cell proliferation, it is reasonable to hypothesize that as a subset of tumors is under a constitutive antiviral state, these tumors need to overcome this restriction by silencing the antiviral signaling to expand further. In doing so, the tumors would inadvertently acquire a new vulnerability to viral infection. Thus, the viral-mimicry state of cancer cells provides an explanation for the source of tumor inflammation/antiviral response that imposes a selection pressure favoring the expansion of IFN/antiviral signaling-defective cancer clones. Various oncolytic viruses were successfully developed by exploiting this defect by disrupting viral genes responsible for suppressing the cell-autonomous antiviral signaling, creating viruses that

cannot replicate in normal cells with an intact antiviral response, but that can infect cancerous cells with defective IFN pathway. The most successful examples of this strategy are the disruption of the ICP34.5 of HSV1 or the matrix protein M of VSV[141,153]. Nonetheless, residual antiviral activity from the cancer cells or surrounding stromal cells might still hamper OV infection[154] and can be further inhibited to enhance OV efficacy[155,156].

Another acquired vulnerability of cancer cells for viral infection is their frequent dysregulated cellular metabolism. Cancer cells are generally in a sustained proliferating state and thus need to maintain an abundance pool of macromolecules to support cell division, including deoxynucleoside triphosphates (dNTPs) and proteins. On the other hand, DNA viruses such as HSV1 and VACV also require a large amount of dNTP to synthesize their genomes. The wild-type strains of these viruses can stimulate the dNTP pools in the infected cell with specialized viral proteins such as viral ribonucleotide reductases in HSV1 and VACV[157,158]. In addition, certain viruses also encode the enzyme thymidine kinase that involves in the conversion of thymidine to thymidine monophosphate, an important step in generating thymidine triphosphates, which are required for DNA synthesis[159,160]. Thus, wild-type strains of these viruses can infect quiescent, non-dividing cells. However, disruption of these genes introduces a restriction for the attenuated viruses to only grow in dividing cells, increasing the selectivity of the OVs towards cancer cells[134,161]. Perhaps one of the most important metabolic reprogramming of cancer cells is their dysregulated translation control, which emerges as a major driver of tumorigenesis[162]. The increased demand for protein synthesis of cancerous transformation drives aberrant signaling in various pathways that converge on translation control, including MYC[163] and PI3K/mTORC1[164] signaling axes. Many viruses also stimulate host protein synthesis via modulating mTORC1 to support replication, suggesting that the overactive mTORC1 signaling in cancer cells provides a

favorable condition for OV infection. Additionally, various genetic disruptions to attenuate OV toxicity target translation modifier viral proteins. For example, the HSV1 protein US3 serves as a modulator of PI3K/mTORC1 signaling[83]. A US3-deficient strain of HSV1 was shown to preferentially replicate in cancer cells and to sensitize infected cancer cells to PI3K inhibitors[165]. Deletion of the PKR antagonist ICP34.5 is a common genetic mutation in oncolytic HSV1. It is noteworthy to mention that this deletion can give rise to an additional mutation that modulates host translation control: it may set another PKR antagonist gene, US11, under the transcription control of the immediate early promoter of UL47 and compensates for the loss of ICP34.5 activity[130,166]. Similarly, MYC overexpression in cancer cells was also reported to favor OV infection[167]. These observations suggest that the elevated protein synthesis environment in cancer cells makes them more susceptible to virus replication.

Cancer cells often have defects in cell cycle checkpoints to enter perpetual cycles of division. In normal cells, senescence and apoptosis can be induced in the case of excessive proliferation signaling, perhaps as a cellular defense mechanism against dysregulated growth[138]. However, in the process of tumorigenesis, many cell cycle regulators such as TP53/p53, retinoblastoma (RB), MYC or RAS are found to be commonly mutated to remove this constraint on tumor expansion[168]. Interestingly, many viruses also favor dividing cells where the activation of proliferation signaling pathways and high DNA synthesis rate and the deactivation of the death pathways occur to maintain the infected cells in a highly proliferative state[169–172]. For example, adenovirus activates proliferation in infected cells by E1A-mediated inhibition of RB, while direct binding and inactivation of p53 by E1B circumvent the induction of apoptosis induced by cell cycle progression in infected cells[173]. Deletion of E1B generated an oncolytic adenovirus that is restricted to p53-deficient tumor cells[174,175]. Similarly, vaccinia virus encodes anti-apoptotic proteins SPI-1 (B22R

gene) and SPI-2 (B13R); deletion of both genes inhibits virus replication in normal cells but not cancer cells[176].

1.3.3. Engineering oncolytic viruses

Although wild-type viruses were found to have a certain degree of selectivity toward cancer cells, it was known very early that they could cause severe side effects due to their natural virulence. Additionally, there are various beneficial properties of the infected cell, such as the induction of the inflammatory response or cell death pathway that the virus deliberately suppresses, potentially diminishing the benefit of OV infection on tumor clearance. Therefore, most modern OVs are engineered viruses whose genomes are modified via either disruption of virulence/immune suppressor genes or the addition of therapeutic transgenes to achieve improved selectivity or clinical efficacy. Some viruses are also engineered to express reporter transgenes for monitoring virus replication and spread kinetics *in vivo*[131].

A successful approach to generate safer OVs is to disrupt virulence genes that are corresponding to cellular processes commonly disrupted or dysregulated in tumor cells. Gene deletions for adapting OVs to the dysregulated metabolism, cell proliferation and death, and defective antiviral response of cancer cells are described in the previous section. Additionally, a transcriptional restriction can be used to implement tumor selectivity, in which a tumor-specific promoter is placed in control of a virus essential gene. For example, the telomerase promoter is active in some cancer cells to sustain telomere maintenance. Introducing the TERT (telomerase reverse transcriptase) promoter to control the expression of the adenovirus E1A and E1B attenuates replication in normal cells, yet retains infectivity in a subset of cancer cells[177]. Similarly, the prostate-specific promoter was used to generate a prostate cancer-specific oncolytic HSV1[178].

Moreover, miRNAs can also be used to de-target viruses from normal cells by incorporating binding sites of miRNAs that are abundant in normal tissues but lacking in tumor cells[179,180]. As virus tropism can be determined at the entry step, there are also attempts to retarget OVs to cancer cells using tumor-specific cell surface receptors. For example, MeV has been engineered to bind to CD38 or EGFR, receptors that are overexpressed in various malignancies[181], while adenovirus can be engineered to bind the integrin receptors that are overexpressed in vascular endothelial cells near tumor tissues[182]. Lastly, translation targeting is also used to engineer OVs, such as the incorporation of an IRES from human rhinovirus type 2 that is inhibited in neuron to attenuate neurotoxicity of poliovirus type 1, or the use of the 5'UTR of fibroblast growth factor (FGF) to control the expression of HSV1 ICP27[178,183].

Another common approach in engineering OVs is the incorporation of transgenes to introduce or enhance a desired property of OVs. Increasing OV-induced antitumor immunity is perhaps the most important therapeutic avenue. As tumor microenvironment can be immunosuppressive, various cytokines and chemokines can be used to "arm" OVs, most successfully is the cytokine GM-CSF that was inserted into the genome of the FDA-approved T-VEC, but also IL2, IL12 or CCL5, to name a few[184]. These cytokines and chemokines reverse the immunosuppressive environment of the tumor, attracting as well as stimulating immune cells and lowering the threshold to mount an antitumor immune response. Additionally, tumor-associated antigens (TAAs) can be incorporated into an OV genome, turning the virus into a live tumor vaccine to train the immune system on recognizing the cancer antigens of interest[185,186]. Another approach is to further enhance OV's capacity to kill infected cancer cells by inserting cytotoxic genes such as tumor suppressors, proapoptotic genes or prodrug conversion genes. A number of tumor suppressors, including *p53* or *pten,* were incorporated into OV genomes in several studies,

of which *p53* seemed to show promising effects in enhancing apoptosis of infected cells[187–189]. Alternatively, a prodrug conversion enzyme can be included in the virus genome to convert a non-toxic prodrug into a cytotoxic compound, specifically in infected cells. For example, the gene cytosine deaminase (CD) converts the prodrug 5-fluorocytosine (5-FC) into the toxic 5-fluorouracil (5-FU). Infection of HSV1 carrying this gene, in combination with 5-FC treatment, reduced tumor growth while remaining safe in a mouse model[190]. Non-invasive monitoring of virus kinetic in patients is a challenge that can be overcome by using viruses expressing certain reporters. For instance, the sodium iodide symporter NIS, normally expressed in the thyroid gland, is responsible for the accumulation of iodide in the cells. Infection of cancer cells with a MeV expressing NIS, in combination with the radioactive ^{131}I treatment, was explored not only as an approach of targeted radiotherapy toward infected cancer cells, but also provided a non-invasive glimpse into the distribution of infected cells in the body through monitoring ^{131}I concentration using gamma camera imaging[191].

1.3.4. The knowledge gap of translation regulation in virus-host interaction and OV design: challenges and potentials

The understanding of translation control in a biological process tends to lag behind that of transcription control, perhaps due to relatively more sophisticated techniques required to study translation control. For instance, high-throughput sequencing was first used to study the transcriptome (RNA-seq) *circa* mid 2000[192]; however, the equivalent technique to study the translatome (Ribo-seq) was only develop by Ingolia *et al.* in 2009[32]. Regarding virus-host interaction, the transcription regulations of the infected cells are understood in a relatively more detailed manner as compared to the translation regulations. Hundreds to thousands of ISGs, genes that are transcriptionally induced by the antiviral state and contribute to the restriction of virus

replication, have been identified[193,194]. However, the translatome of the infected cell is less well understood. The development of Ribo-seq has resulted in a cascade of high-profile studies on the translation landscape of the antiviral state, which reveals a complexity that rivals transcription disturbance of viral infection[195–197]. Non-canonical translation that expands the coding capacity of the viral genome was discovered in different viruses such as HCMV[198], Kaposi's sarcoma-associated herpes virus[199] and most recently SARS-CoV-2[200]. More importantly, translatome analyses have identified host processes that were previously unknown to be associated with virus-host interaction[197]. Additionally, recent evidence has emerged that ISGs expression is perhaps inhibited at the translation level by multiple viruses, including SARS-CoV-2[201], potentially compromising their antiviral function. It is also currently unknown if a subset of antiviral genes that are translationally induced exist, disruption of which could potentially improve OV spread in tumors similar to the case of blocking ISGs. Regarding the virus, viral genes are regularly categorized into different classes based on their temporal transcription regulation, such as the case for HSV1 immediate-early (IE), early, and late genes. Based on this knowledge, strong viral promoters (such as the HCMV IE promoter) were identified and adapted for optimal transcription rate of transgenes in infected cells. However, not much is understood about how these transcripts are translated in the modified environment of the infected-cell due to both host and virus-mediated translation modulation. Thus, whether transgene transcripts are optimally translated not known, nor has their translation been optimized in the current OV platforms.

Adaptation of our understanding of the translation regulation during virus-host interaction can benefit virotherapy in several ways: it can improve the replication of virotherapeutics (virus-based therapeutic agents) in the targeted tissues/cells, optimize the expression of transgenes in cells infected by the therapeutic viruses, and even provide a novel approach to engineer tissue/cell

specificity based on the specific translation environment of the targeted hosts. Regarding virus-host interaction, a number of reports (including my published study in Chapter 2 of this thesis), observed translational de-repression of antiviral genes during virus infection, revealing a new layer of gene expression regulation of the antiviral state. More importantly, it is likely that new antiviral genes will be identified in the future by analyzing the translationally induced genes[202]. As dampening the transcriptionally induced ISGs was shown to be an efficient method to increase OV efficacy[155,203], it is reasonable to speculate that similar approaches to restrict translationally stimulated antiviral genes can be beneficial for the field of OVs. Regarding virus engineering, it was shown that a virus ultimately adapts to the translation condition of host cells, such as the tRNA pools of infected cells[204], raising the interesting possibility of engineering tissue/cell tropism (including oncotropism) using translational adaptation. For example, as miRNA expression is different between different cell types, including tumors, a number of studies have successfully demonstrated enhanced tumor selectivity by incorporating into viral genomes the target sites of miRNAs that are poorly expressed in tumors but highly expressed in normal tissues[179,205]. As cancer cells were shown to possess distinct tRNA pools to support their high growth rate[206], it would be interesting to see if adapting viral codon usage to the cancer-specific tRNA pool could achieve higher infection specificity for OVs.

Perhaps enhancing transgene expression in virotherapy is the aspect that can benefit the most from translation adaptation. Although usage of viral promoters helps achieved very high levels of transcription activity of transgenes, my study in Chapter 3 of this thesis suggests that translation of these transcripts may not be optimal and can be further enhanced by adopting a viral 5'UTR. Additionally, other reports suggest that although a codon usage optimized to that of host cells benefits the expression of mRNAs in uninfected cells, such codon usage can be detrimental for

expression in infected cells, potentially due to the different tRNA pools present in the infected cells[207,208]. Thus, transgene codon optimization towards that of viral genes or of the infected cell conditions might be a better strategy to preserve the fitness of OVs. In summary, the knowledge of the complex translation landscape of the infected cells has expanded significantly recently. This body of knowledge will, in various ways, contribute to the making of better virotherapies that make a substantial impact on how diseases are treated and cured.

1.4. Translation control of the inflammation response via miRNAs

1.4.1. Translation control and the innate immunity

Innate immunity in mammalian cells is a very stringently regulated process: activation of the innate immune response needs to be fast to restrict virus spread as soon as the infection is detected. After the infection is resolved, the immune response also needs to be shut off rapidly to prevent overactive inflammation that can damage the surrounding tissues and cause other inflammatory diseases. Translation control provides a rapid on-off mechanism to control the immune response over transcription control. Indeed, translation regulation was found to be crucial in the activation of the innate immune response, as well as the activation and maturation of various immune cells including T-cells, macrophages, NK cells or neutrophils[209]. A body of research also shows that translation silencing is widespread in gene expression regulation of inflammatory genes[210].

As the master regulator of translation control, it is not surprising that mTORC1 is heavily involved in the immune response. Yet, the role of mTORC1 in immune responses is still an enigmatic question: this complex seems to promote the immune response in some cases but restricts it in other cases. For example, Colina *et al.* showed that mTORC1 regulates the translation of IRF7 via the downstream effectors 4E-BPs, and removing the translation restriction of 4E-BPs

enhanced type I IFN production as well as virus resistance in mouse embryonic fibroblasts[55]. However, mTORC1 activation limits the inflammatory response in phagocytic cells via downregulating the expression of inflammatory cytokines[211]. Similarly, inhibition of mTORC1 activity by rapamycin impairs T-cells proliferation[212,213], yet rapamycin also enhances the differentiation of memory $CD8^+$ T-cells upon virus infection [214]. These multifaceted effects of mTORC1 can be explained by the role of this complex in regulating various factors of these processes, such as KLF2 and CDK1 in the case of T-cell proliferation.

Translation silencing via *cis*-elements also appears to be a widely used mechanism to turn off the expression of inflammatory genes post-transcriptionally. The AU-rich elements (AREs) are commonly found in the 3'UTRs of a subset of mRNAs related to immune and inflammatory responses[215]. The translation repression via AREs depends on other associated RBPs, including hnRNP A1, HuR, TIA-1, TIAR, and TTP. The binding of these RBPs to the ARE motifs resulted in translation repression of associated transcripts[216–219], although the mechanism is still not clearly understood. Another translation repressor element is the IFN-γ-activated inhibitor of translation (GAIT) element found in the 3'UTR of the inflammatory mRNA encoding ceruloplasmin (CP)[220]. This translation repression is carried out by a protein complex that binds to the GAIT element, which includes the ribosomal protein L13a, the glutamyl-prolyl-tRNA synthetase (ERPS), NS-1 associated protein 1 and GAPDH[221,222]. Nevertheless, the most widely found *cis*-elements in the 3'UTR are perhaps miRNA binding sites, which are found to be crucial players in translation control of the immune response and will be discussed in details in the following section[223].

1.4.2. miRNA as a player in translation control of the inflammation response

miRNAs begin as long and primary molecules that are commonly transcribed by RNA polymerase II from either independent miRNA genes or small parts of protein-coding transcripts. They are processed in the nucleus by a complex containing the RNase III-type endonuclease Drosha and DiGeorge syndrome critical region 8 (DGCR8) to form smaller precursor miRNA (pre-miRNA) products. Pre-miRNAs are subsequently exported into the cytoplasm, where their hairpin loops are spliced by Dicer to produced duplex miRNAs. One strand of the miRNA duplex is then incorporated into the RNA-induced silencing complex (RISC), which contains the protein argonaute (AGO2) and glycine-tryptophane protein of 182 kDa (GW182). The RISC complex is then responsible for recognizing and binding to partially complemented miRNA binding sites that are situated mostly in the 3'UTRs of mRNAs. miRNAs can silence gene expression via more than one post-transcriptional mechanism, of which the two main effects of miRNAs on target transcripts are mRNA destabilization and translation inhibition[224]. Full complementary of miRNAs at the binding site causes AGO2 to cleave the target mRNA; however, this process is rarely observed in endogenous miRNAs as most miRNA binding sites are only partially complementary to a given miRNA, and more common in siRNAs. Specifically, the protein GW182 recruits the CCR4-NOT nuclease complex that inhibits translation initiation and deadenylates the mRNA, leading to mRNA degradation[225].

Studying the effects of miRNAs on cellular processes is often complicated by the multi-target mode-of-action of miRNAs: one miRNA can repress multiple target genes simultaneously and one functional gene network can be regulated by a group of miRNAs, thus modulating various cellular processes dependently of each unique condition. Thus, characterizing a miRNA as pro- or anti-inflammatory might not be universal and can be context-dependent. However, there is no

doubt that miRNAs are important players in immunity as various miRNAs have been shown to be involved in different signaling pathways of the immune response[223]. Cells treated with lipopolysaccharide (LPS), a TLR4 ligand, had altered levels of several miRNAs including let-7, miR-9, miR-21, miR-146, miR-147 and miR-155[226–231]. Of these miRNAs, let-7 and miR-21 were in turn found to regulate TLR4 expression while others were involved in regulating the expression of various inflammatory genes. One of the best characterized miRNAs that are involved in immune response signaling is miR-146. This miRNA is upregulated in response to exposure to bacterial PAMPs or pro-inflammatory cytokines[231]. miR-146 then negatively regulates inflammatory signaling, possibly via targeting components of the NF-κB signaling pathway, including tumor necrosis factor receptor (TNFR)-associated factor 6 (TRAF6) and interleukin 1 receptor-associated kinase 1 (IRAK1). On the other hand, miR-155 is an example of pro-inflammatory miRNAs. miR-155 is upregulated in response to LPS and IFN-β, and the expression of this miRNA promotes TNF-α production[230]. miR-155 was shown to impair the expression of the phosphatase SHIP1/INPP5D, a negative regulator of the TLR signaling pathway[232]. Furthermore, miR-155 directly repressed the expression of BCL6, which is an NF-κB antagonist, and thereby enhanced NF-κB activity and pro-inflammatory signals such as CCL2 expression. Thus, current knowledge has identified different miRNAs as important factors in translation control of inflammation signaling and inflammatory-related disease.

1.4.3. Atherosclerosis and inflammation

Whereas virus infection often causes an acute inflammatory response that is resolved after virus clearance, atherosclerosis is a chronic inflammatory disorder that is characterized by non-resolving, maladaptive immune response at the subendothelial space of the arteries[233]. The disease is initiated by the accumulation of low-density lipoproteins (LDL) in arterial sites with disturbed

laminar flow[234]. Here, they are susceptible to chemical modifications such as lipolysis, proteolysis, aggregation and more importantly, oxidation to generate oxidized LDL (oxLDL), which mimic PAMPs or DAMPs and induced a low-grade inflammatory response. This localized inflammation subsequently recruits immune cells and smooth muscle cells, causing accumulation of cellular and extracellular materials in the artery wall that eventually forms atherosclerotic lesions. As chronic inflammation is the main cause of atherosclerosis, resolving or suppressing the localized, dysregulated inflammation is a current therapeutic option for treating atherosclerosis. For instance, one of the many pleiotropic effects that the established atherosclerosis drug statin applies on the atherosclerotic lesion has anti-inflammatory property[234]. Additionally, anti-inflammatory treatments such as the use of anti-IL1β in a large clinical trial have proved to be effective in treating atherosclerosis[235]. HDL mimetics, which are composed of peptides and proteins that bind lipids found in HDL to mimic HDL particles, were shown to provide positive benefits, including anti-inflammatory benefits to atherosclerosis patients[236]. Additionally, anti-inflammatory drugs such as methotrexate are being explored as potential treatments for atherosclerosis[237]. Recently, miRNAs have also emerged as key players in atherosclerotic progression as well as regression[238]. As miRNAs play important roles in regulating the inflammatory response, it is intriguing to elucidate if this regulation contributes to the effects of miRNAs on atherosclerosis, and whether or not there is a translation control component in this signaling network.

1.5. Summary

Translation control plays a crucial role in regulating the antiviral response and inflammatory signaling. In the context of OVs, disturbance of translation control in infected cancer cells shapes the antiviral response as well as viral gene expression. I hypothesized that understanding and applying translation control during virus-host interaction could improve virotherapies for the

treatment of cancer. Profiling of the virus-host interaction at the translation level might reveal residual antiviral activity that could be further suppressed to augment the spread of OVs in cancer cells. On the other hand, understanding the mechanisms of translation induction of viral transcripts can provide a novel method to enhance the expression of transgenes in infected cells. Additionally, I also propose a direct contribution of translation control in miRNA-mediated inflammation signaling in the context of atherosclerosis.

Objective and hypothesis

In my first chapter, I sought to characterize the host translatome in the context of OV-cancer cell interaction. I hypothesized that amongst the translationally regulated genes in the translatome of cancer cells infected with OVs, there are translationally induced antiviral genes that can be disrupted to enhance OV infectivity in cancer cells.

In my second chapter, I focused on virus translation regulation, more specifically on the role of 5'UTRs of HSV1 genes in mediating enhanced translation of these transcripts. I hypothesized that enhanced translation of transgenes expressed from HSV1 genome could be achieved by incorporating these viral 5'UTRs upstream of the CDS.

In my third chapter, I contributed to a project that characterized the effects of miR-223 on macrophage inflammatory responses in the context of atherosclerosis. I hypothesized that miR-223 exerts translational control of cholesterol efflux and inflammatory pathways to protect from atherosclerosis.

CHAPTER 2. Induction of an Alternative mRNA 5' Leader Enhances Translation of the Ciliopathy Gene *Inpp5e* and Resistance to Oncolytic Virus Infection

Authors: Huy-Dung Hoang, Tyson E. Graber, Jian-Jun Jia, Nasana Vaidya, Victoria H. Gilchrist, Xiao Xiang, Wencheng Li, Kyle N. Cowan, Christos G. Gkogkas, Maritza Jaramillo, Seyed Mehdi Jafarnejad, Tommy Alain

Research article (Citations: 6)

Cell Reports, published on December 17, 2019 (Impact factor: 8.109)

2.1. Author contributions

T.A., H.-D.H., T.E.G., and S.M.J. conceived and designed the experiments. H.-D.H. and T.E.G. performed the majority of the experiments, including the functional analysis of the ribosome-profiling data. H.-D.H., T.E.G., and T.A. wrote the manuscript. J.-J.J. produced the viruses and performed the viral titer assays. N.V. performed the heterologous reporter assays. V.H.G. performed the western blotting. X.X. performed qRT-PCR. T.A., C.G.G., and S.M.J. performed the wet component of the ribosome profiling. W.L. performed the ribosome-profiling mapping. K.N.C., M.J., and T.A. reviewed and edited the final manuscript. All of the authors read and approved the final manuscript.

2.2. Abstract

Residual cell-intrinsic innate immunity in cancer cells hampers infection with oncolytic viruses. Translational control of mRNA is an important feature of innate immunity, yet the identity of translationally regulated mRNAs functioning in host defense remains ill-defined. We report the translatomes of resistant murine "4T1" breast cancer cells infected with three of the most clinically advanced oncolytic viruses: herpes simplex virus 1, reovirus, and vaccinia virus. Common among all three infections are translationally de-repressed mRNAs, including *Inpp5e*, encoding an inositol

5-phosphatase that modifies lipid second messenger signaling. We find that viral infection induces the expression of an *Inpp5e* mRNA variant that lacks repressive upstream open reading frames (uORFs) within its 5′ leader and is efficiently translated. Furthermore, we show that INPP5E contributes to antiviral immunity by altering virus attachment. These findings uncover a role for translational control through alternative 5′ leader expression and assign an antiviral function to the ciliopathy gene *Inpp5e*.

Highlights

- Oncolytic virus infection decouples transcription and translation in cancer cells
- Upstream ORFs (uORFs) repress translation of *Inpp5e* mRNA in uninfected cells
- Infection favors a translationally active *Inpp5e* variant lacking intronic uORFs
- *Inpp5e* knockout cells exhibit increased HSV1 attachment and infection

2.3. Introduction

Mammalian cells possess a sophisticated cell-intrinsic innate antiviral program that is activated upon infection. Transcriptional induction of type I interferon expression (IFN-α and -β) and downstream interferon-stimulated genes (ISGs) is a major arm of the innate immune response to infection [239]. Another essential feature of this response is the mRNA translation arm of innate immunity, a reprogramming of protein synthesis to permit the expression of cellular antiviral proteins while concurrently thwarting the production of viral proteins [240]. Translation initiation can be modulated by several eukaryotic initiation factors (eIFs) and RNA-binding proteins (RBPs) [241]. In addition to the m^7G cap structure, which helps recruit eIFs, other *cis*-elements that lie within 5′ leaders, such as 5′ terminal oligopyrimidine (TOP) motifs, upstream open reading frames (uORFs), internal ribosome entry sites (IRESs), RBP binding sites, or localized secondary structure can govern the translational efficiency (TE) of mRNAs[10,242]. During infection, signaling cascades that feed into mRNA translation such as phosphatidylinositol 3-kinase (PI3K)/mammalian target of

rapamycin complex 1 (mTORC1)/(S6K or 4E-BP) and ERK/MNK/eIF4E were shown to enhance the translation of antiviral mRNAs, including *IRF7* and *ISG15* [243,244]. Conversely, translation initiation can be transiently suppressed following infection by preventing efficient ribosome assembly through the activation of eIF2α kinases and subsequent phosphorylation of the α subunit of eIF2 (P-eIF2α)[8]. In contrast, some cellular mRNAs that have uORFs (e.g., *ATF4*;[66]) and/or IRES (e.g., *cIAP1*/*BIRC2*; [245]) in their 5′ leaders display enhanced TE in conditions of high P-eIF2α. Alternative mRNA transcription, splicing, and polyadenylation can also indirectly modify translational output by altering 5′ leaders and 3′ UTRs, thus changing the composition of sequence elements that affect TE [246].

Viruses use a plethora of strategies to maximize TE of their own mRNAs, from evolving 5′ leaders that are better substrates for translation due to the presence of IRES to deploying proteins that shutdown global cellular translation (host shutoff) [240]. Surveying which cellular and viral mRNAs are translated in this highly dynamic environment has been the subject of some recent studies[195,197]. However, these investigations did not specifically address how the translation of mRNAs encoding putative pro- or antiviral effectors could modulate infection. Furthermore, the identification of host mRNAs under translational control during infection could provide targetable strategies to improve antiviral therapies or alleviate viral resistance, an undesirable feature of tumor cells in the context of oncolytic virus therapy, which represents a promising class of cancer therapeutics that relies on natural or engineered cancer cell tropism and mobilization of adaptive, anti-tumor immunity [248].

In this work, we ask which mRNA substrates of translation contribute to the viral resistance of 4T1 breast cancer cells infected with each of three leading oncolytic viruses: herpes simplex virus 1-1716 (HSV1; Sorrento Therapeutics), reovirus type 3 Dearing (also called Reolysin;

reovirus; Oncolytics Biotech), and vaccinia virus JX-594 (VACV; Sillajen). Comparing viral versus mock infected, we identify translationally upregulated host mRNAs common to all three infections. We show that the 5′ leaders of these mRNAs are enriched in uORFs and are translationally repressed in mock conditions but become de-repressed upon infection. This subset includes mRNAs encoding proteins that are associated with primary cilium homeostasis. We characterize the important ciliopathy gene *Inpp5e*, encoding an inositol 5-phosphatase, and describe a virus-induced mRNA variant switch that releases its uORF-mediated translation repression. This response limits viral propagation as cells deficient in INPP5E exhibit increased cell surface attachment of virions and subsequent infection efficiency. These findings highlight the dynamic landscape of alternative 5′ leader usage during viral infection and identify INPP5E as a translationally induced antiviral effector that limits oncolytic virus efficacy.

2.4. Materials and Methods

Key resources table

REAGENT or RESOURCE	SOURCE	IDENTIFIER
Antibodies		
Mouse anti-INPP5E	Abcam	ab69696, RRID:AB_2126254
Rabbit anti-INPP5E	Cohesion Biosciences	CPA3073
Mouse anti- β-actin	Sigma	A5441, AB_476744
Mouse anti-GAPDH	Abcam	Ab8245, RRID:AB_2107448
Rabbit anti-HSV1	Dako	B011402
Mouse anti-HSV1 ICP0	Santa Cruz	11060, RRID:AB_673704
Bacterial and Virus Strains		
HSV1 (HSV1716, strain 17 – g34.5 deleted)	Sorrento Therapeutic, San Diego, US	N/A
VACV (Jennerex-594, strain Wyeth, Tk-deleted expressing GM-CSF)	Sillagen, Seoul, Republic of Korea	N/A

REAGENT or RESOURCE	SOURCE	IDENTIFIER
Reovirus (Reolysin, Type 3 Dearing)	Oncolytics Biotech, Calgary, Canada	N/A
VSVΔ51-RFP (ΔM51 with insertion of RFP marker	Stojdl *et al*., 2003[141]	N/A
HSV1-K26-GFP (HSV1 with insertion of GFP to vp26)	Desai and Person, 1998[249]	N/A
Biological Samples		
DMEM	Fisher	SH30022FS
RPMI	Fisher	SH30027FS
FBS	Sigma	F1051
Penicillin/Streptomycin	Fisher	sv30010
Chemicals, Peptides, and Recombinant Proteins		
High Molecular Weight poly(I:C)	InvivoGen	tlrl-pic

REAGENT or RESOURCE	SOURCE	IDENTIFIER
Lipofectamine 2000	Fisher	11668019
EasyTagTM Express Protein Labeling Mix	Perkin Elmer	NEG772002MC
Critical Commercial Assays		
Cell Proliferation Kit I – MTT	Roche	11465007001
CAT ELISA	Roche	11363727001
Deposited Data		
Ribosome footprint of infected cancer cells	This study	GEO: GSE137757
RNaseq of transcriptome of infected cancer cells	This study	GEO: GSE137757
Experimental Models: Cell Lines		
4T1	ATCC	CRL-2539, RRID:CVCL_0125
HEK293T	ATCC	CRL-3216, CVCL_0063

REAGENT or RESOURCE	SOURCE	IDENTIFIER
CT-2A	Laboratory of D. Stojdl	N/A
PKR-null/WT MEFs	Laboratory of A. Koromilas	N/A
NIH 3T3	ATCC	CRL-1658, CVCL_0594
Oligonucleotides		
See Table S4	N/A	N/A
Recombinant DNA		
shNTC plasmid DNA (MISSION® pLKO.1-puro Non-Mammalian shRNA Control Plasmid DNA)	Sigma	SHC002
shINPP5E plasmid DNA (MISSION® shRNA plasmid DNA)	Sigma	TRCN0000080705
shBBS9 plasmid DNA (MISSION® shRNA plasmid DNA)	Sigma	TRCN0000182387

REAGENT or RESOURCE	SOURCE	IDENTIFIER
shUSP18 plasmid DNA (MISSION® shRNA plasmid DNA)	Sigma	TRCN0000030789
shUSP44 plasmid DNA (MISSION® shRNA plasmid DNA)	Sigma	TRCN0000030879
Software and Algorithms		
FASTX	Laboratory of G. Hannon	http://hannonlab.cshl.edu/fastx_toolkit/
Bowtie2	Langmead and Salzberg, 2012[250]	http://bowtie-bio.sourceforge.net/bowtie2/index.shtml
Venny v2.1	Oliveros, 2007[251]	https://bioinfogp.cnb.csic.es/tools/venny_old/venny.php
BiNGO	Maere *et al*., 2005[252]	http://apps.cytoscape.org/apps/bingo
Cytoscape 3.0	Shannon *et al*., 2003[253]	https://www.cytoscape.org

2.4.1. Cell culture and viruses

Mouse breast carcinoma 4T1, fibroblast NIH 3T3, human HEK293T and monkey Vero cells were obtained from American Type Culture Collection (ATCC). Mouse glioblastoma CT2A was obtained from Dr. David Stojdl (Children's Hospital of Eastern Ontario Research Institute). PKR null and respective wild-type MEFs were obtained from Dr. Antonis Koromilas (Lady Davis Institute). Cells were routinely checked for mycoplasma contamination by cytoplasmic DNA staining. NIH 3T3, HEK293T, Vero, CT2A and MEFs were cultured in Dulbecco's Modified Eagle Medium (DMEM) (Fisher) supplemented with 10% fetal bovine serum (Sigma) and 0.1% penicillin and streptomycin (Life Technologies) at 37°C in 5% CO_2. 4T1 were cultured in Roswell Park Memorial Institute (RPMI) 1640 (Fisher) supplemented with 10% fetal bovine serum (Wisent Bioproducts) and 0.1% penicillin and streptomycin. HSV1 (HSV1-1716, strain 17 – γ34.5 deleted, Sorrento Therapeutics, San Diego, USA), VACV (JX-594 strain Wyeth, Tk-deleted expressing GM-CSF, Jennerex Biotherapeutics / Sillagen, Seoul, Republic of Korea) and Reovirus (Reolysin, Type 3 Dearing, – Oncolytics Biotech, Calgary, Canada) were kindly provided by manufacturers. VSVΔ51-RFP (ΔM51 with insertion of RFP marker) was kindly provided by Dr. John Bell (Ottawa Hospital Research Institute). HSV1-K26-GFP was kindly provided by Dr. Karen Mossman (McMaster University). For propagation of HSV1-1716 and HSV1-K26-GFP, monolayer of Vero cells was inoculated with viruses at a MOI of 0.5 and cultured for 72 hours at 37°C, 5% CO_2. Supernatant was clarified by centrifuge at 500 x g for 5 min, then filtered (0.45 μm). Virus particles in the supernatant were separated from cellular debris by ultracentrifugation at 17500 x g for 90 min over a sucrose cushion (36% sucrose, 10 mM HEPES, 150 mM NaCl, 0.1 mM EDTA, pH 7.3). Pellets were resuspended in 1X HNE buffer (10 mM HEPES, 150 mM NaCl, 0.1 mM EDTA, pH 7.3) and stored at −80°C. VSVΔ51 propagation was adapted from a

previously described method [254]. Briefly, monolayer of Vero cells was inoculated with VSVΔ51 at MOI of 0.01. Approximately 24 hours post inoculation, supernatant was collected and clarified by centrifugation at 500 x g for 5 min. Cleared supernatant are filtered (0.2 μm), then virus particles were pelleted by ultracentrifugation at 28,000 x g for 90 min. Virus particles in the pellet were resuspended in DMEM media and stored at −80°C. JX-594 and Reovirus were used directly from stock provided by manufacturer.

2.4.2. Lentivirus production and plasmids

The following lentiviral vectors were obtained from Sigma Aldrich: SHC002 (shNTC); TRCN0000080705 (shINPP5E); TRCN0000182387 (shBBS9), TRCN0000030789 (shUSP18), TRCN0000030879 (shUSP44). The lentiviral vectors were co-transfected with the packaging plasmids pLP1, pLP2 and pLP/VSVG (Thermofisher) into HEK293T cells. Lentivirus-containing supernatants were collected at 48 and 72 hours post-transfection and filtered (0.45 μm). The filtrate was applied directly to target cells and integration of the expression cassette was confirmed 72 hours post-transduction by puromycin selection at 2 μg/ml for 4 days. The long mouse *Inpp5e* 5′ leader (nt 1-601) was PCR-amplified from a full-length MGC cDNA clone (GenBank: BC052717; cloneID 6837339 from Dharmacon). This clone is missing the first 31 nucleotides of the annotated long *Inpp5e* mRNA transcript (NM_033134). The 601 nt 5′ leader was cloned into the NotI restriction site of pMC (a kind gift of Dr. Martin Holcik, Carleton University) upstream of the CAT reporter maintaining the same reading frame as the endogenous *Inpp5e* transcript. The short *Inpp5e* leader (found in NM_001290437; nt 1-348) was created from the long-leader CAT construct by a deletion overlap extension cloning strategy. Site-directed mutagenesis was performed to mutate uORF start codons in the long-leader CAT construct. All constructs were verified by Sanger sequencing.

2.4.3. Poly(I:C) treatment

Cells was transfecting with high molecular weight poly(I:C) (InvivoGen) using Lipofectamine 2000 (Thermo Fisher) according to the manufacturer protocol at a ratio of 1:2 μg:μl poly(I:C):lipofectamine. A poly(I:C) concentration of 5 μg/ml was used unless otherwise indicated. For "vehicle" treatments, cells were transfected with lipofectamine 2000 but without poly(I:C).

2.4.4. Polysome profiling

Polysome profiling was conducted as previously described [255]. Briefly, cycloheximide (Bioshop, CAT #66-81-9) was added directly to the culture media to a final concentration of 100 μg/ml and incubated for 5 min. Cells were then washed 3 times with ice cold PBS containing cycloheximide, then were scraped from the dishes and pelleted at 500 x g for 5 min at 4°C. Cells were lysed with hypotonic buffer (5 mM Tris pH 7.5, 2.5 mM $MgCl_2$, 1.5 mM KCl) supplemented with cOmplete Protease Inhibitor Cocktail (Roche) and debris was cleared by centrifugation at 14,000 x g for 5 min, 4°C. Lysates containing ribosome-bound mRNAs were collected, flash frozen, then stored at −80°C. A volume of lysate equal to 10 OD260 units was added on a 10%–50% sucrose gradient and centrifuged at 36,000 rpm in a SW41 bucket rotor for 90 min at 4°C. Fractions were collected using a Brandel Fraction Collector System. RNA was extracted from each fraction using Trizol reagent according to the manufacturer's protocol.

2.4.5. Metabolic labeling and cell viability

Cells were incubated with complete growth media supplementing with EasyTagTM Express Protein Labeling Mix containing both [^{35}S]-L-methionine and [^{35}S]-L-cysteine (PerkinElmer) at 10 μCi/ml for 30 min at 37°C, 5% CO_2. Cells were then lysed in radioimmunoprecipitation assay

(RIPA) buffer (150 mM NaCl, 1.0% IGEPAL-CA-630, 0.5% sodium deoxycholate, 0.1% SDS, 50 mM Tris, pH 8.0). Proteins were then separated on SDS-PAGE and transferred to a nitrocellulose membrane, followed by exposure to autoradiography films. Cell viability was measured 48 hours post-infection using the Cell Proliferation Kit I – MTT (Roche) according to the manufacturer's manual.

2.4.6. Ribosome profiling

Ribosome profiling was performed as previously described on 2 biological replicates [256]. Briefly, polysomes in 4T1 lysates were stabilized with cycloheximide and 4T1 lysates were split into two parallel workflows. RNA-Seq on total RNA from one half of the lysate (see below) while RNase I footprinting was performed on the remaining half to capture RPFs. For RNA-Seq, 150 μg of total RNA was taken for RNA-Seq analysis and Poly-(A)+ mRNA was purified using magnetic oligo-dT DynaBeads (Thermofisher) according to the manufacturer's instructions. Purified RNA was eluted and mixed with an equal volume of 2X alkaline fragmentation solution (2 mM EDTA, 10 mM Na_2CO_3, 90 mM $NaHCO_3$) and incubated for 20 min at 95°C. Fragmentation reactions were mixed with stop/precipitation solution (300 mM NaOAc pH 5.5 and GlycoBlue), followed by isopropanol precipitation by standard methods. Fragmented mRNA samples were size-selected on a denaturing 10% urea-polyacrylamide gel. The area corresponding to 35-50 nucleotides was excised, eluted and precipitated with isopropanol. Isolated RPF RNA (corresponding to 28-32 nt fragments) and total RNA fragments were used to create cDNA libraries as previously described [256]. Ribosomal RNA (rRNA) contamination was reduced by subtractive hybridization using biotinylated oligos that were reverse complements of abundant rRNAs. The mRNA and ribosome-footprint libraries were then amplified by PCR (10 cycles) using indexed primers and sequenced

on the Illumina HiSeq 2000 platform with read length of 50 nucleotides at the McGill University and Génome Québec Innovation Centre.

2.4.7. Mapping and analysis of ribosome profiling data

The adaptor sequence was removed from reads using FASTX [257] and reads that mapped to rDNA sequence by Bowtie 2 [250] were discarded. Reads were then mapped to the mouse genome (mm9) using Bowtie 2. Uniquely mapped reads with MAPQ score ≥ 10 were used for further analysis. For gene expression analysis, reads mapping to the coding region of RefSeq transcripts were used to calculate Reads Per Kilobase per Million total uniquely mapped reads (RPKM). Gene-level RPKMs were obtained by conflating and averaging transcript RPKMs. Genes that showed no expression (0 RPKM) at either the transcription or translation levels in either the mock or infected samples were omitted from further analysis. Translation efficiency was defined by the $\log_2$ ratio of RPF to total RNA RPKMs. For metagene analysis of read distribution around start and stop codons, reads mapped to RefSeq transcripts were used. For a given region, only genes with at least 128 reads whose 5′ end was within the region were used. The 5′ end position of a read was used for the plotting. Subsets of differentially-expressed genes that are common and unique between the three oncolytic viruses were compiled using Venny v2.1 [251].

2.4.8. Functional analysis of DEGs

Differentially-expressed genes that were commonly up- or downregulated in all three virus infections were tested for enrichment ($q < 0.10$) in Gene Ontology (GO) terms using BiNGO (GO terms downloaded October, 2015) [252]. GO networks were plotted with the Enrichment Map plugin within Cytoscape 3.0 [253]. The “R” software package in the RStudio environment or GraphPad

Prism was used for all other data manipulation and plotting. For sequence and RNA binding protein analyses, 5′ leaders and 3′ UTRs annotated in RefSeq were retrieved from UCSC Tables.

2.4.9. Immunocytochemistry

4T1 cells were cultured as indicated on a 10 mm, #1.5 glass coverslip (Electron Microscopy Science). For intracellular staining, cells were washed with ice cold PBS followed by fixation in 4% paraformaldehyde in PHEM buffer (60 mM PIPES, 25 mM HEPES, pH6.9, 10 mM EGTA, 2 mM $MgSO_4$) for 10 min at room temperature. Fixed cells were treated with 50 mM NH_4Cl in PBS to reduce autofluorescence, followed by permeabilization with 0.1% Triton X-100 in PBS for 10 min. Following 3 washes with PBS, the coverslip was then blocked with 5% BSA in PBS, for 30 min. Permeabilized cells were then incubated with the indicated primary antibody in 1% BSA/PBS overnight. Coverslips were washed 3 times for 5 min each with PBS and incubated with 1:10,000 dilution Goat anti-Rabbit IgG (H+L) Highly Cross-Adsorbed Secondary Antibody Alexa Fluor 568 secondary antibody (#A-11036, Invitrogen) for 1 hour at room temperature in the dark. Coverslips were washed 3 × 5 min with PBS and nuclei were stained with 1:200 of NucBlue® Live Ready Probe-variant of Hoechst dye (Life Technologies) in PBS for 5 min. Coverslips were then mounted onto slides using Prolong® Diamond mounting medium (Life Technologies). Confocal imaging was performed using a FV-1000 confocal microscope (Olympus) with a PlanApo N 100X/1.40 oil immersion objective lens (Olympus). Non-confocal fluorescence imaging was performed using an EVOS FL Cell Imaging system (Thermofisher). The following primary antibodies and corresponding dilution are used: 1:100 α-INPP5E (# ab69696, Abcam).

2.4.10. Western blotting

Cells were washed with PBS and lysed in RIPA buffer supplemented with 10 mM NaF, 10 mM Na_2VO_3 and cOmplete Protease Inhibitor Cocktail (Roche). Cell debris was removed by centrifugation at 10,000 x *g*, 10 min, 4°C. Protein concentration of the supernatant was quantified using DC Protein assay (BioRad). Indicated amount of total protein was then loaded onto 10% SDS-polyacrylamide gel and separated by electrophoresis. Separated proteins were transferred to a nitrocellulose or PVDF membrane, then blocked with 5% skim milk in TBS-T buffer (10 mM Tris, 50 mM NaCl, 0.1% Tween-20, pH 7.5). The following primary antibodies and corresponding dilution were used: 1:500 α-INPP5E (#CPA3073, Cohesion Biosciences), 1:10,000 α-β-actin (#A5441, Sigma), 1:5000 α-GAPDH (#ab8245, Abcam), 1:2000 α-pan-HSV1 (#B011402, Dako), 1:2000 α-HSV1-ICP0 (#11060, Santa Cruz).

2.4.11. Quantitative RT-PCR (RT-qPCR) and Droplet Digital RT-PCR (RT-ddPCR)

cDNA was reverse transcribed from total RNA using iScript Advanced cDNA Synthesis Kit (BioRad) according to the manufacturer's protocol. RT-qPCR was performed on cDNA mixed with iQ SyBR Green mix (BioRad) according to the manufacturer's protocol, using a Realplex 2 thermocycler (Eppendorf). The PCR conditions were 95°C for 3 min, followed by 40 cycles of 95°C for 10 s, 60°C for 30 s and 72°C for 30 s. Ct threshold was determined by Realplex software (Eppendorf). For calculating mRNA abundance, the ΔΔCt method relative to *Rps20* expression was used. For calculating short *Inpp5e* variant ratio, the ΔΔCt method relative to total *Inpp5e* expression was used. For the binding assays, RT-qPCR was performed directly on the extracted DNA using the same mix and PCR conditions as in qPCR assays, then the number of HSV1 genome relative to the number of host genome was calculated using the ΔΔCt method

comparing relative abundance between HSV1 *UL30* and mouse *Lmnb2* abundance. For RT-ddPCR, cDNA was mixed with QX200 ddPCR EvaGreen Supermix (Biorad) according to the manufacturer's protocol and droplets were prepared using QX200 droplet generation oil on a QX200 Droplet Generator (Biorad). Droplets were subjected to PCR using a C1000 thermocycler (BioRad) using the cycling conditions: 95°C for 5 min, followed by 45 cycles of 95°C for 30 s at a ramp rate of 2°C/s and 60°C for 1 min at a ramp rate of 2°C/s. Positive/negative droplets were counted by a QX200 Droplet Reader (BioRad). Primers (listed 5′ to 3′) used for qPCR and ddPCR are listed in **Table S2.4**. For the gel-based assessment of 5′ leader expression, PCR was performed on 4T1 cDNA libraries using INPP5Eutr-F: CAGTCGTTGTTCCAGCTGC and INPP5E-shortUTR-R: TGAAAACTCGAGTGGCTCCC. For normalization of the CAT RNA reporter assay (see below), CAT cDNA was amplified using the above-noted ddPCR conditions with previously published primers [258]. Melting curves and agarose electrophoresis were performed to control for PCR specificity in all of the above assays.

2.4.12. CAT translation reporter assays

The CAT assay has been described previously [245]. Briefly, 4T1, CT2A or MEFs were seeded at 3 or $6x10^5$ cells/well in 6-well plates, then co-transfected with 1 μg each of β-Galactosidase- (pBGal, obtained from Dr. Martin Holcik) and CAT-expressing plasmids using Lipofectamine 2000. 24 hours post-transfection, cells were lysed, and CAT expression was quantified using the CAT ELISA (Roche) as per the manufacturer's instructions. β-Galactosidase activity was measured using an ortho-Nitrophenyl-β-galactoside (ONPG) colorimetric assay. In the case of RNA transfection experiments, a T7-flanked long *Inpp5e* 5′ leader was amplified from 1 ng of the appropriate CAT reporter plasmid. This amplicon was used as a template for synthesis of capped and poly(A)-tailed RNA using the T7 HiScribe *in vitro* transcription kit (New England Biolabs)

according to the manufacturer's protocol. 1 μg of RNA was transfected with 2 μL of Lipofectamine 2000, and at 4 hours HSV1 was added into the media at indicated MOIs and incubated for an additional 18 hours. Cells were lysed in 300 μL of CAT lysis buffer, and 30 μL was used to isolate total RNA and prepare cDNA using iScript RT (BioRad). CAT cDNA was amplified by ddPCR using the above-noted primers and conditions. CAT expression was determined as above and normalized to the CAT RNA levels.

2.4.13. CRISPR/Cas9-mediated gene knockout

CRISPR/Cas9 knockout of INPP5E in 4T1 was performed as previously described [259]. Briefly, small guide RNAs (sgRNA) targeting the *Inpp5e* first exon or non-targeting sgRNA (primer sequences in **Table S2.4**) were cloned into the lenti-sgRNA(MS2)-zeomycin backbone (Addgene #61427) using BsmBI. To produce separate Cas9- and sgRNA-expressing lentiviruses, doxycycline-inducible and puromycin expressing pCW-Cas9 (Addgene #50661) or the constitutively expressing sgRNA vector were co-transfected with pLP1, pLP2 and pLP/VSVG (Thermofisher) into HEK293T cells using Lipofectamine 2000 (Invitrogen) according to the manufacturer's protocol. Cells were then transduced with the lentiviral supernatants and double-transductants were selected using puromycin and zeomycin. Cas9 expression was then induced using 1 μg/ml doxycycline for 24 hours. Single-cell clones were obtained by limiting dilution, screened using T7 Endonuclease I (New England Biolabs), and confirmed by Sanger sequencing. CRISPR/Cas9 modification efficiency was quantitated using TIDE, which deduces the frequency of individual insertion-deletion (indel) from Sanger sequencing of a mixed population.

2.4.14. Live cell monitoring of virus spread

Live cells monitoring of virus infection was performed using the IncuCyte Live-Cell Analysis system (Sartorius). Cells were seeded in a 24-well plated at 80% confluency, then infected with viruses at the indicated MOI. Multiple phase contrast and fluorescence images were taken per well every 2 hours. Images were then analyzed using the IncuCyte Zoom software (Sartorius) for GFP cluster integrated intensity (Green calibrated unit x μm^2) as a measurement for virus infection. GFP cluster integrated intensity was calculated using the following customized process definition in IncuCyte ZOOM software: background subtraction using Top-Hat method (disk shape structuring element with radius of 10 μm, threshold of 1.0 green calibrated unit), edge split: Off, Hole Fill: No, Adjust Size: No, Filters: No.

2.4.15. Plaque assays

For titration, Vero cells were cultured to a monolayer. Cells were then incubated with a serial dilution in DMEM of virus-containing supernatant for 1 hours, 37°C, 5% CO_2 with shaking every 10 min. Cells were then washed 3 times with DMEM, then a layer of DMEM + 10% FBS +1% agar was added on top and allowed to solidify. Cells were then cultured at 37°C, 5% CO_2 for 48 hours (VSVΔ51) or 72 hours (HSV1, VACV). Full-well fluorescence images were taken, and fluorescent plaques were counted and used for back calculating original viral titer. For modified plaque assay to compare viral entry and spread (**Figure 2.6D**), monolayers of 4T1 WT or 4T1 $Inpp5e^{CRISPR}$ were cultured, then incubated virus diluted in RPMI media at a MOI of 0.01. Cells were then washed 3 times with RPMI media, then a layer of RPMI + 10% FBS +1% agar was added on top and allowed to solidify. Cell culture, and plaque detection and counting were carried out as described above for standard plaque assays.

2.4.16. Binding assays

The cold binding assay was adapted for HSV1 from a previously described method [260]. Briefly, cells were pre-incubated at 4°C for 30 min, then incubated with HSV1-1716 at the indicated MOI at 4°C for 1 hour. For internalization, cells were incubated for 1 hour at 37°C, washed with PBS pH 3.0 to remove surface bound viruses. gDNA was harvested using the QIAamp DNA Mini Kit (QIAGEN) according to manufacturer's protocol. PCR was performed using primers described above on the DNA.

2.4.17. Quantification and Statistical Analyses

All experiments were performed with at least 3 biological replicates unless otherwise specified in figure legends. Statistical significance was *a priori* set to 0.05. Two-tailed Student's t test or one-way ANOVA with Dunett's post hoc tests were performed where applicable unless otherwise indicated in the figure legend. Error bars indicate standard error of the mean (sem). $^{*}p < 0.05$, $^{**}p < 0.01$, $^{***}p < 0.001$, $^{****}p < 0.0001$, ns, non-significant.

2.4.18. Data and Code Availability

Raw sequence files have been deposited on the NCBI Gene Expression Omnibus (GEO: GSE137757).

2.5. Results

2.5.1. Transcription and translation are uncoupled in response to oncolytic virus infection of 4T1 cells

To assess translationally regulated innate immune genes, we used HSV1, reovirus, and VACV individually to infect 4T1 cells, a murine mammary carcinoma model that is refractory to viral oncolysis and closely resembles stage IV human breast cancer. Each of these viruses has a different rate of infection that eventually results in the shutdown of host cell translation[240]. We therefore selected an effective dose that is cytopathic for 50% (ED_{50}) of 4T1 cells at 48 h post-infection (**Figure 2.1A**). At 18 h post-infection, polysome profiles (**Figure 2.1B**) and ^{35}S-methionine labeling (**Figure 2.1C**) showed robust viral protein synthesis, while that of the host cells was only slightly affected. The majority of cells were infected at this dose and time point, confirmed by co-expression of a virion-derived GFP transgene in the case of HSV1 and VACV (**Figure S2.1A**).

We profiled both the transcriptome and translatome signatures of 4T1 cells, with each individual infection compared to mock-infected controls using the ribosome-profiling method (summarized in **Figure 2.1D**)[32]. By in-parallel sequencing of ribosome-protected footprints (RPFs) and total mRNA (RNA), the ribosome occupancy and thus TE (RPF/RNA) of individual mRNA species was quantitated. In contrast to total RNA read densities, which were constant throughout the exonic regions, RPF densities were found to increase within annotated coding sequences (CDSs) relative to 5′ leaders and 3′ UTRs, which is consistent with ribosomes engaged in translation (**Figure S2.1B**). Regression analysis of reads normalized to CDS length and sequencing depth (reads per kilobase of CDS per million reads sequenced [RPKM]) in two

biological replicates showed a high degree of correlation at both the RNA (i.e., transcriptome) and the RPF (i.e., translatome) genomic levels (**Figure S2.1C**). These data demonstrate that ribosome profiling successfully captured the transcriptional and translational states of the 4T1 genome following challenge with three distinct oncolytic viruses.

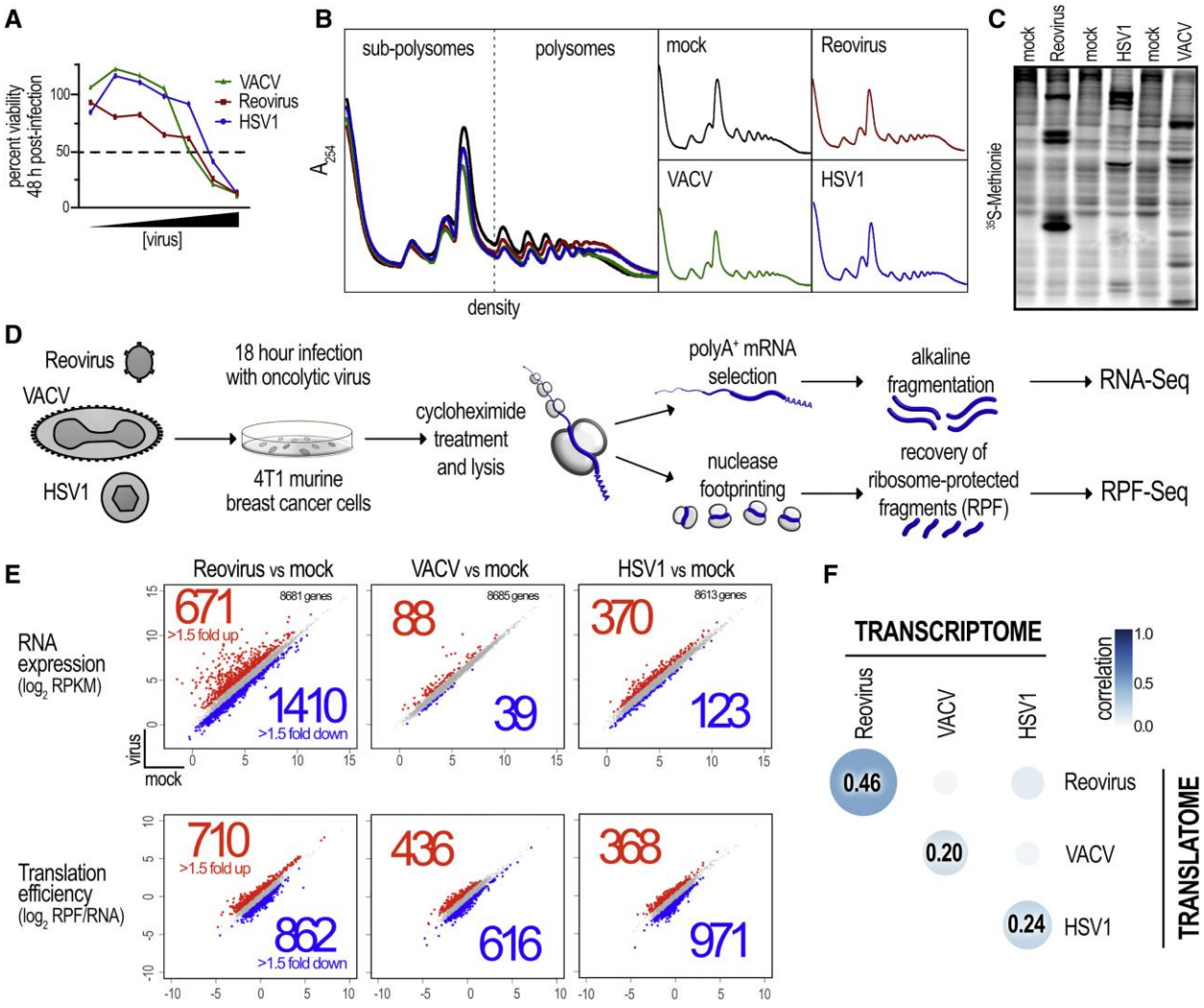

Figure 2.1. Transcription and translation are uncoupled in response to oncolytic virus infection of 4T1 cells.
(A) Infectious dose-response viability curves for the three different viruses used in this study in murine 4T1 breast carcinoma cells.
(B and C) Polysome profiles of virus-infected versus mock-infected 4T1 cells at 18 h post-infection (B) and metabolic labeling with ^{35}S-methionine followed by SDS-PAGE to resolve nascent peptides (C).
(D) Schematic illustration of the ribosome-profiling strategy used in this study.
(E) Differential expression of sequenced genes (total number shown in top right of plots) at both the transcriptional and the translational genome levels. Each point on the plots represents the average RNA expression or TE from two biological replicates. Genes that were up- (red) or downregulated (blue) >1.5-fold were considered to be differentially expressed.
(F) Correlation analysis of RNA-normalized (transcriptome) and RPF-normalized (translatome) abundance between viruses (all relative to mock infected). Pearson's correlation coefficients are presented.

We next determined the differentially expressed genes (DEGs) at the transcriptome and translatome levels in virus- versus mock-infected 4T1 cells (**Table S2.1**). We used a cutoff of 1.5-fold change in expression up or down and found that reovirus modified transcript abundance to a higher degree (24% of sequenced genes) than HSV1 (5.7%) or VACV (1.5%) (**Figure 2.1E**, top). In stark contrast, TEs were perturbed more consistently between all three viruses: reovirus (18% of sequenced genes), VACV (12%), and HSV1 (15%) (**Figure 2.1E**, bottom). We also found a poor correlation between the transcriptome and the translatome (Pearson's correlation coefficients of 0.46, 0.20, and 0.24 for reovirus, VACV, and HSV1 versus mock, respectively) (**Figure 2.1F**). Thus, changes in the transcriptional profile of any given gene is a poor predictor of its TE, a finding that has been replicated in other experimental contexts[16,261].

2.5.2. Genes of the common translatome between all three infections function in pathways not previously associated with viral infections

A primary objective of this study was to identify innate immunity effectors that could function in a general antiviral program during any of the three infections. To this end, we determined the set of DEGs common to all three infections at both the transcriptome and the translatome levels **(Figure 2.2A**; **Table S2.2**). We performed Gene Ontology (GO) functional enrichment analysis on these shared sets and found the expected functional groups at the transcriptional level, including terms encompassing pattern recognition signaling, response to infection, inflammatory response, and nucleic acid binding (**Figure 2.2B**). Of note, many previously validated ISGs [262] were found to be uniquely upregulated at the level of transcription with reovirus, VACV, or HSV1 infection, respectively (**Figure S2.2A**). Moreover, these ISGs populated 38% (13/34) of the transcriptionally upregulated DEGs common to all three infections (**Figure S2.2B**).

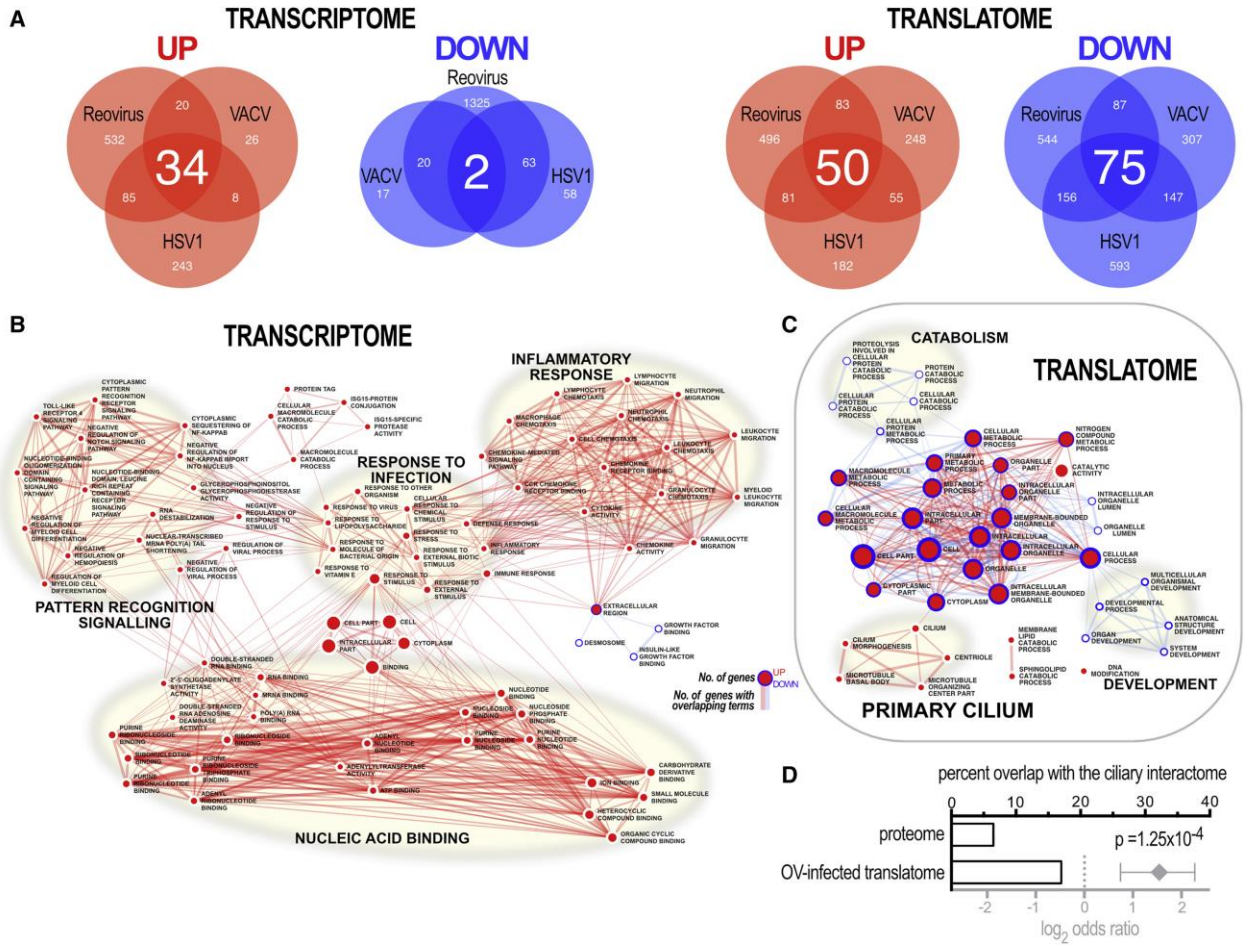

Figure 2.2. Genes of the common translatome between all three infections function in pathways not previously associated with viral infections

(A) Venn diagrams illustrating the common and unique sets of DEGs between viral infections at transcriptional and translational levels.

(B) Network analysis of enriched GO terms for the DEGs commonly regulated by all three oncolytic viruses at the transcriptional level. Generic terms are concentrated at the center and specific terms lie at the extremities. Node diameter and edge thickness are proportional to the number of genes belonging to or overlapping with GO terms, respectively.

(C) As in (B), except at the level of the translatome.

(D) Percentage of the human proteome ("proteome"; 1,319/20,195 proteins) versus the percentage of orthologous genes in the common up and down 4T1 translatomes (OV-infected translatome; 19/112) that overlap with the ciliary interactome [263]. A Fisher's exact test was used to determine statistical significance. The odds ratio is presented with bars representing a 95% confidence interval and indicating an overrepresentation of ciliary proteins in the OV-infected translatome.

Functional enrichment at the level of the common translatome was found to be very different, with few specific GO terms. Translationally downregulated genes fell into categories encompassing catabolic and developmental cellular functions, while the upregulated common set was found to be enriched in genes involved in microtubule organization and the primary cilium, an organelle with a unique cytoskeleton and subcellular proteome that is often referred to as the cell's signaling antenna [263] (**Figure 2.2C**; **Table S2.3**). Confirming the GO analysis, there was significant enrichment ($p = 1.25 \times 10^{-4}$) of genes encoding proteins that constitute the ciliary interactome **(Figure 2.2D)**[263]. Thus, using ribosome profiling, the anticipated transcriptional but unexpected translational signatures of the antiviral state in oncolytic virus-infected 4T1 were obtained. This suggests that viral infection engenders a distinctive reprogramming of cellular translation.

2.5.3. Oncolytic viruses de-repress translation of host mRNAs enriched in uORFs

To characterize the mode of control exerted on the translationally regulated transcripts, we looked for enrichment of RNA-binding protein motifs and microRNA (miRNA) target sequences (**Figures S2.3A** and **S2.3B**). We also surveyed the GC content of these annotated transcripts as well as the lengths of their 5′ leaders, CDSs, and 3′ UTRs, comparing them to all NCBI Reference Sequence (RefSeq) mouse mRNAs. While we found no significant difference in GC content, the shared translationally regulated mRNAs (either up- or downregulated) tended to have shorter 5′ leaders, CDSs, and 3′ UTRs (**Figure 2.3A**). In analyzing the distribution of TEs for the commonly upregulated set of genes, we noted that this subset was dramatically repressed in mock-infected cells compared to the entire sequenced set (**Figure 2.3B**; compare "mock" distributions). This property appeared to be mainly due to lower RPF expression in the upregulated genes (**Figure S2.3C**, center). Viral infection acted to significantly de-repress the translation of these

genes independently of changes at the RNA level (**Figure 2.3B**, shift in distribution denoted by arrow, and **Figure S2.3C**, right). In contrast, the downregulated set of genes followed a mock-infected TE distribution profile that was indistinguishable from the entire set of sequenced genes that shifted to lower TE upon viral infection (**Figure 2.3B**, right, denoted by arrow). Furthermore, a similar analysis performed on the upregulated gene sets uniquely associated with each of the three viruses showed no clear de-repression profile, suggesting that this property is a specific and common cellular response to different viral infections (**Figure 2.3C**, top). Downregulated members of virus-unique sets behaved similarly to the shared set with respect to their TE distributions (**Figure 2.3C**, bottom).

This repression/de-repression profile has previously been ascribed to *cis*-acting mechanisms of translational control involving uORFs. We used an empirically derived list of uORF-containing mouse and human mRNAs[13] and found an overrepresentation in the commonly upregulated set, while no enrichment was seen for the downregulated set (**Figure 2.3D**). Thus, three different viruses were found to commonly affect the translation of transcripts whose 5′ leaders are more likely to contain uORFs, suggesting a universal cellular response to viruses that target cellular mRNAs harboring uORFs.

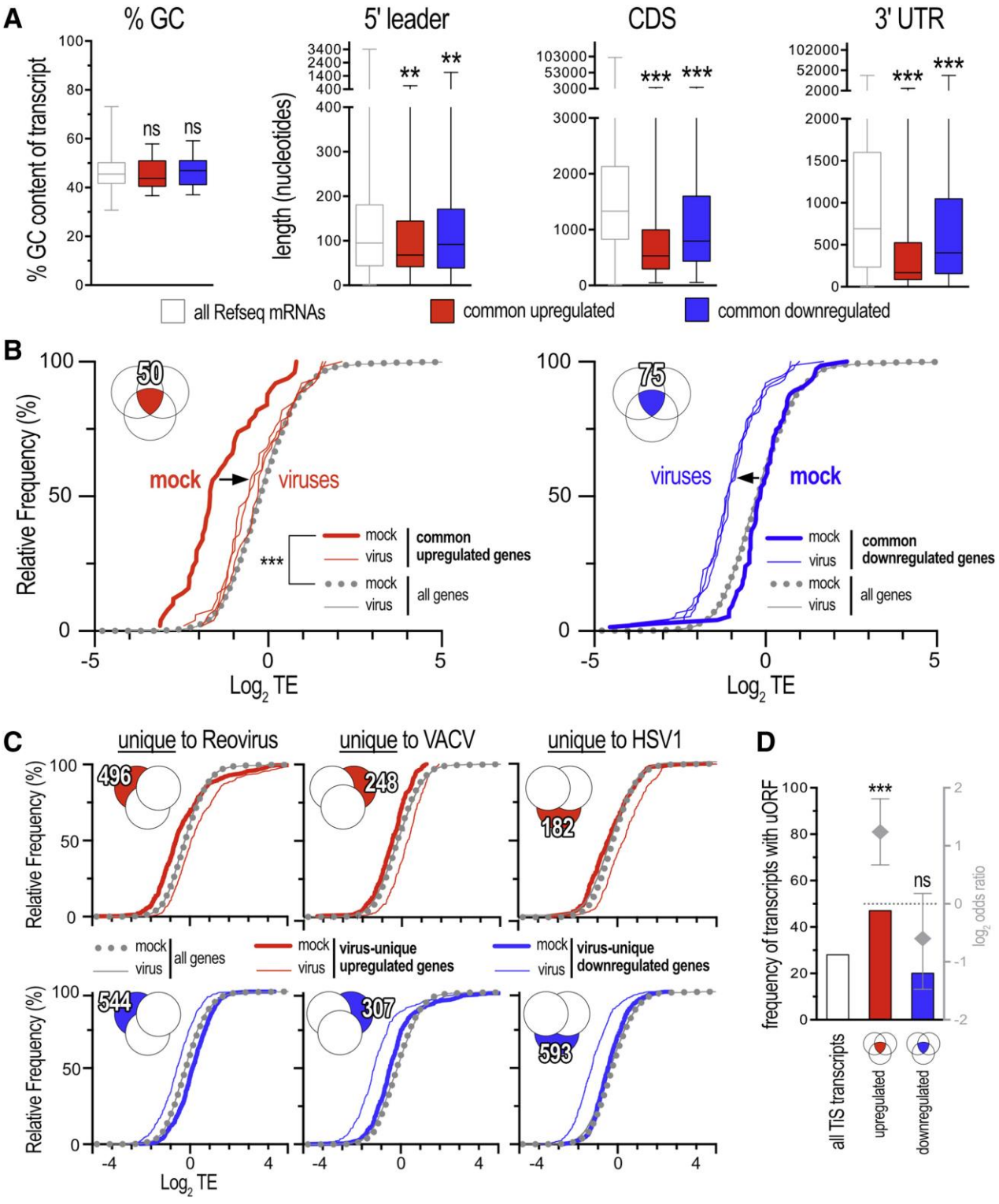
A
% GC
5' leader
CDS
3' UTR
% GC content of transcript
length (nucleotides)
ns
**
***
all Refseq mRNAs
common upregulated
common downregulated
B
Relative Frequency (%)
mock
viruses
50
75
common upregulated genes
common downregulated genes
all genes
Log2 TE
C
unique to Reovirus
unique to VACV
unique to HSV1
496
248
182
544
307
593
virus-unique upregulated genes
virus-unique downregulated genes
D
frequency of transcripts with uORF
log2 odds ratio
all TIS transcripts
upregulated
downregulated

Figure 2.3. Oncolytic viruses de-repress translation of host mRNAs enriched in uORFs
(A) Analysis of RefSeq mRNA sequence characteristics that populate the common translationally regulated gene sets (red or blue bars) compared to the entire RefSeq database (white bars, see 2.4. Materials and Methods for details). Statistical significance was determined using Kruskal-Wallis with Dunn's post hoc testing,
(B) Relative frequency distributions of TE for common upregulated (left) versus downregulated (right) genes show that the former are translationally de-repressed (directional shifts indicated by an arrow). A Mann-Whitney statistical test was used.
(C) Analysis as in (B), but for the translationally regulated gene sets that are unique to each virus.
(D) Frequency of uORFs in all mouse and human transcripts in the TiS database (7,361/26,735; http://tisdb.human.cornell.edu) compared to that present in the translationally upregulated (52/110) and downregulated (17/85) sets of transcripts common to all 3 infections. The increased frequency of uORFs in the commonly upregulated set was found to be significant by Fisher's exact test, with the odds ratios presented with bars representing a 95% confidence interval, indicating overrepresentation of uORF-containing transcripts in the upregulated gene set. $^{**}p<0.01$, $^{***}p<0.001$, ns, non-significant.

2.5.4. INPP5E is translationally induced during the host antiviral response

We next aimed to validate the increased TE of the primary cilium genes identified in the network analysis. One of these included the ciliopathy gene *Inpp5e*, an inositol 5-phosphatase linked to Joubert syndrome [264]. We reasoned that as *Inpp5e* TE is induced during virus infection, the double-stranded RNA (dsRNA) mimic poly(I:C) that induces an antiviral state via activation of IFN regulatory factor 3 (IRF3) and nuclear factor κB (NF-κB) should be able to recapitulate this control of INPP5E expression. While barely detectable in 4T1 cells in control conditions, immunofluorescence (IF) staining of INPP5E notably increased upon poly(I:C) treatment (**Figure 2.4A**, quantified in **Figure 2.4B**), yet *Inpp5e* mRNA abundance trended lower following the same treatment (**Figure 2.4C**). Consistent with the ribosome-profiling results, we observed that INPP5E protein measured by IF in wild-type 4T1 cells ($Inpp5e^{+/+}$) appeared at low levels in mock conditions but is robustly induced upon VACV infection (**Figure 2.4D**, quantified in **Figure 2.4E**). To confirm the specificity of the IF signal, we turned to CRISPR/Cas9 technology to generate two clones of 4T1 cells depleted of INPP5E ($Inpp5e^{CRISPR\#1}$, $Inpp5e^{CRISPR\#2}$). Tracking of indels by decomposition (TIDE) analysis [265] determined that the *Inpp5e* locus was modified at a frequency close to 100% with a mixture of three indels that would be predicted to disrupt expression (**Figures S2.4A–S2.4C**). The VACV-mediated induction of INPP5E protein seen in wild-type cells was lost in $Inpp5e^{CRISPR\#1}$ cells, despite a robust infection marked by strong GFP expression (**Figure 2.4D**, quantified in **Figure 2.4E**). Again, consistent with a post-transcriptional effect, total mRNA levels of *Inpp5e* were unaffected with VACV infection at similar MOI and time point (**Figure 2.4F**). HSV1 gE protein acts as an Fc receptor and binds immunoglobulin G (IgG) of various host species[266], which we used as secondary antibodies for IF detection. Thus, we could not use IF to determine whether HSV1 caused a similar induction of INPP5E. We instead

used western blotting and observed a band (with an apparent molecular weight of 62 kDa) induced with HSV1 infection in 4T1 cells (**Figures 2.4G** and **S2.4D**). Similar to the VACV data, we found that the HSV1-specific signal was lost in *Inpp5e*$^{CRISPR\#1}$ cells, despite a similar expression of HSV1 protein ICP0, indicating specificity for INPP5E (**Figure S2.4D**). The induction of INPP5E occurred in another cancer cell line, the mouse glioblastoma CT2A (**Figure 2.4G**). As was the case for either poly(I:C) or VACV treatments, *Inpp5e* mRNA abundance was not affected by HSV1 infection in either 4T1 or CT2A cells (**Figure 2.4G**).

The above data argue for the post-transcriptional regulation of *Inpp5e* in these contexts; however, post-translational changes such as increased protein stability may explain the increased expression of INPP5E with infection. We therefore determined the TE of *Inpp5e* mRNA using conventional polysome profiling, in which mRNAs are resolved based on the number of associated ribosomes. HSV1 infection (MOI of 5) was found to slightly but consistently reduce global mRNA translation at 4 h post-infection (**Figure 2.4H**, left). Unlike *Actb* mRNA, the majority (~80%) of which was found in the polysome fraction in uninfected CT2A cells, *Inpp5e* resided mainly (~60%) in sub-polysomes, which is indicative of a repressed translation state and consistent with the lack of observable protein seen in our IF and western blotting experiments (**Figure 2.4H**, right). However, the distribution of *Inpp5e* in active polysomes positively shifted from 35.24% ± 6.12% to 59.21% ± 9.53% between mock- versus HSV1-infected cells, while that of *Actb* did not change appreciably (76.49% ± 3.2% and 78.47% ± 6.8%, respectively). Thus, these data demonstrate that *Inpp5e* mRNAs, which are translationally repressed in basal conditions, are under positive translational control during viral infection in cancer cells, despite a general repression of global translation.

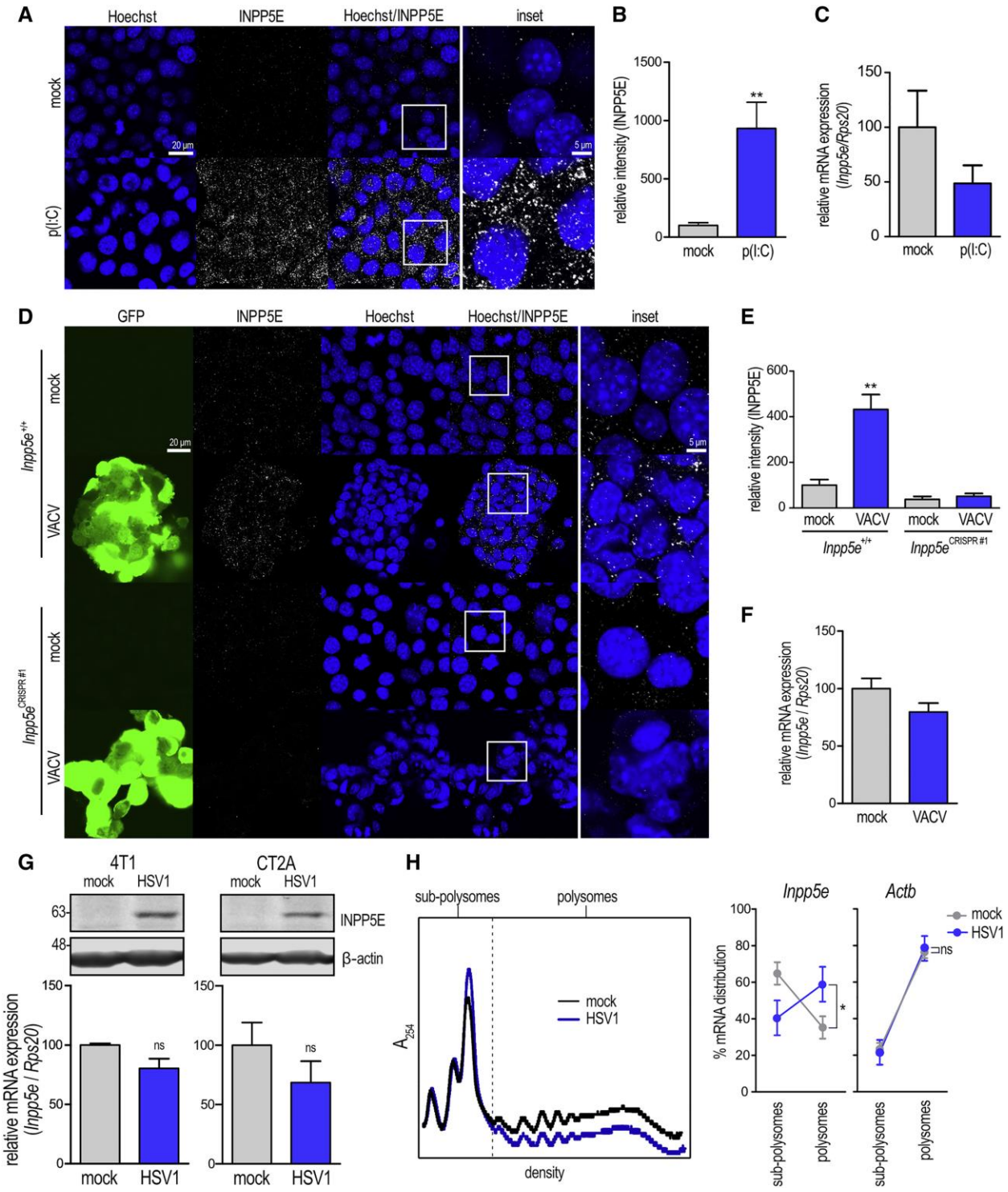
A
Hoechst
INPP5E
Hoechst/INPP5E
inset
mock
p(I:C)
20 µm
5 µm
B
relative intensity (INPP5E)
1500
1000
500
0
**
mock
p(I:C)
C
relative mRNA expression (Inpp5e/Rps20)
150
100
50
0
mock
p(I:C)
D
GFP
INPP5E
Hoechst
Hoechst/INPP5E
inset
Inpp5e+/+
Inpp5eCRISPR#1
mock
VACV
20 µm
5 µm
E
relative intensity (INPP5E)
600
400
200
0
**
mock
VACV
mock
VACV
Inpp5e+/+
Inpp5eCRISPR#1
F
relative mRNA expression (Inpp5e / Rps20)
150
100
50
0
mock
VACV
G
4T1
CT2A
mock
HSV1
63
48
INPP5E
β-actin
relative mRNA expression (Inpp5e / Rps20)
150
100
50
0
ns
mock
HSV1
H
sub-polysomes
polysomes
A254
mock
HSV1
density
Inpp5e
Actb
% mRNA distribution
100
80
60
40
20
0
*
ns
mock
HSV1
sub-polysomes
polysomes

Figure 2.4. INPP5E is translationally induced during the host antiviral response
(A) Representative confocal images of anti-INPP5E stained 4T1 cells treated with poly(I:C) at 5 μg/mL or vehicle for 18 h.
(B) Quantification of the INPP5E IF signal in (A) normalized to mock.
(C) qRT-PCR of *Inpp5e* normalized to *Rps20* mRNA abundance in mock- or poly(I:C)-treated 4T1 cells for 18 h.
(D) As in (A), comparing INPP5E expression in mock-infected *Inpp5e*$^{+/+}$ or *Inpp5e*$^{CRISPR\#1}$ 4T1 cells or cells infected with VACV at 5 MOI.
(E) Quantification of the INPP5E IF signal in (D) (normalized to mock-infected cells).
(F) qRT-PCR of *Inpp5e* mRNA in mock-infected or VACV-infected 4T1 cells at 5 MOI for 24 h.
(G) Top: representative western blots of steady-state INPP5E protein expression in mock-infected and HSV1-infected 4T1 or CT2A cells at 18 h post-infection at 1 MOI. β-Actin is included as a loading control. Apparent molecular weights are indicated to the left in kilodaltons. Bottom: qRT-PCR of *Inpp5e* normalized to *Rps20* mRNA abundance in mock-infected or HSV1-infected cells at 24 h post-infection at 5 MOI in 4T1 and CT2A cells.
(H) Left: representative polysome profiles of mock-infected and HSV1-infected CT2A cells 4 h post-infection at MOI of 5. Right: distribution of *Inpp5e* and *Actb* mRNAs across sub-polysomes (low TE) and polysomes (high TE) in mock-infected versus HSV1-infected samples.
Error bars indicate standard error of the mean (sem). $^{*}p < 0.05$, $^{**}p < 0.01$, ns, non-significant, calculated using two-tailed t test.

2.5.5. Expression of an alternative 5' leader during infection releases Inpp5e from uORF-mediated translational repression

Our data demonstrated that *Inpp5e* translation is normally repressed in 4T1 and CT2A cells, as evidenced by its low TE in mock-infected cells from ribosome profiling, polysome profiling, and the low steady-state protein expression observed by western blotting and IF. Furthermore, the same assays showed that viral infection de-represses *Inpp5e* translation. We therefore hypothesized that this repression/de-repression shift is due to uORF-dependent translational control. There are "long" and "short" mouse *Inpp5e* mRNA variants with long and short 5′ leaders, respectively. The short leader results from a downstream alternative transcription start site (altTSS) and alternative splicing, removing an intron that lies entirely within the 5′ leader. Moreover, the short transcript is predicted to encode a C-terminally truncated protein isoform and is supported in the Sequence Read Archive (SRA) by intron-spanning reads that account for ∼5% of all *Inpp5e* transcripts (**Figure 2.5A**), as well as a single RIKEN clone isolated from neonatal kidney tissue.

A previous genome-wide study of initiating ribosomes listed a putative uORF in both the long and short *Inpp5e* 5′ leaders (**Figure 2.5B**, top schema shows the long and short *Inpp5e* mRNA variant with the location of the putative uORF in dark blue)[13]. Critically, in uninfected 4T1 cells, RPF read densities were concentrated in the *Inpp5e* leader region (**Figure 2.5B**, leader region highlighted in light blue). This density shifted to the main ORF (mORF) upon HSV1, reovirus, or VACV infections, which is strongly suggestive of a regulatory uORF.

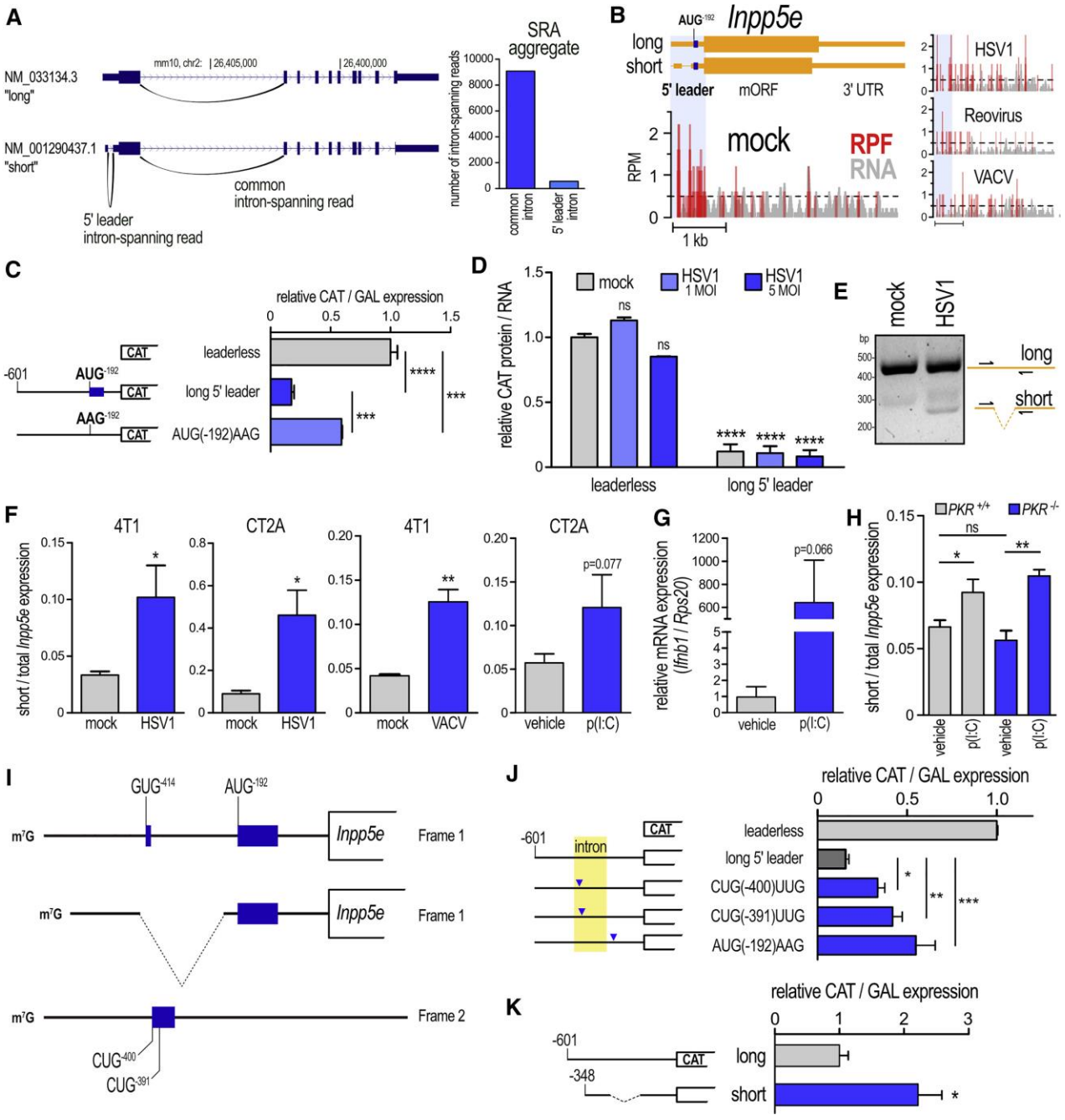
A
mm10, chr2: | 26,405,000 | 26,400,000
NM_033134.3
"long"
NM_001290437.1
"short"
common
intron-spanning read
5' leader
intron-spanning read
SRA
aggregate
number of intron-spanning reads
common intron
5' leader intron
B
Inpp5e
AUG-192
long
short
5' leader
mORF
3' UTR
mock
RPF
RNA
RPM
1 kb
HSV1
Reovirus
VACV
C
relative CAT / GAL expression
CAT
-601
AUG-192
AAG-192
leaderless
long 5' leader
AUG(-192)AAG
D
relative CAT protein / RNA
mock
HSV1 1 MOI
HSV1 5 MOI
ns
leaderless
long 5' leader
E
mock
HSV1
bp
long
short
F
4T1
CT2A
short / total Inpp5e expression
mock
HSV1
VACV
vehicle
p(I:C)
p=0.077
G
relative mRNA expression
(Ifnb1 / Rps20)
p=0.066
H
PKR +/+
PKR -/-
short / total Inpp5e expression
I
GUG-414
AUG-192
m7G
Inpp5e
Frame 1
Frame 2
CUG-400
CUG-391
J
relative CAT / GAL expression
intron
leaderless
long 5' leader
CUG(-400)UUG
CUG(-391)UUG
AUG(-192)AAG
K
relative CAT / GAL expression
-601
-348
long
short

Figure 2.5. Expression of an alternative 5′ leader during infection releases *Inpp5e* from uORF-mediated translational repression

(A) RefSeq-annotated *Inpp5e* transcripts showing "long" and "short" variants. RefSeq accessions are indicated. Deep sequencing reads were aggregated from a pool of samples in the Sequencing Read Archive (SRA; NCBI *Mus musculus* Annotation Release 106) and plotted (right) based on intron-spanning reads from the short 5′ leader intron or the first intron common to both transcripts.

(B) Chromatogram of read densities (reads per million [RPM]) merged from the two biological replicates of ribosome profiling in this study for the *Inpp5e* locus at both RNA and RPF gene expression levels showing a shift in RPF reads from the 5′ leader to the mORF following infection.

(C) Translation reporter assay in 4T1 cells showing that the long *Inpp5e* 5′ leader strongly represses the translation of the CAT ORF. Constructs used are pictured to the left and were co-transfected with a β-galactosidase (GAL) reporter to normalize any differences in transfection. The long leader-mediated repression is substantially weakened with a single mutation that abolishes a uORF start codon (AUG[−192]AAG) demonstrating a bona fide uORF mechanism of translational regulation.

(D) Translation reporter assay as in (C), but in 4T1 cells transfected with *in vitro* transcribed CAT RNA evaluated at 18 h post-HSV1 infection; n = 2 biological replicates.

(E) Agarose gel with resolved PCR amplicons from a 4T1 cDNA library indicates the expression of both the short and long *Inpp5e* 5′ leaders in HSV1-infected cells (a single set of primers flank the 5′ leader intron, pictured at right).

(F) qRT-PCR of short versus total *Inpp5e* mRNA showing an increased expression of the short variant with HSV1 infection after 48 h of infection in either 4T1 or CT2A cells, and VACV-infected 4T1 at 24 h post-infection or poly(I:C)-treated CT2A for 18 h.

(G) qRT-PCR of *Ifnb1* normalized to *Rps20* mRNA expression in CT2A cells treated with poly(I:C) for 18 h.

(H) Poly(I:C)-mediated induction of the short *Inpp5e* variant is PKR independent. Poly(I:C) 8 μg/mL was transfected into $PKR^{+/+}$ or $PKR^{-/-}$ MEFs, and short versus total *Inpp5e* RNA levels were determined by qRT-PCR 18 h later. A two-way ANOVA with Sidak post hoc test was used to determine significance.

(I) Schematic of the *Inpp5e* 5′ leader region in both the long (top) and short (center) mRNA transcript variants in reading frame 1, which encodes INPP5E, and frame 2, which is non-coding (bottom). Putative start codons are indicated, with numbering relative to the first A of the *Inpp5e* AUG start codon in the long variants. Locations of potential uORFs are indicated with dark blue rectangles.

(J) CAT reporter assays were performed as in (C) with uORF start codon mutations (CUG[−400]UUG, CUG[−391]UUG, AUG[−192]AAG; indicated by blue triangles) in the long *Inpp5e* 5′ leader construct.

(K) Translation reporter assay of DNA-transfected 4T1 cells showing that the short *Inpp5e* 5′ leader variant (348 nt) is a markedly better substrate for translation than the long 5′ leader variant (601 nt).

Error bars indicate standard error of the mean (sem). $^{*}p < 0.05$, $^{**}p < 0.01$, $^{***}p < 0.001$, $^{****}p < 0.0001$, ns, non-significant, calculated using two-tailed t test.

To determine the presence of a bona fide uORF, we constructed a heterologous DNA reporter plasmid consisting of the long (601 nt) *Inpp5e* leader inserted in front of an mORF encoding chloramphenicol acetyl transferase (CAT)[245]. We found that the long *Inpp5e* leader confers a very strong repressive effect onto CAT expression, with levels approaching only 20% of that observed in 4T1 cells transfected with a leaderless construct (**Figure 2.5C**). Mutating the methionine-coding AUG start codon of the putative uORF at −192 nt ($uORF^{-192}$; present in both long and short leaders) to AAG rescued CAT expression to ∼60% of the leaderless construct (**Figure 2.5C**). These data show that *Inpp5e* leaders harbor a uORF whose translation represses that of the downstream cistron. This likely explains why this transcript is normally repressed at the level of translation, as seen in the ribosome and polysome profiling experiments.

We next tested whether *Inpp5e* uses a classical uORF de-repression mechanism to modulate its translation during viral infection. In this model, translation of $uORF^{-192}$ would dominate the mORF in basal conditions, while the inverse would prevail with viral infection. However, 4T1 cells transfected with *in vitro* synthesized, capped, and polyadenylated CAT reporter RNA showed no changes in *Inpp5e* leader-dependent translation with HSV1 infection even at high MOI (**Figure 2.5D**). Thus, we were unable to demonstrate that the induction of *Inpp5e* translation during viral infection uses a classical uORF de-repression mechanism.

An alternative possibility is that infection induces a shift in 5′ leader expression, potentially favoring the short variant of *Inpp5e*. By virtue of its lower 5′ leader complexity, this transcript could conceivably display increased TE. In support of this idea, we observed a decrease in the *Inpp5e* 5′ leader:CDS ratio of RNA read densities during virus infection, suggesting a shift in expression to the short 5′ leader variant (**Figure S2.5A**). Using the mixture of isoforms (MISO) algorithm[267], we also found a more generalized alteration of the splicing landscape during infection

with each of the three viruses. We detected 195, 229, and 289 differentially spliced events in reovirus-infected, VACV-infected, or HSV1-infected versus mock-infected 4T1 cells, respectively (**Figures S2.5B** and **S2.5C**). However, MISO was unable to call differentially spliced events in the list of shared translationally regulated genes, potentially due to their low mapping density, as most were found to be rarer mRNAs (**Figure S2.3C**, left).

To monitor the expression of the short and long variants, we designed PCR primers to flank the intron in the 5′ leader and could readily detect the long variant in either mock- or HSV1-infected 4T1 cells, while the short variant was evident only in the latter condition (**Figure 2.5E**). We next repeated the experiment in both 4T1 and CT2A cells using qRT-PCR primers designed to span the exon-exon junction of the short 5′ leader and found that the short variant in uninfected 4T1 or CT2A cells represented 3.32% ± 0.325% and 8.89% ± 1.53%, respectively, of the total abundance of *Inpp5e* mRNA (total *Inpp5e* was detected with primers annealing to a 3′ exon common to both the long and short transcripts) (**Figure 2.5F**). Infection with HSV1 caused a significant increase in the expression of the short variant relative to total *Inpp5e* mRNA levels to 10.19% ± 2.8% and 46.08% ± 11.74% in 4T1 and CT2A, respectively (**Figure 2.5F**). Similarly, VACV infection elevated the short:total *Inpp5e* mRNA ratio from 4.2% ± 0.00037% to 12.5% ± 0.014% in 4T1 cells (**Figure 2.5F**). Moreover, poly(I:C) treatment was also found to consistently enhance short variant expression in CT2A at 8 h post-treatment (**Figure 2.5F**), concomitant with a robust induction *Ifnb1* mRNA expression, which is indicative of a typical response to the dsRNA mimic (**Figure 2.5G**). Protein kinase R (PKR) activation has been previously shown to modulate mRNA splicing[268]; therefore, we asked whether induction of the short *Inpp5e* variant was dependent on this kinase. Although we could recapitulate the poly(I:C)-mediated induction of the short variant in wild-type mouse embryonic fibroblasts (MEFs), there was a similar induction in

their PKR null counterparts, suggesting that induction of this short variant is PKR independent (**Figure 2.5H**).

We reasoned that there may be other uORFs in the 5′ leader intronic region that repress the translation of the mORF and are spliced out during viral infection. Two other ribosome-profiling studies in lipopolysaccharide-treated dendritic cells[269] and SOX-treated keratinocytes[270] showed relatively strong initiating ribosome peaks at two near-cognate CUG start codons at 400 and 391 nt upstream of the main CDS, respectively (referred to here as CUG^{-400} and CUG^{-391}) (**Figure S2.5D**, upper blue track). In addition, elongating ribosome footprints are abundant in the 5′ leader, which is suggestive of active uORF translation (**Figure S2.5D**, lower red track). The putative uORFs starting at CUG^{-400} and CUG^{-391} are 141 and 132 nt in length, respectively, and in-frame with each other but out-of-frame with the other uORFs and the mORF (**Figure 2.5I**). To determine whether these codons are used to initiate the translation of bona fide uORFs, we mutated each of them in the *Inpp5e* long leader CAT construct and determined CAT expression. Mutating the −400 or −391 CUG codon to UUG resulted in a significant enhancement in CAT expression in either construct (**Figure 2.5J**). Thus, near-cognate CUG start codons in the 5′ leader intron contribute to uORF-mediated repression of *Inpp5e* translation.

Finally, we asked whether the short *Inpp5e* transcript variant is a better substrate for translation. Comparison of CAT expression in transfected 4T1 cells revealed that the short (spliced) 5′ leader confers a 2-fold enhancement of CAT expression relative to the long (unspliced) 5′ leader (**Figure 2.5K**). These data expound a complex expression profile for *Inpp5e*; repressive uORFs prevent the inappropriate translation of *Inpp5e* under normal conditions but are removed following viral infection to enhance its translation.

2.5.6. INPP5E functions as an antiviral effector that modifies viral binding

We next investigated the potential function of INPP5E in modulating viral infection using our *Inpp5e*^{CRISPR} cells. These cells exhibited an increased expression of virally expressed GFP following HSV1 infection relative to wild-type 4T1 cells (**Figure 2.6A**). Infection with VSVΔ51 (a negative-sense, single-stranded RNA oncolytic virus candidate) was also enhanced in *Inpp5e*^{CRISPR} cells, although no clear difference was observed with VACV (**Figure 2.6A**). In addition, we knocked down *Inpp5e* expression in CT2A cells using a short hairpin RNA (shRNA) and found an increase in HSV1 protein expression relative to cells expressing non-targeting shRNA (shNTC) (**Figure S2.6A**).

To confirm the microscopy results, we quantified the production of infectious virus particles in the media of infected *Inpp5e*^{CRISPR} 4T1 cells. Cells lacking INPP5E exhibited a 2-log increase in HSV1 viral particle production compared to *Inpp5e*$^{+/+}$ 4T1 cells (**Figure 2.6B**). Although we observed consistent increases in fluorescence with VSVΔ51 by microscopy, there was only a small but significant increase in viral titer (~5-fold increase, $p < 0.001$) and no significant change was observed in VACV titers, suggesting that the INPP5E effect in curtailing infection may be virus specific. Notably, RNA-mediated reduction in BBS9, another ciliary protein under translational control in our screen, also rendered 4T1 cells more permissive to viral infection (**Figures S2.6B** and **S6C**). In contrast, decreasing the expression of two translationally downregulated genes, *Usp18* and *Usp44*, compromised HSV1 infectivity (**Figures S2.6D** and **S2.6E**), suggesting that not only are antiviral genes translationally upregulated but also potential proviral genes are downregulated as part of a concerted effort by the host to quash infection.

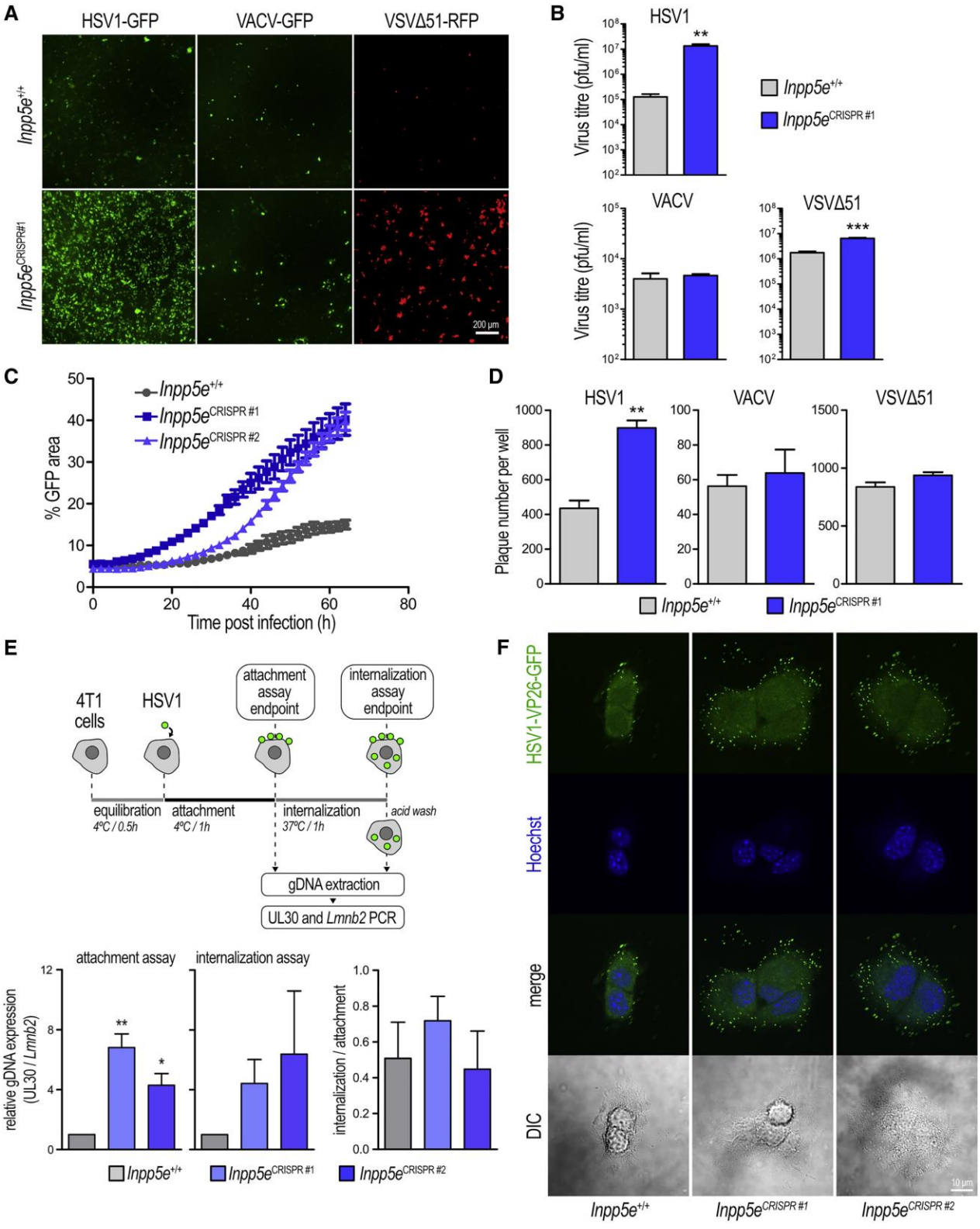
A
HSV1-GFP
VACV-GFP
VSVΔ51-RFP
Inpp5e+/+
Inpp5eCRISPR#1
200 μm
B
HSV1
VACV
VSVΔ51
Virus titre (pfu/ml)
**
***
Inpp5e+/+
Inpp5eCRISPR #1
C
% GFP area
Time post infection (h)
Inpp5e+/+
Inpp5eCRISPR #1
Inpp5eCRISPR #2
D
Plaque number per well
HSV1
VACV
VSVΔ51
Inpp5e+/+
Inpp5eCRISPR #1
E
4T1 cells
HSV1
attachment assay endpoint
internalization assay endpoint
equilibration 4ºC / 0.5h
attachment 4ºC / 1h
internalization 37ºC / 1h
acid wash
gDNA extraction
UL30 and Lmnb2 PCR
attachment assay
internalization assay
relative gDNA expression (UL30 / Lmnb2)
internalization / attachment
Inpp5e+/+
Inpp5eCRISPR #1
Inpp5eCRISPR #2
F
HSV1-VP26-GFP
Hoechst
merge
DIC
10 μm
Inpp5e+/+
Inpp5eCRISPR #1
Inpp5eCRISPR #2

Figure 2.6. INPP5E acts as an antiviral effector that modifies viral binding

(A) Representative fluorescence microscopy images of virus infections at MOI of 0.1 for 24 h (VSVΔ51-RFP) or 48 h (HSV1-GFP and VACV-GFP) in *Inpp5e*$^{CRISPR\#1}$ versus *Inpp5e*$^{+/+}$ 4T1 cells.

(B) Titration of virus obtained from the supernatant of *Inpp5e*$^{CRISPR\#1}$ versus *Inpp5e*$^{+/+}$ 4T1 cells infected with the indicated viruses at 0.01 MOI for 24 h (VSVΔ51-RFP) or 48 h (HSV1 and VACV).

(C) Live-cell measurements of HSV1-GFP infection in both *Inpp5e*^{CRISPR} clones compared to control 4T1. Cells were infected at an MOI of 0.1 and images were taken every 2 h.

(D) Plaque assay in indicated CRISPR cells. Cells were infected with VSVΔ51, HSV1, and VACV at an MOI of 0.01, then plaques were enumerated from full-well fluorescence microscopy images.

(E) Top: schematic of the cold-binding assays. *Inpp5e*^{CRISPR} and *Inpp5e*$^{+/+}$ cells were incubated at 4°C with HSV1 at an MOI of 10 for 1 h (attachment assay) or 4°C for 1 h followed by 37°C for 1 h (internalization assay). Total DNA was extracted and viral UL30 DNA was quantified by qPCR and normalized to cellular *Lmnb2* DNA. Bottom: graphs presenting the effect of *Inpp5e*^{CRISPR} on virus attachment (left), internalization (center), and the contribution of internalization versus attachment in each cell type expressed as a ratio (right).

(F) HSV1-K26-GFP cold-binding assay. As in (E), but using a virus decorated with a GFP-fusion coat protein that allowed the detection of diffraction-limited puncta by confocal microscopy in fixed cells. Images are single confocal slices representing the mid-cell region. Nuclei are stained with Hoechst. DIC, differential interference contrast.

Error bars indicate standard error of the mean (sem). $^{*}p<0.05$, $^{**}p<0.01$, $^{***}p<0.001$, ns, non-significant, calculated using two-tailed *t*-test.

To determine the stage(s) of the viral life cycle that could be affected by *Inpp5e*, we examined whether *Inpp5e*^{CRISPR} cells could support increased viral spread. We infected cells with HSV1-GFP at low MOI (0.1) and measured GFP intensity and area every 2 h using a live-cell-imaging system. By quantitating the area of GFP signal in infected clusters normalized to the total imaged surface area at multiple time points, a more pronounced spread in the two *Inpp5e*^{CRISPR} 4T1 cell lines compared to the control cell line was observed (**Figure 2.6C**). We found that this INPP5E-mediated effect on viral infection was not specific to cancer cells; HSV1 or VSVΔ51 infection also exhibited enhanced spread following shRNA-mediated knockdown of *Inpp5e* in the normal fibroblast cell line NIH 3T3 (**Figures S2.6F** and **S2.6G**). The response in NIH 3T3 was more attenuated than that in 4T1 *Inpp5e*^{CRISPR} cells at 48 h post-infection (compare **Figures 2.6C** and **S2.6F**). However, we cannot rule out the possibility that this was due to residual INPP5E present in the NIH 3T3 cells. As a proxy measurement for viral binding and/or entry, we modified the classical plaque assay by infecting a monolayer of live or *Inpp5e*$^{+/+}$ 4T1 cells in an agar matrix (to prevent cell-to-cell spread of virion) with HSV1, VSVΔ51, or VACV at very low MOI (0.01). *Inpp5e*^{CRISPR} cells generated >2-fold more plaques when exposed to HSV1 in contrast to no change in the number of VACV or VSVΔ51 plaques (**Figure 2.6D**). These data suggest that viral binding and/or entry of HSV1 is enhanced in *Inpp5e*^{CRISPR} cells.

To further investigate the role of INPP5E in early HSV1 infection, we separately assessed cell attachment or internalization of virions using two parallel cold-binding assays (**Figure 2.6E**, schema at top) that quantified virus particles via qPCR of HSV1 genomic DNA (gDNA) copies [271]. In the attachment assay, 6.8- and 4.3-fold more viral DNA was found to be associated with the surface-bound fraction in *Inpp5e*$^{CRISPR\#1}$ and *Inpp5e*$^{CRISPR\#2}$ versus *Inpp5e*$^{+/+}$ cells, respectively (**Figure 2.6E**, lower left). A similar trend was measured with the internalization assay, in which

4.4- and 6.4-fold more viral DNA was found within *Inpp5e*$^{CRISPR\#1}$ and *Inpp5e*$^{CRISPR\#2}$ cells, respectively, relative to control cells (**Figure 2.6E**, lower center). The internalization:attachment ratio did not significantly change in the *Inpp5e*^{CRISPR} cells, indicating that the binding of HSV1 virions to the cell surface is significantly enhanced independently of internalization (**Figure 2.6E**, lower right). Furthermore, in a parallel cold-binding experiment using HSV1 expressing a GFP fusion of the capsid protein VP26, which allows visualization of virions as diffraction-limited puncta, a sizable increase in the number of GFP puncta binding to *Inpp5e*^{CRISPR} cells was observed (**Figure 2.6F**).

These data define translationally regulated antiviral effectors, with the phosphatidylinositol (PI) phosphatase INPP5E being further characterized in our study. While INPP5E is translationally induced by all three of the viruses we assayed, its expression appears to have a pronounced antiviral effect in the context of HSV1 infection, modulating viral attachment to and spread between host cells.

2.6. Discussion

To thwart virus infection, mammalian cells suppress the activity of their mRNA translation machinery, while viruses often attempt to take control of it to maximize translation of their own mRNAs[8,240]. However, the synthesis of antiviral proteins is still needed, and single-gene studies have shown that some of these transcripts are uniquely upregulated at the translation level, distinct from transcriptionally induced ISGs[55, 272]. Our present work reveals a global profile of host cellular mRNAs differentially translated in a breast cancer cell model infected by clinically relevant oncolytic viruses.

We find that translationally regulated mRNAs in this context are functionally enriched in proteins involved in primary cilium homeostasis. Our sentinel gene, *INPP5E,* is a target of genetic

mutation in humans, responsible for ciliopathies such as Joubert syndrome and mental retardation, truncal obesity, retinal dystrophy, and micropenis (MORM) syndrome [273]. Mainly localized at the primary cilium, it has also been observed within the nucleus and at centrioles [274]. Our IF data in poly(I:C)- or VACV-treated cells shows a punctate distribution pattern of induced INPP5E that is reminiscent of vesicles. This is perhaps unsurprising, given the presumed membrane localization of INPP5E, with its C-terminal farnesylation and its role in modifying PI signaling [273]. INPP5E is an inositol 5-polyphosphatase, and therefore likely controls second messenger PI signaling at vesicular structures as it does within the cilium, where it maintains a high concentration of PI-4-phosphate (PI(4)P) relative to $PI(4,5)P_2$, an attribute linked to ciliary stability [275,276]. Another second messenger, PI(5)P, is induced by Newcastle disease virus infection and poly(I:C) and can act as an innate immune effector promoting type I IFN production through the TANK-binding kinase 1 (TBK1)-IRF3 signaling axis [277]. Several viruses activate PI3K signaling pathways [240]; this increases $PI(3,4,5)P_3$ and consequently activates the Akt-mTOR signaling axis, thus modulating infection efficiency. $PI(4,5)P_2$ and $PI(3,4,5)P_3$, two likely INPP5E substrates, are well-known mediators of actin remodeling [278]. We found a positive effect of INPP5E removal on both HSV1 and VSVΔ51 infections, and this may be explained by changes to the actin cytoskeleton (e.g., changes in membrane ruffling that alter viral attachment) [279]. Consistent with this hypothesis, we observed enhanced binding of HSV1 to the cell surface, while internalization remained unaffected. While INPP5E can be localized to the cilium, viral attachment did not appear to be polarized as one would expect if enhanced binding occurred at or near ciliary structures. Thus, INPP5E antiviral activities may be not related to its ciliary localization. Away from the plasma membrane, centrosomal PIs can also be affected by a lack of INPP5E, leading to spindle microtubule destabilization, possibly through an imbalance in $PI(4,5)P_2$ expression [274]. Whether

these mechanisms have a role to play in mediating the enhanced virus binding and infection seen in 4T1 cells is subject to future investigation.

Another ciliary gene we examined, *BBS9*, encodes a protein that serves as a structural component of the BBSome, a stoichiometric, octameric protein complex (composed of BBS1, -2, -5, -7, -8, -9, and -10) charged with receptor cargo destined for the primary cilium [264]; however, others have shown that the BBSome is important in the transport of extra-ciliary cargo to the plasma membrane [280] and in retrograde transport [281]. Mutations in *BBS9* and other *BBS* genes underlie Bardet-Biedel syndrome, a rare pleiotropic disorder that is thought to arise from cilia dysfunction. We have found that akin to INPP5E, BBS9 expression limits HSV1, VACV, and VSVΔ51 infections. Whether impaired BBSome function is responsible for the proviral effect that we observed with BBS9 knockdown in 4T1 cells will require more investigation. BBS9 might instead display BBSome-independent antiviral functions.

We show here that translationally upregulated mRNAs common to all three infections were normally repressed at the level of translation in the uninfected condition. In a search for a mechanistic explanation of this repression-de-repression switch, we noted an enrichment of uORFs in their 5′ leaders, a *cis*-acting sequence element that can confer translational de-repression during the accumulation of P-eIF2α[35]. Further investigation using *Inpp5e* 5′ leader reporter assays revealed no uORF-dependent de-repression during infection. Instead, a variant switch during infection with HSV1 or VACV or upon treatment with the viral mimic poly(I:C) was observed, producing an alternatively transcribed and spliced transcript with a shortened *Inpp5e* 5′ leader. Critically, we found that the spliced 5′ leader intron harbors repressive uORFs, and consequently, the short *Inpp5e* 5′ leader is a better substrate for translation than its longer, unspliced counterpart. We also found enrichment of binding motifs for the splicing factors SRSF1 and SRSF9 in the 5′

leader of translationally regulated genes, again, suggestive of a role for alternative splicing in modifying translation of these genes. Thus, our study presents evidence for a regulatory mechanism in which translational output of an antiviral gene is modulated via a transcript variant shift that increases expression of a normally minor variant that harbors a less translationally repressive leader.

These findings are in line with previous studies proposing a role for regulating protein synthesis via transcript variants [282] and follows the axiom that alternative transcription and splicing increases transcriptome diversity from a more limited and inflexible genome. Clearly, differences in the coding region between transcript variants can produce functionally different protein isoforms, but differences in the non-coding regions (5′ leader and 3′ UTR) similarly confer important changes to protein function by altering protein abundance in time and space [282,283]. These regions contain *cis*-elements that regulate mRNA turnover, location, and/or translation. They can be altered via alternative transcription, splicing, start-site selection, or alternative polyadenylation and termination. Examples of differential transcript variant expression have been reported during infection with various viruses [284,285]. More specifically, RNA sequencing (RNA-seq) has revealed widespread disturbances to host transcription termination caused by HSV1 infection [286] and has identified HSV1 ICP27 protein as a major viral factor responsible for modulating the host transcript variant landscape [287]. Aberrant splicing can lead to defective innate immunity during the host response to virus infection. For instance, the lack of the RNA-binding protein BUD13 causes the retention of the 4th intron in human *IRF7* upon stimulation by poly(I:C) or IFN-α, generating a defective mRNA and impaired antiviral response when challenged with VSV [288]. In the present study, we observed the opposite effect from both a mechanistic and a phenotypic perspective: viral infection or poly(I:C) treatment caused splicing of an intron and potentiation of the host antiviral

response, rather than intron retention and abrogation of that response. The question remains: How does infection signal the switch to an alternative "ribosome-engaged" transcriptome? PKR-mediated splicing has been previously reported [268]; however, we were unable to link PKR activation to our change in variant expression. Further studies will be required to home in on the signaling axis that mediates the increased expression of the short *Inpp5e* transcript.

In summary, we describe herein a post-transcriptional mechanism for the appropriate expression of potent antiviral genes (Figure 2.8). Our data suggest that innate immunity projects a complicated regulatory landscape in which various host and viral factors are translationally modulated through interactions with pre-mRNA and splicing complexes. In cataloging the genes that are part of the translational arm of innate immunity, we have uncovered regulatory nodes that may benefit from future study with the goal of improving cancer therapeutics.

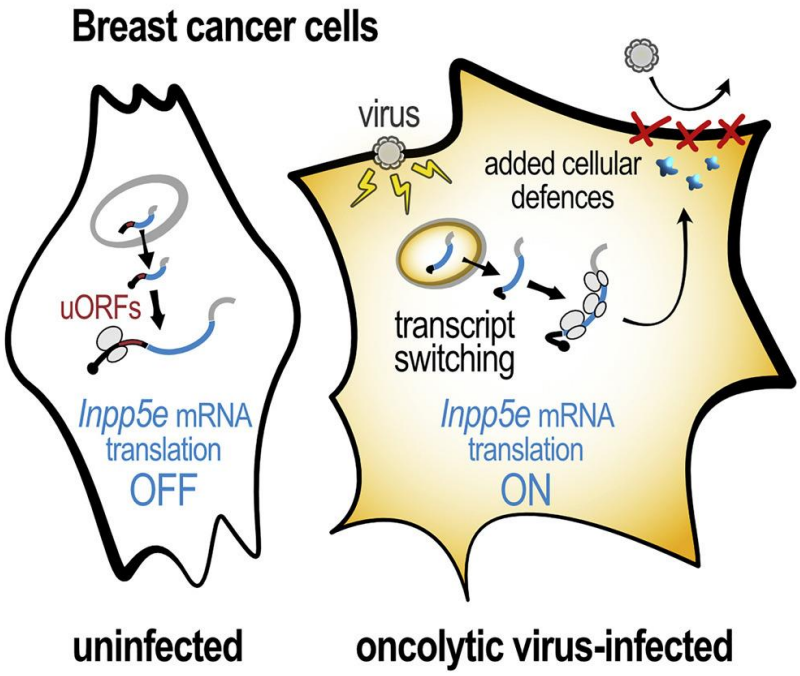

Figure 2.7. Model of translationally induced antiviral genes in cancer cells via isoform switch. In uninfected cells, a long a 5'leader inhibits the translation of *Inpp5e* mRNA. Upon OV infection, a shorter 5'leader is induced and derepress translation of *Inpp5e* mRNA. Expressed INPP5E in turn inhibit viral infection, potentially via modifying virus binding to cell.

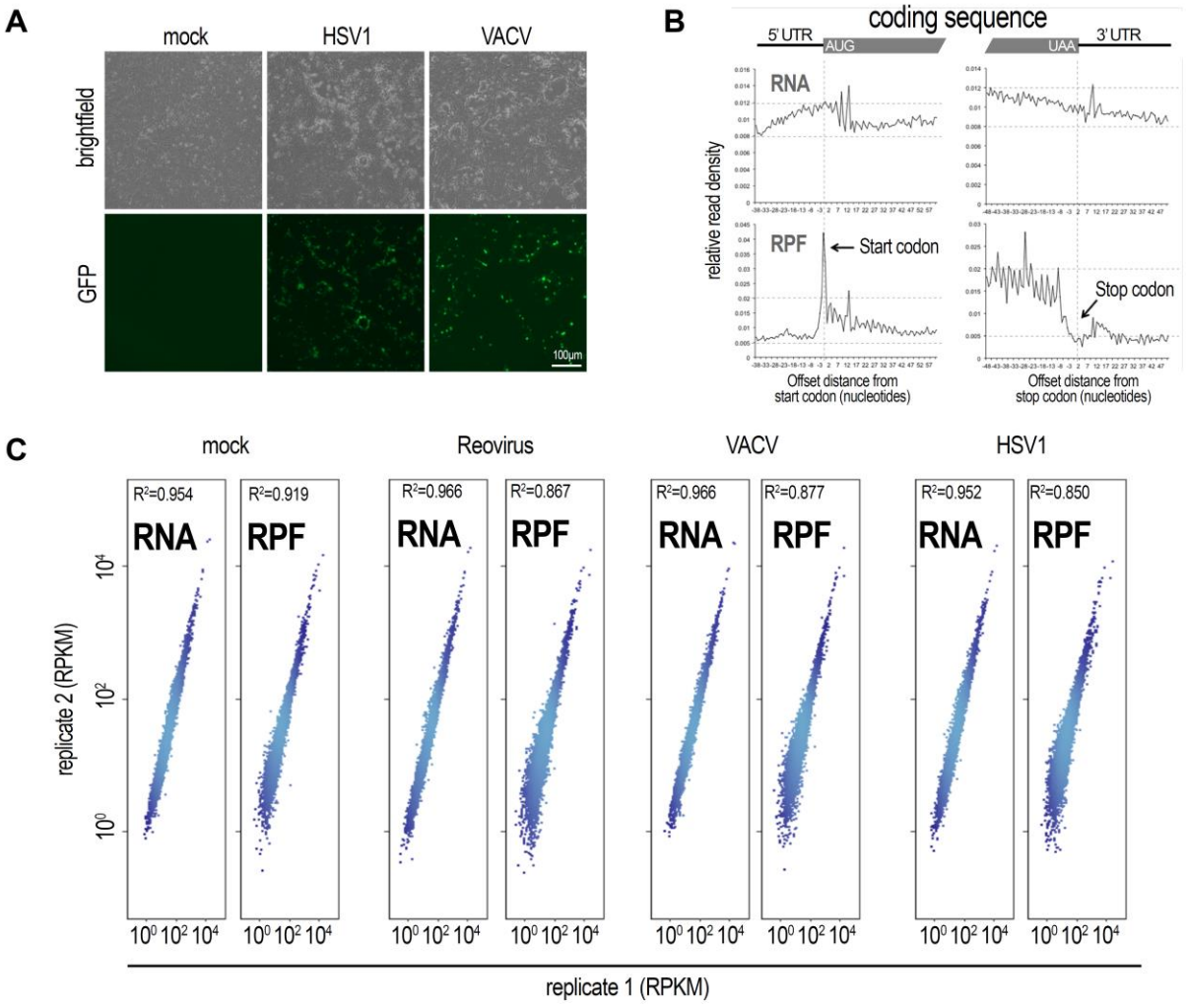

Figure S2.1. Quality control of the ribosome profiling experiments.
(A) Fluorescence microscopy of 4T1 cells mock-infected or infected with an ED_{50} of HSV1 or VACV (note that reovirus does not express a fluorescent reporter).
(B) Metagene analysis of total RNA (top) and RPF read densities (bottom) across a randomized selection of mRNAs demonstrates the ability of the ribosome profiling technique to detect RPFs enriched in the coding sequence of mRNAs.
(C) Scatter plots and correlation analyses of RNA- and RPF-Seq gene expression between biological replicates show a high degree of reproducibility. Linear regression was performed on biological replicate 2 vs 1and the closeness of fit (R^2) to the line of regression is reported, where 1.0 is a perfect fit.

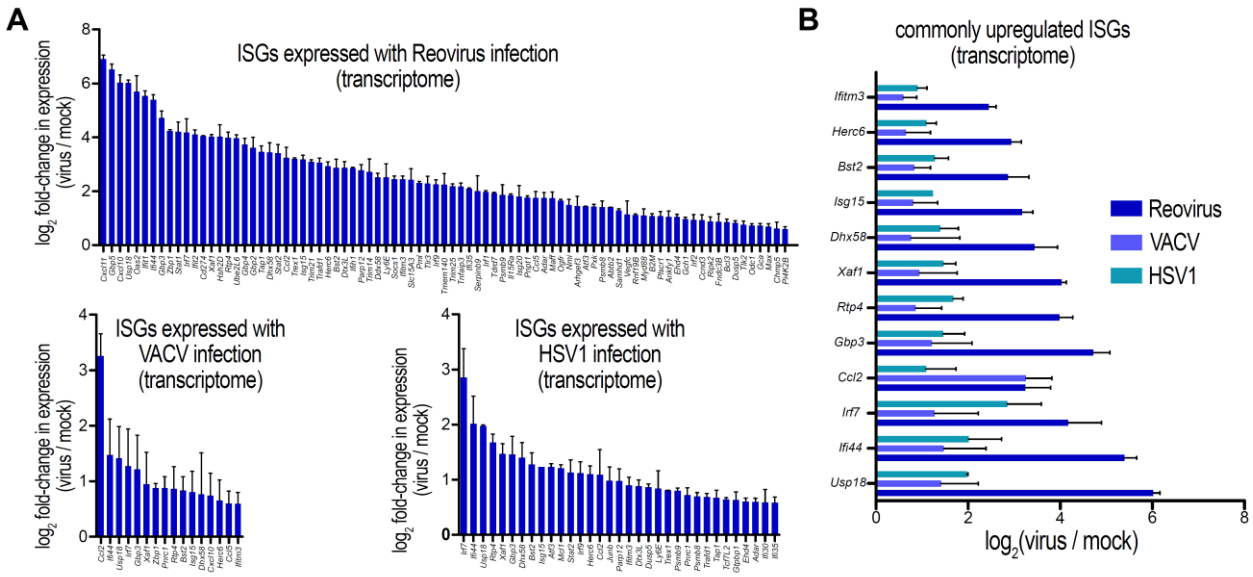

Figure S2.2. The cellular response to infection exhibits an antiviral state at the transcriptional level.

(A) Previously validated ISGs [262] (from a list of 389) found to be upregulated (>2-fold change relative to mock-infected cells) in the transcriptome of 4T1 cells infected with Reovirus, VACV or HSV1.

(B) ISGs from A which were found to be transcriptionally regulated in all three infections.

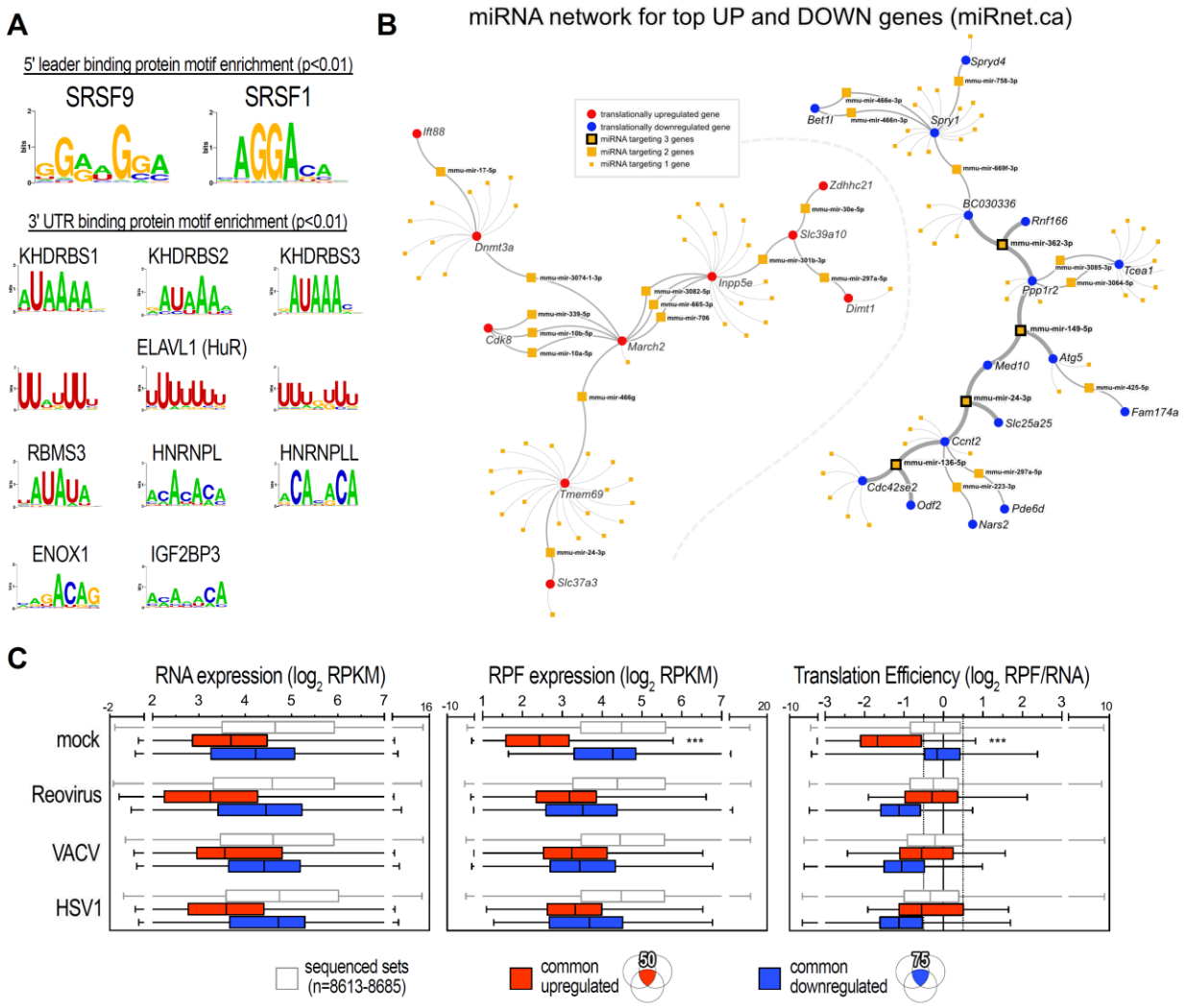

Figure S2.3. Characterizing cis-elements in the common translationally regulated transcripts.
(A) Sequence logos of RNA binding protein motifs enriched in 5'leader and 3'UTR of transcripts comprising the commonly translationally up- and down-regulated list. The CISBP-RNA database [289] was queried using the Analysis of Motif Enrichment (AME), part of the MEME suit [290].
(B) miRNA target analysis was performed using miRNet [291] with the common translationally up or down gene lists and plotted as a network using built-in network visualizer.
(C) Box whisker plots of RNA, RPF expression and TE in each condition for all sequenced genes (white), commonly translationally upregulated (red), or downregulated (blue) genes. Translationally upregulated genes represent a rare subset of mRNAs that are translationally repressed under basal conditions in 4T1 cells (compare white vs red bars of mock expression at both mRNA and RPF genomic level). A Kruskal-Wallis test was used, ***p<0.001.

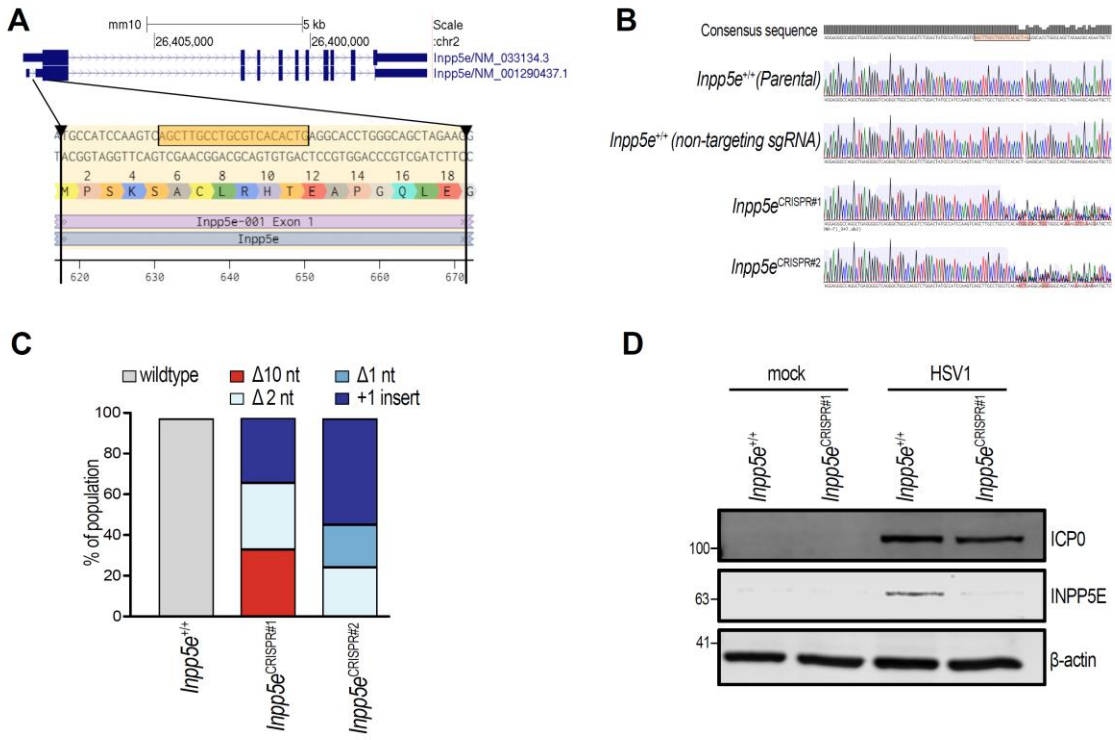

Figure S2.4. CRISPR-Cas9 knock-out of INPP5E in 4T1 cells.
(A) Targeting region and sequence of the synthetic single guide (sgRNA) used to disrupt both *Inpp5e* variants.
(B) Sanger sequencing chromatograms of the wildtype and two *Inpp5e*^{CRISPR} clones. The chromatogram begins at the first nucleotide of the sgRNA sequence. PHRED quality scores are indicated at the top of each chromatogram.
(C) Indel frequency of the two *Inpp5e*^{CRISPR} clones evaluated using the sequence decomposition program TIDE. Types of indel are categorized and plotted as a percentage of the entire population.
(D) Western blot for HSV1 protein ICP0, INPP5E or β-actin from *Inpp5e*$^{+/+}$ or *Inpp5e*$^{CRISPR\#1}$ 4T1 lysates. Cells were infected with HSV1-GFP at a MOI of 5 for 48 hours. Apparent molecular weights are indicated to the left in kDa.

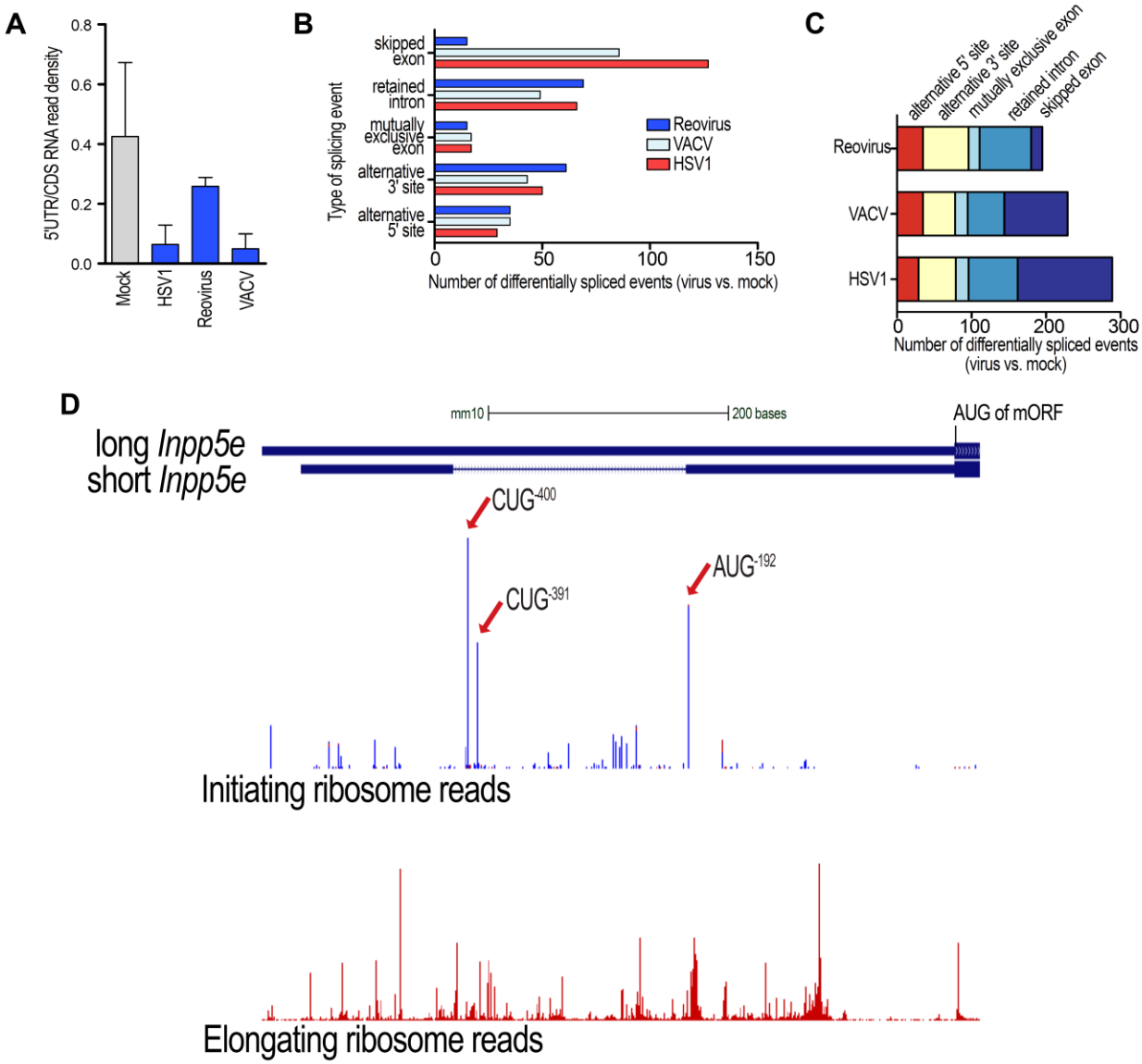

Figure S2.5. Evidence of variant switching with infection.
(A) Coverage ratio of RNA-Seq reads mapping to the 5'leader vs CDS of *Inpp5e* in mock- or virus-infected 4T1 cells.
(B) MISO analysis detects differentially spliced events in the transcriptome of 4T1 infected with Reovirus, VACV or HSV1, grouped by event types
(C) Same analysis as in B but with events classified by viral infection.
(D) Genome Wide Information on Protein Synthesis (GWIPS, https://gwips.ucc.ie) view of the 5'leader region of *Inpp5e* (top) showing initiating ribosome read density (middle; densities are aggregated from all ribosome profiling experiments that assay ribosomes at initiation codons in the database) and elongating ribosome reads (bottom). Red arrows mark initiating ribosome peaks corresponding to the indicated putative uORF start codon.

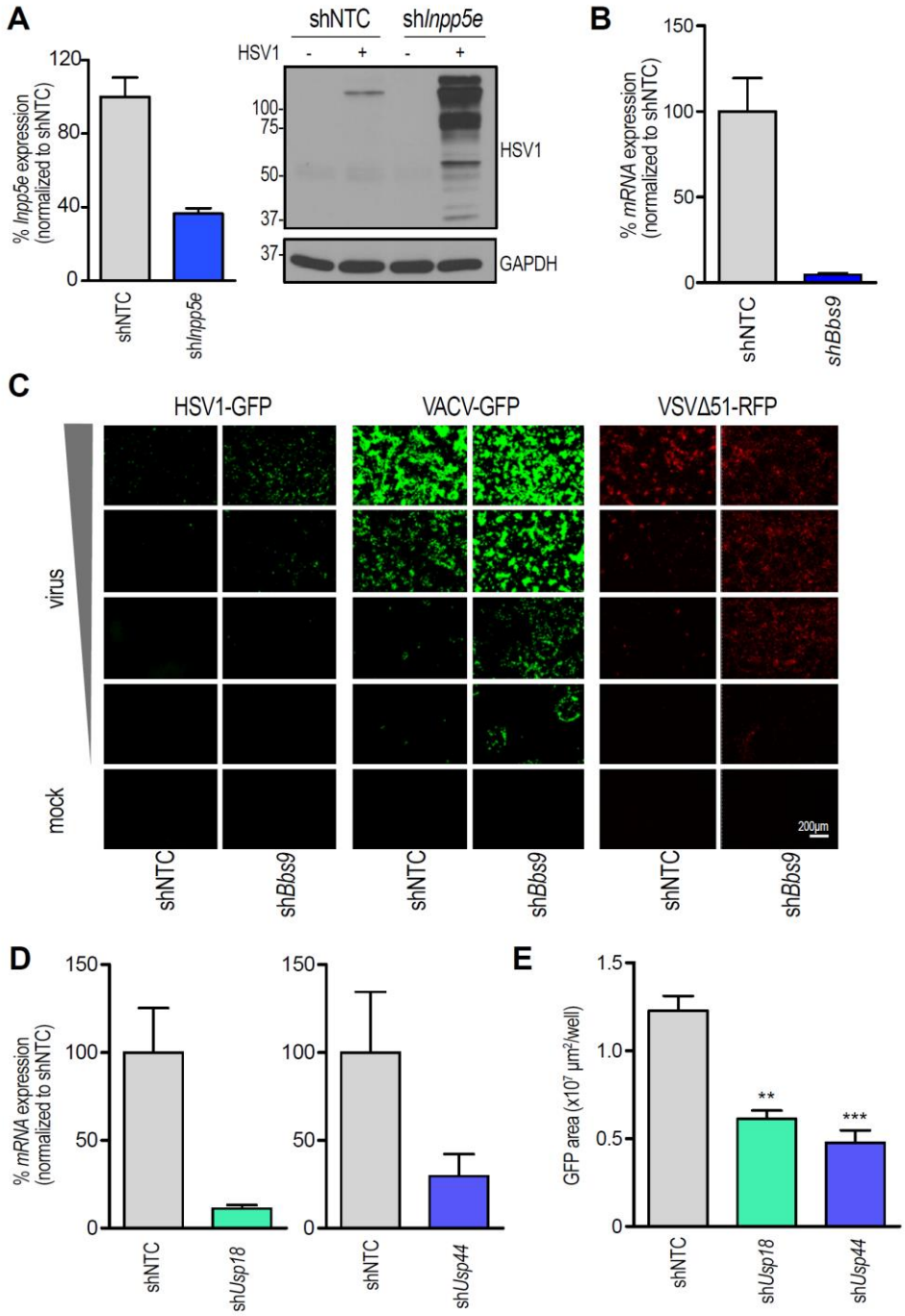

Figure S2.6. Characterizing the role of candidate proteins in modifying viral infection.
(A) Knockdown efficiency using shRNA targeting *Inpp5e* vs. non-targeting control (shNTC) in CT2A cells assessed by RT-qPCR. Western blot of lysates from shNTC vs. *Inpp5e* knockdown CT2A cells infected with HSV1 at a MOI of 0.1 for 48 hours for HSV1 proteins or GAPDH. (B) Knockdown efficiency using shRNA targeting *Bbs9* vs. shNTC as evaluated by RT-qPCR in 4T1 cells.

(C) Representative immunofluorescence images of 4T1 cells stably expressing indicated shRNAs and infected with indicated viruses at increasing MOI.
(D) Knockdown efficiency using shRNA targeting *Usp18* (left) and *Usp44* (right) vs. shNTC in 4T1 cells assayed by RT-qPCR.
(E) Infectivity of HSV1-GFP in 4T1 cells stably expressing shRNA targeting *Usp18*, *Usp44* vs. shNTC as measured by GFP-expressing area.
Error bars represents s.e.m., n=3. One-way ANOVA with Dunnett's post-hoc test was performed in E. **p<0.01, ***p<0.001.

CHAPTER 2

Table S2.1 – S2.3
(Large dataset files attached with this thesis)

Table S2.4. Oligonucleotides used in this study, related to Figures 2.4-6.

Targeted gene	transcript/gene ID	Primer Name	Forward primer sequences (5'-3')	Reverse primer sequences (5'-3')	Description
Inpp5e	NM_033134.3, NM_00129290437.1	mInpp5e	GATCTTTCAGCCTTCTGGCCC	GAGAGCCATGTTTCGGTCTG	PCR primers detecting both isoforms of mouse *Inpp5e* mRNA ("total")
Inpp5e	NM_00129290437.1	Inpp5e-shortUTR	CGGAGGGCGCAGGCAT	TGAAAACTCGAGTGGCTCCC	PCR primers detecting mouse short isoform of *Inpp5e* mRNA
Usp44	NM_001206851.2	mUsp44	TCGGCGACTGATTTTAAGGACA	GCATCTGAAAACTGGGTCTTGG	PCR primers detecting mouse *Usp44* mRNA
Usp18	NM_011909.2	mUsp18	TTCTGCCAACCGAGGAAGAC	TCCAGGTGACCCAACAAACA	PCR primers detecting mouse *Usp18* mRNA
Actb	NM_007393.5	ActB	GGCTCCTAGCACCATGAAGAT	GGGTGTAAAACGCAGCTCAGTAAC	PCR primers detecting mouse *Actb* mRNA
Rps20	NM_026147.6	Rps20	CGCATGCCTACCAAGACTTT	GGCATCTGCAATGGTGACTTC	PCR primers detecting mouse *Rps20* mRNA
UL30	2703462	HSV1UL30	ACATCATCAACTTCGACTGG	CTCAGGTCCTTCTTCTTGTCC	PCR primers detecting HSV1 UL30 DNA
LMNB2	16907	gDNA-Lmnb2	ACCAGGTCGTCTGCTATCCT	TCAGTGGTACCTTCAACGCC	PCR primers detecting mouse Lmnb2 gDNA
Inpp5e	64436	Inpp5e-sgRNA1	CACCGAGCTTGCCTGCGTCACACTG	AAACCAGTGTGACGCAGGCAAGCTC	CRISPR sgRNA targeting mouse Inpp5e
Non-Targeting sgRNA	none	NT-sgRNA	CACCGCGAGGTATTCGGCTCCGCG	AAACCGCGGAGCCGAATACCTCGC	Non-targeting CRISPR sgRNA for mouse

2.7. Acknowledgements

We thank Drs. John Bell, Martin Holcik, Antonis Koromilas, Karen Mossman and David Stojdl for materials used in the experiments. H.-D.H. is a recipient of a University of Ottawa Graduate Scholarship, an Ontario Graduate Scholarship, and a University of Ottawa Faculty of Medicine Destination 2020 Scholarship. This work was supported in part by the Canadian Breast Cancer Foundation/Canadian Cancer Society Research Institute, the Cancer Research Society/CIHR Institute of Cancer Research (grant 22124), the Natural Sciences and Engineering Research Council of Canada (RGPIW-2016-05228), and the Terry Fox Research Institute (New Frontier Program Project Grant, to T.A. and T.E.G.).

CHAPTER 3. A Viral Leader Sequence Enhances Translation of GM-CSF Encoded Within Oncolytic HSV1

Authors: Huy-Dung Hoang, Nasana Vaidya, Victoria H. Gilchrist, Aida Said, Usha Kabilan, Karen Mossman, Seyed Mehdi Jafarnejad, Samuel T. Workenhe, Tyson E. Graber, Tommy Alain

Manuscript ready for submission

3.1. Author contributions

T.A. and H.-D.H. conceived and designed the experiments. H.-D.H. performed the majority of the experiments. H.-D.H. and T.A. wrote the manuscript. N.V. performed the translation reporter assays. V.H.G. performed virus titration. H.-D.H and A.S. performed polysome profiling. U.K. performed the RT-qPCR. S.M.J. performed the wet component of the RNA-Seq. K.M., S.T.W., S.M.J., T.E.G. and T.A. reviewed and edited the final manuscript. All authors read and approved the final manuscript.

3.2. Abstract

Transgenes can be used to deliver therapeutic payloads, improving efficacy profiles of viral-based biomedicines such as engineered oncolytic virus and vaccine platforms. Although they may be highly transcribed within infected cells, their translation can be hampered in this context. Here we determined the transcription start site of the majority of Herpes Simplex Virus-1 (HSV1) genes from RNA-seq read coverage and identified viral leader sequences that confer high mRNA translation efficiency. We found that the leader sequence of the late viral gene US11 enhanced mRNA translation of a downstream transgene within infected cells. By engineering HSV1 with a US11 leader upstream of a sequence encoding GM-CSF, we demonstrated a substantial leader-dependent enhancement in the synthesis of this immune modulator in multiple cellular backgrounds. Our study presents an opportunity to control and enhance therapeutic payload

expression from oncolytic HSV1 platforms by incorporation of the US11 leader sequence into the expression cassette design.

3.3. Introduction

Transgenes are becoming an increasingly important feature of viral-based therapeutics, such as virus-mediated gene deliveries, recombinant vaccines or oncolytic viruses (OVs). In the case of OV platforms, incorporation of an immunomodulatory host gene, tumor-associated antigen gene or suicide gene that can amplify anti-tumor responses or oncolysis is desirable, as are reporter genes to facilitate tracking and dosing (e.g. encoding green fluorescent protein or luciferase) in pre-clinical studies[292,293]. Importantly, high intra-tumoral transgene expression is crucial to the therapeutic efficacies of OVs[184,294], or to elicit an optimal anti-tumor immune response[295].

The design of transgene expression cassettes within viral genomes has not changed significantly from that used for overexpression of GM-CSF from the oncolytic Herpes Simplex Virus-1 (HSV1) genome, resulting in the first FDA-approved OV as a cancer therapeutic[153]; it included a strong promoter, followed by an intron-less open reading frame (ORF) encoding the protein of interest, and ending with a poly(A) signal[296]. Much effort was spent on ensuring high transgene transcription in infected cells by incorporating a strong host promoter such as those from human phosphoglycerate kinase (PGK) or elongation factor 1α (EF1α), or from viruses such as the cytomegalovirus (CMV) immediate early promoter[296]. Any bottlenecks in the subsequent translation of the transgene mRNA into protein, however, have not been thoroughly investigated under the assumption that differences in translation would be nominal if the transcript is highly expressed. The innate antiviral response of the host cell to the presence of a replicating virus challenges this assumption; whereby an infected cell sees dramatic changes in the pool of mRNAs translated, with the replicating virus actively reshaping the host's protein synthesis machinery to

favor the production of viral proteins while impeding that of cellular proteins[8,302]. Thus, the translation rate of a transgene mRNA is likely to be different or suboptimal when comparing uninfected versus infected conditions. Ultimately this could result in poor transgene protein production and consequently reduce the therapeutic efficacy of the replicating viral vector.

Recent studies have revealed various translation enhancer motifs found in the leader sequences of viral mRNAs, including non-templated poly(A) leaders in poxviruses[97,99] or ICP27-interacting motifs that facilitate nuclear export in HSV1 mRNA leaders[128,298]. Viral internal ribosome entry sites (IRESes; *e.g.*, EMCV) are also used in recombinant gene expression contexts to enhance translation[299], yet no transgene translation enhancer has been reported for clinically relevant OVs, including oncolytic poxviruses and HSV1. We reasoned that the synthesis of therapeutic cargos from replicating oncolytic platforms could be enhanced by incorporation of a viral leader sequence that mediates increased translation efficiency of its downstream cistron. Using RNA-seq data of HSV1-infected 4T1 mouse mammary cancer cells, we identified HSV1 leader sequences that mediate high translation efficiency of viral mRNAs during viral replication. The leader of the HSV1 late gene US11 was shown to confer increased translation of a downstream cistron in a heterologous reporter construct and, notably, this effect was only observed during HSV1 infection. Most importantly, an HSV1 engineered to express a cassette containing the US11 leader upstream of the transgene GM-CSF ORF, conferred superior GM-CSF protein expression in several mammalian cell lines. This approach represents a straightforward and effective strategy to assess and characterize viral translation enhancers that are active during viral infection and identifies HSV1 US11 as a leader sequence that can be employed to deliver enhanced levels of therapeutic protein in the OV context and beyond.

3.4. Materials and Methods

3.4.1. Cell culture and viruses

The mouse breast cancer cell line 4T1, as well as HEK293T and Vero cells were acquired from American Tissue Culture Collection. 4T1 was maintained in Roswell Park Memorial Institute (RPMI) 1640 (Fisher) supplemented with 10% fetal bovine serum (FBS) (Sigma-Aldrich) and 1X penicillin/streptomycin (Fisher). HEK293T and Vero cells were maintained in Dulbecco's Modified Eagle Medium (DMEM) (Fisher) supplemented with 10% FBS and 1X penicillin/streptomycin (Fisher). Cells were incubated at 37°C, 5% CO_2 v/v. HSV1716 (HSV1 strain 17 with γ34.5 deleted, Sorrento Therapeutics) was kindly provided by the manufacturers. HSV1 strain KOS was kindly gifted by Dr. Karen Mossman. All HSV1 strains were propagated on Vero cells. A monolayer of Vero cells was inoculated with HSV1 at 0.1 MOI, then cultured for approximately 24-48 hours until close to 100% cytopathic effect was observed. Supernatant was then collected separately, and infected cells were freeze-thawed three times to release intracellular virus. Both the cultured supernatant and the freeze-thawed lysate were clarified by centrifuged at 1000 g, 5 min to remove cell debris. The supernatants were combined and filtered through a 0.45 μm filter. Virus particle was further purified using sucrose cushion by overlaying the supernatant on top of a 36% sucrose cushion in PBS and centrifuge at 18,000 g for 2 hours, 4°C. Virus in the pellet was resuspended in HNE buffer (HEPES 10mM, NaCl 150mM, EDTA 0.1mM, pH 7.2) and stored at -80°C.

3.4.2. Plasmid construction

For the leader translation activity screen using the CAT reporter assay, virus leader sequences were amplified by PCR from cDNA reverse-transcribed from mRNA of HSV1 infected

4T1 cells. Briefly, total RNA was extracted from cell using TRIzol reagent (Fisher), treated with Turbo DNA-free kit (Thermo Fisher) to remove potential contamination of virus genomic DNA, then reverse-transcribed by using the iScript Advanced cDNA Synthesis Kit (BioRad). The forward and reverse primers (NotI_*5'UTR*-F and XhoI_*5'UTR*-R) of each leader also contain the restriction sites of NotI and XhoI, respectively, for subsequent cloning. Amplification specificity was confirmed for each pair of primers by including a negative control cDNA from mRNA of uninfected 4T1. The PCR amplicons were cloned into the CAT reporter plasmid pMCpA (a kind gift from Dr. Martin Holcik, Carleton University) using the NotI-XhoI restriction sites[245]. For inserting transgene expression cassette into HSV1 genome, the cassette was cloned into the pTK-Green plasmid (a kind gift from Dr. Karen Mossman, McMaster University)[300], flanked by two regions of the HSV1 TK gene to allow for homologous recombination. The expression cassette consists of the leader followed by the transgene (firefly luciferase or mouse GM-CSF), the self-cleaving peptide porcine teschovirus-1 2A (P2A) and GFP. The insert was generated by fusion PCR. The virus leader was amplified as described above using a forward primer containing a AgeI cutting site (AgeI_*5'UTR*-F) and a reverse primer with an overlap section of the transgene 5'end (*5'UTR*_LUC-R or *5'UTR*_CSF2-R). The second fragment containing the transgene CDS was amplified using a forward primer (*5'UTR*_LUC-F or *5'UTR*_CSF2-F) and a reverse primer consisted of the CDS 3' end, a GSG linker and a part of the P2A sequence (LUC-GSG-P2A-R). The third fragment containing the GFP was amplified using a forward primer (GSG-P2A-GFP-F) and a reverse primer that include a KpnI cutting side (GFP-KpnI-R). All three fragments were purified using the QIAquick PCR Purification Kit (Qiagen), then used as templates for fusion PCR using the 5'-most (AgeI_*5'UTR*-F) and 3'-most primer (GFP-KpnI-R). The resulting PCR product

was cloned into the pTK-Green using AgeI and XhoI sites. All plasmids were verified by Sanger sequencing. All primer sequences are presented in **Table S3.1**.

3.4.3. RNA-seq mapping and TSS identification

RNA-seq data of 4T1 cells infected by HSV1 was previously published[301]. For mapping of RNA-seq, RNA reads were mapped to the HSV1 reference genome JQ780693.1 using HISAT2[302]. Only one copy of the two flanking inverted repeat regions were used: the TRL region 1-8870 and TRS region 144602-151023 were omitted. Transcription start site (TSS) were manually identified from RNA read coverage, defined by an abrupt increase of read coverage at a base position (shown in **Figure 3.1**). The leader sequence was defined as the sequence from the TSS to the annotated start codon of the associated HSV1 gene, excluding any spliced intron if applicable. For converting leader sequence coverage between different HSV1 reference genomes (JQ780693.1 to JN555585.1), the sequence of the identified leader from JQ780693.1 was aligned to JN555585.1 using NCBI-BLAST (https://blast.ncbi.nlm.nih.gov/Blast.cgi) to find the corresponding coordinates on JN555585.1. Raw data were deposited and analyzed on the Galaxy server (https://galaxyproject.org)[303]. Gene expression level from mapped RNA-seq and Ribo-seq reads was calculated using Cuffdiff[304].

3.4.4. CAT reporter assay

CAT reporter assay was performed as previously described[301]. Cells were seeded at approximately 75% confluency in a 6-well plate and incubated for one day before transfection. In the case of HSV1 infection, cell was infected with HSV1 at 5 MOI 1 hour before transfection. CAT reporter plasmid was co-transfected with β-Galactosidase plasmid (pBGal, a kind gift from Dr. Martin Holcik, Carleton University[305]) at one µg per each plasmid. Cells were lysed 24 hours

post-transfection and assayed for CAT expression using the CAT ELISA kit (Roche). β-Galactosidase activity was also measured from lysate using ortho-Nitrophenyl-β-galactoside (ONPG) colorimetric assay. CAT expression was normalized to β-Galactosidase activity to control for transfection efficiency.

3.4.5. Quantitative RT-PCR

DNase-treated RNA and cDNA were prepared as described above. For RT-qPCR, SsoAdvanced Universal SYBR Green supermix (BioRad) was used with a CFX96 Touch Real-Time PCR Detection System (BioRad). The PCR condition was 95°C for 3 minutes, followed by 40 cycles of 95°C for 10s and 60°C for 30s, and ended with a standard melting curve cycle. Gene expression was calculated using the ΔΔCt method against the indicated reference genes. The list of primers for the genes or sequences of interest is in **Table S3.1**.

3.4.6. Western Blot

Cells were washed once with 1X PBS, then lysed on ice using RIPA buffer (150 mM NaCl, 1.0% IGEPAL® CA-630, 0.5% sodium deoxycholate, 0.1% SDS, 50 mM Tris, 50mM NaF, 15 mM NaVO3, pH 8.0) supplemented with cOmplete Protease Inhibitor Cocktail (Roche). Lysate was centrifuged at 10,000 g, 10 min at 4°C to remove cell debris. Protein concentration was determined using the DC Protein assay kit (BioRad). An indicated amount of total protein was used for SDS-polyacrylamide gel electrophoresis (PAGE) using 10% SDS-polyacrylamide gel. Separated proteins were transferred to PVDF membrane, the membrane was blocked with 5% w/v bovine serum albumin in TBS-T buffer (10 mM Tris, 50 mM NaCl, 0.1% Tween-20, pH 7.5) and then blotted for the indicated antibody. The following antibodies and corresponding dilution were used: anti-GFP (Abclonal, CAT#AE011) at 1:2000, anti-β-actin (Sigma, #A5441) at 1:10,000,

IRDye® 800CW Goat anti-Mouse IgG Secondary Antibody (LICOR, CAT#926-32210) at 1:20,000 and IRDye® 680RD Goat anti-Rabbit IgG Secondary Antibody (LICOR, CAT#926-68071) at 1:20,000.

3.4.7. Live-cell monitoring of GFP expression

Live-cell monitoring of GFP expression was performed using the IncuCyte Live-Cell Monitoring system (Sartorius). Transfection and/or infection were performed as indicated, then cell plates were placed inside the IncuCyte system and monitored at 37°C, 5% CO_2 with phase contrast and fluorescent images taken every 2 hours. Images were then analyzed with the IncuCyte ZOOM software using the following parameter: background subtraction using Top-Hat method (disk shape structuring element with a radius of 10 μm, threshold of 1.0 green calibrated unit), edge split: Off, Hole Fill: No, Adjust Size: No, Filters: No.

3.4.8. Generating recombinant HSV1 viruses

For inserting the expression cassette into HSV1 genome, we targeted the TK gene for insertion as previously described [300]. HSV1 genomic DNA was extracted from purified virus stock using the QIAamp DNA mini kit (Qiagen). HEK293T cells were seeded at 75% confluency one day before in 6-well plates, and then co-transfected with HSV1 gDNA:pTK-Green plasmid at a ratio of 1:40, for a total amount of 1 μg DNA/well, using Lipofectamine 2000 (Thermo Fisher) according to manufacturer protocol. Cells were then cultured for 3-5 days until cytopathic effect was observed. Cells were then freeze-thawed three times, centrifuged at 1000 g, 5 min to remove cell debris and supernatant was collected. Supernatants at various dilutions were then inoculated to a monolayer of Vero cells in order to separate individual plaques overlaid with DMEM supplemented with 10% FBS and 1% carboxymethylcellulose (CMC) to allow for the development

of individual plaques. GFP-positive plaques were selected and subjected to multiple plaque purification rounds until a pure GFP-expressing HSV1 population was obtained. Insertion of the cassette into the HSV1 genome was confirmed first by PCR genotyping using a forward primer on the TK gene (pTK-seq) and a reverse primer on the transgene (CSF2.e-R), followed by Sanger sequencing.

3.4.9. Plaque titration

Virus stock or solution were serially diluted, then inoculated a monolayer of Vero cells and incubated for 1 hour, 37°C, 5% CO_2 with frequent shaking. The virus-containing media was then removed and an overlay of DMEM + 10% FBS + 1% agar was added. Cells were then cultured at 37°C, 5% CO_2 until visible plaques could be observed using a brightfield microscope. Plaques were visualized using crystal violet staining and counted.

3.4.10. Polysome fractionation

Polysome fractionation was performed as previously described[255]. Briefly, cells were treated with cycloheximide (CHX) (Bioshop, CAT #66-81-9) at 100 µg/ml for 5 min to stop ribosome, washed three times with ice-cold PBS supplemented with CHX (100 µg/ml) and lysed using polysome lysis buffer (5 mM Tris pH 7.5, 2.5 mM $MgCl_2$, 1.5 mM KCl, 100 µg/ml CHX, 2 mM DTT, 0.5% Triton X-100, 0.5% sodium deoxycholate) supplemented with 100 units RNAsin Ribonuclease inhibitor (Promega). Cell debris was cleared by centrifugation at 14,000 g for 10 min, 4°C. Supernatant was then loaded on a 10%-50% continuous sucrose gradient and centrifuged at 36,000 rpm, 90 min at 4°C in a SW41Ti rotor. Fractions were then collected, and the OD260 absorbance of fractions was monitored using a Brandel Fraction Collector System (Brandel). RNA

was extracted from each fraction using TRIzol reagent (Thermo Fisher) according to the manufacturer's protocol.

3.4.11. GM-CSF quantification

To measure GM-CSF production from engineered HSV1 infection, cells were seeded at 80-90% confluency and then infected with the indicated HSV1 at an MOI of 5. 24 hours post-infection, culture supernatant was collected and GM-CSF production was measure using the Mouse GM-CSF ELISA Kit (CSF2) (Abcam, CAT#ab100685) according to the manufacturer's protocol.

3.4.12. Single step-growth curve and monitoring HSV1 genes expression

For monitoring virus replication and viral gene transcription during a single-step growth curve, cells were seeded at 80-90% confluency and infected the next day at an MOI of 5. Both cells and culture supernatant were collected at the indicated time points and used for virus titration by plaque assay, or RNA extraction for quantification of viral transcript expressions as described above.

3.4.13. Data and Code Availability

The RNA-seq data was published previously[301] and are available on the NCBI Gene Expression Omnibus (GEO: GSE137757), sample IDs GSM4086602 and GSM4086610 (HSV1 infected mRNA replicate).

3.4.14. Statistical analyses

All experiments were performed in at least three biological replicates. Statistical analyses were performed using GraphPad Prism 8, using the method indicated in figure legends. Error bars

indicate standard error of the mean (SEM). $^{*}p < 0.05$, $^{**}p < 0.01$, $^{***}p < 0.001$, $^{****}p < 0.0001$, ns, non-significant.

3.5. Results

3.5.1. Determining HSV1 mRNA leader sequence

HSV1 is a dsDNA virus enveloped virus with a genome of 153 Kb of two covalently linked segments, the long (L) and short (S) segments, that encode approximately 74 genes. The virus is neurotropic and can enter either a lytic cycle where the active production of viral progeny results in cell death, or a latent state in which most viral gene expression is silenced, with the viral DNA existing in a stable episomal state in latently infected cells for a very long period[306]. It was reported that certain HSV1 transcripts contain a leader sequence, but surprisingly most transcripts have no annotated leader sequences in the commonly accessed NCBI databases for HSV1; only a few HSV1 genes have annotated leaders in public databases (NCBI accession number JQ780693 for strain KOS and JN555585 for strain 17), while several single-gene studies identified and characterized the leader of a limited number of HSV1 genes[307–313] (**see Table S3.1**). One challenge of annotating transcripts on viral genomes based on short-read mapping is the proximity of each gene to its neighboring genes, resulting in overlapping with the UTRs and the coding region of other genes. When a read is mapped to an overlapping region, it is not possible to distinguish which transcript the read belongs. HSV1 genes are encoded on both the positive (+) and negative (-) strands, allowing one additional criterion to separate RNA reads. We previously generated RNA-seq data of HSV1 infected 4T1 murine breast cancer cells[301]. 4T1 cells were infected with an effective dose that caused cytopathic effect in 50% (ED_{50}) of the cells at 48 hours post-infection, and cells were lysed for RNA extraction at 18 hours post-infection. Mapping the HSV1 reads from

this dataset, we were able to distinguish individual transcripts in both the positive and negative strand (**Figure 3.1A**). The RNA-seq mapping strategy also detected the splice junctions of the four known spliced transcripts of HSV1: UL15, US1, US12 and RL2 (**Suppl. Figure 3.1**). Interestingly, we could also detect the intron retention that was previously reported for RL2[314].

Identification of the TSS of viral transcripts from sequencing techniques that yield long reads (such as PacBio methods[315]) or full transcript sequencing (such as the Oxford Nanopore MinION platform[316]) can be easier than RNA-seq that relies on aligning short reads. However, short reads could be used to successfully identify the TSS for non-overlapping HSV1 genes given the high coverage in infected cells by monitoring for a "wall" of stacked short reads that would delineate the 5' end of a transcript[317] (**Figure 3.1B and C**). From RNA-seq data, we detected reads that mapped to the 5' (**Figure 3.1C**) as well as 3' regions of most ORFs (**Figure 3.1D**), confirming that all HSV1 transcripts harbor both a leader and a 3'UTR. Although the 3'UTR regions of a large portion of the viral genes overlapped and were ambiguous with neighboring genes, we observed that the TSS of most viral transcripts can be defined by a sharp increase in read density at a single nucleotide position (**Figure 3.1C**, insets). Even though certain leaders still overlapped with neighboring genes in the HSV1 genome, using this approach, we identified at least one TSS for 61 of 73 HSV1 genes (**Table 3.1**, the read density coverage at each identified 5'TSS are shown in **Suppl. Figure 3.2**). Importantly, when comparing the identified TSSs with those few annotated in NCBI, or more recently identified by long-read sequencing done by Tombacz *et al.*[315] or RNA-seq on enriched 5'end reads by Whisnant *et al.*[317], we found that the coordinates of the TSSs were exact or differed by only a few nucleotides. These studies confirmed that our approach robustly detected HSV1 transcript leaders (**Table 3.1**).

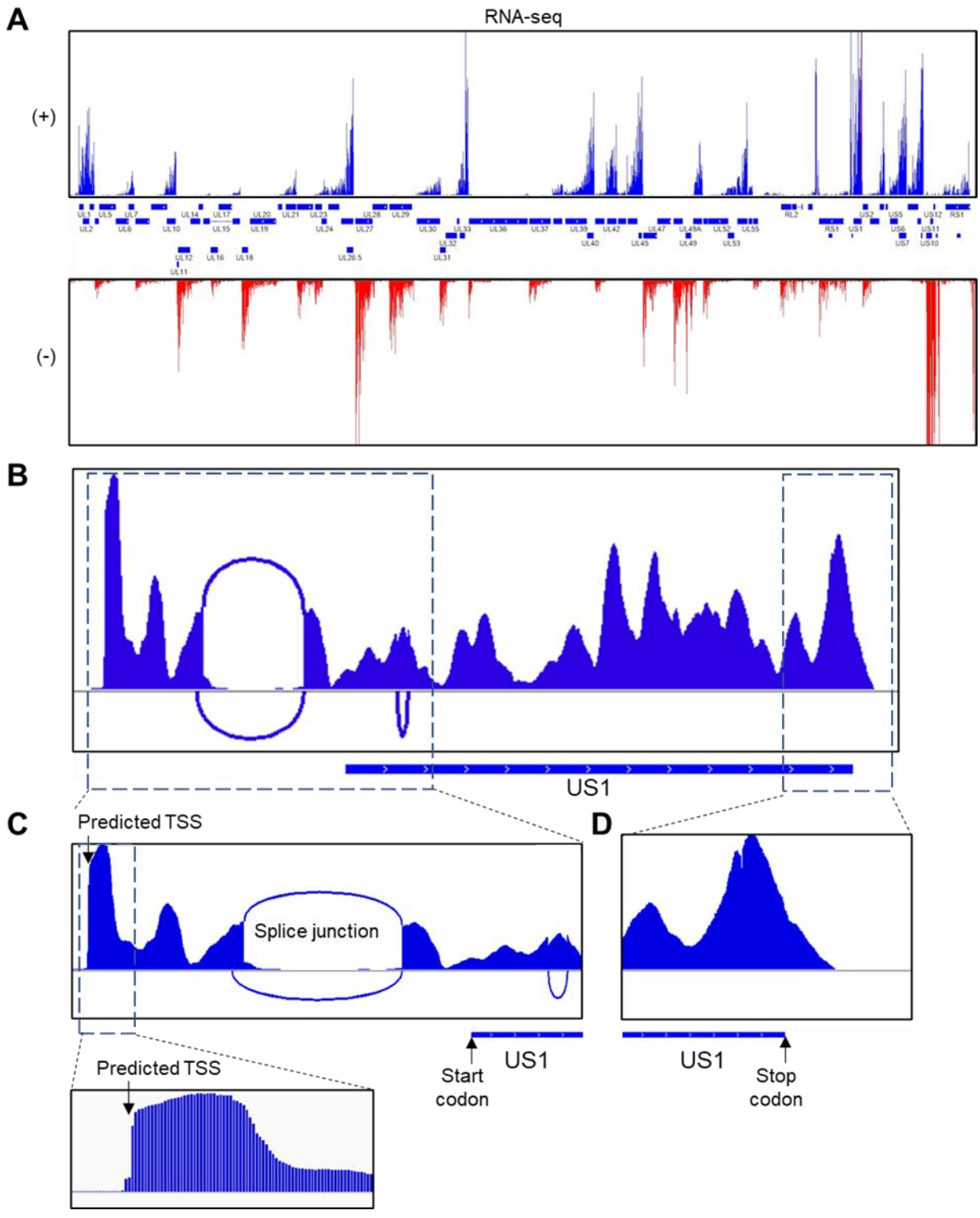
A
RNA-seq
(+)
(-)
B
US1
C
Predicted TSS
Splice junction
Predicted TSS
US1
Start
codon
D
US1
Stop
codon

Figure 3.1. Characterizing HSV1 individual transcript from RNA-seq coverage
(A) Total RNA-seq coverage of the HSV1 genome. RNA-seq data from 4T1 infected with HSV1 were previously published[301]. Strand-specific RNA reads were mapped to HSV1 genome and separated by strand direction to avoid ambiguous mapping of overlapping genes.
(B) Examples of RNA-seq coverage of the US1 gene. Intron-spanning reads were also detected and shown using Sashimi plot.
(C) RNA-seq coverage in the 5' region of US1 gene. The lower plot shows the region of the predicted TSS at nucleotide resolution.
(D) RNA-seq coverage at the 3' region of US1 gene.

3.5.2. The US11 leader enhances translation of downstream ORFs in HSV1-infected cells

Having identified the leader sequences of most HSV1 genes, we next sought one that could enhance the translation output of its associated transcript. We speculated that the leaders of HSV1 late genes that are expressed in an established infection stage should be most adapted to the altered translation control during HSV1 infection, and therefore should have the highest possibility to possess an HSV1 specific translation enhancing effect. Thus, we focused on the leader sequence of late genes. As our data was generated on cells infected at a low HSV1 MOI that might contain multiple stages of infection, we relied on HSV1 gene expression from a previously published study that infected cells at a high MOI and collected RNA-seq data at multiple time points[286] to generate a list of late HSV1 genes (**Suppl. Figure 3.3)**. We next used a plasmid-based translation reporter assay in which the leader of interest is inserted upstream of the chloramphenicol acetyltransferase (CAT) CDS as previously described[318] (**Figure 3.2A**). CAT mRNA is expressed under the control of the strong constitutive CMV promoter and CAT protein expression is measured by ELISA and compared to that expressed from the same construct lacking the leader sequence. HSV1 leader sequences of late viral genes were identified from the RNA-seq data, amplified from a cDNA library generated from HSV1-infected 4T1 cells and cloned into the reporter plasmid (**Suppl. Figure 3.4A**). A previous study reported the virion host shut-off (vhs) protein of HSV1 can promote translation activity of certain cellular IRESes, as well as potentially some HSV1 leader sequences[319]. Thus, we performed the translation reporter assay in both uninfected and HSV1-infected conditions by transfecting cells with the indicated CAT plasmid and a plasmid expressing β-galactosidase to control for transfection efficiency. In the uninfected condition, leaders had both positive and negative effects on reporter expression, although no significant trends were observed.

However, following HSV1 infection, we found that US11 and UL27 leaders significantly enhanced CAT expression (**Figure 3.2B** and **Suppl. Figure 3.4B**) compared to the reporter lacking a leader (leaderless). These observations could not be explained by any leader-mediated increases in CAT mRNA transcription (**Suppl. Figure 3.4C**). We also predicted the folding free energy and potential secondary structure of the US11 and UL27 leaders **(Suppl. Figure 3.4D**) as well as the folding free energy of other screened HSV1 leaders (**Suppl. Figure 3.4E**). We found that despite having the most potent translation enhancement on CAT expression, the leaders of US11 and UL27 have low predicted folding free energy comparing to other HSV1 leaders. This data suggested that the capacity to form a stable secondary structure may not affect the translation activity of HSV1 leaders. Together, these results propose that the leader sequences from HSV1 US11 or UL27 mRNAs can mediate HSV1 infection-dependent increases in protein expression when inserted upstream of a transgene in cells.

We next investigated the effect of HSV1 US11 or UL27 leaders on regulating transgene expression directly from expression cassettes that can be inserted within the virus genome. We used a previously described system to insert a transgene into the HSV1 *tk* locus[300]. Briefly, the pTK plasmid expression cassette includes the CMV promoter, the transgene CDS with or without the leader sequence and an SV40 polyadenylation signal. This plasmid system can then be used to generate recombinant viruses when it is linearized and co-transfected with purified HSV1 genomic DNA, as low-frequency homologous recombination of the expression cassette into the *tk* locus produces virus progenies that harbor a Δ*tk* genotype but express the transgene in an immediate-early manner under the CMV promoter (**Figure 3.2C**). Here we fused the GFP CDS downstream of the transgene CDS, separated by the self-cleaving peptide porcine teschovirus-1 2A (P2A), which causes the translating ribosomes to skip the formation of the peptide bond between the

glycine and proline residue and produce two proteins from one open reading frame[320,321] (**Figure 3.2C**). We generated constructs by fusing either the US11 or UL27 leader (or leaderless) upstream of the transgene CDS of luciferase (LUC) followed by the GFP CDS. This transgene cassette will express GFP and LUC in the infected cell and can be selected using fluorescence microscopy. Furthermore, modulation of transgene expression can also be quantified by measuring GFP fluorescence or luciferase levels. We then first examined whether plasmid expression of the new transgene cassette can reproduce *in vitro* the HSV1 leader-dependent translation enhancement observed in the previous CAT translation reporter setting. Fluorescence microscopy observation and GFP quantification of cells transfected with transgene expression plasmids confirmed that insertion of the US11 leader significantly enhances GFP expression in HSV1 infected cells compared to a leaderless expression cassette (**Figure 3.2D and E**). The US11 leader did not affect GFP expression in uninfected cells, while the UL27 leader yielded a decreased GFP expression compared to the leaderless cassette in both conditions. Western blot confirmed that the increase of GFP fluorescence signal with the US11 leader reflected the increase in GFP protein levels (**Figure 3.2F** and **G**). Importantly, RT-qPCR also showed that incorporation of the US11 leader did not affect transcript levels or splicing of the LUC-P2A-GFP transcript in uninfected compared to HSV1 infected cells (**Figure 3.2H**).

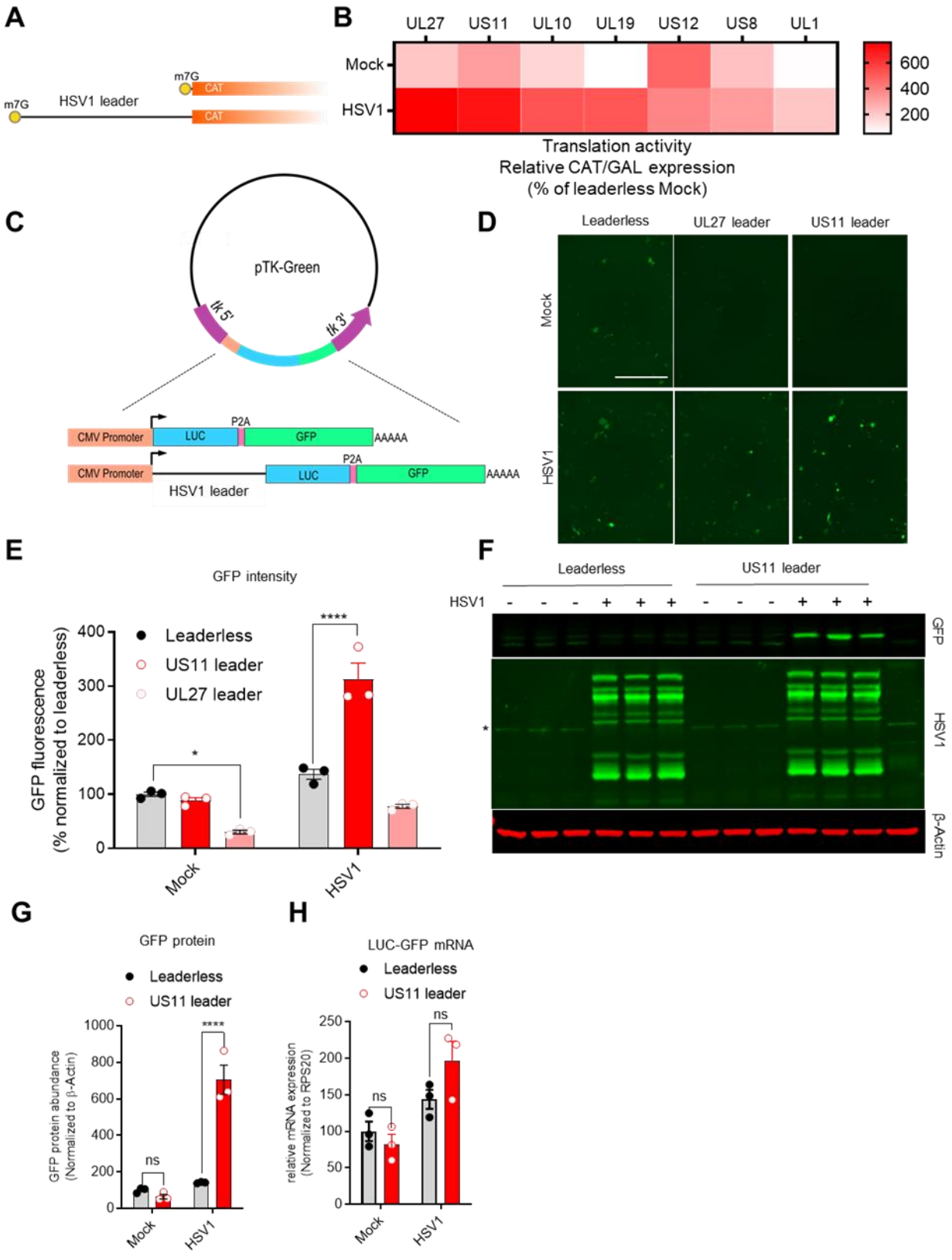
A
m7G
HSV1 leader
CAT
CAT
B
UL27
US11
UL10
UL19
US12
US8
UL1
Mock
HSV1
600
400
200
Translation activity
Relative CAT/GAL expression
(% of leaderless Mock)
C
pTK-Green
tk 5'
tk 3'
CMV Promoter
LUC
P2A
GFP
AAAAA
HSV1 leader
D
Leaderless
UL27 leader
US11 leader
Mock
HSV1
E
GFP intensity
GFP fluorescence
(% normalized to leaderless)
Leaderless
US11 leader
UL27 leader
Mock
HSV1
F
Leaderless
US11 leader
HSV1
GFP
HSV1
β-Actin
G
GFP protein
Leaderless
US11 leader
GFP protein abundance
(Normalized to β-Actin)
ns
H
LUC-GFP mRNA
Leaderless
US11 leader
relative mRNA expression
(Normalized to RPS20)
ns

Figure 3.2. HSV1 US11 and UL27 leader sequences mediate enhanced expression of protein reporters in HSV1-infected mammalian cells.
(A) Schematic diagrams of the mRNAs expressed from CAT reporter construct without/with HSV1 5'UTR.
(B) Translation reporter assay to screen for HSV1 leader sequences that enhance translation during HSV-1 infection. 4T1 cells were transfected with the CAT plasmid and a β-GAL expression plasmid that serve as a transfection control. 8 hours post-transfection, cells were infected with HSV-1716-GFP at an MOI of 5. Cells were lysed 18 hours post-infection and CAT expression was quantified by ELISA, while β-GAL activity was quantified by colorimetric assay using ONPG substrate. Two-way ANOVA with Tukey's *post-hoc* test was performed. Only significant tests were shown. n = at least three biological replicates. Error bars indicate standard error of the mean (sem). $^{*}p < 0.05$, $^{**}p < 0.01$.
(C) Schematic diagram of the pTK-Green plasmid that harbors the HSV1 leader-reporter construct for insertion into the HSV1 TK gene and the resulting transcripts. The ribosome skipping sequence P2A is inserted between the luciferase CDS and GFP CDS, which allowed for the synthesis of 2 proteins from one cistron.
(D) Representative images of GFP expression with/without HSV1 leader in uninfected or infected 4T1. Cells were transfected with LUC-GFP reporter plasmid, then infected with the HSV1 (KOS strain) 4 hours post-transfection at an MOI of 2.5. Images were taken 24 hours post-infection. Scale bar: 400 μm.
(E) Quantification of GFP fluorescence in (B) using the IncuCyte Live Cell Imaging system.
(F) Western Blot of lysate from 293T that is transfected/infected as in (B) against anti-GFP, anti-HSV1 or anti-β-Actin antibodies. (*): non-specific band.
(G) Quantification of GFP expression from the Western Blots in (F).
(F) RT-qPCR quantification of LUC-GFP mRNAs from the same experiment.
Two-way ANOVA with Sidak's *post-hoc* test was performed. n = 3 biological replicates. Error bars indicate standard error of the mean (sem). $*p < 0.05$, $**p < 0.01$, $****p < 0.0001$, ns, non-significant.

3.5.3. The US11 leader enhances transgene protein expression from a recombinant HSV1 genome

Lytic infection by HSV1 induces a profound reprogramming of cellular transcription, splicing and nuclear export[286,287]. Thus, a plasmid-based overexpression reporter assay might be compromised by HSV1 infection and not faithfully reflect the gene expression processes, including mRNA translation, of HSV1-encoded transgenes expressed from the viral genome. We next sought to construct two different recombinant HSV1 strains that express a transgene in *cis*; one harboring the US11 leader upstream of the transgene, with the other lacking this sequence. To demonstrate the potential clinical relevance of enhanced transgene protein expression, we swapped the luciferase CDS with one that encodes murine GM-CSF (*Csf2*), the human homolog of which is currently incorporated into the FDA-approved oncolytic HSV1. Using the co-transfection method to insert the transgene into the HSV1 genome described above (**Figure 3.3A**), we successfully obtained purified colonies of recombinant HSV1 that express GFP. Genotyping the rescued viruses confirmed one virus that expresses the leaderless cassette (HSV1::CSF2-GFP) while two others were obtained that express the US11 leader (HSV1::*us11*-CSF2-GFP) expression cassette (**Figure. 3.3B**). In agreement with the enhanced expression of GFP conferred with the US11 leader in the plasmid-based systems, plaques on Vero cells of HSV1::*us11*-CSF2-GFP showed significantly elevated GFP fluorescence compared to plaques of HSV1::CSF2-GFP (**Figure 3.3C**). Similarly, the leader sequence boosted the production of GM-CSF by approximately seven folds, from 165± 4.8 pg/ml in leaderless expression cassette to 1126 ± 5.6 pg/ml and 1330 ± 13.16 pg/ml (**Figure 3.3D**). To confirm that the enhanced GM-CSF production is not a result of higher viral replication, we measured virus titer kinetics by single-step growth curve and found that both the viruses exhibit comparable replication kinetics (**Figure 3.3E**). RT-qPCR of mRNAs extracted from infected cells

at various time points also confirmed that the presence or absence of the leader sequence did not affect the expression kinetics of an HSV1 transcript (US6, **Figure 3.3F** left panel), nor that of the transgene transcripts expressed in cis (*Csf2* and *gfp*, **Figure 3.3F** middle and right panel) over the course of infection. In order to determine that the transgene enhanced protein production was not cell-type or species-dependent, we infected other cancer cell lines, including the mouse breast cancer cell lines 4T1, the human prostate cancer line DU145 and the human renal cell carcinoma line 786-O, with the two recombinant viruses. Monitoring of GFP fluorescence intensity in these cells over the course of infection revealed a dramatic US11 leader-mediated enhancement of transgene GFP protein expression in all cell lines tested (**Figure S3.5**), suggesting an effect that doesn't rely on cell- or species-specific trans-acting factors or cellular milieu.

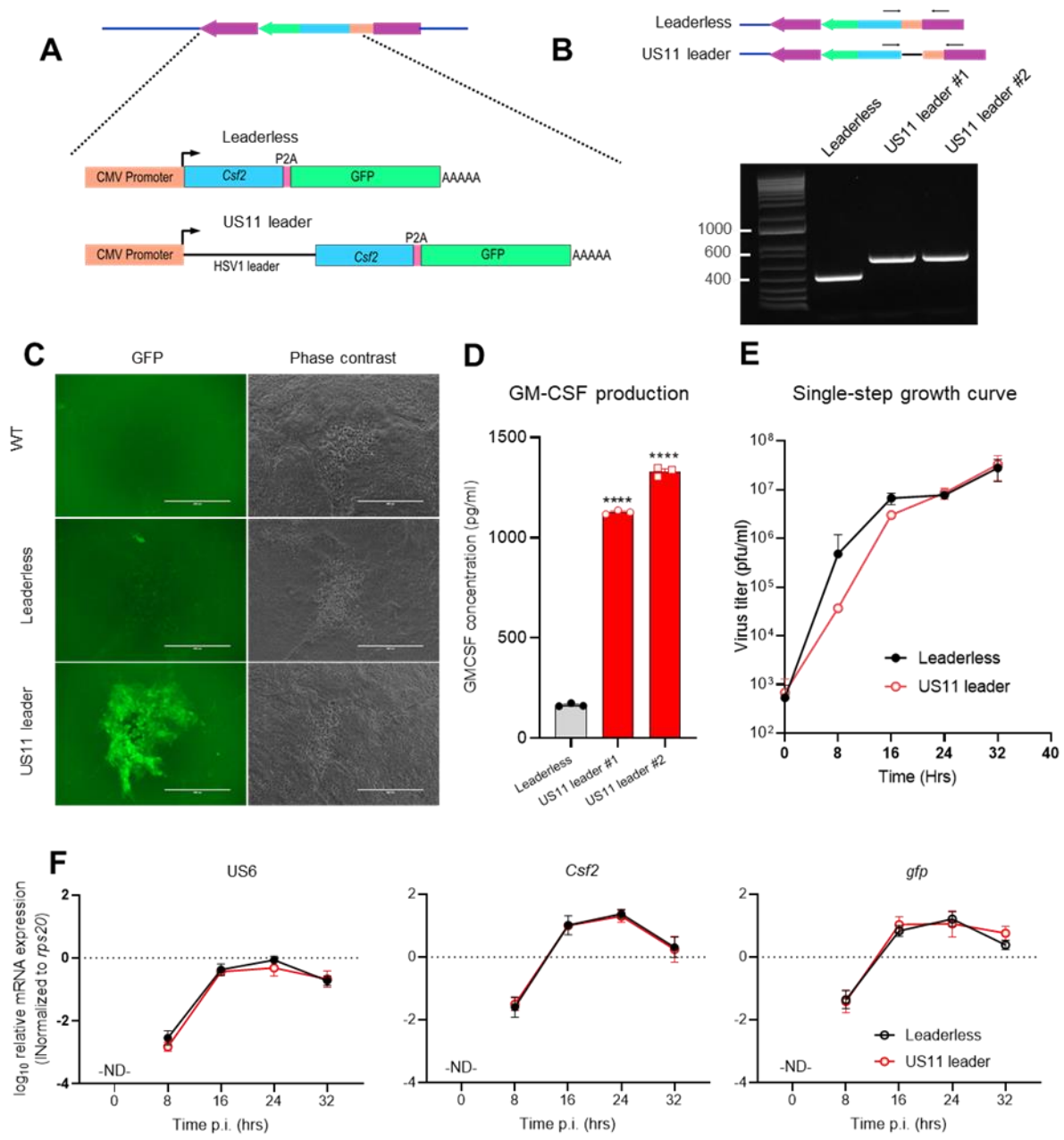

Figure 3.3. A recombinant HSV1 virus exhibits a US11 leader-dependent boost in GM-CSF expression.

(A) Schematic illustration of the expression cassette insertion scheme from the pTK-CSF2::GFP plasmid into HSV1 genome (note that the TK gene is on the minus strand), and the resulting transcripts expressed from the inserted cassette.

(B) Virus genotyping for confirmation of expression cassette insertion. PCR was done using HSV1 gDNA extracted from purified viruses for the confirmation of the insertion of the leaderless-CSF2-GFP cassette (~400 bp) and US11 leader-CSF2-GFP cassette (~600 bp) into the TK region of HSV1 genome.

(C) Fluorescence imaging of individual plaques of wild-type HSV1, HSV1::CSF2-GFP and HSV1::*us11*-CSF2-GFP.
(D) Quantification of GM-CSF production in culture supernatant of Vero cell infected with HSV1 expressing leaderless CSF2-GFP or US11 leader-CSF2-GFP. Monolayer of Vero cells was infected with the indicated virus at an MOI of 5, and the culture supernatant was collected 24 hours post-infection. GM-CSF concentration was quantified by ELISA. One-way ANOVA with Dunnett's *post-hoc* test was performed. n = 3 biological replicates. Error bars indicate standard error of the mean (sem). ∗∗∗∗$p < 0.0001$.
(E) Single-step growth curve of HSV1 expressing leaderless CSF2-GFP and US11 leader-CSF2-GFP. Monolayer of Vero cells was infected at an MOI of 5, then intracellular and supernatant virus was collected and titrated at the indicated time points.
(F) Transcription level of HSV1 endogenous gene (US6) and transgenes. Monolayer of Vero cells was infected at an MOI of 5, then cells were lysed using Trizol at the indicated time points. mRNA abundance was quantified by RT-qPCR and normalized to Rps20.

3.5.3. The US11 5'Leader enhances the expression of transgenes from HSV1 genome

We next sought to validate our strategy by constructing an engineered HSV1 that expresses a transgene from its genome with or without the US11 5'Leader. For this purpose and for clinical relevance, we switched the LUC CDS with the CSF2 CDS, which encodes for the murine GM-CSF, the human GM-CSF transgene is currently incorporated into the FDA-approved oncolytic HSV1. Using the co-transfection method to insert the transgene into the HSV1 genome described before[300] (**Fig. 3.4A**), we successfully obtained purified colonies of recombinant HSV1 that express GFP. Genotyping the viruses using purified virus genomic DNA confirmed that these engineered viruses harbor either the Leaderless-CSF2-GFP (KOS *TK*::Leaderless-Csf2-GFP) or the US11 5'UTR-CSF2-GFP (KOS *TK*::5'Us11-Csf2-GFP) expression cassettes in the CDS of the *tk* gene (**Fig. 3.4B**). In agreement with the enhanced expression of GFP conferred with the US11 5'Leader in the plasmid-based systems, plaques of HSV1-5'Us11-Csf2-GFP showed significantly elevated GFP fluorescence compared to plaques of HSV1-Leaderless-Csf2-GFP (**Fig. 3.4C**). Similarly, the insertion of the US11 5'Leader upstream of the CSF2-GFP transcript greatly enhanced the production of GM-CSF by approximately 7 folds, from 165± 4.8 pg/ml in leaderless expression cassette to 1126 ± 5.6 pg/ml and 1330 ± 13.16 pg/ml for the two HSV1 recombinants harboring the US11 5'Leader (**Fig. 3.4D**). To confirm that the enhanced GM-CSF production is not a result of higher viral replication, we measured virus titer kinetics by single-step growth curve and found that both the Leaderless and US11 5'Leader possess comparable replication kinetic (**Fig 3.4E**). RT-qPCR of mRNAs extracted from infected cells at various time points also confirmed that the insertion of the US11 5'Leader did not affect the expression kinetic of the HSV1 endogenous transcript (US6, **Fig. 3.4F left panel**), nor transgene transcripts expressed from HSV1 genome (*Csf2* and *gfp*, **Fig. 3.4F middle and right panel**), as the transcript levels remained similar between the Leaderless and US11 5'Leader transcripts. In order to confirm that the transgene

enhanced protein production is not cell-type dependent or species-dependent, we infected various other cancer cells lines with the Leaderless and Us11 5'Leader HSV1, including the mouse breast cancer cell lines 4T1, the human prostate cancer line DU145 and the human renal cell carcinoma line 786-O. Monitoring of GFP fluorescence intensity confirmed that the US11 5'Leader-mediated enhancement is observed in all cell lines tested (**Fig. S3.2**), suggesting that the effect can be robustly replicated in different cell types of mouse or human origin.

3.5.4. The HSV1 US11 leader confers increased translation efficiency on the downstream transgene in an HSV1 dependent manner

The leader sequence or the 5'UTR of an mRNA has usually been linked with the regulation of translation control of the transcript. To determine whether the post-transcriptional enhancement of protein expression mediated by the US11 leader is a *bona fide* effect on mRNA translation, we employed the classic polysome profiling technique to compare the translation efficiency of *Csf2* mRNA between HSV1::CSF2-GFP and HSV1::*us11*-CSF2-GFP infected Vero cells at an MOI of 5 (**Figure 3.4A**). Cells were lysed and ribosome-bound mRNAs were resolved on a 10-50% sucrose gradient (**Figure 3.4B**). Transcripts with an increasing number of associated ribosomes migrated to heavier sucrose layers and corresponded to transcripts with a higher translational output. As expected, we found that the *us11*-CSF2-GFP transcript shifted its distribution toward heavier polysome fractions, demonstrating enhanced translation efficiency compared to the leaderless *Csf2-GFP* transcript (**Figure 3.4C and D**). Interestingly, the *US6* and *US11* viral mRNAs are mostly distributed to the heavier polysome fractions (**Figure 3.4C and D**), suggesting that HSV1 transcripts are generally highly translated despite the global shutoff of protein synthesis resulting from HSV1 infection. This data suggests that traditional transgene cassettes that lack *cis*-acting translation enhancing elements may be poorly translated compared to HSV1 endogenous

transcripts. These data clearly show that incorporation of the HSV1 US11 leader can significantly improve translation of a transgene in HSV1 infected cells. Finally, to address whether the translation enhancement mediated by the US11 leader is specific for HSV1 infected cells, or a result of a general antiviral state, we tested GFP expression from the plasmid pTK-Csf2-GFP in Vero cells transfected with the dsRNA mimic poly(I:C), or infected with another virus, VSV. We found that neither poly(I:C) transfection nor VSV infection were capable of inducing GFP from the US11-Csf2-GFP expression plasmid (**Figure 3.4E**). Thus, the enhancement of the US11 leader on gene expression is specific for HSV1 infected cells.

.

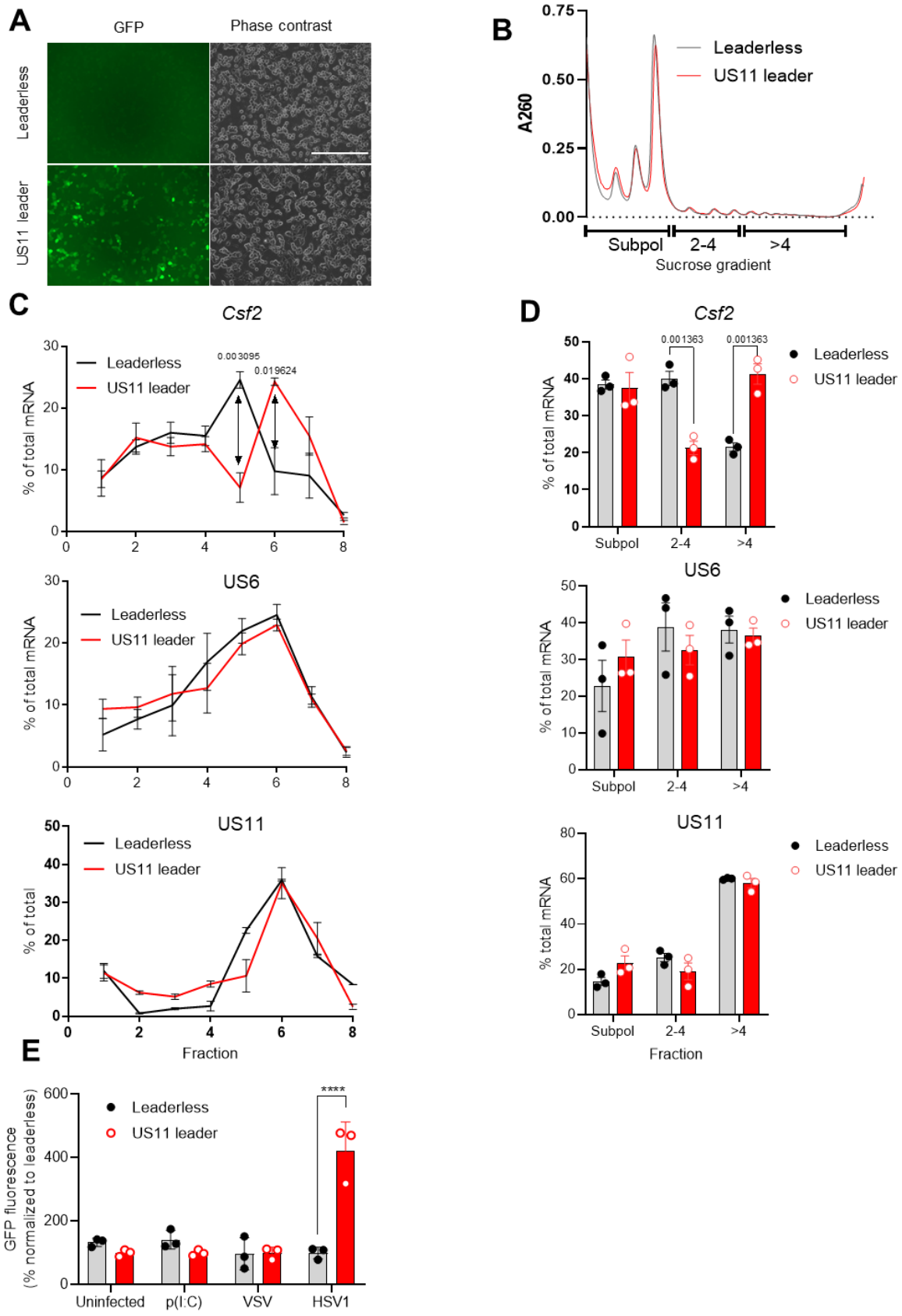
A
GFP
Phase contrast
Leaderless
US11 leader
B
A260
Leaderless
US11 leader
Subpol
2-4
>4
Sucrose gradient
C
Csf2
% of total mRNA
Leaderless
US11 leader
0.003095
0.019624
US6
% of total
US11
Fraction
D
Csf2
0.001363
0.001363
US6
US11
% total mRNA
E
GFP fluorescence (% normalized to leaderless)
****
Uninfected
p(I:C)
VSV
HSV1

Figure 3.4. The HSV1 US11 leader confers increased translation efficiency of the downstream transgene.
(A) Representative fluorescence and phase-contrast images of HSV1 infected Vero cells used for the polysome fractionation experiment in (B) and (C). Scale bar: 400 μm.
(B) Representative polysome traces of Vero cells infected with HSV1 KOS Leaderless-CSF2-GFP or HSV1 KOS US11 leader-CSF2-GFP at an MOI of 5. Cells were lysed at 24 hours post-infection for polysome fractionation.
(C) mRNA distribution in polysome fractions of *Csf2* (upper panel) and the endogenous HSV1 transcripts US6 (middle panel) and US11 (lower panel), quantified by RT-qPCR. Two-sided *t*-test was performed. n = 3 biological replicates. Error bars indicate standard error of the mean (sem). Exact *p*-values were shown where statistically significant.
(D) mRNA distribution in non-translating fraction (Subpolysome), poorly translating fraction (2-4 ribosomes) and highly translated fraction (>4 ribosomes) of *Csf2* (upper panel), US6 (middle panel) and US11 (lower panel) transcripts. Two-sided *t*-test was performed. n = 3 biological replicates. Error bars indicate standard error of the mean (sem). Exact *p*-values were shown where statistically significant.
(E) Quantification of GFP fluorescence in using the IncuCyte Live Cell Imaging system of Vero cells transfected with pTK-CSF2::GFP plasmid with or without US11 leader sequence, co-transfected with poly(I:C) or infected immediately after with VSV or wild-type HSV1 at an MOI of 5.

3.6. Discussion

In this work, we show that incorporating an HSV1 RNA leader sequence enhances downstream transgene protein expression from a recombinant HSV1 virus. Although mammalian leader or other translation enhancing elements are frequently considered in transgene expression cassette designed for transfected cells[322], these might not function well in the context of virus-infected cells. We find that an HSV1 leader sequence that confers efficient translation of its endogenous transcript can also be employed to enhance transgene protein expression in HSV1-infected cells. Our strategy is complementary to those that employ either a strong heterologous promoter to drive transgene expression, or one that inserts the transgene into a highly transcriptionally active region of the HSV1 genome. In an example of the former strategy, Toda *et al.* found that a cassette inserted into the TK region and expressing GM-CSF driven by a CMV promoter yielded approximately 55 pg of GM-CSF per 10^5 Vero cells[323]. In the present study, which also employed a CMV-driven, GM-CSF expression cassette inserted in the TK region of the HSV1 genome, we saw 41.75 ± 2.35 pg GM-CSF per 10^5 Vero cells, a value very close to that previously reported (**Figure 3.3D**; calculated based on 167 ± 9.4 pg/ml of GM-CSF observed in a 12-well plate format at confluency, which typically contains $4x10^5$ cells in 1 ml of culture media). Yet, with the introduction of the US11 leader, a 7-fold increase in GM-CSF production was obtained, representing a significant improvement in transgene protein expression. It is possible that transgene production can be improved even further by combining a strong HSV1 promoter (*e.g.*, the one driving HSV1 RL2 expression[324,325]) with a translation enhancer such as the one found in the US11 leader.

The findings presented here identify *cis*-acting sequences within virus-based therapies that can be exploited to enhance transgene expression. The method relies on a comprehensive

annotation of viral leader sequences through calling TSS by RNA-Seq and mapping translational efficiency across a viral genome by ribosome profiling. In this way, we rapidly identified a defined TSS for 61/73 genes of HSV1. During the lytic cycle, HSV1 expresses its genes in an orderly manner, classified into immediate-early (IE), early (E) and late (L) genes [326]. From this data, we further screened leaders of a subset of late viral genes for translation activity (**Figure 3.2**) using a heterologous translation reporter assay. These leaders belong to HSV1 genes that are highly expressed in the late stage of HSV1 infection, as we reasoned these might be better-tuned to modulate translation at this stage of infection. While we report here the leader of US11 as a significant translation enhancer, there certainly might be other HSV1 leader sequences with translation enhancing activity that might be revealed with a complete screen comparing all HSV1 leaders. Importantly, recent studies that used more specialized techniques for TSS identification such as long-read RNA-seq [315] or cRNA-seq and dRNA-seq[317], were able to detect the primary TSS but also several secondary TSS of alternative transcript variants of HSV1 genes, reporting approximately over 200 potential HSV1 transcripts. Therefore it will be a riveting basic virology question to investigate whether the various HSV1 leaders or alternative leaders mediate an additional layer of temporal regulation on HSV1 gene expression by translation regulation.

What is the mechanism(s) of UL27 and most particularly US11 leader-mediated translation enhancement? The most extensively studied translation enhancer elements of virus origin are IRESes, which support cap-independent translation of viral transcripts[93,327]. While it is unclear whether the HSV1 leaders act as IRESes, viral proteins can also act in-*trans* with leader sequences to modify translational efficiency of a viral mRNA. In poxvirus, non-templated poly(A) sequences are added to the leader of late viral transcripts due to viral polymerase slipping [95], which promotes translation of these viral RNAs [97–99]; this activity is attributed to the phosphorylation of the small

ribosomal protein RACK1 by the virus kinase B1[99]. Recently, it has been shown that the leader of SARS-CoV-2 sgRNA, as well as gRNA also protects viral transcripts from translation shutoff by the virus NS1 protein [328]. Thus, viral leaders are likely enriched in cis-regulatory sequences that have co-evolved with viral trans-acting protein factors that act together to control viral gene expression post-transcriptionally, yet current virus-based therapeutic applications do not effectively employ them. While our study is limited to HSV1 leaders, it will be interesting to determine if the same strategy works for other viral vector and OV backbones, such as AAV, VACV or Adenovirus

In this regard, the HSV1 protein vhs was shown to modulate translation activity of certain host 5'UTRs/IRESes as well HSV1 leader sequences in a cap-independent manner[319,329]. Vhs is a major translation modifier protein of HSV1; it possesses RNase activity toward ssRNA and interacts with the translation initiation complex[330,331], thus mediating the degradation of actively translating mRNAs in infected cells [332]. During the late stage of HSV1 infection, vhs activity is attenuated by the viral proteins VP16 and VP22[333] allowing for productive translation of viral transcripts in a cap-dependent mode. The cap-independent mode of translation employed by the leaders mentioned above might confer an advantage for the associated transcripts in the earlier phase of HSV1 infection. Another HSV1 translation modifier is ICP27, which is crucial for translation of viral mRNAs via facilitating their nuclear export. ICP27 contains an RGG motif at its N-terminal that binds to viral transcripts via GC-rich regions[126], and links the transcripts to the host nuclear export complex via its interaction with the nuclear export factor REF and NXF1[127–129].

In conclusion, our study shows that the HSV1 US11 leader sequence expressed either in-cis or in-trans with HSV1 can be used to greatly enhance transgene protein expression. Our study

exemplified a novel method for optimizing the expression level of a desired transgene using that can be applied to other virus-based therapeutic contexts, including oncolytic viruses, that can substantially improve the therapeutic efficacy of the vector. This finding also invites further study to better understand post-transcriptional gene expression in perturbed cellular conditions, such as the infected cells or stressed cells, which are frequently neglected.

Table 1: HSV-1 TSS identified in this study compared to Tombacz et al., 2017 and Whisnant et al., 2020

	This study				Tombácz et al., 2017		Whisnant et al	
Gene	TSS Location (JQ780693.1)	5'UTR location (JQ780693.1)	5'UTR length	TSS location (JN555585)	TSS location (JN555585)	Difference to our study (nt)	TSS location (JN555585)	Difference to our study (nt)
UL1+	8901	JQ780693.1+:8901-8994	92	9245	9242	3	9245	0
UL2+	9396	JQ780693.1+:9396-9541	145	9740	9739	1	9739	1
UL3+	X				10736			
UL4-	12151	JQ780693.1-:12079-12151	72	12495	12494	1	12494	1
UL5-	X				15581			
UL6+	X				15032			
UL7+	16613	JQ780693.1+:16613-16792	179	16957	16956	1	16956	1
UL8-	20337	JQ780693.1-:20134-20337	203	20680	20677	3	20679	1
UL9-	X				23358			
UL10+	22601	JQ780693.1+:22601-22862	261	22944	22943	1	22943	1
UL11-	25148	JQ780693.1-:24741-25148	407	25499	25498	1	25498	1
UL12-	26695	JQ780693.1-:26537-26695	158	27046	27045	1	27045	1
UL13-	X				28657			
UL14-	X				29249			
UL15+	28451	JQ780693.1+:28451-28670	219	28802	28801	1	28801	1
UL16-	31261	JQ780693.1-:30949-31261	312	31608	31607	1	31607	
UL17-	X				33719			
UL18-	35902	JQ780693.1-:35704-35902	198	36250	36249	1	36247	3
UL19-	40421	JQ780693.1-:40182-40421	239	40768	40768	0	40766	2
UL20-	X				41613			
UL21+	41515	JQ780693.1+:41515-41726	211	41863	41862	1	41862	1
UL22-	46230	JQ780693.1-:46031-46230	199	46582	46581	1	46581	1
UL23-	47558	JQ780693.1-:47451-47558	107	47910	47906	4	47909	1
UL24+	47008	JQ780693.1+:47008-47386	378	47360	47671	-311	47407	-47
UL25+	47722	JQ780693.1+:47722-48461	739	48074	48630	-556	48630	-556
UL26+	50311	JQ780693.1+:50311-50469	158	50664	50659	5	50663	1
UL26.5+	51249	JQ780693.1+:51294-51387	93	51635	51636	-1	51634	1
UL27-	55744	JQ780693.1-:55458-55744	286	56081	56080	1	56080	1
UL29-	61979	JQ780693.1-:61717-61979	262	62312	62312	0	62313	-1
UL30+	X				62605			
UL31-	67123	JQ780693.1-:67044-67123	79	67458	67458	0	67457	1
UL32-	68885	JQ780693.1-:68827-68885	58	69220	69220	0	69219	1
UL33+	68730	JQ780693.1+:68730-68826	96	69065	69065	0	69064	1
UL34+	69107	JQ780693.1+:69107-69298	191	69442	69442	0	69441	1
UL35+	70151	JQ780693.1+:70151-70231	80	70486	70489	-3	70488	-2
UL36-	X				?			
UL37-	83780	JQ780693.1-:83649-83780	131	84215	84215	0	84214	1
UL38+	83958	JQ780693.1+:83958-84088	130	84393	84394	-1	84393	0
UL39+	85774	JQ780693.1+:85774-86000	226	86217	86214	3	86216	1
UL40+	89331	JQ780693.1+:89331-89482	151	89774	89775	-1	89773	1
UL41-	92312	JQ780693.1-:92193-92312	119	92755	92755	0	92753	2
UL42+	924191	JQ780693.1+:92491-92669	178	92934	92936	-2	92934	0
UL43+	94323	JQ780693.1+:94323-94357	34	94765	94653	112	94764	1
UL44+	95723	JQ780693.1+:95723-95865	142	96171	96174	-3	96173	-2
UL45+	95706	JQ780693.1+:95706-97585	79	96154	97953	-1799	97953	-1799
UL46-	X				100995			0
UL47-	102866	JQ780693.1-:102672-102866	194	103312	103311	1	103309	3
UL48-	104814	JQ780693.1-:104635-104814	179	105258	105257	1	105257	1
UL49-	106099	JQ780693.1-:105949-106099	150	106542	106543	-1	106538	4
UL49A-	106686	JQ780693.1-:106551-106686	135	107129	107128	1	107126	3
UL50+	106387	JQ780693.1+:106387-106568	181	106830	106826	4	106829	1
UL51-	108863	JQ780693.1-:108569-108863	294	109306	109305	1	109302	4
UL52+	X				108985			
UL53+	111501	JQ780693.1+:111501-111737	236	111944	111943	1	111943	1
UL54+	113153	JQ780693.1+:113153-113292	139	113596	113598	-2	113598	-2
UL55+	115002	JQ780693.1+:115002-115054	52	115445	115447	-2	115444	1
UL56-	116643	JQ780693.1-:116485-116643	158	117084	117083	1	117083	1
RL2-	123628	JQ780693.1-:123482-123628	146	124258	124256	2	124255	3
RL1-	125310	JQ780693.1-:125206-125310	104	125965	125944	21	125964	1
RS1-	130404	JQ780693.1-:130103-130404	301	131431	131428	3	131429	2
US1+	131098		602					0
		JQ780693.1+:131098-131700	354 (spliced)	132128	132127	1	132129	-1
US2-	134359	JQ780693.1-:133983-134359	376	135307	135306	1	135305	2
US3+	134019	JQ780693.1+:134019-134277	258	134967	134958	9	134966	1
US4+	135787	JQ780693.1+:135787-135799	12	136735	136733	2	136734	1
US5+	X				137625			0
US6+	137395	JQ780693.1+:137395-137476	81	138342	138338	4	138345	-3
US7+	138754	JQ780693.1+:138754-138843	89	139699	139698	1	139699	0
US8+	140208	JQ780693.1+:140208-140282	74	141173	141170	3	141171	2
US8A+	141665	JQ780693.1+:141665-141783	118	142630	142626	4	142629	1
US9+	142287	JQ780693.1+:142287-142352	65	143252	143250	2	143251	1
US10-	144183	JQ780693.1-:144114-144183	69	145169	145171	-2	145168	1
US11-	144480	JQ780693.1-:144265-144480	215	145466	145461	5	145461	5
US12-	145247	JQ780693.1-:144596-145247	319 (spliced)	146069	146068	1	146066	3

Table 3.1: Identified HSV1 TSS in this study, compared to that in two previously published studies by Tombacz *et al*., 2017[315] and Whisnant *et al*., 2020[317]. "X" refers to unidentified TSSs.

Table 3.2: Sequence of HSV1 leader identified in this study (See attached file).

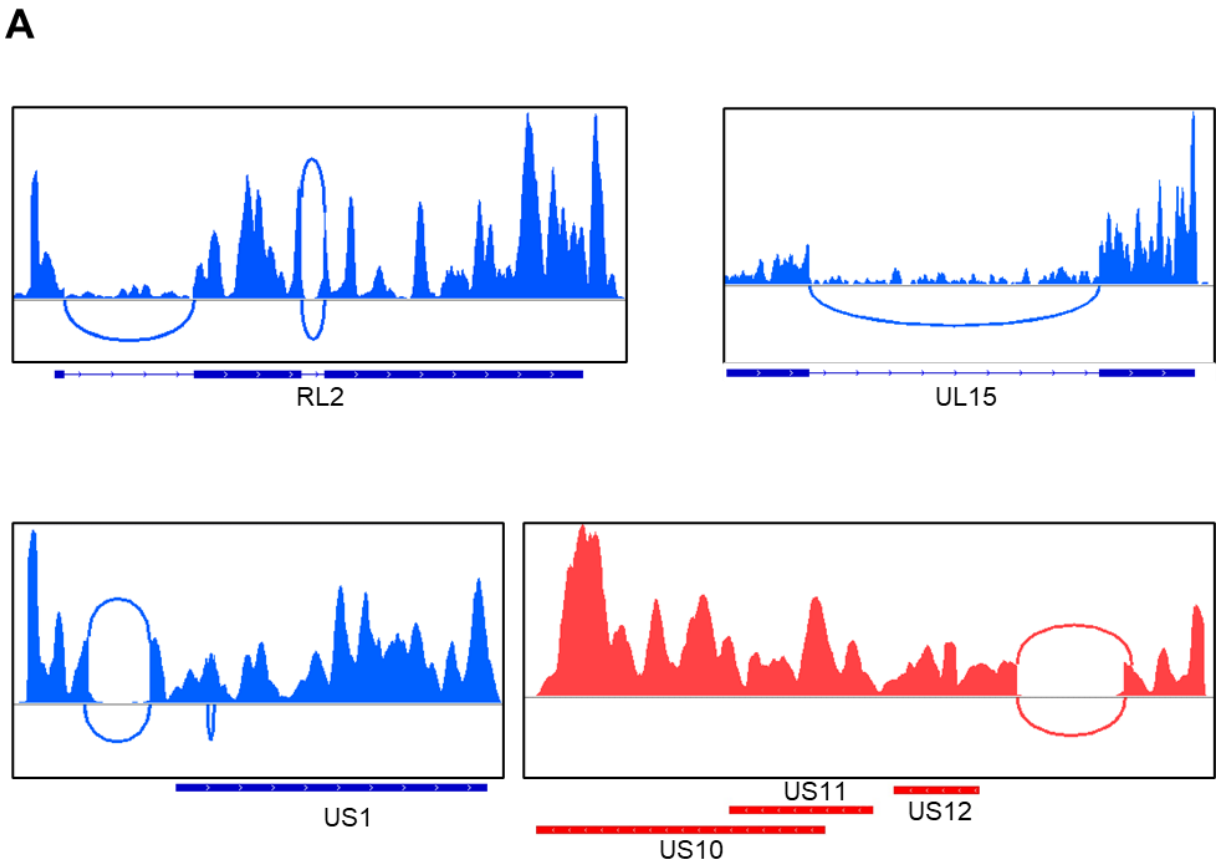

Figure S3.1. Examples of spliced junction detected on known HSV1 spliced transcripts. Individual transcripts (RL2, UL15, US1, US12) identified by RNA-seq coverage on the positive strand (blue) and negative-strand red).

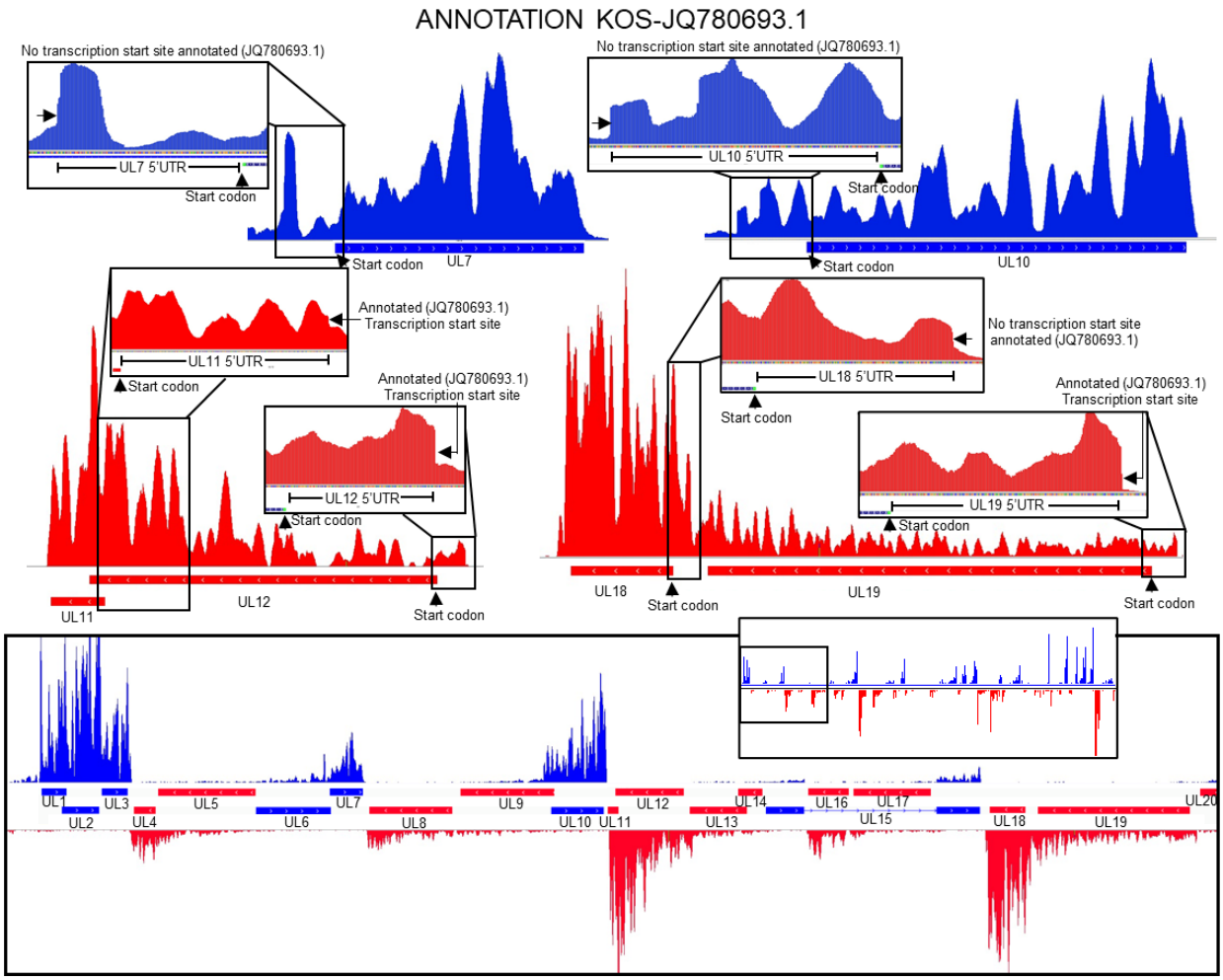

Figure S3.2. Full RNA-seq coverage of HSV1 genome
Total RNA-seq coverage of the HSV1 genome. RNA-seq data from 4T1 infected with HSV1 previously published (Hoang et al., 2019). Strand-specific RNA reads were mapped to HSV1 (JQ780693.1) and separated by direction to avoid ambiguous mapping of overlapping genes. This graph shows the inset for every identified TSSs of all HSV1 genes.

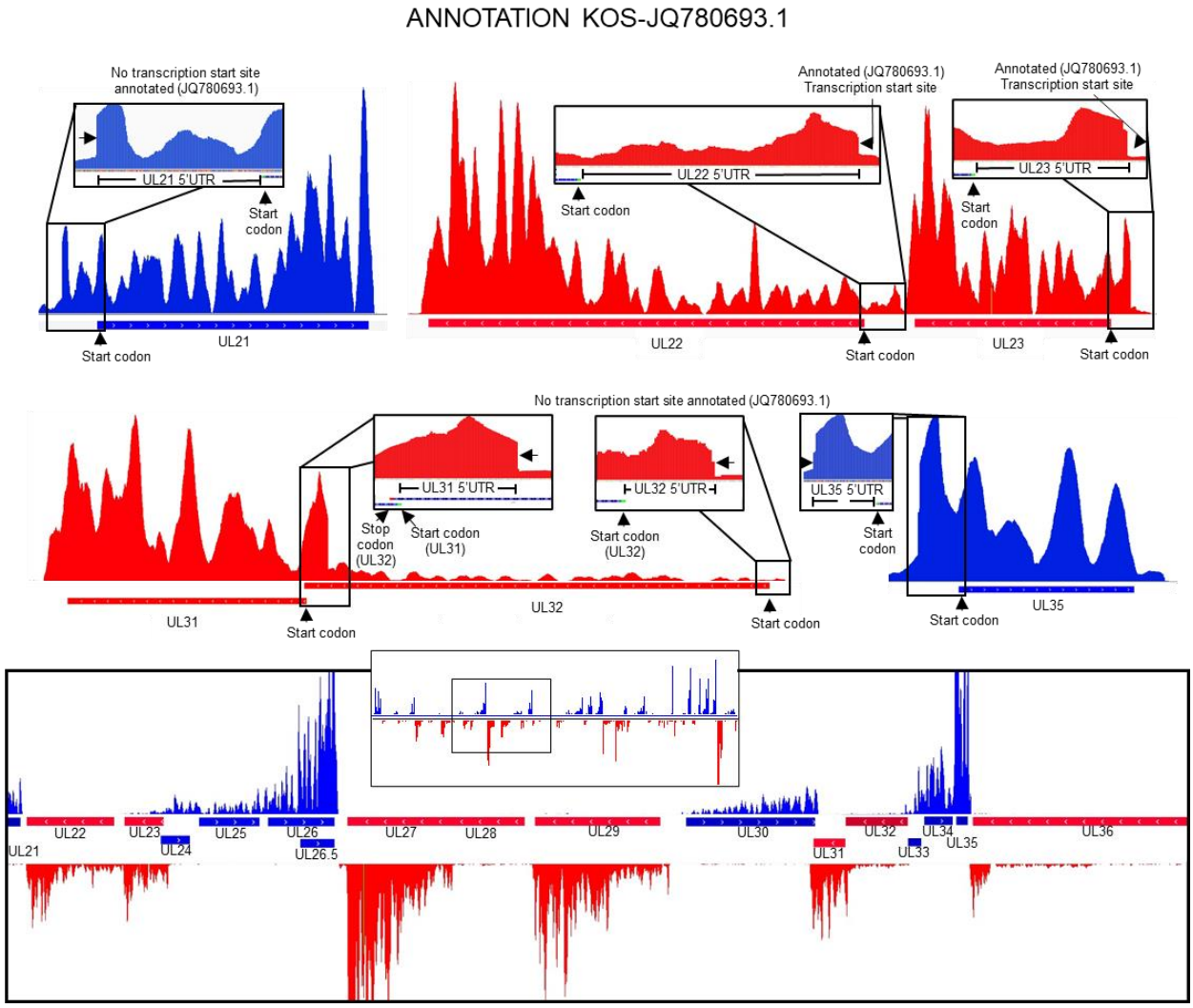

Figure S3.2. Full RNA-seq coverage of HSV1 genome (continued)

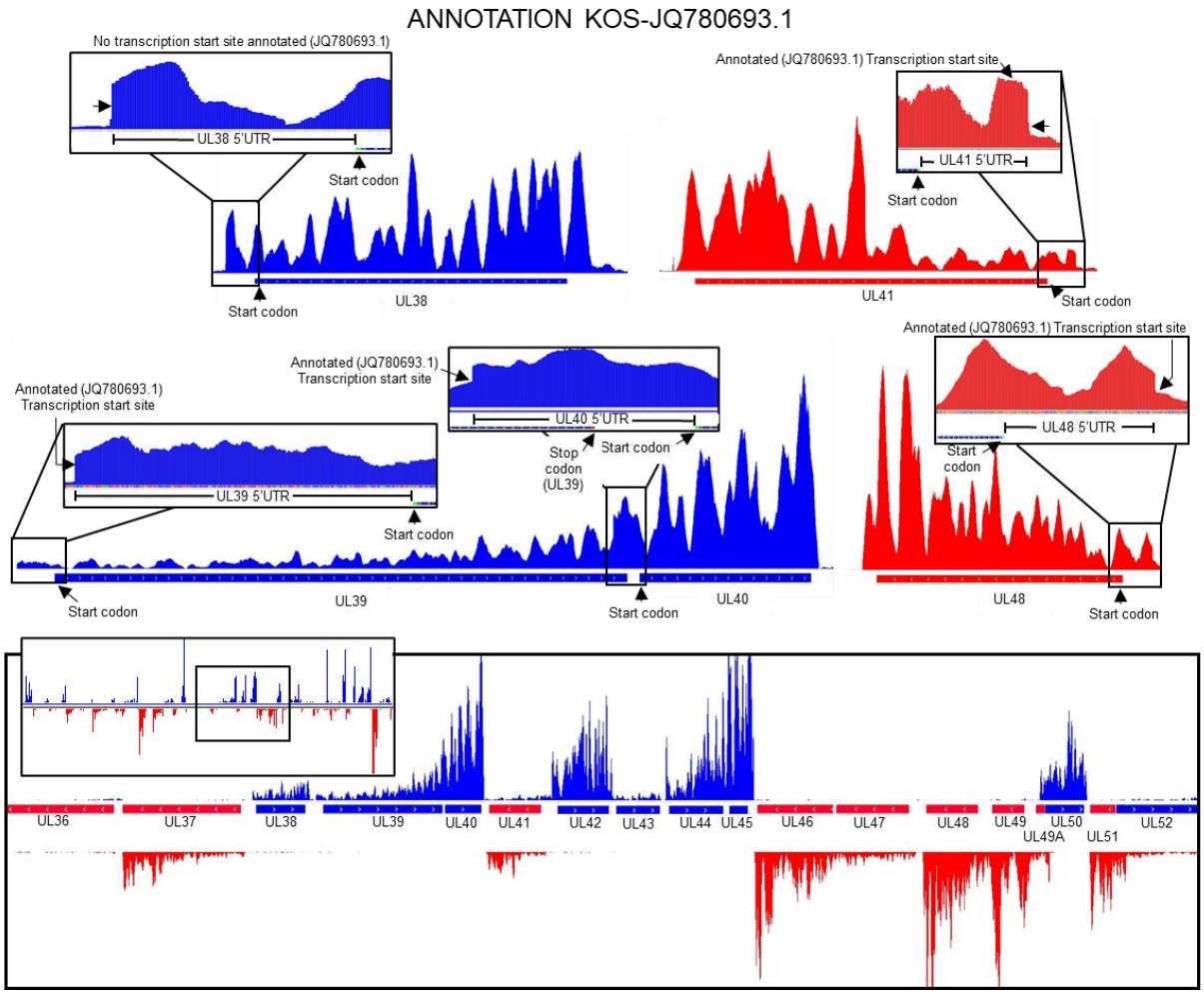

Figure S3.2. Full RNA-seq coverage of HSV1 genome (continued)

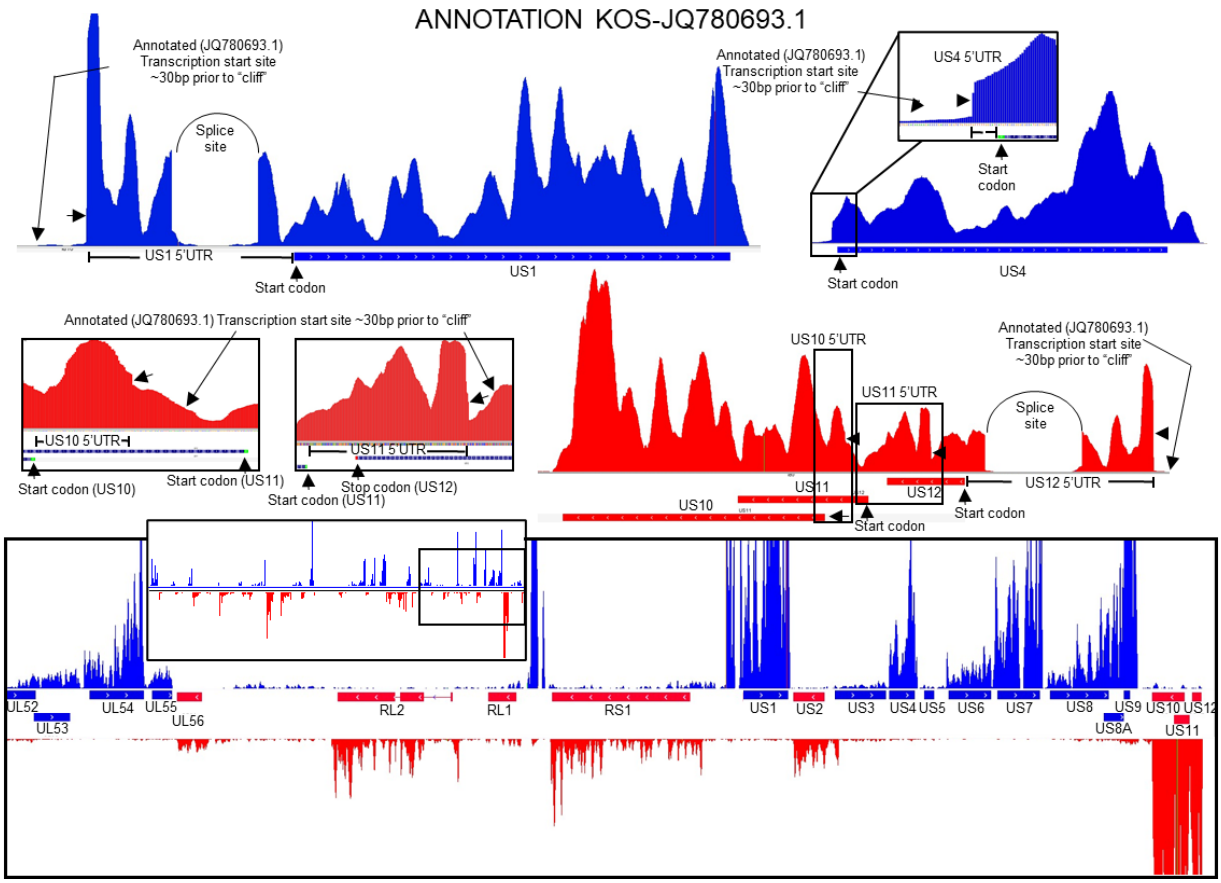

Figure S3.2. Full RNA-seq coverage of HSV1 genome (continued)

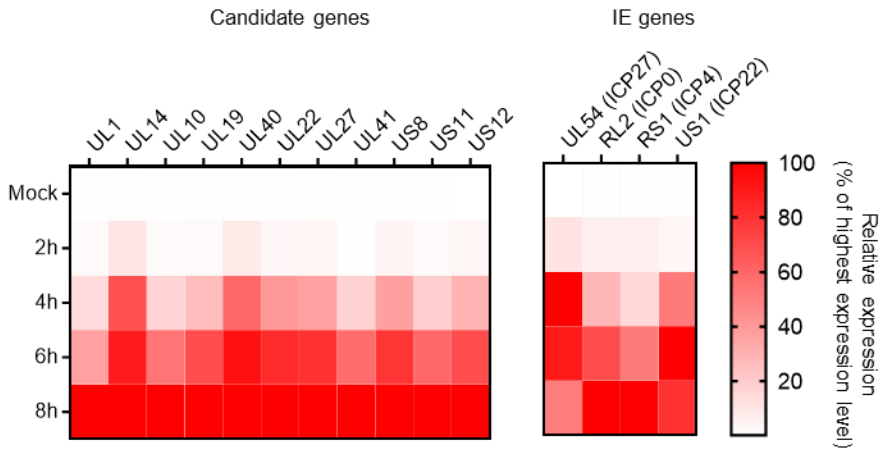

Figure S3.3. Relative mRNA expression level of the 10 late genes selected as candidates (left heatmap), as well as four immediate early genes (right heatmap). HSV1 mRNA expressions were obtained from a previously reported study by Rutkowski *et al.*, 2015[286]. Expression level was normalized as a percentage of the highest expression level across all time points.

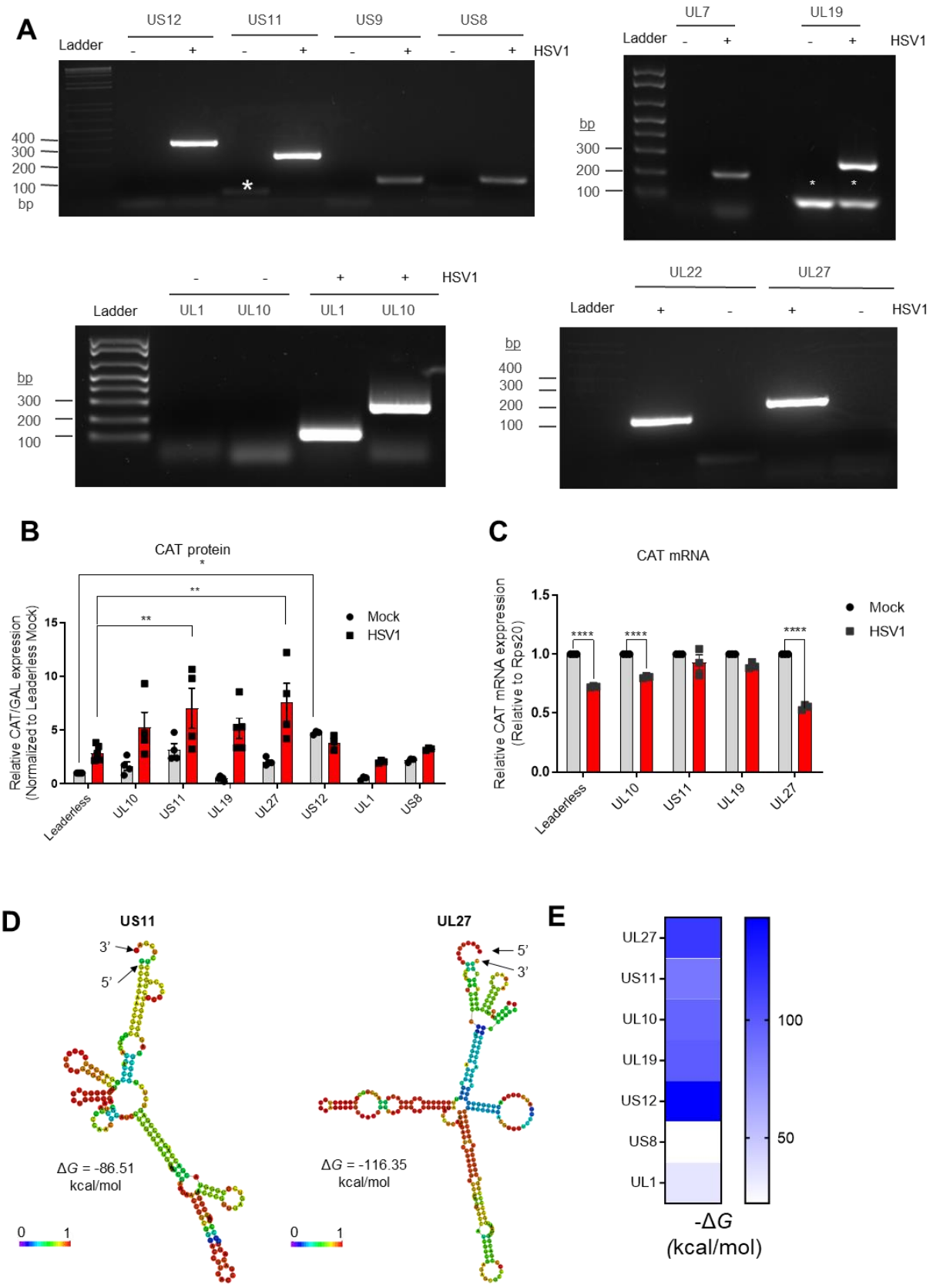
A
US12
US11
US9
US8
Ladder
HSV1
400
300
200
100
bp
UL7
UL19
UL1
UL10
UL22
UL27
B
CAT protein
Relative CAT/GAL expression
(Normalized to Leaderless Mock)
Mock
HSV1
Leaderless
UL10
US11
UL19
UL27
US12
UL1
US8
C
CAT mRNA
Relative CAT mRNA exppression
(Relative to Rps20)
D
US11
UL27
3'
5'
ΔG = -86.51
kcal/mol
ΔG = -116.35
kcal/mol
E
-ΔG
(kcal/mol)

Figure S3.4. Translation reporter screen for HSV1 leader that enhances translation during HSV infection

(A) Agarose gel visualization of other HSV1 5'leaders (including the rest of the 5' leader in Figure 3.2) amplified from total RNA of HSV1 infected cells. Negative controls (RNA from uninfected cells) confirmed the specificity of the PCRs products for HSV1 transcripts only. (*): non-specific band.

(B) Translation reporter assay to screen for HSV1 leaders that enhance translation during HSV1 infection. 4T1 cells were co-transfected with the CAT and β-GAL expression plasmids, the latter serving as a transfection control. 8 hours post-transfection, cells were infected with HSV-1716-GFP at an MOI of 5. Cells were lysed 18 hours post-infection and CAT expression was quantified by ELISA, while β-GAL activity was quantified by colorimetric assay using ONPG substrate. Two-way ANOVA with Tukey's *post-hoc* test was performed. Only significant tests were shown. n = at least 3 biological replicates. Error bars indicate standard error of the mean (sem). $*p < 0.05$, $**p < 0.01$.

(C) Relative CAT mRNA expression from CAT translation reporter assay. 4T1 cells were transfected/infected as in (C), then lysed using Trizol. RT-qPCR was then used to quantified mRNA expression of CAT mRNA normalized to the expression of the housekeeping gene *Rps20*. Two-way ANOVA with Sidak's *post-hoc* test was performed. n = 3 biological replicates. Only significant tests were shown. Error bars indicate standard error of the mean (sem). $*p < 0.05$, $**p < 0.01$, $****p < 0.0001$.

(D) Predicted secondary structure and folding free energy of US11 (left panel) and UL27 (right panel) leaders using Vienna RNAfold[33]. Color scale bars represent base-pairing probabilities.

(E) Heatmap representing folding free energy of candidate HSV1 leaders, calculated using Vienna RNAfold.

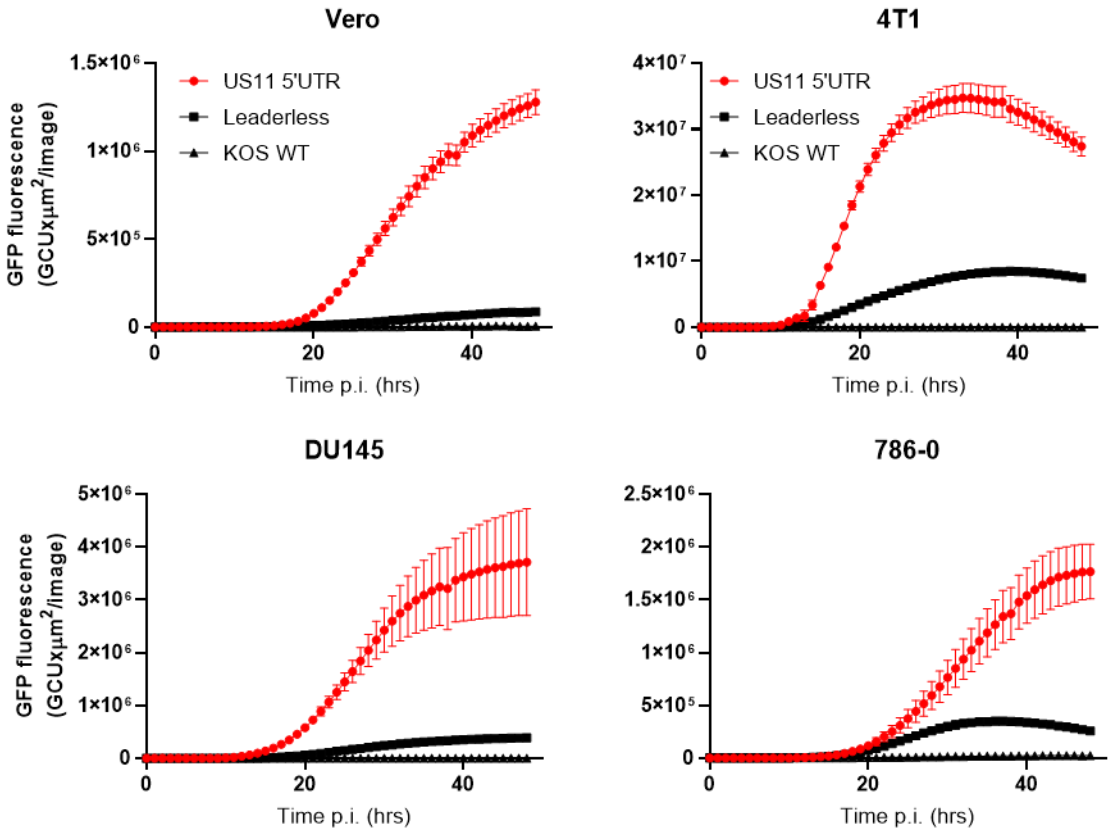

Figure S3.5. US11 leader enhancement is robust in different cell types and species.
A monolayer of the African green monkey kidney cell line Vero, mouse breast cancer cell line 4T1, human pancreatic cancer cell line DU145 and human renal carcinoma cell lines 786-O was infected with HSV1 KOS leaderless or HSV1 US11 5'leader at an MOI of 0.1, then GFP fluorescence intensity was observed for 48 hours using the IncuCyte live-cell imaging system.

Table S3.1. Oligonucleotides used in this study

Primer Name	Primer sequences (5'-3')	Description	Source
NotI_UL10utr_F	GGTGGTGCGGCCGCACACTCGTGTCCGGAGAGTGGATCG	CAT reporter cloning	This study
XhoI_UL10utr_R	GGTGGTCTCGAGTGGGGACGACGAGTGCGAACAGTACAC		
HindIII_US11utr_F	GGTGGTAAGCTTGGCCAGAACCGCCGTGCA		
NotI_US11utr_R	GGTGGTGCGGCCGCCTCGAGAGACACGGGGGGGAAC		
NotI_UL19utr_F	GGTGGTGCGGCCGCGGTCTGTTGGGGACACTGGGTTCTCCT		
XhoI_UL19utr_R	GGTGGTCTCGAGGGGGTCGCGTGGAGATCGGCT		
HindIII_UL27utr_F	GGTGGTAAGCTTACACTCTTTGCCTCGGTCTACC		
NotI_UL27utr-R	GGTGGTGCGGCCGCGGCGGGACTACGGGGG		
NotI_US12utr_F	GGTGGTGCGGCCGCGCAGACGGCGCCGGCCACGAA		
XhoI_US12utr_R	GGTGGTCTCGAGGCTTTTCCCGACGAGCAGGAAGCGG		
NotI_UL1utr_F	GGTGGTGCGGCCGCGGATACGGGGCTTGTGTGGC		
XhoI_UL1utr_R	GGTGGTCTCGAGAGCGCCTAGGGTCGGCACC		
NotI_US8utr_F	GGTGGTGCGGCCGCTCTTCTGGCGGGTTGGT		
XhoI_US8utr_R	GGTGGTCTCGAGGTCCCGGGGATAGCAG		

Table S3.1. Oligonucleotides used in this study (continued)

Primer Name	Primer sequences (5'-3')	Description	Source
AgeI_US11UTR_F	GTTGTTACCGGTGGCCAGAACCGCCGTGCACG	pTK-green cloning	This study
AgeI_UL27UTR_F	GTTGTTACCGGTACACTCTTTGCCTCGGTCTACC		
US11.e_Luc.s_R	ATGTTTTTGGCGTCTTCCATCTCGAGAGACACGGGGGGG		
UL27.e_Luc.s_R	ATGTTTTTGGCGTCTTCCATGGCGGGACTACGGGGGC		
US11.e_mCSF.s_R	AAGTAAATTCTGCAGCCACATCTCGAGAGACACGGGGGGG		
US11.e_Luc.s_F	CCCCCCCGTGTCTCTCGAGATGGAAGACGCCAAAAACAT		
UL27.e_Luc.s_F	GCCCCCGTAGTCCCGCCATGGAAGACGCCAAAAACAT		
US11.e_mCSF.s_F	CCCCCCCGTGTCTCTCGAGATGTGGCTGCAGAATTTACTT		
Luc.e_(GSG)_P2A_R	AGAAGTTCGTGGCTCCGGATCCCACGGCGATCTTTCCGCC		
Luc.e_(GSG)_P2A_F	GGCGGAAAGATCGCCGTGGGATCCGGAGCCACGAACTTCTC		
(GSG)_P2A_GFP.s_F	GGATCCGGAGCCACGAACTTCTCTCTGTTAAAGCAAGCAGGAGACGTG GAAGAAAACCCCGGTCCTGTGAGCAAGGGC		
GFP.e_KPNI_R	ACCACCGGTACCTTATCTAGATCCGGTGGATC		
No-UTRlig-LUC-F	ATGGAAGACGCCAAAAAC		
No-UTRlig-LUC-R	TAGCGCTAGCGGATCTG		
NoUTR-mCSF-F	ATGTGGCTGCAGAATTTACTTTTC		

Table S3.1. Oligonucleotides used in this study (continued)

Primer Name	Primer sequences (5'-3')	Description	Source
CAT-F	GCGTGTTACGGTGAAAACCT	qPCR	(Riley et al., 2010)[258]
CAT-R	GGGCGAAGAAGTTGTCCATA		(Riley et al., 2010)[258]
GFP-F	CTATGGTGAGCAAGGGCGAG		This study
GFP-R	GGCGGACTTGAAGAAGTCGT		
q-Luc-F	ATCCGGAAGCGACCAACGCC		
q-Luc-R	GTCGGGAAGACCTGCCACGC		
pTK-UTRseq	CGCCCCATTGACGCAAATGG		
mCSF.s-F	ATGTGGCTGCAGAATTTACTT		
mCSF.e-R	AGAAGTTCGTGGCTCCGGATCCTTTTTGGCCTGGTTTTTTG		
US6-F	ACAACCTGACCATCGCTTC		
US6-R	GCCCCCAGAGACTTGTTGTA		
US11-F	GGGCGACCCAGATGTTTACT		
US11-R	GGCTTCAGATGGCTTCGAGA		

3.7. Acknowledgements

H.-D.H. is a recipient of a University of Ottawa Graduate Scholarship, an Ontario Graduate Scholarship, and a University of Ottawa Faculty of Medicine Destination 2020 Scholarship. This work was supported in part by a Terry Fox Research Institute New Project Grant for T.A. and T.E.G., and a Canadian Cancer Society Research Institute Impact Grant (#706852) to T.A., T.E.G and H.-D.H.

CHAPTER 4. miR-223 Exerts Translational Control of Cholesterol Efflux and Inflammatory Pathways to Protect from Atherosclerosis

Authors: My-Anh Nguyen*, Huy-Dung Hoang*, Adil Rasheed, Anne-Claire Duchez, Hailey Wyatt, Mary Lynn Cottee, Tyson E Graber, Leah Susser, Michele Geoffrion, Erin E Mulvihill, Tommy Alain, Katey J Rayner

*These authors contributed equally to this work

Manuscript ready for submission

4.1. Author contributions

M.N., H.-D.H, K.J.R. conceived and designed the experiments. M.N. performed the majority of the *in vitro* and *in vivo* experiments in Figure 4.1-3 and Figure S4.1-3. H.-D.H. performed the ribosome profiling and the analysis in Figure 4.4, 4.5 and Figure S4.4, 4.5. M.N., H.-D.H., T.A. and K.J.R. reviewed and edited the final manuscript. All authors read and approved the final manuscript.

4.2. Abstract

Background: The prevention and treatment of cardiovascular diseases (CVD) has largely focused on lowering circulating cholesterol, yet a significant burden of atherosclerotic disease remains likely driven by residual inflammatory risk. Recently, microRNAs (miRNAs) have emerged as exciting therapeutic targets for CVD. miR-223 is a unique miRNA that regulates cholesterol metabolism and inflammation via targeting different components in both cholesterol biosynthesis pathway and NF-κB signaling pathways; however, its role in atherosclerosis has not been investigated. We **hypothesize** that miR-223 globally regulates core inflammatory pathways in macrophages in response to inflammatory and atherogenic stimuli thus limiting the progression of atherosclerosis.

Methods and Results: Loss of miR-223 in macrophages decreased *Abca1* gene and protein expression as well as cholesterol efflux to apoA1 and enhanced pro-inflammatory in response to inflammatory and atherogenic stimuli. In contrast, overexpression of miR-223 promoted the ability of macrophages to effectively efflux intracellular cholesterol and macrophage polarization toward the anti-inflammatory M2 phenotype. These beneficial effects of miR-223 are dependent on the inhibition of its target gene, the transcription factor *Sp3*. Consistent with the anti-atherogenic effects of miR-223 *in vitro*, mice receiving *miR223*$^{-/-}$ bone marrow (BM) exhibited increased plaque size as well as lipid content and elevated levels of serum inflammatory cytokines (*i.e.*, IL-1β). Deficiency of miR-223 in BM-derived cells also resulted in an increase in circulating pro-atherogenic cells (total monocytes and neutrophils) compared to control mice. Furthermore, the expression of miR-223 target gene (*Sp3*) and pro-inflammatory marker (*Il-6*) were enhanced whereas the expression of *Abca1* and anti-inflammatory marker (*Retnla*) were reduced in aortic arches from mice lacking miR-223 in BM-derived cells. To further understand the molecular mechanisms underlying the potential effects of miR-223 on the development of atherosclerosis *in vivo*, we characterized global translation profile of macrophages isolated from mice receiving wild-type or *miR223*$^{-/-}$ BM using ribosome profiling. In these analyses, we reveal a notable up-regulation of inflammatory signaling and lipid metabolism at the translation level, but less significant at the transcription level, indicating that miR-223 acts as a global regulator of protein translation during atherogenesis.

Conclusions: Our study demonstrates that miR-223 can protect against atherosclerosis by acting as a crucial modulator of macrophage cholesterol efflux and inflammation.

4.3. Introduction

Atherosclerosis is a chronic inflammatory disease that is driven by the interplay of excess cholesterol accumulation in the vessel wall and a maladaptive immune response. It is characterized by retention of cholesterol-rich lipoproteins (LPs) in susceptible areas of the arterial vasculature, followed by chronic endothelial activation and recruitment of circulating monocytes into the vascular intima[233,334,335]. In the subendothelial space, the majority of recruited monocytes differentiate into macrophages, a process driven by macrophage colony-stimulating factor (M-CSF) and other factors[336]. Monocyte-derived macrophages then scavenge retained modified LPs, which eventually transform them into cholesterol-laden foam cells. However, excessive cholesterol uptake, leading to free cholesterol accumulation in macrophage-derived foam cells, triggers the activation of downstream cascades including NOD-, LRR- and pyrin domain-containing protein 3 (NLRP3) inflammasome, Toll-like receptor (TLR) and NFκB signaling pathways, resulting in the secretion of pro-inflammatory mediators (cytokines, chemokines, and reactive oxygen and nitrogen species). These inflammatory signals induce the transmigration of additional inflammatory cells including monocytes into the intima, further aggravating plaque inflammation[234,337–339]. Furthermore, free cholesterol accumulation impairs endoplasmic reticulum (ER) function and activates ER stress responses, which if prolonged and combined with other insults, leads to cell death and the formation of a pro-thrombotic necrotic core[340]. Despite significant achievements in the diagnosis, prevention and treatment, atherosclerosis remains the leading cause of morbidity and mortality worldwide[341]. Traditionally, lipid lowering has been the gold-standard therapy for atherosclerosis, yet a significant burden of atherosclerotic disease remains even in the setting of low plasma cholesterol, likely as a result of residual inflammatory

risk[342,343]. Thus, there is an urgent need to better understand the molecular mechanisms that govern atherogenesis particularly those that drive inflammation.

Over the past decade, microRNAs (miRNAs) have emerged as key modulators and fine-tuners of multiple signaling pathways involved in atherosclerosis[344,345]. miRNAs are defined as highly conserved small RNA sequences of 20 to 23 nucleotides that contain complementary sequences for specific target messenger RNAs (mRNAs). *Via* binding to the 3'-untranslated regions (UTR), miRNAs post-transcriptionally regulate gene expression by degradation and/or translational inhibition of their bound targets. Notably, one miRNA can simultaneously repress multiple target genes through seed-based targeting. In addition, one functional gene network can be regulated by a group of miRNAs, providing a mechanism to coordinate complex gene expression programs and thereby modulate many aspects of cellular homeostasis and physiology[346–348]. Indeed, accumulating evidence has highlighted the importance of miRNAs in regulating lipoprotein homeostasis, vascular inflammation, leukocyte recruitment/activation, and vascular smooth muscle function[349,350], thus controlling each stage of atherosclerosis from development, progression to disruption. One of the first miRNAs to be studied for its role in cholesterol regulation was miR-223-3p (hereafter referred to as miR-223), which controls intracellular cholesterol levels through directly repressing genes involved in cholesterol biosynthesis (3-hydroxy-3-methylglutaryl-CoA synthase 1/HMGCS1) and methylsterol monooxygenase1/SC4MOL) and cholesterol uptake (scavenger receptor class B member 1/SR-BI) in hepatocytes and coronary arterial endothelial cells[351]. In addition to cholesterol metabolism, miR-223 has been shown to suppress TLR4-NF-κB pathway, leading to a reduction in pro-inflammatory cytokine production in LPS activated macrophages[352], possibly as a result of its direct targeting of IKKα and reduction in non-canonical NF-κB activation[353]. This feedback likely

prevents macrophages from becoming overactivated while priming them for future NF-κB signaling events[353]. Finally, genome-wide miRNA screens have identified miR-223 as a negative regulator of NLRP3 inflammasome activation by directly suppressing NLRP3 expression and reducing NLRP3-dependent induction of IL-1β in primary neutrophils[354,355]. Together, these studies have established the importance of miR-223 in cholesterol metabolism and inflammation *in vitro*, yet its role in lipid-driven inflammatory diseases *in vivo* has not been established.

Given the intersection of cholesterol and inflammation in the pathogenesis of atherosclerosis, we set out to determine the contribution of miR-223 in atherosclerosis development, particularly its role in myeloid-derived cells that perpetuate inflammation in the plaque. We find that loss of miR-223 in macrophages promotes a pro-inflammatory phenotype and dampens macrophage cholesterol efflux *in vitro*. These effects of miR-223 are largely dependent on the inhibition of its target gene, the transcription factor Specificity Protein 3 (referred to as *Sp3* in mouse and *SP3* in human). Consistent with pro-atherogenic effects *in vitro*, deletion of miR-223 in bone marrow (BM)-derived cells in *Ldlr*$^{-/-}$ mice fed an atherogenic diet results in an increase in plaque size as well as lipid content, plasma inflammatory cytokines, and circulating pro-atherogenic cells compared to wild-type (WT) controls. Furthermore, the expression of pro-inflammatory markers is enhanced whereas the expression of anti-inflammatory markers is reduced in aortic arches from mice lacking miR-223 in BM-derived cells. Interestingly, we find that miR-223 exerts its anti-atherogenic effects by shifting the overall ribosomal profile of inflammatory and lipid metabolism genes, suggesting that miR-223 acts to globally alter macrophage translational activity in the atherogenic environment. Thus, our study demonstrates that miR-223 can protect against atherosclerosis by acting as a central modulator of macrophage cholesterol efflux and inflammation.

4.4. Materials and Methods

4.4.1. Reagents

Acetylated human LDL (BT-906) and human apoA1 (BT-927) were purchased from Alfa Aesar (Thermo Fisher Scientific Inc.). Control mimic and mmu-miR-223-3p mimic (miRIDIAN microRNA mimic) were obtained from Dharmacon (Horizon Discovery Group). Lipofectamine RNAiMAX (DNase and protease-free) was purchased from Thermo Fisher Scientific Inc. Lipopolysaccharides (LPS) was obtained from Sigma-Aldrich. Recombinant mouse IFN-γ and IL-4 were purchased from R&D Systems. All antibodies and stains used in flow cytometry experiments were obtained from BD Biosciences.

4.4.2. Mice

C57BL6 WT mice were purchased from Charles River Laboratories. *miR223*$^{-/-}$mice (on a C57BL6 background) were kindly provided by Dr. Guo-Chang Fan, University of Cincinnati College of Medicine, United States. *Abca1*$^{-/-}$ mice were kindly provided by Dr. Thomas A. Vallim, University of California Los Angeles, United States. *Ldlr*$^{-/-}$ mice were purchased from Jackson Laboratories and were bred in-house. All animal studies were permitted by the University of Ottawa Animal Care and Use Committee in accordance with the international standards established by the Canadian Council on Animal Care.

4.4.3. Macrophage isolation and polarization

Bone marrow-derived macrophages (BMDMs) were harvested from femurs of different mice and differentiated into macrophages using DMEM supplemented with 10% (v/v) FBS, 20% (v/v) L929 conditioned media and 1% (v/v) P-S for 7 days. To polarize macrophages to M1 or M2,

cells were treated with either 100 ng/ml LPS and 100 ng/ml IFN-γ or 10 ng/ml IL-4, respectively, for 24h.

4.4.4. Cell transfection with miRNA mimics

Macrophages were transfected with control mimic or mmu-miR-223-3p mimic (miRIDIAN microRNA mimic) at a concentration of 100nM using Lipofectamine RNAiMAX as previously described[356–358]. Briefly, transfection of macrophages was performed in OPTIMEM media overnight. The next day, the same volume of DMEM containing 20% (v/v) FBS was added and transfected cells were harvested 72 hours after transfection. Similarly, macrophages were transfected with 25nM negative (non-silencing) control siRNA or *Sp3* siRNA (FlexiTube siRNA – QIAGEN) for 72 hours.

4.4.5. Cholesterol efflux

BMDMs were transfected with control mimic or miR-223 mimic for 48 hours and subsequently, were loaded with 37.5 μg/ml acetylated LDL and labeled with 1 μCi/ml [^{3}H] cholesterol (Perkin Elmer) for 24 hours. The next day, cells were washed extensively with PBS and equilibrated in 2% fatty acid-free BSA in DMEM media for 3 hours before being treated with 25 μg/ml apoA1 (Alfa Aesar) for 6 hours or 24 hours. Medium and cellular [^{3}H] were counted using liquid scintillation counting and expressed as a percentage of total cellular [^{3}H] cholesterol content.

4.4.6. miRNA and gene expression analysis

For miRNA expression analysis, total RNA was isolated using Trizol (Invitrogen) and the expression levels of miRNAs of interest was measured by qRT-PCR using miScript II Reverse

Transcription kit, miScript Primer Assays and Quantitect SYBR Green (Qiagen), in which the expression of candidate miRNAs was normalized to RNA, U6 small nuclear 6, pseudogene (QIAGEN). For gene expression analysis, total RNA was isolated using Trizol and reverse transcribed using iScript Reverse Transcription Supermix for qRT-PCR (Bio-Rad). qRT-PCR was performed using the SsoAdvanced Universal SYBR Green Supermix (Bio-Rad) and gene expression was normalized to *Hprt* and *18S*. The primers used are:

Gene	***Forward***	***Reverse***
Abca1	GCTTGTTGGCCTCAGTTAAGG	GTAGCTCAGGCGTACAGAGAT
Sp3	AATCAAACCTTACTCGCCTCTG	GCACATTAGCGACTACTTGAGTT
Tnfa	CCCTCACACTCAGATCATCT	GCTACGACGTGGGCTACAG
Nos2	CGTTCTCAGCCCAACAATACAAGA	GTGGACGGGTCGATGTCAC
Il1b	GCAACTGTTCCTGAACTCAACT	ATCTTTTGGGGTCCGTCAACT
Il6	TAGTCCTTCCTACCCCAATTTCC	TTGGTCCTTAGCCACTCCTTC
Il10	GCTCTTACTGACTGGCATGAG	CGCAGCTCTAGGAGCATGTG
Arg1	GGTCCACCCTGACCTATGTGT	ACGATGTCTTTGGCAGATATGC
Retnla	CTGGGTTCTCCACCTCTTCA	TGCTGGGATGACTGCTACTG
Pknox1	GGTGGTCACGGAGTTAAAAACA	TCGGCATCCATTGGGGTCT
Rasa1	TGTGGTGATTACTACATTGGTGG	CGCCTTCTATCTTCTACTGGCTC
Nfat5	GTGACTATCCTTCCTAATGCCCT	GGTCTCTGGGTTGTATGCCT

4.4.7. Western blot analysis

Cells were washed in ice-cold PBS and lysed in ice-cold RIPA buffer supplemented with protease inhibitor cocktail (Roche). Proteins (50μg) were subjected to 4-20% SDS-PAGE and transferred to PVDF membranes (Bio-Rad) for immunoblot analysis[357]. PVDF membranes were blocked with 5% (w/v) milk in TBST and incubated overnight with antibodies against ABCA1 (Novus Biologicals) and HSP90 (Santa Cruz Biotechnology). Goat anti-mouse or anti-rabbit IRDye® secondary antibodies were used for detection on a LI-COR Odyssey infrared imaging system (LI-COR Biosciences).

4.4.8. Atherosclerosis PCR pathway array analysis

The purity and integrity of RNA isolated from BMDMs isolated from WT mice or *miR223*$^{-/-}$ mice was confirmed using the Agilent Bioanalyzer (Agilent Technologies) as per the manufacturer's instructions. A total of 1 μg of RNA was reverse transcribed with the RT^2 First Strand kit (Qiagen) and used for the mouse atherosclerosis RT^2 Profiler PCR Array kit (Qiagen) as per manufacturer's instructions. Using the manufacturer's PCR Array Data Analysis software: average data was normalized and used to determine the ΔΔCT. A full table of genes found on this PCR array can be found at https://b2b.qiagen.com/~/media/genetable/pa/mm/03/pamm-038za

4.4.9. Atherosclerosis studies

For BM transplantation study, 14-week-old recipient male and female *Ldlr*$^{-/-}$ mice were subjected to whole-body irradiation (10 Gys) followed by injection of BM donor cells (1 x 10^6 cells) by retro-orbital injection. Mice were randomized to receive either WT or *miR223*$^{-/-}$ bone marrow cells. The mice were allowed to recover for 6 weeks. Mice were then fed an adjusted calories western diet (21% fat, 0.2% cholesterol; Harlan Teklad) for 12 weeks.

Enzymatic cholesterol assays: Plasma was collected from the saphenous vein or by cardiac puncture, and total cholesterol was assayed using the Cholesterol-E kit (Wako).

Flow cytometry: Peripheral blood was collected from the saphenous vein or by cardiac puncture to EDTA-coated microvettes (Sarstedt). For lysing red blood cells, 50ul of whole blood was mixed with 50 ul of deionized water and incubated with 1 ml of 1x PharmLyse (BD Biosciences) for 10 minutes at room temperature. The lysed cells were resuspended in 100 ul of Brilliant Staining Buffer (BD Biosciences). To prevent non-specific antibody binding, the cells were incubated with Fc Block (1ug; BD Biosciences) for 5 minutes at room temperature. The cells

were stained with the following antibodies at 4°C for 20 minutes: B220 BV786 (0.1875 ug/test), Ly6C BV605 (0.75 ug/test), CD8a BV510 (0.1875 ug/test), CD11b BV421 (0.21875 ug/test), CD4 PerCP-Cy5.5 (0.06 ug/test), Ly6G PE-Cy7 (0.25 ug/test), CD45 APC-Cy7 (0.045 ug/test), and CD3e APC (1 ug/test). Staining for dead cells was performed with Fixable Viability Stain 700 (1 ul/test) at 4°C for 30 minutes. Cells were fixed using Cytofix (BD Biosciences) for 15 minutes at 4°C. The cells were resuspended in buffer and sample acquisition was performed on a FACS (fluorescence-activated cell sorting) Aria IIIu flow cytometer (BD Biosciences). The data was analysed using FlowJo (Tree Star). Neutrophils were identified as $CD11b^+$ $Ly6C^+$ $Ly6G^+$, monocytes as $CD11b^+$ $Ly6C^+$, B cells as $B220^+$, and T cells as $CD3e^+$.

Immunohistochemical analysis: Mice were perfused with saline, and aortic root, ascending as well as descending aorta, liver, and spleen were collected as previously described[358,359]. Briefly, the aortic sinus was embedded in optimum cutting temperature (OCT) compound medium, frozen, sectioned (10 μm) and stained for hematoxylin & eosin for quantifications, where a minimum of 8-10 sections per animal were measured across the length of the entire aortic root. For detection of neutral lipid, oil red O staining was performed as previously described[359]. All histological analyses of the aortic sinus were performed in accordance with AHA guidelines[360].

Cytokine assays: Serum cytokines were analyzed using Bio-Plex Pro Mouse Cytokine 23-plex Assay (#M60009RDPD; Bio-Rad) as per manufacturer's instructions.

4.4.10. Gene expression analysis in mouse aorta

The aortic arch was excised from the heart, and tissue segments were homogenized in Trizol (Invitrogen) using microbeads along with the Bullet Blender. Total RNA was reverse transcribed using iScript Reverse Transcription Supermix for qRT-PCR (Bio-Rad). For droplet digital RT-

PCR (ddRT-PCR), cDNA was mixed with QX200 ddPCR EvaGreen Supermix (Bio-Rad) according to the manufacturer's protocol and droplets were prepared using QX200 droplet generation oil on a QX200 Droplet Generator (Bio-Rad). Droplets were subjected to PCR using a C1000 thermocycler (Bio-Rad) using the cycling conditions: 95oC for 5 min, followed by 45 cycles of 95°C for 30 s at a ramp rate of 2°C/s and 60°C for 1 min at a ramp rate of 2°C/s. Positive/negative droplets were counted by a QX200 Droplet Reader (Bio-Rad), and gene expression was normalized to *B2m* and *Actb*.

4.4.11. Ribosome profiling

Ribosome profiling was performed using a modified protocol from previously described protocols on 2 biological replicates[32,301,361]. BMDMs were growth and differentiated on a 15 cm plates. Cells were treated with cycloheximide (100 µg/ml) for 1 minute at 37°C, then lysed using polysome lysis buffer (Tris-HCl 20 mM, NaCl 150 mM, MgCl2 5 mM, Triton X-100 1% v/v, DTT 1 mM, TURBO DNase (Thermo Fisher) 2U/ml, cycloheximide 100 µg/ml). Lysates were split into two parts for two parallel workflows of RNA-Seq and Ribo-Seq. For Ribo-Seq, lysate was digested with 2U of RNAse T1 per 1 µg of total RNA (determined by Ribogreen RNA Assay Kit, Thermo Fisher) on ice for 1 hour. RNAse T1 was selected for treatment of ribosome-mRNA complex as it was shown to be able to effectively convert polysomal mRNA into monosome while preserving the ribosome integrity[362] and confirmed during our optimization with polysomal RNA extract from BMDMs. The resulting monosomes were enriched by size-exclusion chromatography (Illustra MicroSpin S-400 HR columns; GE Healthcare), followed by size selection of ribosome-protected mRNA footprints (RPFs) using a denaturing 15% TBA-Urea gel (Invitrogen). The area corresponding to 28-34 nucleotides was excised and extracted using the Zymo Research small-RNA PAGE recovery kit (Zymo Research) and sent for sequencing at Fasteris SA, Switzerland.

The sequencing facility performed rRNA depletion using the Total RNA Gold kit, prior to sequence on HiSeq 4000 with a read length of 50 nucleotides. For RNA-Seq, total RNA was extracted from the lysate using the Trizol method and the extracted RNA was sent for sequencing at Fasteris SA, Switzerland. Briefly, the sequencing facility prepared the RNA library using the Total RNA library preparation Gold kit (Illumina), then sequenced on the HiSeq 4000 platform with a read length of 150 nucleotides.

For RNA-Seq, reads were mapped to the mouse mm10 genome using HISAT2[302]. Gene expression was calculated with Cufflinks[304] using the comprehensive gene annotation from Gencode for mouse, version M22. For mapping of ribosome footprints, rRNA and tRNA reads were removed by mapping reads to mouse rRNA and tRNA sequences, extracted from UCSC. Unaligned reads were then mapped to the mouse mm10 genome using Bowtie2[250]. Gene expression was then calculated using reads mapped to the CDS regions extracted from the comprehensive gene annotation from Gencode for mouse, version M22.

4.4.12. Statistics

Data shown is either mean ± SEM of at least 3 independent experiments or a single representative experiment that was performed in triplicate. Comparison between 2 groups was made using Student's t-test ($p \leq 0.05$) and comparison between groups was performed by one-way ANOVA ($p \leq 0.05$) using Prism GraphPad, as indicated in the Figure legends.

4.5. Results

4.5.1. miR-223 positively regulates ABCA1 expression and promotes macrophage cholesterol efflux in vitro

ABCA1 plays a key role in stimulating the efflux of cholesterol from macrophages, thereby reducing foam cell formation and the development of atherosclerosis[363–365]. miR-223 has been found to indirectly induce ABCA1 expression and cholesterol efflux in hepatocytes via directly targeting the transcription factor SP3, which acts as a repressor of ABCA1 expression[351,366,367]. To confirm that miR-223 similarly regulates cholesterol efflux in macrophages, we first examined the expression of ABCA1 and *Sp3* in bone marrow-derived macrophages (BMDMs) transfected with miR-223 or isolated from miR223$^{-/-}$mice. As expected, over-expression of miR-223 suppressed, whereas loss of miR-223 elevated, *Sp3* expression (**Figure 4.1A**). In contrast, the expression of ABCA1 decreased or increased when miR-223 was knocked down or over-expressed, respectively (**Figure 4.1B**). We next investigated the effects of this miR-223 on macrophage cholesterol efflux and indicated that macrophages transfected with miR-223 exhibited enhanced cholesterol efflux to apoA1 relative to control (25.3 ± 3.2% for control mimic *versus* 34.6 ± 2.0% for miR-223; $p \leq 0.05$) (**Figure 4.1C**).

Atherosclerotic lesions have a highly heterogeneous phenotype as indicated by the simultaneous co-existence of various macrophage subpopulations[368]. To determine whether or not macrophage polarization to a pro-inflammatory M1 or alternative M2 state impacts the effect of miR-223 on cholesterol efflux, we performed cholesterol efflux assays on three well-characterized macrophage subtypes transfected with miR-223 or isolated from *miR223*$^{-/-}$ mice. We confirmed that miR-223 over-expression increased apoA1-mediated cholesterol efflux from different

macrophage subtypes including resting (Mo) macrophages, pro-inflammatory (treated with LPS + IFN-γ, M1) macrophages and anti-inflammatory (treated with IL-4, M2) macrophages. Conversely, Mo macrophages and M2 macrophages, but not M1 macrophages, from *miR223*$^{-/-}$ mice showed decreased cholesterol efflux to apoA1 (**Figure 4.1D**). Supporting the reduced cholesterol efflux capacity of different macrophage subtypes isolated from *miR223*$^{-/-}$ mice was a significant reduction in *Abca1* expression at the mRNA level (**Figure S4.1A**). Interestingly, knockdown of *Sp3* using short interfering RNA (siRNA) relieved the inhibitory effect of miR-223 deficiency on cholesterol efflux (**Figure 4.1E**), indicating that miR-223 regulation of macrophage cholesterol efflux is dependent on *Sp3*. Taken together, these data confirm that miR-223 can indirectly enhance macrophage ABCA1 expression and cholesterol efflux through *Sp3*.

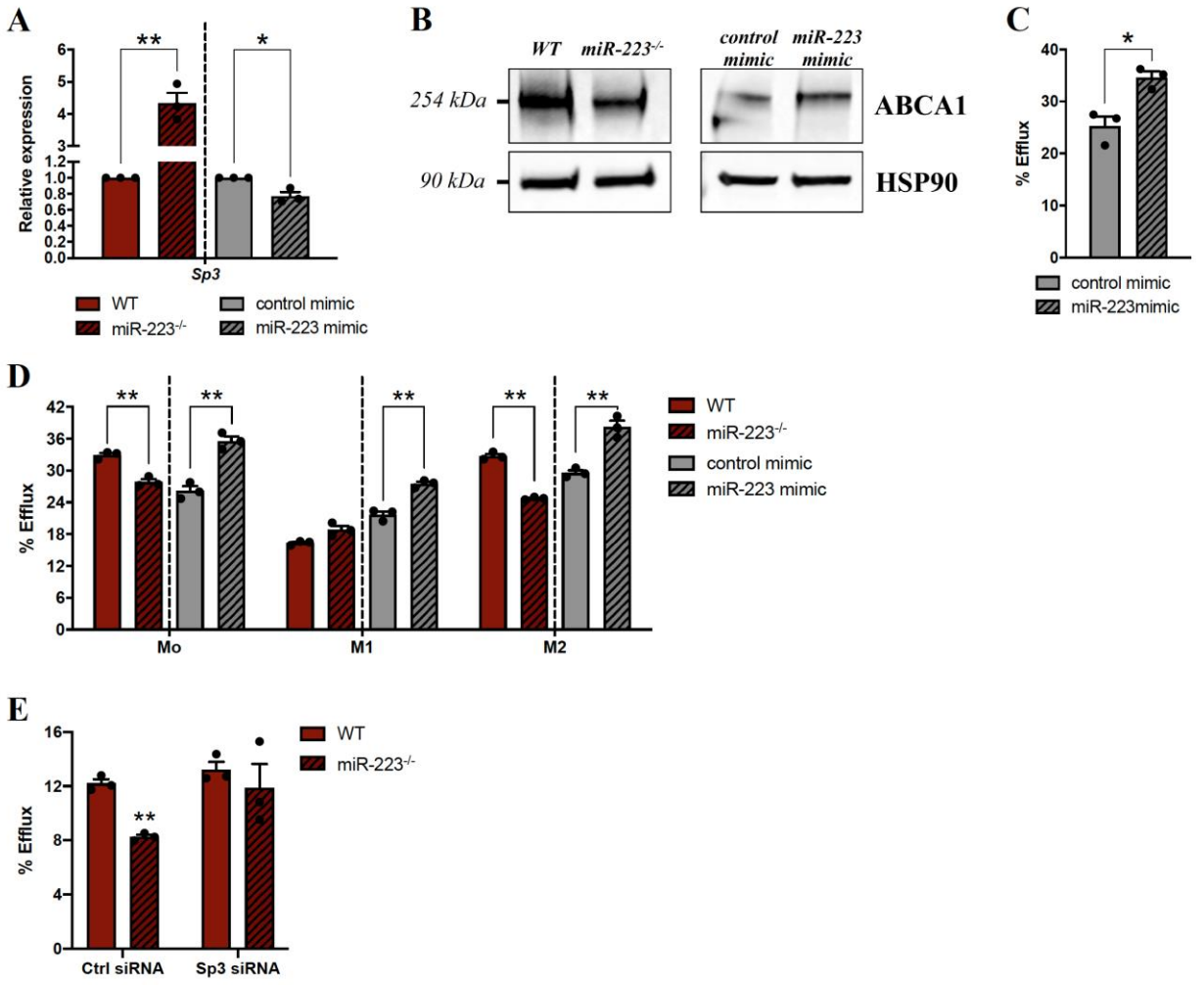

Figure 4.1. miR-223 positively regulates ABCA1 expression and promotes macrophage cholesterol efflux. BMDMs were transfected with control mimic/miR-223 mimic (100 nM) or isolated from WT/miR-223$^{-/-}$ mice. The expression of (**A**) *Sp3* and (**B**) ABCA1 was examined. (**C**) Cholesterol efflux to apoA1 (25 μg/ml) was measured for 24h. Graphs represent the means ± SEM from n=3 independent experiments, *p<0.05 **p<0.01 by Student's t-test. Western blot is representative of a single experiment done in triplicate (n=3) *p<0.05 by Student's t-test. (**D**) BMDMs were cholesterol-loaded and polarized into M1 macrophages or M2 macrophages by induction with LPS (100 ng/ml)/IFN-γ (100 ng/ml) or IL-4 (10 ng/ml), respectively, for 24h. Cholesterol efflux to apoA1 (25 μg/ml) was measured for 24h. **p<0.01 by Student's t-test (**E**) BMDMs isolated from WT/miR-223$^{-/-}$ mice were transfected with control siRNA or *Sp3* siRNA (25nM). Following siRNA transfection, BMDMs were cholesterol-loaded for 24h, and cholesterol efflux to apoA1 (25 μg/ml) was measured for 24h. Graphs represent the experiments performed in triplicate (n=3), **p <0.01 by Student's t-test.

4.5.2. miR-223 suppresses macrophage pro-inflammatory activation and promotes macrophage polarization toward the anti-inflammatory phenotype in vitro

Given the important role of miR-223 in regulating the NF-κB signaling pathway[352,353], we sought to determine if and how miR-223 instructs macrophage inflammatory polarization. We treated BMDMs isolated from *miR223*$^{-/-}$ mice with either LPS + IFNγ (to induce M1) or IL-4 (to induce M2). qRT-PCR analysis showed that pro-inflammatory cytokines *Tnfa*, *Il-1b*, *Il-6*, and *Nos2* were significantly increased in *miR223*$^{-/-}$ macrophages compared with WT cells. In contrast, overexpression of miR-223 in BMDMs repressed the expression of these M1 macrophage markers (**Figure 4.2A**). Expression of M2-associated genes *Il-10*, *Arg1*, and *Retnla*, on the other hand, was decreased in macrophages isolated from *miR223*$^{-/-}$ mice and elevated in macrophages transfected with miR-223 mimic, as compared to control cells (**Figure 4.2B**). Thus, miR-223 can suppress macrophage pro-inflammatory activation while promoting macrophage polarization toward the anti-inflammatory M2 phenotype *in vitro*, in consistent with a previous study[369].

SP3 has been shown to drive the production of inflammatory cytokines in cancer cells via stimulating NFκB-mediated transcription activation[370]. We, therefore, postulated that SP3 might mediate the effects exerted by miR-223 on macrophage polarization. To address this, we first measured the expression of M1 and M2 markers in macrophages where *Sp3* was knocked down by siRNA. Inhibition of *Sp3* resulted in a phenotype similar to that of miR-223 overexpression, with decreased expression levels of M1-associated genes such as *Nos2* and *Tnfa* (**Figure S4.1B**) and increased expression levels of M2-associated genes such as *Arg1* and *Retnla* (**Figure S4.1C**), suggesting that *Sp3* may mediate the effects of miR-223 on macrophage activation. To further confirm the importance of Sp3 in modulating miR-223-controlled macrophage polarization, we performed loss-of-function analyses in *miR223*$^{-/-}$ macrophages by knocking down *Sp3*. In the

absence of *Sp3*, miR-223 deficiency did not alter the expression of M1 markers (*Tnfa*, *Il-1b*, *Il-6*, and *Nos2*, **Figure 4.2C**) or M2 markers *Arg1* and *Retnla* (**Figure 4.2D**). These data confirm that the effect of miR-223 on macrophage polarization is partially attributable to *Sp3*. Because miR-223 can regulate ABCA1 expression, and ABCA1 has been shown to control macrophage inflammatory response by regulating lipid raft, membrane cholesterol[371–375] and inflammasome activation[376], we next tested whether miR-223 can also modulate macrophage inflammation *via Abca1*. Interestingly, the effects of miR-223 overexpression on M2 polarization were blunted in *Abca1*$^{-/-}$ macrophages (**Figure 4.2E**), yet the inhibitory effects on M1 responses were still maintained in the absence of *Abca1* (**Figure 4.2F**). Taken together, these data demonstrate that miR-223 modulates the inflammatory response in both M1 and M2 macrophages primarily *via* regulation of *Sp3* expression.

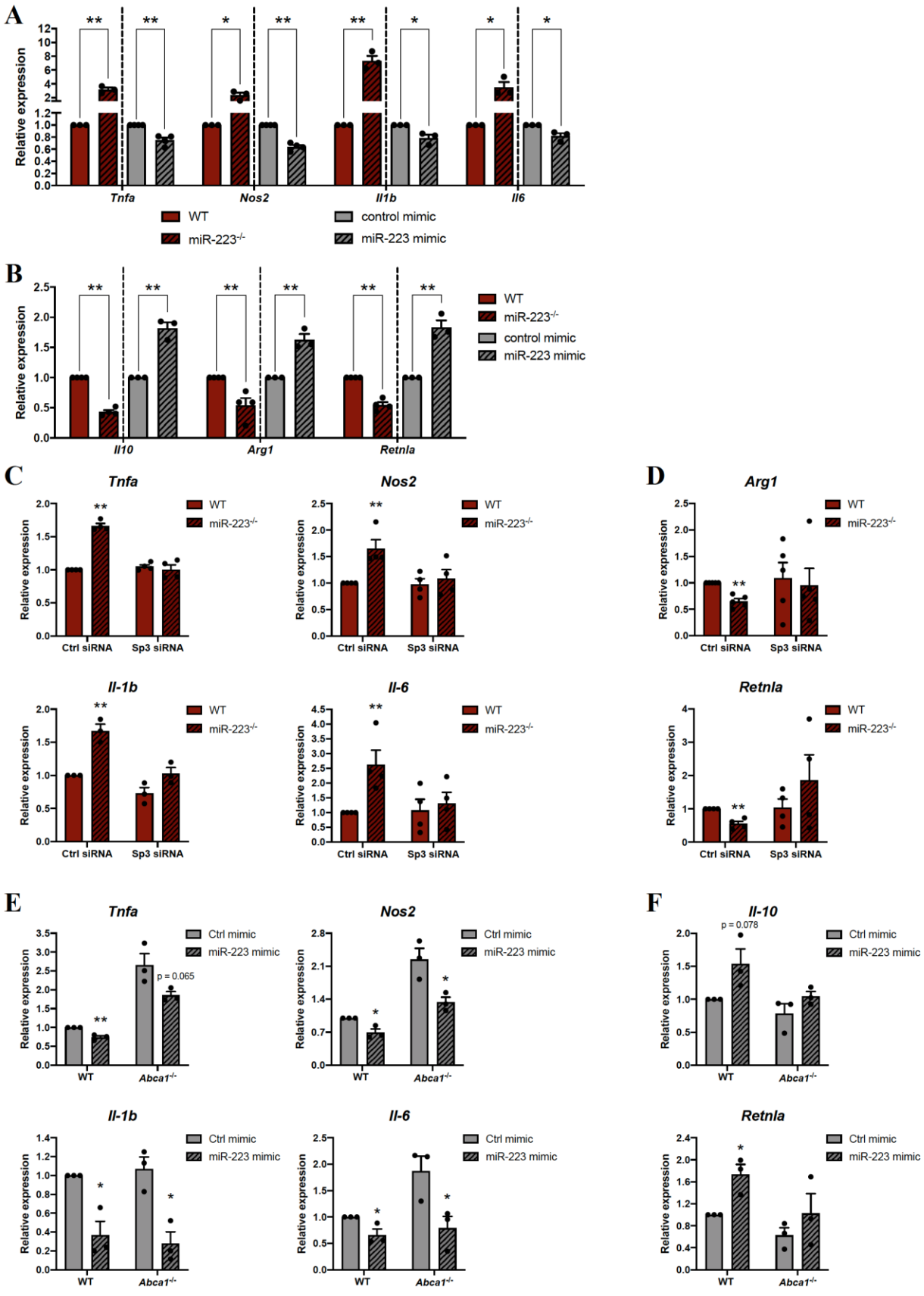
A
Relative expression
Tnfa
Nos2
Il1b
Il6
WT
miR-223-/-
control mimic
miR-223 mimic
B
Relative expression
Il10
Arg1
Retnla
C
Tnfa
Nos2
Il-1b
Il-6
Ctrl siRNA
Sp3 siRNA
D
Arg1
Retnla
E
Tnfa
Nos2
Il-1b
Il-6
Ctrl mimic
miR-223 mimic
p = 0.065
WT
Abca1-/-
F
Il-10
p = 0.078
Retnla

Figure 4.2. miR-223 suppresses macrophage pro-inflammatory activation and promotes macrophage polarization toward the anti-inflammatory phenotype. BMDMs transfected with control mimic/miR-223 mimic (100nM) or isolated from WT/miR-223$^{-/-}$ mice were polarized into either M1 macrophages by induction with LPS (100 ng/ml)/IFN-γ (100 ng/ml) or M2 macrophages by induction with IL-4 (10 ng/ml) for 24h. Expression levels of (**A**) M1 markers (*Tnfa*, *Nos2*, *Il-1b*, *Il-6*) and (**B**) M2 markers (*Il-10*, *Arg1*, *Retnla*) were measured by qPCR. *p<0.05 **p<0.01 by Student's t-test. (**C-D**) Inhibition of SP3 partially relieves the effects of miR-223 on macrophage polarization. BMDMs isolated from WT/miR-223$^{-/-}$ mice were transfected with control siRNA or *Sp3* siRNA (25nM) Expression levels of (**C**) M1 markers (*Tnfa*, *Nos2*, *Il-1b*, *Il-6*) and (**D**) M2 markers (*Arg1*, *Retnla*) were measured by qPCR. *p<0.05 **p<0.01 by Student's t-test. (**E-F**) miR-223 alters M2 activation but not M1 activation dependently of ABCA1. BMDMs isolated from WT/*Abca1*$^{-/-}$ mice were transfected with control mimic or miR-223 mimic (100nM). Expression levels of (**E**) M1 markers (*Tnfa*, *Nos2*, *Il-1b*, *Il-6*) and (**F**) M2 markers (*Il-10*, *Retnla*) were measured by qPCR. Graphs represent the means ± SEM from n=3-4 independent experiments, *p<0.05 **p<0.01 by Student's t-test.

4.5.3. Deletion of miR-223 in BM-derived cells promotes atherogenesis and enhances inflammatory signaling

Considering that miR-223 plays a key role in regulating macrophage cholesterol efflux and inflammation *in vitro*, we next aimed to define the contribution of miR-223 to the pathogenesis of atherosclerosis *in vivo* and the mechanism underlying its effects. To elucidate the role of miR-223 in bone marrow (BM)-derived cells, we lethally irradiated *Ldlr*$^{-/-}$ mice and reconstituted them with WT or *miR223*$^{-/-}$ BM. BM-transplanted mice were then fed a Western-type high cholesterol diet (HCD) for 12 weeks (**Figure 4.3A**). Reconstitution of the hematopoietic compartment after transplantation of WT or *miR223*$^{-/-}$ BM cells appeared normal as circulating levels of leukocytes and lymphocytes were similar between the two groups at 6 weeks after BM transplantation, prior to start of the HCD (**Figure S4.2A**). Examination of aortic root lesions demonstrated male mice lacking miR-223 in BM-derived cells had a 51.3% increase in plaque size relative to control mice (n=6/group, p=0.0729), whereas plaque burden in the aortic root of female mice receiving *miR223*$^{-/-}$ BM was unchanged (**Figure 4.3B**). Quantification of lipid accumulation in aortic sinus lesions by oil red O staining demonstrated a corresponding 20% increase in lipid plaque in mice receiving

miR223$^{-/-}$ BM compared with that of controls (**Figure 4.3C**, $p \leq 0.05$). There were no significant differences in total plasma cholesterol or bodyweight before HCD administration, at early stages (*i.e.,* 6-week HCD), or after 12 weeks of HCD (**Figure S4.2B-C**).

We next assessed systemic inflammation using multiplex immunoassays. We detected higher levels of circulating pro-inflammatory cytokines IL-1β, IL-2, IL-9, IL-12(p70), IL-17A, and GM-CSF in mice receiving *miR223*$^{-/-}$ BM after 12 weeks of HCD (**Figure 4.3E**), while other cytokines such as IL-1α, IL-4, Eotaxin, G-CSF, and MIP-1a remained unchanged (data not shown). Mice lacking miR-223 in BM-derived cells also had increased levels of circulating neutrophils, total monocytes, and Ly6C^{low} monocytes after 12 weeks of HCD (**Figure 4.3D**) whereas there were no differences in circulating levels of other immune cell subsets (**Figure S4.2D**). Assessing circulating levels of leukocytes after 6-week HCD showed similar results (**Figure S4.2E**). These data indicate that the absence of miR-223 from the hematopoietic compartment not only resulted in an increase in lesion lipid accumulation in the aortic sinus but was also accompanied by signs of systemic inflammation.

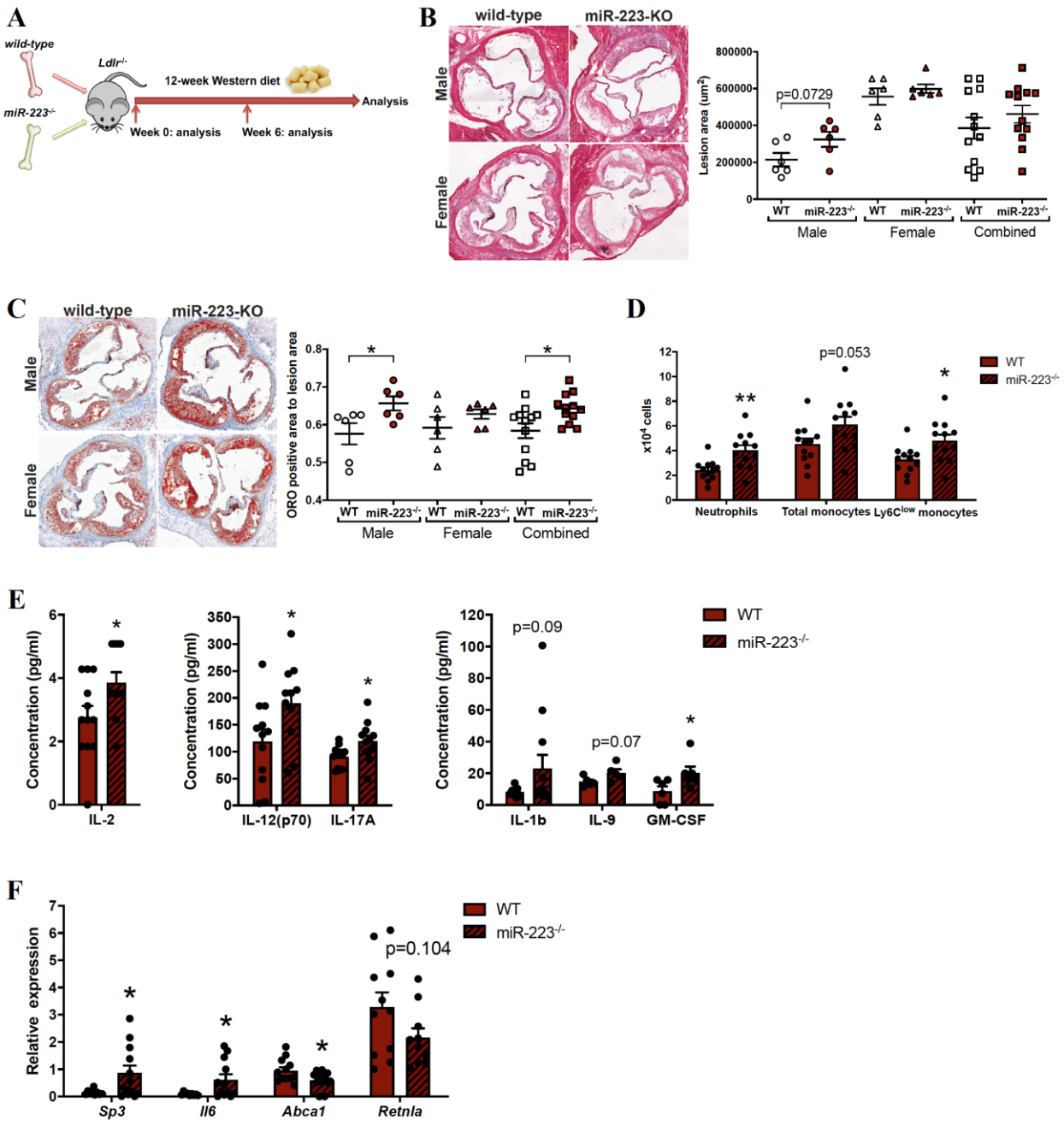

Figure 4.3. Deletion of miR-223 in BM cells promotes atherogenesis and enhances inflammatory signaling. (**A**) *Ldlr*$^{-/-}$ mice (n=6 male and 6 female/group) were lethally irradiated and given BM transplantation from WT or miR-223$^{-/-}$ donors, followed by HCD for 12 weeks. miR-223 deficiency in BM cells increases atherosclerotic plaque (**B**) size and (**C**) lipid content. Aortic sinus lesion areas across the entire aortic root from H&E-stained sections were quantified using ImageJ whereas lipid accumulation in aortic sinus lesions were measured by oil red O staining. Images show representative sections from *Ldlr*$^{-/-}$ mice with WT BM (left) and miR-223$^{-/-}$ BM (right). Data are the mean ± SEM, *p<0.05. (**D**) Circulating levels of leukocytes after 12 weeks of HCD were analyzed by FACS. Data are the mean levels from 9-12 mice per group ±

SEM. *p<0.05 **p<0.01, compared with of mice receiving WT BM. (**E**) Circulating cytokine levels in mice receiving WT BM or miR-223$^{-/-}$ BM (n=9-12 mice per group) were determined by the Bio-Plex Pro Mouse Cytokine 23-plex assay at the end of the 12-week study. Data are the mean ± SEM, *p<0.05. One-Way ANOVA. (**F**) Gene expression in the aorta from *Ldlr*$^{-/-}$ mice receiving WT BM or miR-223$^{-/-}$ BM. The aorta was homogenized using microbeads along with the Bullet Blender. Total RNA was isolated and the expression levels of *Sp3*, *Il6*, *Abca1*, and *Retnla* were measured by ddRT-PCR. Graphs represent means ± SEM from n=9-12 mice per group. *p<0.05, compared with of mice receiving WT BM using One-Way ANOVA.

To further evaluate the inflammatory profile of mice lacking hematopoietic miR-223, we analyzed gene expression in the aorta of mice receiving WT or *miR223*$^{-/-}$ BM after 12 weeks of HCD. Consistent with the *in vitro* data, qRT-PCR analysis demonstrated that the expression *Sp3* and *Il-6* were up-regulated whereas the expression of *Abca1* and *Retnla* were down-regulated in the aorta of mice lacking miR-223 in BM-derived cells (**Figure 4.3F**). On the other hand, other target genes of miR-223 including *Pknox1*[369], *Rasa1* and *Nfat5*[377] did not show significant changes or showed a reduction in mice receiving *miR223*$^{-/-}$ BM (**Figure S4.2F**).

To further characterize the pathways impacted by miR-223, we used a pathway-focused PCR array containing 84 genes related to atherosclerosis. We compared the expression of genes involved in the stress response, apoptosis, cell adhesion molecules, lipid transportation and metabolism, as well as cell growth and proliferation in Mo, M1 and M2 macrophages from WT and *miR223*$^{-/-}$ mice. Lack of miR-223 significantly increased the expression of *Cd44*, *Fga*, *Mmp1a*, *Sod1* and *Tnfaip3*, and decreased the expression of *Bid*, *Csf2*, *Cxcl1*, *Eln*, *Hbegf*, *Icam1*, *Lif*, *Lpl*, *Plin2*, *Serpinb2*, *Tgfb2* and *Tnc* in all macrophage subtypes (**Figure S4.3 and Table 4.1**). Interestingly, we searched for the presence of a miR-223 binding site in the 3'UTR of this group of altered genes using miRSystem[378], but none were identified. This suggests that miR-223 controls the expression of multiple pro-inflammatory genes indirectly and not *via* direct repression

of the 3'UTR, possibly via its regulation of a common regulatory factor such as *Sp3*.

UP-Regulated (miR-223$^{-/-}$ vs. WT)	DOWN-Regulated (miR-223$^{-/-}$ vs. WT)
Cd44, Fga, Mmp1a, Sod1, Tnfaip3	*Bid, Csf2, Cxcl1, Eln, Hbegf, Icam1, Lif, Lpl, Plin2, Serpinb2, Tgfb2, Tnc*

Table 4.1. Most significantly different genes (up- or down-regulated) in miR-223$^{-/-}$ macrophages. Atherosclerosis RT^2 Profiler PCR array was performed using RNA isolated from BMDMs of WT mice or miR-223$^{-/-}$ mice and normalized to housekeeping genes using the ΔΔCt method.

4.5.4. Global analysis of transcription and translation regulation by miR-223 in macrophages

To further understand the molecular mechanisms underlying how miR-223 controls the development of atherosclerosis *in vivo*, we employed ribosome profiling to characterize the global translation profile of macrophages isolated from mice receiving WT or *miR223*$^{-/-}$ BM. Because we found that deletion of miR-223 in BM-derived cells aggravated inflammation and atherosclerosis progression, we compared pro-inflammatory M1 macrophages to resting macrophages (Mo) to better understand the inflammatory pathways that may be activated uniquely in progressing plaques[379]. In this experiment, BMDMs isolated & differentiated from atherogenic mice were lysed to collect cytosolic total RNA, and a fraction of which was used for RNA-seq and the other fraction was used to isolate ribosome-protected fragments (RPF)[32,301,361]. Analysis of the cytosolic lysates from BMDMs (optimization shown in **Figure S4.4A**) demonstrates a strong correlation between biological replicates for both RNA-Seq (RNA) and Ribo-Seq (RPF) gene expression (**Figure S4.4B**). Metagene analysis indicates that RPF densities were significantly higher on the coding regions compared to the 5'-UTR or 3'-UTR, corresponding to the expected position of

translating ribosomes (**Figure S4.4C**). Interestingly, we find a poor correlation between gene expression at the transcription level (RNA-Seq) and the translation level (Ribo-Seq) (**Figure S4.4D**). Specifically, we observe a stronger correlation between RNA and RPF read densities in WT Mo macrophages (Pearson's correlation r=0.67) compared to WT M1 (Pearson's correlation r=0.37) (**Figure 4.4A**) suggesting that mRNA expression alone does not faithfully reflect protein expression and that translation is more active in M1 macrophages. This disturbed translation activity is consistent with previous studies that described the modulation effect of IFNγ or LPS, used during M1 activation, on translation[380,381]. Intriguingly, RNA and RPF densities showed less correlation in the absence of miR-223, as compared to WT, in both Mo and M1 macrophages (r=0.28 and 0.27 for Mo and M1, respectively), suggesting that global translation control is more active in the absence of miR-223 (**Figure 4.4A**). In agreement with the correlation analysis, we found that miR-223 deficiency resulted in modest transcription disturbance in Mo (70 genes up-regulated, 50 genes down-regulated) and M1 (38 genes upregulated, 62 genes down regulated) macrophages, but induced more widespread translation dysregulation (1640 genes up- and 783 genes down-regulated in Mo macrophages, 584 genes up- and 764 genes down-regulated in M1 macrophages) (**Figure 4.4B, Figure S4.4E**). Quantification of global protein synthesis rate by metabolic labelling of newly synthesized protein with puromycin demonstrates an increase in global protein synthesis in M1 compared to Mo BMDMs, but that protein synthesis is more active in *miR223*$^{-/-}$ compared to WT BMDMs (**Figure 4.4C**). Together, these data show that miR-223 alters gene expression in Mo and M1 macrophages primarily via control of translation rather than transcription of genes.

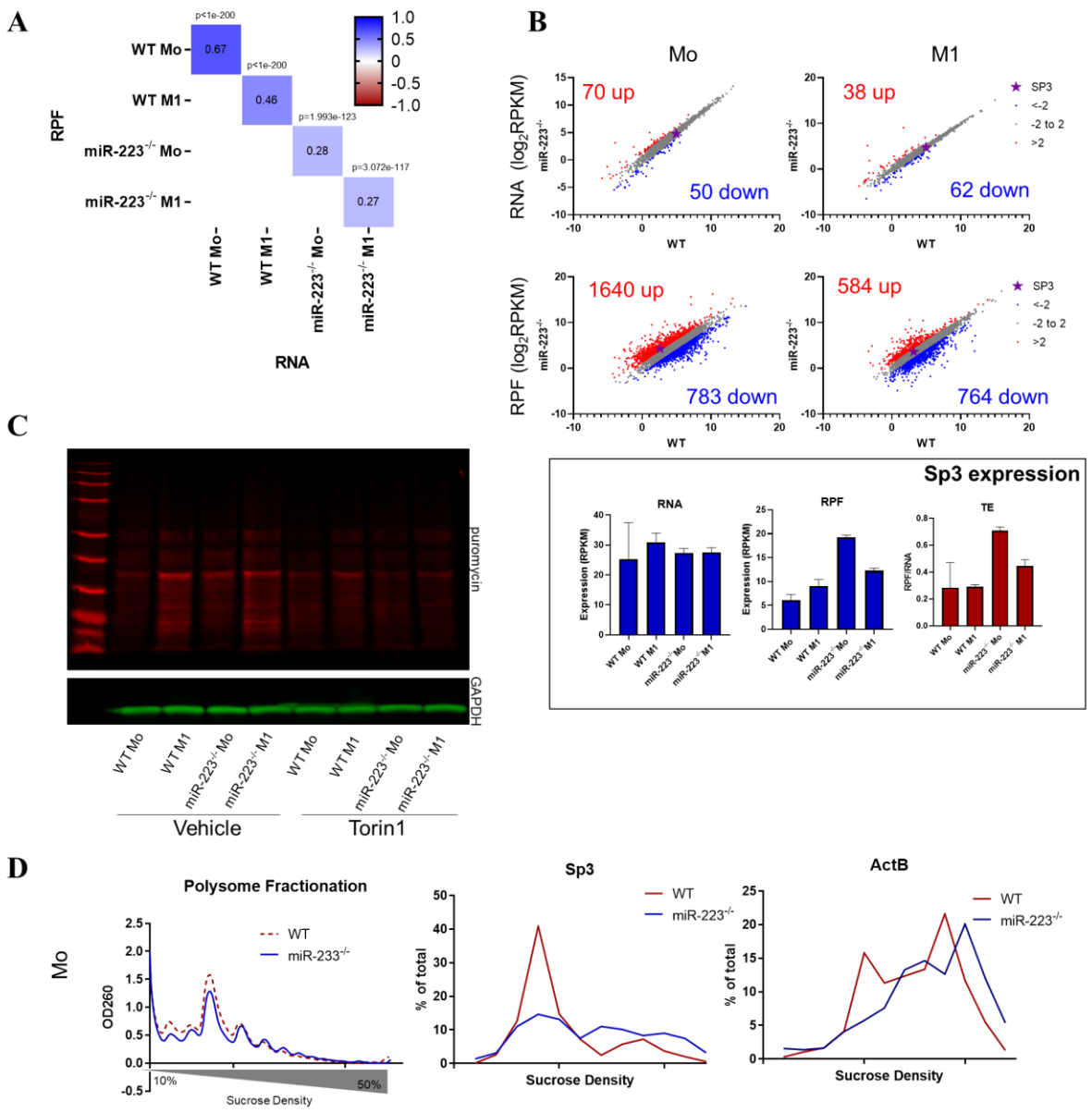

Figure 4.4. Global analysis of transcription and translation regulation in miR-223$^{-/-}$ BMDMs. (**A**) Correlation matrix of RPF (y-axis) and mRNA (x-axis) expression. Numbers show Pearson's correlation for each pair of RPF-RNA. *p*-value for each comparison was shown on top of each cell. Average expression level of each gene was used. (**B**) Upper panels: scatter showing the expression level of individual genes in miR-223$^{-/-}$ (y-axis) *vs* WT (x-axis) BMDMs at the mRNA or RPF level as indicated. Lower panels: Graphs of expression *Sp3* mRNA measured at the RNA or RPF levels, or translation efficiency (RPF/RNA). (**C**) Puromycin metabolic labeling of newly synthesized protein of WT or miR-223$^{-/-}$ BMDMs. Torin1 (300 nM) was used to inhibit mTORC1-dependent protein synthesis as a control. (**D**) Polysome fractionation analysis of translation activity in WT *vs* miR-223$^{-/-}$ Mo BMDMs. Left panel: polysome traces of cytoplasmic RNA extract on a linear 10-50% sucrose gradient. Middle and Right graphs: Distribution of *Sp3* or *ActB* mRNA across sucrose gradient, quantified by RT-qPCR.

Because our Ribo-Seq and RNA-Seq data indicated that changes in WT and *miR223*$^{-/-}$ macrophages were mainly at the translation level, we examined *Sp3* as a specific miR-223 target and investigated its relative translation efficiency in macrophages. Deficiency of miR-223 enhanced the expression of its target gene *Sp3* predominantly at the translation level but not at the transcription level (RNA, RPF and translation efficiency, right panel of **Figure 4.4C**). To confirm the translational regulation of *Sp3* by miR-223, we performed polysome fractionation to resolve polysome-bound mRNAs, where translating ribosomes bound to transcripts increase their overall polysomal density on a sucrose gradient. Consistent with a disturbance in global translation and enhanced global protein synthesis, the absorbance trace at 260 nm (A260) indicates an increased accumulation of 80S ribosomes in WT compared to *miR223*$^{-/-}$ macrophages (**Figure 4.4D**, left panel). We also find *Sp3* mRNA distributed predominantly to the monosome fraction in WT macrophages, while shifted more toward polysome fractions in *miR223*$^{-/-}$ macrophages, indicating augmented translation in the absence of miR-223 (**Figure 4.4D**, middle panel). In comparison, the translationally active *ActB* mRNA was primarily distributed to the polysome fractions, although slightly shifted to the higher polysome fractions in *miR223*$^{-/-}$ macrophages (**Figure 4.4D**, right panel), perhaps as a consequence of the changes in global translation observed.

Next, we sought to understand the putative consequences of this global change in translation upon miR-223 ablation using Ingenuity Pathway Analysis (IPA) on differentially expressed genes (DEGs) captured at the transcriptome and translatome level. IPA analysis revealed that the most significantly altered processes/functions (ranked by Benjamini-Hochberg p-values) are related to hematopoietic development and function, including “Development of hematopoietic system”, “Development of bone marrow” for DEGs at the RNA level and “Quantity of blood cells”, “Quantity of leukocyte” for DEGs at the RPF level (**Figure S4.5A**), consistent with the

hematopoietic-specific role of miR-223 described previously[382,383]. We focused on processes and functions in "Disease and Disorder" to detect potential pathological effects of miR-223 deficiency in macrophages and found that the top enriched annotation associated with processes/functions related to inflammatory response or inflammation-related processes (**Figure 4.5A**). When comparing the degree and directionality (activation or inhibition) of changes in inflammatory response networks (as measured by B-H p-values and activation z-score by IPA), activation of the inflammatory response in *miR223*$^{-/-}$ macrophages was more pronounced at the RPF (translation) level than at the RNA (transcription) level, especially in Mo macrophages (**Figure 4.5B**). Individual genes associated with inflammatory response also showed more profound changes in expression at the RPF level than at the RNA level (**Figure 4.5C**). Additionally, we noted genes categorized as "Lipid metabolism" were also altered at the translation level by miR-223 deficiency in Mo macrophages (**Figure S4.5B**). Thus, data from our transcriptional and translational profiling confirmed that miR-223 knockout aggravates inflammatory signaling in macrophages, and identifies miR-223 as a global regulator of translational control of inflammatory genes.

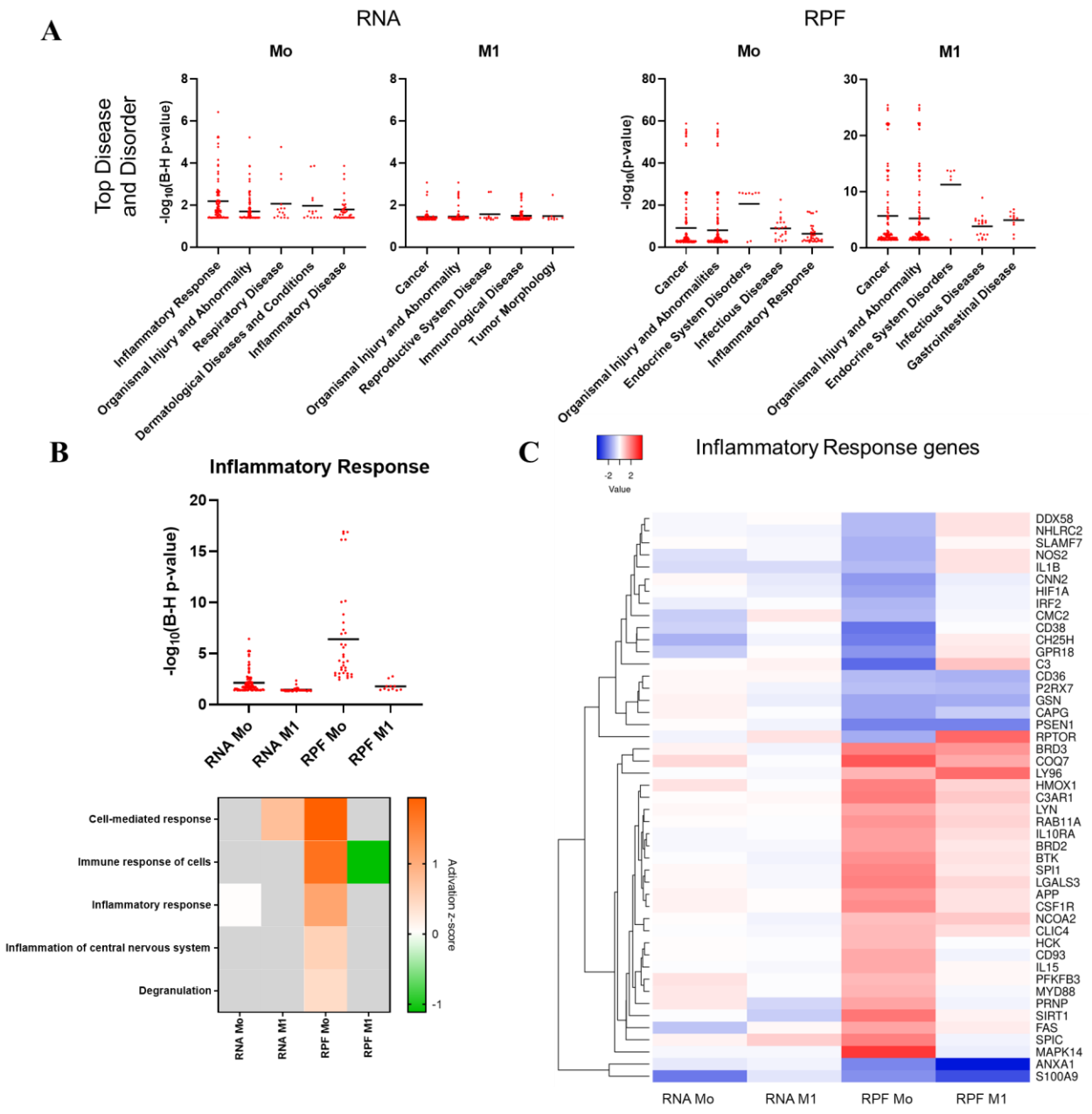

Figure 4.5. Ingenuity Pathway Analysis revealed activation of inflammation signaling at the transcription and translation level in BMDMs. (**A**) Scatter plot of Benjamini-Hochberg (B-H) p-value of significantly differentially regulated processes/functions in Disease and Disorder analysis in the transcriptome and translatome of miR-223$^{-/-}$ compared to WT BMDMs. B-H p-value cut-off of 0.05 (-log$_{10}$(B-H p-value) >1.3) was applied and all accepted processes/functions were shown as individual dots. (**B**) Top plot: scatter plot of B-H p-values of significantly differentially regulated processes/functions in the Inflammatory Response sub-category in miR-223$^{-/-}$ BMDMs compared to that of WT BMDMs. A B-H p-value cut-off of 0.05 (-log$_{10}$(B-H p-value) > 1.3) was applied, and all accepted processes/functions were shown as individual plots. Bottom plot: activation z-score of top 5 differentially regulated pathways in the Inflammatory

Response category in miR-223$^{-/-}$ BMDMs compared to that of WT BMDMs. The cell is grey when an activation z-score cannot be determined by IPA. (**C**) Heatmap of average KO/WT fold change of representative inflammatory response genes at the RNA and RPF level. All genes associated with all processes/functions in (B) were combined, then their clustering was calculated based on their fold change (KO/WT) values using the Average Linkage method.

4.6. Discussion

Since their discovery in *C. elegans*, miRNAs have shown to play important roles in modulating atherogenesis, with many miRNAs dysregulated in different disease states and alterations in miRNA expression associated with atherosclerosis progression[238,350]. Previous studies demonstrated that miR-223 is key to the regulation of the inflammatory response[352–355]. In addition, miR-223 serves as a critical regulator of hepatic cholesterol metabolism[351]. Nonetheless, the contribution of miR-223, particularly macrophage miR-223, to the development of atherosclerosis has not been investigated. In this study, we demonstrate that *in vitro*, miR-223 indeed promotes macrophage cholesterol efflux and macrophage polarization toward the anti-inflammatory M2 phenotype; in contrast, loss of miR-223 attenuates cholesterol efflux and enhances the pro-inflammatory responses. Remarkably, miR-223 appears to control inflammatory responses and lipid homeostasis primarily via regulation of translation, rather than transcription, as revealed by major changes in the ribosomal profile of miR-223-deficient cells. These beneficial effects of miR-223 appear to be partially dependent on the inhibition of its target gene, the transcription factor *Sp3*. *In vivo*, deficiency of miR-223 in BM-derived cells can accelerate the development of atherosclerosis lesions by increasing vascular lipid accumulation and exaggerating the inflammatory response to an HCD. Our study places miR-223 as a translational hub of cholesterol and inflammatory responses in atherosclerosis.

The efficacy of macrophages to efflux and remove intracellular cholesterol is crucial to attenuate lipid accumulation and atherosclerosis formation[364], and as such, targeting ABCA1 and macrophage cholesterol efflux has been a major focus for the prevention and treatment of atherosclerosis. Multiple miRNAs such as miR-33[356,359], miR-144[384,385], miR-148a[386,387], and miR-302a[388] have been found to regulate cholesterol efflux. However, most of them suppress *Abca1* expression and inhibit macrophage cholesterol efflux, thereby accelerating atherosclerosis progression. miR-223 is one of a few miRNAs whose activation, rather than inhibition, can increase *Abca1* expression, promote cholesterol efflux and protect against atherosclerosis. Consistent with studies in hepatocytes[351], we show that miR-223 can enhance the ability of macrophages to efflux intracellular cholesterol *via* up-regulating *Abca1*. More importantly, miR-223 can promote *Abca1* and cholesterol efflux independently of macrophage polarization status. *In vivo*, mice lacking miR-223 in BM-derived cells exhibited increased lipid accumulation in the aortic sinus and decreased *Abca1* gene expression in the aorta arch, further confirming the role of miR-223 in regulating macrophage cholesterol efflux. Interestingly, recent work from our lab indicates that miR-223 delivered *via* nanoparticles can promote cholesterol removal from macrophage-derived foam cells to the liver or intestine for excretion[389], again highlighting the therapeutic potential of this miRNA in reducing vascular lipid accumulation and inflammation during atherosclerosis.

Our study also shows that deficiency of miR-223 in BM-derived cells exacerbate atherosclerosis progression in male mice, but not female mice. Our data aligns with various studies that observed the male-specific effect of modulating inflammation responses on atherosclerosis development[390–394]. Interestingly, macrophage-specific deletion of *Abca1* have also been shown to exert the sex-specific effect on atherogenesis, although in the opposite direction, where *Abca1*

deficiency resulted in an increase in atherosclerosis mainly in female mice[395–397]. The reasons for the difference between male and female mice lacking miR-223 in BM cells are not clear, although the gene encoding miR-223 is located within the q12 locus of the X chromosome, suggesting a role for sex chromosomes on miR-223 function[398]. In addition, sex hormones are known to affect endothelial and macrophage function during atherogenesis[399–401]. Further studies are needed to dissect the mechanism for these sex-specific differences in miR-223 in atherosclerosis.

Macrophages are central players in the development of atherosclerosis. Although macrophages have a wide phenotypic range, for simplicity, they can be classified into two groups: classically activated M1 macrophages and alternatively activated M2 macrophages[402,403]. Macrophage polarization *in vitro* and in mouse models of atherosclerosis have indicated that increasing macrophage activation toward the M1 phenotype or inhibiting macrophage activation toward M2 can promote plaque inflammation and potentiate atherosclerosis[392,394,404–407]. In contrast, driving plaque macrophages to M2-like cells by the administration of IL-13 can attenuate atherosclerosis progression[408]. Therefore, targeting macrophage polarization would be beneficial for the prevention of atherosclerosis. Our study places miR-223 as a central regulator that instructs macrophage polarization. Loss of miR-223 promotes macrophage activation toward the pro-inflammatory phenotype (M1) and suppress macrophage anti-inflammatory activation (M2) *in vitro* and *in vivo*, which is supported by an increase and a decrease in the expression of the M1 marker *Il-6* and the M2 marker *Retnla*, respectively. Our findings are consistent with the observation that ablation of miR-223 expression in mice fed a high-fat diet exacerbated obesity-associated adipose tissue inflammation by enhancing classic proinflammatory responses[369]. We also found that miR-223 loss led to higher levels of cytokines IL-1β[390,409], IL-2[410], IL-9[411,412], IL-12(p70)[413,414], IL-17A[415,416], and GM-CSF[417], which are known to exert pro-inflammatory and pro-

atherogenic effects, and enhanced levels of circulating leukocytes (*i.e.* neutrophils, total monocytes). Several studies have shown that increased lipid raft formation and membrane cholesterol accumulation in ABCA1-deficient macrophages can account for the enhanced inflammatory responses in response to LPS or other TLR ligands[371–374,376], thereby indicating a role of ABCA1 in modulating macrophage inflammatory response. Here, we determine that miR-223 deficiency indeed promotes the pro-inflammatory responses *in vitro* and *in vivo* via both of enhancing the expression of its target gene *Sp3* and *via* suppressing the expression of *Abca1*. It was shown that miR-223 can regulate macrophage responses via directly targeting *Pknox1, Rasa1*, and *Nfat5*[369,377]. However, we observed no difference the expression of *Pknox1, Rasa1*, and *Nfat5* in aortic arches from mice lacking miR-223 in BM-derived cells, suggesting that these genes may not mediate the effects of miR-223 on macrophage activation in our atherosclerosis model. On the other hand, the expression of *Sp3,* another direct target of miR-223[351], was increased in aortic arches from mice receiving *miR223*$^{-/-}$ BM. SP3 was shown to drive the production of inflammatory cytokines including TNFα in cancer cells by promoting NFκB-mediated transcription activation[370]. In addition, knockdown of *Sp3* using RNA interference resulted in a phenotype similar to that of miR-223 overexpression, with decreased expression levels of M1-associated genes and increased expression levels of M2-associated genes, suggesting that the effects of miR-223 on macrophage polarization may be dependent on the inhibition of *Sp3* in our model.

MicroRNAs can control gene expression at the translation level via inhibition of translation initiation, followed by induction of transcript decay[224,418,419]. Our study incorporated genome-wide profiling of translation control using ribosome profiling, which revealed that miR-223 regulates inflammation extensively at the translation level and emphasizes the importance of characterizing the effect of miRNAs at both transcription and translation level to fully capture their impact on

gene expression. While the precise mechanisms for this global control of inflammatory gene translation are not known, it was suggested that the presence of AU-rich elements (AREs), *cis*-elements commonly found in the 3'UTR of cytokine and inflammatory transcripts[420], synergizes with miR-223 to inhibit translation [421]. It suggests a potential sequence-dependent mode for miR-223 to favor direct translation inhibition of inflammatory transcripts. miR-223 also inhibits mTORC1[422], the master regulator of mammalian cap-dependent translation, which has also been shown to be crucial for macrophage polarization [380,423], as well as significantly contribute to the regulation of inflammation signaling [55,272]. Thus, it is possible that mTORC1 plays a partial role in mediating miR-223 effect on translation control of inflammatory response in BMDM. These data, together with the findings herein, strongly suggest that miR-223 acts as a key component of inflammatory signaling in atherosclerotic macrophages.

In conclusion, our study provides evidence that miR-223 can reduce susceptibility to atherosclerosis by acting as a crucial modulator of macrophage cholesterol efflux and inflammation via globally controlling cholesterol and inflammatory gene expression. As such, systemic delivery or macrophage-specific delivery of miR-223 using viral-based vectors, nanoparticles, or extracellular vesicles could be a promising therapeutic strategy to combat inflammation in the atherosclerotic plaque.

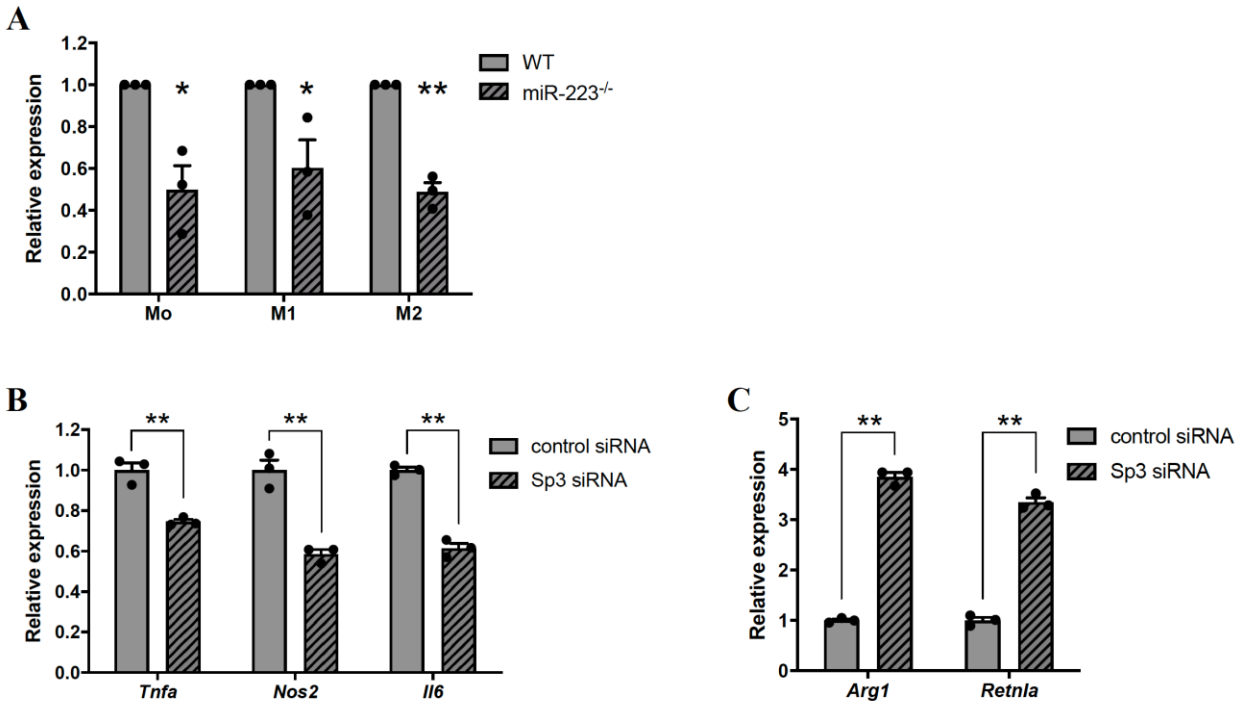

Figure S4.1. The expression of *Abca1* and macrophage activation markers. (A) *Abca1* expression at the RNA level in different macrophage subtypes isolated from miR-223$^{-/-}$ mice. BMDMs isolated from WT/miR-223$^{-/-}$ mice were polarized into M1 macrophages or M2 macrophages by induction with LPS (100 ng/ml)/IFN-γ (100 ng/ml) or IL-4 (10 ng/ml), respectively, for 24h. Total RNA was isolated and the expression levels of *Abca1* were measured by qPCR. (B-C) Inhibition of SP3 decreases the expression of M1 markers whereas increases the expression of M2 markers. BMDMs transfected with control siRNA or *Sp3* siRNA at a concentration of 25nM using Lipofectamine RNAiMAX. Total RNA was isolated and the expression levels of (B) M1 markers (*Tnfa*, *Nos2*, *Il-6*) and (C) M2 markers (*Arg1*, *Retnla*) were measured by qPCR. Graphs represent the experiments performed in triplicate (n=3), *p<0.05 **p <0.01 by Student's t-test.

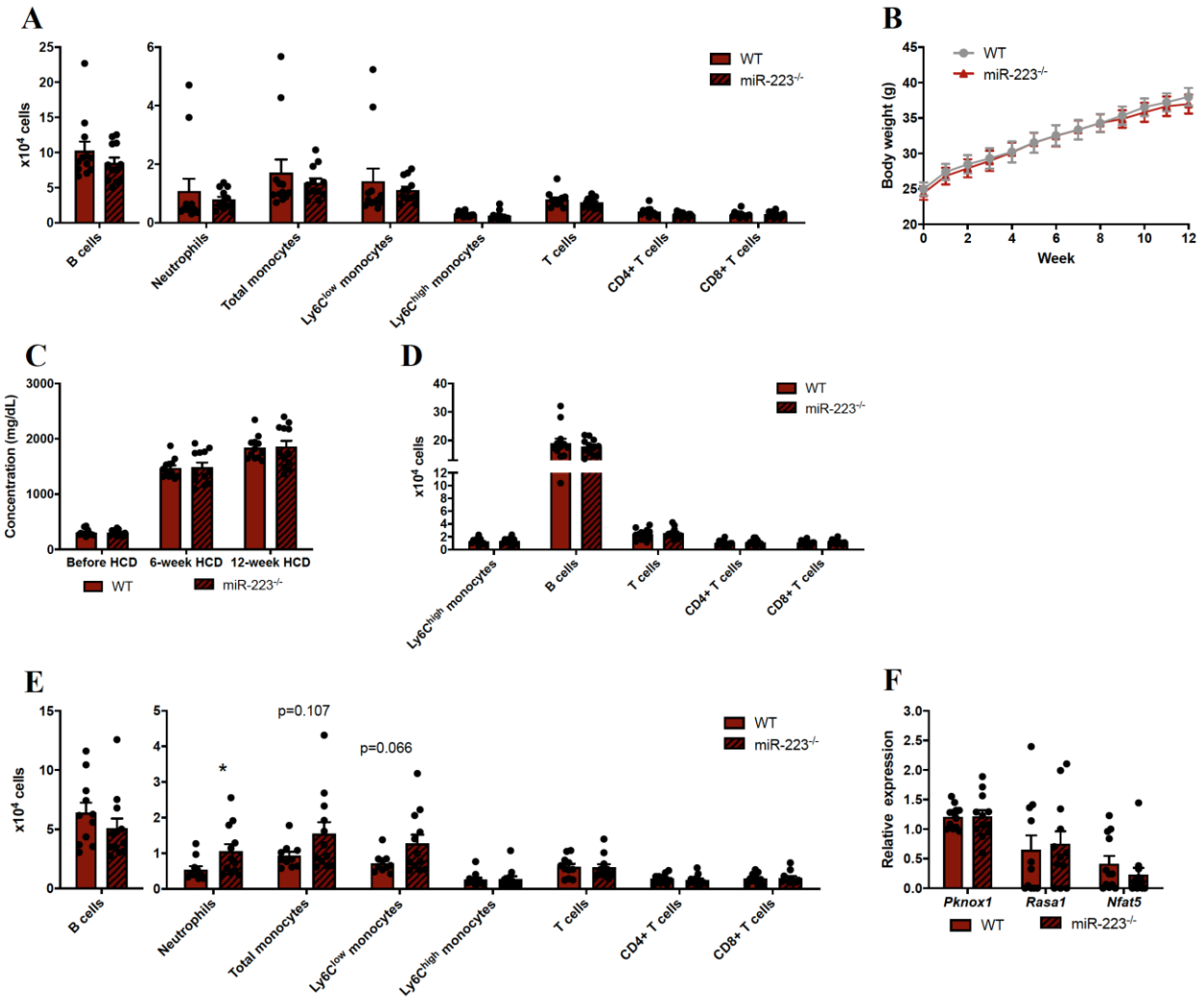

Figure S4.2. Body weight, plasma cholesterol and circulating levels of most leukocytes and lymphocytes are unchanged in mice receiving miR-223 BM. (**A**) Circulating levels of leukocytes before HCD administration were analyzed by FACS. Data are the mean levels from 9-12 mice per group ± SEM. Data were compared using a Student's t-test. (**B-C**) No major difference in (**B**) body weight and (**C**) total plasma cholesterol was noted between mice receiving WT BM or miR-223$^{-/-}$ BM. Data were compared using a Student's t-test. (**D-E**) Circulating levels of leukocytes and lymphocytes after (**D**) 12 weeks of HCD and (**E**) 6 weeks of HCD were analyzed by FACS. Data are the mean levels from 9-12 mice per group ± SEM. Data were compared using a Student's t-test. (**F**) The expression of *Pknox1*, *Rasa1*, and *Nfat5* in the aorta isolated from mice receiving WT BM or miR-223$^{-/-}$ BM. The aorta was homogenized using microbeads along with the Bullet Blender. Total RNA was isolated and gene expression levels were measured by ddRT-PCR. Graphs represent means ± SEM from n=9-12 mice per group. Data were compared using a Student's t-test.

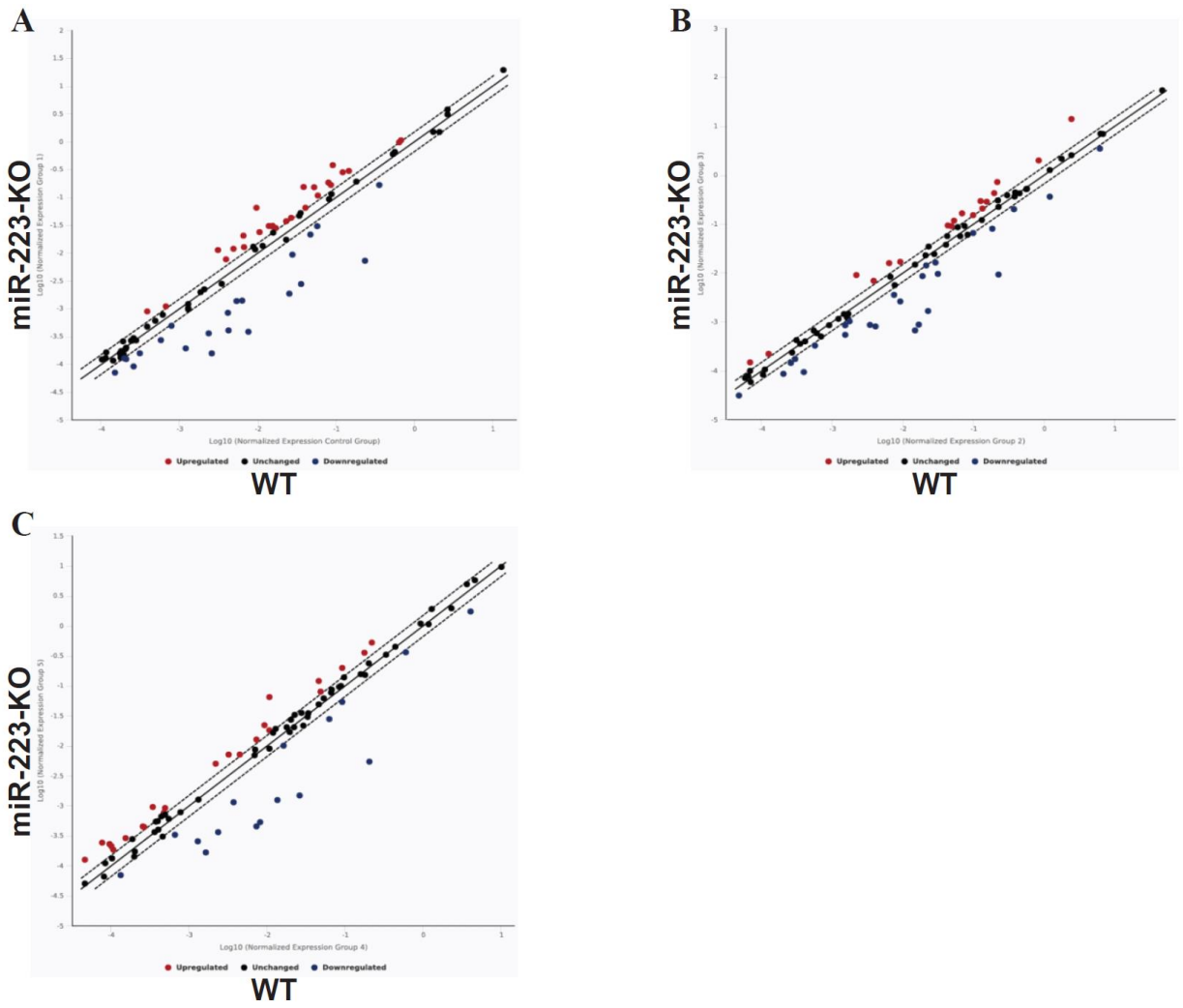

Figure S4.3. Indirect regulation of atherosclerosis gene expression by miR-223. Atherosclerosis RT^2 Profiler PCR array was performed using RNA isolated from (**A**) resting Mo macrophages, (**B**) pro-inflammatory M1 macrophages and (**C**) anti-inflammatory M2 macrophages of WT mice or miR-223$^{-/-}$ mice and normalized to housekeeping genes using the ΔΔCt method. Graph depicts gene expression of WT (x-axis) *versus* miR-223$^{-/-}$ (y-axis). Red and blue symbols represent the up- and down-regulated genes (greater than 2-fold) in miR-223$^{-/-}$ compared to controls, respectively.

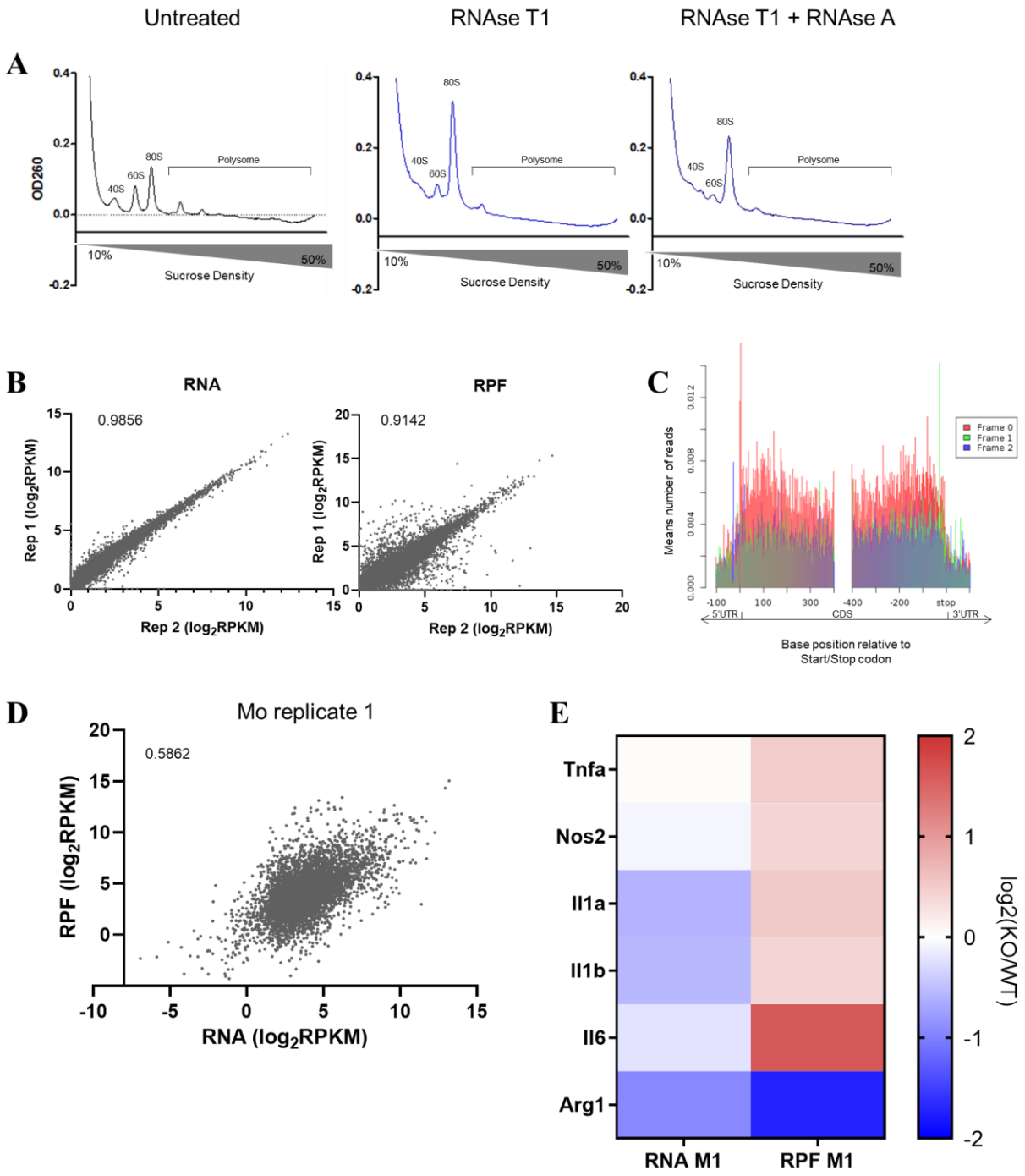

Figure S4.4. RNAseq and Riboseq analysis of gene expression in BMDMs. (**A**) Optimization of different RNAses for ribosome footprinting. Cytosolic lysate was treated with the indicated RNAses, then resolved on 10-50% sucrose gradient. RNAse T1 was chosen as it showed thorough digestion of polysomal RNA without degrading the 80S monosome peak. (**B**) Reproducibility of RNA and RFP densities between two biological replicates from independent mice. Pearson's correlation scores are shown on the top left corner of each plot. (**C**) Metagene analysis to shown mapping density of 28-nt RPF reads at the 5'UTR-CDS and CDS-3'UTR regions. A merged dataset from all Riboseq samples was used. Frame 0 is the reading frame of the CDS, frame 1 and

frame 2 is the +1 and +2 frames, respectively. (**D**) Scatter plot of representative correlation between ribosome footprint (y-axis) and mRNA abundance (x-axis) in one biological replicate. Pearson's correlation was shown on the top left corner of the graph. (**E**) Heatmap of average miR-223-KO/WT fold change of expression at the RNA and RPF level of representative M1 and M2 markers.

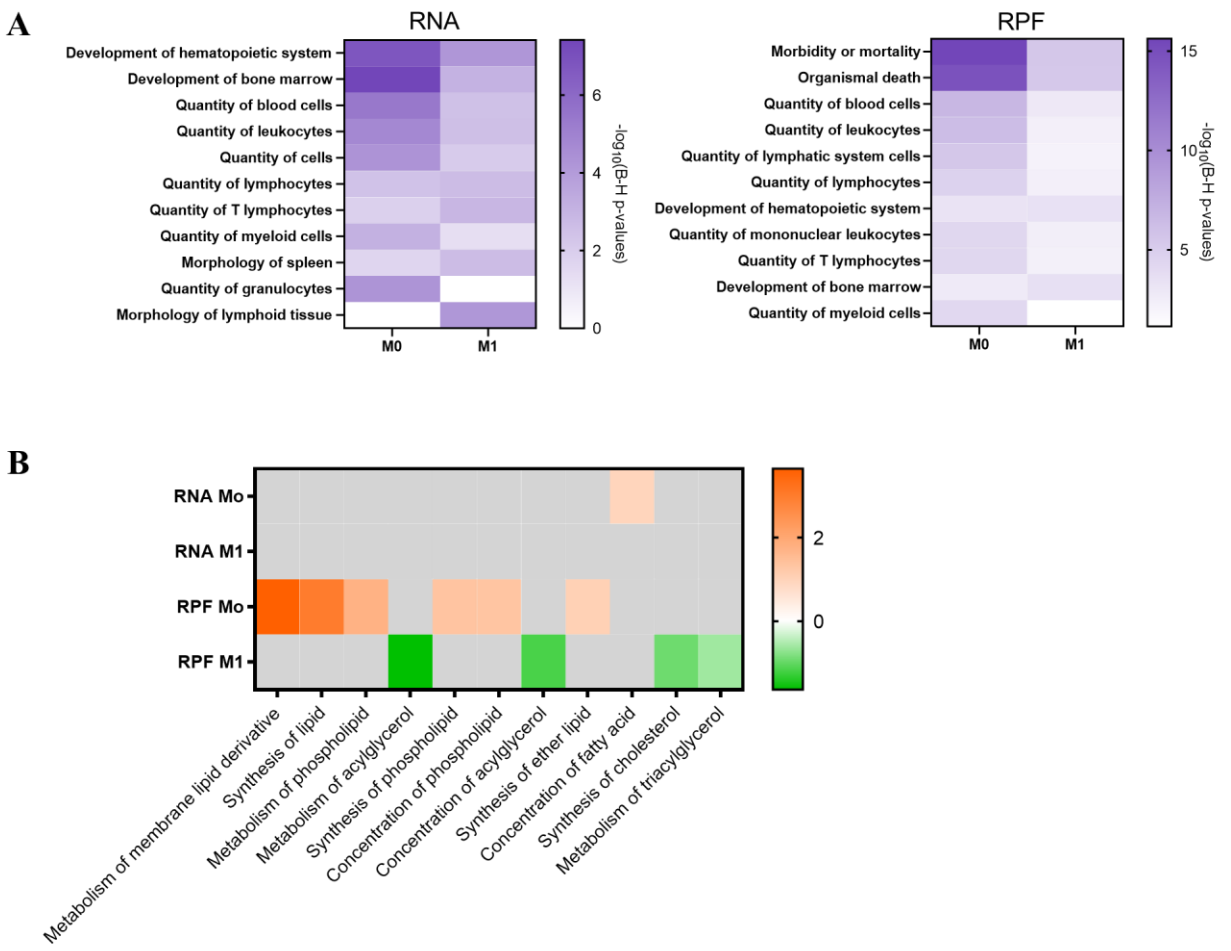

Figure S4.5. Ingenuity Pathway Analysis characterizes the effect of miR-223 removal on BMDMs. (**A**) Heatmap of top differentially regulated processes/functions in Physiological System Development and Function in miR-223$^{-/-}$ BMDMs compared to that of WT BMDMs at the mRNA and RPF level ranked by B-H p-values. A B-H p-value cut-off of 0.05 (-log$_{10}$(B-H p-value) >1.3) was applied and the top 10 processes/functions accepted in Mo or M1 samples, ranked by B-H p-value, were charted for their B-H p-value. (**B**) Activation z-score of top 10 differentially regulated processes/functions in the Lipid Metabolism category in miR-223$^{-/-}$ BMDMs compared to that of WT BMDMs. A B-H p-value cut-off of 0.05 (-log$_{10}$(B-H p-value) >1.3) was applied, then the top 10 differentially processes/function, ranked by activation z-score, were charted for their z-score.

4.7. Acknowledgements

CHAPTER 5. General Discussion

OVs are gaining momentum to become a potent therapeutic option for the treatment of cancer. The first turning point of OVs came in the last decade of the 20th century with the application of genetic engineering of wild-type viruses that introduced for the first time the capacity to modify virus tropism towards the specific metabolism and cellular condition of cancer cells[134]. Since then, our understanding of the virus-host interaction, tumor cell biology and the tumor microenvironment has expanded exponentially. This expansion in turn provides new insights to further adapt OVs to cancer cells. Novel tumor-fighting characteristics have also been introduced into OV, such as antitumor immune response or expression of cytotoxic genes. Translation control has always been a complex layer of virus-host interaction, with both parties evolving a myriad of strategies to fight for control of the translation apparatus while suppressing the translation of the opponent. Although this layer was evident since the beginning of translation control research, recent development of innovative techniques (such as ribosome profiling), as well as the discovery of other layers of gene regulations mechanisms in mammalian cells (such as miRNAs, tRNA fragments or RNA m6A-methylation), have demonstrated the vast uncharted landscape of translation control mechanisms in infected cells. The newly acquired knowledge that the field has and is still generating warrants efforts to deploy novel strategies to improve the safety and efficacy of OVs.

In this thesis, I first set out to explore the host translatome of a resistant breast cancer cell line infected with OVs to discover translationally-regulated OV-resistant genes that could be targeted to improve OV infectivity in cancer cells (**Chapter 2**). I identified a subset of these genes, and focused on the disruption of one candidate, the inositol phosphatase INPP5E, which rendered breast cancer cells more susceptible to OV infection. I also discovered the mechanism of

translation upregulation of *Inpp5e* during infection via the upregulation of an alternative transcript variant containing a more translationally active 5'UTR during the antiviral state. In the second project, I sought to find a viral 5'UTR that can improve transgene expression when incorporated into an expression cassette in an OV genome (**Chapter 3**). I repurposed the RNA-seq data I had generated earlier to identify the transcription start sites (TSS) of most HSV1 transcripts and revealed their 5'UTRs. I subsequently screened a subset of 5'UTRs for their translation activity in uninfected cells. I found that the 5'UTR of the HSV1 US11 gene, when being fused to another transcript, could enhance translation of that transgene specifically in HSV1 infected cells. In my last study, I explored the mechanisms of miR-223-mediated suppression of inflammation in macrophages in the context of atherosclerosis progression. I found that this miRNA suppressed translation control of a subset of inflammatory genes, as well as the inflammatory signaling-related transcription factor SP3. In summary, the results of my thesis exemplified the benefits of applying translation control to potentially improve OVs for cancer treatment. Additionally, my work emphasized the importance of translation control in studying virus-host interaction, as well as inflammatory-related diseases such as atherosclerosis. To the extent of my knowledge, *Inpp5e* is the first described translationally induced antiviral gene. Furthermore, my transgene-enhancing approach is novel and can be rapidly implemented in the clinic. The discovery of the translation component of miR-223-mediated immune suppression also opens the possibility of using translation suppressing drugs in treating atherosclerosis.

5.1. Enhancing therapeutic efficacy of OVs via targeting *Inpp5e* and other translationally induced antiviral genes

Although cancer cells are generally better hosts for virus infection, residual antiviral activity persists in these cells and suppressing these activities has been proven to be a promising approach

to OV research and development. Perhaps the use of viral sensitizers – compounds that enhance OV infectivity in tumors – is the best example of this approach. Unbiased *in vitro* screening identified small molecule compounds that were capable of boosting the infectivity of oncolytic VSV in various tumor models, but not in primary tissue[156,424]. The lead compound was further shown to disrupt the host antiviral response. Other compounds that potentiate OV efficiency were also reported, including vanadium compounds and dimethyl fumarate, which act via suppressing type I interferon signaling[155,425]. These studies support the notion that residual antiviral activity of cancer cells contributes to resistance to OV infection in tumor cells. These observations also raise the question: are there other unknown antiviral genes that contribute to cancer cell's resistance to OV and can be inhibited to benefit OV spread?

My first project identified INPP5E as a phosphatase that is involved in the cellular antiviral response. Removal of this gene makes a normally OV-resistant breast cancer cell line vulnerable to various OVs. The ensuing step of this project is to develop therapeutically applicable methods to inhibit INPP5E and further validation of their effect in *in vivo* models. There is currently no report of a specific inhibitor of INPP5E, however pharmacological inhibitors of inositol 5-phosphatases have been previously described, yet with various degree of selectivity[426]. Particularly, this study reported a class of chemical scaffold that possesses specific inhibition toward the phosphatase INPP5B. Thus, further screening or scaffold modification could potentially generate INPP5E-specific inhibitors. Of consideration, INPP5E was shown to be involved in various cellular processes, from autophagy[427], AKT/mTORC1 signaling[428] to primary cilia formation[273,429]. Mutations of *Inpp5e* have been linked to several developmental defects such as Joubert syndrome and mental retardation, truncal obesity, retinal dystrophy, and micropenis (MORM) syndrome.

Therefore, whole-body inhibition of INPP5E might yield negative side effects, and a more localized approach to suppress INPP5E activity within the tumors might be better appreciated.

In my study, I found that the antiviral effect of *Inpp5e* appeared to be more efficient against specific viruses, with a strong effect against HSV1 and VSV, but limited to no effect against VACV and Reovirus. It would be interesting to test other viruses in the *Inpp5e* KO cell models. Interestingly, although endogenously expressed INPP5E was not reported with antiviral function before, overexpression of INPP5E (formerly known as polyphosphoinositide 5-phosphatase IV - 5ptaseIV) was shown to inhibit HIV-1, albeit via a slightly different mechanism of depleting phosphatidyl-inositol-4,5-biphosphate (PI(4,5)P2) and impairing virus release[430,431]. Thus, the substrate specificity of INPP5E is not restricted to PI(3,4,5)P3, and it might affect more than one step in the virus life cycle. Considering the pleiotropic function of INPP5E, it might be possible that this phosphatase affects OV efficacy via other functions in addition to virus-host interaction, such as modification of the immune response. Notably, it has recently been reported that INPP5E supports the function of immune synapse in T-cells and thus may be important for mounting antitumor immune response[432]. Further work would be needed to determine whether there might be a trade-off between enhancing virus spread and dampening antitumor response if INPP5E is targeted in OV therapy.

A potential localized approach would be to incorporate RNA-interference (RNAi) that targets *Inpp5e* mRNA into the OV genome. Expression of shRNAs from OVs was previously reported for several viruses including HSV1 and Adenovirus (Ad)[433,434]. In the case of oncolytic adenovirus, the short hairpin designed to target VEGF was shown to be capable of inhibiting angiogenesis *in vitro* and *in vivo*, attesting that RNA-interference can be functionally applied in OV platforms. A similar *Inpp5e*-targeting shRNA or artificial miRNA expression cassette could

be inserted into OV genome for the purpose of suppressing gene expression of *Inpp5e*. However, as INPP5E was shown in my study to inhibit OV infectivity at the entry step, it would be important to confirm if INPP5E is upregulated only in the infected cell, or is also upregulated in adjacent cells due to IFN signaling. If the latter occurs, RNA-interference might not be an effective approach as the suppression would be limited to the infected cells only. It has been shown that miRNAs and siRNAs can be transferred via extracellular vesicles[357], and specific miRNAs can be engineered to be preferentially packaged into extracellular vesicles via the incorporation of an RNA-stem loop[435]. These developments could be considered for the distribution of OV-expressed RNAi against *Inpp5e* to the neighboring cells.

5.2. Translational derepression/upregulation as a novel mechanism for antiviral gene expression

How the intrinsic immunity protects cells from virus infection remains a fascinating basic virology question that has implications not only for OV development, but also in the larger context of the interaction of our society with viruses, including our current response to pandemic events. It is now clear that mammalian cells devote extensive efforts to fighting viruses, as illustrated by the complex network of antiviral genes that exist in every cell of the body. Most antiviral genes have been identified via their transcription upregulation upon virus infection or activation of IFN signaling due to infection of neighboring cells. It is estimated that up to 10% of genes in the mammalian genome are subjected to IFN-mediated transcription regulation[436]. These genes, termed ISGs, have only been characterized in details in the last decade and reveal a wide array of mechanisms of action toward every step of a virus life cycle, from attachment, entry, protein production, virion assembly to egress[193,194]. Yet, as genome-wide transcription profiling is the widely used screening method to identify potential antiviral genes, the current knowledge has been

biased toward the subset of transcriptionally induced genes. By doing so, the field has potentially overlooked antiviral genes that are induced at the post-transcriptional levels, including translation control. Consequently, a substantial fraction of the antiviral state might remain to be discovered.

The work presented in my thesis raises an interesting fundamental question: can antiviral genes be upregulated at the translation level, and what mechanism(s) regulate such induction in response to virus infection? Although no translationally regulated antiviral gene was previously reported, examples of translation upregulation as a method of gene expression regulation have been extensively described in other cellular conditions, many of which are related to the antiviral state. For instance, gene expression regulation by uORFs is an example of translation control in stress conditions. Present in up to 50% of all 5'UTRs in the mammalian genome[13,437], these small open reading frames normally suppress translation of a given transcript, but can also act as stress response elements to induce gene expression in P-eIF2α conditions[438]. Interestingly, as discussed in the **Introduction**, a virus infection also activates the ISR and phosphorylation of eIF2α, which can upregulate the translation of certain uORF-containing transcripts. It is noteworthy to mention that I did detect an enrichment of uORFs in the 5'UTRs of translationally upregulated genes in my study. The 5'UTR of *Inpp5e* also contains several uORFs; however, I did not detect a de-repression of this 5'UTR during virus infection but rather a transcript variant shift toward a more translationally active short 5'UTR, ruling out the uORF-related de-repression mechanism for *Inpp5e* 5'UTR. However, it is highly possible that other uORF-containing 5'UTRs can be de-repressed during viral stress. Additionally, a subset of cellular transcripts contains IRES-like activity in their 5'UTRs that maintains translation during cellular conditions where protein synthesis is turned off[439–441]. For example, during mitosis when protein synthesis is tuned down, Qin and Sarnow found a subset of mRNAs that maintain polyribosome association, in which the

5'UTRs of six of them (Cyr61, NPM1, NAP1L1, ABETA, hnRNPA/B and Vimentin) were shown to possess IRES-like activity[440]. Similarly, during the stress condition of hypoxia, the 5'UTR of the angiogenic factor VEGF also shifts toward a cap-independent mode of translation[441]. Thus, these cellular IRESes provide a mechanism for the cells to tune down global protein synthesis to avoid further aggravate the stress conditions, while maintaining the translation of a subset of stress-related transcripts in an attempt to resolve the cause of stress. However, it is noteworthy to mention that the identified cellular IRESes so far generally show weaker activity compared to viral IRESes. Also, the use of bi-cistronic assays as standard methods for IRES discovery are known to confound mis-splicing and cryptic promoter activity, rendering the confirmation of cellular IRESes less certain than their viral counterparts[439].

It has emerged recently that the canonical cap-dependent mode of initiation does not uniformly promote mRNA translation but rather possesses a preference for a subset of mRNAs. Additionally, the composition of the translation initiation complex can change depending on the cellular states, and such changes could alter the transcript preference of cap-dependent translation initiation. The most intriguing case previously reported is the use of the alternative translation initiation factor eIF2A in cancer cells to drive tumorigenesis via recognition of alternative translation start sites. The initiation factor eIF2 is generally responsible for forming the ternary complex and delivering Met-tRNAi for initiation. However, mammalian cells also encode an alternative translation initiation factor called eIF2A, which is capable of interacting with tRNAi[442]. The function of eIF2A is generally obsolete in normal conditions where eIF2 is the main provider of tRNAi, but a recent study has shown that eIF2A is important to drive unconventional translation initiation in malignant cells where eIF2 activity is restricted due to phosphorylation of its eIF2α subunit[270]. In this study, eIF2A-mediated translation initiation tends to favor non-canonical

translation initiation sites in the 5'UTRs, suboptimal initiation sites that are ignored by eIF2-mediated translation initiation and are enriched in the 5'UTRs of a subset of oncogenic mRNAs. In this context, phosphorylation of eIF2α is described as the switch towards another alternative mode of translation that drives the use of non-AUG start codons, which interestingly are used by the majority of uORFs. This draws a strong potential link between the unconventional eIF2A translation initiation and the antiviral state where eIF2α is phosphorylated by the ISR. It will be a promising avenue for future studies to elucidate if there are alternative modes of translation initiation, mediated by eIF2A or other uncharacterized alternative translation initiation factors, used during different antiviral states.

Translation derepression during the antiviral state might not be a direct consequence of translation initiation, but rather a change in mRNA structure unrelated to the CDS region. A typical mammalian gene can generally be transcribed and spliced into multiple transcript variants, which differ in their 5'UTRs, CDSs or 3'UTRs due to a combination of alternative transcription start sites, splicing and termination. While differences in the CDS directly alter the protein product, differences in the UTRs could have implications on the stability and translation of the transcript, the latter of which would be independent of transcript abundance. As described in the introduction, the 5'UTRs of a mammalian mRNA contain various translation modifier elements, including uORFs, IRESes, secondary structures and other motifs[10]. The 3'UTR also contains poly(A) tail and potential miRNA binding sites or other motifs that can modify translation. Importantly, it has been described that the translational output of transcript variants of a gene can differ widely, and changing the transcript variant ratio maybe a powerful mechanism of regulating gene expression[282,443]. As it is the transcript variant ratio, not transcript abundance *per se*, that is changed during this process, it may not be captured efficiently when using transcription-profiling

techniques. Additionally, it is known that the antiviral state includes a major reprogramming of transcription regulation and splicing due to the activation of various IFN-induced transcription signaling. Thus, it is possible that this transcription program might also modulate the transcript variant ratio of a subset of antiviral genes via changing the use of transcription start sites rather than transcriptional output and thus producing alternative 5'UTRs that are more translationally active. Furthermore, splicing has been shown to be heavily disturbed in the infected cells due to activity of viral proteins (for example, the HSV1 ICP27[287]) or host proteins (for example, the RNA-protein BUD13[288]), potentially changing the 5'UTR during transcript maturation. Finally, the 3'UTR can also be affected by a viral infection, such as in the case of HSV1 infection whereby disruptions of transcription termination and polyadenylation occur[286]. These studies emphasize that the transcript variant signature is crucial to completely capture the gene expression landscape in a specific condition. Alternative transcript variant usage also presents the fascinating intersection of transcription and translation regulation.

5.3. Translational adaptation as an approach to tailor oncolytic viruses

In my second project, I provided an example of how adaptation to specific translation conditions can improve gene expression and benefit OV design: by incorporating a viral 5'UTR upstream of the transgene CDS, I showed that transgene expression was significantly improved in HSV1-infected cells. Furthermore, the application of translation control is not limited to improving gene expression: other substantial OV improvements might be possible if the OV is adapted further to the translation conditions of the infected cells and/or cancer cells, including increase oncotropism and safety profile.

For example, the codon usage of virus and its corresponding host presents an interesting paradox with important implications in virotherapy design. Codon usage refers to the frequency of

alternative codons encoding for the same amino acid in an mRNA. Codon usage tends to be specific for each organism and may evolve to adapt to the specific tRNA pools available for protein synthesis in the cells. Suboptimal codon usage was shown in various studies to slow translation elongation via ribosome stalling, a phenomenon that is also observed during depletion of certain amino acids[444,445]. A virus infection introduces an interesting problem: as the virus usurps the host translational resources, including the tRNA pools, its transcripts should be under a strong selection pressure to conform to the codon usage of the host. Surprisingly, it was shown that mammalian and human viruses do not share a very similar codon usage with that of their hosts[446–448]. This dissimilarity might be explained in part by the hypothesis that the host possesses distinct tRNA pools unique for the antiviral state, and the codon usage of viruses may have evolved to adapt to this specific state rather than the general tRNA pools of normal, uninfected conditions. This hypothesis was actually showcased in a report studying the codon adaptation of the influenza virus strain H3N2 during its endemic circulation in the human population since 1968[204]. The study found that the codon adaptation index (CAI) of the virus gene PB1 to host, a measure of the similarity between codon usage, became lower during the virus adaptation to the human population. The authors found that the virus-infected cells possess a different tRNA pool, of which when compared to the virus CAI, showed an increased similarity. This suggests that tRNA pool during the antiviral state is the potential target of virus codon adaptation. Applying to virotherapy design, the virus-host codon usage dynamic poses an interesting question: during transgene design, should the transgene codon usage conform to that of the host, or that of the virus? Previous work has shown that the host codon usage might not be the ideal target for transgene optimization: in a study using adenovirus for gene therapy, the fiber protein of the virus was codon-optimized toward the codon usage of human in an attempt to improve virus replication[207]. Surprisingly, although the codon-

optimized version of the fiber protein is expressed much better in various uninfected human cell lines, this version of fiber protein is detrimental for viral fitness when incorporated into the adenovirus genome. Thus, it is a cautionary tale that transgene codon usage should be adapted toward that of the virus overall genome, or perhaps a distinct antiviral state.

The success of cancer therapeutics relies on the distinction between normal and cancerous cells. The development of tumor specificity of OVs has mainly focused on finding conditions that are unique for cancer cells, such as specific gene mutations or distinct receptor/surface marker profiles that OVs can be tailored towards. The specific tRNA state hypothesis raises another intriguing possibility: is there a specific tRNA pool unique for cancer cells, which the codon usage of the transgene or even the OV genomes can be optimized toward to enhance specificity? It was reported that proliferating cells, including cancerous cells, do possess a different tRNA pool compared to differentiating cells, and this pool is supportive for a subset of proliferating-related mRNAs[206]. Although the evidence and data are still scarce regarding the specific tRNA pools of cancer cells, the application of this knowledge could help enhance tumor specificity of different OVs, and hence the safety profile of these viral therapeutics.

Finally, there are emerging mechanisms that have recently been reported to contribute to the translation landscape of the infected cells. tRNA fragments, cleavage products of tRNAs, were recently reported as novel regulators of mRNA translation[449–451]. tRNA fragments have already been reported to affect virus infectivity in the case of respiratory syncytial virus, suggesting that this class of molecules mediates virus-host interaction[452,453]. Another emerging mechanism to regulate gene expression is epi-transcriptomic modification, referring to modifications of mRNAs after transcription. m6A-methylation is currently the most extensively studied event of epi-transcriptomic modification, and was reported to affect translation via nuclear export, translation

initiation and mRNA stability[208]. Interestingly, m6A is also observed on viral transcripts[454–457], and this modification was shown to have a complex effect on the virus life cycle[458,459]. Thus, it may prove important that these additional layers of translation control are understood and considered during future OV development, so that optimization towards efficacy, specificity and safety can be optimal.

5.4. On the effect of miRNA-mediated translation control of the immune response

In my third Chapter, I characterized the translatome of wild-type and *miR-223*$^{-/-}$ macrophages in order to determine the effect of this miRNA on the inflammation signaling during atherosclerosis development. A translation effect on gene expression was observed for genes enriched in inflammatory signaling, emphasizing the translationally inhibitory effect of this miRNA, especially on inflammation[418]. Although miRNAs are known to inhibit translation, this effect is normally limited to a small set of mRNAs that harbor the specific miRNA binding sites in their 3'UTRs. However, I observed a global derepression of translation in *miR-223*$^{-/-}$ macrophage, first from ribosome profiling data and also by metabolic labeling of newly synthesized protein. This global effect of miR-223 on translation control is clearly unusual and warrants further efforts for investigation. My observation might be explained by a previous study on the function of miR-223 in hepatocellular carcinoma, which interestingly found that miR-223 negatively regulates mTORC1 phosphorylation and function via targeting Rab1, an activator of mTOR during amino acid stimulation[422]. Although this study focused on the effect of mTOR inhibition on apoptosis, the authors also found that overexpression of miR-223 downregulates phosphorylation of S6K, suggesting that removal of this miRNA can result in activation of the mTORC1/S6K1 axis that modulates global protein synthesis. Thus, it is possible that miR-223 might alter global translation control by indirectly inhibiting mTORC1 activity. It is also

interesting to see whether the pro-inflammatory effect of miR-223 deletion is mediated through this derepression of mTORC1. More importantly, if this hypothesis is confirmed, it might lay the foundation for the use of mTORC1 inhibitors to control such inflammatory signaling, which was shown in my last Chapter to be important for atherosclerosis development.

5.5. Conclusion

My studies emphasize the importance of translation control in studying oncolytic viruses as well as inflammatory-related diseases such as atherosclerosis. During a virus infection, a subset of antiviral genes is translationally induced, adding an extra layer of protection against virus infection on top of transcriptionally induced ISGs. My work has uncovered that inhibiting translationally regulated antiviral genes can expose hidden vulnerabilities of cancer cells to OV infection. In addition, my thesis describes that viruses such as HSV1 likely evolved and adapted their 5'UTR of viral transcripts to the disturbed translation control environment of the infected cells. I have demonstrated that incorporating a viral 5'UTR in front of a transgene CDS, encoded within HSV1 genome, is a powerful method to enhance transgene expression translationally. I propose that this approach could further improve the antitumor effect of OVs. Lastly, I have shown that a miRNA ameliorates atherosclerosis via suppressing the inflammatory response at the translation level. My high-throughput approach reveals an unexpected genome-wide landscape of translation modulation resulting from the removal of one miRNA. This work again emphasizes the translation control aspect of miRNAs in regulating gene expression, as well as the importance of global gene expression analysis at the translation level to fully capture the effect of miRNA-mediated modulation. Altogether, my studies show that translation control represents an important target to improve the therapeutic regimen for various diseases and clinical contexts, including OVs and inflammatory diseases.

REFERENCES

1. Lu, P., Vogel, C., Wang, R., Yao, X. & Marcotte, E. M. Absolute protein expression profiling estimates the relative contributions of transcriptional and translational regulation. *Nat. Biotechnol.* **25**, 117–124 (2007).
2. Gygi, S. P., Rochon, Y., Franza, B. R. & Aebersold, R. Correlation between Protein and mRNA Abundance in Yeast. *Mol. Cell. Biol.* **19**, 1720–1730 (1999).
3. Schmidt, M. W., Houseman, A., Ivanov, A. R. & Wolf, D. A. Comparative proteomic and transcriptomic profiling of the fission yeast Schizosaccharomyces pombe. *Mol. Syst. Biol.* **3**, (2007).
4. Baerenfaller, K. *et al.* Genome-scale proteomics reveals Arabidopsis thaliana gene models and proteome dynamics. *Science (80-.).* **320**, 938–941 (2008).
5. Schrimpf, S. P. *et al.* Comparative functional analysis of the Caenorhabditis elegans and Drosophila melanogaster proteomes. *PLoS Biol.* **7**, 0616–0627 (2009).
6. Schwanhäusser, B., Gossen, M., Dittmar, G. & Selbach, M. Global analysis of cellular protein translation by pulsed SILAC. *Proteomics* **9**, 205–209 (2009).
7. Tahmasebi, S., Sonenberg, N., Hershey, J. W. B. & Mathews, M. B. Protein synthesis and translational control: A historical perspective. *Cold Spring Harb. Perspect. Biol.* **11**, a035584 (2019).
8. Hoang, H. D., Graber, T. E. & Alain, T. Battling for Ribosomes: Translational Control at the Forefront of the Antiviral Response. *Journal of Molecular Biology* **430**, 1965–1992 (2018).
9. Tahmasebi, S., Khoutorsky, A., Mathews, M. B. & Sonenberg, N. Translation deregulation in human disease. *Nature Reviews Molecular Cell Biology* **19**, 791–807 (2018).
10. Leppek, K., Das, R. & Barna, M. Functional 5′ UTR mRNA structures in eukaryotic translation regulation and how to find them. *Nature Reviews Molecular Cell Biology* **19**, 158–174 (2018).
11. Matoulkova, E., Michalova, E., Vojtesek, B. & Hrstka, R. The role of the 3′ untranslated region in post-transcriptional regulation of protein expression in mammalian cells. *RNA Biology* **9**, 563–576 (2012).
12. Kumar, P., Hellen, C. U. T. & Pestova, T. V. Toward the mechanism of eIF4F-mediated ribosomal attachment to mammalian capped mRNAs. *Genes Dev.* **30**, 1573–1588 (2016).
13. Lee, S. *et al.* Global mapping of translation initiation sites in mammalian cells at single-nucleotide resolution. *Proc. Natl. Acad. Sci. U. S. A.* **109**, (2012).
14. Starck, S. R. *et al.* Leucine-tRNA initiates at CUG start codons for protein synthesis and presentation by MHC class I. *Science* **336**, 1719–23 (2012).
15. Dever, T. E. & Green, R. The elongation, termination, and recycling phases of translation in eukaryotes. *Cold Spring Harb. Perspect. Biol.* **4**, 1–16 (2012).
16. Schwanhausser, B. *et al.* Global quantification of mammalian gene expression control. *Nature* **473**, 337–342 (2011).
17. Kim, D. H. *et al.* mTOR interacts with raptor to form a nutrient-sensitive complex that signals to the cell growth machinery. *Cell* **110**, 163–175 (2002).
18. Kim, D. H. *et al.* GβL, a positive regulator of the rapamycin-sensitive pathway required for the nutrient-sensitive interaction between raptor and mTOR. *Mol. Cell* **11**, 895–904 (2003).
19. Hara, K. *et al.* Raptor, a binding partner of target of rapamycin (TOR), mediates TOR action. *Cell* **110**, 177–189 (2002).

20. Saxton, R. A. & Sabatini, D. M. mTOR Signaling in Growth, Metabolism, and Disease. *Cell* **168**, 960–976 (2017).
21. Holz, M. K., Ballif, B. A., Gygi, S. P. & Blenis, J. mTOR and S6K1 mediate assembly of the translation preinitiation complex through dynamic protein interchange and ordered phosphorylation events. *Cell* **123**, 569–580 (2005).
22. Gingras, A. C. *et al.* Regulation of 4E-BP1 phosphorylation: A novel two step mechanism. *Genes Dev.* **13**, 1422–1437 (1999).
23. Thoreen, C. C. *et al.* A unifying model for mTORC1-mediated regulation of mRNA translation. *Nature* **485**, 109–113 (2012).
24. Fonseca, B. D. *et al.* La-related Protein 1 (LARP1) Represses Terminal Oligopyrimidine (TOP) mRNA Translation Downstream of mTOR Complex 1 (mTORC1). *J. Biol. Chem.* **290**, 15996–6020 (2015).
25. Dorrello, N. V. *et al.* S6k1- and βTRCP-mediated degradation of PDCD4 promotes protein translation and cell growth. *Science (80-.).* **314**, 467–471 (2006).
26. Fonseca, B. D. *et al.* The ever-evolving role of mTOR in translation. *Seminars in Cell and Developmental Biology* **36**, 102–112 (2014).
27. Fonseca, B. D., Lahr, R. M., Damgaard, C. K., Alain, T. & Berman, A. J. LARP1 on TOP of ribosome production. *Wiley Interdisciplinary Reviews: RNA* **9**, e1480 (2018).
28. Lahr, R. M. *et al.* La-related protein 1 (LARP1) binds the mRNA cap, blocking eIF4F assembly on TOP mRNAs. *Elife* **6**, (2017).
29. Aoki, K. *et al.* LARP1 specifically recognizes the 3′ terminus of poly(A) mRNA. *FEBS Lett.* **587**, 2173–2178 (2013).
30. Jia, J.-J. *et al.* mTORC1 promotes TOP mRNA translation through site-specific phosphorylation of LARP1. *Nucleic Acids Res.* (2021). doi:10.1093/nar/gkaa1239
31. Meyuhas, O. & Kahan, T. The race to decipher the top secrets of TOP mRNAs. *Biochimica et Biophysica Acta - Gene Regulatory Mechanisms* **1849**, 801–811 (2015).
32. Ingolia, N. T., Ghaemmaghami, S., Newman, J. R. S. & Weissman, J. S. Genome-wide analysis in vivo of translation with nucleotide resolution using ribosome profiling. *Science (80-.).* **324**, 218–223 (2009).
33. Johnstone, T. G., Bazzini, A. A. & Giraldez, A. J. Upstream ORF s are prevalent translational repressors in vertebrates . *EMBO J.* **35**, 706–723 (2016).
34. Morris, D. R. & Geballe, A. P. Upstream Open Reading Frames as Regulators of mRNA Translation. *Mol. Cell. Biol.* **20**, 8635–8642 (2000).
35. Barbosa, C., Peixeiro, I. & Romão, L. Gene expression regulation by upstream open reading frames and human disease. *PLoS Genet.* **9**, e1003529 (2013).
36. Kieft, J. S. Viral IRES RNA structures and ribosome interactions. *Trends in Biochemical Sciences* **33**, 274–283 (2008).
37. Yang, Y. & Wang, Z. IRES-mediated cap-independent translation, a path leading to hidden proteome. *J. Mol. Cell Biol.* **11**, 911–919 (2019).
38. Spriggs, K. A., Stoneley, M., Bushell, M. & Willis, A. E. Re-programming of translation following cell stress allows IRES-mediated translation to predominate. *Biol. Cell* **100**, 27–38 (2008).
39. Graber, T. E. & Holcik, M. Cap-independent regulation of gene expression in apoptosis. *Mol. Biosyst.* **3**, 825–834 (2007).
40. Pakos-Zebrucka, K. *et al.* The integrated stress response. *EMBO Rep.* **17**, 1374–1395 (2016).
41. Vazquez de Aldana, C. R., Wek, R. C., Segundo, P. S., Truesdell, A. G. & Hinnebusch, A.

G. Multicopy tRNA genes functionally suppress mutations in yeast eIF-2 alpha kinase GCN2: evidence for separate pathways coupling GCN4 expression to unchanged tRNA. *Mol. Cell. Biol.* **14**, 7920–7932 (1994).
42. Deng, J. *et al.* Activation of GCN2 in UV-irradiated cells inhibits translation. *Curr. Biol.* **12**, 1279–86 (2002).
43. Clemens, M. J. PKR - A protein kinase regulated by double-stranded RNA. *Int. J. Biochem. Cell Biol.* **29**, 945–949 (1997).
44. Carrara, M., Prischi, F., Nowak, P. R., Kopp, M. C. & Ali, M. M. U. Noncanonical binding of BiP ATPase domain to Ire1 and Perk is dissociated by unfolded protein CH1 to initiate ER stress signaling. *Elife* **2015**, (2015).
45. Bertolotti, A., Zhang, Y., Hendershot, L. M., Harding, H. P. & Ron, D. Dynamic interaction of BiP and ER stress transducers in the unfolded-protein response. *Nat. Cell Biol.* **2**, 326–332 (2000).
46. Gardner, B. M. & Walter, P. Unfolded proteins are Ire1-activating ligands that directly induce the unfolded protein response. *Science (80-.).* **333**, 1891–1894 (2011).
47. Young, S. K. & Wek, R. C. Upstream open reading frames differentially regulate genespecific translation in the integrated stress response. *Journal of Biological Chemistry* **291**, 16927–16935 (2016).
48. Andreev, D. E. *et al.* Translation of 5' leaders is pervasive in genes resistant to eIF2 repression. *Elife* **2015**, (2015).
49. Fruman, D. A. & Rommel, C. PI3K and cancer: Lessons, challenges and opportunities. *Nat. Rev. Drug Discov.* **13**, 140–156 (2014).
50. Kang, Y. *et al.* Transient activation of the PI3K/Akt pathway promotes Newcastle disease virus replication and enhances anti-apoptotic signaling responses. *Oncotarget* **8**, 23551–23563 (2017).
51. Soares, J. A. P. *et al.* Activation of the PI3K/Akt Pathway Early during Vaccinia and Cowpox Virus Infections Is Required for both Host Survival and Viral Replication. *J. Virol.* **83**, 6883–6899 (2009).
52. Zhu, L. *et al.* Biphasic activation of PI3K/Akt and MAPK/Erk1/2 signaling pathways in bovine herpesvirus type 1 infection of MDBK cells. *Vet. Res.* **42**, 57 (2011).
53. Weichhart, T., Hengstschläger, M. & Linke, M. Regulation of innate immune cell function by mTOR. *Nature Reviews Immunology* **15**, 599–614 (2015).
54. Kaur, S. *et al.* Regulatory effects of mammalian target of rapamycin-activated pathways in type I and II interferon signaling. *J. Biol. Chem.* **282**, 1757–68 (2007).
55. Colina, R. *et al.* Translational control of the innate immune response through IRF-7. *Nature* **452**, 323–328 (2008).
56. Cao, W. *et al.* Toll-like receptor-mediated induction of type I interferon in plasmacytoid dendritic cells requires the rapamycin-sensitive PI(3)K-mTOR-p70S6K pathway. *Nat. Immunol.* **9**, 1157–64 (2008).
57. Alain, T. *et al.* Vesicular stomatitis virus oncolysis is potentiated by impairing mTORC1-dependent type I IFN production. **107**, 1576–1581 (2010).
58. Dauber, B. & Wolff, T. Activation of the Antiviral Kinase PKR and Viral Countermeasures. *Viruses* **1**, 523–544 (2009).
59. Nallagatla, S. R. *et al.* 5'-triphosphate-dependent activation of PKR by RNAs with short stem-loops. *Science* **318**, 1455–8 (2007).
60. Dey, M., Mann, B. R., Anshu, A. & Mannan, M. A. U. Activation of protein kinase PKR

requires dimerization-induced cis-phosphorylation within the activation loop. *J. Biol. Chem.* **289**, 5747–5757 (2014).
61. Zhang, L. & Wang, A. Virus-induced ER stress and the unfolded protein response. *Front. Plant Sci.* **3**, 293 (2012).
62. Berlanga, J. J. *et al.* Antiviral effect of the mammalian translation initiation factor 2α kinase GCN2 against RNA viruses. *EMBO J.* **25**, 1730–1740 (2006).
63. Won, S. *et al.* Increased susceptibility to DNA virus infection in mice with a GCN2 mutation. *J. Virol.* **86**, 1802–8 (2012).
64. Zang, S. *et al.* HRI of Epinephelus coioides is a critical factor in the grouper immune response to RGNNV infection. *Fish Shellfish Immunol.* **87**, 659–668 (2019).
65. Perkins, D. J. & Barber, G. N. Defects in translational regulation mediated by the alpha subunit of eukaryotic initiation factor 2 inhibit antiviral activity and facilitate the malignant transformation of human fibroblasts. *Mol. Cell. Biol.* **24**, 2025–40 (2004).
66. Blais, J. D. *et al.* Activating transcription factor 4 is translationally regulated by hypoxic stress. *Mol. Cell. Biol.* **24**, 7469–82 (2004).
67. Lee, Y.-Y., Cevallos, R. C. & Jan, E. An upstream open reading frame regulates translation of GADD34 during cellular stresses that induce eIF2alpha phosphorylation. *J. Biol. Chem.* **284**, 6661–73 (2009).
68. Palam, L. R., Baird, T. D. & Wek, R. C. Phosphorylation of eIF2 facilitates ribosomal bypass of an inhibitory upstream ORF to enhance CHOP translation. *J. Biol. Chem.* **286**, 10939–49 (2011).
69. Xuan, B., Qian, Z., Torigoi, E. & Yu, D. Human cytomegalovirus protein pUL38 induces ATF4 expression, inhibits persistent JNK phosphorylation, and suppresses endoplasmic reticulum stress-induced cell death. *J. Virol.* **83**, 3463–74 (2009).
70. Shabman, R. S. *et al.* An upstream open reading frame modulates ebola virus polymerase translation and virus replication. *PLoS Pathog.* **9**, e1003147 (2013).
71. Ruggieri, A. *et al.* Dynamic Oscillation of Translation and Stress Granule Formation Mark the Cellular Response to Virus Infection. *Cell Host Microbe* **12**, 71–85 (2012).
72. White, J. P., Cardenas, A. M., Marissen, W. E. & Lloyd, R. E. Inhibition of Cytoplasmic mRNA Stress Granule Formation by a Viral Proteinase. *Cell Host Microbe* **2**, 295–305 (2007).
73. Li, W. *et al.* Cell proteins TIA-1 and TIAR interact with the 3' stem-loop of the West Nile virus complementary minus-strand RNA and facilitate virus replication. *J. Virol.* **76**, 11989–2000 (2002).
74. Albornoz, A., Carletti, T., Corazza, G. & Marcello, A. The stress granule component TIA-1 binds tick-borne encephalitis virus RNA and is recruited to perinuclear sites of viral replication to inhibit viral translation. *J. Virol.* **88**, 6611–22 (2014).
75. Nikolic, J., Civas, A., Lama, Z., Lagaudrière-Gesbert, C. & Blondel, D. Rabies Virus Infection Induces the Formation of Stress Granules Closely Connected to the Viral Factories. *PLoS Pathog.* **12**, e1005942 (2016).
76. Simpson-Holley, M. *et al.* Formation of antiviral cytoplasmic granules during orthopoxvirus infection. *J. Virol.* **85**, 1581–93 (2011).
77. Diamond, M. S. & Farzan, M. The broad-spectrum antiviral functions of IFIT and IFITM proteins. *Nat. Rev. Immunol.* **13**, 46–57 (2013).
78. Brennan-Laun, S. E., Ezelle, H. J., Li, X.-L. & Hassel, B. A. RNase-L control of cellular mRNAs: roles in biologic functions and mechanisms of substrate targeting. *J. Interferon*

Cytokine Res. **34**, 275–88 (2014).
79. Okumura, F., Zou, W. & Zhang, D.-E. ISG15 modification of the eIF4E cognate 4EHP enhances cap structure-binding activity of 4EHP. *Genes Dev.* **21**, 255–60 (2007).
80. Connor, J. H. & Lyles, D. S. Inhibition of host and viral translation during vesicular stomatitis virus infection: eIF2 is responsible for the inhibition of viral but not host translation. *J. Biol. Chem.* **280**, 13512–13519 (2005).
81. Connor, J. H. & Lyles, D. S. Vesicular stomatitis virus infection alters the eIF4F translation initiation complex and causes dephosphorylation of the eIF4E binding protein 4E-BP1. *J. Virol.* **76**, 10177–87 (2002).
82. Dunn, E. F. & Connor, J. H. Dominant Inhibition of Akt/Protein Kinase B Signaling by the Matrix Protein of a Negative-Strand RNA Virus. *J. Virol.* **85**, 422–431 (2011).
83. Chuluunbaatar, U. *et al.* Constitutive mTORC1 activation by a herpesvirus Akt surrogate stimulates mRNA translation and viral replication. **24**, 2627–2639 (2010).
84. Moorman, N. J. *et al.* Human Cytomegalovirus Protein UL38 Inhibits Host Cell Stress Responses by Antagonizing the Tuberous Sclerosis Protein Complex. *Cell Host Microbe* **3**, 253–262 (2008).
85. Ehrhardt, C. *et al.* Influenza A virus NS1 protein activates the PI3K/Akt pathway to mediate antiapoptotic signaling responses. *J. Virol.* **81**, 3058–67 (2007).
86. CSH, T., P, O., Teo, C. S. H. & O'Hare, P. A bimodal switch in global protein translation coupled to eIF4H relocalisation during advancing cell-cell transmission of herpes simplex virus. **14**, e1007196 (2018).
87. Bovee, M. L., Lamphear, B. J., Rhoads, R. E. & Lloyd, R. E. Direct cleavage of elF4G by poliovirus 2A protease is inefficient in vitro. *Virology* **245**, 241–9 (1998).
88. Alvarez, E., Menéndez-Arias, L. & Carrasco, L. The eukaryotic translation initiation factor 4GI is cleaved by different retroviral proteases. *J. Virol.* **77**, 12392–400 (2003).
89. Piron, M., Vende, P., Cohen, J. & Poncet, D. Rotavirus RNA-binding protein NSP3 interacts with eIF4GI and evicts the poly(A) binding protein from eIF4F. *EMBO J.* **17**, 5811–5821 (1998).
90. Goodfellow, I. *et al.* Calicivirus translation initiation requires an interaction between VPg and eIF 4 E. *EMBO Rep.* **6**, 968–72 (2005).
91. Borah, S., Darricarrère, N., Darnell, A., Myoung, J. & Steitz, J. A. A viral nuclear noncoding RNA binds re-localized poly(A) binding protein and is required for late KSHV gene expression. *PLoS Pathog.* **7**, e1002300 (2011).
92. Kanno, T., Sato, Y., Sata, T. & Katano, H. Expression of Kaposi's sarcoma-associated herpesvirus-encoded K10/10.1 protein in tissues and its interaction with poly(A)-binding protein. *Virology* **352**, 100–9 (2006).
93. Mailliot, J. & Martin, F. Viral internal ribosomal entry sites: four classes for one goal. *Wiley Interdiscip. Rev. RNA* **9**, e1458 (2018).
94. Ahn, B. Y. & Moss, B. Capped poly(A) leaders of variable lengths at the 5' ends of vaccinia virus late mRNAs. *J. Virol.* **63**, 226–232 (1989).
95. Schwer, B., Visca, P., Vos, J. C. & Stunnenberg, H. G. Discontinuous transcription or RNA processing of vaccinia virus late messengers results in a 5′ poly(A) leader. *Cell* **50**, 163–169 (1987).
96. Ink, B. S. & Pickup, D. J. Vaccinia virus directs the synthesis of early mRNAs containing 5′ poly(A) sequences. *Proc. Natl. Acad. Sci. U. S. A.* **87**, 1536–1540 (1990).
97. Dhungel, P., Cao, S. & Yang, Z. The 5'-poly(A) leader of poxvirus mRNA confers a

translational advantage that can be achieved in cells with impaired cap-dependent translation. *PLoS Pathog.* **13**, e1006602 (2017).
98. Shirokikh, N. E. & Spirin, A. S. Poly(A) leader of eukaryotic mRNA bypasses the dependence of translation on initiation factors. *Proc. Natl. Acad. Sci. U. S. A.* **105**, 10738–10743 (2008).
99. Jha, S. *et al.* Trans-kingdom mimicry underlies ribosome customization by a poxvirus kinase. *Nature* **546**, 651–655 (2017).
100. Inoue, Y. *et al.* Selective translation of the measles virus nucleocapsid mRNA by La protein. *Front. Microbiol.* **2**, (2011).
101. Khoo, D., Perez, C. & Mohr, I. Characterization of RNA Determinants Recognized by the Arginine- and Proline-Rich Region of Us11, a Herpes Simplex Virus Type 1-Encoded Double-Stranded RNA Binding Protein That Prevents PKR Activation. *J. Virol.* **76**, 11971–11981 (2002).
102. Bierle, C. J., Semmens, K. M. & Geballe, A. P. Double-stranded RNA binding by the human cytomegalovirus PKR antagonist TRS1. *Virology* **442**, 28–37 (2013).
103. Hatada, E. & Fukuda, R. Binding of influenza a virus NS1 protein to dsRNA in vitro. *J. Gen. Virol.* **73**, 3325–3329 (1992).
104. Yue, Z. & Shatkin, A. J. Double-Stranded RNA-Dependent Protein Kinase (PKR) Is Regulated by Reovirus Structural Proteins. *Virology* **234**, 364–371 (1997).
105. Romano, P. R. *et al.* Inhibition of double-stranded RNA-dependent protein kinase PKR by vaccinia virus E3: role of complex formation and the E3 N-terminal domain. *Mol. Cell. Biol.* **18**, 7304–16 (1998).
106. Vyas, J., Elia, A. & Clemens, M. J. Inhibition of the protein kinase PKR by the internal ribosome entry site of hepatitis C virus genomic RNA. *RNA* **9**, 858–70 (2003).
107. Ghadge, G. D., Swaminathan, S., Katze, M. G. & Thimmapaya, B. Binding of the adenovirus VAI RNA to the interferon-induced 68-kDa protein kinase correlates with function. *Proc. Natl. Acad. Sci. U. S. A.* **88**, 7140–4 (1991).
108. Clarke, P. A., Schwemmle, M., Schickinger, J., Hilse, K. & Clemens, M. J. Binding of Epstein-Barr virus small RNA EBER-1 to the double-stranded RNA-activated protein kinase DAI. *Nucleic Acids Res.* **19**, 243–8 (1991).
109. Gale, M. J., Korth, M. J. & Katze, M. G. Repression of the PKR protein kinase by the hepatitis C virus NS5A protein: a potential mechanism of interferon resistance. *Clin. Diagn. Virol.* **10**, 157–62 (1998).
110. Spurgeon, M. E. & Ornelles, D. A. The adenovirus E1B 55-kilodalton and E4 open reading frame 6 proteins limit phosphorylation of eIF2alpha during the late phase of infection. *J. Virol.* **83**, 9970–82 (2009).
111. Burýsek, L. & Pitha, P. M. Latently expressed human herpesvirus 8-encoded interferon regulatory factor 2 inhibits double-stranded RNA-activated protein kinase. *J. Virol.* **75**, 2345–52 (2001).
112. Van Opdenbosch, N., Van den Broeke, C., De Regge, N., Tabares, E. & Favoreel, H. W. The IE180 Protein of Pseudorabies Virus Suppresses Phosphorylation of Translation Initiation Factor eIF2 . *J. Virol.* **86**, 7235–7240 (2012).
113. He, B., Gross, M. & Roizman, B. The gamma(1)34.5 protein of herpes simplex virus 1 complexes with protein phosphatase 1alpha to dephosphorylate the alpha subunit of the eukaryotic translation initiation factor 2 and preclude the shutoff of protein synthesis by double-stranded RNA-activa. *Proc. Natl. Acad. Sci. U. S. A.* **94**, 843–8 (1997).

114. Zhang, F., Moon, A., Childs, K., Goodbourn, S. & Dixon, L. K. The African Swine Fever Virus DP71L Protein Recruits the Protein Phosphatase 1 Catalytic Subunit To Dephosphorylate eIF2α and Inhibits CHOP Induction but Is Dispensable for These Activities during Virus Infection. *J. Virol.* **84**, 10681–10689 (2010).
115. Kazemi, S. *et al.* Control of alpha subunit of eukaryotic translation initiation factor 2 (eIF2 alpha) phosphorylation by the human papillomavirus type 18 E6 oncoprotein: implications for eIF2 alpha-dependent gene expression and cell death. *Mol. Cell. Biol.* **24**, 3415–29 (2004).
116. Katsafanas, G. C. & Moss, B. Colocalization of transcription and translation within cytoplasmic poxvirus factories coordinates viral expression and subjugates host functions. *Cell Host Microbe* **2**, 221–8 (2007).
117. David, A. *et al.* RNA binding targets aminoacyl-tRNA synthetases to translating ribosomes. *J. Biol. Chem.* **286**, 20688–20700 (2011).
118. Desmet, E. A., Anguish, L. J. & Parker, J. S. L. Virus-mediated compartmentalization of the host translational machinery. *MBio* **5**, (2014).
119. Satterly, N. *et al.* Influenza virus targets the mRNA export machinery and the nuclear pore complex. *Proc. Natl. Acad. Sci. U. S. A.* **104**, 1853–1858 (2007).
120. Glodowski, D. R., Petersen, J. M. & Dahlberg, J. E. Complex nuclear localization signals in the matrix protein of vesicular stomatitis virus. *J. Biol. Chem.* **277**, 46864–46870 (2002).
121. Faria, P. A. *et al.* VSV Disrupts the Rae1/mrnp41 mRNA Nuclear Export Pathway. *Mol. Cell* **17**, 93–102 (2005).
122. García-Sastre, A. Induction and evasion of type I interferon responses by influenza viruses. *Virus Research* **162**, 12–18 (2011).
123. Ahmed, M. *et al.* Ability of the Matrix Protein of Vesicular Stomatitis Virus To Suppress Beta Interferon Gene Expression Is Genetically Correlated with the Inhibition of Host RNA and Protein Synthesis. *J. Virol.* **77**, 4646–4657 (2003).
124. Petersen, J. M., Her, L.-S., Varvel, V., Lund, E. & Dahlberg, J. E. The Matrix Protein of Vesicular Stomatitis Virus Inhibits Nucleocytoplasmic Transport When It Is in the Nucleus and Associated with Nuclear Pore Complexes. *Mol. Cell. Biol.* **20**, 8590–8601 (2000).
125. Malim, M. H., Hauber, J., Le, S. Y., Maizel, J. V. & Cullen, B. R. The HIV-1 rev trans-activator acts through a structured target sequence to activate nuclear export of unspliced viral mRNA. *Nature* **338**, 254–257 (1989).
126. Corbin-Lickfett, K. A., Chen, I. H. B., Cocco, M. J. & Sandri-Goldin, R. M. The HSV-1 ICP27 RGG box specifically binds flexible, GC-rich sequences but not G-quartet structures. *Nucleic Acids Res.* **37**, 7290–7301 (2009).
127. Koffa, M. D. *et al.* Herpes simplex virus ICP27 protein provides viral mRNAs with access to the cellular mRNA export pathway. *EMBO J.* **20**, 5769–5778 (2001).
128. Sandri-Goldin, R. M. ICP27 mediates HSV RNA export by shuttling through a leucine-rich nuclear export signal and binding viral intronless RNAs through an RGG motif. *Genes Dev.* **12**, 868–79 (1998).
129. Chen, I.-H. B., Li, L., Silva, L. & Sandri-Goldin, R. M. ICP27 Recruits Aly/REF but Not TAP/NXF1 to Herpes Simplex Virus Type 1 Transcription Sites although TAP/NXF1 Is Required for ICP27 Export. *J. Virol.* **79**, 3949–3961 (2005).
130. Kohlhapp, F. J. & Kaufman, H. L. Molecular pathways: Mechanism of action for talimogene laherparepvec, a new oncolytic virus immunotherapy. *Clin. Cancer Res.* **22**, 1048–1054 (2016).

131. Russell, S. J., Peng, K. & Bell, J. C. Oncolytic virotherapy. *Nat. Biotechnol.* **30**, 658–670 (2012).
132. Southam, C. M. DIVISION OF MICROBIOLOGY: PRESENT STATUS OF ONCOLYTIC VIRUS STUDIES*. *Trans. N. Y. Acad. Sci.* **22**, 657–673 (1960).
133. Asada, T. Treatment of human cancer with mumps virus. *Cancer* **34**, 1907–1928 (1974).
134. Martuza, R. L., Malick, A., Markert, J. M., Ruffner, K. L. & Coen, D. M. Experimental therapy of human glioma by means of a genetically engineered virus mutant. *Science (80-.).* **252**, 854–856 (1991).
135. Macedo, N., Miller, D. M., Haq, R. & Kaufman, H. L. Clinical landscape of oncolytic virus research in 2020. *Journal for ImmunoTherapy of Cancer* **8**, 1486 (2020).
136. Seymour, L. W. & Fisher, K. D. Oncolytic viruses: Finally delivering. *British Journal of Cancer* **114**, 357–361 (2016).
137. Andtbacka, R. H. I. *et al.* Final analyses of OPTiM: A randomized phase III trial of talimogene laherparepvec versus granulocyte-macrophage colony-stimulating factor in unresectable stage III-IV melanoma. *J. Immunother. Cancer* **7**, (2019).
138. Hanahan, D. & Weinberg, R. A. Hallmarks of Cancer: The Next Generation. *Cell* **144**, 646–674 (2011).
139. Ilkow, C. S., Swift, S. L., Bell, J. C. & Diallo, J. S. From Scourge to Cure: Tumour-Selective Viral Pathogenesis as a New Strategy against Cancer. *PLoS Pathogens* **10**, (2014).
140. von Locquenghien, M., Rozalén, C. & Celià-Terrassa, T. Interferons in cancer immunoediting: Sculpting metastasis and immunotherapy response. *Journal of Clinical Investigation* **131**, (2021).
141. Stojdl, D. F. *et al.* VSV strains with defects in their ability to shutdown innate immunity are potent systemic anti-cancer agents. *Cancer Cell* **4**, 263–275 (2003).
142. Bello, M. J. *et al.* Molecular analysis of genomic abnormalities in human gliomas. *Cancer Genet. Cytogenet.* **73**, 122–129 (1994).
143. Linge, C., Gewert, D., Rossmann, C., Crowe, J. S. & Bishop, J. A. N. Interferon System Defects in Human Malignant Melanoma. *Cancer Res.* **55**, 4099–4104 (1995).
144. Lu, R., Au, W. C., Yeow, W. S., Hageman, N. & Pitha, P. M. Regulation of the promoter activity of interferon regulatory factor-7 gene. Activation by interferon and silencing by hypermethylation. *J. Biol. Chem.* **275**, 31805–31812 (2000).
145. Matin, S. F. *et al.* Impaired α-interferon signaling in transitional cell carcinoma: Lack of p48 expression in 5637 cells. *Cancer Res.* **61**, 2261–2266 (2001).
146. Angelova, M. *et al.* Evolution of Metastases in Space and Time under Immune Selection. *Cell* **175**, 751-765.e16 (2018).
147. Williams, J. B. *et al.* Tumor heterogeneity and clonal cooperation influence the immune selection of IFN-γ-signaling mutant cancer cells. *Nat. Commun.* **11**, 1–14 (2020).
148. Weichselbaum, R. R. *et al.* An interferon-related gene signature for DNA damage resistance is a predictive marker for chemotherapy and radiation for breast cancer. *Proc. Natl. Acad. Sci. U. S. A.* **105**, 18490–18495 (2008).
149. Roulois, D. *et al.* DNA-Demethylating Agents Target Colorectal Cancer Cells by Inducing Viral Mimicry by Endogenous Transcripts. *Cell* **162**, 961–973 (2015).
150. Deblois, G. *et al.* Epigenetic Switch–Induced Viral Mimicry Evasion in Chemotherapy-Resistant Breast Cancer. *Cancer Discov.* **10**, 1312–1329 (2020).
151. Nabet, B. Y. *et al.* Exosome RNA Unshielding Couples Stromal Activation to Pattern Recognition Receptor Signaling in Cancer. *Cell* **170**, 352-366.e13 (2017).

152. Boelens, M. C. *et al.* Exosome transfer from stromal to breast cancer cells regulates therapy resistance pathways. *Cell* **159**, 499–513 (2014).
153. Liu, B. L. *et al.* ICP34.5 deleted herpes simplex virus with enhanced oncolytic, immune stimulating, and anti-tumour properties. *Gene Therapy* **10**, 292–303 (2003).
154. Liu, Y. P., Suksanpaisan, L., Steele, M. B., Russell, S. J. & Peng, K. W. Induction of antiviral genes by the tumor microenvironment confers resistance to virotherapy. *Sci. Rep.* **3**, (2013).
155. Selman, M. *et al.* Dimethyl fumarate potentiates oncolytic virotherapy through NF-B inhibition. *Sci. Transl. Med.* **10**, 1613 (2018).
156. Diallo, J. S. *et al.* A high-throughput pharmacoviral approach identifies novel oncolytic virus sensitizers. *Mol. Ther.* **18**, 1123–1129 (2010).
157. Slabaugh, M., Roseman, N., Davis, R. & Mathews, C. Vaccinia virus-encoded ribonucleotide reductase: sequence conservation of the gene for the small subunit and its amplification in hydroxyurea-resistant mutants. *J. Virol.* **62**, 519–527 (1988).
158. Frame, M. C., Marsden, H. S. & Dutia, B. M. The ribonucleotide reductase induced by herpes simplex virus type 1 involves minimally a complex of two polypeptides (136K and 38K). *J. Gen. Virol.* **66**, 1581–1587 (1985).
159. Chen, M. S., Summers, W. P., Walker, J., Summers, W. C. & Prusoff, W. H. Characterization of pyrimidine deoxyribonucleoside kinase (thymidine kinase) and thymidylate kinase as a multifunctional enzyme in cells transformed by herpes simplex virus type 1 and in cells infected with mutant strains of herpes simplex virus. *J. Virol.* **30**, 942–945 (1979).
160. Black, M. E. & Hruby, D. E. Structure and function of vaccinia virus thymidine kinase: Biomedical relevance and implications for antiviral drug design. *Rev. Med. Virol.* **1**, 235–245 (1991).
161. Kim, J. H. *et al.* Systemic Armed Oncolytic and Immunologic Therapy for Cancer with JX-594, a Targeted Poxvirus Expressing GM-CSF. *Mol. Ther.* **14**, 361–370 (2006).
162. Xu, Y. & Ruggero, D. The Role of Translation Control in Tumorigenesis and Its Therapeutic Implications. *Annual Review of Cancer Biology* **4**, 437–457 (2020).
163. Iritani, B. M. & Eisenman, R. N. c-Myc enhances protein synthesis and cell size during B lymphocyte development. *Proc. Natl. Acad. Sci. U. S. A.* **96**, 13180–13185 (1999).
164. Zoncu, R., Efeyan, A. & Sabatini, D. M. MTOR: From growth signal integration to cancer, diabetes and ageing. *Nature Reviews Molecular Cell Biology* **12**, 21–35 (2011).
165. Liu, T. C., Wakimoto, H., Martuza, R. L. & Rabkin, S. D. Herpes simplex virus Us3(-) mutant as oncolytic strategy and synergizes with phosphatidylinositol 3-kinase-Akt-targeting molecular therapeutics. *Clin. Cancer Res.* **13**, 5897–5902 (2007).
166. Mohr, I. *et al.* A Herpes Simplex Virus Type 1 γ34.5 Second-Site Suppressor Mutant That Exhibits Enhanced Growth in Cultured Glioblastoma Cells Is Severely Attenuated in Animals. *J. Virol.* **75**, 5189–5196 (2001).
167. Corredor, J. C. *et al.* N-Myc expression enhances the oncolytic effects of vesicular stomatitis virus in human neuroblastoma cells. *Mol. Ther. - Oncolytics* **3**, 16005 (2016).
168. Kastan, M. B. & Bartek, J. Cell-cycle checkpoints and cancer. *Nature* **432**, 316–323 (2004).
169. Fan, Y., Sanyal, S. & Bruzzone, R. Breaking Bad: How Viruses Subvert the Cell Cycle. *Frontiers in cellular and infection microbiology* **8**, 396 (2018).
170. Poggioli, G. J. *et al.* Reovirus-Induced Alterations in Gene Expression Related to Cell Cycle Regulation. *J. Virol.* **76**, 2585–2594 (2002).

171. Yoo, N. K., Pyo, C. W., Kim, Y., Ahn, B. Y. & Choi, S. Y. Vaccinia virus-mediated cell cycle alteration involves inactivation of tumour suppressors associated with Brf1 and TBP. *Cell. Microbiol.* **10**, 583–592 (2008).
172. Flemington, E. K. Herpesvirus Lytic Replication and the Cell Cycle: Arresting New Developments. *J. Virol.* **75**, 4475–4481 (2001).
173. Bandara, L. R. & La Thangue, N. B. Adenovirus E1a prevents the retinoblastoma gene product from complexing with a cellular transcription factor. *Nature* **351**, 494–497 (1991).
174. McCormick, F. Interactions between adenovirus proteins and the p53 pathway: The development of ONYX-015. *Semin. Cancer Biol.* **10**, 453–459 (2000).
175. Martin, M. E. D. & Berk, A. J. Adenovirus E1B 55K Represses p53 Activation In Vitro. *J. Virol.* **72**, 3146–3154 (1998).
176. Guo, Z. S. *et al.* The enhanced tumor selectivity of an oncolytic vaccinia lacking the host range and antiapoptosis genes SPI-1 and SPI-2. *Cancer Res.* **65**, 9991–9998 (2005).
177. Fujiwara, T., Urata, Y. & Tanaka, N. Telomerase-Specific Oncolytic Virotherapy for Human Cancer with the hTERT Promoter. *Curr. Cancer Drug Targets* **7**, 191–201 (2007).
178. Lee, C. Y. *et al.* Transcriptional and translational dual-regulated oncolytic herpes simplex virus type 1 for targeting prostate tumors. *Mol. Ther.* **18**, 929–935 (2010).
179. Leber, M. F. *et al.* MicroRNA-sensitive oncolytic measles viruses for cancer-specific vector tropism. *Mol. Ther.* **19**, 1097–1106 (2011).
180. Cawood, R., Wong, S. L., Di, Y., Baban, D. F. & Seymour, L. W. MicroRNA controlled adenovirus mediates anti-cancer efficacy without affecting endogenous microRNA activity. *PLoS One* **6**, (2011).
181. Nakamura, T. *et al.* Rescue and propagation of fully retargeted oncolytic measles viruses. *Nat. Biotechnol.* **23**, 209–214 (2005).
182. Ong, H. T. *et al.* Intravascularly administered RGD-displaying measles viruses bind to and infect neovessel endothelial cells in vivo. *Mol. Ther.* **17**, 1012–1021 (2009).
183. Yang, X. *et al.* Evaluation of IRES-mediated, cell-type-specific cytotoxicity of poliovirus using a colorimetric cell proliferation assay. *J. Virol. Methods* **155**, 44–54 (2009).
184. Pearl, T. M., Markert, J. M., Cassady, K. A. & Ghonime, M. G. Oncolytic Virus-Based Cytokine Expression to Improve Immune Activity in Brain and Solid Tumors. *Molecular Therapy - Oncolytics* **13**, 14–21 (2019).
185. Sorensen, M. R., Holst, P. J., Steffensen, M. A., Christensen, J. P. & Thomsen, A. R. Adenoviral vaccination combined with CD40 stimulation and CTLA-4 blockage can lead to complete tumor regression in a murine melanoma model. *Vaccine* **28**, 6757–6764 (2010).
186. Pol, J. G. *et al.* Preclinical evaluation of a MAGE-A3 vaccination utilizing the oncolytic Maraba virus currently in first-in-human trials. *Oncoimmunology* **8**, (2019).
187. Bressy, C., Hastie, E. & Grdzelishvili, V. Z. Combining Oncolytic Virotherapy with p53 Tumor Suppressor Gene Therapy. *Molecular Therapy - Oncolytics* **5**, 20–40 (2017).
188. Russell, L. *et al.* PTEN expression by an oncolytic herpesvirus directs T-cell mediated tumor clearance. *Nat. Commun.* **9**, 1–16 (2018).
189. Ding, M. *et al.* Prostate Cancer-Specific and Potent Antitumor Effect of a DD3-Controlled Oncolytic Virus Harboring the PTEN Gene. *PLoS One* **7**, e35153 (2012).
190. Guffey, M. B. *et al.* Engineered herpes simplex virus expressing bacterial cytosine deaminase for experimental therapy of brain tumors. *Cancer Gene Ther.* **14**, 45–56 (2007).
191. Dingli, D. *et al.* Image-guided radiovirotherapy for multiple myeloma using a recombinant measles virus expressing the thyroidal sodium iodide symporter. *Blood* **103**, 1641–1646

(2004).
192. Bainbridge, M. N. *et al.* Analysis of the prostate cancer cell line LNCaP transcriptome using a sequencing-by-synthesis approach. *BMC Genomics* **7**, 246 (2006).
193. Schoggins, J. W. & Rice, C. M. Interferon-stimulated genes and their antiviral effector functions. *Current Opinion in Virology* **1**, 519–525 (2011).
194. Schoggins, J. W. Interferon-Stimulated Genes: What Do They All Do? *Annu. Rev. Virol.* **6**, 567–584 (2019).
195. Tirosh, O. *et al.* The Transcription and Translation Landscapes during Human Cytomegalovirus Infection Reveal Novel Host-Pathogen Interactions. *PLoS Pathog.* **11**, 1–29 (2015).
196. Stern-Ginossar, N. & Ingolia, N. T. Ribosome Profiling as a Tool to Decipher Viral Complexity. *Annual Review of Virology* **2**, 335–349 (2015).
197. Dai, A. *et al.* Ribosome Profiling Reveals Translational Upregulation of Cellular Oxidative Phosphorylation mRNAs during Vaccinia Virus-Induced Host Shutoff. *J. Virol.* **91**, 1858–1874 (2017).
198. Stern-Ginossar, N. *et al.* Decoding human cytomegalovirus. *Science (80-.).* **338**, 1088–1093 (2012).
199. Arias, C. *et al.* KSHV 2.0: A Comprehensive Annotation of the Kaposi's Sarcoma-Associated Herpesvirus Genome Using Next-Generation Sequencing Reveals Novel Genomic and Functional Features. *PLoS Pathog.* **10**, e1003847 (2014).
200. Finkel, Y. *et al.* The coding capacity of SARS-CoV-2. *Nature* **589**, 125–130 (2021).
201. Puray-Chavez, M. *et al.* The translational landscape of SARS-CoV-2 and infected cells. *bioRxiv* (2020). doi:10.1101/2020.11.03.367516
202. Li, M. M. H., MacDonald, M. R. & Rice, C. M. To translate, or not to translate: viral and host mRNA regulation by interferon-stimulated genes. *Trends Cell Biol.* **25**, 320–9 (2015).
203. Nguyên, T. L. A. *et al.* Chemical targeting of the innate antiviral response by histone deacetylase inhibitors renders refractory cancers sensitive to viral oncolysis. *Proc. Natl. Acad. Sci. U. S. A.* **105**, 14981–14986 (2008).
204. Smith, B. L., Chen, G., Wilke, C. O. & Krug, R. M. Avian influenza virus PB1 gene in H3N2 viruses evolved in humans to reduce interferon inhibition by skewing codon usage toward interferon-altered tRNA pools. *MBio* **9**, (2018).
205. Leber, M. F. *et al.* Enhanced Control of Oncolytic Measles Virus Using MicroRNA Target Sites. *Mol. Ther. - Oncolytics* **9**, 30–40 (2018).
206. Gingold, H. *et al.* A dual program for translation regulation in cellular proliferation and differentiation. *Cell* **158**, 1281–1292 (2014).
207. Villanueva, E., Martí-Solano, M. & Fillat, C. Codon optimization of the adenoviral fiber negatively impacts structural protein expression and viral fitness. *Sci. Rep.* **6**, 1–10 (2016).
208. Hoang, H. D., Neault, S., Pelin, A. & Alain, T. Emerging translation strategies during virus–host interaction. *Wiley Interdisciplinary Reviews: RNA* (2020). doi:10.1002/wrna.1619
209. Jones, R. G. & Pearce, E. J. MenTORing Immunity: mTOR Signaling in the Development and Function of Tissue-Resident Immune Cells. *Immunity* **46**, 730–742 (2017).
210. Mazumder, B., Li, X. & Barik, S. Translation Control: A Multifaceted Regulator of Inflammatory Response. *J. Immunol.* **184**, 3311–3319 (2010).
211. Weichhart, T. *et al.* The TSC-mTOR Signaling Pathway Regulates the Innate Inflammatory Response. *Immunity* **29**, 565–577 (2008).
212. Sinclair, L. V. *et al.* Phosphatidylinositol-3-OH kinase and nutrient-sensing mTOR

pathways control T lymphocyte trafficking. *Nat. Immunol.* **9**, 513–521 (2008).
213. Morice, W. G., Brunn, G. J., Wiederrecht, G., Siekierka, J. J. & Abraham, R. T. Rapamycin-induced inhibition of p34cdc2 kinase activation is associated with G1/S-phase growth arrest in T lymphocytes. *J. Biol. Chem.* **268**, 3734–8 (1993).
214. Araki, K. *et al.* mTOR regulates memory CD8 T-cell differentiation. *Nature* **460**, 108–112 (2009).
215. Bakheet, T., Frevel, M., Williams, B. R. G., Greer, W. & Khabar, K. S. A. ARED: Human AU-rich element-containing mRNA database reveals an unexpectedly diverse functional repertoire of encoded proteins. *Nucleic Acids Res.* **29**, 246–254 (2001).
216. Buxadé, M. *et al.* The Mnks are novel components in the control of TNFα biosynthesis and phosphorylate and regulate hnRNP A1. *Immunity* **23**, 177–189 (2005).
217. Piecyk, M. *et al.* TIA-1 is a translational silencer that selectively regulates the expression of TNF-α. *EMBO J.* **19**, 4154–4163 (2000).
218. Gueydan, C. *et al.* Identification of TIAR as a protein binding to the translational regulatory AU-rich element of tumor necrosis factor α mRNA. *J. Biol. Chem.* **274**, 2322–2326 (1999).
219. Kedersha, N. L., Gupta, M., Li, W., Miller, I. & Anderson, P. RNA-binding proteins TIA-1 and TIAR link the phosphorylation of eIF-2α to the assembly of mammalian stress granules. *J. Cell Biol.* **147**, 1431–1441 (1999).
220. Sampath, P., Mazumder, B., Seshadri, V. & Fox, P. L. Transcript-Selective Translational Silencing by Gamma Interferon Is Directed by a Novel Structural Element in the Ceruloplasmin mRNA 3′ Untranslated Region. *Mol. Cell. Biol.* **23**, 1509–1519 (2003).
221. Sampath, P. *et al.* Noncanonical function of glutamyl-prolyl-tRNA synthetase: Gene-specific silencing of translation. *Cell* **119**, 195–208 (2004).
222. Mazumder, B. *et al.* Regulated release of L13a from the 60S ribosomal subunit as a mechanism of transcript-specific translational control. *Cell* **115**, 187–198 (2003).
223. Plank, M., Maltby, S., Mattes, J. & Foster, P. S. Targeting translational control as a novel way to treat inflammatory disease: the emerging role of microRNAs. *Clin. Exp. Allergy* **43**, 981–99 (2013).
224. Djuranovic, S., Nahvi, A. & Green, R. miRNA-mediated gene silencing by translational repression followed by mRNA deadenylation and decay. *Science (80-.).* **336**, 237–240 (2012).
225. Hafner, M., Ascano, M. & Tuschl, T. New insights in the mechanism of microRNA-mediated target repression. *Nature Structural and Molecular Biology* **18**, 1181–1182 (2011).
226. Chen, X. M., Splinter, P. L., O'Hara, S. P. & LaRusso, N. F. A cellular micro-RNA, let-7i, regulates toll-like receptor 4 expression and contributes to cholangiocyte immune responses against Cryptosporidium parvum infection. *J. Biol. Chem.* **282**, 28929–28938 (2007).
227. Bazzoni, F. *et al.* Induction and regulatory function of miR-9 in human monocytes and neutrophils exposed to proinflammatory signals. *Proc. Natl. Acad. Sci. U. S. A.* **106**, 5282–5287 (2009).
228. Sheedy, F. J. *et al.* Negative regulation of TLR4 via targeting of the proinflammatory tumor suppressor PDCD4 by the microRNA miR-21. *Nat. Immunol.* **11**, 141–147 (2010).
229. Liu, G. *et al.* miR-147, a microRNA that is induced upon toll-like receptor stimulation, regulates murine macrophage inflammatory responses. *Proc. Natl. Acad. Sci. U. S. A.* **106**, 15819–15824 (2009).
230. Tili, E. *et al.* Modulation of miR-155 and miR-125b Levels following Lipopolysaccharide/TNF-α Stimulation and Their Possible Roles in Regulating the

Response to Endotoxin Shock. *J. Immunol.* **179**, 5082–5089 (2007).
231. Taganov, K. D., Boldin, M. P., Chang, K. J. & Baltimore, D. NF-κB-dependent induction of microRNA miR-146, an inhibitor targeted to signaling proteins of innate immune responses. *Proc. Natl. Acad. Sci. U. S. A.* **103**, 12481–12486 (2006).
232. Kurowska-Stolarska, M. *et al.* MicroRNA-155 as a proinflammatory regulator in clinical and experimental arthritis. *Proc. Natl. Acad. Sci. U. S. A.* **108**, 11193–11198 (2011).
233. Tabas, I., García-Cardeña, G. & Owens, G. K. Recent insights into the cellular biology of atherosclerosis. *Journal of Cell Biology* **209**, 13–22 (2015).
234. Moore, K. J. & Tabas, I. Macrophages in the pathogenesis of atherosclerosis. *Cell* **145**, 341–355 (2011).
235. Mai, W. & Liao, Y. Targeting IL-1β in the Treatment of Atherosclerosis. *Frontiers in Immunology* **11**, (2020).
236. Navab, M. *et al.* Structure and function of HDL mimetics. *Arteriosclerosis, Thrombosis, and Vascular Biology* **30**, 164–168 (2010).
237. Klingenberg, R. & Hansson, G. K. Treating inflammation in atherosclerotic cardiovascular disease: Emerging therapies. *European Heart Journal* **30**, 2838–2844 (2009).
238. Feinberg, M. W. & Moore, K. J. MicroRNA Regulation of Atherosclerosis. *Circ. Res.* **118**, 703–720 (2016).
239. Schneider, W. M., Chevillotte, M. D. & Rice, C. M. Interferon-stimulated genes: a complex web of host defenses. *Annu. Rev. Immunol.* **32**, 513–45 (2014).
240. Walsh, D., Mathews, M. B. & Mohr, I. Tinkering with translation: Protein synthesis in virus-infected cells. *Cold Spring Harb. Perspect. Biol.* **5**, a012351 (2013).
241. Sonenberg, N. & Hinnebusch, A. G. Regulation of translation initiation in eukaryotes: mechanisms and biological targets. *Cell* **136**, 731–45 (2009).
242. Shi, Z. & Barna, M. Translating the Genome in Time and Space: Specialized Ribosomes, RNA Regulons, and RNA-Binding Proteins. *Annu. Rev. Cell Dev. Biol.* **31**, 31–54 (2015).
243. Colina, R. *et al.* Translational control of the innate immune response through IRF-7. *Nature* **452**, 323–328 (2008).
244. Zakaria, C. *et al.* Active-site mTOR inhibitors augment HSV1-dICP0 infection in cancer cells via dysregulated eIF4E/4E-BP axis. *PLOS Pathog.* **14**, e1007264 (2018).
245. Graber, T. E., Baird, S. D., Kao, P. N., Mathews, M. B. & Holcik, M. NF45 functions as an IRES trans-acting factor that is required for translation of cIAP1 during the unfolded protein response. *Cell Death Differ* **17**, 719–729 (2010).
246. Wang, X., Hou, J., Quedenau, C. & Chen, W. Pervasive isoform-specific translational regulation via alternative transcription start sites in mammals. *Mol. Syst. Biol.* **12**, 875 (2016).
247. Tirosh, O. *et al.* The Transcription and Translation Landscapes during Human Cytomegalovirus Infection Reveal Novel Host-Pathogen Interactions. *PLoS Pathog.* **11**, e1005288 (2015).
248. Harrington, K., Freeman, D. J., Kelly, B., Harper, J. & Soria, J. C. Optimizing oncolytic virotherapy in cancer treatment. *Nature Reviews Drug Discovery* (2019). doi:10.1038/s41573-019-0029-0
249. Desai, P. & Person, S. Incorporation of the green fluorescent protein into the herpes simplex virus type 1 capsid. *J. Virol.* **72**, 7563–8 (1998).
250. Langmead, B. & Salzberg, S. L. Fast gapped-read alignment with Bowtie 2. *Nat. Methods* **9**, 357–359 (2012).

251. Oliveros, J. C. -Venny-. Venn Diagrams for comparing lists. By Juan Carlos Oliveros. (2007). Available at: http://bioinfogp.cnb.csic.es/tools/venny_old/venny.php. (Accessed: 1st January 2007)
252. Maere, S., Heymans, K. & Kuiper, M. BiNGO: a Cytoscape plugin to assess overrepresentation of Gene Ontology categories in Biological Networks. *Bioinformatics* **21**, 3448–3449 (2005).
253. Shannon, P. *et al.* Cytoscape: A Software Environment for Integrated Models of Biomolecular Interaction Networks. *Genome Res.* **13**, 2498–2504 (2003).
254. Diallo, J.-S., Vähä-Koskela, M., Le Boeuf, F. & Bell, J. Propagation, Purification, and In Vivo Testing of Oncolytic Vesicular Stomatitis Virus Strains. in *Methods in molecular biology (Clifton, N.J.)* **797**, 127–140 (2012).
255. Gandin, V. *et al.* Polysome fractionation and analysis of mammalian translatomes on a genome-wide scale. *J. Vis. Exp.* (2014). doi:10.3791/51455
256. Jafarnejad, S. M. *et al.* Translational control of ERK signaling through miRNA/4EHP-directed silencing. *Elife* **7**, (2018).
257. Gordon, A. FASTQ/A short-reads pre-processing tools. (2010). Available at: http://hannonlab.cshl.edu/fastx_toolkit/. (Accessed: 1st January 2010)
258. Riley, A., Jordan, L. E. & Holcik, M. Distinct 5′ UTRs regulate XIAP expression under normal growth conditions and during cellular stress. *Nucleic Acids Res.* **38**, 4665–4674 (2010).
259. Sanjana, N. E., Shalem, O. & Zhang, F. Improved vectors and genome-wide libraries for CRISPR screening. *Nat. Methods* **11**, 783–784 (2014).
260. Abernathy, E. *et al.* Gammaherpesviral Gene Expression and Virion Composition Are Broadly Controlled by Accelerated mRNA Degradation. *PLoS Pathog.* **10**, e1003882 (2014).
261. Tebaldi, T. *et al.* Widespread uncoupling between transcriptome and translatome variations after a stimulus in mammalian cells. *BMC Genomics* **13**, 220 (2012).
262. Schoggins, J. W. *et al.* A diverse range of gene products are effectors of the type I interferon antiviral response. *Nature* **472**, 481–485 (2011).
263. Boldt, K. *et al.* An organelle-specific protein landscape identifies novel diseases and molecular mechanisms. *Nat Commun* **7**, 11491 (2016).
264. Nachury, M. V *et al.* A core complex of BBS proteins cooperates with the GTPase Rab8 to promote ciliary membrane biogenesis. *Cell* **129**, 1201–13 (2007).
265. Brinkman, E. K., Chen, T., Amendola, M. & van Steensel, B. Easy quantitative assessment of genome editing by sequence trace decomposition. *Nucleic Acids Res.* **42**, e168–e168 (2014).
266. Johansson, P. J., Myhre, E. B. & Blomberg, J. Specificity of Fc receptors induced by herpes simplex virus type 1: comparison of immunoglobulin G from different animal species. *J. Virol.* **56**, 489–94 (1985).
267. Katz, Y., Wang, E. T., Airoldi, E. M. & Burge, C. B. Analysis and design of RNA sequencing experiments for identifying isoform regulation. *Nat. Methods* **7**, 1009–1015 (2010).
268. Ilan, L. *et al.* PKR activation and eIF2α phosphorylation mediate human globin mRNA splicing at spliceosome assembly. *Cell Res.* **27**, 688–704 (2017).
269. Fields, A. P. *et al.* A Regression-Based Analysis of Ribosome-Profiling Data Reveals a Conserved Complexity to Mammalian Translation. *Mol. Cell* **60**, 816–827 (2015).

270. Sendoel, A. *et al.* Translation from unconventional 5′ start sites drives tumour initiation. *Nature* (2017). doi:10.1038/nature21036
271. Mar, K. B. *et al.* LY6E mediates an evolutionarily conserved enhancement of virus infection by targeting a late entry step. *Nat. Commun.* **9**, 3603 (2018).
272. Herdy, B. *et al.* Translational control of the activation of transcription factor NF-kappaB and production of type I interferon by phosphorylation of the translation factor eIF4E. *Nat Immunol* **13**, 543–550 (2012).
273. Jacoby, M. *et al.* INPP5E mutations cause primary cilium signaling defects, ciliary instability and ciliopathies in human and mouse. *Nat. Genet.* **41**, 1027–1031 (2009).
274. Sierra Potchanant, E. A. *et al.* INPP5E Preserves Genomic Stability through Regulation of Mitosis. *Mol. Cell. Biol.* **37**, (2017).
275. Dyson, J. M. *et al.* INPP5E regulates phosphoinositide-dependent cilia transition zone function. *J. Cell Biol.* **216**, 247–263 (2017).
276. Phua, S. C. *et al.* Dynamic Remodeling of Membrane Composition Drives Cell Cycle through Primary Cilia Excision. *Cell* **168**, 264-279.e15 (2017).
277. Kawasaki, T., Takemura, N., Standley, D. M., Akira, S. & Kawai, T. The Second Messenger Phosphatidylinositol-5-Phosphate Facilitates Antiviral Innate Immune Signaling. *Cell Host Microbe* **14**, 148–158 (2013).
278. Saarikangas, J., Zhao, H. & Lappalainen, P. Regulation of the Actin Cytoskeleton-Plasma Membrane Interplay by Phosphoinositides. *Physiol. Rev.* **90**, 259–289 (2010).
279. Taylor, M. P., Koyuncu, O. O. & Enquist, L. W. Subversion of the actin cytoskeleton during viral infection. *Nat. Rev. Microbiol.* **9**, 427–439 (2011).
280. Starks, R. D. *et al.* Regulation of Insulin Receptor Trafficking by Bardet Biedl Syndrome Proteins. *PLOS Genet.* **11**, e1005311 (2015).
281. Yen, H.-J. *et al.* Bardet–Biedl syndrome genes are important in retrograde intracellular trafficking and Kupffer's vesicle cilia function. *Hum. Mol. Genet.* **15**, 667–677 (2006).
282. Floor, S. N. & Doudna, J. A. Tunable protein synthesis by transcript isoforms in human cells. *Elife* **5**, e10921 (2016).
283. Mayr, C. & Bartel, D. P. Widespread Shortening of 3′UTRs by Alternative Cleavage and Polyadenylation Activates Oncogenes in Cancer Cells. *Cell* **138**, 673–684 (2009).
284. Ku, C.-C. *et al.* Herpes simplex virus-1 induces expression of a novel MxA isoform that enhances viral replication. *Immunol. Cell Biol.* **89**, 173–182 (2011).
285. Wang, P.-H. *et al.* A novel transcript isoform of STING that sequesters cGAMP and dominantly inhibits innate nucleic acid sensing. *Nucleic Acids Res.* (2018). doi:10.1093/nar/gky186
286. Rutkowski, A. J. *et al.* Widespread disruption of host transcription termination in HSV-1 infection. *Nat. Commun.* **6**, 7126 (2015).
287. Tang, S., Patel, A. & Krause, P. R. Herpes simplex virus ICP27 regulates alternative pre-mRNA polyadenylation and splicing in a sequence-dependent manner. *Proc. Natl. Acad. Sci.* **113**, 12256–12261 (2016).
288. Frankiw, L. *et al.* BUD13 Promotes a Type I Interferon Response by Countering Intron Retention in Irf7. *Mol. Cell* (2019). doi:10.1016/J.MOLCEL.2018.11.038
289. Ray, D. *et al.* A compendium of RNA-binding motifs for decoding gene regulation. *Nature* **499**, 172–177 (2013).
290. Bailey, T. L., Johnson, J., Grant, C. E. & Noble, W. S. The MEME Suite. *Nucleic Acids Res.* **43**, W39-49 (2015).

291. Fan, Y. *et al.* miRNet - dissecting miRNA-target interactions and functional associations through network-based visual analysis. *Nucleic Acids Res* **44**, W135-41 (2016).
292. Zhang, Q. & Liu, F. Advances and potential pitfalls of oncolytic viruses expressing immunomodulatory transgene therapy for malignant gliomas. *Cell Death and Disease* **11**, 1–11 (2020).
293. Zheng, M., Huang, J., Tong, A. & Yang, H. Oncolytic Viruses for Cancer Therapy: Barriers and Recent Advances. *Molecular Therapy - Oncolytics* **15**, 234–247 (2019).
294. Conner, J. & Braidwood, L. Expression of inhibitor of growth 4 by HSV1716 improves oncolytic potency and enhances efficacy. *Cancer Gene Ther.* **19**, 499–507 (2012).
295. Serafini, P. *et al.* High-dose granulocyte-macrophage colony-stimulating factor-producing vaccines impair the immune response through the recruitment of myeloid suppressor cells. *Cancer Res.* **64**, 6337–6343 (2004).
296. Cripe, T. P. *et al.* Pediatric cancer gone viral. Part I: Strategies for utilizing oncolytic herpes simplex virus-1 in children. *Molecular Therapy - Oncolytics* **2**, 15015 (2015).
297. Walsh, D. & Mohr, I. Viral subversion of the host protein synthesis machinery. *Nat Rev Microbiol* **9**, 860–875 (2011).
298. Mears, W. E. & Rice, S. A. The RGG box motif of the herpes simplex virus ICP27 protein mediates an RNA-binding activity and determines in vivo methylation. *J. Virol.* **70**, (1996).
299. Rivera, A. A. *et al.* Mode of transgene expression after fusion to early or late viral genes of a conditionally replicating adenovirus via an optimized internal ribosome entry site in vitro and in vivo. *Virology* **320**, 121–134 (2004).
300. Minaker, R. L., Mossman, K. L. & Smiley, J. R. Functional inaccessibility of quiescent herpes simplex virus genomes. *Virol. J.* **2**, (2005).
301. Hoang, H. D. *et al.* Induction of an Alternative mRNA 5′ Leader Enhances Translation of the Ciliopathy Gene Inpp5e and Resistance to Oncolytic Virus Infection. *Cell Rep.* **29**, 4010-4023.e5 (2019).
302. Kim, D., Langmead, B. & Salzberg, S. L. HISAT: A fast spliced aligner with low memory requirements. *Nat. Methods* **12**, 357–360 (2015).
303. Afgan, E. *et al.* The Galaxy platform for accessible, reproducible and collaborative biomedical analyses: 2018 update. *Nucleic Acids Res.* **46**, W537–W544 (2018).
304. Trapnell, C. *et al.* Transcript assembly and quantification by RNA-Seq reveals unannotated transcripts and isoform switching during cell differentiation. *Nat. Biotechnol.* **28**, 511–515 (2010).
305. Graber, T. E., Baird, S. D., Kao, P. N., Mathews, M. B. & Holcik, M. NF45 functions as an IRES trans-acting factor that is required for translation of cIAP1 during the unfolded protein response. *Cell Death Differ.* **17**, 719–29 (2010).
306. Taylor, T. J., Brockman, M. A., McNamee, E. E. & Knipe, D. M. Herpes simplex virus. *Frontiers in bioscience : a journal and virtual library* **7**, (2002).
307. Huang, C. J. & Wagner, E. K. The herpes simplex virus type 1 major capsid protein (VP5-UL19) promoter contains two cis-acting elements influencing late expression. *J. Virol.* **68**, 5738–5747 (1994).
308. Steffy, K. R. & Weir, J. P. Upstream promoter elements of the herpes simplex virus type 1 glycoprotein H gene. *J. Virol.* **65**, 972–975 (1991).
309. Pederson, N. E., Person, S. & Homa, F. L. Analysis of the gB promoter of herpes simplex virus type 1: high-level expression requires both an 89-base-pair promoter fragment and a nontranslated leader sequence. *J. Virol.* **66**, (1992).

310. Goodart, S. A., Guzowski, J. F., Rice, M. K. & Wagner, E. K. Effect of genomic location on expression of beta-galactosidase mRNA controlled by the herpes simplex virus type 1 UL38 promoter. *J. Virol.* **66**, 2973–2981 (1992).
311. Mavromara-Nazos, P. & Roizman, B. Delineation of regulatory domains of early (β) and late (γ2) genes by construction of chimeric genes expressed in herpes simplex virus 1 genomes. *Proc. Natl. Acad. Sci. U. S. A.* **86**, 4071–4075 (1989).
312. Rixon, F. J. & Clements, J. B. Detailed structural analysis of two spliced HSV-1 immediate-early mRNAs. *Nucleic Acids Res.* **10**, 2241–2256 (1982).
313. Greco, A. *et al.* The DNA sequence coding for the 5' untranslated region of herpes simplex virus type 1 ICP22 mRNA mediates a high level of gene expression. *J. Gen. Virol.* **75**, 1693–1702 (1994).
314. Tang, S., Patel, A. & Krause, P. R. Hidden regulation of herpes simplex virus 1 pre-mRNA splicing and polyadenylation by virally encoded immediate early gene ICP27. *PLOS Pathog.* **15**, e1007884 (2019).
315. Tombácz, D. *et al.* Long-Read Isoform Sequencing Reveals a Hidden Complexity of the Transcriptional Landscape of Herpes Simplex Virus Type 1. *Front. Microbiol.* **8**, 1079 (2017).
316. Tombácz, D. *et al.* Multiple Long-Read Sequencing Survey of Herpes Simplex Virus Dynamic Transcriptome. *Front. Genet.* **10**, 834 (2019).
317. Whisnant, A. W. *et al.* Integrative functional genomics decodes herpes simplex virus 1. *Nat. Commun.* **11**, 1–14 (2020).
318. Zhao, T. T. *et al.* hnRNP A1 regulates UV-induced NF-κB signalling through destabilization of cIAP1 mRNA. *Cell Death Differ.* **16**, 244–252 (2009).
319. Saffran, H. A., Read, G. S. & Smiley, J. R. Evidence for Translational Regulation by the Herpes Simplex Virus Virion Host Shutoff Protein. *J. Virol.* **84**, 6041–6049 (2010).
320. Donnelly, M. L. L. *et al.* Analysis of the aphthovirus 2A/2B polyprotein 'cleavage' mechanism indicates not a proteolytic reaction, but a novel translational effect: A putative ribosomal 'skip'. *J. Gen. Virol.* **82**, 1013–1025 (2001).
321. Kim, J. H. *et al.* High cleavage efficiency of a 2A peptide derived from porcine teschovirus-1 in human cell lines, zebrafish and mice. *PLoS One* **6**, (2011).
322. Pfeiffer, B. D., Truman, J. W. & Rubin, G. M. Using translational enhancers to increase transgene expression in Drosophila. *Proc. Natl. Acad. Sci. U. S. A.* **109**, 6626–6631 (2012).
323. Toda, M., Martuza, R. L. & Rabkin, S. D. Tumor growth inhibition by intratumoral inoculation of defective herpes simplex virus vectors expressing granulocyte - Macrophage colony-stimulating factor. *Mol. Ther.* **2**, 324–329 (2000).
324. Thomas, S. *et al.* Development of a new fusion-enhanced oncolytic immunotherapy platform based on herpes simplex virus type 1. *J. Immunother. Cancer* **7**, 214 (2019).
325. Malhotra, S. *et al.* Use of an oncolytic virus secreting GM-CSF as combined oncolytic and immunotherapy for treatment of colorectal and hepatic adenocarcinomas. *Surgery* **141**, 520–529 (2007).
326. Honess, R. W. & Roizman, B. Regulation of Herpesvirus Macromolecular Synthesis I. Cascade Regulation of the Synthesis of Three Groups of Viral Proteins 1. *J. Virol.* **14**, 8–19 (1974).
327. Lee, K. M., Chen, C. J. & Shih, S. R. Regulation Mechanisms of Viral IRES-Driven Translation. *Trends in Microbiology* **25**, 546–561 (2017).
328. Finkel, Y. *et al.* SARS-CoV-2 utilizes a multipronged strategy to suppress host 2 protein

synthesis Introduction. *bioRxiv* 2020.11.25.398578 (2020). doi:10.1101/2020.11.25.398578

329. Dauber, B., Saffran, H. A. & Smiley, J. R. The Herpes Simplex Virus 1 Virion Host Shutoff Protein Enhances Translation of Viral Late mRNAs by Preventing mRNA Overload. *J. Virol.* **88**, 9624–9632 (2014).
330. Doepker, R. C., Hsu, W.-L., Saffran, H. A. & Smiley, J. R. Herpes Simplex Virus Virion Host Shutoff Protein Is Stimulated by Translation Initiation Factors eIF4B and eIF4H. *J. Virol.* **78**, 4684–4699 (2004).
331. Feng, P., Everly, D. N. & Read, G. S. mRNA Decay during Herpes Simplex Virus (HSV) Infections: Protein-Protein Interactions Involving the HSV Virion Host Shutoff Protein and Translation Factors eIF4H and eIF4A. *J. Virol.* **79**, 9651–9664 (2005).
332. Taddeo, B., Zhang, W. & Roizman, B. The virion-packaged endoribonuclease of herpes simplex virus 1 cleaves mRNA in polyribosomes. *Proc. Natl. Acad. Sci. U. S. A.* **106**, 12139–12144 (2009).
333. Taddeo, B., Sciortino, M. T., Zhang, W. & Roizman, B. Interaction of herpes simplex virus RNase with VP16 and VP22 is required for the accumulation of the protein but not for accumulation of mRNA. *Proc. Natl. Acad. Sci. U. S. A.* **104**, 12163–12168 (2007).
334. Lusis, A. J. Atherosclerosis. *Nature* **407**, 233–241 (2000).
335. Weber, C. & Noels, H. Atherosclerosis: Current pathogenesis and therapeutic options. *Nature Medicine* **17**, 1410–1422 (2011).
336. Di Gregoli, K. & Johnson, J. L. Role of colony-stimulating factors in atherosclerosis. *Current Opinion in Lipidology* **23**, 412–421 (2012).
337. Moore, K. J., Sheedy, F. J. & Fisher, E. A. Macrophages in atherosclerosis: A dynamic balance. *Nature Reviews Immunology* **13**, 709–721 (2013).
338. Duewell, P. *et al.* NLRP3 inflammasomes are required for atherogenesis and activated by cholesterol crystals. *Nature* **464**, 1357–1361 (2010).
339. Maxfield, F. R. & Tabas, I. Role of cholesterol and lipid organization in disease. *Nature* **438**, 612–621 (2005).
340. Feng, B. *et al.* The endoplasmic reticulum is the site of cholesterol-induced cytotoxicity in macrophages. *Nat. Cell Biol.* **5**, 781–792 (2003).
341. Roth, G. A. *et al.* Global, regional, and national age-sex-specific mortality for 282 causes of death in 195 countries and territories, 1980–2017: a systematic analysis for the Global Burden of Disease Study 2017. *Lancet* **392**, 1736–1788 (2018).
342. Nabel, E. G. & Braunwald, E. A Tale of Coronary Artery Disease and Myocardial Infarction. *N. Engl. J. Med.* **366**, 54–63 (2012).
343. Yang, Q. *et al.* Assessing potential population impact of statin treatment for primary prevention of atherosclerotic cardiovascular diseases in the USA: population-based modelling study. *BMJ Open* **7**, e011684 (2017).
344. Madrigal-Matute, J., Rotllan, N., Aranda, J. F. & Fernández-Hernando, C. MicroRNAs and atherosclerosis. *Current atherosclerosis reports* **15**, (2013).
345. Nguyen, M. A., Karunakaran, D. & Rayner, K. J. Unlocking the Door to New Therapies in Cardiovascular Disease: MicroRNAs Hold the Key. *Current Cardiology Reports* **16**, 1–12 (2014).
346. Kim, V. N. MicroRNA biogenesis: Coordinated cropping and dicing. *Nature Reviews Molecular Cell Biology* **6**, 376–385 (2005).
347. Huntzinger, E. & Izaurralde, E. Gene silencing by microRNAs: Contributions of

translational repression and mRNA decay. *Nature Reviews Genetics* **12**, 99–110 (2011).
348. He, L. & Hannon, G. J. MicroRNAs: Small RNAs with a big role in gene regulation. *Nature Reviews Genetics* **5**, 522–531 (2004).
349. Feinberg, M. W. & Moore, K. J. MicroRNA Regulation of Atherosclerosis. *Circ. Res.* **118**, 703–720 (2016).
350. Lu, Y., Thavarajah, T., Gu, W., Cai, J. & Xu, Q. Impact of miRNA in Atherosclerosis. *Arteriosclerosis, thrombosis, and vascular biology* **38**, e159–e170 (2018).
351. Vickers, K. C. *et al.* MicroRNA-223 coordinates cholesterol homeostasis. *Proc. Natl. Acad. Sci. U. S. A.* **111**, 14518–14523 (2014).
352. Wang, J. *et al.* miR-223 inhibits lipid deposition and inflammation by suppressing toll-like receptor 4 signaling in macrophages. *Int. J. Mol. Sci.* **16**, 24965–24982 (2015).
353. Li, T. *et al.* MicroRNAs modulate the noncanonical transcription factor NF-κB pathway by regulating expression of the kinase IKKα during macrophage differentiation. *Nat. Immunol.* **11**, 799–805 (2010).
354. Haneklaus, M. *et al.* Cutting Edge: miR-223 and EBV miR-BART15 Regulate the NLRP3 Inflammasome and IL-1β Production. *J. Immunol.* **189**, 3795–3799 (2012).
355. Bauernfeind, F. *et al.* NLRP3 inflammasome activity is negatively controlled by miR-223. *J. Immunol.* **189**, 4175–81 (2012).
356. Rayner, K. J. *et al.* MiR-33 contributes to the regulation of cholesterol homeostasis. *Science (80-.).* **328**, 1570–1573 (2010).
357. Nguyen, M. A. *et al.* Extracellular Vesicles Secreted by Atherogenic Macrophages Transfer MicroRNA to Inhibit Cell Migration. *Arterioscler. Thromb. Vasc. Biol.* **38**, 49–63 (2018).
358. Karunakaran, D. *et al.* Macrophage Mitochondrial Energy Status Regulates Cholesterol Efflux and Is Enhanced by Anti-miR33 in Atherosclerosis. *Circ. Res.* **117**, 266–278 (2015).
359. Rayner, K. J. *et al.* Antagonism of miR-33 in mice promotes reverse cholesterol transport and regression of atherosclerosis. *J. Clin. Invest.* **121**, 2921–2931 (2011).
360. Daugherty, A. *et al.* Recommendation on design, execution, and reporting of animal atherosclerosis studies: A scientific statement from the American Heart Association. *Circulation Research* **121**, e53–e79 (2017).
361. Jafarnejad, S. M. *et al.* Translational control of ERK signaling through miRNA/4EHP-directed silencing. *Elife* **7**, e35034 (2018).
362. Gerashchenko, M. V. & Gladyshev, V. N. Ribonuclease selection for ribosome profiling. *Nucleic Acids Res.* **45**, e6 (2017).
363. Feig, J. E. Regression of atherosclerosis: Insights from animal and clinical studies. *Annals of Global Health* **80**, 13–23 (2014).
364. Tall, A. R., Yvan-Charvet, L., Terasaka, N., Pagler, T. & Wang, N. HDL, ABC Transporters, and Cholesterol Efflux: Implications for the Treatment of Atherosclerosis. *Cell Metabolism* **7**, 365–375 (2008).
365. Yvan-Charvet, L., Wang, N. & Tall, A. R. Role of HDL, ABCA1, and ABCG1 transporters in cholesterol efflux and immune responses. *Arteriosclerosis, Thrombosis, and Vascular Biology* **30**, 139–143 (2010).
366. Langmann, T. *et al.* Identification of sterol-independent regulatory elements in the human ATP-binding cassette transporter A1 promoter. Role of Sp1/3, E-box binding factors, and an oncostatin M-responsive element. *J. Biol. Chem.* **277**, 14443–14450 (2002).
367. Thymiakou, E., Zannis, V. I. & Kardassis, D. Physical and functional interactions between liver X receptor/retinoid X receptor and Sp1 modulate the transcriptional induction of the

human ATP binding cassette transporter A1 gene by oxysterols and retinoids. *Biochemistry* **46**, 11473–11483 (2007).
368. Chinetti-Gbaguidi, G., Colin, S. & Staels, B. Macrophage subsets in atherosclerosis. *Nature Reviews Cardiology* **12**, 10–17 (2015).
369. Zhuang, G. *et al.* A novel regulator of macrophage activation: MiR-223 in obesity-associated adipose tissue inflammation. *Circulation* **125**, 2892–2903 (2012).
370. Beug, S. T. *et al.* The transcription factor SP3 drives TNF- expression in response to Smac mimetics. *Sci. Signal.* **12**, (2019).
371. Yvan-Charvet, L. *et al.* Increased inflammatory gene expression in ABC transporter-deficient macrophages: Free cholesterol accumulation, increased signaling via toll-like receptors, and neutrophil infiltration of atherosclerotic lesions. *Circulation* **118**, 1837–1847 (2008).
372. Zhu, X. *et al.* Macrophage ABCA1 reduces MyD88-dependent toll-like receptor trafficking to lipid rafts by reduction of lipid raft cholesterol. *J. Lipid Res.* **51**, 3196–3206 (2010).
373. Mogilenko, D. A. *et al.* Endogenous apolipoprotein A-I stabilizes ATP-binding cassette transporter A1 and modulates Toll-like receptor 4 signaling in human macrophages. *FASEB J.* **26**, 2019–2030 (2012).
374. Koseki, M. *et al.* Increased lipid rafts and accelerated lipopolysaccharide-induced tumor necrosis factor-α secretion in Abca1-deficient macrophages. *J. Lipid Res.* **48**, 299–306 (2007).
375. Zhu, X. *et al.* Increased cellular free cholesterol in macrophage-specific Abca1 knock-out mice enhances pro-inflammatory response of macrophages. *J. Biol. Chem.* **283**, 22930–22941 (2008).
376. Westerterp, M. *et al.* Cholesterol efflux pathways suppress inflammasome activation, NETosis, and atherogenesis. *Circulation* **138**, 898–912 (2018).
377. Ying, W. *et al.* MicroRNA-223 is a crucial mediator of PPARγ-regulated alternative macrophage activation. *J. Clin. Invest.* **125**, 4149–4159 (2015).
378. Lu, T. P. *et al.* MiRSystem: An integrated system for characterizing enriched functions and pathways of microRNA targets. *PLoS One* **7**, (2012).
379. Barrett, T. J. Macrophages in Atherosclerosis Regression. *Arteriosclerosis, thrombosis, and vascular biology* **40**, 20–33 (2020).
380. Su, X. *et al.* Interferon-γ regulates cellular metabolism and mRNA translation to potentiate macrophage activation. *Nat. Immunol.* **16**, 838–849 (2015).
381. Schott, J. *et al.* Translational Regulation of Specific mRNAs Controls Feedback Inhibition and Survival during Macrophage Activation. *PLoS Genet.* **10**, (2014).
382. Fazi, F. *et al.* A minicircuitry comprised of microRNA-223 and transcription factors NFI-A and C/EBPα regulates human granulopoiesis. *Cell* **123**, 819–831 (2005).
383. Sun, W. *et al.* MiR-223 and miR-142 attenuate hematopoietic cell proliferation, and miR-223 positively regulates miR-142 through LMO2 isoforms and CEBP-B. *Cell Res.* **20**, 1158–1169 (2010).
384. De Aguiar Vallim, T. Q. *et al.* MicroRNA-144 regulates hepatic ATP binding cassette transporter A1 and plasma high-density lipoprotein after activation of the nuclear receptor farnesoid x receptor. *Circ. Res.* **112**, 1602–1612 (2013).
385. Ramírez, C. M. *et al.* Control of cholesterol metabolism and plasma high-density lipoprotein levels by microRNA-144. *Circ. Res.* **112**, 1592–1601 (2013).
386. Goedeke, L. *et al.* MicroRNA-148a regulates LDL receptor and ABCA1 expression to

control circulating lipoprotein levels. *Nat. Med.* **21**, 1280–1288 (2015).
387. Wagschal, A. *et al.* Genome-wide identification of microRNAs regulating cholesterol and triglyceride homeostasis. *Nat. Med.* **21**, 1290–1297 (2015).
388. Meiler, S., Baumer, Y., Toulmin, E., Seng, K. & Boisvert, W. A. MicroRNA 302a is a novel modulator of cholesterol homeostasis and atherosclerosis. *Arterioscler. Thromb. Vasc. Biol.* **35**, 323–331 (2015).
389. Nguyen, M. A. *et al.* Delivery of MicroRNAs by Chitosan Nanoparticles to Functionally Alter Macrophage Cholesterol Efflux in Vitro and in Vivo. *ACS Nano* **13**, 6491–6505 (2019).
390. Kirii, H. *et al.* Lack of interleukin-1ß decreases the severity of atherosclerosis in apoE-deficient mice. *Arterioscler. Thromb. Vasc. Biol.* **23**, 656–660 (2003).
391. Merhi-Soussi, F. *et al.* Interleukin-1 plays a major role in vascular inflammation and atherosclerosis in male apolipoprotein E-knockout mice. *Cardiovasc. Res.* **66**, 583–593 (2005).
392. Whitman, S. C., Ravisankar, P., Elam, H. & Daugherty, A. Exogenous interferon-γ enhances atherosclerosis in apolipoprotein E-/- mice. *Am. J. Pathol.* **157**, 1819–1824 (2000).
393. Whitman, S. C. A practical approach to using mice in atherosclerosis research. *Clin. Biochem. Rev.* **25**, 81–93 (2004).
394. Hamers, A. A. J. *et al.* Bone marrow-specific deficiency of nuclear receptor Nur77 enhances atherosclerosis. *Circ. Res.* **110**, 428–438 (2012).
395. Aiello, R. J. *et al.* Increased atherosclerosis in hyperlipidemic mice with inactivation of ABCA1 in macrophages. *Arterioscler. Thromb. Vasc. Biol.* **22**, 630–637 (2002).
396. Westerterp, M. *et al.* Deficiency of ATP-binding cassette transporters a1 and g1 in macrophages increases inflammation and accelerates atherosclerosis in mice. *Circ. Res.* **112**, 1456–1465 (2013).
397. Van Eck, M. *et al.* Leukocyte ABCA1 controls susceptibility to atherosclerosis and macrophage recruitment into tissues. *Proc. Natl. Acad. Sci. U. S. A.* **99**, 6298–6303 (2002).
398. Rodríguez, A. E. *et al.* Molecular Characterization of Chronic Lymphocytic Leukemia Patients with a High Number of Losses in 13q14. *PLoS One* **7**, (2012).
399. Huang, A. & Kaley, G. Gender-specific regulation of cardiovascular function: Estrogen as key player. *Microcirculation* **11**, 9–38 (2004).
400. Ng, M. K. C. *et al.* Androgens up-regulate atherosclerosis-related genes in macrophages from males but not females: Molecular insights into gender differences in atherosclerosis. *J. Am. Coll. Cardiol.* **42**, 1306–1313 (2003).
401. Ling, S. *et al.* Testosterone (T) enhances apoptosis-related damage in human vascular endothelial cells. *Endocrinology* **143**, 1119–1125 (2002).
402. Gordon, S. & Taylor, P. R. Monocyte and macrophage heterogeneity. *Nature Reviews Immunology* **5**, 953–964 (2005).
403. Wynn, T. A., Chawla, A. & Pollard, J. W. Macrophage biology in development, homeostasis and disease. *Nature* **496**, 445–455 (2013).
404. Buono, C. *et al.* Influence of interferon-γ on the extent and phenotype of diet-induced atherosclerosis in the LDLR-deficient mouse. *Arterioscler. Thromb. Vasc. Biol.* **23**, 454–460 (2003).
405. Gupta, S. *et al.* IFN-γ, potentiates atherosclerosis in ApoE knock-out mice. *J. Clin. Invest.* **99**, 2752–2761 (1997).
406. Hanna, R. N. *et al.* NR4A1 (Nur77) deletion polarizes macrophages toward an

inflammatory phenotype and increases atherosclerosis. *Circ. Res.* **110**, 416–427 (2012).
407. Liao, X. *et al.* Krüppel-like factor 4 regulates macrophage polarization. *J. Clin. Invest.* **121**, 2736–2749 (2011).
408. Cardilo-Reis, L. *et al.* Interleukin-13 protects from atherosclerosis and modulates plaque composition by skewing the macrophage phenotype. *EMBO Mol. Med.* **4**, 1072–1086 (2012).
409. Bhaskar, V. *et al.* Monoclonal antibodies targeting IL-1 beta reduce biomarkers of atherosclerosis in vitro and inhibit atherosclerotic plaque formation in Apolipoprotein E-deficient mice. *Atherosclerosis* **216**, 313–320 (2011).
410. Upadhya, S., Mooteri, S., Peckham, N. & Pai, R. G. Atherogenic effect of interleukin-2 and antiatherogenic effect of interleukin-2 antibody in apo-E-deficient mice. *Angiology* **55**, 289–294 (2004).
411. Zhang, W. *et al.* IL-9 aggravates the development of atherosclerosis in ApoE-/-mice. *Cardiovasc. Res.* **106**, 453–464 (2015).
412. Li, Q. *et al.* Increased Th9 cells and IL-9 levels accelerate disease progression in experimental atherosclerosis. *Am. J. Transl. Res.* **9**, 1335–1343 (2017).
413. Hauer, A. D. *et al.* Blockade of interleukin-12 function by protein vaccination attenuates atherosclerosis. *Circulation* **112**, 1054–1062 (2005).
414. Lee, T. S., Yen, H. C., Pan, C. C. & Chau, L. Y. The role of interleukin 12 in the development of atherosclerosis in apoE-deficient mice. *Arterioscler. Thromb. Vasc. Biol.* **19**, 734–742 (1999).
415. Erbel, C. *et al.* Inhibition of IL-17A Attenuates Atherosclerotic Lesion Development in ApoE-Deficient Mice. *J. Immunol.* **183**, 8167–8175 (2009).
416. Smith, E. *et al.* Blockade of interleukin-17A results in reduced atherosclerosis in apolipoprotein E-deficient mice. *Circulation* **121**, 1746–1755 (2010).
417. Subramanian, M., Thorp, E. & Tabas, I. Identification of a non-growth factor role for GM-CSF in advanced atherosclerosis: Promotion of macrophage apoptosis and plaque necrosis through IL-23 signaling. *Circ. Res.* **116**, e13–e24 (2015).
418. Bazzini, A. A., Lee, M. T. & Giraldez, A. J. Ribosome profiling shows that miR-430 reduces translation before causing mRNA decay in Zebrafish. *Science (80-.).* **336**, 233–237 (2012).
419. Guo, H., Ingolia, N. T., Weissman, J. S. & Bartel, D. P. Mammalian microRNAs predominantly act to decrease target mRNA levels. *Nature* **466**, 835–840 (2010).
420. Turner, M. & DÍaz-Muñoz, M. D. RNA-binding proteins control gene expression and cell fate in the immune system review-article. *Nature Immunology* **19**, 120–129 (2018).
421. Sun, G., Li, H. & Rossi, J. J. Sequence context outside the target region influences the effectiveness of miR-223 target sites in the RhoB 3′UTR. *Nucleic Acids Res.* **38**, 239–252 (2009).
422. Dong, Z. *et al.* MiR-223 modulates hepatocellular carcinoma cell proliferation through promoting apoptosis via the Rab1-mediated mTOR activation. *Biochem. Biophys. Res. Commun.* **483**, 630–637 (2017).
423. Kimura, T. *et al.* Polarization of M2 macrophages requires Lamtor1 that integrates cytokine and amino-acid signals. *Nat. Commun.* **7**, (2016).
424. Dornan, M. H. *et al.* First-in-class small molecule potentiators of cancer virotherapy. *Sci. Rep.* **6**, 26786 (2016).
425. Selman, M. *et al.* Multi-modal Potentiation of Oncolytic Virotherapy by Vanadium Compounds. *Mol. Ther.* **26**, 56–69 (2018).

426. Pirruccello, M. *et al.* Identification of inhibitors of inositol 5-phosphatases through multiple screening strategies. *ACS Chem. Biol.* **9**, 1359–1368 (2014).
427. Hasegawa, J. *et al.* Autophagosome–lysosome fusion in neurons requires INPP5E, a protein associated with Joubert syndrome. *EMBO J.* **35**, 1853–1867 (2016).
428. Hakim, S. *et al.* Inpp5e suppresses polycystic kidney disease via inhibition of PI3K/Akt-dependent mTORC1 signaling. *Hum. Mol. Genet.* **25**, 2295–2313 (2016).
429. Bielas, S. L. *et al.* Mutations in INPP5E, encoding inositol polyphosphate-5-phosphatase E, link phosphatidyl inositol signaling to the ciliopathies. *Nat. Genet.* **41**, 1032–1036 (2009).
430. Ono, A., Ablan, S. D., Lockett, S. J., Nagashima, K. & Freed, E. O. Phosphatidylinositol (4,5) bisphosphate regulates HIV-1 Gag targeting to the plasma membrane. *Proc. Natl. Acad. Sci. U. S. A.* **101**, 14889–14894 (2004).
431. Inlora, J., Chukkapalli, V., Bedi, S. & Ono, A. Molecular Determinants Directing HIV-1 Gag Assembly to Virus-Containing Compartments in Primary Macrophages. *J. Virol.* **90**, 8509–8519 (2016).
432. Chiu, Y. *et al.* INPP5E regulates CD3ζ enrichment at the immune synapse by phosphoinositide distribution control. *bioRxiv* 2021.01.06.425541 (2021). doi:10.1101/2021.01.06.425541
433. Yoo, J. Y. *et al.* VEGF-specific short hairpin RNA-expressing oncolytic adenovirus elicits potent inhibition of angiogenesis and tumor growth. *Mol. Ther.* **15**, 295–302 (2007).
434. Anesti, A. M., Simpson, G. R., Price, T., Pandha, H. S. & Coffin, R. S. Expression of RNA interference triggers from an oncolytic herpes simplex virus results in specific silencing in tumour cells in vitro and tumours in vivo. *BMC Cancer* **10**, 486 (2010).
435. Reshke, R. *et al.* Reduction of the therapeutic dose of silencing RNA by packaging it in extracellular vesicles via a pre-microRNA backbone. *Nat. Biomed. Eng.* **4**, 52–68 (2020).
436. Shaw, A. E. *et al.* Fundamental properties of the mammalian innate immune system revealed by multispecies comparison of type I interferon responses. *PLOS Biol.* **15**, e2004086 (2017).
437. Fritsch, C. *et al.* Genome-wide search for novel human uORFs and N-terminal protein extensions using ribosomal footprinting. *Genome Res.* **22**, 2208–2218 (2012).
438. Barbosa, C., Peixeiro, I. & Romão, L. Gene Expression Regulation by Upstream Open Reading Frames and Human Disease. *PLoS Genet.* **9**, e1003529 (2013).
439. Jackson, R. J. The current status of vertebrate cellular mRNA IRESs. *Cold Spring Harb. Perspect. Biol.* **5**, a011569 (2013).
440. Qin, X. & Sarnow, P. Preferential Translation of Internal Ribosome Entry Site-containing mRNAs during the Mitotic Cycle in Mammalian Cells. *J. Biol. Chem.* **279**, 13721–13728 (2004).
441. Braunstein, S. *et al.* A Hypoxia-Controlled Cap-Dependent to Cap-Independent Translation Switch in Breast Cancer. *Mol. Cell* **28**, 501–512 (2007).
442. Zoll, W. L., Horton, L. E., Komar, A. A., Hensold, J. O. & Merrick, W. C. Characterization of mammalian eIF2A and identification of the yeast homolog. *J. Biol. Chem.* **277**, 37079–37087 (2002).
443. Cheng, Z. *et al.* Pervasive, Coordinated Protein-Level Changes Driven by Transcript Isoform Switching during Meiosis. *Cell* **172**, 910-914.e16 (2018).
444. Darnell, A. M., Subramaniam, A. R. & O'shea, E. K. Translational Control through Differential Ribosome Pausing during Amino Acid Limitation in Mammalian Cells. *Mol. Cell* **71**, 229-243.e11 (2018).

445. Gardin, J. *et al.* Measurement of average decoding rates of the 61 sense codons in vivo. *Elife* **3**, (2014).
446. Bahir, I., Fromer, M., Prat, Y. & Linial, M. Viral adaptation to host: A proteome-based analysis of codon usage and amino acid preferences. *Mol. Syst. Biol.* **5**, (2009).
447. Bradel-Tretheway, B. G., Zhen, Z. & Dewhurst, S. Effects of codon-optimization on protein expression by the human herpesvirus 6 and 7 U51 open reading frame. *J. Virol. Methods* **111**, 145–56 (2003).
448. Ngumbela, K. C. *et al.* Quantitative effect of suboptimal codon usage on translational efficiency of mRNA encoding HIV-1 Gag in intact T cells. *PLoS One* **3**, e2356 (2008).
449. Zhang, S., Sun, L. & Kragler, F. The phloem-delivered RNA pool contains small noncoding RNAs and interferes with translation. *Plant Physiol.* **150**, 378–387 (2009).
450. Yamasaki, S., Ivanov, P., Hu, G. F. & Anderson, P. Angiogenin cleaves tRNA and promotes stress-induced translational repression. *J. Cell Biol.* **185**, 35–42 (2009).
451. Ivanov, P., Emara, M. M., Villen, J., Gygi, S. P. & Anderson, P. Angiogenin-Induced tRNA Fragments Inhibit Translation Initiation. *Mol. Cell* **43**, 613–623 (2011).
452. Wang, Q. *et al.* Identification and functional characterization of tRNA-derived RNA fragments (tRFs) in respiratory syncytial virus infection. *Mol. Ther.* **21**, 368–379 (2013).
453. Deng, J. *et al.* Respiratory Syncytial Virus Utilizes a tRNA Fragment to Suppress Antiviral Responses Through a Novel Targeting Mechanism. *Mol. Ther.* **23**, 1622–1629 (2015).
454. Kane, S. E. & Beemon, K. Precise localization of m6A in Rous sarcoma virus RNA reveals clustering of methylation sites: implications for RNA processing. *Mol. Cell. Biol.* **5**, 2298–2306 (1985).
455. Krug, R. M., Morgan, M. A. & Shatkin, A. J. Influenza viral mRNA contains internal N6-methyladenosine and 5'-terminal 7-methylguanosine in cap structures. *J. Virol.* **20**, 45–53 (1976).
456. Hesser, C. R., Karijolich, J., Dominissini, D., He, C. & Glaunsinger, B. A. N6-methyladenosine modification and the YTHDF2 reader protein play cell type specific roles in lytic viral gene expression during Kaposi's sarcoma-associated herpesvirus infection. *PLoS Pathog.* **14**, (2018).
457. Tsai, K., Courtney, D. G. & Cullen, B. R. Addition of m6A to SV40 late mRNAs enhances viral structural gene expression and replication. *PLoS Pathog.* **14**, e1006919 (2018).
458. Lichinchi, G. *et al.* Dynamics of the human and viral m(6)A RNA methylomes during HIV-1 infection of T cells. *Nat. Microbiol.* **1**, 16011 (2016).
459. Dang, W. *et al.* N6-methyladenosine and viral infection. *Front. Microbiol.* **10**, (2019).

APPENDICES

6.1 Quercetin Induces Pannexin 1 Expression via an Alternative Transcript with a Translationally Active 5'Leader in Rhabdomyosarcoma (Co-First Author article)

Quercetin Induces Pannexin 1 Expression via an Alternative Transcript with a Translationally Active 5'Leader in Rhabdomyosarcoma

Xiao Xiang[1,2,5], Huy-Dung Hoang[1,3,5], Victoria Gilchrist[1,3], Stéphanie Langlois[1,4], Tommy Alain[1,3] and Kyle N. Cowan[1,2,4].

Affiliations:

[1]Molecular Biomedicine Program, Children's Hospital of Eastern Ontario, Ottawa, Ontario, Canada

[2]Department of Cellular and Molecular Medicine, University of Ottawa, Ottawa, Ontario, Canada

[3]Department of Biochemistry, Microbiology and Immunology, University of Ottawa, Ottawa, Ontario, Canada

[4]Department of Surgery, Children's Hospital of Eastern Ontario, University of Ottawa, Ottawa, Ontario, Canada

[5]These authors contributed equally

Running title: PANX1 Regulation in Rhabdomyosarcoma

Financial Support: The Cancer Research Society (CRS, Operating Grant 19080 and Operating Grant 21453; K.N. Cowan), Ontario Graduate Scholarship (OGS, X. Xiang and H.D. Hoang), Queen Elizabeth II Graduate Scholarship in Science and Technology (QEII-GSST, X. Xiang), University of Ottawa Destination 2020 (X. Xiang and H.D. Hoang)

CHAPTER 6

6.1.1 Abstract

Rhabdomyosarcoma (RMS) is a deadly childhood neoplasm of presumed skeletal muscle origin. We have shown that the expression of the ion channel Pannexin 1 (PANX1) is strongly repressed in RMS cells, and that its upregulation dramatically inhibits tumor progression. PANX1 is dynamically expressed during the development of various tissues including skeletal muscle, but the underlining mechanisms by which PANX1 protein levels are controlled, especially in RMS, remain largely unknown. Here we show that both RMS and normal skeletal muscle express comparable amount of *PANX1* mRNAs, but surprisingly the canonical 5' untranslated region (5'UTR) or 5'leader of the transcript is completely lost in RMS cells. We uncover that quercetin, a natural plant flavonoid, increases PANX1 protein levels by inducing re-expression of a 5'leader-containing *PANX1* transcript variant that is efficiently translated. Mechanistically, abolishing CREB and ETV4 transcription factor binding sites in the *PANX1* promoter significantly reduced the luciferase reporter activities and *PANX1* 5'UTR levels, and we show that quercetin enriched the binding of ETV4, but not CREB, to its consensus element in the *PANX1* promoter. Furthermore, quercetin treatment promoted partial myogenic differentiation of RMS cells and both prevented RMS 3D *in vitro* tumor formation while inducing complete regression of established *in vitro* tumors. Collectively, our results demonstrate the tumor-suppressive effects of quercetin in RMS and present a hitherto undescribed mechanism of PANX1 regulation via ETV4-mediated transcription of a translationally-functional 5'leader-containing *PANX1* mRNA.

Keywords: Pannexin; Rhabdomyosarcoma; Quercetin; 5' untranslated region; RNA sequencing; Polysome profiling; Transcription; Alternative transcription; Translation

6.1.2. Introduction

Pannexin 1 (PANX1; known as Panx1 in rodents) is a ubiquitous transmembrane glycoprotein that oligomerizes to form single membrane channels [476–479]. PANX1 channels allow the passage of ions, metabolites, and small molecules up to 1 kDa in size, and are considered major conduits for ATP release from various cell types [480]. We have previously shown that PANX1 levels are highly upregulated in differentiating primary human skeletal muscle myoblasts (HSMM) [481]. Notably, ectopic expression of PANX1 in undifferentiated HSMM promoted their myogenic differentiation while blockade of PANX1 channels using pharmacological agents inhibited this process [481]. A similar upregulation of Panx1 levels was measured during their development and regeneration following injury in mice [482]. Together, our results established PANX1 as an important regulator of skeletal muscle myogenic differentiation [483], which also prompted us to investigate the role of PANX1 in rhabdomyosarcoma (RMS), a childhood neoplasm thought to arise from muscle progenitors due to impaired myogenic differentiation [484–486]. Interestingly, we detected low levels of PANX1 in RMS tissue specimens and patient-derived cell lines and showed that re-introduction of PANX1 in RMS cells dramatically suppressed their malignant properties *in vitro* and *in vivo* [487]. Subsequently, our study of the PANX1 transcriptome and interactome in RMS further implicated PANX1 in the regulation of genes involved in various key cellular processes, such as migration and apoptosis, and uncovered its tumor-inhibitory interaction with the neuroblast differentiation-associated protein AHNAK, respectively (Xiang et al., 2021).

RMS is the most common soft tissue sarcoma in children and adolescents with two major histological subtypes, termed embryonal RMS (eRMS) and alveolar RMS (aRMS), which together make up more than 80% of all RMS [488]. eRMS, the most common subtype, has a more favorable prognosis whereas aRMS is more aggressive and often leads to a poor clinical outcome [488–490].

While the molecular pathogenesis of eRMS and aRMS remains unclear, cytogenetic studies have revealed recurrent loss of heterozygosity at the 11p15 locus in eRMS and chromosomal translocations of t(2;13)(q35;q14) or t(1;13)(p36;q14) in aRMS resulting in paired homeobox (PAX)-forkhead box protein O1 (FOXO1) oncoproteins, PAX3- or PAX7-FOXO1 [491,492]. These genetic alterations have been associated with dysregulation of transcriptional, epigenetic, and molecular signalling mechanisms in many cellular processes, including proliferation and myogenic differentiation, in RMS [491]. Despite aggressive treatment modalities, the overall survival rate of patients with metastatic or relapsed RMS has remained below 30% for over 30 years, underlining the urgency for better clinical management [490,493]. Thus far, our findings strongly suggest that upregulating PANX1 is a promising therapeutic strategy for RMS [487]. As PANX1 levels are low in RMS compared to normal skeletal muscle, understanding the regulation or deregulation of *PANX1* transcriptional and translational control in RMS may reveal novel therapeutic targets.

PANX1/Panx1 levels are dynamically regulated during development and in pathologic states. In murine cortex, cerebellum, and retina, Panx1 levels peaked at embryonic day 18 and dramatically decreased upon birth and continued to decline into adulthood [494]. This gradual decline in Panx1 levels was also reported in the rat brain [495] and observed during differentiation of neural crest-like cells [494] *in vitro*. On the contrary, Panx1 levels increased in primary adipose-derived stromal cells upon induction into an adipogenic lineage [496]. Under pathological conditions, Panx1 levels were down-regulated in C6 glioma cells as compared to normal astrocytes, and its ectopic expression reduced glioma tumor growth *in vivo* [497]. By contrast, upregulation of PANX1/Panx1 levels was positively associated with both human and murine melanoma progression while shRNA-mediated knockdown of PANX1/Panx1 levels led to attenuation of the disease [498,499]. This

dynamic variation of PANX1 levels across different tissue types or pathological conditions suggests tissue- or disease-dependent transcriptional or translational regulation [500], however, studies demonstrating the mechanisms by which this regulation occurs have not been. Thus far, *Panx1* transcriptional regulation has only been comprehensively studied in the rat epididymis, where *Panx1* was shown to have an evolutionarily conserved promoter located in CpG islands under the control of methylation and the transcription factors CREB and ETV4 [501].

Recently, a genome-wide drug screen in murine neuronal cells revealed quercetin, a naturally occurring flavonoid present in vegetables and fruit [502], as an up-regulator of *Panx1* mRNA levels [503]. Thus provided a pharmacological agent that could facilitate the investigation into the molecular mechanism of *PANX1* regulation in RMS. In the current study, using patient-derived Rh18 (eRMS) and Rh30 (aRMS) cell lines [504], we show that *PANX1* transcripts in RMS cells are devoid of their putative 5'UTR (untranslated region) as compared to skeletal muscle tissue and differentiated HSMM, and that the presence of the *PANX1* 5'UTR corresponds to its protein expression in RMS cells and HSMM. After confirming that quercetin upregulates PANX1 protein expression in RMS cells, we reveal that this occurs through the restoration of transcription of a translationally functional *PANX1* mRNA containing a 5'leader. We further demonstrate that the transcription of this *PANX1* mRNA variant in RMS cells is dependent upon the binding of transcription factor ETV4 to the *PANX1* promoter. Collectively, our results show for the first time the involvement of *PANX1* 5'UTR in regulating its mRNA translation.

6.1.3. Materials and Methods

Cell Culture, Drug Treatment and Transfection

Human rhabdomyosarcoma cell lines Rh18 (eRMS) and Rh30 (aRMS) lines were obtained from Dr. P. Houghton (St. Jude Children's Hospital, Memphis, TN). Stable Rh18 and Rh30 cell lines were generated using the SparQ Cumate Switch Inducible System (System Biosciences, CA) as described previously [487]. All RMS cell lines were maintained in RPMI-1640 medium supplemented with 10% FBS and 1% penicillin/streptomycin while the stable RMS cell lines were supplemented additionally with 100 µg/mL geneticin (Life Technologies, CA), and 2 µg/mL puromycin (Corning, NY). Primary human skeletal muscle myoblasts (HSMM) (Lonza, Walkersville, MD) were maintained in Clonetics SkGM™ medium supplemented with the SkGM™ SingleQuots™ kit (Lonza) as specified by the supplier. The HSMM were differentiated by switching to DMEM medium with 2% horse serum [481]. Quercetin was purchased from Sigma-Aldrich (St. Louis, MO) and prepared in DMSO. Quercetin was refreshed in culture medium every 24 hours. All transfections were performed with Lipofectamine 2000 Reagent (Thermo Scientific, Waltham, MA).

Western Blotting

Cells were lysed in IP lysis buffer (150 mM NaCl, 10 mM Tris-HCl, pH 7.4, 1 mM EDTA, 0.5% NP-40, and 1% Triton X-100) as previously described [505]. The lysates were separated in 10% SDS-PAGE and transferred to PVDF membranes. The proteins were immunoblotted with anti-PANX1 (1:2000, Sigma-Aldrich, Cat#: HPA016930), anti-MYOD (1:1000, Santa Cruz, TX, Cat#: sc-377460), anti-MYOG (1:1000, Santa Cruz, Cat#: sc-12732), anti-MHC (1:2000, R&D Systems, Minneapolis, MN, Cat#: MAB4470), anti-CREB (1:1000, Cell Signaling Technology, Danvers, MA, Cat#: 4820S), anti-pCREB (1:1000, Cell Signaling Technology, Cat#: 9198S) or anti-GAPDH (1:5000, Advanced ImmunoChemical, Long Beach, CA, Cat#: 2RGM2) and then with Alexa 680- (1:5000, Thermo Scientific) or infrared fluorescent-labeled secondary antibodies

IRDye 800 (1:5000, Rockland Immunochemicals, Pottstown, PA). The membranes were scanned on a LI-COR infrared-imaging system (LI-COR Biosciences, Lincoln, NE) and the densitometric units of the unsaturated images was quantified with the accompanying Odyssey V3.0 software.

RNA Sequencing and Data Analysis

Total RNA was extracted from Rh30 cells using RNeasy Mini Kit (Qiagen, Germantown, MD) and submitted to Princess Margaret Genomics Centre (Toronto, ON, Canada) for RNA-seq analysis on an Illumina HiSeq2000 sequencing platform as previously described (Xiang et al., 2020). The RNA Integrity Number (RIN) was 10 for all sequenced samples. Total purity filtered reads sequenced generated were 80,991,098, 93,328,541, and 156,294,622 for the biological replicates. Overall read quality was checked using FASTQC v.0.11.2 RNA-SeQC (v1.1.7) software. Raw sequence data, in the form of FASTQ files, was aligned to the human genome (hg19, iGenome GTF definition file) using the BOWTIE/TOPHAT pipeline (BOWTIE v2.2.3, TOPHAT 2.0.13) [506]. Accessory programs for the alignment stage included SAMTOOLS (v1.0) and CUTADAPT (v1.7.1).

Polysome profiling

Polysome profiling was performed as previously described (Gandin et al., 2014). Briefly, cells were treated with cycloheximide (CHX) (Bioshop, Canada) at 100 µg/ml for 5 minutes to fix translating ribosome. Cells were washed three times with ice cold PBS containing CHX, then lysed using hypotonic buffer (5 mM Tris pH 7.5, 2.5 mM $MgCl_2$, 1.5 mM KCl, 2.5 mM DTT, 100U RNAsin nuclease inhibitor (Promega), 0.5% Triton X-100, 0.5% sodium deoxycholate). Cell debris was pelleted by centrifugation at 17,000 g, 10 minutes at 4°C and supernatant was transferred to a new tube. An equivalent of 10 OD at 260 nm of supernatant was then added on top

of a continuous 10-50% sucrose gradient and centrifuged at 221,000 g (36,000 rpm) for 2 hours at 4ºC. Fractions were then collected using a BR-188 Density Gradient Fractionation System (Brandel) and RNA was extracted using Trizol (Thermo Fisher) according to the manufacturer protocol.

RT-qPCR

Total RNA was extracted using RNeasy Mini kit (Qiagen, Germantown, MD), DNase-treated with TURBO DNA-free™ kit (Thermo Scientific) and reverse transcribed into cDNA using High-Capacity cDNA Reverse Transcription kit (Thermo Scientific). Quantitative PCR of the synthesized cDNA was performed on a CFX96 Touch Real-Time PCR Detection System (Bio-Rad, Hercules, CA) using SsoAdvanced™ Universal SYBR® Green Supermix (Bio-Rad). All primers were validated to have an amplification efficiency of 90 – 100% when used at 500 nM (see Supplemental Table S1 for primer sequences) with their respective qPCR program. All qPCR assays were performed using the following program unless otherwise specified: 95 ℃ for 3 min followed by 45 cycles of 95 ℃ for 10 sec, 58 ℃ for 15 sec and 72 ℃ for 50 sec). Relative expression was determined using the comparative Ct method.

5' Rapid Amplification of cDNA End (RACE)

Rh30 (aRMS) cells were treated with 10 µM quercetin or DMSO for 24 hours. Total RNA was collected and DNase-treated as described previously. Reverse transcription of 5' capped poly (A) RNA was performed with TELO™ PRIME Full-Length cDNA Amplification V2 kit following manufacturer's instructions. Briefly, 2 µg of DNase-treated total RNA was first reverse transcribed using an OligodT primer to form a cDNA/RNA hybrid strand. A double-stranded adapter with a 5' C overhang was then ligated to the 5' end of the capped cDNA/RNA by base

pairing to the 5’ G in the cap structure while leaving all 5’ uncapped cDNA/RNA unmodified. Full double-strand cDNA was then synthesized from the 5’ capped RNA using a primer containing the 5’ adapter sequence. Endpoint PCR using a forward primer with the 5’ adaptor sequence and a reverse primer specific to exon 2 of PANX1 (Supplemental Table S1) were used to amplified full length PANX1 cDNA for 21 PCR cycles without allowing the amplification to reach saturation (determined by a separate qPCR analysis under identical conditions). The PCR products were resolved on a 2% agarose gel with GelRed™ (Biotium, Fremont, CA) and visualized on a Gel Doc XR+ Documentation System (Bio-Rad). All PCR programs were set up according to the manufacturer’s instructions.

CAT Translation Reporter Assay

CAT translation reporter assay was performed as previously described (Graber et al., 2010). Briefly, cells were seeded at 75% confluency in a 6-well plate, then transfected with 1 µg each of pBGal (expressing β-galactosidase, a generous gift from Dr. Martin Holcik at Carleton University) and the pMCpA plasmid expressing the CAT open reading frame under the CMV promoter followed by the 5’UTR of interest using Lipofectamine 2000 (Thermo Fisher). 24 hours post transfection, CAT expression in transfected cells was measured using the CAT ELISA kit (Roche) according to the manufacturer’s instruction, while β-galactosidase activity was measured by the ortho-Nitrophenyl-β-galactoside (ONPG) colorimetric assay. CAT expression was then normalized to β-galactosidase to control for transfection efficiency.

PANX1 Promoter Cloning, Plasmid Construction and Site-directed Mutagenesis

Total genomic DNA was extracted from primary HSMM cells using QIAamp DNA Mini kit (Qiagen). Two segments of PANX1 promoter from positions -2697 to -1642 and -1616 to +37 as

well as their deletion mutants from positions -926, -581 and -475 to +37 (relative to its ATG start codon) were PCR amplified (95 ℃ for 3 min followed by 32 cycles of 95 ℃ for 15 sec, 60 ℃ for 15 sec and 72 ℃ for 90) using PCR Master Mix (Promega, Madison, WI), purified with QIAquick PCR Purification kit (Qiagen), and subcloned into the KpnI-XhoI sites in pGL3-Basic vector (Promega). Mutations at the CREB and ETV4 consensus sites on PANX1 promoter (-581 to +37) in pGL3 vector were introduced using the Quick-Change Site-directed Mutagenesis kit (Agilent Technologies, Santa Clara, CA) following the manufacturer's instructions. All plasmid constructs were verified by Sanger sequencing. All restriction enzymes were purchased from New England Biolabs (Ipswich, MA). See **Table S6.1.1** for primer sequences.

Immunofluorescence Microscopy

Rh30 cells on glass coverslips were treated with 10 μM quercetin or DMSO for 24 hours and then fixed with 3.7% paraformaldehyde for 20 min at room temperature. The fixed cells were washed with PBS, and then blocked and permeabilized in 2% BSA with 0.1% Triton X-100 for 1 hour at room temperature. The cells were labeled with previously described primary antibodies against PANX1 (1:200) and ETV4 (1:50) at 4 ℃ overnight and then with Alexa 488 or 594 conjugated secondary antibodies (1:500) at room temperature for 1 hour. The coverslips were mounted with DAPI Fluoromount-G (Southern Biotech, Birmingham, AL) and visualized using EVOS Cell Imaging System (Thermo Fisher) with a 20X objective.

Dual-luciferase Reporter Assay

Rh18 (eRMS) and Rh30 (aRMS) cells were transfected in 96-well plates with 100 ng pGL3-PANX1 promoter constructs or a promoterless pGL3-Basic negative and 100 ng pRL-TK (Promega) for 48 hours and analyzed using Dual-Glo® Luciferase Assay System (Promega) on a

Synergy HTX plate reader (BioTek Instruments, Winooski, VT). Rh18 and Rh30 cells were also transfected in parallel with 1 µg pGL3 constructs and 1 µg pRL-TK in 6-well plates for 48 hours before subjected to total RNA extraction for qPCR analyses of Firefly Luciferase and PANX1 5' UTR transcript levels (95 ℃ for 3 min followed by 45 cycles of 95 ℃ for 3 sec and 60 ℃ for 30 sec) with primers described in Supplemental Table S1.

Chromatin Immunoprecipitation

Rh30 (aRMS) cells were treated with 10 µM quercetin or DMSO for 24 hours and subjected to chromatin immunoprecipitation using EZ-ChIP kit (Millipore, Billerica, MA) according to manufacturer's instructions. Briefly, the cells were fixed with 1% formaldehyde for 10 minutes at room temperature and quenched with 125 mM glycine. The cells were pelleted, and then lysed at 1×10^7 cells/mL of SDS lysis buffer (1% SDS, 10 mM EDTA, and 50 mM Tris, pH 8.1) containing protease inhibitors. The cell lysates were sonicated by a VCX 130 sonicator (Sonics & Materials, Newtown, CT) mounted with a 2 mm tip for 15 sets of 10 s pulses at 30% of maximum power (50 Watts) to shear the crosslinked chromatin into 200 – 1000 bp fragments. Each immunoprecipitation was performed with 100 µL of sonicated chromatin, which was equivalent to 1×10^6 cells. The chromatin was diluted to 1 mL with the dilution buffer and precleared with 60 µL of protein G agarose beads for 1 hour at 4 ℃. A 20 µL aliquot of precleared chromatin was removed and set aside to be used as input in subsequent analysis. The precleared chromatin was then incubated with 1 µg anti-RNA Polymerase II (positive control), 1 µg mouse IgG (negative control), 10 µg anti-ETV4 (Santa Cruz; Cat#: sc-113X) or 10 µg anti-CREB (Santa Cruz; Cat#: sc-377154X) overnight at 4 ℃ on a rotator. The chromatin/DNA immunocomplexes were captured with 60 µL of protein G agarose beads for 1 hour at 4 ℃. The protein G agarose beads were washed, and the captured chromatin was eluted and purified for subsequent qPCR analysis (95 ℃ for 3 min

followed by 45 cycles of 95 ℃ for 3 sec and 60 ℃ for 30 sec) using primers described in Supplemental Table S1.

3D Spheroid Assay

3D spheroid formation and regression assays were performed and quantified using IncuCyte ZOOM™ Live Cell Imaging System (Essen Bioscience, MI) and its accompanying software as previously described [487]

Statistics

The data were analyzed for statistical significance using unpaired two-tailed Student's t-tests, multiple unpaired Student's t-test with Holm-Sidak correction, and analysis of variance (ANOVA) followed by Tukey's post-hoc tests.

6.1.4. Results

PANX1 5'UTR and Protein Levels are Positively Correlated in RMS and HSMM

We have previously detected PANX1 transcript and protein in undifferentiated HSMM and patient-derived RMS cell lines, but their levels are significantly lower than those in differentiated HSMM [481,487]. Since re-introduction of PANX1 in RMS cells vastly reduced their malignant properties [487], we performed RNA-sequencing (RNA-seq) to further study the transcriptomic changes elicited by PANX1 in Rh30 (aRMS) cells as this subtype of RMS remains particularly challenging to treat [493]. To our surprise, the RNA-seq result from wild-type Rh30 cells revealed an abundance of endogenous PANX1 transcripts which mapped to all five exons with the exception of the 5'UTR region (Fig. 1A). Further analyses of RNA-seq data on adult skeletal muscle tissue specimens deposited in the Gene Expression Omnibus (GEO) database, however, showed a clear

mapping of PANX1 transcripts onto its 5'UTR region (Fig. 1A). When normalized to the total RNA-seq reads of the PANX1 coding sequence (CDS), the 5'UTR reads in differentiated HSMM were comparable to the CDS reads, while no 5'UTR read was detected in RNA samples from Rh30 cells, suggesting that PANX1 mRNAs in Rh30 cells do not contain a 5'leader region (Fig. 1B). Using PANX1 5' UTR specific primers and a series of PANX1 exon-exon junction primers, qPCR analyses corroborated the previous RNA-seq results showing that the difference in PANX1 transcript levels between Rh18 (eRMS), or Rh30 cells, and differentiated HSMM was the most dramatic in the 5'UTR region, and this difference gradually diminished from exon 1 to 5 (Fig. 1C). Moreover, Western blotting analysis in parallel showed significantly higher PANX1 protein levels in differentiated HSMM as compared to that of Rh18 and Rh30 cells as well as its undifferentiated counterparts (Fig. 1D and E). An immunoreactive band around 65 kDa was recognized by our anti-PANX1 antibodies in all but differentiated HSMM (Fig. 1D, arrowhead). However, further Western blotting analysis indicated that it corresponded to a non-specific immunoreactive species, as siRNA targeting PANX1 induced a clear knockdown of PANX1 (normally identified between ~39.5 to ~49.9 kDa as a result of various post-translational modifications such as glycosylation and phosphorylation [507]) in Rh30 cells while no change in the levels of the 65 kDa immunoreactive band was observed (Fig. 1F). Taken together, our data show that as compared to HSMM, the PANX1 transcripts expressed in RMS cells are devoid of a 5'leader region and this correlates with protein expression. Thus, the 5'UTR region of the PANX1 transcript may be important for its regulation in tissues.

Quercetin Enhances PANX1 mRNA Translation in RMS Cells

A recent screen using a pool of clinically approved drugs identified quercetin as an up-regulator of Panx1 transcript levels in murine neuronal cells [503], which provided a potential tool to

modulate PANX1 expression in RMS. As a proof of principle experiment, we treated Rh18 and Rh30 cells with increasing dosages of quercetin and subjected them to Western blotting analyses. Interestingly, quercetin treatment induced a dosage-dependent increase in PANX1 protein levels in Rh18 cells in which 50 μM of quercetin induced a statistically significant and maximal increase of PANX1 (Fig. 2A). In Rh30 cells, 10 μM of quercetin was able to elicit maximal induction of PANX1 expression (Fig. 2B). Thus, 50 μM and 10 μM were chosen as quercetin concentrations for treating Rh18 and Rh30 cells in the downstream experiments, respectively. We assessed the change in PANX1 transcript levels using both primers specific to exon 1. Remarkably, quercetin treatment in both Rh18 and Rh30 cells did not lead to a significant increase in PANX1 transcript levels as measured at exon region 1 (Fig. 2C). This prompted us to investigate whether quercetin treatment could instead modulate PANX1 mRNA translation. Using polysome fractionation [508], ribosome-associated mRNA from Rh30 cells with and without quercetin treatment was resolved on a continuous sucrose gradient where polysome-bound mRNA sedimented according to their density, which increases with the number of bound ribosomes and correlates with their translation rate (Fig. 2D). While there was no discernable change of the global translation profiles in Rh30 cells with or without quercetin (Fig. 2D), the distribution of PANX1 transcripts with quercetin treatment shifted towards the polysome fractions 5 – 8 when analyzed by qPCR (Fig. 2E). We further grouped the fractions into translationally inactive subpolysomes (fractions 1 – 4) and translationally active polysomes (fractions 5 – 8) for comparison. As expected, quercetin treatment induced a significant increase of the proportion of PANX1 transcripts in the polysome fraction and a significant corresponding decrease of those in the subpolysome fraction (Fig. 2F). In contrast, the distribution of GAPDH transcripts across polysome fractions (Fig. 2G) and when comparing their proportions between subpolysome and polysome fractions (Fig. 2H), both showed no change

upon quercetin treatment. Collectively, our data indicate that quercetin induced PANX1 expression in Rh30 cells by enhancing its translation.

Quercetin Induced Transcription of a Translationally-efficient PANX1 5' Leader-containing Transcript Variant

As the 5'UTR is an important regulator of translation of the downstream gene [509,510], we thus performed qPCR analyses of Rh18 and Rh30 cells to determine whether quercetin treatment in these cells could restore the expression of 5'leader-containing PANX1 transcripts. By analyzing the overall ratio of PANX1 in these cells, we found that the presence of transcripts containing the 5'UTR of PANX1 significantly increased in both quercetin-treated Rh18 and Rh30 as compared to their respective DMSO vehicle controls (Fig. 3A). To further investigate the quercetin-induction of 5'leader PANX1 transcripts, we performed 5'RACE (Rapid Amplification of cDNA Ends) using Rh30 cells with and without quercetin treatment. To this end, we first ligated a universal 5'adapter sequence to the 5'capped mature RNA and then reverse transcribed the full-length mRNA into cDNA sequentially using a polyA reverse primer followed by a forward primer that recognized the 5' universal adapter (Fig. 3B). Next, we PCR amplified the PANX1 5'leader using the universal adapter forward primer and a reverse primer that was designed to anneal to a position 305 bp downstream of the start codon on PANX1 cDNA (Fig. 3B). Intriguingly, agarose gel electrophoresis analysis showed multiple bands of PCR products, which suggests that PANX1 mRNAs in Rh30 possess multiple alternative 5'UTRs of distinct lengths (Fig 3C). Notably, we did not detect any discernable band at the size corresponding to the annotated PANX1 full-length 5'UTR (approximately 780 bp). Instead, most amplicons from both DMSO and quercetin treated Rh30 cells were detected between 260 and 300 bp, suggesting that the majority of PANX1 transcripts in Rh30 cells are truncated at the 5'end of their open reading frame (ORF) (Fig. 3C).

This was consistent with the lack of 5'UTR reads in our RNAseq data shown previously. We termed these bands collectively as PANX1b (Fig. 3C). Interestingly, quercetin-treated Rh30 cells also showed two additional bands: one at approximately 350 bp (PANX1a) and the other at slightly higher than 200 bp (PANX1c) (Fig. 3C), indicating that hitherto undescribed 5'UTR-containing PANX1 transcript variants emerge upon quercetin treatment (Fig. 3D). This observation was also consistent with the increase in PANX1 5'UTR levels detected earlier in Rh30 cells following quercetin treatment (Fig. 3A). Next, we explored whether the various PANX1 5'leaders had a differential effect on the translation of PANX1 mRNA. Using the public TSS database defined by CAGE/nanoCAGE (FANTOM Consortium and the RIKEN PMI and CLST [DGT] 2014), we found 6 other putative alternative transcription start sites (aTSS) from the annotated TSS for the PANX1 gene locust that generated sequentially shorter 5'UTRs, which we numbered as aTSS1-6 (Fig. 3E). Intriguingly, the aTSS6, which initiated transcription 43 bp upstream of the start codon and yielded the shortest 5'UTR, corresponded to the 5'UTR of the PANX1a transcript that we had detected previously from our 5'RACE analysis in Rh30 cells after quercetin treatment. This further supports the existence of a novel PANX1 transcript variant. Next, we cloned the full-length as well as the alternative 5'UTRs of PANX1 from the public 5'CAGE database into a translation reporter assay system, which used chloramphenicol acetyl transferase as the reporter gene [309]. Unexpectedly, the full length PANX1 5'UTR from the canonical TSS showed a strong repression on chloramphenicol acetyltransferase (CAT) reporter expression as compared to a 5'UTR-less construct. Furthermore, the shorter alternative 5'UTRs showed no improvement in CAT reporter activity until reaching the aTSS6 with the 43 bp-5'UTR upstream of the start codon which dramatically increased CAT reporter activities in both Rh18 (Fig. 3F) and Rh30 (Fig. 3G) cells.

Taken together, our data suggest that quercetin enhances PANX1 translation by inducing the expression of an alternative PANX1 transcript with a 43 bp long 5'UTR.

CREB and ETV4 Binding Sites Within the PANX1 Promoter Regulate its 5'UTR Expression

As the first step towards understanding the mechanism of PANX1 alternative transcription, we turned our attention to the evolutionarily conserved PANX1 promoter sequence. Due to its length, the PANX1 promoter was separated into two sections (-2697 – -1642 and -1616 – +38) and cloned into the pGL3-basic vector. Our results from dual luciferase reporter assays showed no change in luciferase activities from the PANX1 promoter section -2697 to -1642 (Fig. 4A). However, sequential removal of nucleotides at the 5' end of PANX1 promoter section -1616 to +38 caused a gradual increase in luciferase activity that peaked at position -581, which was almost completely abolished by a further removal of 106 bp to position -475 in both Rh18 and Rh30 cells (Fig. 4A). Interestingly, embedded in this 106 bp sequence were putative binding sites for CREB and ETV4 which were previously shown to regulate Panx1 transcription in rat epididymal tissue [501]. Therefore, constructs containing the PANX1 promoter sequence from positions -581 (CREB-ETV4) and -475 (delCREB-delETV4) were chosen for further analyses (Fig. 4A). Subsequent dual luciferase reporter assays and qPCR analyses in parallel showed that delCREB-delETV4 caused a dramatic reduction of luciferase activities in Rh18 and Rh30 cells as compared to those containing CREB-ETV4 (Fig. 4B), while both PANX1 promoter constructs produced comparable levels of Firefly Luciferase transcripts in Rh18 and Rh30 cells (Fig. 4C), suggesting a reduction at the translational level. As we previously showed that the PANX1 5'UTR regulated the translation of the downstream gene, we further compared its expression levels from both PANX1 promoter constructs in Rh18 and Rh30 cells. Interestingly, we observed a significant reduction in the PANX1 5'UTR levels measured at positions -309, -257, -156 and -113 relative to the ATG in the

absence of CREB and ETV4 sites as compared to their counterparts (Fig. 4D). Collectively, our data indicate that a 106 bp portion of the PANX1 promoter containing consensus sites for the transcription factors CREB and ETV4 is important for PANX1 5'UTR expression, which allows translation of the downstream coding sequence.

PANX1 Expression in RMS Requires CREB and ETV4 Consensus Sites

Next, we sought to further verify the importance of CREB and ETV4 consensus sites in regulating PANX1 5'UTR transcription and its translation. To this end, we performed site-directed mutagenesis to disrupt the putative consensus nucleotide sequences in the CREB binding site alone (mutCREB-ETV4) or the ETV4 binding site alone (CREB-mutETV4) or both CREB and ETV4 binding sites (mutCREB-mutETV4) from the CREB-ETV4 PANX1 promoter construct in pGL3 vector. Using the newly generated site-mutant constructs, and CREB-ETV4 and delCREB-delETV4 as positive and negative controls, we subjected Rh18 and Rh30 cells to a dual luciferase reporter assay. As observed previously, delCREB-delETV4 PANX1 promoter construct dramatically reduced the luciferase activities in both Rh18 (Fig. 5A) and Rh30 (Fig. 5B) cells as compared to those from CREB-ETV4. Interestingly, while the CREB site mutation alone did not change luciferase activities, the ETV4 site mutation alone (CREB-mutETV4) and the CREB-ETV4 dual site mutation (mutCREB-mutETV4) both induced similar yet significant reductions in luciferase activities as compared to the positive controls in Rh18 (Fig. 5A) and Rh30 (Fig. 5B). Similar to previous findings, none of the PANX1 promoter site-mutation or deletion constructs significantly changed the levels of Firefly Luciferase reporter gene transcript in both Rh18 (Fig. 5C) and Rh30 (Fig. 5D) cells. However, it is worth noting that mutation of the CREB binding site showed a trend towards an increase in Firefly Luciferase transcripts, which was more evident in Rh18 (Fig. 5C) than in Rh30 (Fig. 5D) cells. Moreover, dual CREB-ETV4 site mutation also

significantly reduced the 5' portion of the Firefly Luciferase reporter gene transcript that contained the PANX1 5'UTR in Rh18 (Fig. 5E) and Rh30 (Fig. 5F) cells. As we have shown here that quercetin upregulates PANX1 5'UTR containing transcript levels leading to enhanced PANX1 translation, we next tested if quercetin could also increase PANX1 promoter activity. Our further dual luciferase reporter assays showed a trend towards a moderate increase in luciferase activities in all PANX1 promoter constructs used after quercetin treatment in Rh18 cells (Fig. 5G). However, we observed a significant increase in luciferase activities following quercetin treatment with CREB-ETV4 and mutCREB-ETV4 constructs in Rh30 cells (Fig. 5H). This increase was no longer statistically significant when the ETV4 site was mutated or CREB and ETV4 sites were both deleted (Fig. 5H). Altogether, these results further suggest the involvement of transcription factors CREB and ETV4 in regulating the transcription of PANX1 from its 5'UTR which controls its translation.

ETV4 Binding to its Consensus Site in the PANX1 Promoter is Enhanced in Quercetin-treated Rh30 cells and During Skeletal Muscle Myogenic Differentiation

In order to confirm that the transcription factors CREB and ETV4 are activated by quercetin and are part of the signalling mechanism to upregulate PANX1 expression in RMS cells, we selected Rh30 cells for further analysis. Both total CREB and phosphorylated CREB (ser133) were detected in Rh30 cells (Fig. 6A), but phosphorylated CREB levels following quercetin treatment were similar to the control (Fig. 6B). Immunofluorescence labeling showed ETV4 (red) in the nuclei of Rh30 cells treated with either DMSO (Fig. 6C) or quercetin (Fig. 6D). However, only quercetin-treated Rh30 cells showed clear co-labeling of PANX1 (green) and ETV4 (Fig. 6D), which was not observed in the DMSO-treated control cells (Fig. 6C). More importantly, although subsequent chromatin immunoprecipitation (ChIP) assays showed no change in CREB binding to

its consensus site on the PANX1 promoter in quercetin-treated Rh30 cells as compared to their DMSO controls (Fig. 6E, left panel), ETV4 binding was significantly enriched by quercetin (Fig. 6E, right panel). As PANX1 levels were highly upregulated during HSMM differentiation [481], we suspected that ETV4 binding on the PANX1 promoter would also be enriched during this process. We thus differentiated HSMM for 6 days and subjected them, as well as their undifferentiated counterparts, to a ChIP assay. Indeed, the ChIP assay results showed a clear enrichment of ETV4 binding to the PANX1 promoter in differentiated HSMM as compared to undifferentiated cells (Fig. 6F). Collectively, these data suggest that the mechanism by which quercetin upregulates PANX1 translation in RMS cells involves the binding of ETV4 to its promoter region and the transcription of a translation-efficient 5'leader-containing PANX1 mRNA.

Quercetin Induces Partial Myogenic Differentiation of RMS Cells, and Prevents Formation and Induces Regression of Established 3D In Vitro Tumors

Since quercetin has been shown to suppress various malignancies [511–514], we next wanted to determine whether quercetin could also induce tumor-suppression in RMS cells. Given its ability to upregulate PANX1, which was previously shown to induce partial myogenic differentiation and inhibit the progression of 3D spheroids in RMS cells [487], we subjected Rh18 and Rh30 cells to similar tests after quercetin treatment. Following 24-hour exposure to quercetin, both Rh18 (Fig. 7A) and Rh30 (Fig. 7B) cells became elongated as compared to their respective DMSO-treated controls, which is indicative of myogenic differentiation [483]. Consistent with this, subsequent Western blotting analyses and their corresponding quantification further showed a significant upregulation of MyoD levels and a trend towards an increase in MYOG after treatment with quercetin at 10 μM in both Rh18 and Rh30 cells (Fig. 7A and 7B). However, this increase in MyoD and MYOG was not observed in either cell line treated with higher concentrations of

quercetin, which was likely the result of concurrently occurring apoptosis (data not shown). Next, we assessed the effect of quercetin in Rh18 and Rh30 3D spheroid formation and regression. To enable the accurate quantification of spheroid size, stable Rh18 and Rh30 cells engineered to constitutively express GFP were used, a previously described [487]. In order to assess the effect of quercetin in spheroid formation and growth, stable Rh18 and Rh30 cells were treated with quercetin for 24 hours prior to induction of spheroid formation. Quercetin treatment induced a dose-dependent inhibitory effect on Rh18 (Fig. 7C) and Rh30 (Fig. 7D) spheroid formation and growth, completely abolishing their formation at the 50-100 µM range. Similarly, when Rh18 (Fig. 7E) and Rh30 (Fig. 7F) cells were exposed to quercetin after having been allowed to develop into established spheroids, a dramatic dose-dependent regression was observed. Notably, treatment of 100 µM of quercetin, a well tolerated dosage in normal human cells [515], completely obliterated both Rh18 (Fig. 7E) and Rh30 (Fig. 7F) spheroids. Together, these data demonstrate the tumour-suppressive effects of quercetin in RMS and further support its potential use as a therapeutic agent for this childhood malignancy.

6.1.5. Discussion

Despite the last five decades of research, clinical outcomes for patients with metastatic RMS remains unacceptably poor in the vulnerable patient population [490,493,516]. A major obstacle is the current limitation of therapeutic options, with treatment chemotherapy remaining largely the same having had only minor modifications in dosage, duration, and route of administration [517]. Previous work from our laboratory has revealed that PANX1 is down-regulated in RMS and established upregulation of PANX1 as a potential new therapeutic approach [487]. In this study, we investigated the transcriptional and translational regulation of *PANX1* in RMS using quercetin as a pharmacological up-regulator of PANX1 expression. We present here a correlation between the

levels of 5'UTR containing *PANX1* transcripts and PANX1 protein in skeletal muscle and RMS. We show that quercetin increases PANX1 levels in RMS cells by enriching the binding of the transcription factor ETV4 to the *PANX1* promoter, which induces the expression of an alternative *PANX1* mRNA transcript variant containing a translationally competent 5'leader. Moreover, we also demonstrate the tumor-suppressive effects of quercetin in RMS and the possibility for future clinic translation.

Our initial RNA-seq and RT-qPCR data revealed a unique transcriptional profile of *PANX1* in RMS where the majority of transcription starts sporadically around the ATG start codon without a defined TSS. The *PANX1*/*Panx1* promoters have been shown to reside in CpG islands and lack core promoter elements [501]. Such promoters generally have dispersed transcription initiation [518,519]. Our data also suggest a considerable basal level of *PANX1* transcription in RMS cells. However, due to the lack of the *PANX1* 5'UTR, or in most cases the ATG start codon, they are deficient in the necessary message for translation into functional full-length PANX1 protein. Indeed, PANX1 levels in RMS are significantly lower than those of differentiated HSMM. Skeletal muscle differentiation is an intricately regulated process which involves precise temporal regulation of genes including *PANX1* [481,483]. Thus, it is not surprising to see such aberrant transcription of *PANX1* in RMS as their myogenic differentiation program is largely impaired [520]. Our observation adds to a growing body of literature that has identified the dynamic regulation of transcript variants, not just transcript abundance, to play an important role in eukaryotic gene expression via altering the translational output of each transcript [521,522]. It also raises the intriguing question as to whether dynamic 5'UTR regulation might contribute to PANX1 protein expression during muscle development.

Recently, RNA-seq data from Hadwen et al. (2018) showed that quercetin induced *Panx1* mRNA levels in murine primary cerebral cultures. We further substantiate this data here by showing that quercetin induces PANX1 protein expression in RMS. However, as opposed to an induction of *PANX1* mRNA levels, quercetin-induced PANX1 expression at the translational level. This was supported by a shift in *PANX1* mRNA towards more translationally active polysome fractions upon treatment with quercetin. While total PANX1 mRNA levels stayed unchanged, we detected an increase of transcripts containing a 5'leader region, suggesting possible alternative transcription of *PANX1*. Thus, we performed 5'RACE to reveal potential aTSSs. Our results from 5'RACE of *PANX1* in Rh30 (aRMS) cells are also in accordance with our alignment of RNA-seq reads which reveal a broad band between ~260 to 300 bp indicative of *PANX1* transcripts with 5' truncation. However, we also identified two additional distinct bands following quercetin treatment that are ~350 bp (*PANX1a*) and ~230 bp (*PANX1c*) long. While *PANX1b* and *PANX1c* are truncated beyond the first ATG start codon, *PANX1a* represents a potentially translatable full-length mRNA. Notably, our survey of various *PANX1* 5'UTR lengths (between position -476 and -43 relative to the ATG start codon), which represent multiple potential alternative TSSs based on aggregated CAGE data, shows that the 5'UTR from *PANX1a* (43 bp) is the most translationally active. Alternative transcription of *Panx1* have been reported in rat epididymis which leads to three different *Panx1* mRNA transcript variants with 393 bp-, 429 bp- and 443 bp-long 5'UTR, respectively [501]. Although the translational activities of these *Panx1* 5'UTRs were not studied in rat epididymis, their protein product Panx1 has been detected in the same tissue [523] suggesting that they are translationally active. These data indicate potential tissue-dependent translational activity of the *PANX1* 5'UTR resulting in dynamic regulation of PANX1 expression [481,494–496].

The *PANX1* promoter is evolutionarily conserved between human and rodents especially in the region containing consensus sites for CREB and ETV4 [501]. Interestingly, we find that quercetin upregulates PANX1 in RMS through a mechanism of alternative transcription of *PANX1* involving ETV4. ETV4 (ETS variant 4), also known as PEA3, is a member of PEA3 (polyomavirus enhancer activator 3) subfamily of ETS transcription factors (Xin et al., 1992; Higashino et al., 1993). ETV4 has been detected in skeletal muscle and shown to be critically involved in myogenic differentiation [524]. The transactivity of ETV4 is enhanced by MEF2 and, more importantly, over-expression of ETV4 accelerates myogenic differentiation and blocking ETV4 function inhibits this process [524]. The functional role of ETV4 thus closely resembles that of PANX1 in skeletal muscle [481]. Similar to PANX1, ETV4 expression in RMS is generally low [525]. This correlation between ETV4 and PANX1 levels also remains in breast cancer [526,527], prostate cancer [528,529], and melanoma [499,530], which further broadens the contextual implications of ETV4 for PANX1 expression. Our data also suggests the involvement of other transcription factors as abolishing the ETV4 binding site does not completely prevent the increase in reporter activity by quercetin. One potential candidate is interferon response factor 2 (IRF-2), an important regulator of skeletal myogenesis [531], as removal of its consensus site in the *PANX1* promoter significantly reduced reporter gene transcript levels and activities (data not shown). Thus, future efforts will be directed to deciphering the role of IRF-2 or other potential TFs on *PANX1* promoter regulation.

Moreover, our findings further expand the current functional implications of quercetin by suggesting that it may constitute a potential new therapeutic agent for diseases such as RMS [487], glioma [497], and hearing loss [532] where upregulation of PANX1 has been shown to be potentially beneficial. Quercetin is widely studied owing to its anti-oxidant, anti-inflammatory, anti-cancer, and chemopreventive properties [511–513,533]. As a polyphenol, quercetin can readily cross the nuclear

envelope and modulate gene expression by altering the structure of transcription factors or directly interacting with the *cis* elements on DNA [534–537]. Notably, quercetin has various protective roles in skeletal muscle [538–540]. It has been recently shown to upregulate myocyte enhancer factor 2C (*MEF2C*) [541], an important myogenic factor in skeletal muscle differentiation [542] that is dysregulated in RMS [543,544].

Interestingly, we also observed that quercetin treated RMS cells became elongated which was accompanied by upregulation of both myogenic markers, MyoD and MYOG, suggesting partial myogenic differentiation [487,545]. An earlier study also reported a dose-dependent inhibition of proliferation and morphological changes in RD cells, an eRMS cell line, after 48 hours in the presence of 30 - 130 µM of quercetin [546]. However, it was unclear if the morphological changes in RD cells resembled myogenic differentiation [546]. Notably, the quercetin-induced partial myogenic differentiation of RMS cells were only observed in low concentrations, and counter intuitively, treatment with higher concentrations of quercetin did not further change MyoD or MYOG levels in either Rh18 or Rh30 cells. This may be due to the biphasic effect of quercetin. Indeed, multiple reports have shown that low dosages of quercetin elicit changes in various biochemical pathways while higher concentrations induce cytotoxicity and cell death [547]. More importantly, quercetin treatment resulted in a dose-dependent growth inhibition and regression of Rh18 and Rh30 3D tumor spheroids. Remarkably, quercetin inhibited tumor RMS spheroid growth and induced complete regression of established RMS tumor spheroids when used at concentrations well tolerated by normal human cells [515], which suggest that quercetin treatment engaged a mechanism of tumor-suppression specific to RMS cells. As PANX1 expression alone promptly inhibited 3D spheroid formation and induced their regression in both Rh18 and Rh30 cells [487], our results suggest a possible quercetin tumor-suppressive mechanism involving PANX1. However, further

investigation is needed to establish the functional link between quercetin and PANX1. In addition, our results also warrant future studies to further assess the tumor-suppressive effects of quercetin in RMS with *in vivo* mouse models. Results from these studies will facilitate the process of drug repurposing of quercetin for treatment of RMS and accelerate its potential clinical translation.

Taken together, we present a mechanism of quercetin-induced PANX1 expression in RMS leading to induction of RMS differentiation, inhibition of 3D tumor spheroid growth, and regression of established *in vitro* tumors (Fig. 8). We have found that the majority of *PANX1* transcripts in RMS are truncated at their 5' ends thus lacking the putative 5'UTR leading to low PANX1 levels. Quercetin treatment enhances the binding of ETV4 to the PANX1 promoter, which induces the transcription of a *PANX1* mRNA transcript variant that contains a translationally active 5'UTR leading to an increase in PANX1 levels. To our knowledge, our results constitute the first evidence for upregulation of PANX1 by a pharmacological agent in human disease as well as the first report of a mechanism of PANX1 regulation via alternative transcription and 5'UTR usage. Collectively, our findings further establish quercetin as a potential therapeutic agent for treatment of RMS.

6.1.6. Acknowledgements

We thank Dr. P. Houghton for providing us with the RMS patient-derived cell lines.

Fig. 1

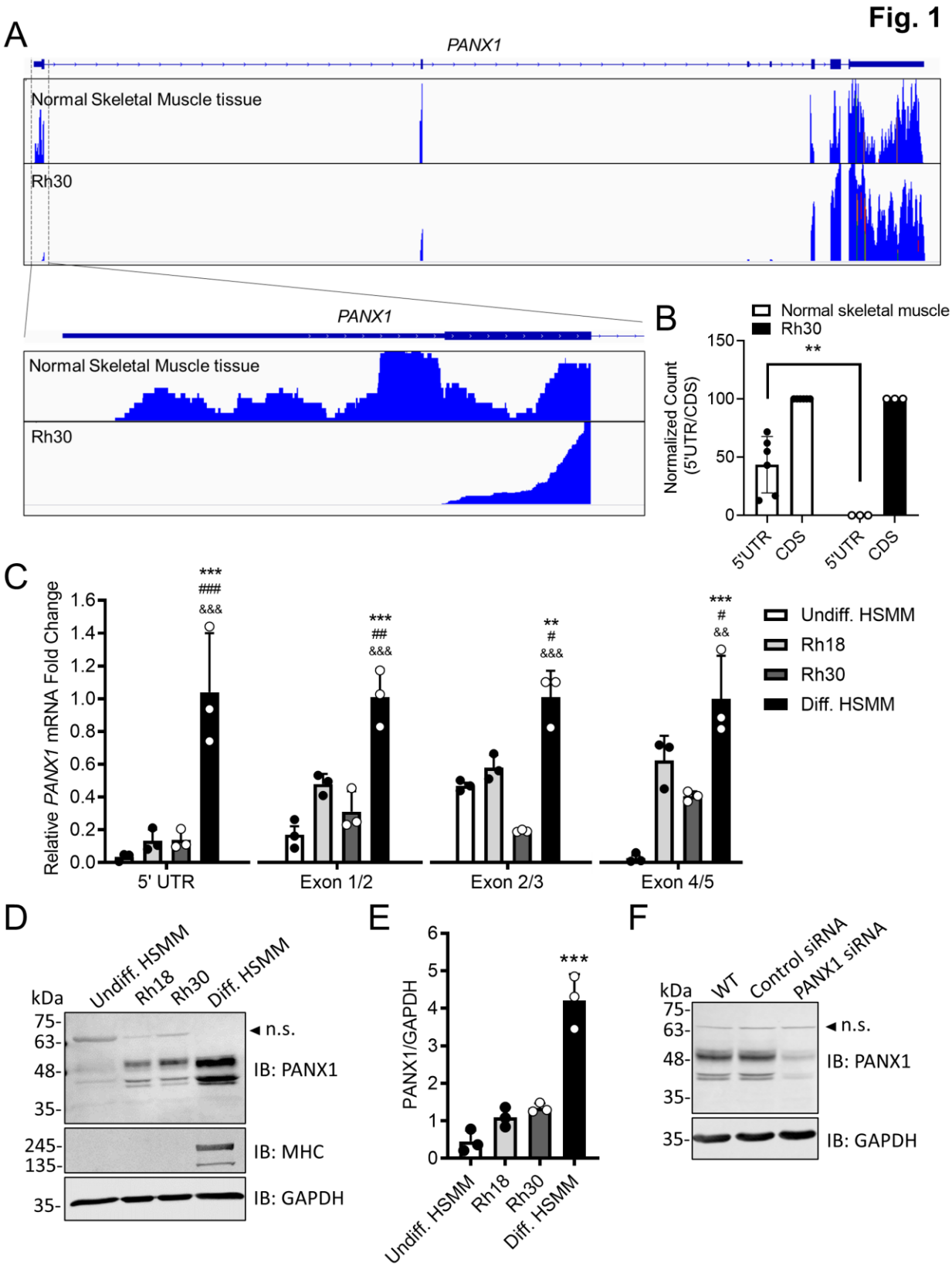
A
PANX1
Normal Skeletal Muscle tissue
Rh30
PANX1
Normal Skeletal Muscle tissue
Rh30
B
Normal skeletal muscle
Rh30
**
Normalized Count (5'UTR/CDS)
150
100
50
0
5'UTR
CDS
5'UTR
CDS
C
Relative PANX1 mRNA Fold Change
1.6
1.4
1.2
1.0
0.8
0.6
0.4
0.2
0.0
***
###
&&&
***
##
&&&
**
#
&&&
***
#
&&
5' UTR
Exon 1/2
Exon 2/3
Exon 4/5
Undiff. HSMM
Rh18
Rh30
Diff. HSMM
D
kDa
Undiff. HSMM
Rh18
Rh30
Diff. HSMM
75-
63-
48-
35-
◄ n.s.
IB: PANX1
245-
135-
IB: MHC
35-
IB: GAPDH
E
PANX1/GAPDH
6
5
4
3
2
1
0
***
Undiff. HSMM
Rh18
Rh30
Diff. HSMM
F
kDa
WT
Control siRNA
PANX1 siRNA
75-
63-
48-
35-
◄ n.s.
IB: PANX1
35-
IB: GAPDH

Fig 1. PANX1 5' UTR Expression Correlates with its Protein Abundance. (A) RNA-seq reads mapped to the 5'UTR and exon 1 regions of *PANX1* from representative RNA libraries prepared from three biological replicates of Rh30 (aRMS) cells and as compared to representative RNA libraries from six normal human skeletal muscle tissue samples retrieved from Ryan et al., *JCI Insight* 2018. **(B)** Ratio of normalized counts of RNA-seq reads mapped to the 5'UTR region over the CDS region of *PANX1*. Note that there is no read mapped to the 5'UTR region of *PANX1* in Rh30 RNA samples. All normal skeletal muscle RNA-seq reads were retrieved from Ryan et al., *JCI Insight* 2018. **(C)** RT-qPCR of *PANX1* from Rh18 (eRMS) (n=3) and Rh30 cells (n=3) using primers specific to its 5' UTR (-276 to +1 relative to the *PANX1* ATG start codon) and exon-exon junctions. Undifferentiated (n=3) and differentiated (n=3) human skeletal muscle myoblasts (HSMM) were used as controls. Results from each amplified region was normalized independently to their differentiated (Diff. HSMM) HSMM controls in the respective *PANX1* mRNA regions. ** $P < 0.01$ and *** $P < 0.001$ compared to Undiff. HSMM; # $P < 0.05$, ## $P < 0.01$ and ### $P < 0.001$ compared to Rh18; && $P < 0.01$ and &&& $P < 0.001$ compared to Rh30. **(D)** Representative Western blots and their quantification (n=3) **(E)** showing levels of myosin heavy chain (MHC), a marker for terminal myogenic differentiation of HSMM, and PANX1. GAPDH was used as loading control. Arrowhead indicates a non-specific immunoreactive band (n.s.), which was further confirmed by **(F)** Western blotting analysis (n=3) of Rh30 cells 72 hours post siRNA-mediated knockdown of PANX1. Both wildtype Rh30 cells (WT) and Rh30 cells transfected with a scrambled siRNA sequence (Control siRNA) were used as controls. GAPDH was used as loading control. Arrowhead highlights the non-specific immunoreactive band (n.s.) also seen in **(D)**. *** $P < 0.001$ compared to Undiff. HSMM, Rh18 and Rh30. Results are expressed as mean ± s.d.

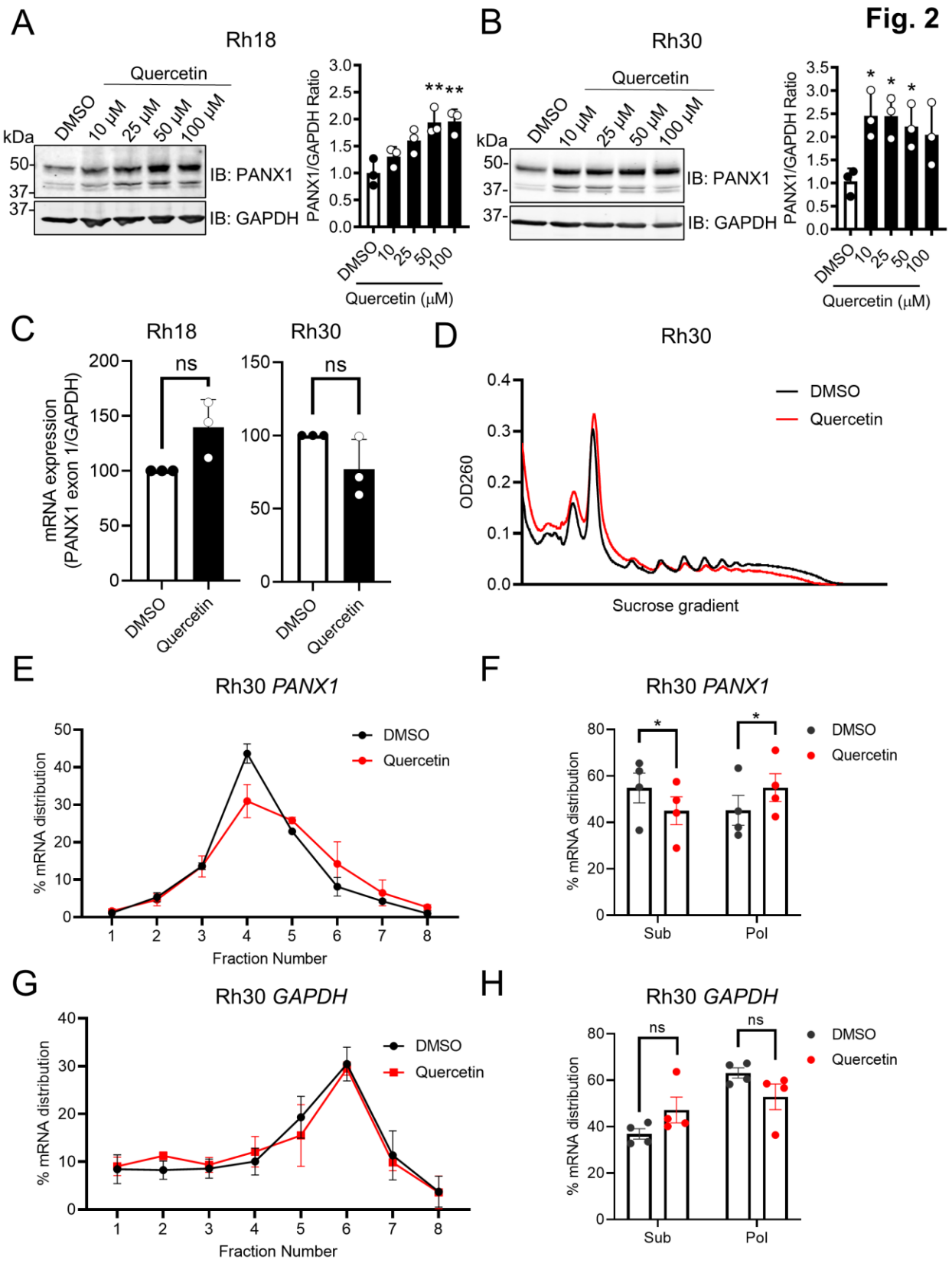
Fig. 2
A
Rh18
Quercetin
DMSO
10 μM
25 μM
50 μM
100 μM
kDa
50-
37-
37-
IB: PANX1
IB: GAPDH
PANX1/GAPDH Ratio
Quercetin (μM)
B
Rh30
C
Rh18
Rh30
mRNA expression (PANX1 exon 1/GAPDH)
ns
D
Rh30
DMSO
Quercetin
OD260
Sucrose gradient
E
Rh30 PANX1
% mRNA distribution
Fraction Number
F
Rh30 PANX1
Sub
Pol
G
Rh30 GAPDH
H
Rh30 GAPDH

Fig 2. Quercetin Upregulates the Translation of PANX1 mRNA in RMS cells. Rh18 (eRMS) and Rh30 (aRMS) cells were treated with increasing dosages of quercetin or its vehicle control (DMSO) for 24 hours. DMSO concentration corresponded to the highest dosage of quercetin. Representative Western blots and quantification for PANX1 in Rh18 (n=3) **(A)** and Rh30 (n=3) **(B)** cells are shown. * $P < 0.05$ and ** $P < 0.01$ compared to DMSO. GAPDH was used as loading control. **(C)** RT-qPCR analysis of *PANX1* transcript levels in Rh18 (n=3) and Rh30 (n=3) using primers specific to its exon 1 region. Results are relative to *GAPDH* transcript levels. ns: not significant. qPCR program: 95 ˚C for 3 min followed by 40 cycles of 95 ˚C for 15 sec, 60 ˚C for 30 sec. **(D)** Representative polysome traces of Rh30 cells treated with quercetin or DMSO. RT-qPCR analysis (n=4) showing **(E)** distribution of *PANX1* mRNA levels in polysome fractions and **(F)** their proportions in subpolysomes (fractions 1 – 4) and polysomes (fractions 5 – 8) fractions from DMSO- or quercetin-treated Rh30 cells. Results are expressed as the percentage of total *PANX1* mRNA. * $P < 0.05$. RT-qPCR analysis (n=4) showing **(G)** distribution of *GAPDH* mRNA levels in polysome fractions and **(H)** their proportions in combined subpolysomes (fractions 1 – 4) (translationally inactive) and polysomes (fractions 5 – 8) (translationally active) fractions from the DMSO- or quercetin-treated Rh30 cells in **(E)** and **(F)**. Results are expressed as the percentage of total *GAPDH* mRNA. Results are expressed as mean ± s.d. ns: not significant.

Fig. 3

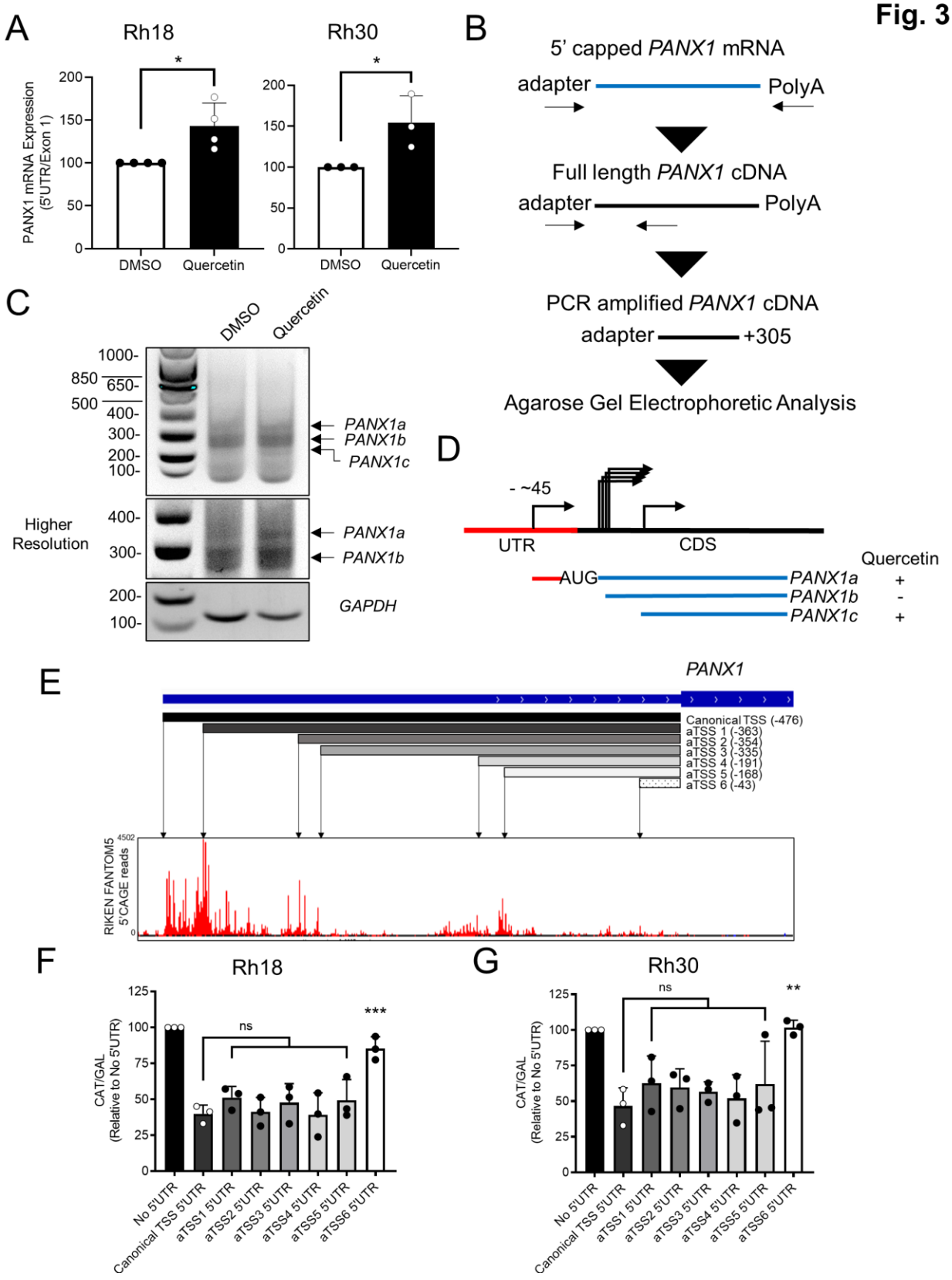
A
Rh18
Rh30
PANX1 mRNA Expression (5'UTR/Exon 1)
DMSO
Quercetin
B
5' capped PANX1 mRNA
adapter
PolyA
Full length PANX1 cDNA
PCR amplified PANX1 cDNA
+305
Agarose Gel Electrophoretic Analysis
C
Higher Resolution
PANX1a
PANX1b
PANX1c
GAPDH
D
- ~45
UTR
CDS
AUG
Quercetin
E
PANX1
Canonical TSS (-476)
aTSS 1 (-363)
aTSS 2 (-354)
aTSS 3 (-335)
aTSS 4 (-191)
aTSS 5 (-168)
aTSS 6 (-43)
RIKEN FANTOM5 5'CAGE reads
F
Rh18
CAT/GAL (Relative to No 5'UTR)
ns
***
No 5'UTR
Canonical TSS 5'UTR
aTSS1 5'UTR
aTSS2 5'UTR
aTSS3 5'UTR
aTSS4 5'UTR
aTSS5 5'UTR
aTSS6 5'UTR
G
Rh30
ns
**

Fig 3. Quercetin Induces the Transcription of a Translation-Competent Variant of 5' UTR Containing *PANX1* mRNA in RMS cells. (A) RT-qPCR analysis (n=3) of *PANX1* transcript levels using primers specific to its 5' UTR region from DMSO- or quercetin-treated Rh18 (eRMS) and Rh30 (aRMS) cells. Results are relative to *GAPDH* transcript levels. * $P < 0.05$ compared to DMSO. qPCR program: 95 ˚C for 3 min followed by 40 cycles of 95 ˚C for 15 sec, 60 ˚C for 30 sec. **(B)** Schematic representation of the RACE workflow and regions amplified by PCR. A PCR product of 305 bps was expected for an intact *PANX1* cDNA from its ATG start codon. **(C)** Agarose gel electrophoresis analysis (n=2 technical replicates) of the RACE products from Rh30 cells 24 hours post quercetin treatment or its DMSO control. A higher resolution of the agarose gel image highlighting the 5' UTR containing *PANX1* mRNA variant (*PANX1a*) is shown below. GAPDH was used as control. **(D)** Schematic interpretation of the RACE products from **(C)** in which the 5' UTR containing *PANX1* cDNA (*PANX1a*) and a truncated transcript variant (*PANX1c*) induced by quercetin treatment are shown in addition to the quercetin-independent transcript variants collectively named *PANX1b*. **(E)** Aggregated CAGE reads mapped to the 5'UTR region of *PANX1* showing the canonical as well as six alternative transcription start sites (TSS). Data were retrieved from Riken FANTOM 5 track hub on hg38 genome and reviewed in UCSC genome browser. Translation reporter assay in Rh18 (n=3) **(F)** and Rh30 (n=3) **(G)** cells showing the translational activity of indicated *PANX1* putative 5'UTRs. Plasmids encoding the indicated 5'UTRs fused to a CAT CDS were co-transfected with β-galactosidase (GAL) to control transfection efficiency. CAT expression was measured by CAT ELISA kit, then normalized to the expression of a CAT mRNA without 5'UTR. ** $P<0.01$, *** $P<0.001$ compared to the canonical TSS 5' UTR. Results are expressed as mean ± s.d. ns: not significant.

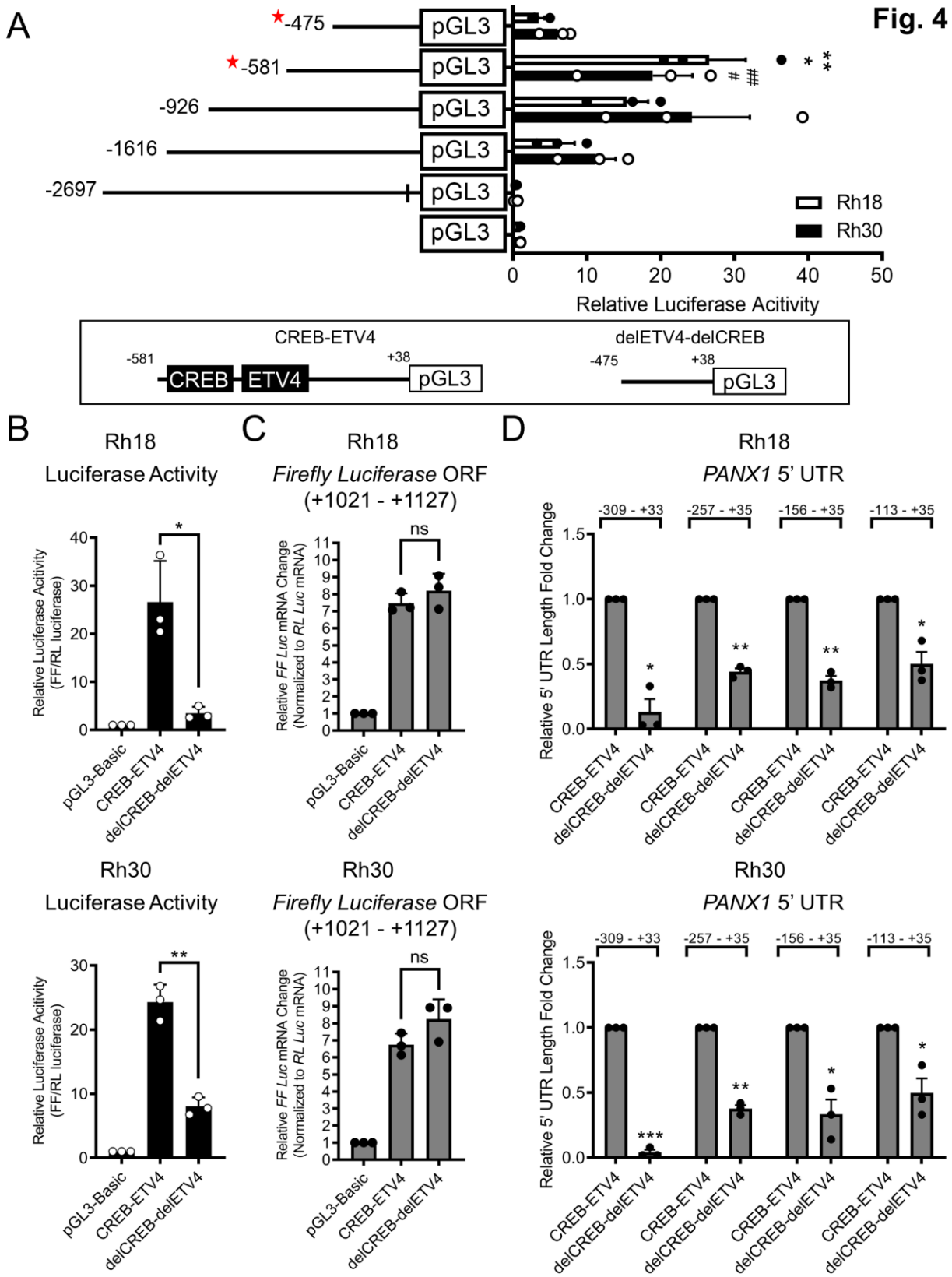
A
Fig. 4
-475
-581
-926
-1616
-2697
pGL3
Rh18
Rh30
0
10
20
30
40
50
Relative Luciferase Acitivity
CREB-ETV4
-581
CREB
ETV4
+38
pGL3
delETV4-delCREB
-475
+38
pGL3
B
Rh18
Luciferase Activity
Relative Luciferase Acitivity (FF/RL luciferase)
pGL3-Basic
CREB-ETV4
delCREB-delETV4
C
Rh18
Firefly Luciferase ORF
(+1021 - +1127)
Relative FF Luc mRNA Change (Normalized to RL Luc mRNA)
ns
D
Rh18
PANX1 5' UTR
-309 - +33
-257 - +35
-156 - +35
-113 - +35
Relative 5' UTR Length Fold Change
CREB-ETV4
delCREB-delETV4
Rh30
Luciferase Activity
Firefly Luciferase ORF
(+1021 - +1127)
PANX1 5' UTR

Fig 4. A Region of the *PANX1* Promoter Containing CREB and ETV4 Consensus Sites Regulates Transcription of its 5' UTR. *PANX1* promoter fragment from -2697 to -1642 as well as promoter fragments from -1616, -926, -581 and -475 to +38 relative to the ATG start codon were PCR amplified from primary HSMM cells and subcloned into the pGL3-basic plasmid. The pGL3 plasmids with *PANX1* promoter fragments were then co-transfected with pRL-TK into Rh18 (eRMS) and Rh30 (aRMS) for 48 hours prior to downstream assays. **(A)** Luciferase activities from pGL3 carrying various portions of the *PANX1* promoter in Rh18 (n=3) and Rh30 (n=3) cells relative to pRL-TK. Red stars highlight the two *PANX1* promoter clones shown in the schematic diagrams below which were selected for further analyses. *, # $P < 0.05$ compared to -1616 - + 38 and **, ## $P < 0.01$ compared to -475 - + 38. The pGL3-Basic or pGL3 carrying *PANX1* promoter fragments from -581 - + 38 (CREB-ETV4) or -475 - + 38 (delETV4-delCREB) were co-transfected with pRL-TK into Rh18 and Rh30 cells for 48 hours and subjected to dual luciferase reporter assay (n=3) **(B)** and RT-qPCR analyses (n=3) for **(C)** *Firefly Luciferase* (*FF*) mRNA and **(D)** *PANX1* 5'UTR levels. * $P < 0.05$ and ** $P < 0.01$ in **(B)**. ns indicates not significant in **(C)**. Each indicated amplified region was normalized separately to CREB-ETV4 in **(D)** where * $P < 0.05$, ** $P < 0.01$ and *** $P < 0.001$ compared to their respective ETV4-CREB controls. Results are expressed as mean ± s.d.

Fig. 5

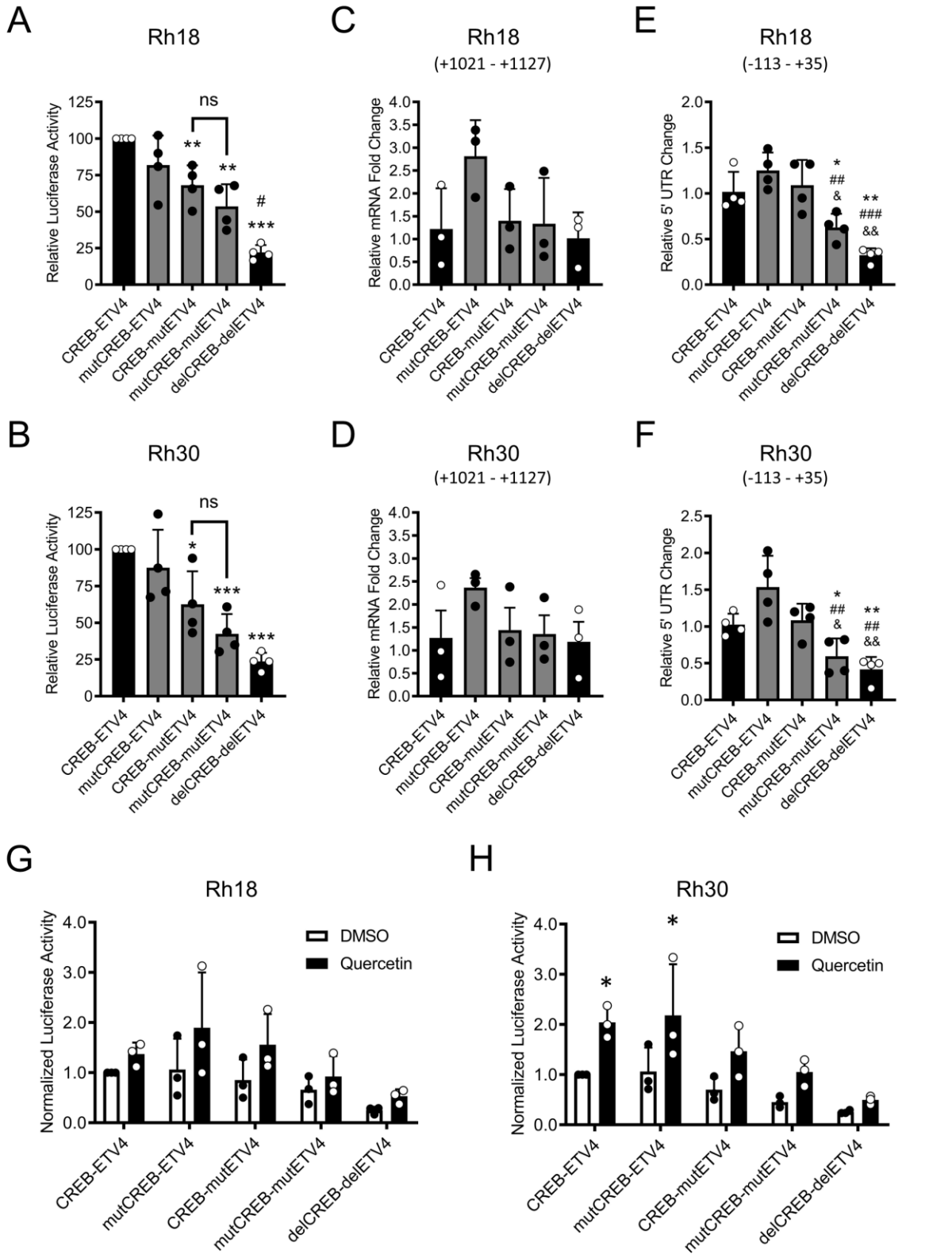
A
Rh18
Relative Luciferase Activity
ns
CREB-ETV4
mutCREB-ETV4
CREB-mutETV4
mutCREB-mutETV4
delCREB-delETV4
C
Rh18
(+1021 - +1127)
Relative mRNA Fold Change
E
Rh18
(-113 - +35)
Relative 5' UTR Change
B
Rh30
D
Rh30
(+1021 - +1127)
F
Rh30
(-113 - +35)
G
Rh18
Normalized Luciferase Activity
DMSO
Quercetin
H
Rh30

Fig 5. CREB and ETV4 Consensus Sites in the *PANX1* Promoter Regulate PANX1 Expression in RMS cells. Rh18 (eRMS) and Rh30 (aRMS) cells were co-transfected with pRL-TK and pGL3 vectors containing one of the following constructs: the wildtype *PANX1* promoter (CREB-ETV4) or the *PANX1* promoter with point mutations in CREB (mutCREB-ETV4), ETV4 (CREB-mutETV4), or both sites (mutCREB-mutETV4). The pGL3 vector containing *PANX1* promoter with dual site deletion (delCREB-delETV4) was also included as a negative control. After 48 hours, cells were analyzed by dual luciferase reporter assays (n=4) **(A and B)** and then with RT-qPCR (n=4) for *FF* (amplified at +1021 - +1127 from *FF* ATG start codon) **(C and D)** or *PANX1* 5'UTR (amplified at -113 - +35 from *PANX1* ATG start codon) **(E and F)**. Dual luciferase reporter assays (n=3) were also performed in cells 48 hours post co-transfection following 24-hour DMSO or quercetin treatment prior to analysis **(G and H)**. In **(A)** and **(B)**, * $P < 0.05$, ** $P < 0.01$ and *** $P < 0.001$ compared to CREB-ETV4; # $P < 0.05$ compared to mutCREB-mutEVT4; ns = not significant. In **(E)** and **(F)**, * $P < 0.05$ and ** $P < 0.01$ compared to CREB-ETV4; ## $P < 0.01$ and ### $P < 0.001$ compared to mutCREB-ETV4; & $P < 0.05$ and && $P < 0.01$ compared to CREB-mutETV4. In **(H)**, * $P < 0.05$ compared to DMSO. pRL-TK was used as an internal normalizer in all results shown. Results are expressed as mean ± s.d.

Fig. 6

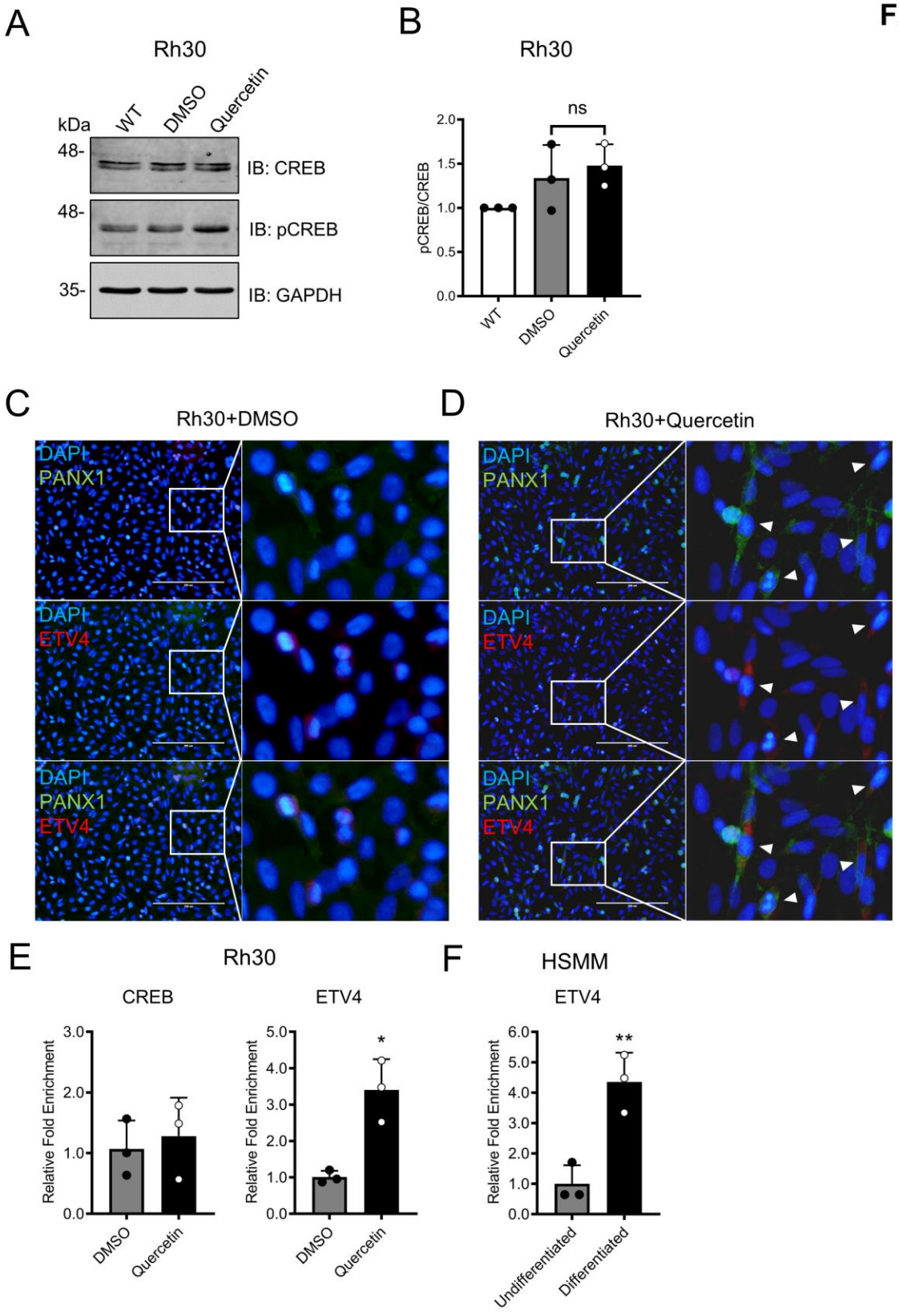
A
Rh30
kDa
WT
DMSO
Quercetin
48-
IB: CREB
48-
IB: pCREB
35-
IB: GAPDH
B
Rh30
ns
pCREB/CREB
2.0
1.5
1.0
0.5
0.0
WT
DMSO
Quercetin
C
Rh30+DMSO
DAPI
PANX1
DAPI
ETV4
DAPI
PANX1
ETV4
D
Rh30+Quercetin
DAPI
PANX1
DAPI
ETV4
DAPI
PANX1
ETV4
E
Rh30
CREB
ETV4
Relative Fold Enrichment
3.0
2.0
1.0
0.0
5.0
4.0
3.0
2.0
1.0
0.0
*
DMSO
Quercetin
DMSO
Quercetin
F
HSMM
ETV4
Relative Fold Enrichment
6.0
5.0
4.0
3.0
2.0
1.0
0.0
**
Undifferentiated
Differentiated

Fig 6. Quercetin Enhances the Binding of ETV4 to its Consensus Site in the *PANX1* Promoter. Rh30 (aRMS) cells were treated with quercetin or DMSO for 24 hours and then subjected to various analyses. **(A)** Representative Western blot for CREB and pCREB. GAPDH was used as a loading control. **(B)** Quantification (n=3) of pCREB levels (relative to CREB) from **(A)**. Results were normalized to untreated Rh30 cells (WT: wild-type). N.S. = not significant. **(C and D)** Representative immunofluorescence (IF) images showing DAPI (blue), PANX1 (green) and ETV4 (red). Images were taken with a 20X objective. Arrowheads indicate PANX1 and ETV4 dual-positive Rh30 cells. Bar = 200 μm. **(E)** Chromatin Immunoprecipitation (ChIP) of CREB and ETV4 in Rh30 cells (n=3) showing enrichment of transcriptional factor binding to their respective consensus site in the *PANX1* promoter. * $P < 0.05$ compared to DMSO. **(F)** ChIP assay results (n=3) of undifferentiated and differentiated HSMM. HSMM cells were induced to differentiate by serum-withdrawal for 6 days prior to analysis. ** $P < 0.01$ compared to Undifferentiated. Results are expressed as mean ± s.d.

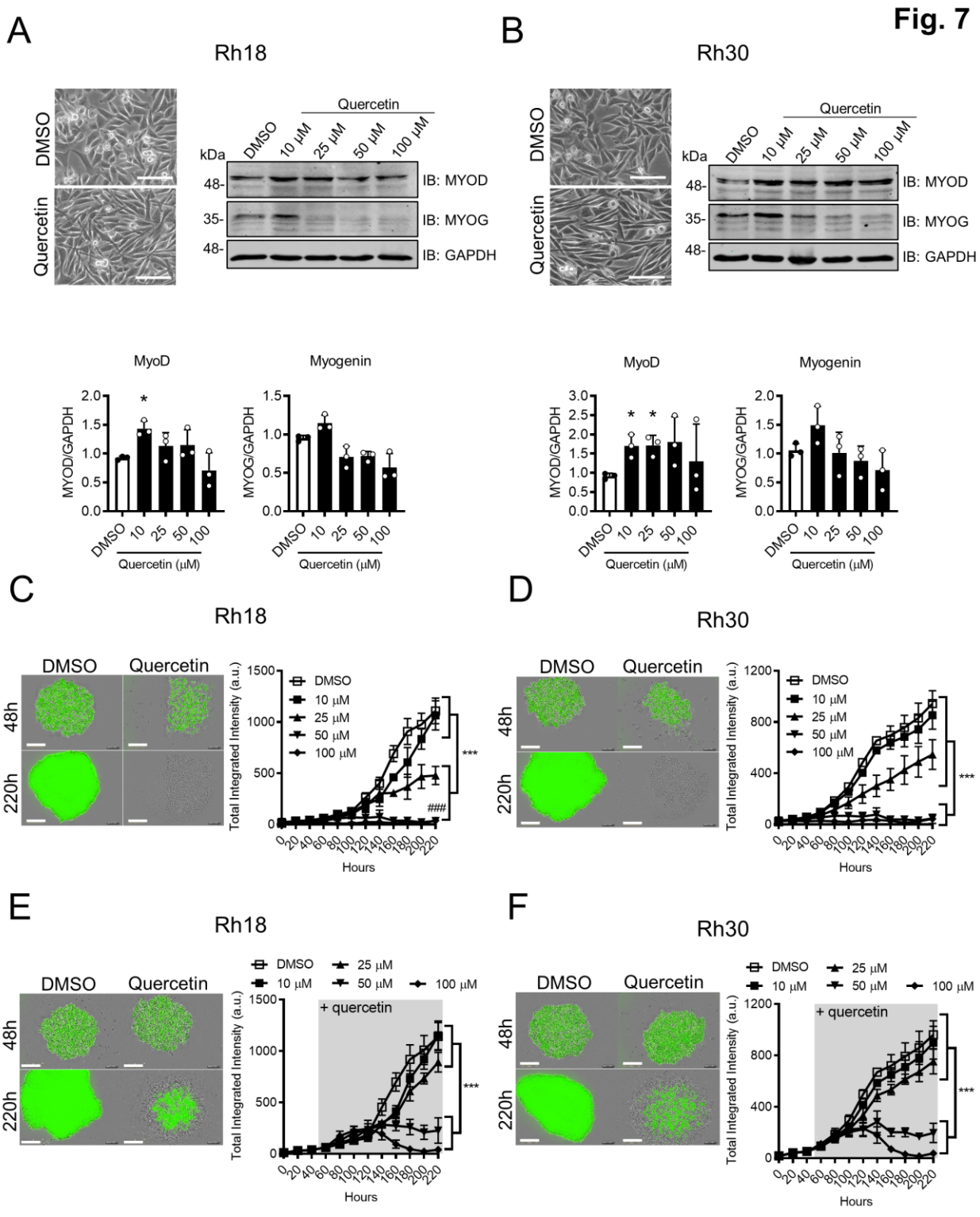
Fig. 7
A
Rh18
DMSO
Quercetin
kDa
Quercetin
DMSO
10 μM
25 μM
50 μM
100 μM
48-
35-
48-
IB: MYOD
IB: MYOG
IB: GAPDH
B
Rh30
MyoD
Myogenin
MYOD/GAPDH
MYOG/GAPDH
Quercetin (μM)
C
Rh18
D
Rh30
48h
220h
Total Integrated Intensity (a.u.)
Hours
###
***
E
Rh18
F
Rh30
+ quercetin

Fig 7. Quercetin Induces Partial Differentiation of RMS Cells, and Both Inhibits Formation of and Induces Regression of their Established 3D *In Vitro* Tumors. Representative images, Western blots, and their quantifications for myogenic markers, MYOD and MYOG, from Rh18 (eRMS) (n=3) (A) and Rh30 (aRMS) (n=3) (B) cells 24 h post quercetin treatment. DMSO was used as vehicle control. Bar = 100 μm. GAPDH was used as a loading control. * $P < 0.05$ compared to DMSO. Rh18 and Rh30 cells stably expressing GFP were subjected to 3D spheroid formation and regression assays. The GFP fluorescence, a surrogate measurement of spheroid size, was monitored over 220 h. In 3D spheroid formation and growth assay, Rh18 and Rh30 cells were pre-treated with quercetin or DMSO for 24 h. Representative images of Rh18 and Rh30 cells treated with 50 μM quercetin at 48 and 220 h are shown. The changes in total integrated intensities for Rh18 (n=3) (C) and Rh30 (n=3) (D) spheroids treated with the indicated dosages of quercetin are summarized to the right. In 3D spheroid regression assays, Rh18 and Rh30 cells were treated with quercetin 48 h post spheroid formation. Representative images of Rh18 (E) and Rh30 (F) cells treated with 50 μM of quercetin at 48 h (the time of treatment initiation) and 220 h are shown. Changes in total integrated intensities of Rh18 (n=3) (E) and Rh30 (n=3) (F) spheroids treated with the indicated dosages of quercetin are summarized to the right. *** $P < 0.001$ between indicated groups. ### $P < 0.001$ compared to 25 μM. Bar = 300 μm. Results are expressed as mean + or ± s.d.

Fig. 8

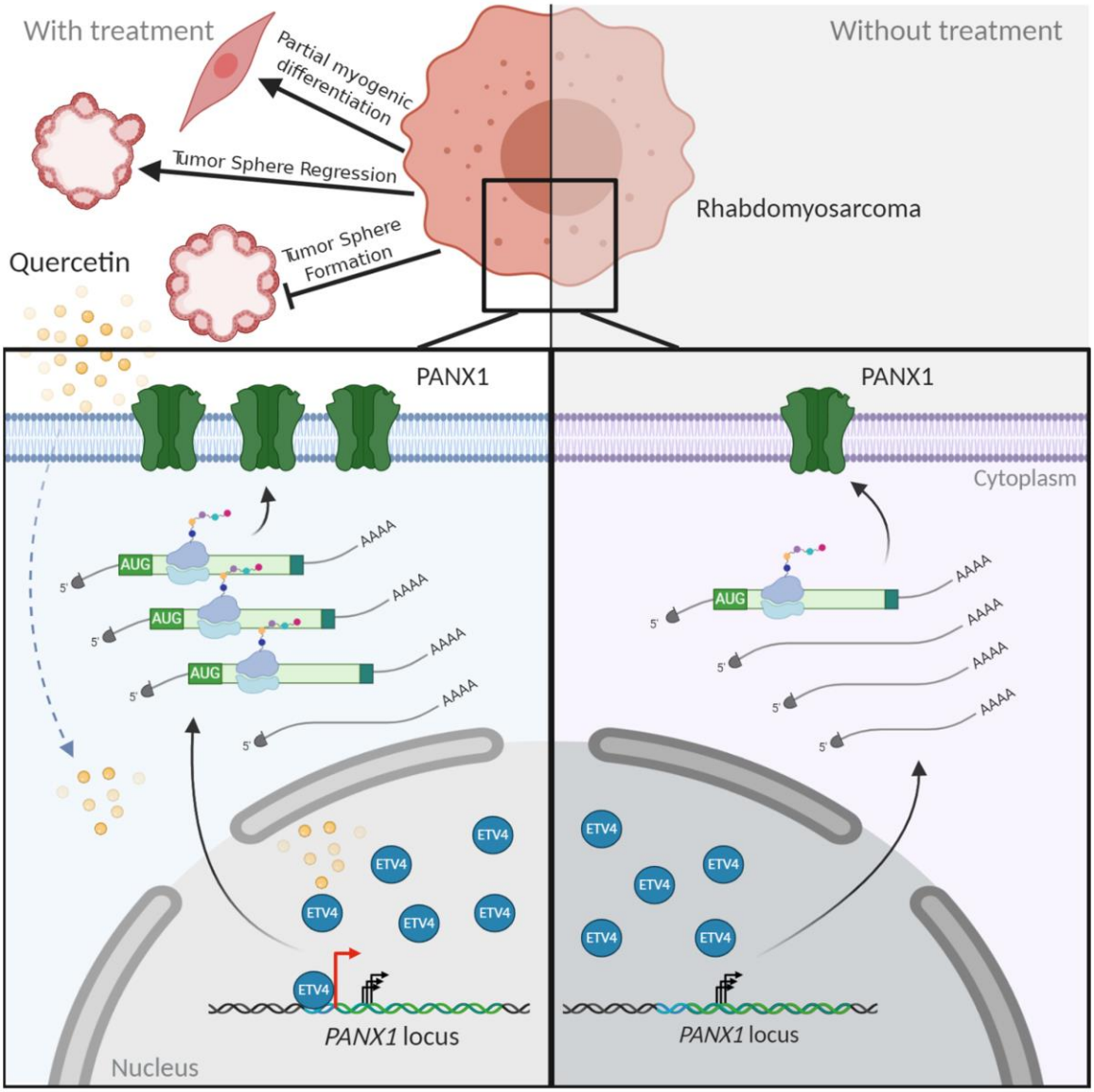
With treatment
Without treatment
Partial myogenic differentiation
Tumor Sphere Regression
Rhabdomyosarcoma
Quercetin
Tumor Sphere Formation
PANX1
PANX1
Cytoplasm
AUG
AAAA
5'
ETV4
PANX1 locus
PANX1 locus
Nucleus

Fig 8. Quercetin-Induced Transcriptional and Translational Control of *PANX1* in RMS. Under normal culture conditions, the majority of basal *PANX1* transcription starts after the ATG start codon generating truncated mRNA of varying lengths that are not readily translated into PANX1 protein. Quercetin treatment enhances the binding of ETV4 to its consensus site in *PANX1* promoter, which allows the transcription of a variant of the *PANX1* transcript containing a short (~43 bp) fragment of its putative 5' UTR. This 5' UTR containing variant of the full length *PANX1* transcript can be readily bound by ribosomes resulting in an enhancement in its translation. This results in an increase in PANX1 levels and alleviation of RMS malignant properties, which suggests that repurposing of quercetin for RMS may constitute a potential new therapeutic strategy for this neoplasm. Moreover, the switch in *PANX1* transcription from producing various translationally incompetent mRNA to a more translatable 5' UTR containing variant of mRNA may have implications in the rapid modulation of PANX1 levels observed during tissue development and homeostasis, and by contrast, the dysregulation of which may lead to pathological conditions.

6.1.7. References

1. Ruan, Z., Orozco, I. J., Du, J. & Lü, W. Structures of human pannexin 1 reveal ion pathways and mechanism of gating. *Nature* (2020). doi:10.1038/s41586-020-2357-y
2. Deng, Z. *et al.* Cryo-EM structures of the ATP release channel pannexin 1. *Nat. Struct. Mol. Biol.* **27**, 373–381 (2020).
3. Jin, Q. *et al.* Cryo-EM structures of human pannexin 1 channel. *Cell Res.* **30**, 449–451 (2020).
4. Michalski, K. *et al.* The Cryo-EM structure of a pannexin 1 reveals unique motifs for ion selection and inhibition. *Elife* **9**, 9–11 (2020).
5. Bao, L., Locovei, S. & Dahl, G. Pannexin membrane channels are mechanosensitive conduits for ATP. *FEBS Lett.* **572**, 65–68 (2004).
6. Langlois, S. *et al.* Pannexin 1 and pannexin 3 channels regulate skeletal muscle myoblast proliferation and differentiation. *J. Biol. Chem.* **289**, 30717–30731 (2014).
7. Pham, T. Le *et al.* Expression of Pannexin 1 and Pannexin 3 during skeletal muscle development, regeneration, and Duchenne muscular dystrophy. *J. Cell. Physiol.* **233**, 7057–7070 (2018).
8. Langlois, S. & Cowan, K. N. Regulation of Skeletal Muscle Myoblast Differentiation and Proliferation by Pannexins. *Adv. Exp. Med. Biol.* **925**, 57–73 (2017).
9. Lav, R., Heera, R. & Cherian, L. M. Decoding the 'embryonic' nature of embryonal rhabdomyosarcoma. *J. Dev. Orig. Health Dis.* 1–6 (2015). doi:10.1017/S204017441500015X
10. Charytonowicz, E., Cordon-Cardo, C., Matushansky, I. & Ziman, M. Alveolar rhabdomyosarcoma: Is the cell of origin a mesenchymal stem cell? *Cancer Lett.* **279**, 126–

136 (2009).

11. Monti, E. & Fanzani, A. Uncovering metabolism in rhabdomyosarcoma. *Cell Cycle* **4101**, 00–00 (2015).

12. Xiang, X. *et al.* Pannexin 1 inhibits rhabdomyosarcoma progression through a mechanism independent of its canonical channel function. *Oncogenesis* **7**, (2018).

13. Amer, K. M. *et al.* Epidemiology, Incidence, and Survival of Rhabdomyosarcoma Subtypes: SEER and ICES Database Analysis. *J. Orthop. Res.* **37**, 2226–2230 (2019).

14. Punyko, J. a *et al.* Long-term survival probabilities for childhood rhabdomyosarcoma. A population-based evaluation. *Cancer* **103**, 1475–83 (2005).

15. Oberlin, O. *et al.* Prognostic factors in metastatic rhabdomyosarcomas: results of a pooled analysis from United States and European cooperative groups. *J. Clin. Oncol.* **26**, 2384–9 (2008).

16. Shern, J. F. *et al.* Comprehensive genomic analysis of rhabdomyosarcoma reveals a landscape of alterations affecting a common genetic axis in fusion-positive and fusion-negative tumors. *Cancer Discov.* **4**, 216–31 (2014).

17. Dobson, C. C., Langlois, S., Grynspan, D. & Cowan, K. N. Engaging Cell Death Pathways for the Treatment of Rhabdomyosarcoma. *Crit. Rev. Oncog.* **21**, 221–239 (2016).

18. Hettmer, S. *et al.* Rhabdomyosarcoma: Current Challenges and Their Implications for Developing Therapies. *Cold Spring Harb. Perspect. Med.* **4**, a025650 (2014).

19. Ray, A., Zoidl, G., Weickert, S., Wahle, P. & Dermietzel, R. Site-specific and developmental expression of pannexin1 in the mouse nervous system. *Eur. J. Neurosci.* **21**, 3277–3290 (2005).

20. Vogt, A., Hormuzdi, S. G. & Monyer, H. Pannexin1 and Pannexin2 expression in the developing and mature rat brain. *Mol. Brain Res.* **141**, 113–120 (2005).

21. Lee, V. *et al.* Pannexin 1 regulates adipose stromal cell differentiation and fat accumulation. *Sci. Rep.* 1–14 (2018). doi:10.1038/s41598-018-34234-9

22. Lai, C. P. K. *et al.* Tumor-suppressive effects of pannexin 1 in C6 glioma cells. *Cancer Res.* **67**, 1545–1554 (2007).

23. Penuela, S. *et al.* Loss of pannexin 1 attenuates melanoma progression by reversion to a melanocytic phenotype. *J. Biol. Chem.* **287**, 29184–29193 (2012).

24. Freeman, T. J. *et al.* Inhibition of pannexin 1 reduces the tumorigenic properties of human melanoma cells. *Cancers (Basel).* **11**, 1–24 (2019).

25. Boyce, A. K. J., Epp, A. L., Nagarajan, A. & Swayne, L. A. Transcriptional and post-translational regulation of pannexins. *Biochim. Biophys. Acta - Biomembr.* **1860**, 72–82 (2018).

26. Dufresne, J. & Cyr, D. G. Regulation of the Pannexin-1 Promoter in the Rat Epididymis.

Biol. Reprod. **91**, 143–143 (2014).

27. Tang, S. M. *et al.* Pharmacological basis and new insights of quercetin action in respect to its anti-cancer effects. *Biomed. Pharmacother.* **121**, 109604 (2020).

28. Hadwen, J. *et al.* Transcriptomic RNAseq drug screen in cerebrocortical cultures: toward novel neurogenetic disease therapies. *Hum. Mol. Genet.* **27**, 3206–3217 (2018).

29. Hinson, A. R. P. *et al.* Human rhabdomyosarcoma cell lines for rhabdomyosarcoma research: utility and pitfalls. *Front. Oncol.* **3**, 183 (2013).

30. Cowan, K. N., Langlois, S., Penuela, S., Cowan, B. J. & Laird, D. W. Pannexin1 and Pannexin3 exhibit distinct localization patterns in human skin appendages and are regulated during keratinocyte differentiation and carcinogenesis. *Cell Commun. Adhes.* **19**, 45–53 (2012).

31. Trapnell, C. *et al.* Differential gene and transcript expression analysis of RNA-seq experiments with TopHat and Cufflinks. *Nat. Protoc.* **7**, 562–578 (2012).

32. Penuela, S. *et al.* Diverse post-translational modifications of the pannexin family of channel-forming proteins. *Channels (Austin).* **8**, 124–30 (2014).

33. Gandin, V. *et al.* Polysome fractionation and analysis of mammalian translatomes on a genome-wide scale. *J. Vis. Exp.* 1–9 (2014). doi:10.3791/51455

34. Hinnebusch, A. G., Ivanov, I. P. & Sonenberg, N. Translational control by 5'-untranslated regions of eukaryotic mRNAs. *Science* **352**, 1413–6 (2016).

35. Araujo, P. R. *et al.* Before It Gets Started: Regulating Translation at the 5' UTR. *Comp. Funct. Genomics* **2012**, 475731 (2012).

36. Graber, T. E., Baird, S. D., Kao, P. N., Mathews, M. B. & Holcik, M. NF45 functions as an IRES trans-acting factor that is required for translation of cIAP1 during the unfolded protein response. *Cell Death Differ.* **17**, 719–29 (2010).

37. Cossarizza, A. *et al.* Quercetin and cancer chemoprevention. *Evidence-based Complement. Altern. Med.* **2011**, (2011).

38. Rauf, A. *et al.* Anticancer potential of quercetin: A comprehensive review. *Phyther. Res.* **32**, 2109–2130 (2018).

39. Reyes-Farias, M. & Carrasco-Pozo, C. The anti-cancer effect of quercetin: Molecular implications in cancer metabolism. *Int. J. Mol. Sci.* **20**, 1–19 (2019).

40. Shafabakhsh, R. & Asemi, Z. Quercetin: A natural compound for ovarian cancer treatment. *J. Ovarian Res.* **12**, 1–9 (2019).

41. Matsuo, M., Sasaki, N., Saga, K. & Kaneko, T. Cytotoxicity of flavonoids toward cultured normal human cells. *Biol. Pharm. Bull.* **28**, 253–259 (2005).

42. Yohe, M. E. *et al.* Insights into pediatric rhabdomyosarcoma research: Challenges and goals. *Pediatr. Blood Cancer* 1–10 (2019). doi:10.1002/pbc.27869

43. Chen, C., Dorado Garcia, H., Scheer, M. & Henssen, A. G. Current and Future Treatment

Strategies for Rhabdomyosarcoma. *Front. Oncol.* **9**, 1–18 (2019).

44. Zhang, L., Yu, H., Wang, P., Ding, Q. & Wang, Z. Screening of transcription factors with transcriptional initiation activity. *Gene* **531**, 64–70 (2013).

45. Butler, J. E. F. & Kadonaga, J. T. The RNA polymerase II core promoter: A key component in the regulation of gene expression. *Genes Dev.* **16**, 2583–2592 (2002).

46. Keller, C. & Guttridge, D. C. Mechanisms of impaired differentiation in rhabdomyosarcoma. *FEBS J.* **280**, 4323–4334 (2013).

47. Floor, S. N. & Doudna, J. A. Tunable protein synthesis by transcript isoforms in human cells. *Elife* **5**, (2016).

48. Cheng, Z. *et al.* Pervasive, Coordinated Protein-Level Changes Driven by Transcript Isoform Switching during Meiosis. *Cell* **172**, 910-923.e16 (2018).

49. Turmel, P. *et al.* Characterization of pannexin1 and pannexin3 and their regulation by androgens in the male reproductive tract of the adult rat. *Mol. Reprod. Dev.* **78**, 124–138 (2011).

50. Taylor, J. M. *et al.* A role for the ETS domain transcription factor PEA3 in myogenic differentiation. *Mol. Cell. Biol.* **17**, 5550–5558 (1997).

51. Le Guellec, S. *et al.* ETV4 is a useful marker for the diagnosis of CIC-rearranged undifferentiated round-cell sarcomas: A study of 127 cases including mimicking lesions. *Mod. Pathol.* **29**, 1523–1531 (2016).

52. Qin, L. *et al.* The AIB1 Oncogene Promotes Breast Cancer Metastasis by Activation of PEA3-Mediated Matrix Metalloproteinase 2 (MMP2) and MMP9 Expression. *Mol. Cell. Biol.* **28**, 5937–5950 (2008).

53. Wu, D., Li, L. & Chen, L. A new perspective of mechanosensitive pannexin-1 channels in cancer metastasis: clues for the treatment of other stress-induced diseases. *Acta Biochim. Biophys. Sin. (Shanghai).* gmw018 (2016). doi:10.1093/abbs/gmw018

54. Tomlins, S. A. *et al.* TMPRSS2:ETV4 gene fusions define a third molecular subtype of prostate cancer. *Cancer Res.* **66**, 3396–3400 (2006).

55. Vanden Abeele, F. *et al.* Functional implications of calcium permeability of the channel formed by pannexin 1. *J. Cell Biol.* **174**, 535–546 (2006).

56. Li, S. *et al.* Requirement of PEA3 for transcriptional activation of FAK gene in tumor metastasis. *PLoS One* **8**, 1–13 (2013).

57. Jesse, T. & LaChance, R. Interferon regulatory factor-2 is a transcriptional activator in muscle where it regulates expression of vascular cell adhesion molecule-1. *J. cell …* **140**, 1265–1276 (1998).

58. Zhao, H.-B., Zhu, Y., Liang, C. & Chen, J. Pannexin 1 deficiency can induce hearing loss. *Biochem. Biophys. Res. Commun.* 1–5 (2015). doi:10.1016/j.bbrc.2015.05.049

59. Escribano-Ferrer, E., Queralt Regué, J., Garcia-Sala, X., Boix Montanés, A. & Lamuela-

Raventos, R. M. In vivo anti-inflammatory and antiallergic activity of pure naringenin, naringenin chalcone, and quercetin in Mice. *J. Nat. Prod.* **82**, 177–182 (2019).

60. Giuliani, C. *et al.* The flavonoid quercetin regulates growth and gene expression in rat FRTL-5 thyroid cells. *Endocrinology* **149**, 84–92 (2008).

61. Arif, H., Rehmani, N., Farhan, M., Ahmad, A. & Hadi, S. M. Mobilization of copper ions by flavonoids in human peripheral lymphocytes leads to oxidative DNA breakage: A structure activity study. *Int. J. Mol. Sci.* **16**, 26754–26769 (2015).

62. Srivastava, S. *et al.* Quercetin, a natural flavonoid interacts with DNA, arrests cell cycle and causes tumor regression by activating mitochondrial pathway of apoptosis. *Sci. Rep.* **6**, 1–13 (2016).

63. Srivastava, N. S. & Srivastava, R. A. K. Curcumin and quercetin synergistically inhibit cancer cell proliferation in multiple cancer cells and modulate Wnt/β-catenin signaling and apoptotic pathways in A375 cells. *Phytomedicine* **52**, 117–128 (2019).

64. Le, N. H. *et al.* Quercetin protects against obesity-induced skeletal muscle inflammation and atrophy. *Mediators Inflamm.* **2014**, (2014).

65. Ekinci Akdemir, F. N., Gülçin, İ., Karagöz, B. & Soslu, R. Quercetin protects rat skeletal muscle from ischemia reperfusion injury. *J. Enzyme Inhib. Med. Chem.* **31**, 162–166 (2016).

66. Spaulding, H. R., Ballmann, C. G., Quindry, J. C. & Selsby, J. T. Long-Term quercetin dietary enrichment partially protects dystrophic skeletal muscle. *PLoS One* **11**, 1–18 (2016).

67. Atrahimovich, D. *et al.* Genome-wide localization of the polyphenol quercetin in human monocytes. *BMC Genomics* **20**, 1–9 (2019).

68. Potthoff, M. J. *et al.* Regulation of Skeletal Muscle Sarcomere Integrity and Postnatal Muscle Function by Mef2c. *Mol. Cell. Biol.* **27**, 8143–8151 (2007).

69. Zhang, M., Zhu, B. & Davie, J. Alternative splicing of MEF2C pre-mRNA controls its activity in normal myogenesis and promotes tumorigenicity in rhabdomyosarcoma cells. *J. Biol. Chem.* **290**, 310–324 (2015).

70. Ignatius, M. S. *et al.* The NOTCH1/SNAIL1/MEF2C Pathway Regulates Growth and Self-Renewal in Embryonal Rhabdomyosarcoma. *Cell Rep.* **19**, 2304–2318 (2017).

71. Lukasiewicz, E. & Miekus, K. Inhibition of rhabdomyosarcoma's metastatic behavior through downregulation of MET receptor signaling. *Folia Histochem. ...* **47**, 485–489 (2009).

72. Jagadeeswaran, R., Thirunavukkarasu, C., Gunasekaran, P., Ramamurty, N. & Sakthisekaran, D. In vitro studies on the selective cytotoxic effect of crocetin and quercetin. *Fitoterapia* **71**, 395–399 (2000).

73. Gibellini, L. *et al.* Interfering with ROS metabolism in cancer cells: The potential role of quercetin. *Cancers (Basel).* **2**, 1288–1311 (2010).

6.2. Battling for Ribosomes: Translational Control at the Forefront of the Antiviral Response

Authors: Huy-Dung Hoang, Tyson E. Graber, Tommy Alain

Review article (Citations: 16)
Journal of Molecular Biology, published on July 2018 (Impact Factor: 4.76)

6.2.1 Author contributions

H.-D.H and T.E.G. wrote the article; H.-D.H, T.E.G. and T.A. reviewed and edited the final manuscript.

6.2.2. Abstract

Highlights

- Viruses battle for control over the cellular protein synthesis machinery.
- The host cell fights back by controlling which mRNAs are translated.
- Technical advances will identify new roles for translation in innate immunity.

In the early stages of infection, gaining control of the cellular protein synthesis machinery including its ribosomes is the ultimate combat objective for a virus. To successfully replicate, viruses unequivocally need to usurp and redeploy this machinery for translation of their own mRNA. In response, the host triggers global shutdown of translation while paradoxically allowing swift synthesis of antiviral proteins as a strategy to limit collateral damage. This fundamental conflict at the level of translational control defines the outcome of infection. As part of this special issue on molecular mechanisms of early virus–host cell interactions, we review the current state of knowledge regarding translational control during viral infection with specific emphasis on protein kinase RNA-activated and mammalian target of rapamycin-mediated mechanisms. We also

describe recent technological advances that will allow unprecedented insight into how viruses and host cells battle for ribosomes.

Keywords

Virus; mTOR; protein synthesis; stress granules; ribosome profiling.

6.2.3. Parasitizing protein synthesis

Protein synthesis is mediated by the ribosome, a complex and fine-tuned molecular machine made up of many ribosomal proteins and ribosomal RNAs (rRNA). This machinery translates genetically encoded information present in mRNA sequences into proteins using amino acids conjugated to transfer RNAs (tRNAs) as intermediates. Moreover, dozens of trans-acting proteins and RNA elements add to the intricacy of the control of mRNA translation in cells. Viruses are obligate parasites of cells because they have an absolute need for the ribosomes of their host to replicate. Indeed, the specificity of translational control for different cellular mRNA substrates is dictated by *cis*-acting sequence features, which are also present in viral mRNAs. In perhaps a quirk of evolution where virally encoded protein synthesis machineries never saw the light of day, viruses instead have set up complex combat strategies to usurp ribosomes within their cellular hosts. In response, host cells have evolved a plethora of defensive tactics to protect their own translation machinery, forming an important component of cell autonomous innate immunity. Early in infection, cellular strategies to prevent viruses from replicating include specifically translating mRNAs that encode for antiviral factors and transiently shutting down global translation. To begin to understand how this battle can unfold, we must review how ribosomes are used to translate information encoded in mRNAs.

6.2.4. A brief introduction to eukaryotic mRNA translation

Translation of mRNAs that originate from both eukaryotic cells and viruses can be divided into three mechanistically distinct steps: initiation, elongation, and termination. Canonical eukaryotic initiation involves the recruitment and assembly of the 40S (small) and 60S (large) ribosomal subunits to form the 80S ribosome at the AUG initiation codon. This highly regulated process is mediated by several eukaryotic initiation factors (eIFs) (reviewed in Refs. [548], [549]).

Initiation begins at the 7-methylguanosine (m^7G) cap structure located at the 5' terminus of an mRNA with the binding of the multi-protein eIF4F complex: a cap-binding protein eIF4E which anchors the complex to the 5' terminus, a RNA helicase eIF4A which helps to unwind RNA secondary structure that might be present with the 5' untranslated region (UTR), and eIF4G, an adaptor protein that serves as a scaffold for the initiation complex (**Fig. 1.1**). The 40S ribosomal subunit needs to be charged prior to initiation with the initiator methionyl-tRNA ($Met\text{-}tRNA_i$) in a GTP-dependent process that is regulated by the heterotrimeric GTPase eIF2. eIF1, eIF1A, eIF5, and eIF3 stimulate binding of a ternary complex (TC) consisting of eIF2-GTP•Met-tRNAi to the 40S subunit, forming a 43S pre-initiation complex. This complex is then recruited to the eIF4F-bound mRNA mediated by interactions between eIF4F and eIF3. The complexity of translation initiation regulation is underscored by the fact that the 3' end of an mRNA can also dictate the efficiency of initiation. Indeed, interaction between eIF4G at the 5' end and poly-A binding proteins (PABPs) at the 3' end, likely through mRNA circularization, serves to synergistically and potently enhance initiation[550].

Next, the 43S complex scans along the 5' UTR in an ATP-dependent process with the help of eIF4A, whose ATP-dependent helicase activity is enhanced by eIF4G together with the

accessory proteins eIF4B or eIF4H, resolving any RNA secondary structure and displacing RNA binding proteins that might prevent ribosomal scanning[551]. While eIF4A is a defining component of the cap-binding eIF4F complex, other helicases such as DHX29, which remodels the 40S ribosomal subunit to facilitate travel along a structured 5' UTR, contribute to the processivity of the pre-initiation complex[552]. Other DEAD/H-box RNA helicases might promote initiation, especially on particular mRNA substrates or in specific cellular contexts and future studies will be needed to solidify their role in translation. Following scanning, recognition of an AUG codon in appropriate Kozak sequence context (typically GCCRCCAUGG, where R is any purine) through anticodon base-pairing renders a 48S initiation complex; the eIFs including the eIF2 TC are then released in a coordinated fashion concomitant with recruitment of the 60S ribosomal subunit (promoted by eIF5 and eIF5B) forming an elongation-competent 80S monosome (reviewed in Refs. [551], [553]).

Translation elongation and termination are comparatively simple in both their molecular players and known control points. The elongation step involves the delivery of aminoacyl-tRNA at the A-site of the 80S ribosome by eukaryotic elongation factor (eEF) 1A followed by ribosome-catalyzed peptide bond formation (**Fig. 1.1**). The GTP-dependent translocase eEF2 promotes movement of the ribosome by one codon toward the 3' end of the mRNA, thus shifting the peptidyl-tRNA to the P-site with deacylated tRNA now occupying the E-site and freeing the A-site for the next cycle of elongation (reviewed in Refs. [551], [15]).

The termination step occurs when the 80S ribosome reaches a stop codon (UAG, UGA or UAA). Eukaryotic release factor (eRF) 1, which mimics tRNA in shape, associates with the GTPase eRF3 that together with GTP form the termination TC. This complex is recruited into the empty A-site of the ribosome (Fig. 1). Upon eRF3-mediated GTP hydrolysis, eRF1 deacylates the

peptidyl-tRNA, releasing the completed polypeptide chain and leaving the 80S ribosome bound to the mRNA. Following termination, ribosomes must be dissociated from the mRNA and recycled. Ribosome recycling is mediated by several protein factors which could be considered a fourth step of translation and the reader is directed toward an excellent review on the subject by Dever and Green (reviewed in Refs. [551], [15]).

Translation control in eukaryotes occurs mainly at the initiation step. Some of the major regulation points involve eIF4F and eIF2. eIF4E can be bound by 4E binding proteins (4E-BPs), which increases the former's affinity for the m7G cap but competes for eIF4G binding, preventing formation of the eIF4F complex[554–556]. Sequential phosphorylation of 4E-BPs by the mammalian target of rapamycin complex 1 (mTORC1; made-up of mTOR, the regulatory-associated protein of mTOR RAPTOR and mLST8) results in their release from eIF4E, allowing normal eIF4F complex assembly on the mRNA[557]. Various stress conditions including viral infection are also known to inhibit translation initiation via phosphorylation of the alpha subunit of eIF2 which blocks eIF2 TC formation. We will visit these important control points in more detail later in the review.

Protein synthesis can also be regulated at the elongation step; eEF2, which regulates ribosome translocation, can be phosphorylated by eEF2 kinase (eEF2K) at Thr56, resulting in decreased affinity for the ribosome[558,559]. Although initiation is often viewed as the major rate-limiting step of mRNA translation, recent work has uncovered specific cellular contexts in which elongation acts as the control point in translation. eEF2K is phosphorylated and inactivated in an mTORC1-dependent fashion[560,561], and a study in intestinal epithelial cells found that genetic removal of APC, a tumor suppressor that is often mutated in colorectal cancer, enhances elongation rates in an mTORC1-dependent manner[562]. mTORC1-dependent control of elongation is also

critical for a specific type of synaptic plasticity occurring in pyramidal neurons[563]. In addition, the regulation of tRNA pools, which directly affect elongation rate, was found to be differentially regulated in proliferating and differentiating cells[206]. Thus, translation control at the elongation step is a promising avenue for future research and it is likely to play a major role in the virus–host context. While little is known about how viruses or other stresses might affect translation elongation, even less is known about how termination might be affected by these conditions.

As we have seen so far, the translation machinery and particularly the initiation step of protein synthesis is a complex choreography of multiple factors coming together in harmony. We will now discuss how upstream inputs from the cellular environment, in particular during viral infection, disrupt this peaceful molecular ballet.

6.2.5. Translational control at the forefront of the antiviral response

As protein synthesis is one of the most energy intensive processes in an eukaryotic cell[564,565], the cell has developed an extensive network of signaling to rapidly and systematically alter the protein synthesis machinery to quickly adapt to environment stimuli (reviewed in Ref. [[549]]). Such a heavily regulated network also provides a critical layer of defense for fighting against parasitic pathogens. Switching off the translation machinery will effectively prevent any further propagation of the pathogen, yet it needs to be used with precaution so that production of host antiviral and cellular homeostasis proteins is still effective. To achieve this degree of control, cell autonomous innate immunity mechanisms have evolved to sense invaders and regulate translation in order to increase its chances at resolving the infection.

Recognizing viral attack

The earliest exposure of the host cell to virus is at the plasma membrane or within the endocytic compartments that the virus uses for entry and transport. Recognizing viral attack falls upon three main classes of pattern-recognition receptors (PRRs) that are part of the cell's autonomous innate immune response: Toll-like, RIG-I-like, and cytosolic nucleic acid-sensing receptors. One major outcome of any PRR activity is the induction of interferon regulatory factors (IRF)-3, IRF-7, or nuclear factor kappa-light-chain-enhancer of activated B cells (NF-κB) that leads to transcriptional upregulation of interferon (IFN)-β. IFN-β in turn upregulates interferon stimulated genes (ISGs) in the infected cell or neighboring cells to prevent virus replication[566].

It is critical to understand that although early detection may be transient and insufficient to mount an effective antiviral response, downstream induction of ISGs effectively amplifies the response to infection at the level of translation. Furthermore, paracrine interferon signaling can impart an early warning to neighboring, uninfected cells allowing them to fully and effectively bring up their defenses prior to imminent viral incursion. Indeed, IFNs clearly affect translational in addition to transcriptional signaling pathways through activation of IFN receptors[567]. How exactly then does virus infection and/or IFNs trigger changes in mRNA translation?

Activation of PI3K–AKT–mTORC1signaling

At the center of the mRNA translation signaling network lies the multi-protein complex mTORC1, which integrates upstream signals from the cellular environment (**Fig. 1.3**). At the apex of the signaling cascade, the family of phosphoinositide 3-kinases (PI3Ks) is activated and recruited to the plasma membrane by receptor tyrosine kinases and G protein-coupled receptors but can also be activated by acute viral infection[568]. Here, PI3K generates phosphatidylinositol-(3,4,5)-triphosphate (PIP3) lipid rafts that serve as a docking point for AKT (also known as protein kinase B), which when bound to these phosphoinositides can be activated through the AKT kinases

PDK1/2 and mTORC2 (a second mTOR complex that does not directly target translation)[569]. Interestingly, studies on Newcastle disease virus (NDV), vaccinia virus (VV), or bovine herpes virus type 1 (BHV-1), to name but a few, have found that infection triggers a period of transient AKT activity as early as 1 h post-infection that later becomes sustained[50–52]. Importantly, these studies have shown that an acute infection with primary inoculum is sufficient to drive the first phase of transient AKT activity as it is present in cells treated with replication-incompetent, UV-inactivated virus. Downstream of AKT lies the tuberous sclerosis complex (TSC) 1 and 2, a negative regulator of Ras homologue enriched in brain (RHEB) which is an activator of mTORC1. Phosphorylation of TSC2 by AKT leads to the inability of the TSC1–TSC2 complex to perform its GTPase activating protein (GAP) activity on RHEB-GTP and allows the now active RHEB to phosphorylate and stimulate mTORC1 activity[570].

Several studies demonstrate that mTORC1 is a critical factor in mediating a translation arm of the innate immune response. For example, cells deficient in the TSC1–TSC2 complex, and thus having increased mTORC1 activity, lead to enhanced expression of the ISGs, ISG15 and C-X-C motif chemokine ligand (CXCL10)[54]. In the same study, these proteins were also found to be induced in MEFs lacking 4E-BP1 and did not display any difference in their mRNA expression, suggesting that translation or post-translation mechanisms were involved. It is also clear that mTOR is involved in mediating the production of type-I interferons (i.e., IFN-α or IFN-β) and other cytokines when PRRs are activated. Stimulation of plasmacytoid dendritic cells with a toll-like receptor 9 (TLR9) agonist induces both IFN-α/β production along with other cytokines, and IFN-α secretion in particular was shown to be ablated by rapamycin, a specific allosteric inhibitor of mTORC1[56]. Interestingly, IFN-β induction in this study appeared to be suppressed by rapamycin but not completely blocked, suggesting mTOR-independent effects (or at least mTORC1-

independent effects as mTORC2 may not be fully inhibited under these conditions). In the same study, Cao et al. found that rapamycin suppressed IFN-α secretion in both vesicular stomatitis virus (VSV) and Yellow Fever virus-infected cells. That VSV infection is highly sensitive to IFNs underpins its use as an oncolytic agent for the treatment of malignancies, as many cancer cells have an impaired IFN response and are therefore permissive to viral infection[571]. Neighboring, non-transformed tissues can, however, mount an effective innate immune response to thwart a viral attack. However, some tumor cell types such as malignant gliomas maintain a type I IFN response; this can be blunted by rapamycin, allowing improved oncolysis in a mouse xenograft model when combined with VSV or myxoma virus (MV) that can be attributed to enhanced viral replication[57,572].

We have seen that mTORC1 and its upstream signaling effectors are important targets of viral infection and that mTORC1-dependent translation of ISGs is an important feature of the innate immune response. Specificity of mTORC1-dependent translational control lies in its two major families of downstream effectors: the paralogous 4E-BPs (4E-BP1, 2, 3) and the ribosomal protein S6 kinases (S6K1 and S6K2). It is noteworthy that La-related protein 1 (LARP1) has recently been found to be a direct target of mTORC1 and functions by interacting with terminal oligo-pyrimidine (TOP) motif-containing mRNAs and repressing their translation[24,28]. However, there is a dearth of information regarding the role of LARP1 in host–virus translation control and future studies are needed to address its role in innate immunity. We will next explore the links between 4E-BPs, S6Ks, and the regulation of cell autonomous innate immunity in response to viral infection.

Downstream of mTORC1: 4E-BPs

4E-BP1 and 4E-BP2 are expressed in most cell types, while 4E-BP3 is generally poorly expressed at the protein level, but can be induced during prolonged mTORC1 inhibition[573]. The 4E-BPs, when in their hypophosphorylated state, interact with the eIF4E cap-binding protein and strongly repress cap-dependent translation initiation. mTORC1 activity induces sequential hyperphosphorylation of 4E-BPs, freeing eIF4E and thus promoting cap-dependent translation initiation[574]. This control appears to be critical in establishing a proper innate immune response to viral infection as 4E-BP1/2 double knockout MEFs (4E-BP3 is poorly expressed in MEFs) and animals were found to be resistant to VSV infection, and this phenomenon was mediated by enhanced translation of *Irf7*, a key transcription factor that activates expression of type I IFNs[55]. Interestingly, 4E-BP1/2 double knockout animals were also resistant to the parasite Leishmania due to enhanced type I IFN responses[575]. Type I and II IFNs can generally cause hyperphosphorylation of 4E-BP1 in an mTOR-dependent manner and this correlates with increased ISG expression that is independent of transcription[576]. Intriguingly, haploinsufficiency of 4E-BP in MEFs (i.e., as found in either 4E-BP1 or 4E-BP2 knockout cells) is sufficient to impair VSV infection through increased IFN secretion, although removing 4E-BP2 had a more profound effect than 4E-BP1 on viral titers (5-log *versus* 2-log decrease)[577]. The significance of this difference is unknown, although it may have to do with differences in tissue expression or activity. Critically, while genetic ablation of both 4E-BP1 and 4E-BP2 is sufficient to cause a small increase in ISG15 and CXCL10 protein levels, stimulation with IFN-α causes a super-induction of these two ISGs at the protein level[54], suggesting two convergent pathways contributing to this phenotype. Indeed, a subsequent study by the same lab indicates that the S6Ks, which we will review in the next section, are involved in enhancing IFN-stimulated translation of ISGs[578].

Downstream of mTORC1: S6Ks

The p70 S6 kinases (S6K1 and S6K2) are also important mTORC1 effectors that target translation initiation by indirectly regulating eIF4A activity through PDCD4 and eIF4B, or elongation by regulating eEF2 activity via eEF2K (**Fig. 1.3.**; reviewed in Ref. [579]). S6Ks also phosphorylate the ribosomal protein S6 (RPS6), a component of the 40S ribosomal subunit; however, the role for RPS6 phosphorylation in general protein synthesis is not defined (reviewed in Ref. [580]). Complicating matters considerably is the fact that S6K targets can also be regulated through parallel pathways involving the p90 ribosomal S6 kinase (RSK) family of kinases (RSK1–4). For example, both RSKs and S6Ks target Ser422 of eIF4B[581]. Highlighting this complexity, IFN-α or -β can activate S6K1-mediated phosphorylation of its target eIF4B in a PI3K-mTOR-dependent manner in MEFs; yet, Ser422-eIF4B phosphorylation in KT1 hematopoietic cells appears to require RSK1 (but not RSK2 or S6K1)[576,578]. In the same study, Kroczynska *et al.* [578] showed that in MEFs lacking both S6K1 and S6K2, IFN–mediated recruitment of *Isg15* mRNA to polysomes is impaired, demonstrating that S6Ks in this context are required for proper translation of at least one ISG when mTORC1 is activated. Exactly why there is a tissue-dependent effect was not immediately clear as differential expression of RSKs and S6Ks could not explain their observations. Recent data, however, invoke the presence of another protein, S6 kinase 1 Aly/REF-like target (SKAR), downstream of both S6K1 and RSK1 whose activity is cell type dependent and enhances *Isg15* translation in an IFN-dependent manner[582].

S6Ks are therefore hypothesized to enhance the IFN response and consequently should create an environment that is hostile to viral infection. Indeed, S6K1/2 double knockout MEFs infected with VSV exhibited much higher titers of virus and this was due to decreased expression of ISGs[57]. Interestingly, S6K1/2 were shown to also function independently from their canonical roles in translation in the context of viral infection and adds yet another layer of complexity. Wang

et al.[583] found that S6K1 (and to a lesser extent S6K2) participates as an adaptor protein in a ternary complex together with the ISG signaling molecules STING and TBK1. This complex, which was unaffected by rapamycin treatment, phosphorylates and activates the ISG transcription factor IRF3 which in turn activates transcription of ISGs. It is important to note, however, that this mechanism does not preclude the translation activity of S6Ks from modulating the innate immune response.

Activation of eIF4E via MAPK/ERK signaling

We have seen that eIF4E is regulated by 4E-BPs; however, direct phosphorylation by the mitogen-associated protein kinase (MAPK) interacting protein kinase 1 and 2 (MNK1 and 2), acting downstream of ERK and p38 MAPK, can also modulate eIF4E activity (Fig. 1.3)[584–586]. MNK1 interaction with eIF4G positions it in proximity to eIF4E and this is crucial for MNK1 kinase activity at Ser209 of eIF4E[587,588]. The role of eIF4E phosphorylation in cap-dependent translation is still unclear, with studies reporting both an increase[589–592] and decrease[593–595] in protein synthesis following eIF4E phosphorylation. In the context of virus infection, these two MAPK signaling pathways are known to be activated during certain viral infections[596–598]. Importantly, the phosphorylation of eIF4E was found to be critical for translation of the inhibitor of NF-κB (IκBα kinase) mRNA which resulted in an impaired type I IFN response due to uncontrolled NF-κB activity when eIF4E phospho-null cells were challenged with several different viruses or the viral dsRNA mimic poly(I:C)[438]. Notably, chemical inhibition of MNK1 or MNK2 impairs replication of herpes simplex virus type 1 (HSV-1), human cytomegalovirus (HCMV), and VV[591,599,600], or suppresses the reactivation of Kaposi's sarcoma-associated herpesvirus (KSHV)[601]. Similarly, chemical inhibition or antisense oligonucleotide depletion of MAPK in HIV-1 infection decreased infectivity, although it did not affect Gag or Env protein levels, suggesting that MAPK might not contribute significantly to HIV-1 protein production[602]. Thus, the contribution of

MAPK/MNK signaling to protein synthesis during infection remains poorly defined and can be variable between different viral contexts.

Inhibition of viral mRNA translation through ISG positive feedback loops

IFNs can provide a positive feedback loop, allowing a super-induction of ISGs. Importantly, some ISGs have been found to have antiviral functions that directly or indirectly target the translation machinery in an attempt to minimize the synthesis of viral proteins. For instance, the IFN-induced proteins with tetratricopeptide repeats (IFITs) modify pre-initiation complexes through their binding to eIF3 subunits (reviewed in Ref. [77]). The endoribonuclease RNase L, which can be activated through IFN- and dsRNA-induced oligoadenylate synthetases, indirectly arrests translation of both viral and host transcripts by degrading rRNA and mRNA[78]. The RNA substrate specificities of RNase L have remained elusive; however, recent evidence now indicates that RNase L may exert more immediate effects on translation through cleavage of tRNA, which results in global translation arrest even when rRNA and mRNAs remained intact[603]. Given that tRNA has been observed within VV factories, it would be of interest to determine if the former is preferentially targeted by RNase L over cytoplasmic tRNA pools during infection. Another example is ISG-15, a ubiquitin-like protein that affects protein modifications analogous to ubiquitylation (called ISGylation) and has been shown to ISGylate the cap-binding protein eIF4E homologous protein (4EHP)[79]. This is important as 4EHP, which is thought to repress cap-dependent translation by mediating translational silencing via miRNAs[375,604,605], is normally a weak cap-binding protein relative to eIF4E. ISGylation, however, was suggested to enhance 4EHP cap-binding activity and therefore could repress or modulate translation of subsets of mRNAs during stress, such as during hypoxia[606]. Perhaps the best known ISG that negatively affects

translation is protein kinase RNA-activated (PKR), and we will visit its mechanism of action in more detail below.

The integrated stress response

Outside of the mTORC1 signaling pathway, the most well-characterized mechanism of translational control in response to infection is the integrated stress response (ISR). The ISR consists of input collected from upstream stress (e.g., viral infection) signaling and converges to affect phosphorylation of the α-subunit of eIF2 (P-eIF2α), which triggers a block in general translation while favoring that of select transcripts. The magnitude and duration of this response modifies the cellular outcome (**Fig. 1.3**). It is important to emphasize that the ISR also triggers transcriptional reprogramming and selective proteolysis; however, we will focus here on the translation arm of the ISR. This particular ISR signaling arm can be mediated by any or all of four eIF2α kinases: heme-regulated inhibitor (HRI), general control nonderepressible 2 (GCN2), PKR, and PKR-like endoplasmic reticulum (ER) kinase (PERK). HRI is activated by oxidative stress, heme deprivation, and osmotic stress[607]. GCN2 is activated by UV light or amino acid deprivation[42]. PKR is activated by binding to dsRNA, an intermediate or final product of viral replication[608]. PERK is activated by unfolded proteins within the ER lumen which can occur during ER stress[609]. As the reader can appreciate, all of these kinases could be activated during viral infections as their activity is modified by infection cues such as amino acid starvation and oxidative stress. For instance, GCN2 can act in a similar manner to PKR, sensing the structured genomic RNA of Sindbis virus (SV) and possibly that of VV and VSV. Indeed, NIH3T3 cells expressing a kinase-dead form of GCN2 fail to maintain host protection from SV infection[62]. Likewise, the DNA virus mouse cytomegalovirus (MCMV) induces P-eIF2α in a GCN2-dependent manner, and a GCN2 loss-of-function mutation increases susceptibility to infection

with MCMV or adenovirus *in vivo*[63]. ER stress is a common feature of infection with replicating viruses, where viral envelope proteins overwhelm the folding capacity of the ER resulting in PERK activation and subsequent eIF2α phosphorylation[61]. However, PKR by virtue of its ability to sense a wide array of foreign nucleic acid is well placed as a first responder to *acute* viral infection, which we will discuss further in the next section.

The PKR-eIF2 signaling arm reprograms translation

The appearance of dsRNA in the cytoplasm is a universal signal of viral infection, as it makes up the genomes of many viruses and is produced during ssRNA or DNA virus genome replication. PKR senses dsRNA and 5′ triphosphate-capped ssRNA, both of which are not normally present in the cytoplasm[58,59]. Sensing is mediated by the two dsRNA binding domains (dsRBM1 and dsRBM2) of PKR and activity is regulated by a single kinase domain. Inactive, unphosphorylated PKR exists as a monomer with the two dsRBMs forming a loop that masks the kinase domain. Upon binding of dsRNA, PKR dimerizes and autophosphorylation triggers its kinase activity[60]. Activated PKR in turn will phosphorylate eIF2α. Indeed, treatment of MEFs with poly(I:C) mimics viral dsRNA exposure and induces P-eIF2α in a PKR-dependent manner[610].

As we have seen earlier, eIF2-GTP participates in eIF2 TC formation and is thus critical for translation initiation. Once GTP is hydrolyzed the eIF2-GDP product binds the guanosine exchange factor (GEF) eIF2B which recycles eIF2 TC activity (**Fig. 1.3**). Critically, P-eIF2α is a competitive inhibitor of eIF2B GEF activity, thus blocking eIF2 TC formation and subsequently impairing translation initiation[611]. Of note, PKR also plays a translation-independent role in modifying infection by activating the NF-κB signaling pathway, causing its nuclear translocation and transcriptional upregulation of *IFNB1* and other antiviral and antiproliferative genes, thus enhancing the IFN response[612–615].

P-eIF2α-mediated attenuation of translation ostensibly limits viral spread by preventing viral RNA translation. Indeed, overexpression of a P-eIF2α mimetic (S51D) blocks VSV replication[65]. During P-eIF2α-mediated global translation suppression, there is a group of transcripts that are paradoxically induced, the main mechanism of which involves the presence of upstream open reading frames (uORFs) in their 5′ UTRs. These sequence features consist of short ORFs whose initiation codon lies upstream of that of the main ORF. uORFs can lie entirely within a 5′ UTR or overlap with the main ORF. As such, uORFs compete for pre-initiation complexes, effectively initiating their own translation in lieu of the main ORF. In contrast, an increase in P-eIF2α switches translation to the main, downstream ORF. There are multiple models proposed about how this comes about and there are likely multiple contributing mechanisms. Two mechanisms that are likely in play with a scarcity of eIF2 TC are enhanced ribosome bypass and leaky scanning. This takes us beyond the scope of this review and the reader is directed to an excellent review by Barbosa *et al.*[35] covering these concepts in-depth. Of the stress response transcripts that are upregulated in a uORF-dependent manner, some have pro-survival (ATF4) and pro-apoptotic (GADD34 and CHOP) functions[66–68,616]. Given the important function of these transcripts in cellular homeostasis, one might expect that their upregulation in the presence of high P-eIF2α can have important implications on viral propagation and is therefore an attractive target for viral manipulation. Indeed, the UL38 protein of HCMV promotes infected-host survival via translational induction of ATF4 expression. Mutation of UL38 attenuates the virus, while expression of UL38 alone confers resistance to ER-stress related cell death by activating the unfolded protein response and inducing ATF4 expression[69]. In the same study, overexpression of ATF4 rescues viral attenuation caused by the UL38 mutation, suggesting that translational induction of ATF4 by stress is important for chronic infection by HCMV. Interestingly, certain

viruses have co-opted uORF-mediated translation regulation, possibly to favor the expression of specific viral genes in the context of low eIF2 TC. For instance, the 5′ UTR of the Ebola virus polymerase L mRNA contains a repressive uORF that overlaps with the main ORF and responds to P-eIF2α[70]. Notably, Shabman *et al*. also showed uORF-mediated regulation in Ebola VP35, VP30 and VP24 5′UTRs, suggesting that this may be a pervasive mechanism of regulating gene expression for this particular virus. Moreover, they showed that removing this regulatory mechanism by mutating the uORF initiation codon in the L mRNA resulted in a modestly attenuated virus, suggesting that uORF-dependent translation is important for optimal Ebola infection.

uORFs cannot be the only mechanism by which translation is maintained during viral infection. This is evident from the translational induction of ISGs such as *ISG15*, *CSCL10*, and *IRF7*, which do not appear to be controlled through an uORF-mediated mechanism. Accumulating evidence shows that certain antiviral mRNAs can be still efficiently translated even when PKR is activated. This phenomenon depends on the activity of the ISR-induced GADD34, a regulatory subunit of protein phosphatase 1 (PP1) which binds PP1 and targets its activity to P-eIF2α[610,617]. The GADD34 5′ UTR contains two uORFs that inhibit translation of the main ORF in normal conditions, but enhance it under conditions of high P-eIF2α, thus acting in a feedback loop to ensure that it is only translated under the latter condition[67]. Interestingly, single cell monitoring of MEFs treated with poly(I:C) revealed that global protein synthesis oscillates between “ON” and “OFF” phases in a GADD34-dependent manner that is inversely correlated with P-eIF2α expression[618]. Dalet *et al*. showed that the ON phase correlates with a burst of IFN-β production, and one can speculate that these phasic short bursts of host translation mediate an effective response to viral infection by striking the right balance in maintaining a brake on viral

mRNA translation while at the same time synthesizing critical antiviral proteins and/or maintaining synthesis of homeostatic proteins.

Many questions remain concerning the molecular details of host–virus interactions during the ISR that could be answered using genome-wide translation (translatome) profiling of infections over multiple timepoints: What are the sub-populations of mRNAs being translated during the ON and OFF phases? Alternatively, do antiviral mRNAs compete better for translation initiation factors under these conditions than viral mRNAs? Later in this review, we will see that some viruses deploy mechanisms to reverse P-eIF2α: Does this inadvertently allow translation of host antiviral mRNAs?

Occluding viral RNA translation via stress granules

P-eIF2α and the resulting depletion in eIF2 TC on pre-initiation complexes can cause them to stall on 5′ UTRs[619]. This initiation stall causes any downstream, elongating ribosomes on an mRNA substrate to "run-off," leaving a naked transcript. This invites the recruitment of RNA binding proteins that are prone to aggregation, causing the stalled initiation complexes to condense into stress granules (SG). The most well-described SG-associated RNA binding proteins are T-cell internal antigen 1 (TIA1), TIA1-related protein (TIAR), and Ras-GTPase activating protein SH3 domain-binding protein 1 (G3BP1). TIA1 and TIAR consist of three RNA binding domains followed by a glutamine-rich prion-like domain, the latter of which is necessary for SG nucleation[620]. G3BP1 can also induce SG formation through self-oligomerization, an activity that is inhibited by Ser149 phosphorylation[621,622]. SG nucleation can also occur in an P-eIF2α-independent manner, as they form when cells are depleted of other initiation factors such as eIF4B, eIF4H or PABP, presumably because stalled translation initiation is a universal signal for the recruitment of SG condensing proteins[623].

Transient accumulation of SG during many different viral infections suggests that they may play a role in mediating the innate immune response[71,72]. Supporting this view, viruses have developed mechanisms to inhibit SG formation[72]. One way that SGs might enhance innate immunity is by decreasing the threshold of PRR activation through increased, localized concentrations of viral nucleic acids and proteins. Supporting this idea, cells infected with NS1-mutant influenza A virus (wild-type virus does not form SGs) were found to have viral mRNA enriched in SGs relative to the cytoplasm together with several antiviral proteins, including RIG-I, LGP2, and MDA5[624]. PKR is also re-localized to SGs upon infection with an SG-permissible mutant strain of mengovirus via its interaction with G3BP1 and Caprin-1[625]. Moreover, the IFN response is interrupted when SG formation is blocked, as depleting G3BP1 impairs IFN-β production in response to either virus infection or treatment with poly(I:C)[624]. These observations suggest that SG formation is important for the optimal activation of the antiviral response.

Another means by which SGs could boost innate immunity is by disrupting translation of viral mRNAs, perhaps via RNA sequestration. It has been observed that chemical induction of SGs inhibits synthesis of both viral and host mRNAs[626,627]. As viral mRNA was also found in SGs during influenza infection, there is a possibility that it is actively sequestered there[624]. Indeed, TIA1 and TIAR have been shown to directly bind to the 3′ stem-loops of West Nile virus (WNV) and tick born encephalitis virus (TBEV) RNAs, suggesting that these complexes could serve as SG nucleation points[73,74]. However, knockout of TIAR or TIA-1 negatively affects WNV infectivity[73]. In the case of TBEV infection, knockout of TIA-1 enhances replication, while TIAR knockout impairs infection. Similarly, G3BP1 has been shown to interact with HIV-1 RNA and knockdown enhances HIV-1 replication[628]. These disparate effects between SG proteins on viral infections could simply be due to the fact that these RNA-binding proteins have a direct role in

enhancing viral replication in addition to serving as SG nucleation factors. In addition, many viruses such as rabies, VV, or reovirus form viral factories; these intracellular foci enriched in viral genomes and transcripts act as privileged sites of viral transcription and translation[629,630]. The high concentration of unprotected RNA in these foci might serve as an SG nucleation point which could affect virus propagation. Indeed, a study on mouse fibroblasts infected with rabies virus found that a sub-population of SGs are closely associated with viral factories, while depleting TIA-1 enhances viral replication, suggesting that these SGs have a negative impact on virus propagation[75]. Similarly, G3BP1 and Caprin-1 were co-purified with the VV viral factory-associated protein VITF-2, which suggests a direct link between viral factories and the SG nucleation machinery[631]. Importantly, VV viral factory-associated SGs seem to be non-canonical as they are not enriched in small ribosomal subunits and still form in the presence of cycloheximide (CHX), which normally prevents SG nucleation; suggesting that this particular atypical SG is not formed by mRNAs stalled at initiation[76]. Whether or not SGs form a functional connection with other types of viral factories remains unknown.

The timing and duration of SG formation in the context of viral infection might be an important factor in their ability to limit infection. How early are they induced in the infection cycle? As SG formation largely relies on PKR activation, it is assumed that DNA and ssRNA viruses do not trigger SGs until the replication step, thus limiting any negative impact SGs might have on early infection for these viruses. However, dsRNA viruses could possibly induce SGs via PKR much earlier, before virus replication. Indeed, in a study on reovirus, chemical inhibition of viral uncoating prevented SG formation; yet UV-inactivated virus or infection in the presence of the protein synthesis inhibitor puromycin, still triggered SGs[632]. These experiments propose that genomic dsRNA from the primary viral inoculum can be responsible for an early activation of SG

in the infection cycle and may contribute to limiting the cellular sequelae of infection. Together, these findings suggest that SGs play an important role in the innate immune response, possibly by limiting translation of viral RNAs.

6.2.6. Viruses fight back: Viral manipulation of host translation

Viruses gain control of the host translation machinery by (1) blocking the cellular antiviral response and (2) redirecting host translation to prioritize that of viral mRNAs. Viruses have devised an impressive number of strategies to counteract translation arrest by P-eIF2α and reorganize translation substrate specificities in order to maximize viral protein synthesis. Virtually every virus has effectors that can manipulate host translation machinery, and every step of translation control can be targeted, which has been well reviewed elsewhere[608]. We also invite the reader to review virus-induced changes in codon usage and miRNA homeostasis that modulate the translational response to infection[633,634]. Here, we will focus on the viral strategies that modulate the PKR-eIF2 signaling arm, as well as mTORC1 signaling and their downstream effects on translation.

Targeting AKT–mTORC1 signaling

As we have seen at the beginning of this review, the PI3K–AKT–mTORC1 pathway is activated with viral infection, either as a cellular response or affected by viral proteins. Some viruses inhibit host translation by targeting AKT–mTORC1 signaling. For instance, the VSV M protein can inhibit AKT phosphorylation[80], resulting in accumulation of hypophosphorylated 4E-BP1 and thus likely inhibiting eIF4E-dependent translation initiation[81]. In contrast to inhibition of this pathway, PI3K is a target of activation by various viral proteins, such as adenovirus E4 ORF1 product, influenza virus NS1 protein, Epstein–Barr virus LMP2A, and KSHV GPCR protein[85,635–

[637]. AKT is activated by the myxoma virus ankyrin repeat M-T5 protein[638]. The inhibitory TSC1–TSC2 complex is blocked by HSV-1 US3, HCMV UL38, and human papilloma virus (HPV) E6[83,84,639]. So far, no evidence of direct viral protein engagement of RHEB has been documented, although RHEB has been shown to be required for efficient HCMV replication and, more intriguingly, is found to be associated with mTOR in HCMV perinuclear assembly compartments[640]. In contrast, adenovirus E4 ORF4 protein is able to activate mTORC1 in an RHEB-independent manner[641]. The importance of mTORC1 activation in viral infection is also emphasized by the fact that active site mTOR inhibitors, which target both mTORC1 and mTORC2, inhibit replication of HCMV[642]. As such, AKT–mTORC1 inhibitors have potential to be used as antiviral reagents[643], such as the use of an AKT inhibitor peptide to block influenza virus replication[644]. AKT inhibitors have already been used in the clinic as antitumor agents[645] and therefore might be attractive candidates for future clinical trials investigating their antiviral efficacy. In summary, more than a decade of intensive research has consolidated the fact that AKT–mTORC1 is a prime target of viruses in its battle plan to gain control of the ribosome, and this knowledge has potential to be translated into the clinic.

Targeting the cap-dependent translation initiation complex

Targeting the cap-dependent translation initiation complex is a major strategy employed by viruses to usurp host translation. For instance, the calicivirus VPg protein facilitates recruitment of eIF4E to the viral mRNA[90]. eIF4G is degraded by a range of viral proteases and can be altered so as to affect its interaction with other cellular or viral initiation factors[87–89,646,647]. PABP activity is targeted for inhibition from a surprisingly large number of virus effectors[89,91,92,648–650]. Components of the eIF3 complex are also binding targets of viral effectors, which results in impaired host translation[651–654]. Instead of targeting cap-dependent translation initiation factor

activity per se, some viral proteins act as sinks for these translation factors, affecting their localization to facilitate viral mRNA translation. For example, influenza virus PB2 polymerase subunit binds eIF4G and the 5′ cap, facilitating recruitment of the eIF4F complex[655]. Poxviruses and Asfarviruses replicate in cytoplasmic viral factories which sequester eIF4E and eIF4G, thus placing them in proximity with viral mRNAs[116,600,656,657].

Many RNA viruses bypass the need for cap-dependent translation initiation entirely. Such "cap-independent" translation initiation is mediated by viral 5′ UTRs harboring a structured RNA sequence element that is conserved through sequence co-variation and acts as an internal ribosome entry site (IRES)[658]. Viral IRES can be divided into four classes ordered by increasing complexity of structural features and decreasing eIF requirements. We will briefly outline these classes below; however, the reader is directed to excellent in-depth and recent reviews on this topic by Asnani *et al* or Mailliot and Martin[93,659].

Type I IRES (e.g., found in enteroviruses such as poliovirus, PV) consist of simple hairpin secondary structures; apart from eIF4E, they require all canonical eIFs to mediate recruitment of the ribosome followed by scanning along the 5′ UTR prior to reaching the downstream initiation codon. Critically, in cells infected with these viruses, eIF4G is cleaved by viral proteases, precluding its interaction with eIF4E at the cap[660,661]. This effectively blocks cap-dependent (i.e., host) protein synthesis while favoring that of IRES-containing viral mRNAs. Type II IRES (e.g., found in EMCV, FMDV, TMEV) require the eIFs (again, apart from eIF4E) but are able to forgo the scanning requirement allowing ribosomes to be directly recruited to the initiation codon.

Type III IRES (also referred to as Type IV, see discussion about Hepatitis A below) can be found in viruses like HCV and BVDV and possess more complex structures such as pseudoknots.

These IRES need a minimal set of eIFs (eIF2, eIF3, eIF5), bypassing the scanning requirement through direct recruitment of the ribosome to the initiation codon. Finally, Type IV IRES (sometimes called Type V and found in intergenic regions of, e.g., CrPV) are the most structurally and functionally sophisticated; restricted to intergenic regions of viral polycistronic mRNAs, they are imbued with the ability to effectively recruit ribosomes without any need for eIFs, an AUG codon or Met-tRNA$_i$ to initiate translation. It is important to note that different classes of IRES can exist within the same polycistronic viral RNA, such as CrPV which sports a Type III in the 5′ UTR of ORF1 and a Type IV between ORF1 and ORF2[662].

Hepatitis A (HAV) is a misfit IRES. It was previously classified as a lone Type III IRES due to its lack of activity in rabbit reticulocyte lysate (RRL), which is a feature that distinguishes it from Type I and II IRES. A newer IRES classification system which we use here has removed this class and moved up what used to be referred to as Type IV and V IRES to Types III and IV. HAV IRES activity in RRL requires both intact eIF4G and its interaction with eIF4E making it somewhat unique[663,664]. However, more recent experiments performed in intact cells have found that the HAV IRES behaves more like a Type 1 IRES, requiring cleavage of eIF4G[665]. Remarkably, it seems that in the context of HAV and PV IRES, eIF4E can behave independently of the cap, acting to enhance both eIF4A activity and eIF4G processing, and positively effecting IRES activity[666].

Many other viral IRES do not fit into any of these categories and perhaps additional classes will be distilled as new IRES and their mechanisms are identified. Some IRES do not even reside entirely within a 5′ UTR and can straddle the downstream ORF such as in HCV[667]. HIV-1 or HIV-2 exhibit complex post-transcriptional regulation and their mRNAs (e.g., gag) harbor IRES within ORFs as well as 5′ UTRs[668,669].

Critically, IRES activity can be regulated through interaction with proteins other than eIFs. These IRES trans-acting factors (ITAFs) are thought to act as a bridge, mediating the interaction between ribosome and IRES, and/or as RNA chaperones, molding an IRES into a form that can more efficiently recruit the ribosome. A detailed inventory and discussion about ITAFs is beyond the scope of this review; however, we point the reader to an excellent current review on the topic[338] and we will examine one interesting set of ITAFs below. ITAFs are actually host RNA-binding proteins that normally function in a variety of roles, including RNA splicing, transport, and stability and they have thus been co-opted by viruses. However, cellular IRES also exist, and although their structural cores are comparatively less conserved and more dynamic than their viral counterparts, they too are subject to regulation by the same ITAFs[658]. Indeed, the heterodimer of NF45 and NF90 acts as a transcription factor[670] and NF45 regulates RNA splicing[671], but these proteins can moonlight as both cellular and viral ITAFs. NF45 but not NF90 was found to be required for IRES-mediated translation of the anti-apoptotic protein cIAP1 during ER stress and also positively affects IRES-mediated translation of other mRNAs that together maintain proper control of the cell cycle[309,672]. What is interesting about these particular ITAFs is that while NF45 enhances the activity of these cellular IRES, the NF45/NF90 heterodimer effectively represses human rhinovirus type 2 (HRV2) IRES activity in neurons[673].

As we have seen, the cell has its own IRES mechanisms to thwart productive infection when cap-dependent mechanisms are impaired. However, the constellation of robust viral IRES mechanisms is expert at subverting the cap-dependent translation machinery and improving the translational efficiency of viral proteins.

Counteracting eIF2α phosphorylation

Despite the ability of viral IRES to recruit the ribosome, eIF2 TC is still needed for initiation in many viral contexts and this is depleted during the ISR. Not surprisingly, certain viruses can also bypass this requirement: The swine fever virus IRES can use eIF5B, an analogue of the bacterial initiation factor 2 (IF2), instead of eIF2 for $tRNA_i$ delivery[674]. Similarly, the HCV IRES uses eIF2 TC under normal conditions, but through a poorly understood mechanism favors eIF5B TC when eIF2α is phosphorylated[675,676]. It is noteworthy that the X-linked inhibitor of apoptosis (XIAP), an IRES-containing cellular mRNA, can use an eIF5B TC mechanism when cells are treated with poly(I:C)[677]. Interestingly, a recent, unbiased mass spectrometry screen of translation factors that are differentially regulated during hypoxia found that cells reprogram translation initiation to a eIF5B-dependent mode in this context, suggesting that eIF5B is an important player for $tRNA_i$ delivery during stress conditions[678]. It is likely then that both cap-dependent and cap-independent eIF5B mechanisms of $tRNA_i$ delivery exist and more work will have to be done to determine if viral infections can (1) increase eIF5B TC activity, and (2) take advantage of this reprograming. Other outstanding questions are: What factors (cellular and/or viral) favor the use of eIF5B, and which mRNAs are targeted under different viral infections?

Viruses have been shown to prevent or reverse P-eIF2α using their own effectors that target eIF2α kinases. HSV-1, HCMV, MCMV, EBV, influenza virus, reovirus, and VV all express dsRNA binding proteins that act like sponges by titrating away dsRNA and preventing PKR activation[101–105,679,680]. Viruses can also restrict the production of dsRNA, thus precluding PKR activation[681]. Remarkably, binding of certain structured viral RNAs (HCV IRES, Adenovirus VA, and EBV EBER-1/2) antagonize rather than activate PKR[106–108]. Other viruses encode proteins that directly bind and inhibit PKR activity[109–112]. For instance, the K3L protein of VV has dual activities, binding to both PKR and HRI as a pseudosubstrate, preventing activation of these

eIF2α kinases[682]. The HIV-1 protein Tat can also bind to PKR preventing dimerization and autophosphorylation[683]. PERK can also be targeted by viruses. Both E2 protein of HCV and glycoprotein B of HSV-1 bind to PERK and inhibit its activity[684,685]. Lastly, certain viral proteins act analogously to GADD34, by increasing PP1 activity and enhancing dephosphorylation of eIF2α[113–115].

It has been discussed in the previous section that SGs form due to accumulation of P-eIF2α. As SGs may serve a role in innate immunity, they are also targeted by many viruses. Wild-type influenza virus does not trigger SG accumulation, yet when the NS1 protein is mutated, infection induces SGs in a PKR-dependent manner and correlates with P-eIF2α, suggesting that NS1 suppresses SG by inhibiting PKR activity[626]. PV is also capable of inhibiting SG formation by cleaving G3BP1 with its 3C Protease[72]. HSV-2 virion host shut off (Vhs) protein also inhibits SG formation, a function that is associated with its endoribonuclease activity[686]. Importantly, these studies found that restoring SGs either by preventing G3BP1 cleavage (PV infection) or by preventing expression of NS1 (influenza infection) severely impairs virus replication[72,626]. HIV-1 was shown to be capable of preventing SG formation via its Gag protein in a manner dependent on the RNA binding protein Staufen 1 and this has effects on viral assembly[687–689]. In contrast, HIV-2 infection readily induces SG and localization of its genomic RNA therein; this is potentially due to limited expression of HIV-2 Gag polyprotein as low-level expression of ectopic Gag can restore cytoplasmic localization of viral RNA[690]. Zika virus also inhibits P-eIF2α accumulation and SG formation via its capsid proteins NS3 and NS4A[691,692]. Ebola virus protein VP35 inhibits SGs as well, perhaps via the sequestering of SG proteins in viral inclusion bodies[693,694]. Thus, SG appears to be an important aspect of the eIF2α-dependent stress response in virus-infected cells, one which many viruses have evolved sophisticated mechanisms to counteract.

Translation compartmentalization in virus factories

Viral infection not only affects *how* and *when* translation occurs in the cell but can also modify *where* it takes place. Up until now, the only known virus-induced event that has a clear link to translation re-localization is the formation of viral factories. These entities are specialized subcellular microenvironments resulting from reorganization of cellular membranes and are enriched in viral genomes and proteins (as well as select host proteins)[695]. Being shielded from the host antiviral response, they favor viral replication.

A study of poxviruses viral factories found selective enrichment of translation factors eIF4E and eIF4G[116], suggesting that they can serve as a platform for compartmentalized viral mRNA translation. In agreement with this model, imaging protein synthesis *in cellulo* using ribopuromycylation (RPM; **Table 6.1.**) showed higher translation activity inside VV viral factories compared to the cytoplasm[117]. Similarly, a study using reovirus found that translation activity occurs inside viral factories, together with an enrichment of translation initiation, elongation and termination factors[118]. This study also found that most of the RPM signal and translation factors seem to localize to the periphery of the viral factory, suggesting spatial organization of mRNA translation therein. Thus, translation compartmentalization is yet another method that viruses might use to support selective translation of viral mRNA over host mRNA in infected cells. Using new spatially sensitive techniques such as RPM will yield exciting new models of how viruses create specialized sites of translation. One cannot help but surmise that the privileged sites of translation that are observed in viral factories are intimately linked to the mTOR signaling machinery as has been seen with colocalized RHEB and mTOR at the periphery of HCMV assembly compartments[640].

6.2.7. Studying translation during viral infection: Technological progress and limits

Assessing changes in the nascent proteome

The last decade has seen a blossoming of tools for studying translational control—some of which have already been applied to virology. We summarize these techniques in **Table 6.1**. To begin with, the sensitivity of non-radioactive labeling of nascent peptides (so-called "metabolic labeling") has matured to a point that they are now reliably used. For example, bio-orthogonal (i.e., a chemical modification that does not interfere with the original biological activity of a molecule) amino acids such as azidohomoalanine (AHA), can be used to pulse-label cells and allows for covalent conjugation with a fluorophore following fixation or cell lysis (BONCAT, also referred to as FUNCAT)[696]. A slight twist on this technique allows for biotin conjugation and subsequent analysis of the biotinylated nascent peptides by mass spectrometry[697].

The aminoacyl-tRNA mimic puromycin acts to block translation elongation by entering the ribosome and covalently binding to the C-terminus of the nascent peptide chain. This property makes it an ideal compound to mark actively translated peptides and antibodies targeting puromycin can then be used to identify these peptides by standard Western blotting, fluorescence-activated cell sorting (FACs), or immunofluorescence (the SUnSET technique)[698]. Spatial localization using puromycylation is problematic, however, as the reaction at the ribosome is a chain-terminating event, where the puromycylated peptide is released from the ribosome, causing the former to diffuse in live cells and the latter to slip off the mRNA. A powerful adaptation of this technique, RPM, relies on co-incubation of cells with emetine, which acts to lock the ribosome on the mRNA and prevents puromycylated peptides from diffusing away from the ribosome[699,700]. Puromycin analogues can also be employed in a similar manner to BONCAT/FUNCAT. For

example, OP-puro has been developed to allow covalent incorporation of labels such as fluorophores[701]. Alternatively, biotin-puromycylation has been successfully employed in lysed cells to assess nascent peptide chain populations by mass spectrometry (PUNCH-P)[702].

Metabolic labeling of nascent peptides by [^{35}S]-methionine has been the gold standard method to monitor mRNA translation for many decades[80,703]. Isotope-based methods, however, prove more useful with stable isotope labeling by amino acid in cell culture (SILAC) for differential steady-state protein expression. Recently, the technique has been adapted with pulse-labeling cells to ascertain differential changes in nascent peptide synthesis (pSILAC), although the lack of sensitivity with SILAC labeling means that poorly translated proteins may be missed[704]. Howden *et al*. took these techniques one step further by combining the sensitivity of the BONCAT labeling method with the quantitative power of SILAC (QuaNCAT)[705] or pSILAC[706].

Profiling the translatome using deep sequencing techniques

Arguably, the platform that has caused a transformational shift in the study of translational control is deep sequencing. Traditionally, global analysis of changes in the translational efficiency (TE) of mRNAs (i.e., the translatome) was determined by probing polysome fractions (isolated by the classical polysome profiling technique which sediments translating *versus* non-translating mRNAs based on the number of associated ribosomes) with oligonucleotide DNA microarrays[508,707]. With the advent of massively parallel short sequencing, it was realized that translating ribosomes, which mask a specific region of mRNA with a defined periodicity (i.e., codon periodicity), would be especially amenable to this platform and the concept of ribosome profiling was born[32]. Following CHX treatment of cells to freeze translating ribosomes and digestion of naked single-stranded mRNA by ribonucleases, ribosome-masked "footprints" (~ 28–30 nucleotides in the case of footprints from cyclohexmide-associated ribosomes) can be

sequenced in a high-throughput manner (Ribo-Seq)[708]. Ribo-Seq is captured in parallel with standard RNA-Seq to assess both translational and transcriptional changes, respectively. Normally, the TE of any particular transcript can be expressed by the relative Ribo-Seq/RNA-Seq expression ratio.

Ribosome profiling not only reveals the TE for the annotated genome but gives an unprecedented codon resolution of the translatome that allows the investigator to infer sites of novel translation and even translation dynamics. Interestingly, ribosome profiling has already revealed a high degree of ribosome occupancy at genomic sites that were previously thought to be ribosome deserts, such as annotated UTRs and long non-coding RNAs (lncRNA)[709]. One implication of this finding is the mapping of many new uORFs, revealing a previously uncharted world of potential short peptides with as yet unknown function[709,710].

One caveat of the technique is the difficulty in differentiating between translating-ribosome and artifactual footprints. Indeed, more and more ribosome footprints have been found in non-coding regions[709] and it raises the question of whether these footprints truly belong to actively elongating ribosomes or just non-functional ribosomes or other RNA binding proteins. In addition, stalled ribosomes, those that are not actively incorporating amino acids[563,711], might still be producing footprints but do not contribute to translational activity. Highlighting the importance of algorithm design in the analysis of ribosome profiling data, a *posthoc* analysis method has been recently proposed to distinguish actively translated ribosomes *versus* artifact and allows for identification of novel ORFs; RiboTaper relies on the identification of a 3-nucleotide (codon) periodicity in-frame with the P-site of ribosome footprints, which correlates with the annotated or predicted ORF[712].

Another twist on ribosome profiling allows empirical identification of novel ORFs by replacing CHX with homoharringtonine (HHT) or lactimidomycin (LTM). These latter two inhibitors selectively stall only those ribosomes engaged at the initiation codon. While the mechanism by which HHT achieves this selectivity is still unknown[713,714], LTM has been shown to function by occluding the empty tRNA exit site within the ribosome during the first round of elongation, blocking its translocation and creating well-defined ribosome footprints at *bona fide* initiation codons[32,715]. Downstream elongating ribosomes do not have LTM-accessible tRNA exit sites and thus run-off the mRNA. This newer method combined with CHX-based ribosome profiling can enhance our ability to identify and annotate novel ORFs. To further increase the ORF prediction fidelity afforded by this technique, Fields *et al.*[710] designed ORF-RATER, which integrates ribosome profiling data from standard, CHX protocols and run-off experiments using HHT or LTM, and employs a linear regression model to better predict ORFs that are actively translated. These new tools have allowed unprecedented surveys of translation substrates in many cellular contexts, and as we will see in the next section, virus-infected cells have only recently been probed using ribosome profiling strategies.

Ribosome profiling in virology

In the last 5 years, ribosome profiling has been used to study the dynamic interaction between viruses and their hosts. HCMV was the first virus to be extensively examined by ribosome profiling[198]. Stern-Ginossar *et al*. used HHT and LTM to identify translation initiation sites in parallel with standard ribosome profiling across three different timepoints to reveal hundreds of previously unannotated HCMV ORFs and alternative transcription start sites, thus providing an unprecedented clarity to the infection kinetics of this virus. In addition, ribosome profiling has clearly shown that HCMV RNAs are better translated compared to the global translation signature

of host mRNAs at the late stage of infection[195]. Tirosh *et al.*[195] combined ribosome profiling with mass spectrometry revealing a group of host proteins being targeted for degradation during HCMV infection. The transcriptome and translatome of KSHV has also been extensively characterized using ribosome profiling[199]. From this study, the authors found translation activity in previously annotated non-coding regions (e.g., the KSHV lncRNA *Pan*) and identified novel short ORFs including uORFs in the viral genome. Interestingly, the authors found that the alternative initiation codon CUG is used in 28% of all translation start sites within the viral translatome at 72 h post-infection, although the functional implications of this usage are unclear. This finding strengthens a model in which the virus takes advantage of changes to the host translational machinery in response to viral attack by ensuring that its own messages are efficiently translated. On the other hand, a ribosome profiling study in influenza virus-infected cells found that viral RNA is not preferentially translated and host shut-off is instead a numbers game, caused by viral mRNA overtaking the mRNA pool[716]. Ribosome profiling has also been performed on VV to construct snapshots of the viral translatome at several time points after infection[717]. Dai *et al.*[197] also conducted ribosome profiling in VV-infected cells, but critically, with a focus on host mRNAs. Their study found that host transcripts involved in the oxidative phosphorylation pathway are favorably translated during infection, which correlates with an increase in their protein expression and oxidative phosphorylation activity. Together, these observations have proposed that a subset of host mRNAs are still actively translated during periods of global translation shutoff induced by viruses. There is a clear and pressing need to apply this technique to more viral and host contexts in order to better understand the underlying mechanisms that contribute to and modify infections from the perspective of both the host and the virus.

Toward single-cell and mRNA resolutions

Ribosome profiling provides us with an unmatched breadth of data regarding the translation dynamics of a population of RNAs and can tell us how their associated ribosomes might be distributed across their ORFs. However, as these are population distributions of cells and/or transcripts within cells, information about how any individual cell or transcripts might differ or be controlled at the level of translation is lost. This is especially true in the viral context, where infected-cell heterogeneity could produce diluted phenotypes that can be easily missed in a population-level study. Single-cell and tissue-specific ribosome profiling (e.g., using a TRAP[718] or RiboTag[719] approach) will likely overcome this issue, allowing the investigator to stratify infections between sub-populations of cells or to ensure that only the translatome of a specific cell type is monitored.

Sub-populations of localized viral transcripts might be subject to the conditions of microenvironments within the cell that are undetectable even with single-cell resolution. Indeed, it has become clear that the TE of certain transcripts depends on their localization[720–723]. Temporal dynamics have also been generally ascribed to population-wide translation events (e.g., the TE of a given transcript increases by 2-fold in 10 min following a given treatment). However, these spatiotemporal dynamics are only an average of a signal that is stochastic at the single mRNA level due to the "bursty" nature of both transcription and translation[724]. Thus, spatiotemporal regulation of mRNA translation is an important aspect of cellular translation regulation that has yet to be adequately investigated in the context of viral infection.

Assaying translation with single-molecule resolution and real-time kinetics is problematic. Translation output from a single reporter mRNA (e.g., GFP protein) is impossible to detect using current imaging technologies. Notwithstanding this, the entire protein needs to be synthesized and properly folded prior to detection which substantially reduces temporal resolution of translation

dynamics. Recently, a series of four publications have described elegant methods to overcome these obstacles. These methods record translation of individual transcripts in real time with subcellular resolution and have the potential to profoundly impact our current understanding of translation regulation during virus infection[725–728]. These studies employed similar strategies, borrowed from the MS2-MS2 coat system, a well-used method to track individual mRNAs with subcellular resolution. This older method uses genetically encoded reporter RNAs with multiple MS2 bacteriophage coat protein binding protein sites. Cells expressing MS2 coat protein fused with a fluorescent reporter will mark these RNAs and the multiple binding sites allow fluorescence to reach the level of detection by standard diffraction-limited microscopy[729]. All of these nascent peptide live-tracking techniques require multiple antibody epitopes that are genetically inserted into the coding sequence of the transcript of interest. As the reporter ORF is translated by multiple ribosomes (i.e., a polysome), these multiple epitopes per nascent peptide chain emerge and bind to fluorescently tagged antibodies. This real-time nascent peptide tagging is combined with the fluorescent RNA reporter system (e.g., MS2-MS2) to report both the location and real-time translation status of the transcript under scrutiny by measuring colocalization in live cells.

By transiently expressing the tagged nascent peptide in U2OS cells, Morisaki *et al.*[725] successfully visualized and characterized the dynamics of polysomes, and detected rare events in which polysomes were made up of two distinct mRNAs. Using a different tagging system transduced by virus, Wu *et al.*[726] observed that ER–bound peptides are translated when the ribosome reaches the ER membrane and could even determine the elongation rate of individual transcripts by combining with photobleaching. In addition, when applying their system to primary neurons,they found that translation of mRNAs is suppressed in distal dendrites, suggesting that

translation activity depends on distance from the cell body. However, another flavor of this system allowed Wang *et al*.[552,727] to visualize and quantify translation activity being repressed during environmental stress. Remarkably, in the same context, they were also able to visualize the upregulation of a reporter designed with a 5′ UTR harboring the ATF4 uORFs, discussed earlier in this review, confirming the previously ascribed translation regulation mediated by these sequence elements. Moreover, they were able to observe a bursty translation phenotype under conditions of stress. Finally, the system used by Yan *et al*.[728] allowed them to estimate the number of individual ribosomes on a given fluorescent puncta by comparing the signal from individual foci to that of diffuse reporter signal in the same cell. Based on this estimation, they observed a wide distribution of ribosome densities for populations of homomeric mRNAs in a cell, suggesting that even a single mRNA species can vary tremendously in translation rates depending on the intracellular context.

One challenge that emerges from this work so far is the difficulty in live tracking of individual polysomes due to high diffusion speed and both lateral and axial overlap with other, neighboring polysomes. Yan *et al*.[728] mitigate this problem by adding membrane docking sequence elements into the reporter ORF, but this is at the cost of compromising spatial resolution of the transcript of interest. Future improvements in imaging technology might provide a technical solution for such caveats.

6.2.8. Perspectives

In this review, we have summarized data that together overwhelmingly support the idea that translation regulation is at the forefront of the host response to virus infection. This constitutes a translation arm of the cellular innate immune response (**Fig. 1.3**). As we have tried to impress upon

the reader, translation regulation in an infected cell is highly dynamic and continuously altered in response to extra- and intra-cellular stimuli. However, there is a need for more knowledge about how the translation of cellular and viral mRNAs is controlled in these contexts. Current *in vitro* systems do not faithfully recapitulate the *in vivo* environment, and it is in the latter case where micro-environmental cues such as nutrient, oxygen, and cytokine concentrations might dramatically alter translational control. Indeed, IFN-mediated para/autocrine signaling, which is often optimized and homogeneous in culture, is variable in time and space in the context of heterogeneous cell populations in tissue. As the techniques to study translation mature and become more robust, we expect that future experimental designs will be able to incorporate 3D cell culture and tissue models with the goal of better understanding translation in heterogeneous infected-cells.

An arsenal of techniques has been developed in recent years that allows for the study of cellular translation activity at unprecedented scale (genome-level) and spatiotemporal resolutions (real-time kinetics of translation activity on single mRNAs). Of all the techniques described, ribosome profiling has so far proven instrumental to the study of translation regulation during virus infection. In the near future, identifying and characterizing host cell translatomes using this method during different viral infections is a readily achievable and worthy goal, just as transcriptomic studies were instrumental in revealing a large number of ISGs that have important functions in host–virus interactions. Beyond a small number of viral and host contexts, very little is known about which mRNAs are translated and at what efficiency beyond what can be inferred from other stress conditions that activate similar pathways (e.g., ER stress). Thus, identifying the list of translationally regulated antiviral genes might uncover important innate immunity mediators that are overlooked with the more traditional transcriptomic approach.

It is increasingly apparent that certain subcellular compartments also contribute to the altered translation landscape of infected cells. The virus and/or IFN-triggered ISR stimulates SG assembly, yet there are also ample data demonstrating that viruses deploy multiple strategies to block their formation. Although there is evidence of recruitment of viral RNA to SG, which can be viewed as an antiviral response of the host cell, it is not clear if this can specifically impact replication efficiency of a virus through limiting translation of viral mRNA.

New techniques that assess translation *in situ* have shown that viral factories can be recognized as a privileged site where the translation machinery is enriched, effectively exhausting cytosolic translation factors. However, there is limited information yet available that could hint at the specifics of the translation program inside these privileged sites. Are the ribosomes there modified in some way to take on specialized roles? Are non-canonical initiation complexes participating in viral translation at these sites? Do *cis*-acting viral UTR sequences dictate the fate of viral TE inside and outside of viral factories? Conversely, what is the impact on depletion of translation factors, including ribosomes, from the cytoplasmic pool on host mRNA translation?

The advent of single-cell ribosome profiling and the ability to monitor translation in real-time using nascent peptide imaging techniques will also be invaluable in the heterogeneous context of viral infections. We expect that with advances in gene editing technology and super-resolution imaging in the next 5 years, investigators will be able to reliably probe the translation dynamics of viral and cellular mRNAs that they are interested in. Just beyond the horizon lies even more powerful methods that will excite and entice new investigators to the field. Third-generation, long-read sequencing techniques might allow massively parallel monitoring of *in vitro* translation in real-time. One can imagine that advances in dye-free Coherent Anti-stokes Raman Scattering (CARS) microscopy in conjunction with machine learning will permit the real-time monitoring of

translation on multiple mRNA species *in cellulo*, thus preserving both temporal and spatial information. Indeed, these techniques will help us understand how battles for the ribosome are fought and will grant us ways to design new armor with which to fight viral infection or alter the cellular innate immune response.

6.2.9. Acknowledgments

We apologize for not being able to cite all of the studies on translation control related to virus infection due to space restrictions. We thank Drs. Bruno Fonseca and Stéphanie Pontier for critical comments on this manuscript. H.D.H. is a recipient of a University of Ottawa Graduate Scholarship, Ontario Graduate Scholarship, and University of Ottawa Faculty of Medicine Destination 2020 Scholarship. This work was supported in part by the Canadian Breast Cancer Foundation/Canadian Cancer Society Research Institute, the Cancer Research Society/CIHR Institute of Cancer Research (grant #22124), the Natural Sciences and Engineering Research Council of Canada (RGPIW-2016-05228), and the Terry Fox Research Institute (New Frontier Program Project Grant) to T.A. and T.E.G.

Table 6.1. Techniques to monitor translation during viral infection.

Biological scale	Method name	Description	Advantages	Limitations
Nascent proteome	BONCAT (bio-orthogonal non-canonical amino acid tagging)[697]	• Incorporation of modified amino acids amenable to click chemistry (e.g., AHA) into nascent peptide chains • Click chemistry allows covalent binding to biotin after cell lysis. • Biotinylated nascent peptides analyzed by mass spectrometry	• Bio-orthogonality reduces chances of artifacts	• Methionine depletion may induce cell stress which can alter mRNA translation and cause erroneous results in the context of viral infection.
	pSILAC (pulsed stable isotope labeling with amino acids in cell culture)[704]	• Modified SILAC in which medium/heavy radio-isotopes incorporated into amino acids are incubated for a short period of time to measure nascent peptide synthesis • Radio-labeled peptides are isolated	• Sensitive to small changes in nascent peptide synthesis between uninfected and infected conditions	• Acute (seconds-minutes) effects of viral infection on translation may be missed.

Biological scale	Method name	Description	Advantages	Limitations
		and differential mass spectrometry performed.		
	QuaNCAT (quantitative non-canonical amino acid tagging)[705]	• Combined BONCAT (reporting nascent peptide synthesis) with SILAC (reporting steady-state protein levels)	• High sensitivity of BONCAT for nascent peptide tagging allows for short labeling times, while the high sensitivity of SILAC for detecting differential translation allows for reliable quantitation of translational output. • Bagert *et al.*[706] have also coupled BONCAT to pSILAC in order to minimize artifacts associated with using either technique in isolation.	• Combined disadvantages of BONCAT and SILAC: requires methionine depletion and is an endpoint technique
	PUNCH-P (puromycin-associated nascent chain proteomics)[702]	• *In vitro* incorporation of biotinylated puromycin into the nascent polypeptide chain	• Increased sensitivity *versus* BONCAT • Ex vivo labeling allows this technique to be easily applied to tissue samples.	• Requirement of the reaction to take place in cell lysates might lead to artifacts especially in the

Biological scale	Method name	Description	Advantages	Limitations
		• Biotin-puromycylated peptides are isolated and analyzed by mass spectrometry.		context of viral infection where localized translational control might predominate.
Translatome	Polysome profiling[508,707]	• Resolving mRNAs across sucrose density gradients based on the number of bound ribosomes. Increasing number of bound ribosomes is usually associated with increased translational efficiency. • mRNA isolated from gradient fractions is probed by RNA-Seq or similar (e.g., cDNA microarray or nanoString™). • Can also be used to profile translational	• Goldstandard for assessing translational efficiency of specific transcripts. Currently (ca. 2018) a more affordable alternative to ribosome profiling	• Difficult to resolve small changes (e.g., ± 1 ribosome) of highly translated mRNA

Biological scale	Method name	Description	Advantages	Limitations
		efficiency of a single mRNA		
	Ribosome profiling[32]	• Ribosome-protected fragments of mRNA are isolated and deep-sequenced (Ribo-Seq) in parallel with total mRNA (RNA-Seq) to measure ribosome density as a function of transcriptional output (translational efficiency).	• Genome-wide translational profiles (translatomes) with codon resolution	• Currently (ca. 2018) expensive with a high learning curve for new users that is largely due to poor access to required bioinformatics tools • Standard ribosome profiling is an endpoint assay and ignores ribosome transit times: Slowed or stalled higher-order polysomes can be erroneously interpreted as highly

Biological scale	Method name	Description	Advantages	Limitations
				translated, while fast, monosomal translation would also be misinterpreted.
	TRAP (translating ribosome affinity purification)[718] or RiboTag[719]	• Conditional expression of a reporter-tagged ribosomal protein (RPL10-eGFP in the case of TRAP or HA-tagged RPL22a for RiboTag) in knock-in mice allows cell type-specific affinity purification of polysomes. • Subsequent probing of isolated polysomes can be done on a gene-by-gene basis or by cDNA microarray or RNA-Seq analysis.	• *In vivo*, cell type-specific translational profiling	• Requires animal husbandry

Biological scale	Method name	Description	Advantages	Limitations
Single cell	BONCAT/FUNCAT (fluorescent non-canonical amino acid tagging)[696]	• Incorporation of modified amino acids amenable to click chemistry (e.g., AHA) into nascent peptide chains • Click chemistry allows covalent binding to a fluorophore after cell lysis.	• Sub-cellular localization of translation activity could be informative in the context of viral infection.	• Methionine depletion may induce cell stress which can cause erroneous results in the context of viral infection. • Diffusion of labeled nascent peptide chains could lead to misinterpretation of location of translation activity, limiting its use in this form.
	SUnSET[698] (surface sensing of translation) or equivalent	• Label nascent peptides with puromycin, then using anti-puromycin antibody to detect newly synthesized membrane proteins using FACS • A common	• Inexpensive and achieves similar sensitivity to standard metabolic labeling with radio-isotopes	• Cannot assess spatial resolution of translation activity due to surface secretion (FACS analysis) or diffusion of puromycylated

Biological scale	Method name	Description	Advantages	Limitations
		variation of this technique probes for intracellular puromycylated proteins by Western or by immunofluorescence.		peptides • Puromycin labeling is not sensitive enough to detect changes in protein synthesis during energy starvation[730].
	OPP[701] (*O*-propargyl-puromycin)	• Alkyl-bearing puromycin analogue allows puromycylation followed by covalent linking to fluorescent dye or equivalent by click chemistry.	• Does not require anti-puromycin antibody	• Lack of spatial resolution as with SUnSET technique • Similar limitations to those in SUnSET
	RPM[699,700] (ribopuromycylation)	• Combined with inhibitors of elongation, puromycylated peptides are trapped at ribosomes engaged in translation.	• Has a distinct advantage over other puromycylation techniques in that it is spatially sensitive. RPM signal is localized to polysomes • Has been used to look at	• Cannot be used for live cell studies and does not have real-time resolution

Biological scale	Method name	Description	Advantages	Limitations
		• Puromycylated ribosomes are detected with an anti-puromycin antibody to resolve the site of translation.	sites of translation in viral factories[117]	
Real-time, single-RNA molecule	Nascent peptide live-tracking techniques: NCT[725], SINAPS[726], SunTag variations[727,728].	• Detection of translation activity by colocalizing mRNA and nascent polypeptides bound to reporter antibodies • mRNA is labeled with an MS2–MS2 system, while the nascent peptide expresses repeated epitope tags that bind multiple antibodies fused to fluorescent reporters in order to distinguish active translation from diffuse fluorescent reporter molecules.	• Offers the highest spatiotemporal resolution of RNA translation	• Limited to genetically modified ORFs • Cannot be used to profile large numbers of mRNA species

6.2.10. References

1. Sonenberg, N. & Hinnebusch, A. G. Regulation of Translation Initiation in Eukaryotes: Mechanisms and Biological Targets. *Cell* **136**, 731–745 (2009).
2. Hinnebusch, A. G. & Lorsch, J. R. The mechanism of eukaryotic translation initiation: New insights and challenges. *Cold Spring Harb. Perspect. Biol.* **4**, a011544 (2012).
3. Kahvejian, A., Svitkin, Y. V., Sukarieh, R., M'Boutchou, M. N. & Sonenberg, N. Mammalian poly(A)-binding protein is a eukaryotic translation initiation factor, which acts via multiple mechanisms. *Genes Dev.* **19**, 104–113 (2005).
4. Jackson, R. J., Hellen, C. U. T. & Pestova, T. V. The mechanism of eukaryotic translation initiation and principles of its regulation. *Nature Reviews Molecular Cell Biology* **11**, 113–127 (2010).
5. Parsyan, A. *et al.* mRNA helicases: the tacticians of translational control. *Nat. Rev. Mol. Cell Biol.* **12**, 235–45 (2011).
6. Kozak, M. Possible role of flanking nucleotides in recognition of the AUG initiator codon by eukaryotic ribosomes. *Nucleic Acids Res.* **9**, 5233–52 (1981).
7. Dever, T. E. & Green, R. The elongation, termination, and recycling phases of translation in eukaryotes. *Cold Spring Harb. Perspect. Biol.* **4**, 1–16 (2012).
8. Ptushkina, M., von der Haar, T., Karim, M. M., Hughes, J. M. X. & McCarthy, J. E. G. Repressor binding to a dorsal regulatory site traps human eIF4E in a high cap-affinity state. *EMBO J.* **18**, 4068–4075 (1999).
9. Marcotrigiano, J., Gingras, A. C., Sonenberg, N. & Burley, S. K. Cap-dependent translation initiation in eukaryotes is regulated by a molecular mimic of eIF4G. *Mol. Cell* **3**, 707–16 (1999).
10. Mader, S., Lee, H., Pause, A. & Sonenberg, N. The translation initiation factor eIF-4E binds to a common motif shared by the translation factor eIF-4 gamma and the translational repressors 4E-binding proteins. *Mol. Cell. Biol.* **15**, 4990–7 (1995).
11. Gingras, A. C. *et al.* Regulation of 4E-BP1 phosphorylation: a novel two-step mechanism. *Genes Dev.* **13**, 1422–37 (1999).
12. Carlberg, U., Nilsson, A. & Nygård, O. Functional properties of phosphorylated elongation factor 2. *Eur. J. Biochem.* **191**, 639–45 (1990).
13. Ryazanov, A. G., Shestakova, E. A. & Natapov, P. G. Phosphorylation of elongation factor 2 by EF-2 kinase affects rate of translation. *Nature* **334**, 170–173 (1988).
14. Wang, X. *et al.* Regulation of elongation factor 2 kinase by p90RSK1 and p70 S6 kinase. *EMBO J.* **20**, 4370–4379 (2001).
15. Browne, G. J. & Proud, C. G. A novel mTOR-regulated phosphorylation site in elongation factor 2 kinase modulates the activity of the kinase and its binding to calmodulin. *Mol. Cell. Biol.* **24**, 2986–97 (2004).
16. Faller, W. J. *et al.* mTORC1-mediated translational elongation limits intestinal tumour initiation and growth. *Nature* **517**, 497–500 (2015).
17. Graber, T. E. *et al.* Reactivation of stalled polyribosomes in synaptic plasticity. *Proc. Natl.*

Acad. Sci. U. S. A. **110**, 16205–10 (2013).
18. Gingold, H. *et al.* A dual program for translation regulation in cellular proliferation and differentiation. *Cell* **158**, 1281–1292 (2014).
19. Buttgereit, F. & Brand, M. D. A hierarchy of ATP-consuming processes in mammalian cells. *Biochem. J.* **312**, 163–167 (1995).
20. Roux, P. P. & Topisirovic, I. Regulation of mRNA translation by signaling pathways. *Cold Spring Harb. Perspect. Biol.* **4**, (2012).
21. Bowie, A. G. & Unterholzner, L. Viral evasion and subversion of pattern-recognition receptor signalling. *Nat. Rev. Immunol.* **8**, 911–22 (2008).
22. Joshi, S., Kaur, S., Kroczynska, B. & Platanias, L. C. Mechanisms of mRNA translation of interferon stimulated genes. *Cytokine* **52**, 123–7 (2010).
23. Cooray, S. The pivotal role of phosphatidylinositol 3-kinase-Akt signal transduction in virus survival. *J. Gen. Virol.* **85**, 1065–76 (2004).
24. Manning, B. D. & Toker, A. AKT/PKB Signaling: Navigating the Network. *Cell* **169**, 381–405 (2017).
25. Kang, Y. *et al.* Transient activation of the PI3K/Akt pathway promotes Newcastle disease virus replication and enhances anti-apoptotic signaling responses. *Oncotarget* **8**, 23551–23563 (2017).
26. Soares, J. A. P. *et al.* Activation of the PI3K/Akt Pathway Early during Vaccinia and Cowpox Virus Infections Is Required for both Host Survival and Viral Replication. *J. Virol.* **83**, 6883–6899 (2009).
27. Zhu, L. *et al.* Biphasic activation of PI3K/Akt and MAPK/Erk1/2 signaling pathways in bovine herpesvirus type 1 infection of MDBK cells. *Vet. Res.* **42**, 57 (2011).
28. Menon, S. *et al.* Spatial control of the TSC complex integrates insulin and nutrient regulation of mTORC1 at the lysosome. *Cell* **156**, 771–85 (2014).
29. Kaur, S. *et al.* Regulatory effects of mammalian target of rapamycin-activated pathways in type I and II interferon signaling. *J. Biol. Chem.* **282**, 1757–68 (2007).
30. Cao, W. *et al.* Toll-like receptor-mediated induction of type I interferon in plasmacytoid dendritic cells requires the rapamycin-sensitive PI(3)K-mTOR-p70S6K pathway. *Nat. Immunol.* **9**, 1157–64 (2008).
31. Stojdl, D. F. *et al.* Exploiting tumor-specific defects in the interferon pathway with a previously unknown oncolytic virus. *Nat. Med.* **6**, 821–5 (2000).
32. Alain, T. *et al.* Vesicular stomatitis virus oncolysis is potentiated by impairing mTORC1-dependent type I IFN production. **107**, 1576–1581 (2010).
33. Lun, X. Q. *et al.* Targeting human medulloblastoma: oncolytic virotherapy with myxoma virus is enhanced by rapamycin. *Cancer Res.* **67**, 8818–27 (2007).
34. Lahr, R. M. *et al.* La-related protein 1 (LARP1) binds the mRNA cap, blocking eIF4F assembly on TOP mRNAs. *Elife* **6**, (2017).
35. Fonseca, B. D. *et al.* La-related Protein 1 (LARP1) Represses Terminal Oligopyrimidine (TOP) mRNA Translation Downstream of mTOR Complex 1 (mTORC1). *J. Biol. Chem.* **290**, 15996–6020 (2015).
36. Tsukumo, Y., Alain, T., Fonseca, B. D., Nadon, R. & Sonenberg, N. Translation control during prolonged mTORC1 inhibition mediated by 4E-BP3. *Nat. Commun.* **7**, 11776 (2016).
37. Gingras, A. C. *et al.* Hierarchical phosphorylation of the translation inhibitor 4E-BP1. *Genes Dev.* **15**, 2852–64 (2001).

38. Colina, R. *et al.* Translational control of the innate immune response through IRF-7. *Nature* **452**, 323–328 (2008).
39. Jaramillo, M. *et al.* Leishmania repression of host translation through mTOR cleavage is required for parasite survival and infection. *Cell Host Microbe* **9**, 331–41 (2011).
40. Lekmine, F. *et al.* Activation of the p70 S6 kinase and phosphorylation of the 4E-BP1 repressor of mRNA translation by type I interferons. *J. Biol. Chem.* **278**, 27772–27780 (2003).
41. Nehdi, A. *et al.* Deficiency in Either 4E-BP1 or 4E-BP2 Augments Innate Antiviral Immune Responses. *PLoS One* **9**, e114854 (2014).
42. Kroczynska, B. *et al.* Interferon-dependent engagement of eukaryotic initiation factor 4B via S6 kinase (S6K)- and ribosomal protein S6K-mediated signals. *Mol. Cell. Biol.* **29**, 2865–75 (2009).
43. Magnuson, B., Ekim, B. & Fingar, D. C. Regulation and function of ribosomal protein S6 kinase (S6K) within mTOR signalling networks. *Biochem. J.* **441**, 1–21 (2012).
44. Meyuhas, O. Ribosomal Protein S6 Phosphorylation: Four Decades of Research. *Int. Rev. Cell Mol. Biol.* **320**, 41–73 (2015).
45. Shahbazian, D. *et al.* The mTOR/PI3K and MAPK pathways converge on eIF4B to control its phosphorylation and activity. *EMBO J.* **25**, 2781–2791 (2006).
46. Kroczynska, B. *et al.* Regulatory effects of SKAR in interferon α signaling and its role in the generation of type I IFN responses. *Proc. Natl. Acad. Sci. U. S. A.* **111**, 11377–82 (2014).
47. Wang, F. *et al.* S6K-STING interaction regulates cytosolic DNA-mediated activation of the transcription factor IRF3. *Nat. Immunol.* **17**, 514–522 (2016).
48. Ueda, T., Watanabe-Fukunaga, R., Fukuyama, H., Nagata, S. & Fukunaga, R. Mnk2 and Mnk1 are essential for constitutive and inducible phosphorylation of eukaryotic initiation factor 4E but not for cell growth or development. *Mol. Cell. Biol.* **24**, 6539–49 (2004).
49. Waskiewicz, A. J. *et al.* Phosphorylation of the cap-binding protein eukaryotic translation initiation factor 4E by protein kinase Mnk1 in vivo. *Mol. Cell. Biol.* **19**, 1871–80 (1999).
50. Waskiewicz, A. J., Flynn, A., Proud, C. G. & Cooper, J. A. Mitogen-activated protein kinases activate the serine/threonine kinases Mnk1 and Mnk2. *EMBO J.* **16**, 1909–20 (1997).
51. Pyronnet, S. *et al.* Human eukaryotic translation initiation factor 4G (eIF4G) recruits mnk1 to phosphorylate eIF4E. *EMBO J.* **18**, 270–9 (1999).
52. Shveygert, M., Kaiser, C., Bradrick, S. S. & Gromeier, M. Regulation of eukaryotic initiation factor 4E (eIF4E) phosphorylation by mitogen-activated protein kinase occurs through modulation of Mnk1-eIF4G interaction. *Mol. Cell. Biol.* **30**, 5160–7 (2010).
53. Kaspar, R. L., Rychlik, W., White, M. W., Rhoads, R. E. & Morris, D. R. Simultaneous cytoplasmic redistribution of ribosomal protein L32 mRNA and phosphorylation of eukaryotic initiation factor 4E after mitogenic stimulation of Swiss 3T3 cells. *J. Biol. Chem.* **265**, 3619–22 (1990).
54. Manzella, J. M., Rychlik, W., Rhoads, R. E., Hershey, J. W. & Blackshear, P. J. Insulin induction of ornithine decarboxylase. Importance of mRNA secondary structure and phosphorylation of eucaryotic initiation factors eIF-4B and eIF-4E. *J. Biol. Chem.* **266**, 2383–9 (1991).
55. Walsh, D. & Mohr, I. Phosphorylation of eIF4E by Mnk-1 enhances HSV-1 translation and replication in quiescent cells. **1**, 660–672 (2004).

56. Woods, A. *et al.* LKB1 is the upstream kinase in the AMP-activated protein kinase cascade. *Curr. Biol.* **13**, 2004–8 (2003).
57. Knauf, U., Tschopp, C. & Gram, H. Negative regulation of protein translation by mitogen-activated protein kinase-interacting kinases 1 and 2. *Mol. Cell. Biol.* **21**, 5500–11 (2001).
58. Morley, S. J. & Naegele, S. Phosphorylation of eukaryotic initiation factor (eIF) 4E is not required for de novo protein synthesis following recovery from hypertonic stress in human kidney cells. *J. Biol. Chem.* **277**, 32855–9 (2002).
59. Naegele, S. & Morley, S. J. Molecular cross-talk between MEK1/2 and mTOR signaling during recovery of 293 cells from hypertonic stress. *J. Biol. Chem.* **279**, 46023–34 (2004).
60. Hargett, D., McLean, T. & Bachenheimer, S. L. Herpes simplex virus ICP27 activation of stress kinases JNK and p38. *J. Virol.* **79**, 8348–60 (2005).
61. Mikkelsen, S. S. *et al.* RIG-I-mediated activation of p38 MAPK is essential for viral induction of interferon and activation of dendritic cells: dependence on TRAF2 and TAK1. *J. Biol. Chem.* **284**, 10774–82 (2009).
62. Hirasawa, K. *et al.* Effect of p38 mitogen-activated protein kinase on the replication of encephalomyocarditis virus. *J. Virol.* **77**, 5649–56 (2003).
63. Herdy, B. *et al.* Translational control of the activation of transcription factor NF-κB and production of type I interferon by phosphorylation of the translation factor eIF4E. *Nat. Immunol.* **13**, 543–550 (2012).
64. Walsh, D., Perez, C., Notary, J. & Mohr, I. Regulation of the translation initiation factor eIF4F by multiple mechanisms in human cytomegalovirus-infected cells. *J. Virol.* **79**, 8057–64 (2005).
65. Walsh, D. *et al.* Eukaryotic translation initiation factor 4F architectural alterations accompany translation initiation factor redistribution in poxvirus-infected cells. *Mol. Cell. Biol.* **28**, 2648–58 (2008).
66. Arias, C., Walsh, D., Harbell, J., Wilson, A. C. & Mohr, I. Activation of host translational control pathways by a viral developmental switch. *PLoS Pathog.* **5**, e1000334 (2009).
67. Yang, X. & Gabuzda, D. Regulation of human immunodeficiency virus type 1 infectivity by the ERK mitogen-activated protein kinase signaling pathway. *J. Virol.* **73**, 3460–6 (1999).
68. Diamond, M. S. & Farzan, M. The broad-spectrum antiviral functions of IFIT and IFITM proteins. *Nat. Rev. Immunol.* **13**, 46–57 (2013).
69. Brennan-Laun, S. E., Ezelle, H. J., Li, X.-L. & Hassel, B. A. RNase-L control of cellular mRNAs: roles in biologic functions and mechanisms of substrate targeting. *J. Interferon Cytokine Res.* **34**, 275–88 (2014).
70. Donovan, J., Rath, S., Kolet-Mandrikov, D. & Korennykh, A. Rapid RNase L-driven arrest of protein synthesis in the dsRNA response without degradation of translation machinery. *RNA* **23**, 1660–1671 (2017).
71. Okumura, F., Zou, W. & Zhang, D.-E. ISG15 modification of the eIF4E cognate 4EHP enhances cap structure-binding activity of 4EHP. *Genes Dev.* **21**, 255–60 (2007).
72. Chapat, C. *et al.* Cap-binding protein 4EHP effects translation silencing by microRNAs. *Proc. Natl. Acad. Sci. U. S. A.* **114**, 5425–5430 (2017).
73. Chen, S. & Gao, G. MicroRNAs recruit eIF4E2 to repress translation of target mRNAs. *Protein Cell* **8**, 750–761 (2017).
74. Jafarnejad, S. M. *et al.* Translational control of ERK signaling through miRNA/4EHP-directed silencing. *Elife* **7**, e35034 (2018).

75. Uniacke, J. *et al.* An oxygen-regulated switch in the protein synthesis machinery. *Nature* **486**, 126–9 (2012).
76. Lu, L., Han, A. P. & Chen, J. J. Translation initiation control by heme-regulated eukaryotic initiation factor 2alpha kinase in erythroid cells under cytoplasmic stresses. *Mol. Cell. Biol.* **21**, 7971–80 (2001).
77. Deng, J. *et al.* Activation of GCN2 in UV-irradiated cells inhibits translation. *Curr. Biol.* **12**, 1279–86 (2002).
78. Walsh, D. & Mohr, I. Viral subversion of the host protein synthesis machinery. *Nat. Rev. Microbiol.* **9**, 860–875 (2011).
79. Harding, H. P., Zhang, Y. & Ron, D. Protein translation and folding are coupled by an endoplasmic-reticulum-resident kinase. *Nature* **397**, 271–274 (1999).
80. Berlanga, J. J. *et al.* Antiviral effect of the mammalian translation initiation factor 2α kinase GCN2 against RNA viruses. *EMBO J.* **25**, 1730–1740 (2006).
81. Won, S. *et al.* Increased susceptibility to DNA virus infection in mice with a GCN2 mutation. *J. Virol.* **86**, 1802–8 (2012).
82. Zhang, L. & Wang, A. Virus-induced ER stress and the unfolded protein response. *Front. Plant Sci.* **3**, 293 (2012).
83. Dauber, B. & Wolff, T. Activation of the Antiviral Kinase PKR and Viral Countermeasures. *Viruses* **1**, 523–544 (2009).
84. Nallagatla, S. R. *et al.* 5'-triphosphate-dependent activation of PKR by RNAs with short stem-loops. *Science* **318**, 1455–8 (2007).
85. Dey, M., Mann, B. R., Anshu, A. & Mannan, M. A. U. Activation of protein kinase PKR requires dimerization-induced cis-phosphorylation within the activation loop. *J. Biol. Chem.* **289**, 5747–5757 (2014).
86. Clavarino, G. *et al.* Induction of GADD34 is necessary for dsRNA-dependent interferon-β production and participates in the control of Chikungunya virus infection. *PLoS Pathog.* **8**, (2012).
87. Bogorad, A. M., Lin, K. Y. & Marintchev, A. Novel mechanisms of eIF2B action and regulation by eIF2α phosphorylation. *Nucleic Acids Res.* **45**, 11962–11979 (2017).
88. Zamanian-Daryoush, M., Mogensen, T. H., DiDonato, J. A. & Williams, B. R. NF-kappaB activation by double-stranded-RNA-activated protein kinase (PKR) is mediated through NF-kappaB-inducing kinase and IkappaB kinase. *Mol. Cell. Biol.* **20**, 1278–90 (2000).
89. Bonnet, M. C., Weil, R., Dam, E., Hovanessian, A. G. & Meurs, E. F. PKR stimulates NF-kappaB irrespective of its kinase function by interacting with the IkappaB kinase complex. *Mol. Cell. Biol.* **20**, 4532–42 (2000).
90. Chu, W. M. *et al.* JNK2 and IKKbeta are required for activating the innate response to viral infection. *Immunity* **11**, 721–31 (1999).
91. Kumar, A. *et al.* Deficient cytokine signaling in mouse embryo fibroblasts with a targeted deletion in the PKR gene: role of IRF-1 and NF-kappaB. *EMBO J.* **16**, 406–16 (1997).
92. Perkins, D. J. & Barber, G. N. Defects in translational regulation mediated by the alpha subunit of eukaryotic initiation factor 2 inhibit antiviral activity and facilitate the malignant transformation of human fibroblasts. *Mol. Cell. Biol.* **24**, 2025–40 (2004).
93. Barbosa, C., Peixeiro, I. & Romão, L. Gene expression regulation by upstream open reading frames and human disease. *PLoS Genet.* **9**, e1003529 (2013).
94. Lewerenz, J. *et al.* Mutation of ATF4 mediates resistance of neuronal cell lines against

oxidative stress by inducing xCT expression. *Cell Death Differ.* **19**, 847–58 (2012).
95. Blais, J. D. *et al.* Activating transcription factor 4 is translationally regulated by hypoxic stress. *Mol. Cell. Biol.* **24**, 7469–82 (2004).
96. Lee, Y.-Y., Cevallos, R. C. & Jan, E. An upstream open reading frame regulates translation of GADD34 during cellular stresses that induce eIF2alpha phosphorylation. *J. Biol. Chem.* **284**, 6661–73 (2009).
97. Palam, L. R., Baird, T. D. & Wek, R. C. Phosphorylation of eIF2 facilitates ribosomal bypass of an inhibitory upstream ORF to enhance CHOP translation. *J. Biol. Chem.* **286**, 10939–49 (2011).
98. Xuan, B., Qian, Z., Torigoi, E. & Yu, D. Human cytomegalovirus protein pUL38 induces ATF4 expression, inhibits persistent JNK phosphorylation, and suppresses endoplasmic reticulum stress-induced cell death. *J. Virol.* **83**, 3463–74 (2009).
99. Shabman, R. S. *et al.* An upstream open reading frame modulates ebola virus polymerase translation and virus replication. *PLoS Pathog.* **9**, e1003147 (2013).
100. Clavarino, G. *et al.* Protein phosphatase 1 subunit Ppp1r15a/GADD34 regulates cytokine production in polyinosinic:polycytidylic acid-stimulated dendritic cells. *Proc. Natl. Acad. Sci. U. S. A.* **109**, 3006–11 (2012).
101. Dalet, A. *et al.* Protein synthesis inhibition and GADD34 control IFN-β heterogeneous expression in response to dsRNA. *EMBO J.* **36**, 761–782 (2017).
102. Kedersha, N. *et al.* Evidence that ternary complex (eIF2-GTP-tRNA(i)(Met))-deficient preinitiation complexes are core constituents of mammalian stress granules. *Mol. Biol. Cell* **13**, 195–210 (2002).
103. Gilks, N. *et al.* Stress granule assembly is mediated by prion-like aggregation of TIA-1. *Mol. Biol. Cell* **15**, 5383–5398 (2004).
104. Tourrière, H. *et al.* The RasGAP-associated endoribonuclease G3BP assembles stress granules. *J. Cell Biol.* **160**, 823–831 (2003).
105. Matsuki, H. *et al.* Both G3BP1 and G3BP2 contribute to stress granule formation. *Genes to Cells* **18**, 135–146 (2013).
106. Mokas, S. *et al.* Uncoupling stress granule assembly and translation initiation inhibition. *Mol. Biol. Cell* **20**, 2673–2683 (2009).
107. Ruggieri, A. *et al.* Dynamic Oscillation of Translation and Stress Granule Formation Mark the Cellular Response to Virus Infection. *Cell Host Microbe* **12**, 71–85 (2012).
108. White, J. P., Cardenas, A. M., Marissen, W. E. & Lloyd, R. E. Inhibition of Cytoplasmic mRNA Stress Granule Formation by a Viral Proteinase. *Cell Host Microbe* **2**, 295–305 (2007).
109. Onomoto, K. *et al.* Critical role of an antiviral stress granule containing RIG-I and PKR in viral detection and innate immunity. *PLoS One* **7**, e43031 (2012).
110. Reineke, L. C., Kedersha, N., Langereis, M. A., van Kuppeveld, F. J. M. & Lloyd, R. E. Stress granules regulate double-stranded RNA-dependent protein kinase activation through a complex containing G3BP1 and Caprin1. *MBio* **6**, e02486 (2015).
111. Khaperskyy, D. A., Hatchette, T. F. & McCormick, C. Influenza A virus inhibits cytoplasmic stress granule formation. *FASEB J.* **26**, 1629–1639 (2012).
112. Khaperskyy, D. A. *et al.* Influenza A Virus Host Shutoff Disables Antiviral Stress-Induced Translation Arrest. *PLoS Pathog.* **10**, e1004217 (2014).
113. Li, W. *et al.* Cell proteins TIA-1 and TIAR interact with the 3' stem-loop of the West Nile virus complementary minus-strand RNA and facilitate virus replication. *J. Virol.* **76**,

11989–2000 (2002).
114. Albornoz, A., Carletti, T., Corazza, G. & Marcello, A. The stress granule component TIA-1 binds tick-borne encephalitis virus RNA and is recruited to perinuclear sites of viral replication to inhibit viral translation. *J. Virol.* **88**, 6611–22 (2014).
115. Cobos Jiménez, V. *et al.* G3BP1 restricts HIV-1 replication in macrophages and T-cells by sequestering viral RNA. *Virology* **486**, 94–104 (2015).
116. Nikolic, J. *et al.* Negri bodies are viral factories with properties of liquid organelles. *Nat. Commun.* **8**, 58 (2017).
117. Liem, J. & Liu, J. Stress Beyond Translation: Poxviruses and More. *Viruses* **8**, 169 (2016).
118. Nikolic, J., Civas, A., Lama, Z., Lagaudrière-Gesbert, C. & Blondel, D. Rabies Virus Infection Induces the Formation of Stress Granules Closely Connected to the Viral Factories. *PLoS Pathog.* **12**, e1005942 (2016).
119. Katsafanas, G. C. & Moss, B. Vaccinia virus intermediate stage transcription is complemented by Ras-GTPase-activating protein SH3 domain-binding protein (G3BP) and cytoplasmic activation/proliferation-associated protein (p137) individually or as a heterodimer. *J. Biol. Chem.* **279**, 52210–7 (2004).
120. Simpson-Holley, M. *et al.* Formation of antiviral cytoplasmic granules during orthopoxvirus infection. *J. Virol.* **85**, 1581–93 (2011).
121. Qin, Q., Hastings, C. & Miller, C. L. Mammalian orthoreovirus particles induce and are recruited into stress granules at early times postinfection. *J. Virol.* **83**, 11090–101 (2009).
122. Kirchner, S. & Ignatova, Z. Emerging roles of tRNA in adaptive translation, signalling dynamics and disease. *Nat. Rev. Genet.* **16**, 98–112 (2015).
123. Trobaugh, D. W. & Klimstra, W. B. MicroRNA Regulation of RNA Virus Replication and Pathogenesis. *Trends Mol. Med.* **23**, 80–93 (2017).
124. Connor, J. H. & Lyles, D. S. Inhibition of host and viral translation during vesicular stomatitis virus infection: eIF2 is responsible for the inhibition of viral but not host translation. *J. Biol. Chem.* **280**, 13512–13519 (2005).
125. Connor, J. H. & Lyles, D. S. Vesicular stomatitis virus infection alters the eIF4F translation initiation complex and causes dephosphorylation of the eIF4E binding protein 4E-BP1. *J. Virol.* **76**, 10177–87 (2002).
126. Couty, J. P., Geras-Raaka, E., Weksler, B. B. & Gershengorn, M. C. Kaposi's sarcoma-associated herpesvirus G protein-coupled receptor signals through multiple pathways in endothelial cells. *J. Biol. Chem.* **276**, 33805–11 (2001).
127. Portis, T. & Longnecker, R. Epstein-Barr virus (EBV) LMP2A mediates B-lymphocyte survival through constitutive activation of the Ras/PI3K/Akt pathway. *Oncogene* **23**, 8619–8628 (2004).
128. Ehrhardt, C. *et al.* Influenza A virus NS1 protein activates the PI3K/Akt pathway to mediate antiapoptotic signaling responses. *J. Virol.* **81**, 3058–67 (2007).
129. Frese, K. K. *et al.* Selective PDZ protein-dependent stimulation of phosphatidylinositol 3-kinase by the adenovirus E4-ORF1 oncoprotein. *Oncogene* **22**, 710–721 (2003).
130. Werden, S. J. *et al.* The Myxoma Virus M-T5 Ankyrin Repeat Host Range Protein Is a Novel Adaptor That Coordinately Links the Cellular Signaling Pathways Mediated by Akt and Skp1 in Virus-Infected Cells. *J. Virol.* **83**, 12068–12083 (2009).
131. Chuluunbaatar, U. *et al.* Constitutive mTORC1 activation by a herpesvirus Akt surrogate stimulates mRNA translation and viral replication. **24**, 2627–2639 (2010).
132. Moorman, N. J. *et al.* Human Cytomegalovirus Protein UL38 Inhibits Host Cell Stress

Responses by Antagonizing the Tuberous Sclerosis Protein Complex. *Cell Host Microbe* **3**, 253–262 (2008).
133. Lu, Z. *et al.* Human papillomavirus 16 E6 oncoprotein interferences with insulin signaling pathway by binding to tuberin. *J. Biol. Chem.* **279**, 35664–35670 (2004).
134. Clippinger, A. J., Maguire, T. G. & Alwine, J. C. Human cytomegalovirus infection maintains mTOR activity and its perinuclear localization during amino acid deprivation. *J. Virol.* **85**, 9369–76 (2011).
135. O'Shea, C. *et al.* Adenoviral proteins mimic nutrient/growth signals to activate the mTOR pathway for viral replication. *EMBO J.* **24**, 1211–21 (2005).
136. Moorman, N. J. & Shenk, T. Rapamycin-resistant mTORC1 kinase activity is required for herpesvirus replication. *J. Virol.* **84**, 5260–9 (2010).
137. Zhu, J.-D., Meng, W., Wang, X.-J. & Wang, H.-C. R. Broad-spectrum antiviral agents. *Front. Microbiol.* **6**, 517 (2015).
138. Hirata, N. *et al.* Inhibition of Akt kinase activity suppresses entry and replication of influenza virus. *Biochem. Biophys. Res. Commun.* **450**, 891–898 (2014).
139. Porta, C., Paglino, C. & Mosca, A. Targeting PI3K/Akt/mTOR Signaling in Cancer. *Front. Oncol.* **4**, 64 (2014).
140. Goodfellow, I. *et al.* Calicivirus translation initiation requires an interaction between VPg and eIF 4 E. *EMBO Rep.* **6**, 968–72 (2005).
141. Bovee, M. L., Lamphear, B. J., Rhoads, R. E. & Lloyd, R. E. Direct cleavage of elF4G by poliovirus 2A protease is inefficient in vitro. *Virology* **245**, 241–9 (1998).
142. Belsham, G. J., McInerney, G. M. & Ross-Smith, N. Foot-and-mouth disease virus 3C protease induces cleavage of translation initiation factors eIF4A and eIF4G within infected cells. *J. Virol.* **74**, 272–80 (2000).
143. Alvarez, E., Menéndez-Arias, L. & Carrasco, L. The eukaryotic translation initiation factor 4GI is cleaved by different retroviral proteases. *J. Virol.* **77**, 12392–400 (2003).
144. Piron, M., Vende, P., Cohen, J. & Poncet, D. Rotavirus RNA-binding protein NSP3 interacts with eIF4GI and evicts the poly(A) binding protein from eIF4F. *EMBO J.* **17**, 5811–5821 (1998).
145. Walsh, D. & Mohr, I. Assembly of an active translation initiation factor complex by a viral protein. *Genes Dev.* **20**, 461–72 (2006).
146. Borah, S., Darricarrère, N., Darnell, A., Myoung, J. & Steitz, J. A. A viral nuclear noncoding RNA binds re-localized poly(A) binding protein and is required for late KSHV gene expression. *PLoS Pathog.* **7**, e1002300 (2011).
147. Kanno, T., Sato, Y., Sata, T. & Katano, H. Expression of Kaposi's sarcoma-associated herpesvirus-encoded K10/10.1 protein in tissues and its interaction with poly(A)-binding protein. *Virology* **352**, 100–9 (2006).
148. Aoyagi, M., Gaspar, M. & Shenk, T. E. Human cytomegalovirus UL69 protein facilitates translation by associating with the mRNA cap-binding complex and excluding 4EBP1. *Proc. Natl. Acad. Sci. U. S. A.* **107**, 2640–5 (2010).
149. Kuyumcu-Martinez, M. *et al.* Calicivirus 3C-like proteinase inhibits cellular translation by cleavage of poly(A)-binding protein. *J. Virol.* **78**, 8172–82 (2004).
150. Fontaine-Rodriguez, E. C., Taylor, T. J., Olesky, M. & Knipe, D. M. Proteomics of herpes simplex virus infected cell protein 27: association with translation initiation factors. *Virology* **330**, 487–92 (2004).
151. Komarova, A. V. *et al.* Rabies virus matrix protein interplay with eIF3, new insights into

rabies virus pathogenesis. *Nucleic Acids Res.* **35**, 1522–32 (2007).
152. Sato, H. *et al.* Measles virus N protein inhibits host translation by binding to eIF3-p40. *J. Virol.* **81**, 11569–76 (2007).
153. Xiao, H., Xu, L. H., Yamada, Y. & Liu, D. X. Coronavirus spike protein inhibits host cell translation by interaction with eIF3f. *PLoS One* **3**, e1494 (2008).
154. Daughenbaugh, K. F., Fraser, C. S., Hershey, J. W. B. & Hardy, M. E. The genome-linked protein VPg of the Norwalk virus binds eIF3, suggesting its role in translation initiation complex recruitment. *EMBO J.* **22**, 2852–9 (2003).
155. Yángüez, E. *et al.* Functional impairment of eIF4A and eIF4G factors correlates with inhibition of influenza virus mRNA translation. *Virology* **413**, 93–102 (2011).
156. Castelló, A. *et al.* Regulation of host translational machinery by African swine fever virus. *PLoS Pathog.* **5**, e1000562 (2009).
157. Zaborowska, I. & Walsh, D. PI3K signaling regulates rapamycin-insensitive translation initiation complex formation in vaccinia virus-infected cells. *J. Virol.* **83**, 3988–92 (2009).
158. Katsafanas, G. C. & Moss, B. Colocalization of transcription and translation within cytoplasmic poxvirus factories coordinates viral expression and subjugates host functions. *Cell Host Microbe* **2**, 221–8 (2007).
159. Baird, S. D., Turcotte, M., Korneluk, R. G. & Holcik, M. Searching for IRES. *RNA* **12**, 1755–85 (2006).
160. Asnani, M., Kumar, P. & Hellen, C. U. T. Widespread distribution and structural diversity of Type IV IRESs in members of Picornaviridae. *Virology* **478**, 61–74 (2015).
161. Mailliot, J. & Martin, F. Viral internal ribosomal entry sites: four classes for one goal. *Wiley Interdiscip. Rev. RNA* **9**, e1458 (2018).
162. Etchison, D., Milburn, S. C., Edery, I., Sonenberg, N. & Hershey, J. W. Inhibition of HeLa cell protein synthesis following poliovirus infection correlates with the proteolysis of a 220,000-dalton polypeptide associated with eucaryotic initiation factor 3 and a cap binding protein complex. *J. Biol. Chem.* **257**, 14806–10 (1982).
163. Ventoso, I., MacMillan, S. E., Hershey, J. W. . & Carrasco, L. Poliovirus 2A proteinase cleaves directly the eIF-4G subunit of eIF-4F complex. *FEBS Lett.* **435**, 79–83 (1998).
164. Gross, L. *et al.* The IRES5'UTR of the dicistrovirus cricket paralysis virus is a type III IRES containing an essential pseudoknot structure. *Nucleic Acids Res.* **45**, 8993–9004 (2017).
165. Borman, A. M. & Kean, K. M. Intact Eukaryotic Initiation Factor 4G Is Required for Hepatitis A Virus Internal Initiation of Translation. *Virology* **237**, 129–136 (1997).
166. Ali, I. K., McKendrick, L., Morley, S. J. & Jackson, R. J. Activity of the hepatitis A virus IRES requires association between the cap-binding translation initiation factor (eIF4E) and eIF4G. *J. Virol.* **75**, 7854–63 (2001).
167. Redondo, N. *et al.* Translation Directed by Hepatitis A Virus IRES in the Absence of Active eIF4F Complex and eIF2. *PLoS One* **7**, e52065 (2012).
168. Avanzino, B. C., Fuchs, G. & Fraser, C. S. Cellular cap-binding protein, eIF4E, promotes picornavirus genome restructuring and translation. *Proc. Natl. Acad. Sci.* **114**, 9611–9616 (2017).
169. Honda, M. *et al.* Structural Requirements for Initiation of Translation by Internal Ribosome Entry within Genome-Length Hepatitis C Virus RNA. *Virology* **222**, 31–42 (1996).
170. Buck, C. B. *et al.* The Human Immunodeficiency Virus Type 1 gag Gene Encodes an

Internal Ribosome Entry Site. *J. Virol.* **75**, 181–191 (2001).
171. Herbreteau, C. H. *et al.* HIV-2 genomic RNA contains a novel type of IRES located downstream of its initiation codon. *Nat. Struct. Mol. Biol.* **12**, 1001–7 (2005).
172. Lee, K. M., Chen, C. J. & Shih, S. R. Regulation Mechanisms of Viral IRES-Driven Translation. *Trends in Microbiology* **25**, 546–561 (2017).
173. Kao, P. N. *et al.* Cloning and expression of cyclosporin A- and FK506-sensitive nuclear factor of activated T-cells: NF45 and NF90. *J. Biol. Chem.* **269**, 20691–9 (1994).
174. Marchesini, M. *et al.* ILF2 Is a Regulator of RNA Splicing and DNA Damage Response in 1q21-Amplified Multiple Myeloma. *Cancer Cell* **32**, 88-100.e6 (2017).
175. Graber, T. E., Baird, S. D., Kao, P. N., Mathews, M. B. & Holcik, M. NF45 functions as an IRES trans-acting factor that is required for translation of cIAP1 during the unfolded protein response. *Cell Death Differ.* **17**, 719–29 (2010).
176. Faye, M. D. *et al.* Nucleotide Composition of Cellular Internal Ribosome Entry Sites Defines Dependence on NF45 and Predicts a Posttranscriptional Mitotic Regulon. *Mol. Cell. Biol.* **33**, 307–318 (2013).
177. Merrill, M. K. & Gromeier, M. The Double-Stranded RNA Binding Protein 76:NF45 Heterodimer Inhibits Translation Initiation at the Rhinovirus Type 2 Internal Ribosome Entry Site. *J. Virol.* **80**, 6936–6942 (2006).
178. Pestova, T. V, de Breyne, S., Pisarev, A. V, Abaeva, I. S. & Hellen, C. U. T. eIF2-dependent and eIF2-independent modes of initiation on the CSFV IRES: a common role of domain II. *EMBO J.* **27**, 1060–72 (2008).
179. Terenin, I. M., Dmitriev, S. E., Andreev, D. E. & Shatsky, I. N. Eukaryotic translation initiation machinery can operate in a bacterial-like mode without eIF2. *Nat. Struct. Mol. Biol.* **15**, 836–41 (2008).
180. Kim, J. H., Park, S. M., Park, J. H., Keum, S. J. & Jang, S. K. eIF2A mediates translation of hepatitis C viral mRNA under stress conditions. *EMBO J.* **30**, 2454–2464 (2011).
181. Thakor, N. & Holcik, M. IRES-mediated translation of cellular messenger RNA operates in eIF2α- independent manner during stress. *Nucleic Acids Res.* **40**, 541–52 (2012).
182. Ho, J. J. D. *et al.* Oxygen-Sensitive Remodeling of Central Carbon Metabolism by Archaic eIF5B. *Cell Rep.* **22**, 17–26 (2018).
183. Khoo, D., Perez, C. & Mohr, I. Characterization of RNA Determinants Recognized by the Arginine- and Proline-Rich Region of Us11, a Herpes Simplex Virus Type 1-Encoded Double-Stranded RNA Binding Protein That Prevents PKR Activation. *J. Virol.* **76**, 11971–11981 (2002).
184. Bierle, C. J., Semmens, K. M. & Geballe, A. P. Double-stranded RNA binding by the human cytomegalovirus PKR antagonist TRS1. *Virology* **442**, 28–37 (2013).
185. Child, S. J., Hanson, L. K., Brown, C. E., Janzen, D. M. & Geballe, A. P. Double-stranded RNA binding by a heterodimeric complex of murine cytomegalovirus m142 and m143 proteins. *J. Virol.* **80**, 10173–80 (2006).
186. Poppers, J., Mulvey, M., Perez, C., Khoo, D. & Mohr, I. Identification of a Lytic-Cycle Epstein-Barr Virus Gene Product That Can Regulate PKR Activation. *J. Virol.* **77**, 228–236 (2003).
187. Hatada, E. & Fukuda, R. Binding of influenza a virus NS1 protein to dsRNA in vitro. *J. Gen. Virol.* **73**, 3325–3329 (1992).
188. Yue, Z. & Shatkin, A. J. Double-Stranded RNA-Dependent Protein Kinase (PKR) Is Regulated by Reovirus Structural Proteins. *Virology* **234**, 364–371 (1997).

189. Romano, P. R. *et al.* Inhibition of double-stranded RNA-dependent protein kinase PKR by vaccinia virus E3: role of complex formation and the E3 N-terminal domain. *Mol. Cell. Biol.* **18**, 7304–16 (1998).
190. Takeuchi, K., Komatsu, T., Kitagawa, Y., Sada, K. & Gotoh, B. Sendai Virus C Protein Plays a Role in Restricting PKR Activation by Limiting the Generation of Intracellular Double-Stranded RNA. *J. Virol.* **82**, 10102–10110 (2008).
191. Vyas, J., Elia, A. & Clemens, M. J. Inhibition of the protein kinase PKR by the internal ribosome entry site of hepatitis C virus genomic RNA. *RNA* **9**, 858–70 (2003).
192. Ghadge, G. D., Swaminathan, S., Katze, M. G. & Thimmapaya, B. Binding of the adenovirus VAI RNA to the interferon-induced 68-kDa protein kinase correlates with function. *Proc. Natl. Acad. Sci. U. S. A.* **88**, 7140–4 (1991).
193. Clarke, P. A., Schwemmle, M., Schickinger, J., Hilse, K. & Clemens, M. J. Binding of Epstein-Barr virus small RNA EBER-1 to the double-stranded RNA-activated protein kinase DAI. *Nucleic Acids Res.* **19**, 243–8 (1991).
194. Gale, M. J., Korth, M. J. & Katze, M. G. Repression of the PKR protein kinase by the hepatitis C virus NS5A protein: a potential mechanism of interferon resistance. *Clin. Diagn. Virol.* **10**, 157–62 (1998).
195. Spurgeon, M. E. & Ornelles, D. A. The adenovirus E1B 55-kilodalton and E4 open reading frame 6 proteins limit phosphorylation of eIF2alpha during the late phase of infection. *J. Virol.* **83**, 9970–82 (2009).
196. Burýsek, L. & Pitha, P. M. Latently expressed human herpesvirus 8-encoded interferon regulatory factor 2 inhibits double-stranded RNA-activated protein kinase. *J. Virol.* **75**, 2345–52 (2001).
197. Van Opdenbosch, N., Van den Broeke, C., De Regge, N., Tabares, E. & Favoreel, H. W. The IE180 Protein of Pseudorabies Virus Suppresses Phosphorylation of Translation Initiation Factor eIF2 . *J. Virol.* **86**, 7235–7240 (2012).
198. Carroll, K., Elroy-Stein, O., Moss, B. & Jagus, R. Recombinant vaccinia virus K3L gene product prevents activation of double-stranded RNA-dependent, initiation factor 2 alpha-specific protein kinase. *J. Biol. Chem.* **268**, 12837–42 (1993).
199. McMillan, N. A. J. *et al.* HIV-1 Tat Directly Interacts with the Interferon-Induced, Double-Stranded RNA-Dependent Kinase, PKR. *Virology* **213**, 413–424 (1995).
200. Pavio, N., Romano, P. R., Graczyk, T. M., Feinstone, S. M. & Taylor, D. R. Protein Synthesis and Endoplasmic Reticulum Stress Can Be Modulated by the Hepatitis C Virus Envelope Protein E2 through the Eukaryotic Initiation Factor 2 Kinase PERK. *J. Virol.* **77**, 3578–3585 (2003).
201. Mulvey, M., Arias, C. & Mohr, I. Maintenance of endoplasmic reticulum (ER) homeostasis in herpes simplex virus type 1-infected cells through the association of a viral glycoprotein with PERK, a cellular ER stress sensor. *J. Virol.* **81**, 3377–90 (2007).
202. He, B., Gross, M. & Roizman, B. The gamma(1)34.5 protein of herpes simplex virus 1 complexes with protein phosphatase 1alpha to dephosphorylate the alpha subunit of the eukaryotic translation initiation factor 2 and preclude the shutoff of protein synthesis by double-stranded RNA-activa. *Proc. Natl. Acad. Sci. U. S. A.* **94**, 843–8 (1997).
203. Zhang, F., Moon, A., Childs, K., Goodbourn, S. & Dixon, L. K. The African Swine Fever Virus DP71L Protein Recruits the Protein Phosphatase 1 Catalytic Subunit To Dephosphorylate eIF2α and Inhibits CHOP Induction but Is Dispensable for These Activities during Virus Infection. *J. Virol.* **84**, 10681–10689 (2010).

204. Kazemi, S. *et al.* Control of alpha subunit of eukaryotic translation initiation factor 2 (eIF2 alpha) phosphorylation by the human papillomavirus type 18 E6 oncoprotein: implications for eIF2 alpha-dependent gene expression and cell death. *Mol. Cell. Biol.* **24**, 3415–29 (2004).
205. Finnen, R. L., Zhu, M., Li, J., Romo, D. & Banfield, B. W. Herpes Simplex Virus 2 Virion Host Shutoff Endoribonuclease Activity Is Required To Disrupt Stress Granule Formation. *J. Virol.* **90**, 7943–55 (2016).
206. Cinti, A., Sage, V. Le, Ghanem, M. & Mouland, A. J. HIV-1 Gag Blocks Selenite-Induced Stress Granule Assembly by Altering the mRNA Cap-Binding Complex. *MBio* **7**, e00329 (2016).
207. Valiente-Echeverría, F. *et al.* eEF2 and Ras-GAP SH3 domain-binding protein (G3BP1) modulate stress granule assembly during HIV-1 infection. *Nat. Commun.* **5**, 4819 (2014).
208. Rao, S. *et al.* HIV-1 NC-induced stress granule assembly and translation arrest are inhibited by the dsRNA binding protein Staufen1. *RNA* **24**, 219–236 (2018).
209. Soto-Rifo, R. *et al.* HIV-2 genomic RNA accumulates in stress granules in the absence of active translation. *Nucleic Acids Res.* **42**, 12861–75 (2014).
210. Amorim, R., Temzi, A., Griffin, B. D. & Mouland, A. J. Zika virus inhibits eIF2α-dependent stress granule assembly. *PLoS Negl. Trop. Dis.* **11**, e0005775 (2017).
211. Hou, S. *et al.* Zika virus hijacks stress granule proteins and modulates the host stress response. *J. Virol.* JVI.00474-17 (2017). doi:10.1128/JVI.00474-17
212. Le Sage, V. *et al.* Ebola virus VP35 blocks stress granule assembly. *Virology* **502**, 73–83 (2017).
213. Nelson, E. V *et al.* Ebola Virus Does Not Induce Stress Granule Formation during Infection and Sequesters Stress Granule Proteins within Viral Inclusions. *J. Virol.* **90**, 7268–84 (2016).
214. Netherton, C. L. & Wileman, T. Virus factories, double membrane vesicles and viroplasm generated in animal cells. *Current Opinion in Virology* **1**, 381–387 (2011).
215. David, A. *et al.* RNA binding targets aminoacyl-tRNA synthetases to translating ribosomes. *J. Biol. Chem.* **286**, 20688–20700 (2011).
216. Desmet, E. A., Anguish, L. J. & Parker, J. S. L. Virus-mediated compartmentalization of the host translational machinery. *MBio* **5**, (2014).
217. Dieterich, D. C. *et al.* In situ visualization and dynamics of newly synthesized proteins in rat hippocampal neurons. *Nat. Neurosci.* **13**, 897–905 (2010).
218. Dieterich, D. C., Link, A. J., Graumann, J., Tirrell, D. A. & Schuman, E. M. Selective identification of newly synthesized proteins in mammalian cells using bioorthogonal noncanonical amino acid tagging (BONCAT). *Proc. Natl. Acad. Sci. U. S. A.* **103**, 9482–7 (2006).
219. Schmidt, E. K., Clavarino, G., Ceppi, M. & Pierre, P. SUnSET, a nonradioactive method to monitor protein synthesis. *Nat. Methods* **6**, 275–277 (2009).
220. David, A. *et al.* Nuclear translation visualized by ribosome-bound nascent chain puromycylation. *J. Cell Biol.* **197**, 45–57 (2012).
221. David, A., Bennink, J. R. & Yewdell, J. W. Emetine optimally facilitates nascent chain puromycylation and potentiates the ribopuromycylation method (RPM) applied to inert cells. *Histochem. Cell Biol.* **139**, 501–4 (2013).
222. Liu, J., Xu, Y., Stoleru, D. & Salic, A. Imaging protein synthesis in cells and tissues with an alkyne analog of puromycin. *Proc. Natl. Acad. Sci. U. S. A.* **109**, 413–8 (2012).

223. Aviner, R., Geiger, T. & Elroy-Stein, O. Novel proteomic approach (PUNCH-P) reveals cell cycle-specific fluctuations in mRNA translation. *Genes Dev.* **27**, 1834–1844 (2013).
224. Kallin, B., Luka, J. & Klein, G. Immunochemical characterization of Epstein-Barr virus-associated early and late antigens in n-butyrate-treated P3HR-1 cells. *J. Virol.* **32**, 710–6 (1979).
225. Schwanhäusser, B., Gossen, M., Dittmar, G. & Selbach, M. Global analysis of cellular protein translation by pulsed SILAC. *Proteomics* **9**, 205–209 (2009).
226. Howden, A. J. M. *et al.* QuaNCAT: quantitating proteome dynamics in primary cells. *Nat. Methods* **10**, 343–6 (2013).
227. Bagert, J. D. *et al.* Quantitative, Time-Resolved Proteomic Analysis by Combining Bioorthogonal Noncanonical Amino Acid Tagging and Pulsed Stable Isotope Labeling by Amino Acids in Cell Culture. *Mol. Cell. Proteomics* **13**, 1352–1358 (2014).
228. Faye, M. D., Graber, T. E. & Holcik, M. Assessment of selective mRNA translation in mammalian cells by polysome profiling. *J. Vis. Exp.* e52295 (2014). doi:10.3791/52295
229. Gandin, V. *et al.* Polysome fractionation and analysis of mammalian translatomes on a genome-wide scale. *J. Vis. Exp.* 1–9 (2014). doi:10.3791/51455
230. Ingolia, N. T., Ghaemmaghami, S., Newman, J. R. S. & Weissman, J. S. Genome-wide analysis in vivo of translation with nucleotide resolution using ribosome profiling. *Science (80-.).* **324**, 218–223 (2009).
231. Lareau, L. F., Hite, D. H., Hogan, G. J. & Brown, P. O. Distinct stages of the translation elongation cycle revealed by sequencing ribosome-protected mRNA fragments. *Elife* **3**, e01257 (2014).
232. Ingolia, N. T. *et al.* Ribosome profiling reveals pervasive translation outside of annotated protein-coding genes. *Cell Rep.* **8**, 1365–79 (2014).
233. Fields, A. P. *et al.* A Regression-Based Analysis of Ribosome-Profiling Data Reveals a Conserved Complexity to Mammalian Translation. *Mol. Cell* **60**, 816–827 (2015).
234. Richter, J. D. & Coller, J. Pausing on Polyribosomes: Make Way for Elongation in Translational Control. *Cell* **163**, 292–300 (2015).
235. Calviello, L. *et al.* Detecting actively translated open reading frames in ribosome profiling data. *Nat. Methods* **13**, 165–70 (2016).
236. Fresno, M., Jiménez, A. & Vázquez, D. Inhibition of translation in eukaryotic systems by harringtonine. *Eur. J. Biochem.* **72**, 323–30 (1977).
237. Huang, M. T. Harringtonine, an inhibitor of initiation of protein biosynthesis. *Mol. Pharmacol.* **11**, 511–9 (1975).
238. Schneider-Poetsch, T. *et al.* Inhibition of eukaryotic translation elongation by cycloheximide and lactimidomycin. *Nat. Chem. Biol.* **6**, 209–217 (2010).
239. Stern-Ginossar, N. *et al.* Decoding human cytomegalovirus. *Science (80-.).* **338**, 1088–1093 (2012).
240. Tirosh, O. *et al.* The Transcription and Translation Landscapes during Human Cytomegalovirus Infection Reveal Novel Host-Pathogen Interactions. *PLoS Pathog.* **11**, 1–29 (2015).
241. Arias, C. *et al.* KSHV 2.0: A Comprehensive Annotation of the Kaposi's Sarcoma-Associated Herpesvirus Genome Using Next-Generation Sequencing Reveals Novel Genomic and Functional Features. *PLoS Pathog.* **10**, e1003847 (2014).
242. Bercovich-Kinori, A. *et al.* A systematic view on influenza induced host shutoff. *Elife* **5**, e18311 (2016).

243. Yang, Z. *et al.* Deciphering poxvirus gene expression by RNA sequencing and ribosome profiling. *J. Virol.* **89**, 6874–86 (2015).
244. Dai, A. *et al.* Ribosome Profiling Reveals Translational Upregulation of Cellular Oxidative Phosphorylation mRNAs during Vaccinia Virus-Induced Host Shutoff. *J. Virol.* **91**, 1858–1874 (2017).
245. Heiman, M. *et al.* A translational profiling approach for the molecular characterization of CNS cell types. *Cell* **135**, 738–48 (2008).
246. Sanz, E. *et al.* Cell-type-specific isolation of ribosome-associated mRNA from complex tissues. *Proc. Natl. Acad. Sci. U. S. A.* **106**, 13939–44 (2009).
247. Besse, F. & Ephrussi, A. Translational control of localized mRNAs: restricting protein synthesis in space and time. *Nat. Rev. Mol. Cell Biol.* **9**, 971–80 (2008).
248. Buxbaum, A. R., Haimovich, G. & Singer, R. H. In the right place at the right time: visualizing and understanding mRNA localization. *Nat. Rev. Mol. Cell Biol.* **16**, 95–109 (2015).
249. Holt, C. E. & Schuman, E. M. The central dogma decentralized: new perspectives on RNA function and local translation in neurons. *Neuron* **80**, 648–57 (2013).
250. Graber, T. E. *et al.* UPF1 Governs Synaptic Plasticity through Association with a STAU2 RNA Granule. *J. Neurosci.* **37**, 9116–9131 (2017).
251. Cai, L., Friedman, N. & Xie, X. S. Stochastic protein expression in individual cells at the single molecule level. *Nature* **440**, 358–62 (2006).
252. Morisaki, T. *et al.* Real-time quantification of single RNA translation dynamics in living cells. *Science* **352**, 1425–9 (2016).
253. Wu, B., Eliscovich, C., Yoon, Y. J. & Singer, R. H. Translation dynamics of single mRNAs in live cells and neurons. *Science* **352**, 1430–5 (2016).
254. Wang, C., Han, B., Zhou, R. & Zhuang, X. Real-Time Imaging of Translation on Single mRNA Transcripts in Live Cells. *Cell* **165**, 990–1001 (2016).
255. Yan, X., Hoek, T. A., Vale, R. D. & Tanenbaum, M. E. Dynamics of Translation of Single mRNA Molecules In Vivo. *Cell* **165**, 976–989 (2016).
256. Mannack, L. V. J. C., Eising, S. & Rentmeister, A. Current techniques for visualizing RNA in cells. *F1000Research* **5**, 775 (2016).
257. Marciano, R., Leprivier, G. & Rotblat, B. Puromycin labeling does not allow protein synthesis to be measured in energy-starved cells. *Cell Death Dis.* **9**, 39 (2018).

6.3. Emerging translation strategies during virus–host interaction

Authors: Huy-Dung Hoang, Serge Neault, Adrian Pelin, Tommy Alain

Review article (Citations: 1)
Wiley Interdisciplinary Reviews RNA, published on August 2020 (Impact Factor: 6.84)

6.3.1 Author contributions

H.-D.H conceptualized and wrote the majority of the article; S.N. and A.P. contribute to section 6.3.4.4. H.-D.H, S.N., A.P. and T.A. reviewed and edited the final manuscript.

6.3.2. Abstract

Translation control is crucial during virus–host interaction. On one hand, viruses completely rely on the protein synthesis machinery of host cells to propagate and have evolved various mechanisms to redirect the host's ribosomes toward their viral mRNAs. On the other hand, the host rewires its translation program in an attempt to contain and suppress the virus early on during infection; the antiviral program includes specific control on protein synthesis to translate several antiviral mRNAs involved in quenching the infection. As the infection progresses, host translation is in turn inhibited in order to limit viral propagation. We have learnt of very diverse strategies that both parties utilize to gain or retain control over the protein synthesis machinery. Yet novel strategies continue to be discovered, attesting for the importance of mRNA translation in virus–host interaction. This review focuses on recently described translation strategies employed by both hosts and viruses. These discoveries provide additional pieces in the understanding of the complex virus–host translation landscape.

6.3.3. Introduction

6.3.3.1. Basis of eukaryotic mRNA translation

A typical mammalian mRNA consists of a 7-methylguanosine cap (m7G) at the 5′termini, a 5′ untranslated region (5′UTR), a coding sequence (CDS) that starts with a start codon and ends with an in-frame stop codon, a 3′ untranslated region (3′UTR), and a poly(A) tail[548]. Viral mRNAs follow the same arrangement principles but with some particularities (described below and reviewed in more details in Jan, Mohr, & Walsh, 2016[731]). Despite the distinctions, translation in mammalian cells for both host and virus mRNAs follows the same three fundamental steps: initiation, elongation, and termination. If translation occurs via the canonical cap-dependent mechanism, initiation begins with the recruitment of the eIF4F complex, which includes the cap-binding protein eIF4E, the scaffold protein eIF4G, the RNA helicase eIF4A, to the 5′end of the mRNA via the eIF4E–m7G cap interaction. The eIF4F complex recruits the 43S preinitiation complex, consisting of eIF2-GTP.Met-tRNAi.40S ribosomal subunit, to the 5′UTR. If the mRNA is translated via cap-independent mechanisms, other translation factors can come into play to recruit the ribosome to the mRNA, often involving internal ribosome entry sites (IRES)[93]. Either following cap-dependent or -independent initiation, the subsequent steps follow the same principles. The 43S preinitiation complex begins to scan the 5′UTR with the help of eIF4A ATP-dependent helicase activity to resolve secondary structure. Scanning stops when the 43S complex recognizes a start codon via anticodon-base pairing with Met-tRNAi. Although the cognate AUG is the dominant start codon of choice, approximately 60% of mammalian translation initiation occurs at noncognate start codons (which include CUG, GUG, or UUG)[732], potentially using other initiator tRNAs than Met-tRNAi[733]. The eIFs are then released and the 60S ribosomal subunit is recruited to the 40S ribosomal subunit, forming an elongation competent 80S monosome[548,551].

Elongation then begins with a continuous supply of aminoacyl-tRNA to the A site of the 80S monosome by the eukaryotic elongation factor (eEF) 1A. Peptide bond formation between amino acids in the P site and the A site is catalyzed, while the translocase eEF2 “rachet” the ribosome by one codon in the 3′ direction. The uncharged tRNA is then moved to the E site while the peptidyl-tRNA transfers to the P site, leaving the A site unoccupied for the next cycle of elongation. When the ribosome reaches a stop codon (UAG, UGA, or UAA), the eukaryotic release factors eRF1.eRF3.GTP is recruited to the A site instead of a charged tRNA to initiate termination. GTP hydrolysis catalyzed by eRF3 causes deacetylation of the peptidyl-tRNA bond, releasing the polypeptide chain from the last tRNA followed by dissociation of the 80S ribosome[15].

6.3.3.2. Translation reprogramming during virus–host interaction

Protein synthesis is a complex cellular process that consumes a large portion of the cell energy expenditure and involves a sophisticated signaling and effector gene network[548,551,564]. Unlike for replication and transcription where viruses can encode their own genes to carry out these functions, the synthesis of viral proteins completely relies on the host translation machinery and represents a major interaction interface that is crucial for virus propagation. Viruses deploy a surprisingly diverse set of strategies to redirect the translation machinery on viral RNAs and shutting down host translation. Simultaneously, the antiviral response depends on the same machinery for translating antiviral transcripts while various translation control mechanisms are also engaged by the host to limit viral infection[8,731,734,735]. In this section, we will attempt to briefly summarize the specific translation strategies employed by host cells and viruses during infection and provide the readers with a nonexhaustive, representative literature list for reference. For comprehensive discussions of established knowledge of translation control in virus–host

interaction, we invite the readers to peruse previous excellent reviews by Jan *et al.*[731] or Walsh *et al.*[735].

A number of signaling pathways impact upon translation control during viral infection. For instance, the PI3K-AKT-mTORC1 pathway regulates cellular metabolism and is one of the main signaling axes that impact mRNA translation, most notably via its principal downstream effectors S6Ks, 4E-BPs, and LARP1[20,27]. The activation of mTORC1 was reported during the antiviral state induced by type I interferon[576]. Similarly, the early events of virus entry were shown to activate this pathway[50–52]. mTORC1 in turn was shown to play an important role in translation of antiviral transcripts, and of crucial antiviral transcription factors[55–57,577,736]. Another translation arm of the antiviral response is the integrated stress response (ISR), a stress-induced pathway that causes protein synthesis shutdown via phosphorylation of the eIF2α by four kinases: heme-regulated inhibitor (HRI), general control non-derepressible 2 (GCN2), protein kinase R (PKR), or PKR-like endoplasmic reticulum (ER) kinase (PERK). The formation of the ternary complex (TC) requires eIF2-GTP that is recycled after translation initiation. Phosphorylation of the α subunit of eIF2 (P-eIF2α) inhibits the recycling step, thus blocking translation initiation by exhausting the cellular pool of active eIF2-GTP. Stimuli from virus infection are known to activate ISR kinases: structured viral genomic RNA of Sindbis virus activates GCN2[62], while the unfolded protein response during virus infection induces PERK[61]. Importantly, the kinase PKR is an interferon stimulated gene (ISG) that is upregulated by type I interferon and is a sensor of double-stranded RNA or 5′triphosphate RNA, nucleic acid products that characterize all virus replication[58,59].

Viruses, in turn, have the capacity to alter the translation environment of the antiviral state. The mTORC1 is a primary target of virus manipulation, inhibited in an attempt to thwart host translation or activated to benefit viral protein production. For example, the matrix protein M of

VSV was shown to inhibit AKT phosphorylation[81], which in turn dampen host protein synthesis including interferon gene expression[123]. In contrast, various components of the PI3K-AKT-mTORC1 signaling have been reported to be activated by viral proteins to benefit virus replication[83–85,636–639,644,737]. The translation initiation complex, the crucial component of cap-dependent translation initiation, is also targeted by viral proteins using numerous mechanisms, including protease degradation of translation initiation factors, inhibition of complex formation, and redirection of these factors toward viral mRNAs[8]. The ISR signaling pathway is no exception and is a frequent subject of virus hijacking to prevent ISR-mediated translation shutdown. The various strategies range from deploying dsRNA-binding protein to shield viral dsRNA from detection by PKR[102–105,680,738,739], expressing proteins that bind directly to ISR kinases to impair their function[109,112,684,740] and enhancing eIF2α dephosphorylation to resolve translation shutdown by P-eIF2α[114,741,742]. The activation of certain aspects of the ISR might also be beneficial for virus replication, such as in the case of SARS-CoV (the strain that caused the 2003 Severe Acute Respiratory Syndrome global outbreak) activating the unfolded protein response via its 8ab protein. When expressing ectopically, 8ab promotes proteolysis of ATF6 to produce the active form that translocates to the nucleus and regulates the transcription program of UPR[743]. Additionally, certain viruses can sustain translation in the suboptimal translation condition of the antiviral state via an IRES, structured RNA sequences that are capable of recruiting ribosome to mRNA with the requirement of only a minimal and incomplete set of eIF, mediating a mode of cap-independent translation initiation[93].

Despite the wealth of knowledge that the field accumulated over the last few decades, the translation landscape of virus–host interaction still contains various uncharted territories that remain to be discovered. With the development of novel techniques to examine previously poorly

understood cellular phenomena, emerging aspects of this crucial virus–host interaction have been revealed (**Figure 6.3.1**), many of them prove no less important in defining the fate of the infected cell. In the following sections, we attempt to review the current state of understanding of the emerging aspects of virus–host interactions.

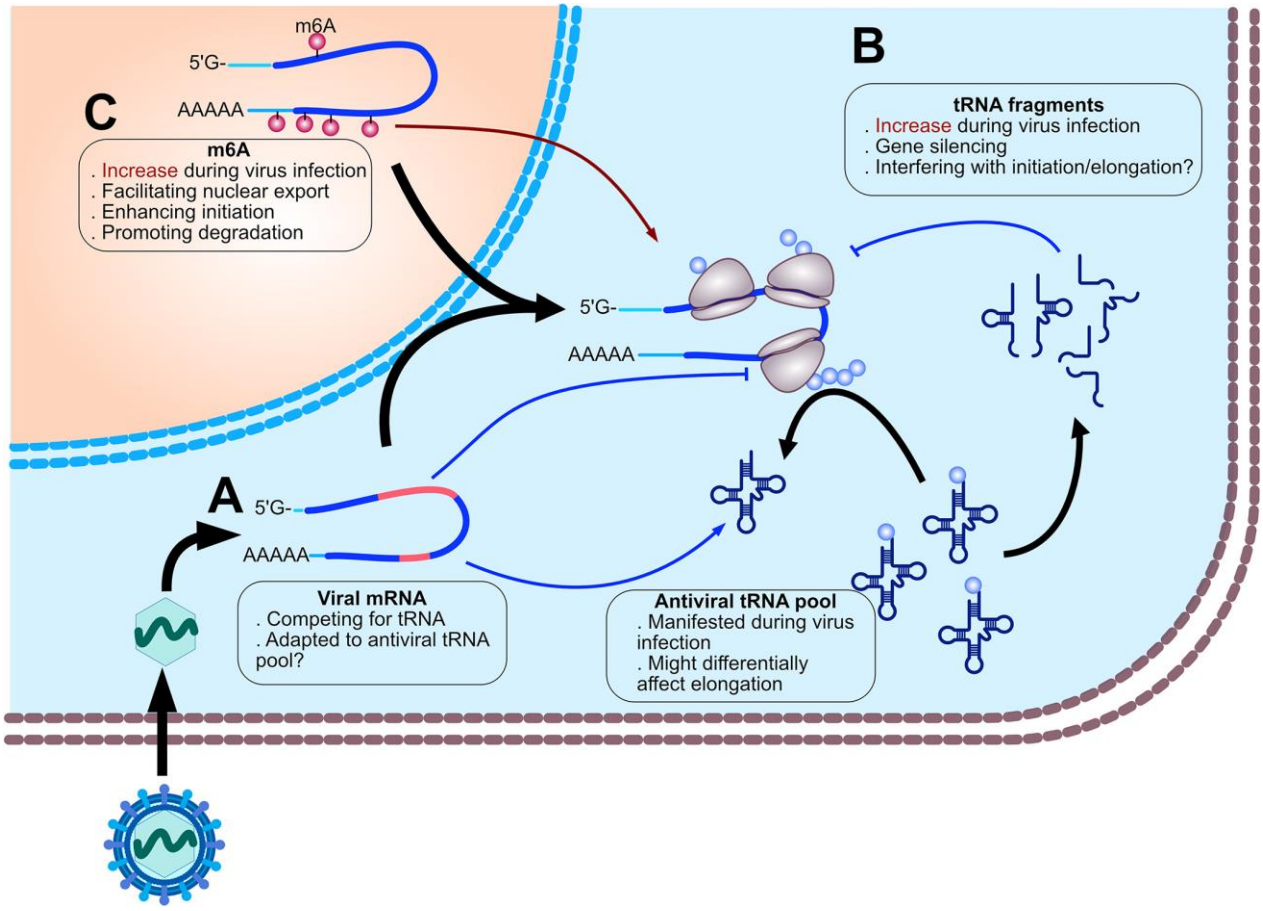

Figure 6.3.1. Emerging mechanisms of translation control during viral infection. (A) Transcription of viral mRNAs and alteration of the tRNA pools during the antiviral state impact translation. Viral mRNAs often possess dissimilar codon usage than that of host mRNAs, consequently altering the tRNA pools by their unique consumption of tRNAs. The antiviral state also changes the composition of the tRNA pools. Ultimately, such altered tRNA pools might affect the elongation rate of a defined subset of mRNAs. (B) tRNA fragments impair translation during viral infection. tRNA fragments abundance increases in infected cells. These fragments might in turn inhibit translation via their interaction with translating ribosomes or via the RNA interference machinery. (C) m6A is a layer of translation control in virus–host interaction. m6A machinery is activated during infection. m6A might enhance or disrupt translation depending on the effector proteins

6.3.4. Emerging translation strategies during virus–host interaction

6.3.4.1. Codon usage and the tRNA pool of the antiviral state

During translation elongation, the ribosome incorporates individual amino acid to the elongating peptide chain from the cytoplasmic pool of amino acyl-tRNA. Although it was generally assumed that the elongation rate in an organism is constant, a ribosome in fact assimilates amino acid at varying rates depending on the codon, the type of amino acid, and the availability of the corresponding amino acyl-tRNA. Suboptimal codon usage, depletion of certain amino acids, or certain codons can slow the elongation rate via ribosome stalling[460,461,744] (**Figure 6.3.2**). Consequently, translation efficiency is a selection pressure that shapes codon usage bias toward the availability of the organism's tRNA pools, such that the codon corresponding to the most abundant tRNAs will be used more frequently[745] (**Figure 6.3.1a**). Recently, it has been revealed that the tRNA pool is not just unique for each species, but is also dynamically altered between different cellular states[206,460]. Virus infection poses a unique challenge for the host tRNA pool: as the virus usurps the host translation machinery, the variety of translating mRNAs degenerates dramatically from tens of thousands of host mRNA species to only a few hundred of virus mRNAs. This environment theoretically imposes a selection pressure for viral genes to conform to the host tRNA pool and thus the host codon usage bias, especially between highly expressed viral genes and the most abundantly expressed tRNAs. Such selection pressure appears to be very strong in shaping bacteriophage codon usage[746–748], while affecting that of avian and mammalian viruses to a lesser extent[462]. Intriguingly, it was reported that HIV and HSV genes employ suboptimal codon usage for human cells[463,464]. Therefore, although it has been clear that viruses have adapted their codon usage to that of their hosts, dissimilarities remain, which raises the following question: are there specific tRNA pools that are manifested during the host's antiviral state, and conversely do

specific viruses actively shape the tRNA pools to suit their replication while thwarting host translation?

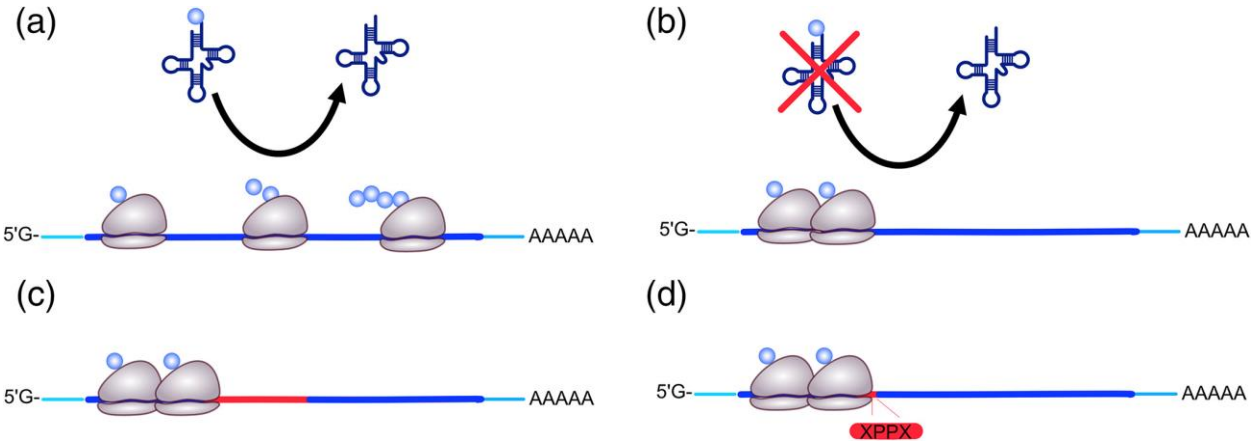

Figure 6.3.2. Various scenarios of stalled elongation. (a) Normal elongating ribosomes. (b) Ribosome stalling due to depletion of certain amino acids or tRNAs. (c) Suboptimal codon usage that requires rare tRNAs for decoding may also cause ribosome stalling. (d) Certain amino acid motifs, such as di-proline (XPPX) depicted here, can also cause ribosome stalling

The altered tRNA pools in infected cells can be initiated by the activation of the antiviral state with interferon. The earliest evidence of antiviral state-specific tRNA pools came from a study in 1976 that reported inhibition of protein synthesis in cell extracts from interferon-treated cells, which was overcome by adding crude tRNA preparations[749]. Additionally, by measuring the incorporation rate of individual amino acid to purified total endogenous tRNA, the authors revealed that interferon treatment impaired amino acylation of a subset of amino acid to tRNAs, most significantly that of leucine, lysine, and serine, proposing that tRNAs corresponding to these amino acids are inactivated. The antiviral state-specific tRNA pool hypothesis was further corroborated by a study that tracked the codon adaptation of the influenza virus gene PB1[204]. Influenza A viruses can exchange gene segments between subtypes; these subtypes in turn are endemic in different host species. The gene fragment encoding the polymerase PB1 was introduced into the human H3N2 influenza viruses in 1968 and since has been proposed to be subjected to selection pressure to conform to human tRNA pools, such adaptation was tracked using PB1 sequence from H3N2 isolates collected over the years. Surprisingly, the author found that as the H3N2 strain continued to circulate seasonally, PB1 codon usage gradually diverged from that of human as evaluated by codon adaptation index (CAI). More astonishingly, H3N2 expressing PB1 gene with codon usage mimicking that of recent strain with low CAI to human replicated better in A549 cell treated with interferon, but not in untreated A549 cells, compared to H3N2 expressing an earlier version of PB1 with a higher CAI to human. To inquire whether interferon treatment induces a different tRNA pool in human cells, the authors performed high-throughput sequencing of tRNA pools and found that expression of certain tRNAs decreased in response to interferon, and the decrease in PB1 CAI to human was inversely correlated with an increase in PB1 codon usage bias adapting to this specific tRNA pool. It is noteworthy to mention that attempts to

optimize PB1 codon usage to the interferon-specific tRNA pool resulted in interferon resistance but a decrease in overall fitness of the new virus, suggesting that other selection pressures are also at play for codon selection. The mechanisms of how interferon could induce changes in the tRNA pool remain an open question. Of the two main classes of interferon, type I and type II IFN, type I IFN has a more prominent antiviral property and activates various transcription programs, primarily via the JAK/STAT signaling pathway[750,751]. These transcription programs upregulate the expression of hundreds to thousands of antiviral genes, termed ISGs[193]. Some of these ISGs are RNAses (Isg20[752], Slfn11[753]) or related to RNAse (Oas1/2/3[754]), of which genes belong to the Schlafen family were shown to be able to degrade tRNAs[755,756]. Thus, it is reasonable to speculate that degrading tRNA via the activation of tRNA-specific RNAses by interferon is a plausible mechanism that shapes the tRNA pool of interferon-treated cells.

Simultaneously with the presence of interferon, the tRNA pool of infected cells can also be actively altered by the virus productive infection. Despite the restricted coding capacity owned by their relatively small genomes, some viruses have been reported to encode tRNA genes and this phenomenon has been reported extensively in bacteriophage and cyanophage[757]. In the specific case of the chlorella virus CVK2, viral tRNAs have been reported to be amino-acylated, strengthening the notion that they contribute to protein synthesis in infected host cells[758]. In the case of mammalian viruses, tRNA genes were previously reported in the genome of murine gamma herpes virus 68[759]. Alternatively, virus infection can favor the usage of specific tRNAs for protein synthesis without affecting total tRNA pools[760]. Although the exact mechanism to select tRNA is not known, certain viruses such as vaccinia virus form virus factories, subcellular entities where viral proteins are translated[117]. It is possible that these virus factories can recruit selective tRNAs to its active translation site, potentially skewing cellular tRNA pools in the process. However, very

little is known about the role of viral tRNA genes or virus-mediated modulation of host tRNA pools, and further investigation is required to obtain a clearer picture of their importance in virus–host interaction.

Despite emerging evidence presented above, we should be cautious in formulating the hypothesis that optimizing translation efficiency is the only direction of the virus codon evolution as suboptimal codon bias persist in many viral genes. Codon usage of a gene can also regulate other gene expression in *trans*, most likely via competing for aa-tRNAs from the common pools. For instance, it has been reported that codon optimization of the late gene (adenovirus genes can be classified as early or late genes based on the temporal dynamic of their expression in the virus life cycle) encoding the fiber protein of adenovirus impaired expression of the more codon-optimized hexon structural protein and ultimately hampered virus replication[207]. Similarly, another study by Chen et al. proposed that virus codon usage bias might differ from that of host to avoid delay in decoding time due to overconsumption and depletion of similar tRNAs[761]. Using ribosome profiling data from various studies to calculate relative codon decoding time of ribosomes[461], the authors found that translation of highly expressed viral genes delayed the decoding time, and such delay correlated with the rarity of host tRNA supply. The authors then ectopically expressed 37 synonymous-codon altered versions of a reporter gene ranging from poorly to highly codon-optimized under a strong expression promoter, together with another reporter gene expressed under a weak promoter. This aimed to recapitulate the effect of highly expressed viral genes (the highly transcribed reporter) of various codon adaptation level on host cells general translation (the poorly transcribed reporter). Interestingly, synonymous codon adaptation to host cells resulted in elevated expression of the highly transcribed reporter gene at the expense of the expression of the poorly transcribed reporter gene. Thus, this report supports the model in which high codon adaptation of

a few very highly expressed mRNAs might be detrimental for translation of the rest of the mRNAs, probably via depletion of the commonly used tRNAs. Together, these reports propose another direction for adaptation of virus codon usage: the whole genome or certain genes might actively be selected to a suboptimal codon usage to avoid depletion of abundantly used tRNAs and subsequently be exposed to translation constraints. Interestingly, as viruses or host actively shutoff protein synthesis, it would be interesting to investigate if suboptimal codon usage can be a viral strategy toward the goal of overloading host translation machinery with suboptimally adapted mRNAs to quickly deplete rare tRNAs. Overall, the data so far paint a complex picture wherein viral genes are under selection pressure to optimize their codons toward a distinct antiviral-state tRNA pool, yet at least a subset of viral genes might preserve a certain degree of dissimilarity in codon usage to avoid directly competing for tRNAs with other viral or host genes. Further understanding of this aspect of virus–host interaction might benefit transgene design for viral vector or engineering a better cancer-specific oncolytic virus that suits a cancer-optimized codon usage.

6.3.4.2. Small tRNA fragments: Stress response element exploited by viruses

Small noncoding RNAs are RNA fragments that are typically <50 nt and inferred to provide a layer of posttranscriptional control. Recently, a group of small noncoding RNA called small tRNA fragments was described, which is the products of cleaved tRNAs in stress condition in various organisms[466,762–765]. Although the nomenclature has yet to be unified, these small tRNA fragments can be classified loosely into two classes depending on the cleavage position on the tRNA. The first class is called tRNA halves (tiRNA), which are 29–50 nt in length, the products of cleavage at the anticodon loop of the tRNA resulting in the 5′ tRNA fragment (5′tiRNA) and the 3′ tRNA fragment (3′tiRNA)[766]. In mammalian cells, the endonuclease angiogenin (ANG) was

found to be responsible for tRNA cleaving to produce tiRNA under various stress condition[466,762]. The second class of small tRNA fragments are tRNA-derived fragments (tRFs), shorter fragments with a length ranging from 14–30 nt. Unbiased short RNA sequencing has discovered this class of RNA fragments that mapped to tRNA loci[764]. Subsequent studies corroborate the existence of this novel small RNA class as a functional cellular biomolecule as evidenced by their importance in cell proliferation[767–769]. tRFs can be further divided into tRF-5, tRF-3, and tRF-1. tRF-5 contains the region from 5′end of tRNA to the D-loop or the region between the D-loop and the anticodon loop, with three specific size ranges of 14–16 nt, 22–24 nt, and 28–30 nt[764,770]. tRF-3 fragment contains the acceptor arms to the TψC loop and are between 18 and 22 nt in length[764]. tRF1 fragments are originated from the 3′end of the primary tRNA transcript, with their 5′end situated after the 3′end of the mature tRNA[764].

The fact that small tRNA fragments are induced during stress suggests that this class of small RNAs might be involved in some aspects of the cellular ISR, which include alteration of protein synthesis. Indeed, it has been found that the partially cleaved product of tRNA with RNAse A can inhibit protein synthesis in yeast and plant[465]. Similarly, Yamasaki *et al.* showed that transfection of tiRNAs derived from angiogenin cleavage inhibits translation in mammalian. These observations allow speculations for a role of small tRNA fragments in translation inhibition. Yet only a small fraction of the tRNA pools are cleaved, thus their levels do not seem to be sufficiently altered to affect the rate of translation elongation[466]. A subsequent study that analyzed the effect of both 5′ and 3′tiRNA on translation using luciferase translation reporter assay revealed that only a subset of tiRNA was capable of inhibiting translation of capped and uncapped mRNA, including 5′tiRNA from Ala-tRNA(GGC), Gly-tRNA(GCC), Gly-tRNA(CCC), and Cys-tRNA(GCA) as well as 3′tiRNA from Pro-tRNA[467]. Among them, 5′tiRNA-Ala was the most potent translation

inhibitor and was further showed to displace eIF4G and eIF4A from capped and uncapped *Renilla* luciferase mRNA when added to an in vitro transcription assay in rabbit reticulocyte lysate. This study attributed the translation repression effect of tiRNA to the terminal oligoguanine (TOG) motif found at the 5′end of $tRNA^{Ala}$ and $tRNA^{Cys}$; mutating this motif ablates the translation inhibition capacity of 5′tiRNA-Ala and 5′tiRNA-Cys, while introducing this motif into 5′tiRNA-Met renders this tiRNA the capacity to inhibit translation. The shorter tRFs were also shown to be capable of inhibiting translation, although in a mechanistically distinct manner than that of tiRNA. Various tRFs have been shown to associate with Argonaut proteins[771–773] and were found to repress the expression of transcripts in a sequence-specific manner[772]. Thus, tRFs might silence gene expression using the RNAi machinery. Intriguingly, data from virus infection discussed in the following paragraph also argue that the same machinery can be employed by tiRNA to inhibit translation. A study of ribosome-associated small RNA (RNome) in the archaeon *Haloferax volcanii* also observed that tRNA fragments can directly bind to ribosomes, which infer another potential mechanism where tRFs directly interfere with ribosome assembly or translation initiation/elongation[774]. Whether such an interaction with ribosomes occurs in mammalian cells, as well as the exact outcome of such an interaction on ribosome function and protein synthesis, are exciting questions open for future investigations.

As small tRNA fragments are induced during various stress conditions, their roles in the landscape of virus–host interaction are becoming clearer (**Figure 6.3.1b**). A number of studies have uncovered the involvement of tRNA fragments in virus infection and host response. Wang et al. reported that respiratory syncytial virus (RSV) infection significantly upregulated the level of 5′tiRNA in infected cells[468]. One of the highly induced 5′tiRNAs, 5′tiRNA-GluCTC, can silence luciferase reporter expression that contains a reverse complementary sequence of this tiRNA in

the 3′UTR. Importantly, treating the cells with an anti-5′tiRNA-GluCTC impaired RSV replication, suggesting that the induction of this tRNA fragment is beneficial for RSV infection. In a follow-up study from the same group, Deng et al. used biotinylated synthetic 5′tiRNA-GluCTC as a bait to search for enriched mRNAs that interact with this tRNA fragment. Combining with the list of genes with decreased abundance upon RSV infection, the author came up with potential targets of 5′tiRNA-GluCTC[469]. One of the candidate genes, APOER2, contains two short regions of 8 and 9 nt that are reverse-complement with 5′tiRNA-GluCTC. Importantly, while RSV infection was found to decrease APOER2 mRNAs abundance, treating infected cells with anti-5′tiRNA-GluCTC rescued this inhibition. Together, these two studies provide evidence that tRNA fragments are an integrated component of the virus–host interaction. While the tRNA fragments investigated in these studies seem to be proviral, as other cellular biomolecules such as miRNA and protein were found to be capable of both proviral and antiviral functions, it is likely that other tRNA fragments could also have antiviral function. Accordingly, other 5′tiRNA fragments that have been shown elsewhere to inhibit cap-dependent translation via displacing of components of the eIF4F complex[467] were also found to be upregulated in RSV-infected cells[468]. Thus, the induction of tRNA fragments by RSV or other viruses could also contribute to a global host-shutoff of protein synthesis, and the implication of this for virus infection is certainly an important subject for further investigations.

As mounting evidence suggests that tRNA fragments can accumulate during viral infection, the mechanisms behind such induction remain currently unaddressed. Although ANG was shown to be the main nuclease that generates tRNA fragments[466,762], ANG expression decreases during interferon treatment, a condition directly linked to virus infection[775–777], suggesting that other endonucleases might contribute to tRNA fragment genesis during virus infection. Aside from ANG,

there are a subset of ISGs that function as RNAses and might produce tRNA fragments from tRNA cleavages. For example, the gene Slfn11 discussed above is an ISG[753] that can also cleave type II tRNA[755]. The schlafen family was recently described to be a family of endonuclease that preferably targets tRNA, degrading from the 3′end and producing intact 5′ fragments. Thus, it is reasonable to speculate that the schlafen family, together with other undiscovered tRNA endonucleases, may contribute to the generation of tRNA fragments during specific virus infection[756]. This might also be another mechanism of schlafen-mediated translation inhibition on top of the reported mechanism of tRNA depletion.

6.3.4.3. m6A methylation: An important epi-transcriptomic modification

Methylation of RNA was first described in 1974 to be a common posttranscriptional modification for ribonucleotide[778,779]. Methylation was reported to occur on 0.2% of all total nucleotide in poly(A) RNAs, of which methylation of adenosine (m6A) accounts for 50% of all methylation[779]. Despite its relatively high occurrence, m6A only emerged recently as an important layer of genomic regulation in mammalian cells[780,781], corresponding with the development of techniques to survey genome-wide m6A methylation[782,783]. Since then, this modification has been reported to be involved in various physiological aspects including stress responses[784], stem cell reprogramming[785], circadian rhythm[786], oocyte maturation[787], and cancer[788]. Mechanistically, m6A was shown to affect splicing[782], cap-dependent translation initiation[789], miRNA processing[790], and mRNA stability[791].

The mechanisms that regulate m6A modification and function involve “writers” (m6A methyltransferases), “erasers” (m6A demethyltransferases), and “readers” (effectors that bind to m6A). Methylation of adenine on mRNA is not random, and it was reported that the motif RRACH (R = purine, H = A, C, or U) is the m6A consensus sequence, and methylation preferentially occurs

on the CDS and 3′UTR, particularly concentrating near the stop codon region[782,783]. The methyltransferase complex METTL3-METTL14, together with the accessory proteins WTAP, KIAA1429, RBM15, and ZC3H13 form a protein complex that adds a methyl group to adenosine residues of nuclear pre-mRNAs[792–798]. Demethylation of m6A was reported to be carried out by FTO or ALKHB5[799,800]. The function of m6A modification on target mRNAs depends on various "readers," effector proteins that are recruited by m6A. The YT521-B homology (YTH) family, its members include YTHDF1, YTHDF2, YTHDF3, YTHDC1, and YTHDC2, is the most well-studied group of reader proteins that regulates the effect of m6A[782,791,801,802]. Binding of some reader proteins enhances translation efficiency, such as the case for YTHDF1 and YTHDF3[801,802]. More specifically, YTHDF1 was reported to enhance ribosome loading on its target mRNAs via interaction with the translation initiation factors eIF3A and eIF3B[802]. In contrast, binding of YTHDF2 to target mRNAs promotes degradation via relocalization to mRNA decay sites such as P-bodies[791]. In another case, nuclear export of target mRNAs was enhanced by YTHDC1 via facilitation of interaction with the splicing factor SRSF3 and nuclear export adaptor NX1[803]. It is likely that other readers will be discovered in the near future that would have a diverse mode of action on mRNA translation and stability.

m6A is an important process in virus–host interaction (**Figure 6.3.1c**). m6A modification on viral mRNAs was first reported over three decades ago for RNA viruses[470,471,804,805] and more recently for DNA viruses[472,473,806]. Methylation of adenosine on viral mRNAs was shown to have complex effects on virus replication from positive to negative, and was recently reviewed elsewhere[475]. Regarding the effect of m6A on translation of viral mRNAs, it was reported that mutation of one methylated adenosine residue on HIV-1 RNA (A7883) results in impaired nuclear export, suggesting one mechanism by which m6A might affect viral mRNA translation[474].

However, considering that m6A has a wide range of effect on mRNA translation, it is highly possible that there are multiple mechanisms influencing viral protein synthesis that remain to be discovered. In addition to m6A modification to viral genes, translation control during host antiviral response can also be modulated via m6A. Indeed, increased N6 methylation might be a response to virus infection, as evidenced in HCMV and HIV-1 infection [474,807]. Interestingly, this upregulation has so far been shown to be negative for the antiviral response, as interferon-β mRNA was found to be m6A-methylated and this modification results in destabilization of this mRNA in an METTL3-YTHDF2-dependent manner[807]. Similarly, the RNA helicase DDX46 was reported to promote demethylation of MAVS, TRAF3, and TRAF6 mRNAs, which encode important signaling proteins for the antiviral response, and this demethylation inhibits their nuclear exports and impairs translation, ultimately decreasing interferon production[808]. In another study, VSV infection was shown to stimulate initially, then to decrease m6A modification in mouse peritoneal macrophage[809]. Demethylations are important for VSV replication, which is partially attributed to the activity of ALKBH5. This demethyltransferase enzyme was in turn shown to remove m6A modification on α-ketoglutarate dehydrogenase (OGDH) mRNAs, an important enzyme of the itaconate metabolic pathway that is required for VSV replication, resulted in increased stability and expression of OGDH mRNAs. However, the current knowledge of m6A in antiviral response does not exclude the possibility that this modification may also serve as a positive contributor for translation of antiviral genes, possibly depending on the specific interaction of individual mRNAs with different readers, an area that should be subject of further investigation.

6.3.4.4. Other potential mechanisms of translation control during virus–host interaction

Aside from the above discussed mechanisms, separated reports indicate that there are other mechanisms at play in the competition for the translation machinery by both the host and the virus

during infection. Although additional studies are required before robust models can be formulated, we feel that it is important to mention these intriguing observations in order to fully capture our current understanding of the translation landscape in virus–host interaction.

Spatial rearrangement of translation activity

mRNA translation can be regulated by spatial distribution of mRNAs[810]. Intriguingly, there is evidence of spatial redistribution of translation activity in infected cells, possibly due to active relocalization of translation factors including those involved in translation initiation and elongation. One line of evidence surrounds the formation of virus factories, active replication sites for viruses that are enriched in host membranes, ribosomes, and proteins, as well as viral nucleic acids and proteins[695]. Using the ribopuromycylation method to visualize subcellular translation activity, it has been reported that the virus factory of vaccinia virus and reovirus possess elevated translation activity compared to the surrounding cytoplasm. This advantage of increased translation was attributed to selective enrichment of tRNA-amino acyl synthetases in the case of vaccinia virus[117] or translation initiation, elongation, termination factor, and ribosomal proteins in the case of reovirus[118].

There are also subcellular locales that house nontranslating mRNAs, namely stress granules (SGs) for stalled mRNAs and processing bodies (PBs) for decaying mRNAs[811]. Of these granules, SG has been reported to be induced during virus infection, suggesting its involvement in virus–host interaction[71,72]. The formation of SG begins with stalled translation initiation on mRNA at the 5′UTR that causes ribosome run-off and exposes the downstream region of the mRNA to various SG-associated RNA-binding proteins TIA1, TIAR, and G3BP1 that subsequently aggregate to form RNA granules[620–622]. Such a mechanism of aggregation based on nucleation on naked single-stranded RNAs, together with the seclusion of various translation initiation factors in the stalled

translation initiation complex, proposes that SG formation might inhibit translation and replication of virus when the cytoplasm is overloaded with abnormal amounts of viral RNA. Intriguingly, viruses seem to evolve mechanisms to suppress SG formation. Okonski and Samuel have shown that SG formation was induced by measles virus (MeV) infection in a PKR-dependent manner[812]. However, MeV with a C protein knockout was a more efficient inducer of SG formation than wild-type MeV. It was determined that the intact C protein would lead to a decrease in PKR expression, which would subsequently allow for SG formation[813]. Similar function has been attributed to the influenza NS1 protein and vaccinia virus E3L protein[76,626]. The exact mechanism as well as the implication of SG suppression by viral proteins remains to be elucidated; nevertheless, this regulation might indicate a method to ensure that the host translation remains functional for the virus' replication.

Modification or exploitation of host translation machinery to favor virus translation

Mammalian mRNAs can contain *cis*-elements that modulate their translation activity in specific conditions. One example is the 5′ terminal oligo pyrimidine (5′TOP) motif that is situated at the 5′end of mRNAs of genes encoding protein components of the translation machinery[31]. TOP mRNAs are suppressed during stress conditions, largely regulated via the mTORC1 signaling pathway through its effector LARP1[23,24]. Intriguingly, mRNAs of certain viruses also contain *cis*-elements that enhance their translations via interaction with host RNA-binding proteins, in some case in an infected cells-specific manner. One example of a viral mRNA *cis*-element that enhances translation was reported in MeV on its nucleocapsid mRNA. It was observed that during a pathogenic MeV infection, the host cell undergoes global translation shutdown attributed to eIF2α phosphorylation[652,814]. Intriguingly, the mRNA of the nucleocapsid coding gene of MeV possesses a short stem-loop structure at its N-5′ terminus residues 1–15[100] that recruit the La/SSB (La)

autoantigen protein, a well-described human translation factor[815]. This in turn promotes the selective translation of N mRNA during a translational shutdown in MeV-infected cells, which is crucial for MeV production since it has been previously shown that the accumulation of N protein within an infected cell is required for efficient viral genome replication[816]. It is noteworthy to mention that LARP1, the RNA-binding protein that represses TOP mRNA translation, also belongs to the La protein family and similarly interacts with its target mRNAs via the 5′ terminal region of the 5′UTR, albeit conferring an opposite effect on translation[27]. Considering that LARP1 was found to be a positive modulator of extracellular hepatitis C virus infection and dengue virus replication[817,818], the role of the La protein family in virus translation might be an interesting subject for further investigation.

Another curious example of viral *cis*-element is the poly(A) leader sequences that are found on mRNAs of vaccinia virus late genes. Vaccinia genes are often described as early or late depending on when they are transcribed during the viral life cycle. Early genes are turned on immediately following entry and include virulence factors that take over the host cell[819], transcription factors for late genes[820], decapping enzymes[821], and genes with unknown function. Later in the viral life cycle, expression of late viral gene products is accompanied by their nontemplated 5′ polyadenylation[822]. First reported three decades ago, these nontemplated poly(A) sequences are added to the 5′end of mRNAs of late vaccinia virus genes, likely due to slipping of vaccinia polymerase at a poly-T motif in the promoter regions[94–96]. These poly(A) leaders promote translation in vaccinia-infected cells in a noncanonical cap-dependent manner that require most of the translation initiation components, but without the essential eIF3 and eIF4F[97,98]. The virus-specific enhancement is attributed to the activity of vaccinia virus kinase B1 that phosphorylates

the host small ribosomal protein RACK1, which enhances ribosome recruitment to poly(A) leader mRNAs[99].

In addition to modifying translation of viral mRNAs, the untranslated regions might also contribute to regulation of host mRNA expression in the antiviral state. It is well known that the 5′ and 3′ untranslated regions of mRNAs are rich in *cis*-elements that regulate their translation[823,824]. Recent studies reported that these untranslated regions are dynamically regulated in various contexts via alternative transcription start site (for 5′UTR) or alternative polyadenylation and termination (for 3′UTR) that consequently modulate gene expression via altered translation efficiency[521,825–827]. Curiously, VSV infection has also been reported to cause widespread shortening of host mRNA 3′UTR via alternative polyadenylation[828]. The shortening events occurred more frequently in genes functioning in antiviral and interferon signaling suggest that such 3′UTR shortening is an integrated antiviral response, potentially to enhance the translation efficiency of the antiviral mRNAs via removal of miRNA-binding site[826,829]. Our group has also reported that virus infection causes an alternative 5′UTR event that enhances the translation of the ciliopathy gene INPP5E, the expression of which inhibits HSV and VSV infection[311]. The canonical 5′UTR of INPP5E mRNA contains multiple uORFs, which strongly inhibits translation of its CDS. Virus infection induces the expression of an alternative, shorter 5′UTR that lacks an intron containing three of the repressive uORFs, thus de-repress the translation of INPP5E in infected conditions. Curiously, the SARS-CoV-2 receptor ACE2 is also an ISG[830] and gene information from NCBI indicates that ACE2 is translated from two transcript variants NM_001371415.1 and NM_021804.3; both possess the same CDS that encode the same protein but the latter harbors a longer 5′UTR with an intron. Thus, it will be intriguing to investigate if the antiviral state alters the transcript ratio of ACE2 or the splicing of the long 5′UTR. Altogether,

these data suggest that the global transcript variants are regulated by the antiviral state, which then affects the translational output of antiviral genes.

6.3.5. Conclusion and perspective

The field of translation control has accumulated extensive insight into the mechanisms of host cell- and virus-mediated translation regulation during infection and the antiviral state, as well as the outcomes of these regulations on the antiviral response and virus propagation. Our understanding so far emphasizes on the translation initiation step with various strategies outlined in Section 6.3.3 of this review, corroborating the importance of initiation in translation control in mammalian cells. However, emerging evidence suggests that there is much to learn about this interface of virus–host interaction. With the extension of our collective capacity to probe into more aspects of translational control such as tRNA pools, posttranscriptional modification, and translation rate, novel layers of regulation are slowly revealed, providing a more complex picture of translational regulation where almost every component of the host protein synthesis machinery can be altered. The advance of the tRNA fragments field adds one previously poorly understood noncoding RNA species, besides miRNA, as a player in translation control, including during virus–host interaction. Much remains to be explored regarding the biogenesis, mechanism of action, and outcome of tRNA fragments in the cells; yet considering the abundance of these tRNA products, such endeavors guarantee interesting discoveries. Recent studies regarding the tRNA pools also suggest a divergence from the constant tRNA pools model and suggest that modulation of tRNA abundance might play a role in host defense, while some antiviral-specific tRNA pools might play a role in shaping virus codon usage. Additionally, as tRNA fragments are generated from cleaved tRNAs, it is likely that the product of degradation of certain tRNAs also regulate translation, delivering a one-two punch to the cell protein synthesis. Last but not least, the revealed

effect of posttranscriptional mRNA modification on mRNA translation as well as its widespread occurrence on viral RNAs, of which m6A is the representative phenomenon, warrants further investigation.

As we advance our knowledge on this complex virus–host translation landscape, we are expanding our fundamental understanding of how one of the most ancient self-replicating organic systems can coexist successfully in a parasitic relationship with the most sophisticated organisms, including us humans. No less important than the fundamental understanding of this interaction, such knowledge will benefit a substantial number of medical applications that are virus-based, ranging from vaccine development, viral vectors to anticancer oncolytic viruses. For instance, in vaccine development, the method of recombinant viral vector vaccine relies on the expression of an antigen from a safe viral vector backbone, and is used to develop successful vaccines or other vaccines currently in clinical trials against various highly pathogenic viruses including SARS-CoV-2. As discussed in Section 6.3.4.1 of this review, the synonymous codon usage of the foreign antigen might need to be harmonized with the viral vector or a specific host tRNA pool to maximize the yield/efficacy depending on the specific application. Another example can be made in the engineering of anticancer oncolytic viruses where human transgenes are frequently incorporated into the virus genome to enhance immunotherapeutic efficacy[136]. The expression of therapeutic transgene as well as the overall fitness of the engineered oncolytic viruses will be enhanced if various translation regulation aspects, including but not limited to proper codon optimization and incorporation of virus-specific untranslated regions, are considered during the optimization process. Clearly these examples are just a minuscule representation of the vast number of potential improvements that translation control can contribute toward, and this will only continue to increase with the expansion of knowledge in this field.

6.3.6. Acknowledgments

We apologize for works that are not discussed and cited in our review due to space constraint. This review is supported in part by funding from the Canadian Breast Cancer Foundation/Canadian Cancer Society, the Natural Sciences and Engineering Research Council of Canada, and the Terry Fox Research Institute to T. A.

6.3.7. References

1. Sonenberg, N. & Hinnebusch, A. G. Regulation of Translation Initiation in Eukaryotes: Mechanisms and Biological Targets. *Cell* **136**, 731–745 (2009).
2. Jan, E., Mohr, I. & Walsh, D. A Cap-to-Tail Guide to mRNA Translation Strategies in Virus-Infected Cells. *Annu. Rev. Virol.* **3**, 283–307 (2016).
3. Mailliot, J. & Martin, F. Viral internal ribosomal entry sites: four classes for one goal. *Wiley Interdiscip. Rev. RNA* **9**, e1458 (2018).
4. Ingolia, N. T., Lareau, L. F. & Weissman, J. S. Ribosome profiling of mouse embryonic stem cells reveals the complexity and dynamics of mammalian proteomes. *Cell* **147**, 789–802 (2011).
5. Kearse, M. G. & Wilusz, J. E. Non-AUG translation: A new start for protein synthesis in eukaryotes. *Genes and Development* **31**, 1717–1731 (2017).
6. Jackson, R. J., Hellen, C. U. T. & Pestova, T. V. The mechanism of eukaryotic translation initiation and principles of its regulation. *Nature Reviews Molecular Cell Biology* **11**, 113–127 (2010).
7. Dever, T. E. & Green, R. The elongation, termination, and recycling phases of translation in eukaryotes. *Cold Spring Harb. Perspect. Biol.* **4**, 1–16 (2012).
8. Buttgereit, F. & Brand, M. D. A hierarchy of ATP-consuming processes in mammalian cells. *Biochem. J.* **312**, 163–167 (1995).
9. Bushell, M. & Sarnow, P. Hijacking the translation apparatus by RNA viruses. *Journal of Cell Biology* **158**, 395–399 (2002).
10. Hoang, H. D., Graber, T. E. & Alain, T. Battling for Ribosomes: Translational Control at the Forefront of the Antiviral Response. *Journal of Molecular Biology* **430**, 1965–1992 (2018).
11. Walsh, D., Mathews, M. B. & Mohr, I. Tinkering with Translation: Protein Synthesis in Virus-Infected Cells. *Cold Spring Harb. Perspect. Biol.* **5**, a012351–a012351 (2013).
12. Fonseca, B. D., Lahr, R. M., Damgaard, C. K., Alain, T. & Berman, A. J. LARP1 on TOP of ribosome production. *Wiley Interdisciplinary Reviews: RNA* **9**, e1480 (2018).
13. Saxton, R. A. & Sabatini, D. M. mTOR Signaling in Growth, Metabolism, and Disease. *Cell* **168**, 960–976 (2017).
14. Lekmine, F. *et al.* Activation of the p70 S6 kinase and phosphorylation of the 4E-BP1

repressor of mRNA translation by type I interferons. *J. Biol. Chem.* **278**, 27772–27780 (2003).
15. Kang, Y. *et al.* Transient activation of the PI3K/Akt pathway promotes Newcastle disease virus replication and enhances anti-apoptotic signaling responses. *Oncotarget* **8**, 23551–23563 (2017).
16. Soares, J. A. P. *et al.* Activation of the PI3K/Akt Pathway Early during Vaccinia and Cowpox Virus Infections Is Required for both Host Survival and Viral Replication. *J. Virol.* **83**, 6883–6899 (2009).
17. Zhu, L. *et al.* Biphasic activation of PI3K/Akt and MAPK/Erk1/2 signaling pathways in bovine herpesvirus type 1 infection of MDBK cells. *Vet. Res.* **42**, 57 (2011).
18. Alain, T. *et al.* Vesicular stomatitis virus oncolysis is potentiated by impairing mTORC1-dependent type I IFN production. **107**, 1576–1581 (2010).
19. Cao, W. *et al.* Toll-like receptor-mediated induction of type I interferon in plasmacytoid dendritic cells requires the rapamycin-sensitive PI(3)K-mTOR-p70S6K pathway. *Nat. Immunol.* **9**, 1157–64 (2008).
20. Colina, R. *et al.* Translational control of the innate immune response through IRF-7. *Nature* **452**, 323–328 (2008).
21. Nehdi, A. *et al.* Deficiency in Either 4E-BP1 or 4E-BP2 Augments Innate Antiviral Immune Responses. *PLoS One* **9**, e114854 (2014).
22. Zakaria, C. *et al.* Active-site mTOR inhibitors augment HSV1-dICP0 infection in cancer cells via dysregulated eIF4E/4E-BP axis. *PLOS Pathog.* **14**, e1007264 (2018).
23. Berlanga, J. J. *et al.* Antiviral effect of the mammalian translation initiation factor 2α kinase GCN2 against RNA viruses. *EMBO J.* **25**, 1730–1740 (2006).
24. Zhang, L. & Wang, A. Virus-induced ER stress and the unfolded protein response. *Front. Plant Sci.* **3**, 293 (2012).
25. Dauber, B. & Wolff, T. Activation of the Antiviral Kinase PKR and Viral Countermeasures. *Viruses* **1**, 523–544 (2009).
26. Nallagatla, S. R. *et al.* 5'-triphosphate-dependent activation of PKR by RNAs with short stem-loops. *Science* **318**, 1455–8 (2007).
27. Connor, J. H. & Lyles, D. S. Vesicular stomatitis virus infection alters the eIF4F translation initiation complex and causes dephosphorylation of the eIF4E binding protein 4E-BP1. *J. Virol.* **76**, 10177–87 (2002).
28. Ahmed, M. *et al.* Ability of the Matrix Protein of Vesicular Stomatitis Virus To Suppress Beta Interferon Gene Expression Is Genetically Correlated with the Inhibition of Host RNA and Protein Synthesis. *J. Virol.* **77**, 4646–4657 (2003).
29. Chuluunbaatar, U. *et al.* Constitutive mTORC1 activation by a herpesvirus Akt surrogate stimulates mRNA translation and viral replication. **24**, 2627–2639 (2010).
30. Couty, J. P., Geras-Raaka, E., Weksler, B. B. & Gershengorn, M. C. Kaposi's Sarcoma-associated Herpesvirus G Protein-coupled Receptor Signals through Multiple Pathways in Endothelial Cells. *J. Biol. Chem.* **276**, 33805–33811 (2001).
31. Ehrhardt, C. *et al.* Influenza A virus NS1 protein activates the PI3K/Akt pathway to mediate antiapoptotic signaling responses. *J. Virol.* **81**, 3058–67 (2007).
32. Frese, K. K. *et al.* Selective PDZ protein-dependent stimulation of phosphatidylinositol 3-kinase by the adenovirus E4-ORF1 oncoprotein. *Oncogene* **22**, 710–721 (2003).
33. Lu, Z. *et al.* Human papillomavirus 16 E6 oncoprotein interferences with insulin signaling pathway by binding to tuberin. *J. Biol. Chem.* **279**, 35664–35670 (2004).

34. Moorman, N. J. *et al.* Human Cytomegalovirus Protein UL38 Inhibits Host Cell Stress Responses by Antagonizing the Tuberous Sclerosis Protein Complex. *Cell Host Microbe* **3**, 253–262 (2008).
35. Portis, T. & Longnecker, R. Epstein-Barr virus (EBV) LMP2A mediates B-lymphocyte survival through constitutive activation of the Ras/PI3K/Akt pathway. *Oncogene* **23**, 8619–8628 (2004).
36. Werden, S. J. *et al.* The Myxoma Virus M-T5 Ankyrin Repeat Host Range Protein Is a Novel Adaptor That Coordinately Links the Cellular Signaling Pathways Mediated by Akt and Skp1 in Virus-Infected Cells. *J. Virol.* **83**, 12068–12083 (2009).
37. Hirata, N. *et al.* Inhibition of Akt kinase activity suppresses entry and replication of influenza virus. *Biochem. Biophys. Res. Commun.* **450**, 891–898 (2014).
38. Child, S. J., Hanson, L. K., Brown, C. E., Janzen, D. M. & Geballe, A. P. Double-Stranded RNA Binding by a Heterodimeric Complex of Murine Cytomegalovirus m142 and m143 Proteins. *J. Virol.* **80**, 10173–10180 (2006).
39. Hatada, E. & Fukuda, R. Binding of influenza a virus NS1 protein to dsRNA in vitro. *J. Gen. Virol.* **73**, 3325–3329 (1992).
40. Poppers, J., Mulvey, M., Perez, C., Khoo, D. & Mohr, I. Identification of a Lytic-Cycle Epstein-Barr Virus Gene Product That Can Regulate PKR Activation. *J. Virol.* **77**, 228–236 (2003).
41. Rabouw, H. H. *et al.* Middle East Respiratory Coronavirus Accessory Protein 4a Inhibits PKR-Mediated Antiviral Stress Responses. *PLOS Pathog.* **12**, e1005982 (2016).
42. Romano, P. R. *et al.* Inhibition of double-stranded RNA-dependent protein kinase PKR by vaccinia virus E3: role of complex formation and the E3 N-terminal domain. *Mol. Cell. Biol.* **18**, 7304–16 (1998).
43. Yue, Z. & Shatkin, A. J. Double-Stranded RNA-Dependent Protein Kinase (PKR) Is Regulated by Reovirus Structural Proteins. *Virology* **234**, 364–371 (1997).
44. Bierle, C. J., Semmens, K. M. & Geballe, A. P. Double-stranded RNA binding by the human cytomegalovirus PKR antagonist TRS1. *Virology* **442**, 28–37 (2013).
45. Carroll, K., Elroy-Stein, O., Moss, B. & Jagus, R. Recombinant vaccinia virus K3L gene product prevents activation of double- stranded RNA-dependent, initiation factor 2α-specific protein kinase. *J. Biol. Chem.* **268**, 12837–12842 (1993).
46. Gale, M. J., Korth, M. J. & Katze, M. G. Repression of the PKR protein kinase by the hepatitis C virus NS5A protein: a potential mechanism of interferon resistance. *Clin. Diagn. Virol.* **10**, 157–62 (1998).
47. Pavio, N., Romano, P. R., Graczyk, T. M., Feinstone, S. M. & Taylor, D. R. Protein Synthesis and Endoplasmic Reticulum Stress Can Be Modulated by the Hepatitis C Virus Envelope Protein E2 through the Eukaryotic Initiation Factor 2 Kinase PERK. *J. Virol.* **77**, 3578–3585 (2003).
48. Van Opdenbosch, N., Van den Broeke, C., De Regge, N., Tabares, E. & Favoreel, H. W. The IE180 Protein of Pseudorabies Virus Suppresses Phosphorylation of Translation Initiation Factor eIF2 . *J. Virol.* **86**, 7235–7240 (2012).
49. He, B., Gross, M. & Roizman, B. The γ134.5 protein of herpes simplex virus 1 complexes with protein phosphatase 1α to dephosphorylate the α subunit of the eukaryotic translation initiation factor 2 and preclude the shutoff of protein synthesis by double-stranded RNA-activated protein kinase. *Proc. Natl. Acad. Sci. U. S. A.* **94**, 843–848 (1997).
50. Kazemi, S. *et al.* Control of Subunit of Eukaryotic Translation Initiation Factor 2 (eIF2)

Phosphorylation by the Human Papillomavirus Type 18 E6 Oncoprotein: Implications for eIF2 -Dependent Gene Expression and Cell Death. *Mol. Cell. Biol.* **24**, 3415–3429 (2004).
51. Zhang, F., Moon, A., Childs, K., Goodbourn, S. & Dixon, L. K. The African Swine Fever Virus DP71L Protein Recruits the Protein Phosphatase 1 Catalytic Subunit To Dephosphorylate eIF2α and Inhibits CHOP Induction but Is Dispensable for These Activities during Virus Infection. *J. Virol.* **84**, 10681–10689 (2010).
52. Sung, S. C., Chao, C. Y., Jeng, K. S., Yang, J. Y. & Lai, M. M. C. The 8ab protein of SARS-CoV is a luminal ER membrane-associated protein and induces the activation of ATF6. *Virology* **387**, 402–413 (2009).
53. Darnell, A. M., Subramaniam, A. R. & O'shea, E. K. Translational Control through Differential Ribosome Pausing during Amino Acid Limitation in Mammalian Cells. *Mol. Cell* **71**, 229-243.e11 (2018).
54. Gardin, J. *et al.* Measurement of average decoding rates of the 61 sense codons in vivo. *Elife* **3**, (2014).
55. Peil, L. *et al.* Distinct XPPX sequence motifs induce ribosome stalling, which is rescued by the translation elongation factor EF-P. *Proc. Natl. Acad. Sci. U. S. A.* **110**, 15265–15270 (2013).
56. Gingold, H. & Pilpel, Y. Determinants of translation efficiency and accuracy. *Mol. Syst. Biol.* **7**, 481 (2011).
57. Gingold, H. *et al.* A dual program for translation regulation in cellular proliferation and differentiation. *Cell* **158**, 1281–1292 (2014).
58. Carbone, A. Codon bias is a major factor explaining phage evolution in translationally biased hosts. *J. Mol. Evol.* **66**, 210–223 (2008).
59. Lucks, J. B., Nelson, D. R., Kudla, G. R. & Plotkin, J. B. Genome Landscapes and Bacteriophage Codon Usage. *PLoS Comput. Biol.* **4**, e1000001 (2008).
60. Sharp, P. M., Rogers, M. S. & McConnell, D. J. Selection pressures on codon usage in the complete genome of bacteriophage T7. *J. Mol. Evol.* **21**, 150–160 (1985).
61. Bahir, I., Fromer, M., Prat, Y. & Linial, M. Viral adaptation to host: A proteome-based analysis of codon usage and amino acid preferences. *Mol. Syst. Biol.* **5**, (2009).
62. Bradel-Tretheway, B. G., Zhen, Z. & Dewhurst, S. Effects of codon-optimization on protein expression by the human herpesvirus 6 and 7 U51 open reading frame. *J. Virol. Methods* **111**, 145–56 (2003).
63. Ngumbela, K. C. *et al.* Quantitative effect of suboptimal codon usage on translational efficiency of mRNA encoding HIV-1 Gag in intact T cells. *PLoS One* **3**, e2356 (2008).
64. Sen, G. C. *et al.* Interferon Treatment of Ehrlich Ascites Tumor Cells: Effects on Exogenous mRNA Translation and tRNA Inactivation in the Cell Extract. *J. Virol.* **17**, 191–203 (1976).
65. Smith, B. L., Chen, G., Wilke, C. O. & Krug, R. M. Avian influenza virus PB1 gene in H3N2 viruses evolved in humans to reduce interferon inhibition by skewing codon usage toward interferon-altered tRNA pools. *MBio* **9**, (2018).
66. Ivashkiv, L. B. & Donlin, L. T. Regulation of type i interferon responses. *Nature Reviews Immunology* **14**, 36–49 (2014).
67. Platanias, L. C. Mechanisms of type-I- and type-II-interferon-mediated signalling. *Nature Reviews Immunology* **5**, 375–386 (2005).
68. Schoggins, J. W. & Rice, C. M. Interferon-stimulated genes and their antiviral effector functions. *Current Opinion in Virology* **1**, 519–525 (2011).

69. Espert, L. *et al.* ISG20, a new interferon-induced RNase specific for single-stranded RNA, defines an alternative antiviral pathway against RNA genomic viruses. *J. Biol. Chem.* **278**, 16151–16158 (2003).
70. Valdez, F. *et al.* Schlafen 11 Restricts Flavivirus Replication. *J. Virol.* **93**, (2019).
71. Kristiansen, H., Gad, H. H., Eskildsen-Larsen, S., Despres, P. & Hartmann, R. The oligoadenylate synthetase family: An ancient protein family with multiple antiviral activities. *Journal of Interferon and Cytokine Research* **31**, 41–47 (2011).
72. Li, M. *et al.* DNA damage-induced cell death relies on SLFN11-dependent cleavage of distinct type II tRNAs. *Nat. Struct. Mol. Biol.* **25**, 1047–1058 (2018).
73. Yang, J. Y. *et al.* Structure of Schlafen13 reveals a new class of tRNA/rRNA- targeting RNase engaged in translational control. *Nat. Commun.* **9**, 1–13 (2018).
74. Albers, S. & Czech, A. Exploiting tRNAs to boost virulence. *Life* **6**, (2016).
75. Nishida, K., Kawasaki, T., Fujie, M., Usami, S. & Yamada, T. Aminoacylation of tRNAs encoded by Chlorella virus CVK2. *Virology* **263**, 220–229 (1999).
76. Virgin, H. W. *et al.* Complete sequence and genomic analysis of murine gammaherpesvirus 68. *J. Virol.* **71**, 5894–5904 (1997).
77. Pavon-Eternod, M. *et al.* Vaccinia and influenza A viruses select rather than adjust tRNAs to optimize translation. *Nucleic Acids Res.* **41**, 1914–21 (2013).
78. David, A. *et al.* RNA binding targets aminoacyl-tRNA synthetases to translating ribosomes. *J. Biol. Chem.* **286**, 20688–20700 (2011).
79. Villanueva, E., Martí-Solano, M. & Fillat, C. Codon optimization of the adenoviral fiber negatively impacts structural protein expression and viral fitness. *Sci. Rep.* **6**, 1–10 (2016).
80. Chen, F. *et al.* Dissimilation of synonymous codon usage bias in virus–host coevolution due to translational selection. *Nat. Ecol. Evol.* 1–12 (2020). doi:10.1038/s41559-020-1124-7
81. Fu, H. *et al.* Stress induces tRNA cleavage by angiogenin in mammalian cells. *FEBS Lett.* **583**, 437–442 (2009).
82. Lee, S. R. & Collins, K. Starvation-induced cleavage of the tRNA anticodon loop in Tetrahymena thermophila. *J. Biol. Chem.* **280**, 42744–42749 (2005).
83. Lee, Y. S., Shibata, Y., Malhotra, A. & Dutta, A. A novel class of small RNAs: tRNA-derived RNA fragments (tRFs). *Genes Dev.* **23**, 2639–2649 (2009).
84. Thompson, D. M., Lu, C., Green, P. J. & Parker, R. tRNA cleavage is a conserved response to oxidative stress in eukaryotes. *RNA* **14**, 2095–2103 (2008).
85. Yamasaki, S., Ivanov, P., Hu, G. F. & Anderson, P. Angiogenin cleaves tRNA and promotes stress-induced translational repression. *J. Cell Biol.* **185**, 35–42 (2009).
86. Thompson, D. M. & Parker, R. Stressing Out over tRNA Cleavage. *Cell* **138**, 215–219 (2009).
87. Cole, C. *et al.* Filtering of deep sequencing data reveals the existence of abundant Dicer-dependent small RNAs derived from tRNAs. *RNA* **15**, 2147–2160 (2009).
88. Couvillion, M. T., Sachidanandam, R. & Collins, K. A growth-essential Tetrahymena Piwi protein carries tRNA fragment cargo. *Genes Dev.* **24**, 2742–2747 (2010).
89. Li, Z. *et al.* Extensive terminal and asymmetric processing of small RNAs from rRNAs, snoRNAs, snRNAs, and tRNAs. *Nucleic Acids Res.* **40**, 6787–99 (2012).
90. Kumar, P., Anaya, J., Mudunuri, S. B. & Dutta, A. Meta-analysis of tRNA derived RNA fragments reveals that they are evolutionarily conserved and associate with AGO proteins to recognize specific RNA targets. *BMC Med.* **12**, 78 (2014).

91. Zhang, S., Sun, L. & Kragler, F. The phloem-delivered RNA pool contains small noncoding RNAs and interferes with translation. *Plant Physiol.* **150**, 378–387 (2009).
92. Ivanov, P., Emara, M. M., Villen, J., Gygi, S. P. & Anderson, P. Angiogenin-Induced tRNA Fragments Inhibit Translation Initiation. *Mol. Cell* **43**, 613–623 (2011).
93. Haussecker, D. *et al.* Human tRNA-derived small RNAs in the global regulation of RNA silencing. *RNA* **16**, 673–695 (2010).
94. Maute, R. L. *et al.* TRNA-derived microRNA modulates proliferation and the DNA damage response and is down-regulated in B cell lymphoma. *Proc. Natl. Acad. Sci. U. S. A.* **110**, 1404–1409 (2013).
95. Yeung, M. L. *et al.* Pyrosequencing of small non-coding RNAs in HIV-1 infected cells: evidence for the processing of a viral-cellular double-stranded RNA hybrid. *Nucleic Acids Res.* **37**, 6575–86 (2009).
96. Gebetsberger, J., Zywicki, M., Künzi, A. & Polacek, N. tRNA-derived fragments target the ribosome and function as regulatory non-coding RNA in Haloferax volcanii. *Archaea* **2012**, 260909 (2012).
97. Wang, Q. *et al.* Identification and functional characterization of tRNA-derived RNA fragments (tRFs) in respiratory syncytial virus infection. *Mol. Ther.* **21**, 368–379 (2013).
98. Deng, J. *et al.* Respiratory Syncytial Virus Utilizes a tRNA Fragment to Suppress Antiviral Responses Through a Novel Targeting Mechanism. *Mol. Ther.* **23**, 1622–1629 (2015).
99. McNab, F. W. *et al.* TPL-2–ERK1/2 Signaling Promotes Host Resistance against Intracellular Bacterial Infection by Negative Regulation of Type I IFN Production. *J. Immunol.* **191**, 1732–1743 (2013).
100. Monocyte responses in the context of Q fever: from a static polarized model to a kinetic model of activation. - PubMed - NCBI. Available at: https://www.ncbi.nlm.nih.gov/pubmed/23801603. (Accessed: 29th March 2020)
101. Rock, R. B. *et al.* Transcriptional response of human microglial cells to interferon-γ. *Genes Immun.* **6**, 712–719 (2005).
102. Desrosiers, R., Friderici, K. & Rottman, F. Identification of methylated nucleosides in messenger RNA from Novikoff hepatoma cells. *Proc. Natl. Acad. Sci. U. S. A.* **71**, 3971–3975 (1974).
103. Wei, C. M., Gershowitz, A. & Moss, B. Methylated nucleotides block 5′ terminus of HeLa cell messenger RNA. *Cell* **4**, 379–386 (1975).
104. He, C. Grand Challenge Commentary: RNA epigenetics? *Nature Chemical Biology* **6**, 863–865 (2010).
105. Nilsen, T. W. Internal mRNA methylation finally finds functions. *Science* **343**, 1207–1208 (2014).
106. Dominissini, D. *et al.* Topology of the human and mouse m6A RNA methylomes revealed by m6A-seq. *Nature* **485**, 201–206 (2012).
107. Meyer, K. D. *et al.* Comprehensive analysis of mRNA methylation reveals enrichment in 3′ UTRs and near stop codons. *Cell* **149**, 1635–1646 (2012).
108. Zhou, J. *et al.* Dynamic m6 A mRNA methylation directs translational control of heat shock response. *Nature* **526**, 591–594 (2015).
109. Chen, T. *et al.* M6A RNA methylation is regulated by microRNAs and promotes reprogramming to pluripotency. *Cell Stem Cell* **16**, 289–301 (2015).
110. Fustin, J. M. *et al.* XRNA-methylation-dependent RNA processing controls the speed of

the circadian clock. *Cell* **155**, 793 (2013).
111. Ivanova, I. *et al.* The RNA m6A Reader YTHDF2 Is Essential for the Post-transcriptional Regulation of the Maternal Transcriptome and Oocyte Competence. *Mol. Cell* **67**, 1059-1067.e4 (2017).
112. Pan, Y., Ma, P., Liu, Y., Li, W. & Shu, Y. Multiple functions of m6A RNA methylation in cancer. *Journal of Hematology and Oncology* **11**, 48 (2018).
113. Meyer, K. D. *et al.* 5′ UTR m6A Promotes Cap-Independent Translation. *Cell* **163**, 999–1010 (2015).
114. Alarcón, C. R., Lee, H., Goodarzi, H., Halberg, N. & Tavazoie, S. F. N6-methyladenosine marks primary microRNAs for processing. *Nature* **519**, 482–485 (2015).
115. Wang, X. *et al.* N 6-methyladenosine-dependent regulation of messenger RNA stability. *Nature* **505**, 117–120 (2014).
116. Guo, J., Tang, H. W., Li, J., Perrimon, N. & Yan, D. Xio is a component of the Drosophila sex determination pathway and RNA N6-methyladenosine methyltransferase complex. *Proc. Natl. Acad. Sci. U. S. A.* **115**, 3674–3679 (2018).
117. Knuckles, P. *et al.* Zc3h13/Flacc is required for adenosine methylation by bridging the mRNA-binding factor RbM15/spenito to the m6 a machinery component Wtap/Fl(2)d. *Genes Dev.* **32**, 415–429 (2018).
118. Kobayashi, M. *et al.* The RNA Methyltransferase Complex of WTAP, METTL3, and METTL14 Regulates Mitotic Clonal Expansion in Adipogenesis. *Mol. Cell. Biol.* **38**, (2018).
119. Patil, D. P. *et al.* M6 A RNA methylation promotes XIST-mediated transcriptional repression. *Nature* **537**, 369–373 (2016).
120. Schwartz, S. *et al.* Perturbation of m6A writers reveals two distinct classes of mRNA methylation at internal and 5' sites. *Cell Rep.* **8**, 284–296 (2014).
121. Wen, J. *et al.* Zc3h13 Regulates Nuclear RNA m6A Methylation and Mouse Embryonic Stem Cell Self-Renewal. *Mol. Cell* **69**, 1028-1038.e6 (2018).
122. Yao, Q. J. *et al.* Mettl3–Mettl14 methyltransferase complex regulates the quiescence of adult hematopoietic stem cells. *Cell Research* **28**, 952–954 (2018).
123. Jia, G. *et al.* N6-Methyladenosine in nuclear RNA is a major substrate of the obesity-associated FTO. *Nat. Chem. Biol.* **7**, 885–887 (2011).
124. Zheng, G. *et al.* ALKBH5 Is a Mammalian RNA Demethylase that Impacts RNA Metabolism and Mouse Fertility. *Mol. Cell* **49**, 18–29 (2013).
125. Shi, H. *et al.* YTHDF3 facilitates translation and decay of N 6-methyladenosine-modified RNA. *Cell Res.* **27**, 315–328 (2017).
126. Wang, X. *et al.* N6-methyladenosine modulates messenger RNA translation efficiency. *Cell* **161**, 1388–1399 (2015).
127. Roundtree, I. A. *et al.* YTHDC1 mediates nuclear export of N6-methyladenosine methylated mRNAs. *Elife* **6**, (2017).
128. Kane, S. E. & Beemon, K. Precise localization of m6A in Rous sarcoma virus RNA reveals clustering of methylation sites: implications for RNA processing. *Mol. Cell. Biol.* **5**, 2298–2306 (1985).
129. Krug, R. M., Morgan, M. A. & Shatkin, A. J. Influenza viral mRNA contains internal N6-methyladenosine and 5'-terminal 7-methylguanosine in cap structures. *J. Virol.* **20**, 45–53 (1976).
130. Stoltzfus, C. M. & Dimock, K. Evidence of methylation of B77 avian sarcoma virus

genome RNA subunits. *J. Virol.* **18**, 586–95 (1976).
131. Thomason, A. R., Brian, D. A., Velicer, L. F. & Rottman, F. M. Methylation of high-molecular-weight subunit RNA of feline leukemia virus. *J. Virol.* **20**, 123–32 (1976).
132. Hesser, C. R., Karijolich, J., Dominissini, D., He, C. & Glaunsinger, B. A. N6-methyladenosine modification and the YTHDF2 reader protein play cell type specific roles in lytic viral gene expression during Kaposi's sarcoma-associated herpesvirus infection. *PLoS Pathog.* **14**, (2018).
133. Tsai, K., Courtney, D. G. & Cullen, B. R. Addition of m6A to SV40 late mRNAs enhances viral structural gene expression and replication. *PLoS Pathog.* **14**, e1006919 (2018).
134. Ye, F., Chen, E. R. & Nilsen, T. W. Kaposi's Sarcoma-Associated Herpesvirus Utilizes and Manipulates RNA N6-Adenosine Methylation To Promote Lytic Replication. *J. Virol.* **91**, (2017).
135. Dang, W. *et al.* N6-methyladenosine and viral infection. *Front. Microbiol.* **10**, (2019).
136. Lichinchi, G. *et al.* Dynamics of the human and viral m(6)A RNA methylomes during HIV-1 infection of T cells. *Nat. Microbiol.* **1**, 16011 (2016).
137. Winkler, R. *et al.* m 6 A modification controls the innate immune response to infection by targeting type I interferons. *Nat. Immunol.* **20**, 173–182 (2019).
138. Zheng, Q., Hou, J., Zhou, Y., Li, Z. & Cao, X. The RNA helicase DDX46 inhibits innate immunity by entrapping m 6 A-demethylated antiviral transcripts in the nucleus. *Nat. Immunol.* **18**, 1094–1103 (2017).
139. Liu, Y. *et al.* N6-methyladenosine RNA modification–mediated cellular metabolism rewiring inhibits viral replication. *Science (80-.).* **365**, 1171–1176 (2019).
140. Martin, K. C. & Ephrussi, A. mRNA Localization: Gene Expression in the Spatial Dimension. *Cell* **136**, 719–730 (2009).
141. Netherton, C. L. & Wileman, T. Virus factories, double membrane vesicles and viroplasm generated in animal cells. *Current Opinion in Virology* **1**, 381–387 (2011).
142. Desmet, E. A., Anguish, L. J. & Parker, J. S. L. Virus-mediated compartmentalization of the host translational machinery. *MBio* **5**, (2014).
143. Anderson, P. & Kedersha, N. RNA granules. *Journal of Cell Biology* **172**, 803–808 (2006).
144. Ruggieri, A. *et al.* Dynamic Oscillation of Translation and Stress Granule Formation Mark the Cellular Response to Virus Infection. *Cell Host Microbe* **12**, 71–85 (2012).
145. White, J. P., Cardenas, A. M., Marissen, W. E. & Lloyd, R. E. Inhibition of Cytoplasmic mRNA Stress Granule Formation by a Viral Proteinase. *Cell Host Microbe* **2**, 295–305 (2007).
146. Gilks, N. *et al.* Stress granule assembly is mediated by prion-like aggregation of TIA-1. *Mol. Biol. Cell* **15**, 5383–5398 (2004).
147. Matsuki, H. *et al.* Both G3BP1 and G3BP2 contribute to stress granule formation. *Genes to Cells* **18**, 135–146 (2013).
148. Tourrière, H. *et al.* The RasGAP-associated endoribonuclease G3BP assembles stress granules. *J. Cell Biol.* **160**, 823–831 (2003).
149. Okonski, K. M. & Samuel, C. E. Stress Granule Formation Induced by Measles Virus Is Protein Kinase PKR Dependent and Impaired by RNA Adenosine Deaminase ADAR1. *J. Virol.* **87**, 756–766 (2013).
150. Jiang, Y., Qin, Y. & Chen, M. Host-pathogen interactions in measles virus replication and

anti-viral immunity. *Viruses* **8**, (2016).
151. Khaperskyy, D. A., Hatchette, T. F. & McCormick, C. Influenza A virus inhibits cytoplasmic stress granule formation. *FASEB J.* **26**, 1629–1639 (2012).
152. Simpson-Holley, M. *et al.* Formation of antiviral cytoplasmic granules during orthopoxvirus infection. *J. Virol.* **85**, 1581–93 (2011).
153. Meyuhas, O. & Kahan, T. The race to decipher the top secrets of TOP mRNAs. *Biochimica et Biophysica Acta - Gene Regulatory Mechanisms* **1849**, 801–811 (2015).
154. Fonseca, B. D. *et al.* La-related Protein 1 (LARP1) Represses Terminal Oligopyrimidine (TOP) mRNA Translation Downstream of mTOR Complex 1 (mTORC1). *J. Biol. Chem.* **290**, 15996–6020 (2015).
155. Thoreen, C. C. *et al.* A unifying model for mTORC1-mediated regulation of mRNA translation. *Nature* **485**, 109–113 (2012).
156. Inoue, Y., Tsukiyama-Kohara, K., Yoneda, M., Sato, H. & Kai, C. Inhibition of host protein synthesis in B95a cells infected with the HL strain of measles virus. *Comp. Immunol. Microbiol. Infect. Dis.* **32**, 29–41 (2009).
157. Sato, H. *et al.* Measles virus N protein inhibits host translation by binding to eIF3-p40. *J. Virol.* **81**, 11569–76 (2007).
158. Inoue, Y. *et al.* Selective translation of the measles virus nucleocapsid mRNA by La protein. *Front. Microbiol.* **2**, (2011).
159. Intine, R. V., Tenenbaum, S. A., Sakulich, A. L., Keene, J. D. & Maraia, R. J. Differential phosphorylation and subcellular localization of La RNPs associated with precursor tRNAs and translation-related mRNAs. *Mol. Cell* **12**, 1301–1307 (2003).
160. Lamb, R. A. & Parks, G. D. Paramyxoviridae: the viruses and their replication. 957–995 (2013).
161. Plissonnier, M. L. *et al.* LARP1 binding to hepatitis C virus particles is correlated with intracellular retention of viral infectivity. *Virus Res.* **271**, 197679 (2019).
162. Suzuki, Y. *et al.* Characterization of RyDEN (C19orf66) as an Interferon-Stimulated Cellular Inhibitor against Dengue Virus Replication. *PLOS Pathog.* **12**, e1005357 (2016).
163. Assarsson, E. *et al.* Kinetic analysis of a complete poxvirus transcriptome reveals an immediate-early class of genes. *Proc. Natl. Acad. Sci. U. S. A.* **105**, 2140–2145 (2008).
164. Rosales, R., Sutter, G. & Moss, B. A cellular factor is required for transcription of vaccinia viral intermediate-stage genes. *Proc. Natl. Acad. Sci. U. S. A.* **91**, 3794–3798 (1994).
165. Liu, S.-W., Wyatt, L. S., Orandle, M. S., Minai, M. & Moss, B. The D10 decapping enzyme of vaccinia virus contributes to decay of cellular and viral mRNAs and to virulence in mice. *J. Virol.* **88**, 202–11 (2014).
166. Yang, Z., Bruno, D. P., Martens, C. A., Porcella, S. F. & Moss, B. Genome-wide analysis of the 5’ and 3’ ends of vaccinia virus early mRNAs delineates regulatory sequences of annotated and anomalous transcripts. *J. Virol.* **85**, 5897–909 (2011).
167. Ahn, B. Y. & Moss, B. Capped poly(A) leaders of variable lengths at the 5’ ends of vaccinia virus late mRNAs. *J. Virol.* **63**, 226–232 (1989).
168. Ink, B. S. & Pickup, D. J. Vaccinia virus directs the synthesis of early mRNAs containing 5′ poly(A) sequences. *Proc. Natl. Acad. Sci. U. S. A.* **87**, 1536–1540 (1990).
169. Schwer, B., Visca, P., Vos, J. C. & Stunnenberg, H. G. Discontinuous transcription or RNA processing of vaccinia virus late messengers results in a 5′ poly(A) leader. *Cell* **50**, 163–169 (1987).

170. Dhungel, P., Cao, S. & Yang, Z. The 5'-poly(A) leader of poxvirus mRNA confers a translational advantage that can be achieved in cells with impaired cap-dependent translation. *PLoS Pathog.* **13**, e1006602 (2017).
171. Shirokikh, N. E. & Spirin, A. S. Poly(A) leader of eukaryotic mRNA bypasses the dependence of translation on initiation factors. *Proc. Natl. Acad. Sci. U. S. A.* **105**, 10738–10743 (2008).
172. Jha, S. *et al.* Trans-kingdom mimicry underlies ribosome customization by a poxvirus kinase. *Nature* **546**, 651–655 (2017).
173. Hinnebusch, A. G., Ivanov, I. P. & Sonenberg, N. Translational control by 5′-untranslated regions of eukaryotic mRNAs. *Science* **352**, 1413–1416 (2016).
174. Mayr, C. Regulation by 3′-Untranslated Regions. *Annu. Rev. Genet.* **51**, 171–194 (2017).
175. Cheng, Z. *et al.* Pervasive, Coordinated Protein-Level Changes Driven by Transcript Isoform Switching during Meiosis In Brief A single transcription factor can coordinate control of both up-and down-regulation of protein production through induction of alternative transcripts. *Cell* **172**, 910–923 (2018).
176. Floor, S. N. & Doudna, J. A. Tunable protein synthesis by transcript isoforms in human cells. *Elife* **5**, (2016).
177. Mayr, C. & Bartel, D. P. Widespread Shortening of 3′UTRs by Alternative Cleavage and Polyadenylation Activates Oncogenes in Cancer Cells. *Cell* **138**, 673–684 (2009).
178. Wang, X., Hou, J., Quedenau, C. & Chen, W. Pervasive isoform-specific translational regulation via alternative transcription start sites in mammals. *Mol. Syst. Biol.* **12**, 875 (2016).
179. Jia, X. *et al.* The role of alternative polyadenylation in the antiviral innate immune response. *Nat. Commun.* **8**, 1–12 (2017).
180. Fu, Y. *et al.* Crosstalk between alternative polyadenylation and miRNAs in the regulation of protein translational efficiency. *Genome Res.* **28**, 1656–1663 (2018).
181. Hoang, H. D. *et al.* Induction of an Alternative mRNA 5′ Leader Enhances Translation of the Ciliopathy Gene Inpp5e and Resistance to Oncolytic Virus Infection. *Cell Rep.* **29**, 4010-4023.e5 (2019).
182. Ziegler, C. G. K. *et al.* SARS-CoV-2 receptor ACE2 is an interferon-stimulated gene in human airway epithelial cells and is detected in specific cell subsets across tissues. *Cell* **0**, (2020).
183. Seymour, L. W. & Fisher, K. D. Oncolytic viruses: Finally delivering. *British Journal of Cancer* **114**, 357–361 (2016).

6.4 Copyrights

Full article reprinted from Cell Reports (**Chapter 2)**:

Hoang, H.-D. *et al.* Induction of an Alternative mRNA 5′ Leader Enhances Translation of the Ciliopathy Gene Inpp5e and Resistance to Oncolytic Virus Infection. *Cell Rep.* **29**, 4010-4023.e5 (2019)

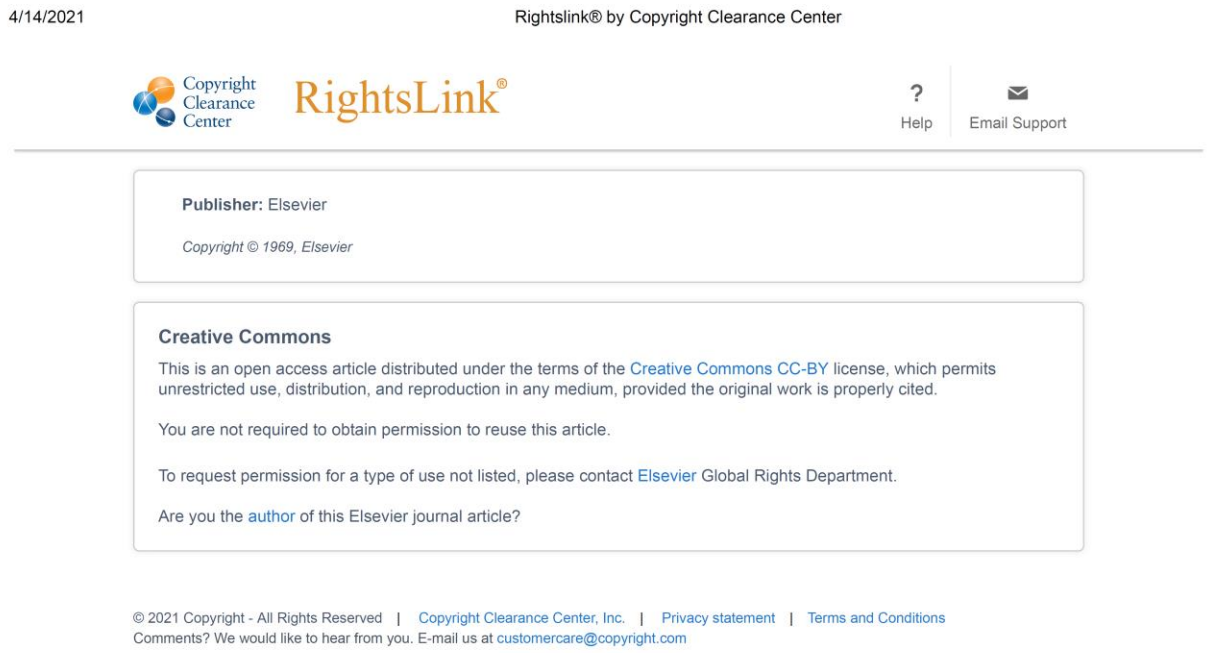

4/14/2021 Rightslink® by Copyright Clearance Center

Copyright Clearance Center RightsLink® ? Help Email Support

Publisher: Elsevier

Copyright © 1969, Elsevier

Creative Commons

This is an open access article distributed under the terms of the Creative Commons CC-BY license, which permits unrestricted use, distribution, and reproduction in any medium, provided the original work is properly cited.

You are not required to obtain permission to reuse this article.

To request permission for a type of use not listed, please contact Elsevier Global Rights Department.

Are you the author of this Elsevier journal article?

© 2021 Copyright - All Rights Reserved | Copyright Clearance Center, Inc. | Privacy statement | Terms and Conditions
Comments? We would like to hear from you. E-mail us at customercare@copyright.com

Figures reprinted from Journal of Molecular Biology (**Figure 1.1** and **1.3**) and full article reprinted from Journal of Molecular Biology (**Apendix 6.2**)

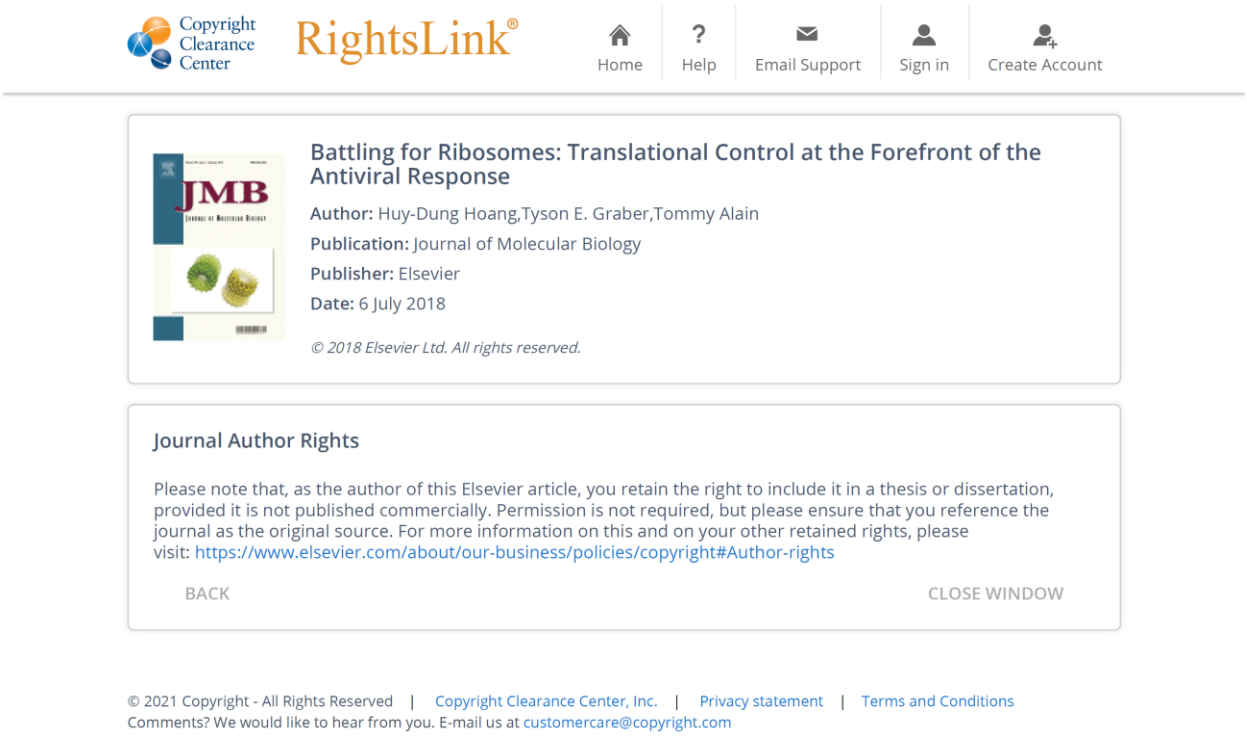

Copyright Clearance Center RightsLink®

Home | Help | Email Support | Sign in | Create Account

Battling for Ribosomes: Translational Control at the Forefront of the Antiviral Response

Author: Huy-Dung Hoang,Tyson E. Graber,Tommy Alain

Publication: Journal of Molecular Biology

Publisher: Elsevier

Date: 6 July 2018

© 2018 Elsevier Ltd. All rights reserved.

Journal Author Rights

Please note that, as the author of this Elsevier article, you retain the right to include it in a thesis or dissertation, provided it is not published commercially. Permission is not required, but please ensure that you reference the journal as the original source. For more information on this and on your other retained rights, please visit: https://www.elsevier.com/about/our-business/policies/copyright#Author-rights

BACK CLOSE WINDOW

© 2021 Copyright - All Rights Reserved | Copyright Clearance Center, Inc. | Privacy statement | Terms and Conditions

Comments? We would like to hear from you. E-mail us at customercare@copyright.com

Full article reprinted from Wiley Interdisciplinary Reviews: RNA (**Appendix 6.3**)

JOHN WILEY AND SONS LICENSE
TERMS AND CONDITIONS

Apr 14, 2021

This Agreement between Mr. Huy-Dung Hoang ("You") and John Wiley and Sons ("John Wiley and Sons") consists of your license details and the terms and conditions provided by John Wiley and Sons and Copyright Clearance Center.

License Number	5047870564357
License date	Apr 14, 2021
Licensed Content Publisher	John Wiley and Sons
Licensed Content Publication	WILEY INTERDISCIPLINARY REVIEWS: RNA
Licensed Content Title	Emerging translation strategies during virus–host interaction
Licensed Content Author	Huy-Dung Hoang, Serge Neault, Adrian Pelin, et al
Licensed Content Date	Aug 5, 2020
Licensed Content Pages	1
Type of use	Dissertation/Thesis
Requestor type	Author of this Wiley article
Format	Print and electronic

Portion	Full article
Will you be translating?	No
Title	Translation control to improve oncolytic virus efficacy and regulate inflammatory diseases
Institution name	University of Ottawa, Ottawa, Canada
Expected presentation date	Jun 2021
Requestor Location	Mr. Huy-Dung Hoang Attn: Mr. Huy-Dung Hoang
Publisher Tax ID	EU826007151
Total	0.00 CAD
Terms and Conditions	

TERMS AND CONDITIONS

This copyrighted material is owned by or exclusively licensed to John Wiley & Sons, Inc. or one of its group companies (each a"Wiley Company") or handled on behalf of a society with which a Wiley Company has exclusive publishing rights in relation to a particular work (collectively "WILEY"). By clicking "accept" in connection with completing this licensing transaction, you agree that the following terms and conditions apply to this transaction (along with the billing and payment terms and conditions established by the Copyright Clearance Center Inc., ("CCC's Billing and Payment terms and conditions"), at the time that you opened your RightsLink account (these are available at any time at http://myaccount.copyright.com).

Terms and Conditions

- The materials you have requested permission to reproduce or reuse (the "Wiley Materials") are protected by copyright.

- You are hereby granted a personal, non-exclusive, non-sub licensable (on a stand-alone basis), non-transferable, worldwide, limited license to reproduce the Wiley Materials for the purpose specified in the licensing process. This license, **and any CONTENT (PDF or image file) purchased as part of your order,** is for a one-time use only and limited to any maximum distribution number specified in the license. The first instance of republication or reuse granted by this license must be completed within two years of the date of the grant of this license (although copies prepared before the end date may be distributed thereafter). The Wiley Materials shall not be used in any other manner or for any other purpose, beyond what is granted in the license. Permission is granted subject to an appropriate acknowledgement given to the author, title of the material/book/journal and the publisher. You shall also duplicate the copyright notice that appears in the Wiley publication in your use of the Wiley Material. Permission is also granted on the understanding that nowhere in the text is a previously published source acknowledged for all or part of this Wiley Material. Any third party content is expressly excluded from this permission.

- With respect to the Wiley Materials, all rights are reserved. Except as expressly granted by the terms of the license, no part of the Wiley Materials may be copied, modified, adapted (except for minor reformatting required by the new Publication), translated, reproduced, transferred or distributed, in any form or by any means, and no derivative works may be made based on the Wiley Materials without the prior permission of the respective copyright owner.**For STM Signatory Publishers clearing permission under the terms of the STM Permissions Guidelines only, the terms of the license are extended to include subsequent editions and for editions in other languages, provided such editions are for the work as a whole in situ and does not involve the separate exploitation of the permitted figures or extracts,** You may not alter, remove or suppress in any manner any copyright, trademark or other notices displayed by the Wiley Materials. You may not license, rent, sell, loan, lease, pledge, offer as security, transfer or assign the Wiley Materials on a stand-alone basis, or any of the rights granted to you hereunder to any other person.

- The Wiley Materials and all of the intellectual property rights therein shall at all times remain the exclusive property of John Wiley & Sons Inc, the Wiley Companies, or their respective licensors, and your interest therein is only that of having possession of and the right to reproduce the Wiley Materials pursuant to Section 2 herein during the continuance of this Agreement. You agree that you own no right, title or interest in or to the Wiley Materials or any of the intellectual property rights therein. You shall have no rights hereunder other than the license as provided for above in Section 2. No right, license or interest to any trademark, trade name, service mark or other branding ("Marks") of WILEY or its licensors is granted hereunder, and you agree that you shall not assert any such right, license or interest with respect thereto

- NEITHER WILEY NOR ITS LICENSORS MAKES ANY WARRANTY OR REPRESENTATION OF ANY KIND TO YOU OR ANY THIRD PARTY, EXPRESS, IMPLIED OR STATUTORY, WITH RESPECT TO THE MATERIALS OR THE ACCURACY OF ANY INFORMATION CONTAINED IN THE MATERIALS, INCLUDING, WITHOUT LIMITATION, ANY IMPLIED WARRANTY OF MERCHANTABILITY, ACCURACY, SATISFACTORY QUALITY, FITNESS FOR A PARTICULAR PURPOSE, USABILITY, INTEGRATION OR NON-INFRINGEMENT AND ALL SUCH WARRANTIES ARE HEREBY EXCLUDED BY WILEY AND ITS LICENSORS AND WAIVED BY YOU.

- WILEY shall have the right to terminate this Agreement immediately upon breach of this Agreement by you.

- You shall indemnify, defend and hold harmless WILEY, its Licensors and their respective directors, officers, agents and employees, from and against any actual or threatened claims, demands, causes of action or proceedings arising from any breach of this Agreement by you.

- IN NO EVENT SHALL WILEY OR ITS LICENSORS BE LIABLE TO YOU OR ANY OTHER PARTY OR ANY OTHER PERSON OR ENTITY FOR ANY SPECIAL, CONSEQUENTIAL, INCIDENTAL, INDIRECT, EXEMPLARY OR PUNITIVE DAMAGES, HOWEVER CAUSED, ARISING OUT OF OR IN CONNECTION WITH THE DOWNLOADING, PROVISIONING, VIEWING OR USE OF THE MATERIALS REGARDLESS OF THE FORM OF ACTION, WHETHER FOR BREACH OF CONTRACT, BREACH OF WARRANTY, TORT, NEGLIGENCE, INFRINGEMENT OR OTHERWISE (INCLUDING, WITHOUT LIMITATION, DAMAGES BASED ON LOSS OF PROFITS, DATA, FILES, USE, BUSINESS OPPORTUNITY OR CLAIMS OF THIRD PARTIES), AND WHETHER OR NOT THE PARTY HAS BEEN ADVISED OF THE POSSIBILITY OF SUCH DAMAGES. THIS LIMITATION SHALL APPLY NOTWITHSTANDING ANY FAILURE OF ESSENTIAL PURPOSE OF ANY LIMITED REMEDY PROVIDED HEREIN.

- Should any provision of this Agreement be held by a court of competent jurisdiction to be illegal, invalid, or unenforceable, that provision shall be deemed amended to achieve as nearly as possible the same economic effect as the original provision, and the legality, validity and enforceability of the remaining provisions of this Agreement shall not be affected or impaired thereby.

- The failure of either party to enforce any term or condition of this Agreement shall not constitute a waiver of either party's right to enforce each and every term and condition of this Agreement. No breach under this agreement shall be deemed waived or excused by either party unless such waiver or consent is in writing signed by the party granting such waiver or consent. The waiver by or consent of a party to a breach of any provision of this Agreement shall not operate or be construed as a waiver of or consent to any other or subsequent breach by such other party.

- This Agreement may not be assigned (including by operation of law or otherwise) by you without WILEY's prior written consent.

- Any fee required for this permission shall be non-refundable after thirty (30) days from receipt by the CCC.

- These terms and conditions together with CCC's Billing and Payment terms and conditions (which are incorporated herein) form the entire agreement between you and WILEY concerning this licensing transaction and (in the absence of fraud) supersedes all prior agreements and representations of the parties, oral or written. This Agreement may not be amended except in writing signed by both parties. This Agreement shall be binding upon and inure to the benefit of the parties' successors, legal representatives, and authorized assigns.

- In the event of any conflict between your obligations established by these terms and conditions and those established by CCC's Billing and Payment terms and conditions,

these terms and conditions shall prevail.

- WILEY expressly reserves all rights not specifically granted in the combination of (i) the license details provided by you and accepted in the course of this licensing transaction, (ii) these terms and conditions and (iii) CCC's Billing and Payment terms and conditions.

- This Agreement will be void if the Type of Use, Format, Circulation, or Requestor Type was misrepresented during the licensing process.

- This Agreement shall be governed by and construed in accordance with the laws of the State of New York, USA, without regards to such state's conflict of law rules. Any legal action, suit or proceeding arising out of or relating to these Terms and Conditions or the breach thereof shall be instituted in a court of competent jurisdiction in New York County in the State of New York in the United States of America and each party hereby consents and submits to the personal jurisdiction of such court, waives any objection to venue in such court and consents to service of process by registered or certified mail, return receipt requested, at the last known address of such party.

WILEY OPEN ACCESS TERMS AND CONDITIONS

Wiley Publishes Open Access Articles in fully Open Access Journals and in Subscription journals offering Online Open. Although most of the fully Open Access journals publish open access articles under the terms of the Creative Commons Attribution (CC BY) License only, the subscription journals and a few of the Open Access Journals offer a choice of Creative Commons Licenses. The license type is clearly identified on the article.

The Creative Commons Attribution License

The Creative Commons Attribution License (CC-BY) allows users to copy, distribute and transmit an article, adapt the article and make commercial use of the article. The CC-BY license permits commercial and non-

Creative Commons Attribution Non-Commercial License

The Creative Commons Attribution Non-Commercial (CC-BY-NC)License permits use, distribution and reproduction in any medium, provided the original work is properly cited and is not used for commercial purposes.(see below)

Creative Commons Attribution-Non-Commercial-NoDerivs License

The Creative Commons Attribution Non-Commercial-NoDerivs License (CC-BY-NC-ND) permits use, distribution and reproduction in any medium, provided the original work is properly cited, is not used for commercial purposes and no modifications or adaptations are made. (see below)

Use by commercial "for-profit" organizations

Use of Wiley Open Access articles for commercial, promotional, or marketing purposes requires further explicit permission from Wiley and will be subject to a fee.

Further details can be found on Wiley Online Library
http://olabout.wiley.com/WileyCDA/Section/id-410895.html

6.5. Curriculum vitae

HUY DUNG HOANG

EDUCATION

Master of Science, Biotechnology **2012-2014**
Graduate school of Agricultural and Life Science, The University of Tokyo, Tokyo, Japan

Bachelor of Science, Biotechnology **2005-2009**
Faculty of Biology, University of Science, Vietnam National University in Ho Chi Minh City, Ho Chi Minh City, Vietnam

HONOURS and AWARDS

Faculty of Medicine Award of Excellence in Graduate Studies, Doctorates **2019**
Faculty of Medicine, University of Ottawa.

BMI Poster Award, 2nd place **2019**
Department of Biochemistry, Microbiology and Immunology, Faculty of Medicine, University of Ottawa

Ontario Graduate Scholarship **2017**
Ministry of Advanced Education and Skill Development, The Government of Ontario

CIHR Travel Award (Travel Award – Institute Community Support) **2016**
CIHR

BioCanRX Travel Award **2016**
BioCanRX, Ottawa, Canada

Faculty of Medicine Destination 2020 Scholarship **2015**
Faculty of Medicine, University of Ottawa

International Admission Scholarship **2015**
Faculty of Graduate and Postdoctoral Studies, University of Ottawa

Certificate of Commendation **2014**
Embassy of the Socialist Republic of Vietnam in Japan (for student with excellent achievement in social activities)

Ajinomoto Scholarship for ASEAN international students **2011-2014**

The Ajinomoto Scholarship Foundation, Japan (approximately USD 21000/year + tuition fee for three years, 1 recipients/country/year for five ASEAN countries)

Faculty Scholarship for Excellence Student **2008**
Faculty of Biology, the University of Science

GRANTS

Canadian Cancer Society Innovation to Impact **2020**
"Bioengineering peak transgene production during viral oncolysis"
Contributed as Additional Author
Amount: $450,000
Duration: 2020 – 2023

RESEARCH EXPERIENCE

PhD candidate **2015-present**
University of Ottawa, Children's Hospital of Eastern Ontario Research Institute

Graduate Student (1 year research student + 2 years M.Sc. student) **2011-2014**
The University of Tokyo, Tokyo, Japan
Project: *Interaction between ER-Golgi cargo receptor and secretory protein, protein secretion optimization*

Research Assistant **2010-2011**
The University of Science, Vietnam National University in Ho Chi Minh City, Ho Chi Minh City, Vietnam
Project: *Immunogenicity of H5N1 HA conserved epitopes predicted in silico*

Undergraduate student **2008-2009**
The University of Science, Vietnam National University in Ho Chi Minh city, Ho Chi Minh city, Vietnam
Project: *Cloning, expressing and purifying of fusion H5N1 hemagglutinin conserved epitopes using E. coli*

TEACHING EXPERIENCE

Teaching assistant **2016-Current**
University of Ottawa, Ottawa, Canada
Introduction to Biochemistry BCH 2333L: Demonstrator/Lab monitor, corrector (Winter 2017)
Introduction to Biochemistry BCH2333A: DGD, corrector (Winter 2016)

Teaching assistant **2012-2014**
The University of Tokyo, Tokyo, Japan
Microbiology Experiment

Teaching assistant **2009-2011**

The University of Science, Vietnam National University-Ho Chi Minh city, Ho Chi Minh city, Vietnam

Experiment in Microbiology

Mentor **2013**

Department of Biotechnology, Laboratory of Microbiology, the University of Tokyo

- Instructed a junior laboratory member with laboratory technique, experiment design and data analysis

PUBLICATIONS

1. Jia, J.-J.; Lahr, R. M.; Solgaard, M. T.; Moraes, B. J.; Pointet, R.; Yang, A.-D.; Celucci, G.; Graber, T. E.; **Hoang, H.-D**.; Niklaus, M. R.; et al. MTORC1 Promotes TOP MRNA Translation through Site-Specific Phosphorylation of LARP1. Nucleic Acids Res. 2021, 49 (6), 3461–3489.
2. Graber, T. E.; Mercier, É.; D'aoust, P. M.; **Hoang, H.-D**.; Tian, X.; Tasneem, S.; Bhatnagar, K.; Delatolla, R. An Allele-Specific Primer Extension Assay to Quantify the Proportion of B.1.1.7-Specific SARS-CoV-2 RNA in Wastewater. medRxiv 2021, 2021.02.22.21252041.
3. Soubeyrand, S.; Nikpay, M.; Lau, P.; Turner, A.; **Hoang, H.-D**.; Alain, T.; McPherson, R. CARMAL Is a Long Non-Coding RNA Locus That Regulates MFGE8 Expression. Front. Genet. 2020, 11, 631.
4. Olagnier, D.; Farahani, E.; Thyrsted, J.; Blay-Cadanet, J.; Herengt, A.; Idorn, M.; Hait, A.; Hernaez, B.; Knudsen, A.; Iversen, M. B.;Schilling, M; Jørgensen, S.E.; Thomsen, M.; Reinert, L.S.; Lappe, M.; **Hoang, H.-D.** et al. SARS-CoV2-Mediated Suppression of NRF2-Signaling Reveals Potent Antiviral and Anti-Inflammatory Activity of 4-Octyl-Itaconate and Dimethyl Fumarate. Nat. Commun. 2020, 11 (1), 1–12.
5. **Hoang, H. D**.; Graber, T. E.; Jia, J. J.; Vaidya, N.; Gilchrist, V. H.; Xiang, X.; Li, W.; Cowan, K. N.; Gkogkas, C. G.; Jaramillo, M.; Jafarnejad, S. M.; Alain, T. Induction of an Alternative MRNA 5′ Leader Enhances Translation of the Ciliopathy Gene Inpp5e and Resistance to Oncolytic Virus Infection. Cell Rep. 2019, 29 (12), 4010-4023.e5.
6. **Hoang, H. D**.; Graber, T. E.; Alain, T. Battling for Ribosomes: Translational Control at the Forefront of the Antiviral Response. Journal of Molecular Biology. Academic Press July 6, 2018, pp 1965–1992.
7. Zakaria, C.; Sean, P.; **Hoang, H.-D**.; Leroux, L.-P.; Watson, M.; Workenhe, S. T.; Hearnden, J.; Pearl, D.; Truong, V. T.; Robichaud, N.; et al. Active-Site MTOR Inhibitors Augment HSV1-DICP0 Infection in Cancer Cells via Dysregulated EIF4E/4E-BP Axis. PLOS Pathog. 2018, 14 (8), e1007264.
8. Graber, T. E.; Freemantle, E.; Anadolu, M. N.; Hébert-Seropian, S.; Macadam, R. L.; Shin, U.; **Hoang, H. D**.; Alain, T.; Lacaille, J. C.; Sossin, W. S. UPF1 Governs Synaptic Plasticity through Association with a STAU2 RNA Granule. J. Neurosci. 2017, 37 (38), 9116–9131.
9. Wang, F.; Alain, T.; Szretter, K. J.; Stephenson, K.; Pol, J. G.; Atherton, M. J.; **Hoang, H. D**.; Fonseca, B. D.; Zakaria, C.; Chen, L.; et al. S6K-STING Interaction Regulates Cytosolic DNA-Mediated Activation of the Transcription Factor IRF3. Nat. Immunol. 2016, 17 (5), 514–522..
10. Fonseca, B. D.; Graber, T. G.; **Hoang, H. D**.; González, A.; Soukas, A. A.; Hernández, G.; Alain, T.; Swift, S. L.; Weisman, R.; Meyer, C.; Robaglia, C.; Avruch, J.; Hall, M. N. Evolution

of TOR and Translation Control. In Evolution of the Protein Synthesis Machinery and Its Regulation; Springer International Publishing, 2016; pp 327–411.
11. Fonseca, B. D.; Zakaria, C.; Jia, J. J.; Graber, T. E.; Svitkin, Y.; Tahmasebi, S.; Healy, D.; **Hoang, H. D.**; Jensen, J. M.; Diao, I. T.; et al. La-Related Protein 1 (LARP1) Represses Terminal Oligopyrimidine (TOP) MRNA Translation Downstream of MTOR Complex 1 (MTORC1). J. Biol. Chem. 2015, 290 (26), 15996–16020.
12. **Hoang, H. D**.; Maruyama, J. I.; Kitamoto, K. Modulating Endoplasmic Reticulum-Golgi Cargo Receptors for Improving Secretion of Carrier-Fused Heterologous Proteins in the Filamentous Fungus Aspergillus Oryzae. Appl. Environ. Microbiol. 2015, 81 (2), 533–543.
13. Tran T.H.K., **Hoang, H.D**., Nguyen T.T.V., Tran L.T. (2011) Assaying immunogenicity of *in silico*-predicted T cell epitope of HA antigen from influenza A/H5N1. *Vietnam Journal of Biotechnology*, 9(4B), 907-913.

CONFERENCES

1. **Hoang, H. D**.; Graber, T. E.; Jia, J. J.; Vaidya, N.; Gilchrist, V. H.; Xiang, X.; Li, W.; Cowan, K. N.; Gkogkas, C. G.; Jaramillo, M.; Jafarnejad, S. M.; Alain, T. (2020). Induction of an Alternative MRNA 5′ Leader Enhances Translation of the Ciliopathy Gene Inpp5e and Resistance to Oncolytic Virus Infection, Invited Oral presentation at the 43rd Annual Meeting of the Molecular Biology Society of Japan, Virtual, hosted at Japan.
2. **Hoang H.D**., Graber T.E., Vaidya N., Jia J.J., Li W., Jafarnejad M., Alain T. (2019) Exploiting translation control during viral oncolysis to enhance therapeutic transgene expression, Poster presentation at the Canadian Cancer Research Conference, Ottawa, Canada.
3. **Hoang H.D**., Graber T.E., Jia J.J., Fonseca B.D., Healy D., Gkogkas C., Sonenberg N., Jafarnejad M., Alain T. (2018) Characterizing the host mRNAs actively translated during viral oncolysis, Oral presentation at the International Oncolytic Virus Conference, Oxford, UK.
4. **Hoang H.D**., Graber T.E., Jia J.J., Fonseca B.D., Healy D., Gkogkas C., Sonenberg N., Jafarnejad M., Alain T. (2017) Characterizing the host mRNAs actively translated during viral oncolysis, poster presentation at the 2017 Summit for Cancer Immunotherapy, Gatineau, Canada.
5. **Hoang H.D**., Graber T.E., Jia J.J., Fonseca B.D., Healy D., Gkogkas C., Sonenberg N., Jafarnejad M., Alain T. (2016) The oncolytic virus translatome: characterizing the host mRNAs actively translated during viral oncolysis, oral presentation at the 2016 International Meeting on Replicating Oncolytic Virus Therapeutics, Vancouver, CA.
6. **Hoang H.D**., Graber T.E., Jia J.J., Fonseca B.D., Healy D., Gkogkas C., Sonenberg N., Jafarnejad M., Alain T. (2015) The oncolytic virus translatome: characterizing the host mRNAs actively translated during viral oncolysis, poster presentation at the 9th International Conference on Oncolytic Virus Therapeutics, Boston, US.
7. **Hoang H.D**., Maruyama J., Kitamoto K. (2013) Identification and functional analysis of ER cargo receptors for secreted proteins in *Aspergillus oryzae*, oral presentation at the 2013 Annual Meeting of the Japan Society for Bioscience, Biotechnology and Agrochemistry, Sendai, Japan.
8. **Hoang H.D**., Maruyama J., Kitamoto K. (2013) Disruption of lectin-type cargo receptor increases recombinant protein production in *Aspergillus oryzae*, poster presentation at the 2013 BIO-UT Symposium, Tokyo, Japan.
9. **Hoang H.D**., Maruyama J., Kitamoto K. (2013) Effect of deleting two putative cargo receptors on heterologous protein production in *Aspergillus oryzae*, poster presentation at the 65th Annual meeting of the Society for Biotechnology, Hiroshima, Japan.

10. **Hoang H.D**., Maruyama J., Kitamoto K. (2013) Involvement of lectin-type cargo receptors in heterologous protein secretion in *Aspergillus oryzae*, poster presentation at the 13th Conference on Fungal Genetics and Molecular Biology, Tsukuba, Japan.

ADMINISTRATIVE EXPERIENCES

CHEO RI representative, Graduate Student Experience Committee **2019**

Communication with BMI Faculty Leadership to improve the BMI graduate students experience. Organize scientific workshops for BMI professors and students.

Administrator, Biomedicine Group **2012-2013**

Biomedicine Group (a group for academic and research experience exchange between Vietnamese students in Biomedical and Biotechnology majors in Tokyo regions)

- Promote academic exchange between other members.
- Drafting group policy, planning activity
- Organizing monthly seminar
- Supervizing the operation of the group fanpage on Facebook

Charter administrative member, Betoaji Charity **2013**

Betoaji (a charity association in Japan founded by Vietnamese students for promoting Vietnam cultural and fund raising for poor children in Vietnam)

- Organizing monthly cultural exchange events
- Helped drafting the organization policy and direction
- Involve in planning and execution other events

REFERENCES

Dr. Tommy ALAIN (PhD thesis supervisor)
Department of Biochemistry, Microbiology and Immunology, University of Ottawa, Ottawa, Canada
Tel: +1-613-737-7600 Ext 4198
Email: tommy@mgcheo3.med.uottawa.ca

Dr. Jun-ichi MARUYAMA (Master thesis mentor)
Department of Biotechnology, Graduate School of Agricultural and Life Science, The University of Tokyo, Japan
Tel: +81-3-5841-5161
Email: amarujun@mail.ecc.u-tokyo.ac.jp